U.PORTO

FEUP FACULDADE DE ENGENHARIA
UNIVERSIDADE DO PORTO

SEISMIC PERFORMANCE ASSESSMENT AND STRENGTHENING TECHNIQUES FOR EXISTING REINFORCED CONCRETE BUILDINGS IN NEPAL

Rakesh Dumaru

Dissertation submitted to the Faculty of Engineering of the University of Porto in fulfilment of the requirements for the degree of Doctor in Civil Engineering.

Supervisor: Humberto Salazar Amorim Varum (Full Professor, FEUP)
Co-supervisor: Hugo Filipe Pinheiro Rodrigues (Adjunct Professor, IPLeiria)

Erasmus Mundus   Smart Link

Acknowledgements

their ideas, experiences, and making my stay fruitful and joyful. I am very thankful to all friends of G212 for making the working environment very friendly and was my nice experience to work with all of them. I would also like to express my special thanks to André Filipe Furtado, João Oliveira, Luis de Matos and Dr. Hossameldeen Ahmed for their valuable help and unconditional support, when I am in trouble. I would also like to thank Mafalda Amorim, Alma Sanchez and Laura Sarchi for always staying beside me as friends and family.

Special thanks to my wife Arati Shrestha and Son Aarush Dumaru, for their unconditional love, support, inspiration and encouragement throughout my research.

Finally, I would like to dedicate my research work to my parents for their unconditional support and inspiration throughout the period.

Dedicated to my father Kanchha Dumaru, mother Krishna Laxmi Dumaru, brother Binod Dumaru, sister-in-law Sita Suwal Dumaru and sisters Bimala and Saru Dumaru

Abstract

The present thesis started with a field reconnaissance conducted two months after the large magnitude earthquake of the 25th April 2015 Gorkha earthquake, Nepal, and the subsequent series of aftershocks that result in more than 9,000 fatalities and additional 22,000 injured, caused by the collapse of the buildings, mainly old masonry constructions and infilled RC framed structures. The collapsed RC structures comprise mainly non-engineered buildings and few pre-engineered buildings. As observed, many failure mechanisms were associated to the irregular distribution of infill panels and to the action of the infills on the response of the RC structure, i.e. soft-storey mechanisms, short-columns, shear failure in the columns. But, in many situations, poor detailing, construction materials and construction quality were observed. RC buildings with a regular distribution of infill walls, and located in one of the most affected areas in Nepal, showed light and moderate damages in the infill walls without damages to the structural elements. This illustrates the positive contribution that infill walls can have. These field observations are aligned with the conclusions of the past six decades of experimental and analytical investigations on the influence of infill panel walls in the response of frame structures that may have important contributions in the structural performance and safety for earthquake demands; however, these studies did not reach a consolidated stage allowing for the derivation of generalized and accurate values and numerical strategies to consider the infill panels in the design and safety assessment of building structures. In addition, the Nepal Building Code (NBC) for ordinary residential buildings, i.e. NBC 205: 1994 and revised NBC 205: 2012, did not introduce the contribution of the infill walls in its design guidelines, but considers the infill walls as non-structural elements, and normally buildings are designed as bare frame structures, which is far from the common construction practice.

Six buildings were selected as case studies, representing three different design approaches, i.e. non-engineered, pre-engineered and well-designed buildings. Besides site reconnaissance, in-situ tests were performed in these buildings, namely Schmidt hammer and ambient vibration tests. Ambient vibration tests allowed to obtain the fundamental

frequencies and the corresponding vibration modes, which was fundamental for model's calibration. One of the case studies is an unfinished pre-engineered building only with the RC elements, which allowed for the calibration of a bare frame model. For this case, the influence of the infill walls distribution on the seismic performance is detailed, based on adaptive pushover analysis and nonlinear time history analysis; it was concluded that the strength of the infilled frame increases approximately 3 to 4 times relatively to the bare frame, and the soft-storey configuration revealed to be much more vulnerable when compared with the fully infilled building.

Different strengthening strategies are investigated, with the aim to reduce the seismic vulnerability of existing buildings, namely studying common practice retrofitting strategies, variations in its distribution and location. Based on the results of the nonlinear time-history analyses, it was concluded that all the retrofit techniques and strategies studied could help in enhancing the seismic performance of typical existing RC buildings, namely in terms of stiffness, strength, ductility and energy dissipation capacity. In addition, a probabilistic cost-benefit analysis was performed for the retrofitting methods and strategies studied, based on the expected annual loss and lifecycle loss, considering the discount rate as 10% p.a. and 25 years as the service life of the retrofitted buildings. The results showed that steel bracing is a suitable retrofitting technique, being, in some case studies, the more efficient in reducing the vulnerability of the building; but the addition of shear wall revealed to be in many situations the more economically beneficial. With the parametric analysis, it was possible to prove that a positive cost-benefit ratio (CBR) could be obtained faster than expected even considering only the direct structural loss, where the CBR for the non-engineered and pre-engineered buildings could be achieved in 19 and 5 years, respectively. In the end, a prototype building was defined and analysed with a plan layout and structural details defined as specified in the revised NBC 205: 2012, for different scenarios associated to the adoption of different dispositions of infill walls and to the construction of additional storeys; results allow to conclude on the seismic vulnerability and collapse mechanisms expected for buildings with those type of constructive options and/or modifications.

Resumo

A presente dissertação teve início com uma inspeção e subsequente campanha experimental realizada em Bhaktapur (Nepal) após o sismo de 25 de Abril de 2015 com epicentro em Gorkha. O referido sismo e as réplicas subsequentes conduziram ao colapso de edifícios, principalmente edifícios antigos de alvenaria e edifícios de betão armado (BA) com paredes de alvenaria, provocando cerca de 9000 mortes e mais de 22000 feridos. Os edifícios de BA destruídos englobam essencialmente edifícios construídos com base no conhecimento empírico local sendo que apenas uma pequena parte constitui edifícios executados com recurso a conhecimento técnico de engenharia. No decurso da inspeção realizada registaram-se diversos mecanismos de rotura, nomeadamente mecanismos associados à distribuição irregular dos painéis de alvenaria e mecanismos provocados pela influência destes painéis na reposta sísmica das estruturas e.g. roturas do tipo soft-storey, pilares curtos e rotura dos pilares por esforço transverso. Para além dos mecanismos mencionados, verificou-se a existência de casos de pormenorização inadequada, materiais de construção de fraca qualidade e execução pouco cuidada. Contudo, a existência de edifícios localizados numa das zonas mais afetadas pelo sismo, sem qualquer dano nos elementos estruturais apresentando apenas danos ligeiros a moderados nos painéis de alvenaria, evidenciaram o efeito benéfico da distribuição regular destes elementos nas estruturas inspecionadas. As observações registadas durante a campanha efetuada, em conjunto com as conclusões retiradas ao longo de seis décadas de trabalhos de investigação, acerca da influência dos painéis de alvenaria na resposta sísmica de estruturas porticadas, revelam a importância destes elementos na performance e segurança estrutural dos edifícios em situações sísmicas. No entanto, os estudos realizados até à presente data não atingiram um nível de conhecimento suficientemente sólido que permita a generalização e aplicação de regras, bem como a definição de estratégias numéricas que possibilitem um dimensionamento e verificação de segurança adequados. Mais ainda, a norma Nepal Building Code (NBC) destinada ao dimensionamento de edifícios residenciais genéricos, i.e. NBC 205:1994 e a NBC 205:2012, não inclui a contribuição de paredes de

alvenaria nas regras de dimensionamento, classificando estes elementos como não-estruturais, pelo que o cálculo de edifícios considerando apenas a estrutura de BA constitui a prática corrente de dimensionamento.

Desta forma, foram selecionados seis edifícios para integrarem um conjunto de casos de estudo, representando três abordagens de dimensionamento distintas, i.e. edifício não-dimensionado, edifício dimensionado por regras simples, e edifício corretamente dimensionado. Os edifícios selecionados foram alvo de uma campanha experimental com recurso a testes in-situ, nomeadamente ensaios de caracterização do betão com recurso ao esclerómetro de Schmidt e ensaios de vibração ambiental. A calibração dos modelos numéricos desenvolvidos foi efetuada com base nos resultados dos ensaios de vibração ambiental. Um dos casos de estudos corresponde a um edifício inacabado constituído apenas pelos elementos estruturais de BA, tendo servido de base para a calibração do modelo numérico correspondente. No caso referido, a influência das paredes de alvenaria foi avaliada através de análises push-over e análises não-lineares do tipo time-history. Os resultados mostram que a consideração dos painéis de alvenaria conduz a uma resistência cerca de 3 a 4 vezes superior à da estrutura constituída apenas pelos elementos de BA, revelando a última uma maior suscetibilidade a modos de rotura por soft-storey.

Mais ainda, foram investigadas diversas técnicas de reforço estrutural, tendo em vista a redução da vulnerabilidade sísmica dos edifícios existentes, com especial enfoque em estratégias de reforço de prática corrente, variando a sua distribuição e localização no edifício. Tendo por base os resultados das análises time-history, concluiu-se que todas as técnicas e estratégias de reforço estudadas conduzem a um desempenho sísmico superior, no que toca a rigidez, resistência, ductilidade e capacidade de dissipação de energia de edifícios típicos de BA. Além disso, foi também realizada uma análise probabilística de custo-benefício das técnicas e estratégias referidas, tendo por base estimativas anuais de perda bem como perdas durante o tempo de serviço, considerando uma taxa de evolução de custos de 10% p.a. e 25 anos de vida útil dos edifícios considerados. Os resultados indicam que o contraventamento das estruturas com recurso a diagonais metálicas constitui uma abordagem de reforço adequada, tendo-se revelado em alguns casos a técnica mais eficiente na redução da vulnerabilidade sísmica dos edifícios. Contudo, a inclusão de paredes de BA revelou ser na generalidade dos casos a técnica com maior benefício económico. Mais ainda, as análises paramétricas efetuadas indicam que um rácio custo-benefício (CBR) positivo pode ser conseguido mais rapidamente do que esperado, mesmo considerando o efeito das perdas estruturais diretas, nos casos em que o CBR para a classe

edifícios não-dimensionados e "pré-dimensionados" foi conseguido em 19 e 5 anos. Finalmente, procedeu-se à análise de um edifício-tipo, dimensionado e pormenorizado de acordo com as regras prescritas na norma NBC 205:2012, tendo-se considerado vários cenários de disposição das paredes de alvenaria assim com a inclusão de pisos adicionais. Os resultados obtidos permitiram retirar conclusões acerca da vulnerabilidade sísmica bem como dos mecanismos de colapso expectáveis para edifícios com tipologia e opções construtivas semelhantes.

Table of Contents

Chapter 7. Cost-benefit Analysis of Retrofitted Non-engineered and Pre-engineered Buildings using Probabilistic Approach   281

Chapter 8. Seismic Fragility Assessment of Revised MRT Buildings considering typical Construction changes   331

Table of Figures

Chapter 1. - Introduction

Chapter 2. – Seismic Performance of Buildings in Nepal after the Gorkha Earthquake

Chapter 3. – Case Study Buildings and Field Tests

Chapter 4. –Literature Review

Chapter 5. – Numerical Analysis and Results Discussion

Chapter 6. – Seismic Retrofitting of the Case Study Buildings

Chapter 7. – Cost-benefit Analysis of Retrofitted Non-engineered and Pre-engineered Buildings using Probabilistic Approach

Chapter 8. – Seismic Fragility Assessment of Revised MRT Buildings considering typical Construction changes

Table of Tables

Chapter 1. – Introduction

Chapter 2. – Seismic Performance of Buildings in Nepal after the Gorkha Earthquake

Chapter 3. – Case Study Buildings and Field Tests

Chapter 4. –Literature Review

Chapter 5. – Numerical Analysis and Results Discussion

Chapter 6. – Seismic Retrofitting of Case Study Buildings

Chapter 7. – Cost-benefit Analysis of Retrofitted Non-engineered and Pre-engineered Buildings using Probabilistic Approach

Chapter 8. – Seismic Fragility Assessment of Revised MRT Buildings considering typical Construction changes

Chapter 1.

Introduction

1.1   General Overview

Nepal is a mountainous country that lies between China in the north and India on the other three sides. The energy generated and stored due to continuous convergence between Indian and Tibetan plates, can be released in the form of large magnitude earthquakes. It is revealed that at least one major earthquake of magnitude > 7.5 can occur in every 70-80 years [1, 2].

Table 1.1 shows approximate recurrence interval of earthquakes in Nepal and the surrounding region between 1911-1991 [3]. It illustrates that the small magnitude earthquakes occur frequently in the interval of less than 2 years. Similarly, Table 1.2 shows the major historical earthquakes recorded in Nepal since 1200 [4]. The 1934 Nepal-Bihar earthquake of magnitude 8.3 was considered the worst earthquake history recorded in Nepal. It caused extensive damages in Nepal and northern Bihar resulting in more than 8,500 fatalities. In addition, almost 20% of the houses collapsed only in Kathmandu Valley and more than 40% were damaged [5]. The first earthquake was recorded in the year 1255 having a magnitude of 7.8, and led to the severe damage and collapse of temples, monuments and traditional houses. It was recorded that one third of the population in Kathmandu Valley was killed including King Sri Abhaya Malla. The human fatalities recorded by major historic earthquakes: dated 1408 of magnitude 8.2 killed more than 2,500 people, earthquake of magnitude 8.8 in the year 1505 resulted almost 6,000 people death, and earthquake of magnitude 8.0 in the year 1681 that killed more than 4,500 people [6].

Table 1.1 - Magnitude-frequency earthquake data in Nepal and surrounding region between (1911-1991) [3]

Earthquake in Richter Scale	5 to 6	6 to 7	7 to 7.5	7.5 to 8	> 8
No. of Events	41	17	10	2	1
Approximate Recurrence Interval (years)	2	5	8	40	81

Table 1.2 - Historical major earthquakes recorded in Nepal since 1200 [4]

Year (AD)	Description
7th June, 1255	Severe damage in Kathmandu with estimated intensity X (Rana, *et al.* (2007)) and a magnitude of 7.8. Destroyed many houses and temples in Nepal and killed one-third of population.
1260	Collapse of many buildings and temples, and subsequent widespread epidemic and famine.
1408	Completely destroyed Rato Matchendranath Temple, and severely damaged and collapsed many buildings and temples in Kathmandu valley.
1681	Heavy collapse and damage of many buildings that caused heavy loss of life in Nepal.
1767	21 aftershocks reported within 24 hours period. No information is available regarding the losses and damages.
1810	21 shocks were recorded over a period of a month. Numbers of casualties were relatively low but some buildings and temples were severely damaged and destroyed.
1823	17 shocks of moderate magnitude were felt in Kathmandu valley. No loss of human life or livestock was recorded.
1833	Two main shocks hit Kathmandu valley, one at 6 pm and other at 11 pm (NST local time). Most of the buildings, houses, public shelters and temples were collapsed. The Dharahara tower was severely damaged. In addition, Thimi and Bhaktapur were completely destroyed. More than 18,000 houses were collapsed throughout Nepal that included 4,214 houses in the Kathmandu Valley only.
1834	Four main shocks reported during June and July. Excessive rain resulted damage to the bridges.
15th January,1934, Great Nepal-Bihar earthquake	The most devastating earthquake recorded in the history of Nepal with magnitude of 8.0 that led highest number of casualties ever in the three cities of Kathmandu valley; namely, Kathmandu, Bhaktapur and Patan. More than 126,000 houses were severely damaged and also more than 80,000 buildings completely collapsed.
1980	Earthquake of magnitude 6.5 with epicentre in Far-western development region of Nepal. 125 people lost their lives, 248 seriously injured; 13,414 buildings severely damaged and 11,604 buildings completely destroyed.
21th August,1988, Udaipur earthquake	Earthquake of magnitude 6.9 affects mostly in the eastern region of Nepal that led to 721 deaths and 6,553 seriously injured, and also damaged more than 65,000 buildings. The estimated loss was 5 billion rupees.
18th September, 2011	Earthquake of magnitude 6.9 with epicentre 272 km east of Kathmandu that caused widespread damage in Nepal. This earthquake caused more than 6,000 houses collapses, as a result 164 people got injured, 3 fatalities and more than 14,000 houses were damaged. (CUEE report 2011-1).
25th April 2015	Earthquake of magnitude 7.8 with epicentre in Gorkha district led to more than 8,000 fatalities and more than 22,000 people got injured. More than 550 earthquakes of magnitude greater than 4 were recorded within 45 days.

The reinforced concrete (RC) frames with unreinforced masonry walls are a common construction practice around the globe and is even more frequent in seismically active regions and developing countries like Nepal. The unreinforced infill masonry walls are usually the combination of solid bricks size (230 x 115 x 75) mm³ connected by a mortar layer (with 10 mm thickness). Generally, the external infill walls were laid in two leaves and one leave for internal infill walls. In this type of construction, no special connections are provided at the interface between infill walls and the surrounding frames. Extensive researches, both experimental and analytical over the past decades examined the influence of infill walls and its interaction with the surrounding frames. It was concluded that infill

wall demonstrates both positive and negative contributions along with RC frame buildings [2, 7-11]. The positive contribution was illustrated by a significant increase in stiffness and strength capacity of the infilled buildings. The negative contribution can be related with the potential structural collapse under soft-storey mechanism due to brittle behaviour of infill walls. In some cases in- and out-of-plane failure of infill walls could also initiate shear failure in the columns and short-column mechanisms. Figure 1.1 presents experimental findings, illustrating the contribution of infill wall on the global in-plane response of infilled RC frames [12]. The lateral strength of infilled frames was found to have increased by almost 0.5-3.5 times compared with corresponding bare framed structures [12]. Similarly, the test results for confined masonry walls also exhibit an adequate increase in shear and flexure strength but a decrease in displacement capacity of the infilled RC buildings [13-17]. Pujol, *et al.* (2008) [18] concluded that the addition of infill panels not only increases stiffness and strength by 500% and 100%, respectively, but also prevents the collapse of the slab. Furthermore, Varum, H. (2003) [8] test results concluded that infill panels protects the frame structures for low to medium ground intensities, and also increases the fundamental frequencies by almost four times compared to the bare frame.

The RC building construction started in Nepal about more than 3 decades ago. The observed element sections and reinforcement details revealed that these structures were designed for carrying gravity loads and did take into account any seismic consideration, exhibiting higher vulnerability to the inhabitants. This could be justified from the observed building damages recorded after 25th April 2015 Gorkha earthquake and subsequent series of small to large magnitude aftershocks, where 6,613 RC buildings collapsed and 16,971 were partially collapsed [19]. The in-situ site survey conducted after Gorkha earthquake also revealed that RC buildings with irregular distribution of masonry infill walls are more likely have various levels of damage states, i.e. most likely extensive damage, and in some cases partial collapse and total collapse states. The collapse of the infilled RC buildings was reported mostly due to soft-storey mechanism, and partial-collapse was mainly due to short-column and shear failure mechanisms as a result of in- and out-of-plane failure of infill walls (see Figure 1.2). Despite these facts, Nepal National building Code (NBC), i.e. NBC 205: 1994 [20] and later revised NBC 205: 2012 [21] guidelines for ordinary residential buildings did not integrate infill panels contribution. In Clause 4.1 and 4.2 of revised NBC 205: 2012 [21], it is clearly stated that the RC buildings should be designed as bare frame for resisting the lateral loads that does not match in real construction site. In

addition, it could be stated that the revised NBC guideline was primarily focused on increasing the structural section sizes and detailing rather than to integrate infill walls influence in the design, whose seismic performance could vary largely with small variation in the infill walls parameters [10]. Therefore, the present study primarily intends to focus on the combined behaviour of the infilled frames and also the study intended to stress to the need of its consideration in the design of RC buildings.
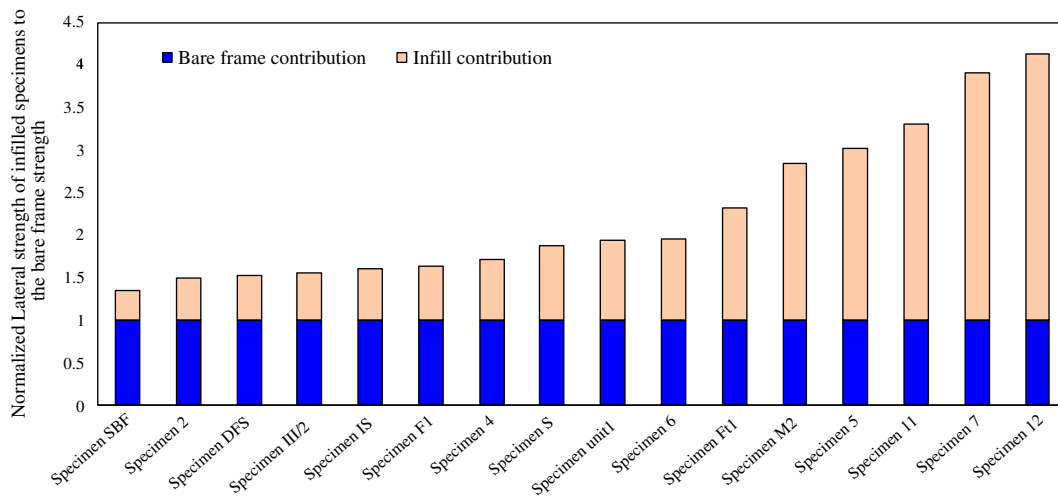
Figure 1.1 – Examples illustrating the contribution of the infill panels for the global infilled RC frames (after Hossameldeen, 2017 [12])

Figure 1.2 – Examples of infill wall negative contributions on infilled RC buildings; (a) Soft-storey, (b) Shear in column, (c) Short-column, (d) In-plane and (e) Out-of-plane failure of infill walls

1.2   Objectives and Overall Strategies

The main objective of the present work is to investigate the seismic performance assessment of the existing RC buildings that represent different design approaches, i.e. non-engineered, pre-engineered and well-designed buildings, and the influence of infill walls in these building typologies.

To attain these objectives, the intended study was carried out in four stages, which include detailed site inspection and field tests, model calibration and performance assessment,

assessment of strengthening solutions with a probabilistic cost-benefit analysis. Therefore, initial site works were carried out to identify the state of structural members, the construction and the material quality deficiencies for the entire selected buildings. Two types of in-situ tests were performed for each case study buildings, i.e. Schmidt hammer tests and ambient vibration tests. In addition, the geometrical and structural element dimensions were also measured for this investigation. The data was used in the second stage to calibrate the developed numerical models. In the second stage, three-dimensional modelling was carried out through finite element software, i.e. SeismoStruct [22] in which the frame elements were modelled as inelastic force-based frame element type and macro-modelling of infill walls with the six struts model proposed by Crisafulli, F. (1997) [11]. The contribution of infill walls and its effect on the frame structures were detailed investigated under nonlinear time history analyses considering an existing bare frame building. The bare frame conclusions will be further reinforced through the study of prototype NBC 205: 2012 building [21]. The incremental dynamic analysis (IDA) and fragility curves were generated and identified seismic vulnerability of case studied buildings.

In the third stage, the buildings illustrating poor seismic performance were strengthened with three retrofit techniques, whose sections and detailing were designed following guidelines procedures. Finally, probabilistic cost-benefit analysis was performed, as it is one of the determining factors to influence decision makers about the benefit of investing money for retrofitting existing buildings. Therefore, the cost-benefit analysis of the retrofitted buildings was performed and compared.

In the last part, a prototype building whose geometrical layout, structural sections and its detailing initially designed for three-storey bare frame building was selected similar to as proposed by NBC 205: 2012 [21] guideline to investigate the adequacy of such assigned structural sections and reinforcement details. Furthermore, the building performance was examined through variable number of storeys and also through different arrangements of infill walls that are commonly practiced. This study aimed to make aware the concerned authorities that structural sections and reinforcement details stated in the current revised NBC 205: 2012 might not be adequate based on the current trend of practice.

The summarized methodologies adopted in the present thesis are presented in Figure 1.3. Here, the seismic capacity and demands characterized in terms of inter-storey drift for the entire case study buildings.
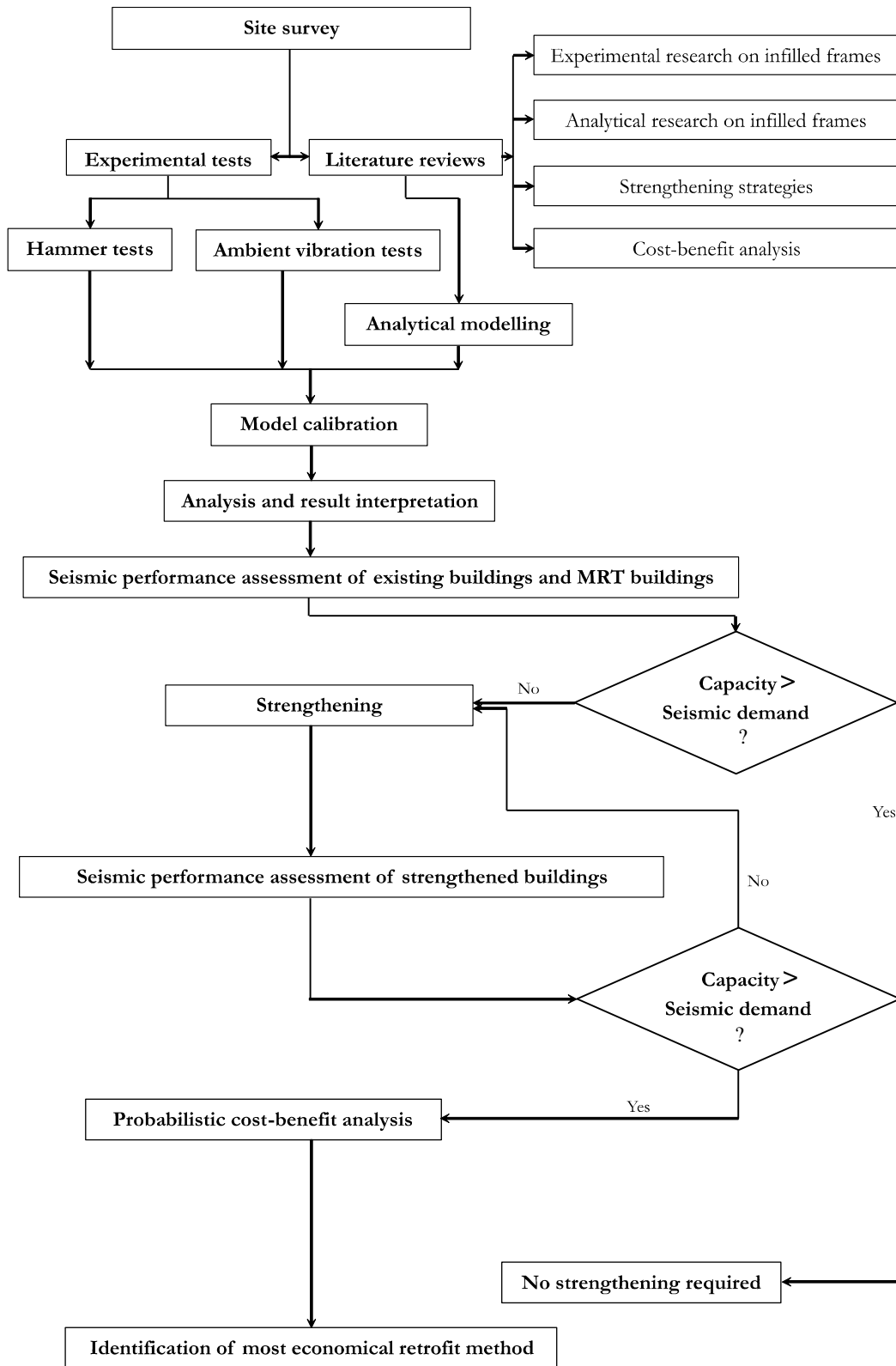
Figure 1.3 – Summary of the research methodology considered in the present thesis

1.3   Thesis Organization

The present work has been structured into nine chapters. The general overview and the objectives of the study are discussed in the present Chapter.

Chapter 2 describes the general construction practice of the RC buildings in Nepal and points out to the need of design codes and guidelines for reducing damages in infilled RC buildings, which eventually minimizes human injuries and casualties. The structural failure caused by the irregular distribution of infill walls, weak-column and strong-beam, and insufficient reinforcement details, as observed in-situ, is also discussed in this chapter. In addition, RC construction defects, such as material quality, insufficient effective cover, exposure of reinforcement, etc. are also discussed in detail. Furthermore, Chapter 2 demonstrates various failure modes observed in the RC buildings, unreinforced masonry buildings, and vernacular and rural constructions, as recorded after Gorkha earthquake.

Chapter 3 presents an overview of all case study buildings, which includes building plan layout, structural details, observed construction drawbacks and state of the building recorded during site survey. The chapter also discusses in-situ tests performed on each case studied building which helps to determine and identify existing concrete strength and dynamic properties of the existing buildings. The concrete strength of the structural elements was identified through Schmidt hammer test that was later calibrated. Similarly, the dynamic properties, such as fundamental frequencies and damping ratio of the case studied buildings after earthquakes were captured through ambient vibration tests. The results were processed using ARTeMIS software, and later used to calibrate numerical models through parametric study. The chapter also presents first three fundamental frequencies and corresponding vibration modes obtained from the eigenvalue analysis. In addition, this chapter also presents standard material properties and general loading conditions to be considered in detailed analysis.

Chapter 4 reviews the past experimental and analytical investigations on the failure modes of the infilled frames, and also the RC frames interaction with infill walls. The chapter also discusses the development of various analytical approaches to capture the structural behaviour of infilled frames, includes micro-modelling and macro-modelling. The macro-modelling is discussed in detail as strength and stiffness methods. Later, the chapter presents the literature reviews on modification of diagonal struts model and multiple struts model to represent more precisely infill walls behaviour with surrounding frames. In

addition, Chapter 4 also discusses various strengthening approaches, its design philosophy and its influence on the existing structures. The strengthening approaches include concrete column jacketing, addition of RC shear walls and steel bracing. The detailed numerical modelling adopted for the frames and infill panels, and various analysis types, thresholds of limit states and literature review on the development of the fragility curves are also integrated in this chapter.

In the first section of Chapter 5, the detailed seismic performance assessment of an existing bare frame building is carried out and the global building performance is later investigated through different arrangements of infill walls throughout the building. The model calibration is initially performed through a parametric study. A detailed seismic performance of bare frame building with various dispositions of infill walls was evaluated under nonlinear static and dynamic time history analyses. The variation in base shear capacity was evaluated through capacity curves and the state of the building and likely damages at particular IMs are investigated through fragility curves. Similarly, the seismic performance of the other existing infilled buildings is also carried out in the similar manner; however, distributions of the infill walls are identical as observed and measured during site inspections.

Chapter 6 presents brief literature reviews in strengthening techniques and adopted material properties, sections and reinforcement details. The existing buildings that are found seismic deficient and highly vulnerable are proposed to be strengthened through three retrofit techniques, such as concrete column jacketing, circular hollow section steel bracing, and RC shear wall. Their layouts, sections and reinforcement details, and number of storeys required to retrofit are discussed in detail in this chapter. Similar to the Chapter 5, the seismic performance of the strengthened buildings are investigated under nonlinear static and dynamic time history analyses. The attained results are demonstrated and discussed in detail in this chapter. The degree of level of damages reduced with the addition of new elements is also investigated in this chapter through a comparative study of fragility and IDA curves.

Chapter 7 presents the detailed probabilistic cost-benefit analysis of retrofitted buildings presented and discussed in Chapter 6. This chapter includes the state-of-art of previous works on the cost-benefit analysis, seismic loss assessment framework and seismic hazard curves for the site and different damage factors. The chapter also includes various empirical equations and various cost-benefit estimation models for estimating the expected

annual loss (EAL), life cycle loss (LCL) and the cost-benefit ratio (CBR). The Chapter discusses the steps considered in the study for the estimation of cost-benefit analysis and results are summarized illustrating the losses that correspond to each damage state, discrete and cumulative distribution of EAL and risk curves. In addition, the sensitivity analysis is also performed for each building to identify the point of pay-back period, and further helps to clarify owners and concerned stakeholders to make conclusive decisions.

Chapter 8 discusses three storeys prototype bare frame building, initially designed and detailed based on revised NBC 205: 2012 guideline. The building is later modified through three infill walls configurations and variable number of storeys, assuming all parameters and material properties remaining constant to represent the real building scenario of the past and present. The study also attempts to acquaint concerned owner, authorities and stakeholders regarding potential vulnerability of the building before and after modifications. It also checks the adequacy and the sufficiency of predefined structural sections and reinforcement details.

The last chapter of the thesis summarizes the main conclusions from the previous chapters and identifies key results, along with the possible recommendations for future researches are also addressed.

Chapter 2.

Seismic Performance of Buildings in Nepal after the Gorkha Earthquake

2.1   Summary

The chapter discusses common RC frame construction practice and structural defects recorded from the site reconnaissance. The global behaviour of existing non-engineered and pre-engineered buildings and likely different failure modes of infill walls and structures as a whole observed after Gorkha earthquake were presented. The need of design codes and its proper implementation are justified through extensive damage. It includes partial or complete collapse of the infill walls and building itself, mainly due to vertical irregularities that leads to stiffness differences between adjacent storeys and subsequent soft-storey mechanisms. This type of failure mechanism was mostly observed in non-engineered structures and in some pre-engineered buildings. Similarly, well-designed buildings also demonstrated significant damages in non-structural elements, particularly in masonry infill walls. The observed extensive damages and large number of collapsed URM buildings and vernacular constructions was likely due to poor construction materials and weak or non-existent connections between the walls and floors or roof, which can lead to improper transmission and distribution of stresses among the various elements. This type of building lack structural integrity between orthogonal walls, and could potentially lead to out-of-plane collapse of masonry walls. Most of the contents discussed in the present chapter were already published in the book entitled "*Impacts and Insights of the Gorkha Earthquake*".

2.2   Introduction

On April 25, 2015, at 11:56 a.m. local time, an earthquake of magnitude, M_w 7.8 hit central, eastern and parts of western Nepal. The mainshock was followed by several strong aftershocks with magnitudes greater than 6.5, the strongest of which was recorded on May

12, 2015 (M_w =7.3). The Kathmandu valley and surrounding areas were mostly affected by the earthquake. The Kathmandu valley contains mainly substandard to pre-engineered RC buildings, along with brick masonry infill and adobe residential buildings, and thousands of heritage sites and monuments. In valley periphery and regions outside the Kathmandu Valley, rubble masonry stone buildings are the most common building type. In addition, hundreds of villages in the regions surrounding the valley are settlements characterized by buildings of vernacular construction, all designed without concerns to seismic activity.

The earthquake caused extensive damage to both recent and older constructions in the Kathmandu Valley that resulted in 8790 casualties and 22,000 injured [6]. According to the Government of Nepal, 498,852 residential buildings collapsed due to mainshock and aftershock seismic sequences and another 256,697 residential buildings were partially damaged. Although the damage was primarily to non-engineered to pre-engineered RC and brick/stone masonry buildings, closer analysis revealed that a significant amount of damage was sustained by a very large number of buildings, while many other building types performed surprisingly well following the earthquake.

A detailed description of the seismic performance of existing buildings in Nepal following the April 2015 Nepal earthquake can provide valuable insights into the seismic risk and future opportunities for retrofit and mitigation, not only in Nepal but also in other seismic regions that may be subjected to similar strong shaking. In this context, this chapter presents a brief overview of the damage observed and recorded during a field reconnaissance survey that was carried out after the two main seismic events. The performance of buildings is discussed, focusing on recent RC buildings construction and briefly on older substandard constructions, urban masonry building stocks as well as rural vernacular constructions. This chapter presents evidences from the field survey to justify the seismic performance as well as to depict the damage modes which can be insightful in the case of earthquake resistant constructions and seismic strengthening strategies worldwide.

2.3   Evolution and Need of Design Code for RC Structures

The RC construction increased drastically over the last few decades in the Kathmandu Valley and other major urban centres in Nepal to meet the rapidly increasing settlement of the region. RC constructions started around four decades ago as an alternative to traditional unreinforced masonry (URM) buildings that lack structural integrity and

ductility. These buildings were designed to carry only vertical loads, without considering lateral seismic forces. These types of buildings were built to satisfy client requirements by contractors based on his past experiences and, in some cases, under the guidance of mid-level technicians and masons, mostly without consulting design professionals. As per National Census of 2011, about 10 % of the building construction in Nepal is RC, with more than 40 % of the total RC construction being concentrated only in the Kathmandu Valley, as shown in Figure 2.1.
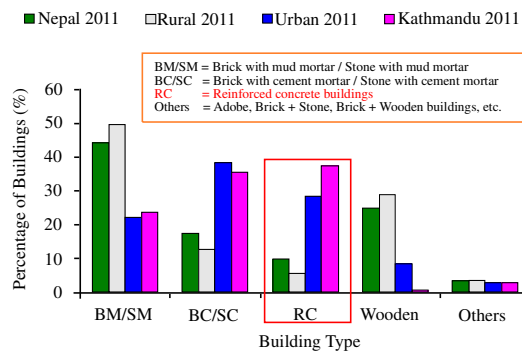
Figure 2.1 – Building types in Nepal [23]

In Nepal, RC buildings constructed before the implementation of design codes are typically characterized by low concrete quality and poor workmanship, often with inadequate column and beam section sizes, insufficient longitudinal reinforcement, large stirrup spacing and weak beam-column joints. Furthermore, such buildings frequently employ unreinforced solid infill panels for external and internal partition walls. These types of buildings are more susceptible to damages as recorded in past earthquakes in the neighbouring countries like India, China, Japan and all around the globe. In addition, the damage to RC buildings resulting in large numbers of injuries and casualties in 1988 Udaipur earthquake drew attention to the need of modifications and improvements in current design practice and methods.

Table 2.1 and Table 2.2 presents the lists of design codes used in Nepal. The primary objective of these design codes is to replace the haphazard RC construction practiced in Nepal, such that these structures satisfy minimum seismic requirement. The buildings design intends to avoid and/or reduce the possible future structural and non-structural losses, which eventually minimizes human injuries and fatalities, and other loss related to monetary values, such as relocation loss, rental loss, business loss, maintenance or replacement loss and so on. In present practice the design codes are utilized for the

approval of architectural drawings by the concerned authorities and later its implementation is uncertain and vague if past and present trends are considered. This explanation will be justified in the following sections through damaged non-engineered and pre-engineered buildings observed after Gorkha earthquake. In the present section, the main design codes commonly practiced for design of RC buildings in Nepal are discussed.

Table 2.1 - List of design codes in Nepal

NBC 000: 1994	Requirements for State-of-the-Art Design: An Introduction
NBC 101: 1994	Materials Specifications
NBC 102: 1994	Unit Weight of Materials
NBC 103: 1994	Occupancy Load
NBC 104: 1994	Wind Load
NBC 105: 1994	Seismic Design of Buildings in Nepal
NBC 106: 1994	Snow Load
NBC 107: 1994	Provisional Recommendation on Fire Safety
NBC 108: 1994	Site Consideration for Seismic Hazards
NBC 109: 1994	Masonry: Unreinforced
NBC 110: 1994	Plain and Reinforced Concrete
NBC 111: 1994	Steel
NBC 112: 1994	Timber
NBC 113: 1994	Aluminium
NBC 114: 1994	Construction Safety
NBC 201: 1994	Mandatory Rules of Thumb: Reinforced Concrete Buildings With Masonry Infill
NBC 202: 1994	Mandatory Rules of Thumb: Load Bearing Masonry
NBC 203: 1994	Guidelines for Earthquake Resistant Building Construction: Low Strength Masonry
NBC 204: 1994	Guidelines for Earthquake Resistant Building Construction: Earthen Building (EB)
NBC 205: 1994	Mandatory Rules of Thumb: Reinforced Concrete Buildings Without Masonry Infill
NBC 206: 2003	Architectural Design Requirements
NBC 207: 2003	Electrical Design Requirements for (Public Buildings)
NBC 208: 2003	Sanitary and Plumbing Design Requirements

Table 2.2 - NBC design codes based on their uses

SN.	Types of Building Code	Purpose
1	International State-of-Art Applicable codes: NBC 000	Applicable to large building structures. The Structures must comply with existing international state-of-the-art building codes.
2	Professionally Engineered Buildings Applicable Codes: NBC 101 NBC 107 NBC 113 NBC102 NBC 108 NBC 114 NBC 103 NBC 109 NBC 206 NBC 104 NBC 110 NBC 207 NBC 105 NBC 111 NBC 208 NBC 106 NBC 112	Buildings designed and constructed under the supervision of engineers, buildings with plinth area more than 1,000 sq. ft., buildings having more than 3 stories, buildings with span more than 4.5 m and buildings with irregular shapes.
3	Mandatory Rules of Thumb Applicable Codes: NBC 201, NBC 202, NBC 205	Buildings of plinth area less than 1,000 sq. ft., less than 3 stories, buildings having span less than 4.5 m and regular buildings designed and constructed by technicians in the areas where professional engineers' service is not available.
4	Guidelines of Remote Rural Buildings (Low Strength Masonry/ Earthen Buildings): NBC 203 and NBC 204	Buildings constructed by local masons in remote areas and not more than 2 stories.

2.3.1 Nepal National Building Code (NBC 205: 1994) and revised NBC 205: 2012

NBC 205: 1994 [20] is also known as Mandatory Rule of Thumb (MRT). It was first prepared in 1993 as a part of a project to formulate a National Building Code for Nepal. Until 1991, Nepal did not have any regulations or documents of its own setting out either requirements or good practice for achieving satisfactory strength and ductility in buildings. The MRT guideline was prepared by a team of subcontractor's within the department of building and Ministry of Housing and Physical Planning (MHPP). The first design code was approved and implemented only in 2004.

MRT guideline is intended for the mid-level technicians (overseers and draughtspersons) who are not trained to undertake independently the structural design of buildings. This guideline can also be utilized by civil engineers for effective design of buildings following design procedures. The MRT guideline offers ready-to-use dimensions for all components, includes detailing of structural and non-structural members for specified building types. The guideline assumes masonry infill walls as non-structural elements, thus its contribution is neglected and buildings are designed as bare frame so that lateral forces are to be resisted by the frame alone.

NBC 205:2012 [21] is a modified form of NBC 205:1994 [20], such that these guidelines are applicable for regular RC buildings up to three storeys. As stated above, previous experimental and numerical investigations concluded that masonry infill walls drastically increases stiffness and strength capacities if the seismic demand does not exceed the deformation capacity of the structure and decreases the deformation capability of the structure with respect to the maximum capacity [2, 7-9]. In addition, infill walls changes the dynamic behaviour of the buildings. However, these facts could not be integrated in the revised MRT building as well, where infill panels were again assumed as non-structural elements. Besides many similarities with previous MRT guideline, the revised MRT introduced some modifications, such as increased the column and beam sections, increased number of longitudinal bars, reduced transverse reinforcement spacing and also improved concrete strength to 20 MPa.

Chaulagain, 2015 [2] performed numerical investigations on the prototype NBC 205:1994 buildings [20], and concluded that column sections and reinforcement details defined in previous MRT guideline is insufficient. Therefore, in the present thesis, the numerical investigation on prototype building designed based on revised MRT guideline [21] was

performed. In addition, the evaluation is extended with various orientations of masonry infill panels and added number of storeys to study its influence on the building performance, which will be discussed in detail in Chapter 8.

2.3.2   NBC 105:1994

NBC 105:1994 guideline [24] provides minimum requirements for seismic design of buildings. The seismic design code is applied in conjunction with Indian Standard (IS 4326:1976) [25], a code of practice for earthquake resistant design and construction of buildings. For earthquake loads the buildings are designed in accordance with either Working stress method or Limit state method, such that the design shall be in accordance with the Limit state method unless specifically noted otherwise. This code intends to design buildings that are not covered by NBC 205:1994 [20] and revised NBC 205:2012 [21], i.e. mostly used for important and high rise buildings. This design code is not applicable for buildings having height greater than 90 m. In addition, the code also does not consider the infill walls contribution, a main limitation of the design code.

2.4 RC Building Construction Practice and Observed Structural Defects

As discussed already, the past constructed infilled RC buildings in the region did not follow any design code. Also site surveys revealed that those designed MRT buildings [20] in most cases range from 3 to 6 storeys, and most likely irregularly infilled. Site reconnaissance also observed structural defects that potentially disturb the load path and others include short-column at the staircase landing, lack of continuity of floor beams at the stair landing that decreases the effectiveness of floor diaphragms, and absence of seismic gap between adjacent buildings that could result in pounding during ground shaking, as illustrated in Figure 2.2. Other detected structural defects included issues related to slender buildings that increased the expected drift demands, and very different floor height and floor elevations between adjacent buildings. The latter increased the propensity for these buildings to strike each other, causing the failure of weak stories and potentially even the collapse of building.

One of the most common construction issues in Nepal is related to the existence of soft-stories that are used for residential and commercial purposes. In the case of residential buildings, there is often an opening on the road-facing side used for retail shops that results

in lower stiffness and strength with respect to upper stories. Commercial and office buildings often do not have ground infill or even sometimes infill at the basement of the structure, the latter for parking and storage purposes, resulting in considerably lower stiffness and strength at the storey, potentially leading to soft-stories during an earthquake. Poor concrete quality and compaction eventually increase the tendency for a brittle failure of structural members. The lack of sufficient effective cover in beam and column may result in the exposure of structural reinforcing steel bars and subsequently lead to corrosion. Such a situation may also indicate that the longitudinal reinforcement from the beam is not properly anchored, causing weak connections at the beam-column joints. The structural deficiencies just mentioned lead to disproportionate effects when these buildings are subjected to moderate to intense earthquakes.

Results from the site survey indicate that most RC buildings in Nepal are of 3-5 stories, with column size varying from (230 x 230) mm², (230 x 300) mm², to more recently (300 x 300) mm², while beam sizes are approximately (230 x 325) mm² including slab thickness ranging 100-150 mm. Most longitudinal reinforcement used in column of size (230 x 230) mm² is 4 Φ 12, with (230 x 300) mm² columns containing 6 Φ 12, and (300 x 300) mm² columns 6 Φ 16 +2 Φ 12. Primitive buildings are characterized by stirrup spacing of 150 mm on centre throughout the column and beam height, whereas more recently constructed buildings possess two types of stirrup spacing: 100 mm on centre up at the bottom and top one third of the column height at each storey and 150 mm on centre for the remainder third of the column height. The characteristic strength of the reinforcement is 415 MPa, with concrete strength for past buildings ranging from 10 to 15 MPa for structural members. No concrete mix design is typically used for concrete, which therefore allows a great variability in measured concrete strengths.

| (a) | (b) | (c) | (d) |
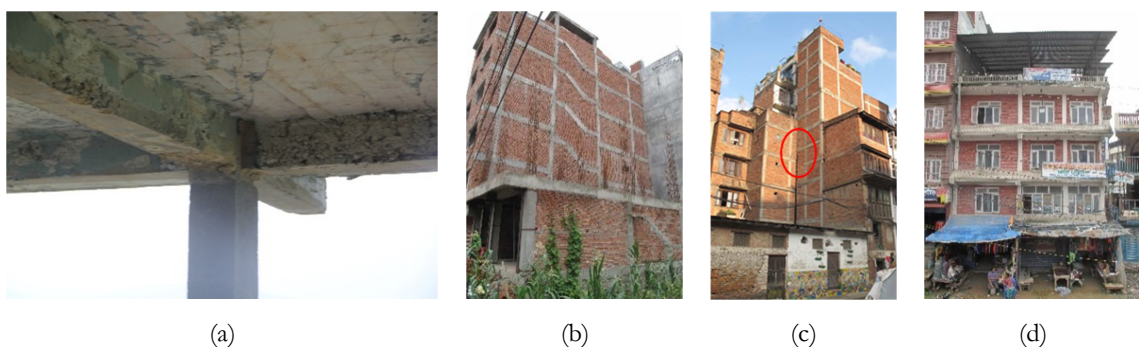
Figure 2.2 – Examples of common RC construction and recorded structural defects; (a) Poor material quality, compaction, and insufficient effective cover in beam and column, (b) Irregular distribution of infill walls and discontinuity of floor beams, (c) Slenderness and vertical irregularity and no seismic gap and (d) Soft-storey at the ground floor

2.5   Typical Failure Modes in RC Buildings Recorded in Gorkha Earthquake

As discussed above, the large mainshock and subsequent aftershocks of Gorkha earthquake are one of the most disastrous earthquakes in the history of Nepal. The recorded mainshock ground acceleration was 0.158g in E-W direction and 0.164g in N-S direction, attained from United States Geological Survey (USGS) stationed at Kanti Path, Kathmandu with latitude 27.7120 N and latitude 85.3160 E. Almost 6,613 RC framed buildings were collapsed and 16,971 buildings were partially damaged [19]. Pokharel, *et al.* (2015) [26] investigated in-situ field survey after Gorkha earthquake. They stressed the major cause of failure of RC structures is due to quality control in the construction site, lack of preparedness and built without code compliance. The paper also stressed on the need of engineered buildings complying with earthquake resistant design to reduce damage caused by future earthquakes. Goda, *et al.* (2015) [27] pointed out that 2015 Gorkha earthquake is not the worst-case scenario, as the earthquake intensity experienced in Kathmandu is not as intense than was expected, i.e. predicted from the probabilistic hazard curve for a site. Therefore, the buildings are recommended to comply with seismic detailing.

Most remarkably, maximum damage in buildings was observed far away from epicentre while only limited or moderate damages near the epicentre [28]. This is due to soil strata of the region and specifically pointed out on the need of research on the soil-structure interaction. The Post Disaster Needs Assessment (PDNA) [29] report concluded that poor rural area is more adversely affected than the town, mainly due to poor construction material and unavailability of skilled labour in the area. The report confirms more than 55% of the casualties were women, mostly working as a household, and finally estimated that more than 7 billion dollars will be required for reconstruction, which is approximately 20% gross domestic product (GDP) of Nepal.

Although the number of RC buildings collapsed is numerically less compared to masonry and other structures, the ratio of number of injuries and fatalities are significantly higher than in masonry structures. Site reconnaissance after Gorkha earthquake demonstrates that most of the collapsed RC structures are non-engineered and some pre-engineered, whereas few pre-engineered structures are partially damaged. Remarkably, non-engineered buildings with regular distribution of infill panels possess only minor cracks although located in most

disastrous area. This illustrates positive contribution of infill panels to frame structures behaving as monolithic in resisting lateral loads. This section discussed the common failure modes observed and recorded during site survey, mainly caused by construction defects and construction trends in Nepal.

2.5.1   Soft-storey failure mechanism

A soft-storey in a multi-storey building is a sudden decrease in lateral stiffness compared to the adjacent floor above it. A soft storey can be defined as a storey that has 70% less stiffness than floor immediately above it or less than 80% as stiff as the average stiffness of the three floors above it. This mechanism takes place if one or more floors have windows, wide doors, large unobstructed commercial spaces or other openings in places where a shear wall would normally be required for stability as a matter of earthquake engineering design. These buildings are likely to have moderate damage to global collapse under moderate to severe earthquakes, known as soft-storey failure mode. This type of failure mechanism is most common in non-engineered and pre-engineered buildings, and few in well-designed buildings as well.

During field reconnaissance, most of the non-engineered and pre-engineered buildings were found to possess irregular distributed infill panels. Similarly, buildings near highways are without infill panels in a complete bay. And in some cases, whole ground floor is without infill panels. This type of construction practice is more common in commercial, high rise, office buildings, etc., where such spaces are usually used for parking and storage purposes. Such buildings are provided with heavy masonry infill walls and other dead and live loads at the consecutive upper floor resulting large stiffness and strength variations between storeys; as a result soft-storey can be expected at the ground floor or at the basement. Soft-storey increases flexibility on that storey, thus decreases the lateral resistance compared to the adjacent floors against earthquakes. Therefore, the overall side to side drift is concentrated on soft-storey, eventually causing the collapse of the structure. This type of infill walls distribution contributes to negative effects in the building. The site survey found that most of the collapsed RC buildings were due to soft-storey effect, mainly on the ground floor and, in some cases, it was detected in the first or second storeys. The soft-storey followed by pounding is also recorded during Gorkha earthquake; some of the collapsed buildings due to this failure mechanism are demonstrated in Figure 2.3.

(a)	(b)	(c)

Figure 2.3 - Examples of buildings subjected to soft-storey collapse during the Nepal earthquake; (a) and (c) Building collapsed due to soft-storey at the ground floor and (b) Soft storey followed by pounding

2.5.2   Short column failure mechanism

In buildings, each storey column suffers the same deformation during ground motion shaking. However, short columns are stiffer than tall columns, and since the force required for the same deformation is larger for stiffer elements, short columns experience large shear forces. If a short column is not designed for such lateral forces or possesses insufficient transverse reinforcement, the element suffers significant damage or even collapses during the earthquake shaking, in what is called a short-column failure. The short column is mostly found in stair portion of the building where stair is landed on the beam at the mid-height of the column, as presented in Figure 2.4 (b). In addition, such failure was also experienced due to the existence of openings in infill walls, as demonstrated in Figure 2.4 (c).

(a)	(b)	(c)

Figure 2.4 – Examples of short-column failure due to the existence of (a) Staircase landing and infill, (b) Stair landing beam and (c) Infill panels with openings

2.5.3   Pounding failure mechanism

Pounding failure observed during the reconnaissance was typically characterized by the lack of seismic gap between adjacent buildings. Each building has its own natural period of vibration, approximately 0.1 N (as per IS 1893:2002) [30] for RC-MRF, where N denotes the number of stories. It is apparent that higher buildings have a longer fundamental period. In addition, the fundamental period of vibration also depends on the stiffness provided by structural and non-structural elements. The typical building type in Kathmandu Valley is inserted in rows of buildings without a sufficient seismic gap, with no uniform inter-storey height or floor height, the number of stories, and structural section sizes. Due to these variations, during ground shaking, such structures vibrate at different periods and phases, increasing the chance that they strike each other in an effect known as pounding. Under such conditions, the probability of collapse of a weak structure is higher. Building failure due to pounding followed by soft-storey collapse is shown in Figure 2.5 (a). Furthermore, a significant difference in floor level elevation between two adjacent buildings can also lead to pounding failure, as illustrated in Figure 2.5 (b).

(a)   (b)

Figure 2.5 - Examples of buildings failure; (a) Pounding followed by soft-storey and (b) Interaction between the buildings due to lack of seismic gap

2.5.4   Beam-column joint failure (Cold Joint Failure)

The so-called beam-column joint failure mechanisms were also observed in Nepal. Beam-column joint failures are associated to the placing of concrete during two different periods, longitudinal reinforcements lapped at the same sections, insufficient transverse

reinforcements and poor reinforcement detailing. The first attributed reason is related to the addition of further 1-3 storeys after 5-10 years the construction of the original building without taking into account the condition of the concrete contact surface, producing weak links with large voids between existing and added concrete. Moreover, for the second attributed reason, the lack of proper lap splicing of reinforcement and insufficient splice lengths explain the beam-column failures, as shown in Figure 2.6.

Lastly the pancake-type failure was observed in several damaged buildings during the reconnaissance performed following the earthquake. This is often attributed to soft-storey mechanisms, but at least in one case, this could be explained by the existence of weak beam-column joints, as presented in Figure 2.6 (b).

(a)   (b)

Figure 2.6 - Failure caused by weak beam-column joint; (a) Poor beam-column reinforcement detailing and (b) Pancake collapse

2.5.5   Strong-beam weak-column mechanism

In older RC building design and construction, it was assumed that the beams should be stronger than the columns. As a result, pre-engineered RC buildings in Nepal possess small column section (230 x 230) mm² when compared to the beam size (230 x 325) mm², leading to the formation of shear failure or formation of plastic hinges in the columns. This design approach along with insufficient stirrup spacing and small diameter results in poor confinement of the RC sections and premature reinforcing steel bar buckling. Figure 2.7 (a) present global collapse of the building due to strong-beam weak-column, and Figure 2.7 (b) demonstrates a local column failure due to large stirrup spacing, insufficient hook length and small stirrup diameter.
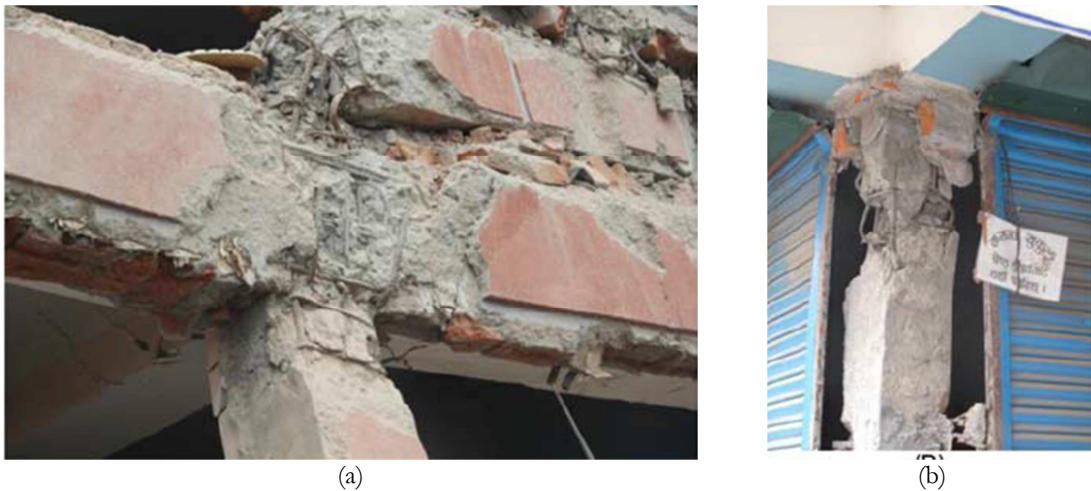
Figure 2.7 – Failure caused by column rebar buckling; (a) Strong-beam and weak-column and insufficient lateral ties detailing and (b) Poor reinforcing steel bar detailing

2.5.6   Detailing problems and construction material quality

Detailing problems recorded during the reconnaissance include insufficient lap-splice lengths that lead to bond-slip failures. For building structures, the modified mandatory rule of thumb (MRT) delineates lap-splice detailing requirements, specifying that column lap-splice should be carried out at floor mid-height. In addition, the lap-splice length should be 60 Φ (bar diameter), and the number of lap-spliced bars should not be more than 50% of the longitudinal reinforcements. However, in Nepal, these guidelines are not enforced on site due to lack of enforcement policies, lack of accountability or even fear of conflicts arises between contractors and engineers. As a result, the lap-splice of the longitudinal reinforcing steel in the columns and beams are often developed near the beam-column joints with an insufficient lap-splice length. Such sections could be the weakest zone of any structural element and failure occurs with concentrations of the deformations at the sections, where bond-slip failures develop as recorded from building damages in Nepal. When seismic stresses act on these sections, the column might fail rupturing concrete and leading to buckling of the longitudinal reinforcing bars. Examples of structures that collapsed during the Gorkha earthquake due to such construction works and poor concrete quality were observed, some of which are demonstrated in Figure 2.8.

(a)   (b)   (c)
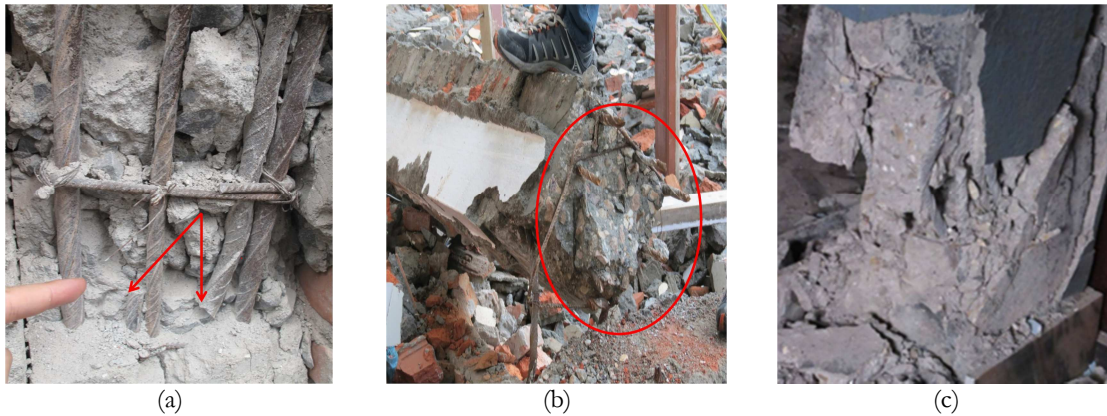
Figure 2.8 – Failure of the structural elements caused by; (a) Insufficient lapping length, (b) All reinforcement lapped at the same section and (c) Poor concrete quality and confinement

2.5.7   Shear failure in column

At the top of columns, shear failures were induced by the presence of a masonry infill panel was a common mode of structural failure seen after the Gorkha earthquake. This is attributed as the infill panel can significantly alter the structural response in terms of stiffness, strength and mode of failure when acted upon seismic actions. This type of failure was observed mostly near beam-column joint. The damage patterns observed are consistent with those expected for strong-infill and weak-frame modes of failure, including in-plane diagonal shear damage to the infill masonry walls and shear failures of RC columns near the beam-column joints. As described before, insufficient shear detailing at column ends were also common, which exacerbates this failure mechanism, as illustrated in Figure 2.9.

(a)   (b)

Figure 2.9 – Examples of shear failure at top of column induced by masonry infill panel; (a) Initiated by the strength difference of the adjacent column and (b) Shear failure at the corner column

2.5.8 In-plane and out-of-plane failure mechanism of masonry infills

Masonry infill panels can increase the seismic capacity of a structure by 3-4 times with respect to that of the RC bare frame [10, 31], thus attracting large seismic forces during earthquake loading. Masonry infill panels consist of brick masonry units and mortar joints. Brick masonry units are usually brittle and weaker in tension than in compression, which results in the infill walls being weaker in a biaxial tension-compression stress state than under biaxial compression-compression stress states. The failure of the infill panel is also influenced by the presence of mortar joints. Depending on the orientation of the mortar joints with respect to the applied loading, failure can take place either in the joint only or via a combined mechanism in the mortar and masonry unit. When the stresses are parallel to the bed joints, failure occurs along the interface of brick and mortar joint. Due to these possible failure modes of the brick and mortar, masonry infill panels are very brittle in nature and in-plane cracking may take place in shear or flexure modes of deformation [32]. Infill walls also experience both in- and out-of-plane forces simultaneously during an earthquake. Examples of in-plane failure caused by flexural cracking and shear cracking are shown in Figure 2.10. These failure mechanisms are commonplace in masonry infill panels found in Kathmandu, as the strength of typical masonry units is weaker at the mortar joint in comparison to the surrounding frame. In contrast, out-of-plane failure was not observed frequently, is most likely due to solid brick being stronger thus arching effect becomes more effective.

| (a) | (b) | (c) |
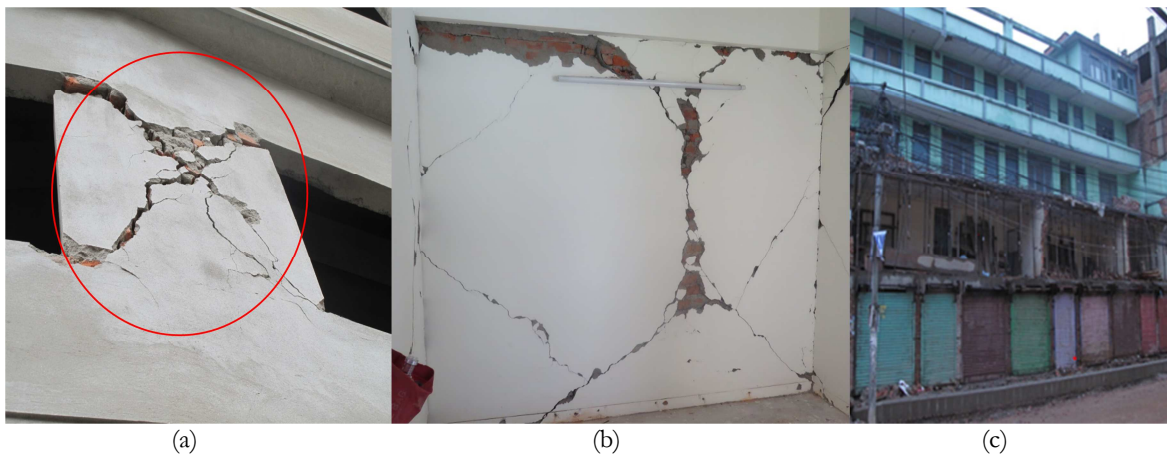
Figure 2.10 – Examples of infill masonry failures due to Gorkha earthquake; (a) and (b) In-plane and (c) Out-of-Plane

2.6   Performance of Unreinforced Masonry (URM) Buildings

2.6.1   Structural description and materials

URM buildings constitute the majority of buildings in Kathmandu and surrounding urban areas. These types of structure can be considered as non-engineered, as they were built before the existence of modern building codes, with most constructed spontaneously without any support from engineers in their design. URM structures are characterized by the use of poor materials, such as solid clay bricks and mud mortar and in a few cases the use of concrete blocks and cement mortar, with material types used varying based on location and building age. For the URM structures, during the reconnaissance survey, the team observed a range of masonry wall thicknesses, varying from 500 to 750 mm, composed of at least a three-leafs wall (three layers of bricks) filled with mud mortar, as shown in Figure 2.11. The façades of traditional buildings are typically made from fire clay bricks with a smooth finish, while the inner face is of sun-dried clay bricks. During the reconnaissance, it was also observed that no connection was used between the layers at the time of construction, frequently resulting in the collapse of external walls, illustrated in Figure 2.12. Some buildings possess very complex wall systems, with an irregular distribution of bricks and a hard to determine or even undetermined number of layers; due to the weak characteristics of the mortar. The seismic behaviour of such buildings is typically very poor.

| (a) | (b) | (c) |
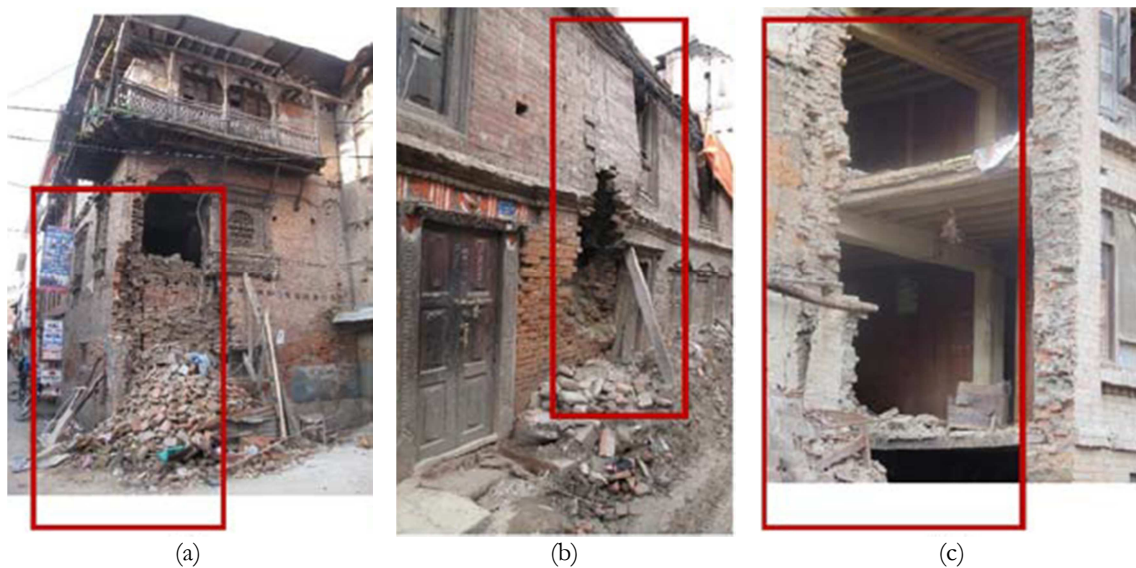
Figure 2.11 - URM earthquake damages and failure modes; (a) Out-of-plane collapse of the façade wall and insufficient connection between timber floor and the masonry walls, (b) Out-of-plane collapse of façade wall with bulging of exterior walls, and (c) Insufficient connection between the floors and the masonry walls and out-of-plane collapse of the façade wall of a 3-storey building

<center>(a)   (b)   (c)</center>

Figure 2.12 - URM buildings construction details; (a) Masonry wall leafs disposition, (b) Connection between the timber floor and the transversal wall and (c) Buildings block

Floors and roofs are built using timber elements, although the former can vary significantly between adjacent and apparently similar buildings. Timber floor joists are common, spanning one or two directions in older buildings, and are built using simple battens or joists upon which timber planks are laid (Figure 2.11 (c)). These in turn, support the final floor finish. Deficient or in some cases, with no connections between these horizontal structural elements and the masonry walls were frequently observed.

URM structures usually comprise 2-5 storeys and are commonly constructed in adjacent blocks. This practice contributed to protect some buildings from collapsing, since the seismic response comprised the entire block, compensating for the insufficient capacity of each individual URM building, as shown in the example in Figure 2.12 (c). Moreover, in the case of multi-storey buildings, masonry wall thickness is not uniform throughout the building height, but rather decreases from the ground to the top storeys, resulting in structural irregularities with elevation. In some cases, it was observed that the ground floor was used for commercial purposes, with the reduction in the number of masonry walls in such floors causing structural irregularity and leading to soft-storey types of collapse [33].

2.6.2   Damages and failure modes

Almost all URM buildings were found not containing reinforcing bands, such as sills, lintels, or gables, at any level. Due to lack of proper bonding in the masonry load bearing

walls, out-of-plane collapses were more commonly observed in the Kathmandu Valley and other settlements. In most URM buildings, the orthogonal walls were found to show incompatible deformations due to lack of any proper connection between two perpendicular walls, exhibiting poor integrity. Furthermore, due to an absence of integration between several members within the building structural components, out-of-plane failures were also more intense than any other types of failure in some of these cases, as shown in Figure 2.11.

Diagonal cracking at the corners of openings and in the centre of wall segments, as illustrated in Figure 2.13, was caused by stress concentration at the corners of windows and doors, as well as the absence of sill and lintel bands. Vertical cracks recorded in the centre, ends, and corners of walls reflect insufficient or absent bonds at continuous vertical joints (wall-to-wall connections).

(a)　　　　　　　　　　　　(b)　　　　　　　　　　　　(c)
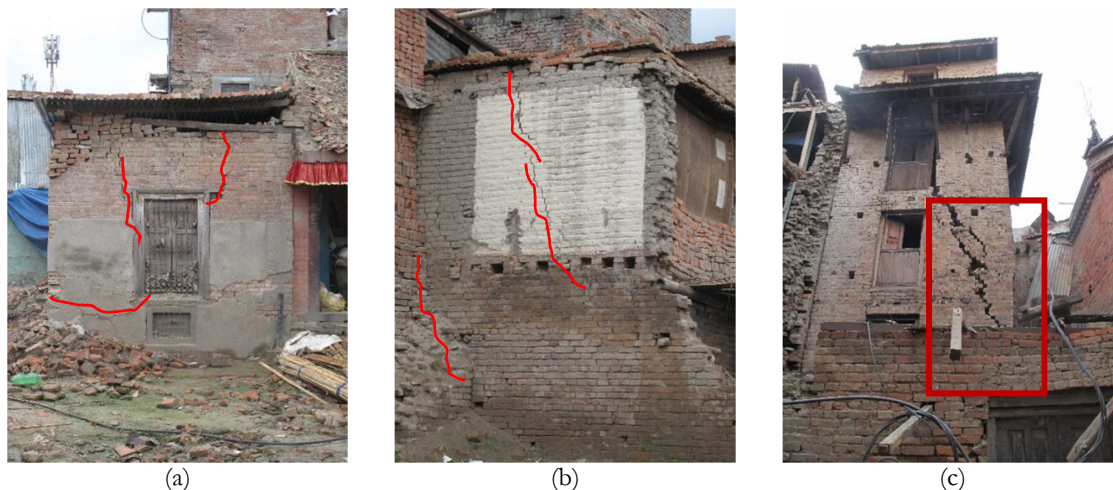
Figure 2.13 - URM earthquake damages and failure modes; (a) Diagonal and upper cracking due to vertical stresses, (b) Diagonal cracking and (c) Diagonal cracking due to the stress accumulation associated with openings

Partial and total collapse of buildings was observed in many areas in Bhaktapur, as illustrated in Figure 2.14, where entire neighbourhoods were destroyed due to the accumulation of various phenomena, such as in- and out-of-plane failures, corner effects, pounding, torsion, and warping failure caused by building irregularities in plan and elevation, reduced space between two adjacent buildings, imbalance in the sizes and positions of openings in walls, and improperly tied roofing material [34].

Figure 2.14 - URM earthquake damages and failure modes; (a) and (b) Partial or total collapse

Finally, as was the case for RC structures, the use of the ground floor for commercial purposes was also observed in URM buildings, creating vertical irregularity in terms of the existence of openings and the placement of interior walls, and leading to the concentration of earthquake damage in this floor, in what is known as the soft-storey failure mechanism, as demonstrated in Figure 2.15 (a). In some cases, this phenomenon also resulted in the total collapse of many buildings across the Kathmandu Valley region. A combination of factors such as the poor quality of material used in construction, building type and lack of structural integrity, resulted in building vulnerability to severe damage and collapse. In addition, walls inadequately anchored to the floor or roof diaphragm exhibited large cracks and in some cases, had collapsed entirely (see Figure 2.15 (b)).

Figure 2.15 – Earthquake damages and failure modes; (a) concentration of the damage in the ground floor due to the openings disposition and (b) Total collapse of the building's façade due to the inadequate anchorage of the floor diaphragm to the wall

2.7 Vernacular and Rural Constructions and Failure Modes

2.7.1 Structural description and materials

Nearly 40% of the total housing stock of Nepal is comprised of rubble stone masonry buildings. Such buildings are non-engineered and owner built constructions built by untrained local masons. The immediate availability of construction materials is of the highest priority during construction. Vernacular constructions do exist, although such buildings are outnumbered by those built using traditional dry stone or mud mortar in rubble stone. The field reconnaissance undertaken in central Nepal after the 2015 Gorkha earthquake revealed that wall thickness typically varies between 390 mm to 530 mm, with two-leaf walls being most common, as demonstrated in Figure 2.16 (a). The material found between the bricklayers also varied, with stone chips observed in the case of dry masonry buildings and segregated mud mortar in the case of mud mortar stone masonry construction. Rural stone masonry constructions in Nepal are predominantly 1-3 storeys structures, with shallow foundations, although a few 4-storey buildings can also be found in the middle mountain region of Nepal. Rural constructions are usually surfaced with mud plasters both internally and externally, however, a countable fraction of such buildings can be found without plastered walls as well. Although such building practice is economic and does not require skilled manpower, the seismic capacity of the resulting building is inherently low and such falls under the EMS-98 vulnerability class A. As sites are selected without any engineering considerations, rural buildings are generally constructed on sloping terrain due to a lack of flat areas in the middle to high mountains of Nepal. Timber joists supported by structural walls are designed to support the floor and roof. Roofing material varies with the elevation and the economic status of the building owner, with the middle mountains characterized by corrugated galvanized iron (CGI) sheets or thatched roofing and the high mountains by heavy stone roofing (sliced stones), shown in Figure 2.16 (c), or mud blocks. Rural stone masonry buildings are typically standalone rectangular constructions with a roof sloping in two directions; masonry partition walls are rarely provided. Where the latter are present, they are generally the same thickness as the structural walls. The field reconnaissance revealed the use of irregularly shaped and sized stones, with timber and bamboo materials limited to elements such as joists, purlins and rafters.

(a)   (b)   (c)

Figure 2.16 - Typical features of rural buildings; (a) Heavy dry stone masonry wall, (b) Two-storied building subject to in- and out-of-plane collapse and (c) Heavy roofing stones

2.7.2   Damages and failure modes

Out of the 474,025 collapsed rural buildings recorded in central Nepal, approximately 90% were constructed of rubble stone, while nearly 70% of the 173,867 damaged buildings were rural stone masonry constructions. It is therefore interesting to note that this type of buildings was more susceptible to collapse than minor to moderate damages after the Gorkha earthquake, a finding similar to that recorded after other events in the region, such as the Bihar-Nepal earthquake of AD 1934 and the Udaipur earthquake of AD 1988. Observation of more than 10,000 rural buildings revealed that their orthogonal walls were behaving discrepantly (see Figure 2.17 (b)), as was the case for URM buildings in the Kathmandu valley, with wall collapse predominantly occurring in the out-of-plane direction (Figure 2.17 (c)) in rural stone masonry buildings. In addition, heavy and united gable construction also led to gable collapses in many buildings in middle mountains (Figure 2.17 (c)). Lack of proper connection between orthogonal walls and lack of maintenance was one of the major causes of damage in most rural settlements in the middle mountains, leading to severe damage and in some cases collapse. Indeed, buildings aged 100 years or more were found to be still, with no periodic strengthening or repairs ever undertaken. Delaminated wall leafs, both internally and externally, revealed that mortar was no longer binding the two units and that leafs were behaving independently. In case of dry stone masonry constructions, walls were composed of stacked a stone in which leafs were not

linked to each other. In summary, the major causes of damage of varying degrees to rural buildings during the Gorkha earthquake included a high weight concentration on the walls and roofs, a lack of structural integrity, heavy gable construction, poor mortar quality, a lack of seismic provisions and detailing, stress concentration in corners and openings, topographical and ridgeline effects, sloping foundation, as well as progressive damage due to continued aftershocks.

| (a) | (b) | (c) |
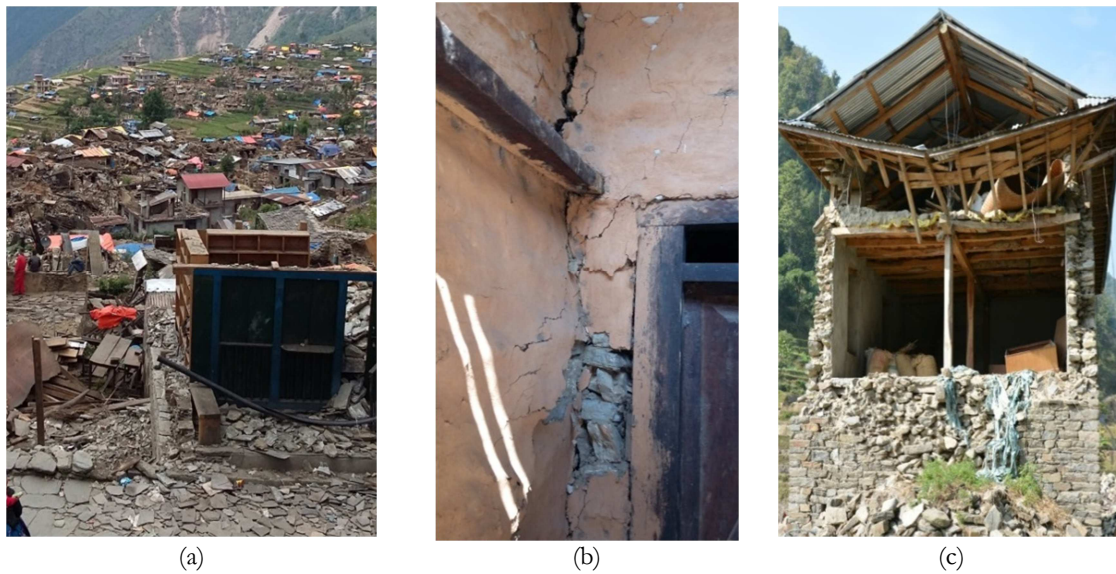
Figure 2.17 - Damage in rural stone masonry buildings; (a) More than 95% of building collapsed in the epicentral Barpak village, (b) Separated orthogonal walls and (c) Out-of-plane collapse of structural and gable end walls

2.8   Other Building Types

As the stone is not abundantly available in the confluence region of the plains and middle mountains of Nepal, timber buildings are typically constructed in these regions. Indeed, nearly 25% of the total housing stock in Nepal consists of timber buildings, while a minor fraction (approximately 2-5%) are constructed of wattle and daub or bamboo. During historic strong to major earthquakes, including the great Bihar-Nepal earthquake of AD 1934, timber, wattle and daub, and bamboo houses have shown excellent seismic performance; a similar situation was also the case after the 2015 Gorkha event, with no cases of damage reported for these types of constructions. Timber houses are typically 1-3 storeys rectangular constructions, with wooden posts and beams used as part of the structural system. The initial stage of timber building construction is similar to that of the RC skeleton system, with wooden frames fixed in place. However, in timber houses, the openings are then filled with knitted bamboo sheets (known locally as ikra) or with wooden planks. Due to their lightweight construction, ductility, and adequate orthogonal

connections, the resilience of such structures has been undeterred during each significant earthquake in Nepal. Wattle and daub buildings are primarily single-storey rectangular constructions, found mainly in the southern plains and lower mountains of Siwalik. Such construction is preferred as a low-cost housing solution in the region due to the wider availability of bamboo than timber. The construction of wattle and daub houses is similar to that of timber buildings. In this construction type, first, bamboo posts are fixed and knitted ikra is placed in the openings between the posts. Thermal insulation is typically achieved using roof tiles, although CGI sheets can also be found. Wattle and daub houses in Nepal have proven similarly resilient against strong major earthquakes, including those of 1934, 1988, and 2015. Both timber and wattle and daub constructions can be classified as belonging to EMS-98 vulnerability class D.

2.9   Conclusions

This chapter provides insight into the damage observed during a field reconnaissance trip following April 25, 2015, Gorkha earthquake in Nepal. RC buildings that were not properly designed to resist the seismic forces suffered extensive damage, including partial or complete collapse, mostly due to vertical irregularities in their construction that caused stiffness difference and subsequent soft-storey mechanisms, as is often associated with non-engineered structures. However, many well-designed tall RC buildings also presented significant non-structural damage, particularly in masonry infill walls. As recorded from the site survey, building damage and collapse is mainly due to the soft-storey mechanism, some due to pounding as a result of soft-storey, few caused by short-column and shear column failure, and detailing problem. The positive and negative contributions of masonry infill panels with RC frame structure as chronicled after Gorkha earthquake signifies the need of its consideration in the design code of buildings, i.e. NBC. The extensive damage and a large number of URM buildings and vernacular constructions that collapsed can be attributed to poor materials and a lack of construction detailing and construction practices that improve the structural behaviour of such buildings when subjected to ground shaking. These buildings often exhibited vulnerabilities related to weak or non-existent connections between the walls and floors or roof, which can lead to improper transmission and distribution of stresses among the various elements. This in turn subjected to out-of-plane demands, causing significant damage and collapse. A timely renovated URM and vernacular building types show better seismic performance without significant damage as

recorded during the survey. Interestingly, it can be noted that wattle and daub houses have proven to be resilient against past major earthquakes recorded that includes those of 1934, 1988, and 2015. The present chapter intends to give overall information building exist in Nepal; however, the further study will be carried out for RC buildings. Thus, the buildings shown and discussed from Section 2.6 to 2.8 will not be addressed further in the thesis.

Chapter 3.

Case Study Buildings and Field Tests

3.1   Introduction

The field survey was conducted after a large-magnitude main shock and a subsequent series of large and smaller-magnitude aftershocks of the 2015 Gorkha earthquake in Nepal, as reported in Chapter 2. In the present study, six reinforced concrete moment-resisting frame (RC-MRF) buildings were selected that are located in Bhaktapur, which represent three design approaches: non-engineered, pre-engineered, and well-designed. The site survey reveals non-engineered, pre-engineered and well-designed buildings composed almost 60-65%, 30-35% and < 5%, respectively, of the total existing RC buildings in Kathmandu Valley. Two buildings representing each design approach were selected to investigate the seismic performance. This involved in-situ experimental tests and numerical analyses. Two experimental investigations were performed, using tests such as Schmidt hammer tests and ambient vibration tests, which will be discussed in detail in the following sections. Similarly, the numerical investigation includes various types of analyses ranging from linear to nonlinear dynamic time history analyses, which will be discussed in detail in Chapter 5. The present study classified buildings in such a way that buildings built before the implementation of any design codes whose structural sections and reinforcement details cover only the carrying of gravity loads are grouped as non-engineered buildings (Common construction practice) and are represented as CCP. The non-engineered buildings selected in the present study were built in late 1990s. Similarly, infilled RC frame buildings having structural section sizes and reinforcement details identical to those defined in MRT guidelines [20] were classified as pre-engineered buildings and are characterized as MRT. The reinforcement details at the site was not possible in these buildings; therefore, details were recorded and presented based on owner assistance, and in one of the building they were recorded through exposed reinforcement at the top floor. The selected buildings were built between the late 2000 and 2015. It is to be noted that the NBC 205: 1994 [20] was implemented and enforced in all municipalities only after 2004, whereas Lalitpur municipality started applying it in 2003. This could create misunderstanding to the readers regarding the building classification. Therefore, it is pointed out that the present study

classified buildings as pre-engineered based on the observed and measured structural sections and reinforcement diameter without taking into consideration if selected buildings were built following design guidelines or not. This is due to various limitations within design guidelines and also to real practices, where it will be difficult or even impossible to find buildings that completely follow design guidelines. Furthermore, some important buildings, such as hospitals and institutional and commercial buildings are required to be designed with special code provision. In other words, buildings that need to contribute to public safety in future earthquakes have to be designed based on response spectra of the site or through dynamic analyses; they are classified as well-designed buildings and are represented as WD. In some cases, residential buildings that reflect unusual design, such as a high number of storeys and large plinth area, are required to be designed based on dynamic analysis and are also classified in this category. It is noteworthy that buildings selected under the well-design approach have considered the structural sections and reinforcement details similar to the approved drawings, which were acquired from the concerned authority. The selected WD buildings were built in late 2000 and are utilized for institutional purposes. The location of the entire case study buildings, set along with the epicentre of the main and major aftershock of the Gorkha earthquake, is shown in Figure 3.1. The selected buildings were subcategorized based on the existing state as damaged and non-damaged (see Table 3.1).
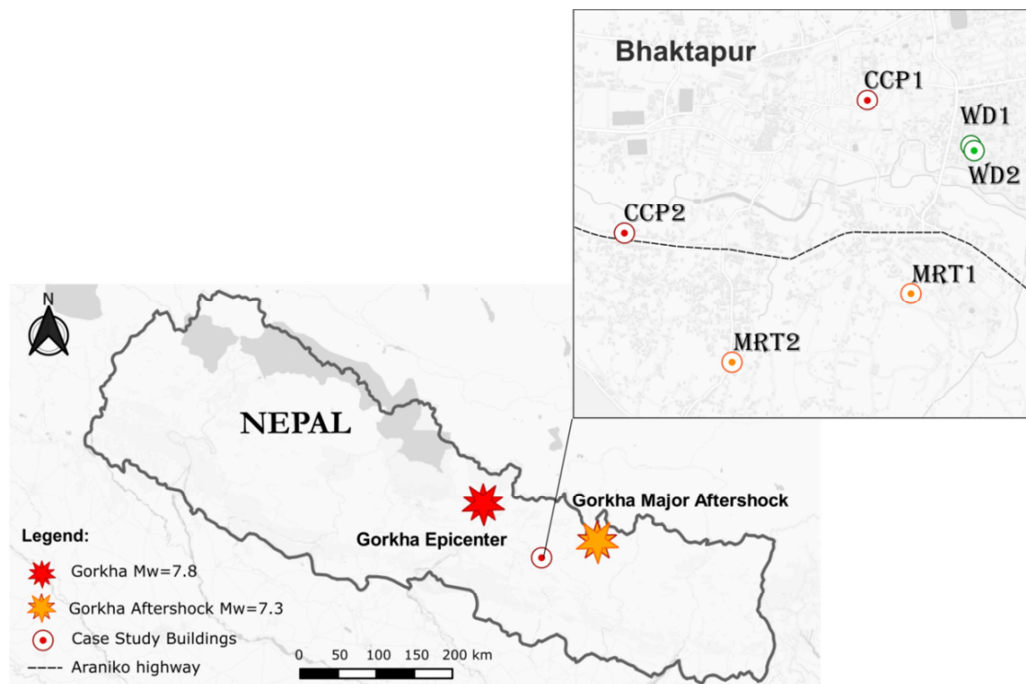
Figure 3.1 – Location of the selected buildings and main aftershocks earthquakes

Table 3.1 – Case study building classification based on the construction practice

Building Class	Damage state	Building Name	Remarks
Non-engineered	Non-damaged	Mitra Chaphakhana (CCP1)	
	Damaged	Suwal House (CCP2)	
Pre-engineered	Non-damaged	Bare Frame (MRT1)	
	Damaged	Twayana House (MRT2)	
Well-designed	Non-damaged	Khwopa Engineering College Block 'C' (WD1)	
	Non-damaged	Khwopa College of Engineering Block 'E' (WD2)	

In the first stage, an exhaustive field survey was carried out and existing buildings were selected that met the research objective. This was followed by visual inspection through which the information on the state of the building was acquired; the inspection included the present condition of RC elements, concrete quality, reinforcements, state of infill panels, and so on, as illustrated in Figure 3.2. Generally, slight to moderate damage was clearly visible in the masonry infill panels, mainly in non-engineered and pre-engineered buildings and few in well-designed buildings. Similarly, in-plane and out-of-plane failure of infill walls was observed in some non-engineered buildings and a few in engineered buildings. This type of infill behaviour could potentially lead to the failure of buildings, mainly under the soft-storey mechanism. Figure 3.2 (a) presents various cracking patterns observed in the masonry infill walls, which include diagonal cracking of the infill wall, corner crushing, and shear sliding. Figure 3.2 (b) presents prevailing construction practices

such that new infill panels were built at the basement at the time of construction. This building was without infill walls at the basement before the earthquake and corner columns suffered extensive damage, most likely due to the irregular arrangement of infill walls. Figure 3.2 (c) shows the state of reinforcement details in the structural elements resulting from insufficient effective cover, poor concrete confinement, poor material quality and poor workmanship. These reflect only some representative damage observed in the existing buildings to justify the need for and significance of the present study. The detailed condition and state of each building will be discussed in the following sections.

| (a) | (b) | (c) |

Figure 3.2 – Typical state of structural and non-structural elements observed during visual inspection; (a) Diagonal cracking, corner crushing and shear cracking on the infill panel, (b) Construction of new infill panel on the open ground storey and (c) Poor concrete quality, poor stirrup spacing and its distribution, and poor concrete compaction

In addition to visual inspection, two types of in-situ field tests were performed on each case-study building: Schmidt hammer tests and ambient vibration tests. The identification and accurate estimation of the superficial characteristic strength of the existing buildings is a very challenging task due to various difficulties associated with the site. The behaviour of the structure is also influenced by the quality of the concrete that depends on the accuracy of an in-situ test. There exist various governing factors that affect the accuracy of the test but mainly depend on the precision of the Schmidt hammer and tested concrete surfaces. The existing concrete strength can be evaluated through destructive tests (such as core tests, pull-out and pull-off tests) and non-destructive tests (NDT). The present study deployed NDT using Schmidt hammer, obtained from Khwopa Engineering College. The Schmidt hammer test is also known as a rebound hammer test, a widely used technique to estimate the in-situ concrete compressive strength of existing buildings. Considerable work has been performed to develop rapid NDT, which provide a reproducible measure of concrete quality in a structure [35]. These test results are affected by various existing parameters, which include aggregate type and size, age, moisture content, and mix proportions [35]. The Schmidt hammer tests were performed on the smooth and plain

surfaces. Figure 3.3 demonstrates representative tests conducted on column, beam, and slab elements during site surveys.

Liu, *et al.* (2009) [36] conducted experimental NDT to estimate the strength of the concrete, where test data were analysed through a regression model. The average accuracy with an error of 5.5% was attained by combining the rebound test value of composite concrete materials and statistical regression analysis. It was concluded from the test results that the accuracy depends upon the input design parameters of materials, such as water-binder ratio, fly ash, slag, chemical admixture, age and moisture content [36]. Similarly, Brencich, *et al.* (2013) [37] carried out experimental tests to calibrate the reliability of the rebound hammer test and concluded that compressive strength estimates might deviate by 70% if parameters such as moisture content, maturity, stress state, etc. are not taken into account [37].
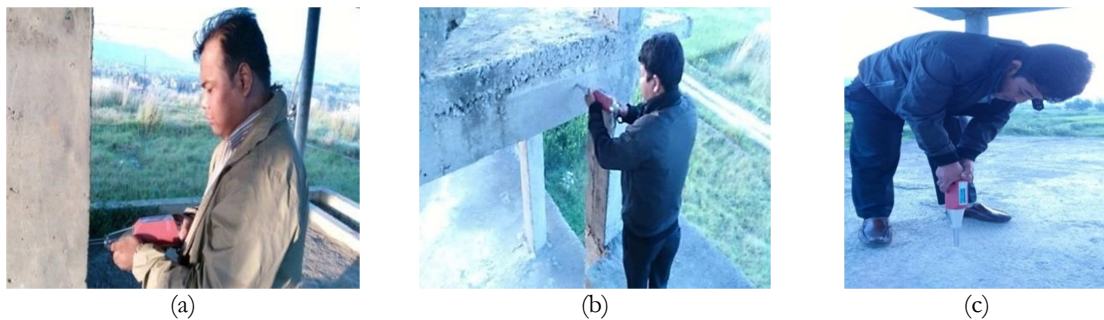
(a)   (b)   (c)
Figure 3.3 – Schmidt hammer test on the structural elements of the bare frame building; (a) Column, (b) Beam, and (c) Slab

Aydin, *et al.* (2010) [38] investigated the correlation between Schmidt hammer results and destructive results through concrete testing on existing buildings. Therefore, some correction factors were proposed that lie between 0.51–0.82 depending upon the strength interval, as presented in Table 3.2.

Table 3.2 – Strength transform factors for Schmidt hammer test used in old concrete [38]

Strength interval MPa	Correction factor number
<10	0.51
10-15	0.62
15-20	0.67
20-25	0.72
25-30	0.75
30-35	0.78
35-40	0.8
40-45	0.81
45-50	0.82

Large dispersions of rebound hammer test results were recorded; thus it can be concluded that Schmidt hammer test results provide only an approximate estimate of the compressive strength of existing concrete. This statement is true when various limitations at the site are considered. These limitations include unavailability of exposed structural elements (i.e. not plastered surface), difficulty in hammering space and the test being limited only to the plain surface. In addition, large dispersions of test results also induce doubt and uncertainty concerning the reliability of the results and method of measurements. It is also noted that the Schmidt hammer test relies only on the plain surface and specific points; thus the accuracy of the result and its representations about building global behaviour create doubts. Considering all of these limitations and drawbacks, it can be stated that Schmidt hammer results provide only rough estimation, and thus these results were calibrated using the correction factor shown in Table 3.2. The present study utilized the NDT results for the calibration of numerical models, which were later adjusted after parametric analysis.

Ambient vibration tests are one of the most useful non-destructive tests; they are dynamic tests performed on existing buildings to acquire the fundamental frequencies and vibration modes. The experimental investigations were performed for all case-studied buildings with the help of the CONSTRUCT-LESE team from the Faculty of Civil Engineering of the University of Porto. Figure 3.4 presents representative ambient vibration tests carried out in the selected buildings and also accelerometers fixed to infill walls to investigate and identify possible structural characteristics like natural frequencies, vibration modes and respective viscous damping parameters of various full-scale existing buildings [39-42]. Ambient vibration tests have been performed by many researchers in the past, particularly in RC buildings and bridges to investigate the fundamental frequencies and state of stresses and other building parameters, some of which are discussed in the following section.

(a)   (b)   (c)
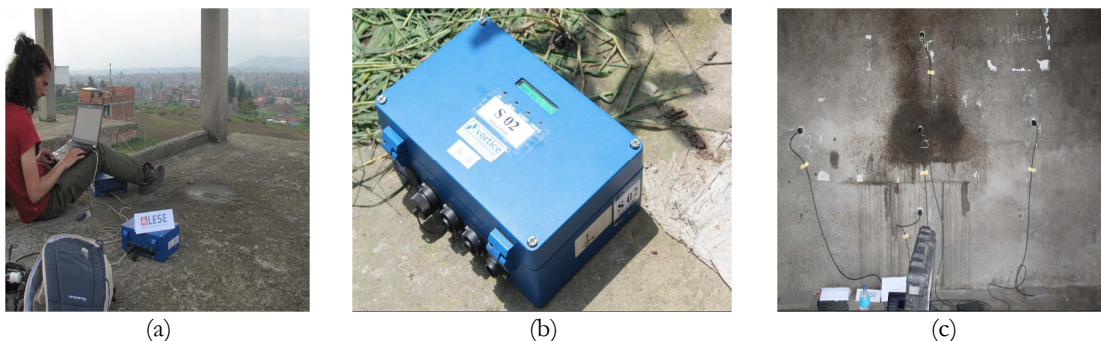
Figure 3.4 – Ambient vibration test set-up; (a) and (b) Seismograph positioned to obtain the translational vibration mode shapes and (c) Infill panel using accelerometers

Ventura, *et al.* (1995) [43] performed ambient vibration tests on fifteen- and forty-eight-storey RC buildings. They established a reliable finite element model that could be effectively useful in large civil engineering structures. The model was acquired through ambient vibration identification techniques with model updating tools. It also revealed a possible accomplishment of an effective model update using results from the natural input modal identification analysis through application in large civil engineering structures. The use of an automatic model-updating tool greatly facilitates determining the modal parameters, which can be modified to achieve a good correlation between experimental and analytical results [43].

Ivanovic, *et al.* (2000) [40] carried out ambient vibration tests on a seven-storey RC frame building in Van Nuys, California, which was damaged in the 17th January 1994 Northridge earthquake and its aftershocks. The study presented apparent frequencies, and two- and three-dimensional mode shapes, i.e. longitudinal, transverse, and vertical vibrations. It suggested the need for high special resolution in order to identify the localized damage in the column and beam. The paper concluded that the moderate and weak damage was not noticeable through ambient vibration surveys, but the loss of axial capacity due to damaged column could be visualized through the vertical response of the columns [40].

Rodrigues, *et al.* (2004) [44] analysed ambient vibration data collected from a one-quarter-scale model of a four-storey building, later utilized for the improvement of frequency domain output-only analysis. The test results concluded that a significant improvement in reducing the noise and quality of frequency domain modal identification can be obtained through the frequency domain identification module [44].

Cunha, *et al.* (2006) [45] discussed the evolution of experimental modal analysis in the civil engineering field from classical input-output modal identification to output-only modal identification techniques. The paper concluded that the technique can be utilized for developing finite element correlation analyses, later can be employed for finite-element updating and validation and also can be implemented in vibration-control devices [45].

Gueguen, *et al.* (2014) [46] presented an inventory of practices and progress made in ambient vibration tests. This was later executed in a structure to represent its elastic dynamic responses, bypassing any hypothesis so as to identify the quality of its materials, design, or the soil-structure interaction. The paper concluded that the ambient vibration test can be regarded as an alternative method to acquire knowledge of existing buildings by

providing building dynamic characteristics and their state for earthquakes. Ambient vibration tests are the least expensive and easiest method to identify the fundamental frequencies, vibration mode shapes, and damping. Similarly, the test records can be utilized for assessing the seismic vulnerability of existing buildings, as frequencies are the dominant parameters that have a direct relationship with earthquake design of the building [46].

Varum, *et al.* (2017) [32] published experimental work on ambient vibration tests performed on seven masonry infills—tests conducted two months after the 2015 Gorkha earthquake. The tests were carried out on three masonry walls that also represent one of the selected case-study buildings in this research, i.e. building CCP2. The masonry infill walls were classified as large, small, and an external infill panel with opening. The tests were performed using five accelerometers, which were positioned in such a way that accelerometers were at approximately one-quarter of the infill height from the ends of infill walls and three at the mid-height, as illustrated in Figure 3.5. The tests showed that the first frequency of the larger wall was unexpectedly 46% less compared to the smaller wall, and the opening reduced the first frequency by 70% [32].

(a)   (b)
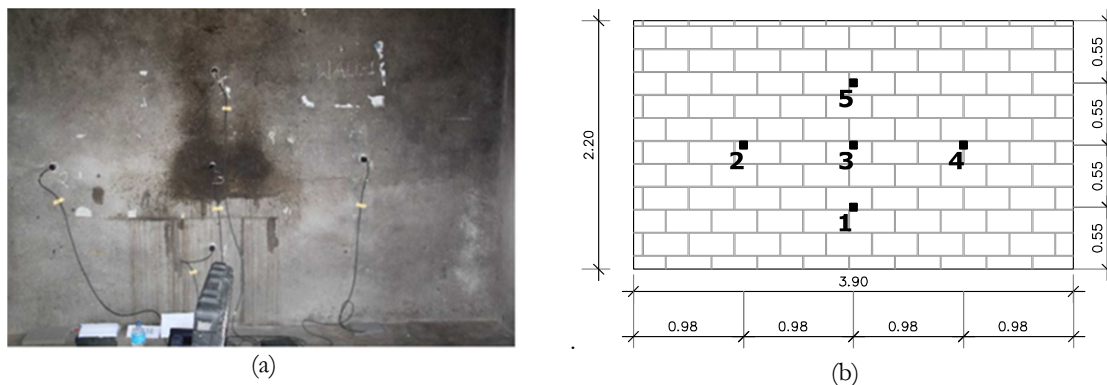
Figure 3.5 – Ambient vibration test on external wall; (a) Geometric dimensions, and (b) Test setup [32]

The recorded data were analysed, and structural modal parameters were identified using output-only modal identification methods. Three types of frequency domain output-only modal identification methods were used: basic frequency domain method (BFD) or peak picking method (PP), frequency domain decomposition method (FDD), and enhanced frequency domain decomposition method (EFDD) [44]. In the BFD method, the averaged normalized power spectra density function (ANPSD) is obtained through normalized auto-spectra, which is averaged later such that all resonance peaks with respect to the vibration modes of a system, can be attained. The half-power bandwidth method is widely used along with the BFD method for the estimation of the damping coefficients [47]. Similarly,

in the FDD method, the spectral density function matrix, at each discrete frequency, is decomposed into singular values and vectors using the SVD algorithm [44]. The mode shapes are estimated as the singular vectors at the peak of each auto power spectral density function corresponding to each mode [44]. Furthermore, the EFDD method is closely related to the FDD method, with some additional procedures to evaluate the damping and to get enhanced estimates of the frequencies and mode shapes of a system [48]. This method enhances the estimation of the mode shapes, considering all the singular vectors within each SDOF auto-spectral density function, weighted with the corresponding singular values. Both the FDD and EFDD methods are widely used due to their availability in the ARTeMIS software [44].

In the following sections, we will discuss detailed information gathered for the selected case-studied buildings, obtained after the Gorkha earthquake that includes non-destructive experimental test set-ups and attained test results. In addition, the recorded data were filtered and calibrated using various software and calibration factors as discussed above.

3.2   Mitra Chaphakhana (CCP1)

3.2.1   General introduction

Mitra Chaphakhana is a three-storey building located in Bhaktapur, Nepal. It was built in 1985 using local knowledge and skill, representing common buildings that were built before implementation of design guidelines. Therefore, the building was classified as non-engineered and named as a CCP1 building. The site survey revealed that the CCP1 building sustained minor damage, particularly in the infill walls. Figure 3.6 presents various elevations of the building, and interestingly, it can be observed that the building did not sustain any structural damage although it is located in one of the most affected areas in Bhaktapur. Therefore, the building was classified as a non-engineered and non-damaged RC building type.

The columns of floor height were erected at the top storey of the building, indicating that a new storey would be added in the near future. This is a multipurpose building, such that the ground floor contains heavy printing machinery that was in operation during the earthquake; the first and second floors are used for occupancy. It is an isolated building with large open spaces on the southern and eastern sides, whereas the western and

northern sides of the building face towards the pedestrian street and have large openings for windows and ventilation, as shown in Figure 3.6 (a) and (b). The masonry infill panels were observed to be internally plastered at the ground and first floor, which helps in identifying minor cracks in the infill walls (see Figure 3.6 (c)).

| (a) | (b) | (c) |

Figure 3.6 – CCP1 building recorded during the reconnaissance after the Gorkha earthquake; (a) and (b) North and South facing, respectively, and (c) State of infill panel and frame elements and their connections

Figure 3.7 demonstrates the floor plan, vertical cross-section, beam plan layout and structural section details. The building is unsymmetrical in plan, having four bays in the N–S (north–south) direction and two bays in the E–W (east–west) direction. The eastern side of the building possesses cantilever projections that could potentially develop torsional behaviour. The uniform inter-storey height of 2.43 m is provided throughout, such that the total height of the building is 9.7 m. Similarly, the total plinth area of the building is approximately 70 m², where it possesses maximum bay length of 2.7 m along the N–S direction and 4.2 m along E–W direction.

During the detailed site survey, the structural elements recorded and measured in situ were seen to possess a uniform cross-section throughout, with column size (230 x 230) mm² and beam section size approximately (230 x 330) mm² including constant slab thickness of 100 mm. The observed structural section indicates that the beam is stronger compared to the column, which illustrates the design philosophy of that time. This shows that non-engineered buildings were built based on strong-beam weak-column concepts. Two types of solid masonry infill walls were used, such that the external infill walls of 230 mm thickness (placed in two layers) were placed at the periphery of the building, with large openings for windows, whereas the internal infill walls of 110 mm thickness were used for internal partitions. These infill walls lack satisfactory bonding with surrounding frames. Slight cracks were detected in the infill walls without any structural damage during the

Gorkha earthquake. This reveals that the frames and infill walls act together as monolithic elements in developing sufficient strength capacity against lateral loads, thus highlighting the positive contribution of infill walls. The stair was landed on the wall, which could reduce potential building failure under short-column. However, the possibility of a short-column mechanism cannot be ignored, which is likely to be instigated by distribution of infill panels. The columns are reinforced with uniform longitudinal bars of 4 Φ 12, and the beams are reinforced with top bars of 3 Φ 12 and bottom bars of 2 Φ 12. Similarly, transverse reinforcement bars having one legged stirrup of Φ 6 mm are uniformly spaced at 150 mm centre throughout the beam and column heights. The characteristic strength of the reinforcement bar was assumed as 415 MPa [20].
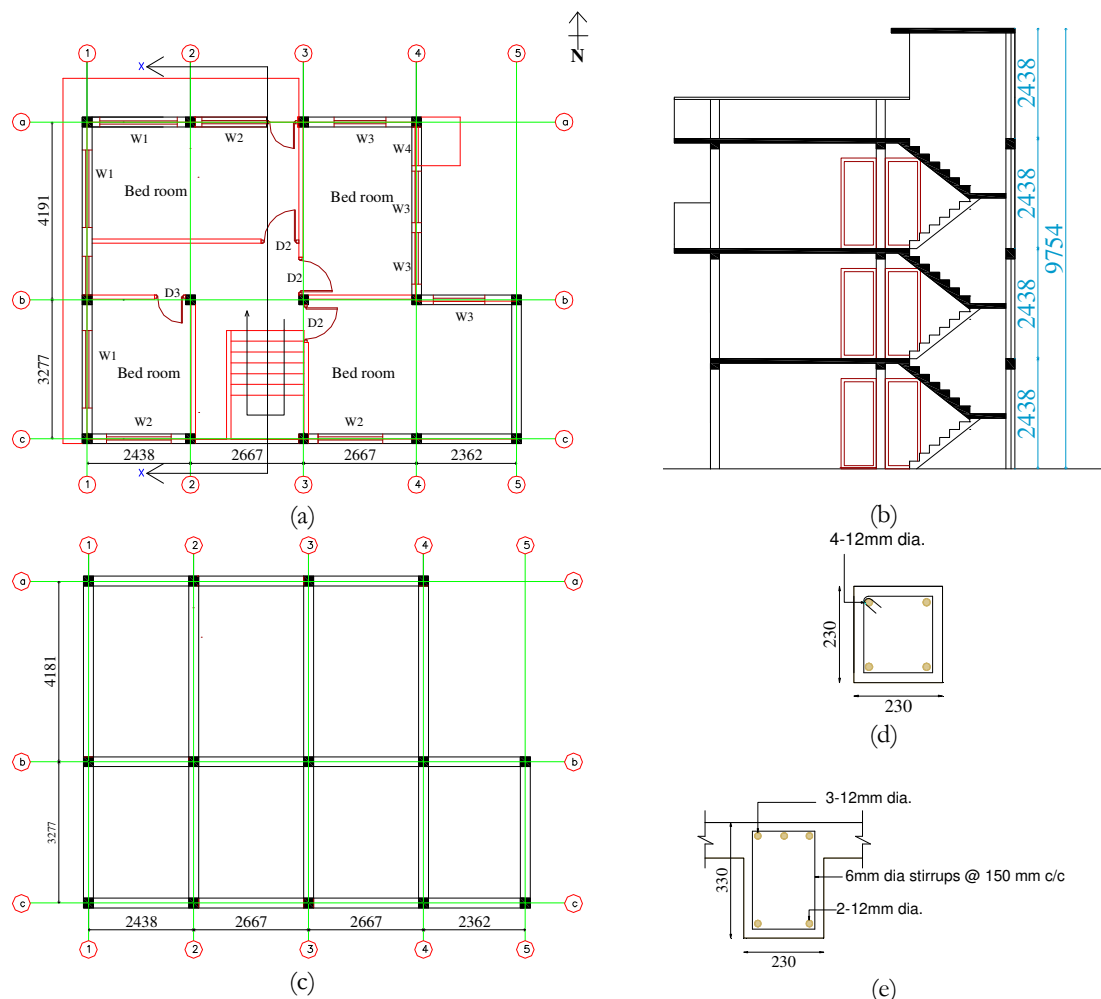
Figure 3.7 – Geometrical details and section layout of the CCP1 building; (a) Typical floor plan, (b) Cross-section, (c) Typical beam and column layout, (d) Typical column section and (e) Typical beam section (all dimensions are in mm)

3.2.2   Field tests

3.2.2.1   Schmidt hammer test

Schmidt hammer tests were performed on beam, column and slab elements of the CCP1 building. At least 16 records were noted in each test set, which were then averaged. Here the highest and lowest deviated test records were neglected. The averaged rebound number or value recorded for the CCP1 is shown in Table 3.3. A correction factor for old concrete was carried out using Table 3.2 [38] to obtain averaged compressive strength. The mean compressive strength of beam, column, and slab was found to be 18.42 MPa, 17.1 MPa, and 15.84 MPa, respectively. These values were rounded to the nearest value to represent in more realistic form; thus the mean concrete strengths for the beam, column and slab were approximately 20 MPa, 15 MPa and 15 MPa, respectively. As discussed above, these concrete compressive strengths may not characterize global concrete strength since the tests were performed only on plain and smooth surface, and only in a few locations. Hence, these values were utilized as preliminary data for parametric analysis.

Table 3.3 - Schmidt hammer test results for the CCP1 building

Reading	Calibrated strength in MPa	Mean concrete Strength MPa	Structural element
27	20.25		
29	21.75		
21	15.12	18.42	Beam
27	20.25		
23	16.56		
23	16.56		
28	21		
29	21.75		
24	17.28		
26	18.72	17.1	Column
23	16.56		
21	15.12		
19	13.68		
18	12.96		
22	15.84		
20	14.4		
25	18	15.84	Slab
23	16.56		
20	14.4		
22	15.84		

3.2.2.2 *Ambient vibration test*

3.2.2.2.1 *Test setups*

The ambient vibration test for the CCP1 building was performed two months after the 2015 Gorkha earthquake using seismographs having three triaxial accelerometers (i.e. GeoSIG GSR-18bit resolution). The data was recorded by PCB electronic accelerometers with force balance ± 5g and sampling frequency of 2048 Hz, and acquisition of data through a cDAQ-9172 system. Figure 3.8 presents the experimental test set-up, where the test began from the top floor. The master (reference) seismograph was placed approximately at the geometrical centre of the building, and the remaining two seismographs were stationed at diagonal corner columns (i.e. slave or mobile seismographs). This test set-up aims to capture the torsional behaviour of the CCP1 building. The orientations of seismographs in each test set-up should be carefully noted so as to manage data accurately and precisely for future analysis. Although the test was performed in two set-ups, it was later detected that one of the seismographs had technical problems that forced only one experimental set-up. This problem could not be identified or noticed during the experimental work, mainly due to limitation numbers for seismographs, which directly or indirectly limited the scope of the data check. The data acquisition for each test set-up was set for 15 minutes. Considering all these limitations, the results presented and interpreted for this building were obtained from a single set-up, thus a precise and optimal building response might not have been achieved.
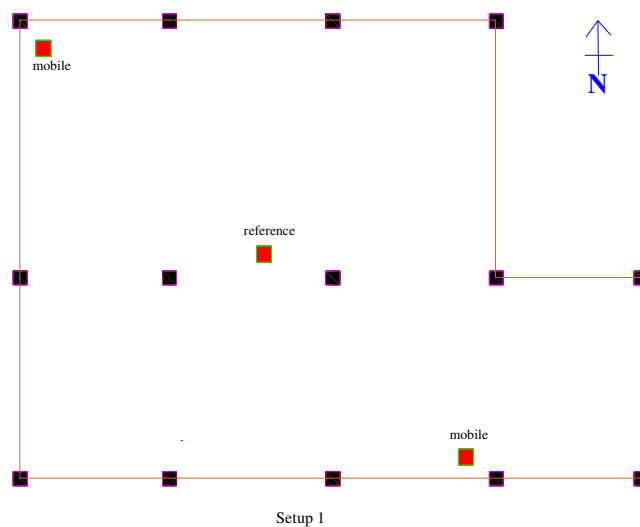
Figure 3.8 – Ambient vibration tests setup for the CCP1 building - schematic layout (not scaled)

3.2.2.2.2   Test results

The recorded raw time series data were analysed using the computer software ARTeMIS [49], an application for operational modal analysis [49]. A Singular Value Decomposition (SVD) of the spectral density matrices was performed to obtain the natural frequencies, damping coefficients and vibration modes. Figure 3.9 presents SVD graph illustrating the fundamental frequencies and corresponding vibration modes for the CCP1 building, which were performed by peak picking stable frequencies. If the multiple test setups are available, then average the first singular value of all test setups and average the second and so on. The first singular value was picked for well-separated modes and in case of close or repeated modes, the second singular value, third singular value etc. were also picked (trial-and-error method). The process was continued while stable frequencies and its pure building responses were not matched.

(a)

(b)
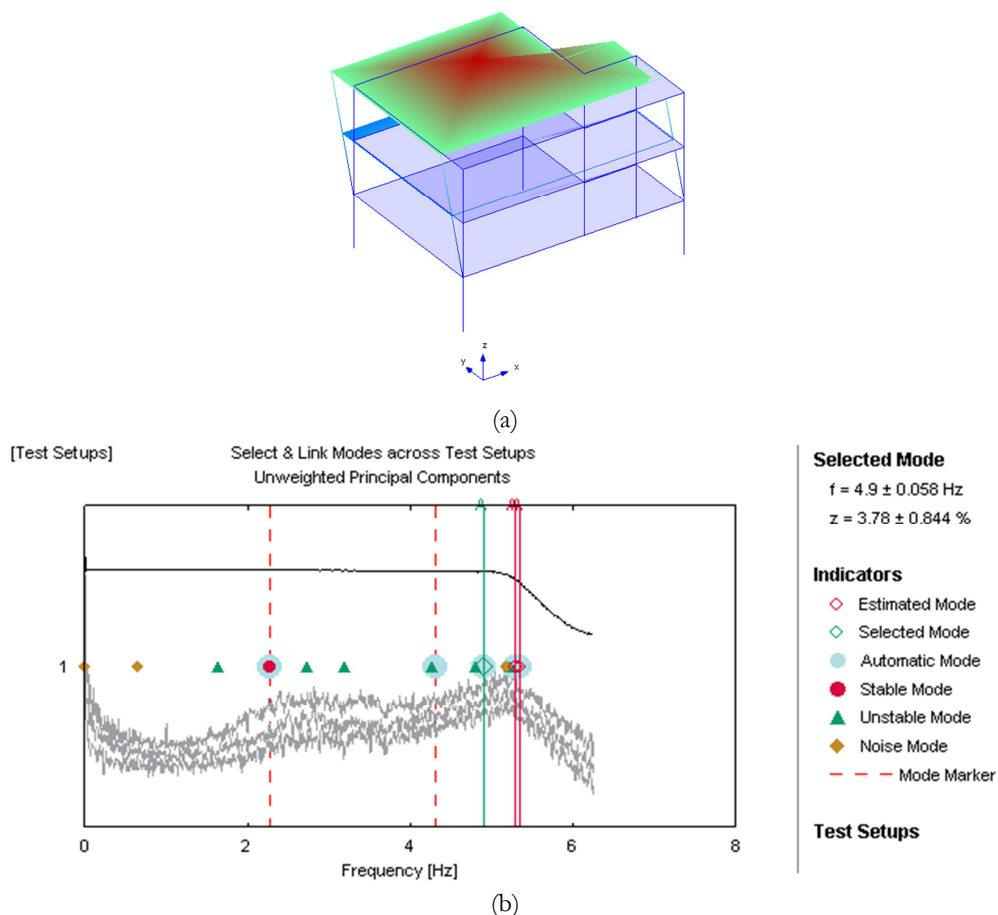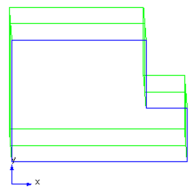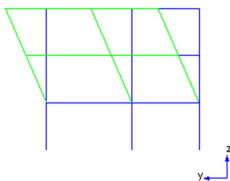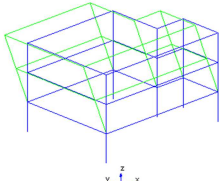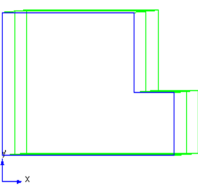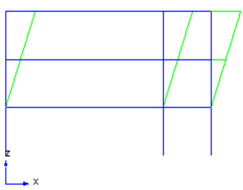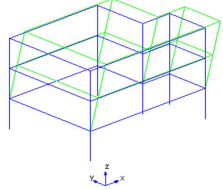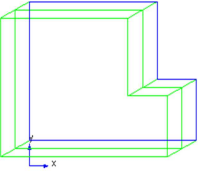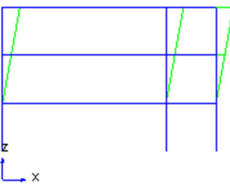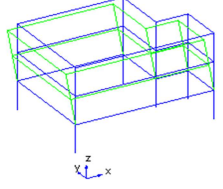
Figure 3.9 – Ambient vibration tests results for the CCP1 building – (a) Vibration modes and (b) Singular value of spectral density matrices

Table 3.4 presents the selected fundamental frequencies and vibration modes demonstrated in top, lateral, and 3-D views. The test results revealed that the CCP1 building shows two vibration modes as translational and a third one as diagonal, as initially expected. The first vibration mode was along the N–S direction, represented as the Y-axis in the ARTeMIS visual interface, whereas the second vibration mode along the E–W direction is represented as the X-axis. The results were obtained from one experimental set-up; thus obtained fundamental frequencies were not utilized for model calibration.

Table 3.4 – Ambient vibration frequency and vibration mode for the CCP1 building

Vibration mode	Fundamental frequency (Hz)	Top view	Lateral view	3-D view
First mode	4.89			
Second mode	5.28			
Third mode	5.34			

3.3   Suwal House (CCP2)

3.3.1   General introduction

The Suwal House is a four-storey ordinary RC frame building infilled with URM panels, and is located in Ghalate, Bhaktapur, Nepal. The building was built in the late 1980s, which also marks the beginning of RC construction in Nepal; thus it is classified as a non-engineered building and denoted as a CCP2 building. The site survey showed that the building sustained structural and non-structural damage, thus it was sub-categorized as damaged. The former damage was clearly visible in the corner columns at the ground floor, as shown in Figure 3.10 (a), where the repair and maintenance work was being carried out in these columns, and the latter damage was related to slight to moderate damage that was noticeable in entire infill walls. Figure 3.10 (c) demonstrates a representative pattern of cracks in the infill walls recorded in this building. The authorized drawings acquired from the owner illustrate that the building was built in two stages. Initially, two storeys were built, and two more storeys were added after 15 years. The building possesses vertical irregularity contributed by irregular distributions of infill panels, such that one complete bay on the road-facing side was without infill walls at the ground floor. This phenomenon could initiate structural damage potentially due to the soft-storey mechanism, which is likely to be a dominant failure mechanism in this particular building. In addition, the vertical irregularity in the building was reinforced by the presence of external infill panels on the projected slab at the northern side of the building, and the presence of wide openings on all sides except the west side could also contribute to this mechanism. Furthermore, the building also possesses parapet walls on the cantilever, as shown in Figure 3.10 (a), and such walls could create eccentricity in the building.

Given these considerations, it can be concluded that the building possesses large vertical irregularities and eccentricities, which could affect the load path and increase torsional behaviour, and eventually increase the seismic vulnerability of the building. This is a multipurpose (commercial and residential) building; the ground and third floors are being used for commercial purposes and the remaining floors are used for residential purposes. As previously stated, the building suffered heavy damage, and it can be expected to collapse in a future earthquake having moderate to large magnitude. To the team's surprise, many people are still living in this building, which illustrates its importance. The concerned

government bodies are requested to force the owner either to demolish the building or perform proper strengthening in order to safeguard the lives of the occupants.

Figure 3.10 – CCP2 building during the site inspection; (a) Geometrical 3-D view, (b) Maintenance work on damaged corner column and (c) Crushing of infill panel and separation of infill panel at the beam interface

Figure 3.11 presents the building geometrical plan, beam plan layout, and reinforcement details in the column, illustrating that the building is rectangular, having two bays along the E–W direction and three bays in the N–S direction. It has a maximum bay length of 4.2 m and 3 m along the N–S and E–W directions, respectively. The total length is 11.16 m along the building's N–S direction and 5.95 m along the E–W direction, such that the total plinth area is approximately 69.60 m². The stair is landed on the beam at the mid-height of the column, which increases a higher probability of short-column mechanism, and the irregular arrangement of infill panels also contributes to this failure mechanism.

The first two floors possess uniform inter-storey height of 2.75 m, and the remaining two storeys have 2.3 m inter-storey height; thus the total height of the building is 10.3 m. The site survey revealed that the building possesses uniform column and beam sections, such that the column section (230 x 230) mm² and beam size (230 x 330) mm² include a constant slab thickness of 100 mm. This shows that the CCP2 building was also built based on a strong-beam weak-column design approach. The reinforcements were not exposed in the structural elements and at the top floor; thus reinforcement detailing in the beam and

column was considered as specified by the owner since the reinforcement detailing was not detailed in the authorized drawings of that time. The column is reinforced with longitudinal bars of 4 Φ 12 and reinforced, in the beam, the top reinforcement is 4 Φ 12 and the bottom reinforcement is 3 Φ 12. In addition, the lateral ties are one-legged of Φ 6 mm uniformly spaced at 150 mm centre throughout the column and beam height. In some un-plastered areas, reinforcement was found exposed as a result of insufficient effective cover, which can cause rusting and potentially result in brittle failure. The building contains two types of solid brick infill panels: the external wall of 230 mm thickness placed at the periphery with large openings for windows, and the internal infill walls of 110 mm thickness that functions as partition walls.

(a)

(b)   (c)
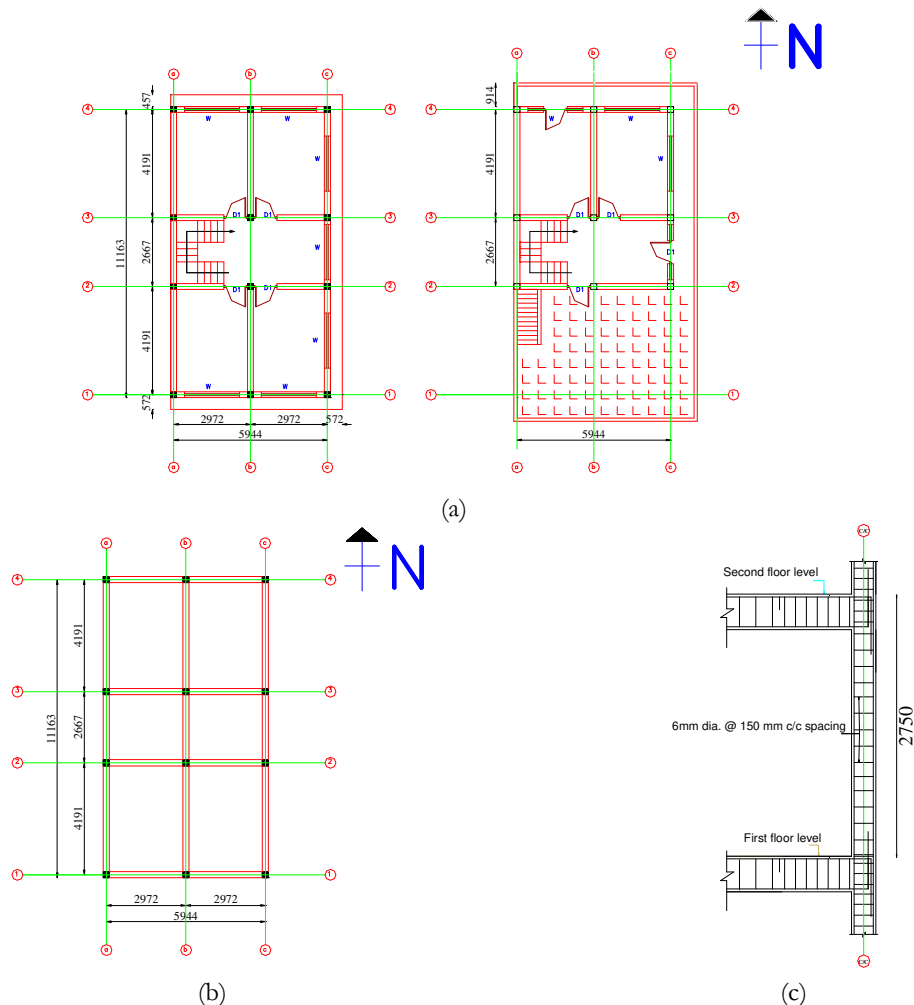
Figure 3.11– Geometrical layout and structural details of the CCP2 building; (a) Typical first and roof floor plans, (b) Column and beam layout and (c) Representative detailing of stirrups in column (all dimensions are in mm)

3.3.2 Field test

3.3.2.1 Schmidt hammer test

In-situ Schmidt hammer tests were conducted on the beam, column and slab elements of the existing CCP2 building, such that tests on the beams and columns were performed near the ends and approximately at the mid-height. At least 18 records were noted for each test set-up, and largely deviated records were ignored; the records were later averaged. These averaged data were calibrated using correction factor for old concrete using Table 3.2 [38]. Table 3.5 presents an average compressive strength for the tested concrete elements, and it was observed that the mean compressive strengths of the beam, column and slab elements were 7.45 MPa, 15.9 MPa and 6.6 MPa, respectively. The obtained strength was then rounded to the nearest value so that it can represent realistic concrete strength. For further study, the compressive strength of concrete for the column, beam and slab was considered as 15 MPa, 10 MPa and 5 MPa, respectively.

Table 3.5 – Schmidt hammer test results for the existing CCP2 building

Reading	Calibrated strength in MPa	Mean Compressive strength (MPa)	Structural element
12	7.44		
12	7.44		
14	8.68		
11	6.82	7.45	Beam
13	8.06		
12	7.44		
10	6.20		
15	9.30		
24	17.28		
30	21.60		
26	18.72		
17	11.39		
26	18.72	15.9	Column
22	15.84		
25	18.00		
22	15.84		
25	18.00		
22	15.84		
16	10.72		
10	6.20		
11	6.82		
10	6.20		
9	5.58	6.6	Slab
13	8.06		
12	7.44		
10	6.20		

3.3.2.2   *Ambient vibration test*

3.3.2.2.1   *Test setup*

The main objective of an ambient vibration test is to investigate a building's overall response as affected after a series of large- and small-magnitude earthquakes. Therefore, to meet the research objective, the dynamic test was conducted in the CCP2 building with the help of seismographs that consisted of three triaxial accelerometers, i.e. the same instruments as used in the CCP1 building. For this building the test was carried out in four set-ups and the acquisition time for each set-up was set at 15 min. The ambient vibration test set-ups for the CCP2 building are demonstrated in Figure 3.12. The seismographs recorded data in three directions, i.e. X, Y, and Z axes; thus the seismograph orientations for each test set-up should be carefully noted to avoid disparity when analysing data.

The test set-up began from the top floor, such that the reference seismograph was stationed at the geometrical centre of the building and was fixed. The slave seismograph (i.e. mobile) was initially placed at the corner column of the top floor along the S–W direction and was represented by set-up 1. Similarly, in set-up 2 the slave seismograph was moved to the N–E corner column of the top floor. The combination of set-ups 1 and 2 helps to capture the torsional response of the building. Likewise, the translational vibration of each storey was acquired by shifting the slave seismograph to the consecutive lower floors and placing it at the geometrical centre, i.e. just below the reference seismograph. In set-ups 3 and 4, the slave (represented by mobile in the figure) seismograph was again moved to lower floors and placed just below the reference seismograph.
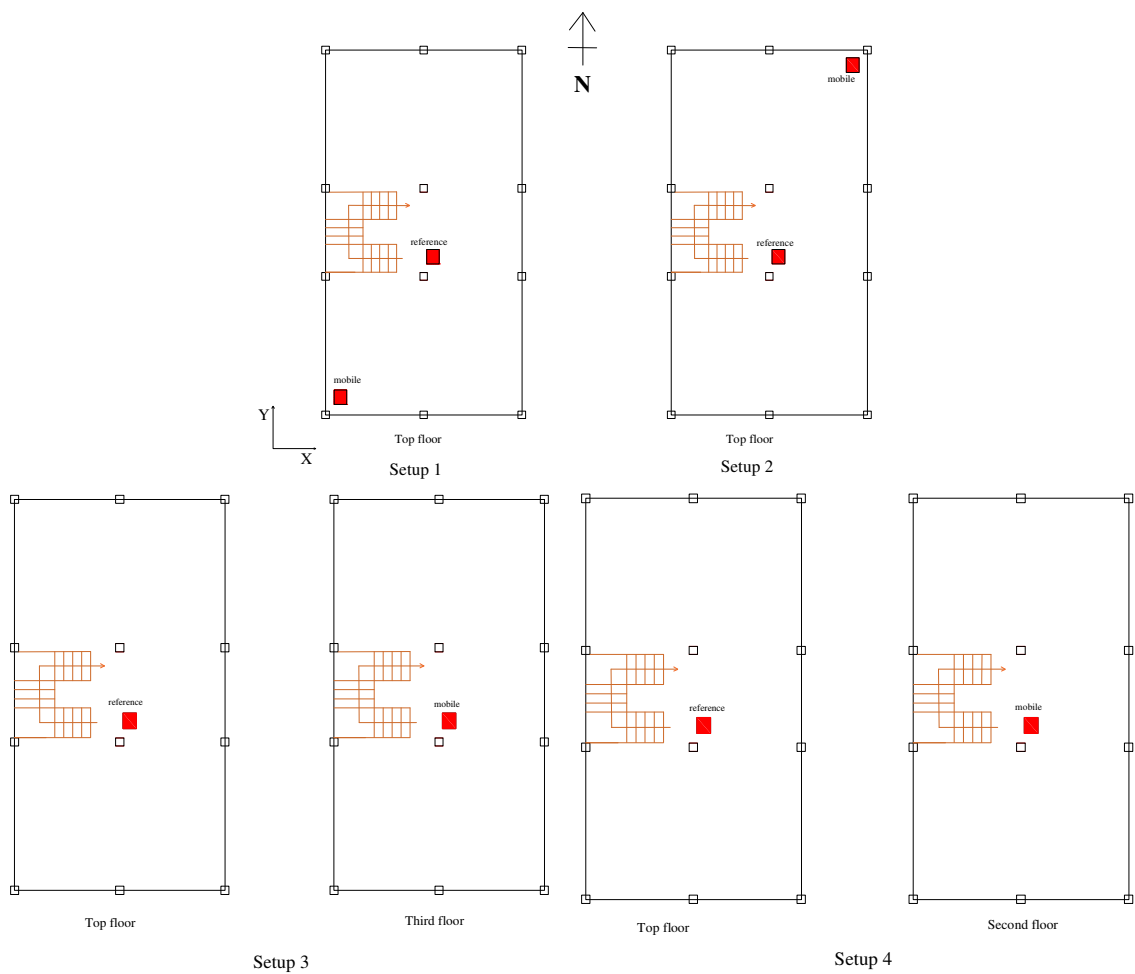
Figure 3.12 – Ambient vibration tests setup for the CCP2 building - schematic layout (not scaled)

3.3.2.2.2   *Test result*

Figure 3.13 shows the ambient vibration mode and the normalized singular values of spectral density matrix for all test set-ups acquired through the ARTeMIS software [49]. The fundamental frequencies of the CCP2 building were identified by the trial-and-error method: picking peak frequencies and comparing them with the corresponding vibration modes and finally checking the agreement between them.

(a)

(b)
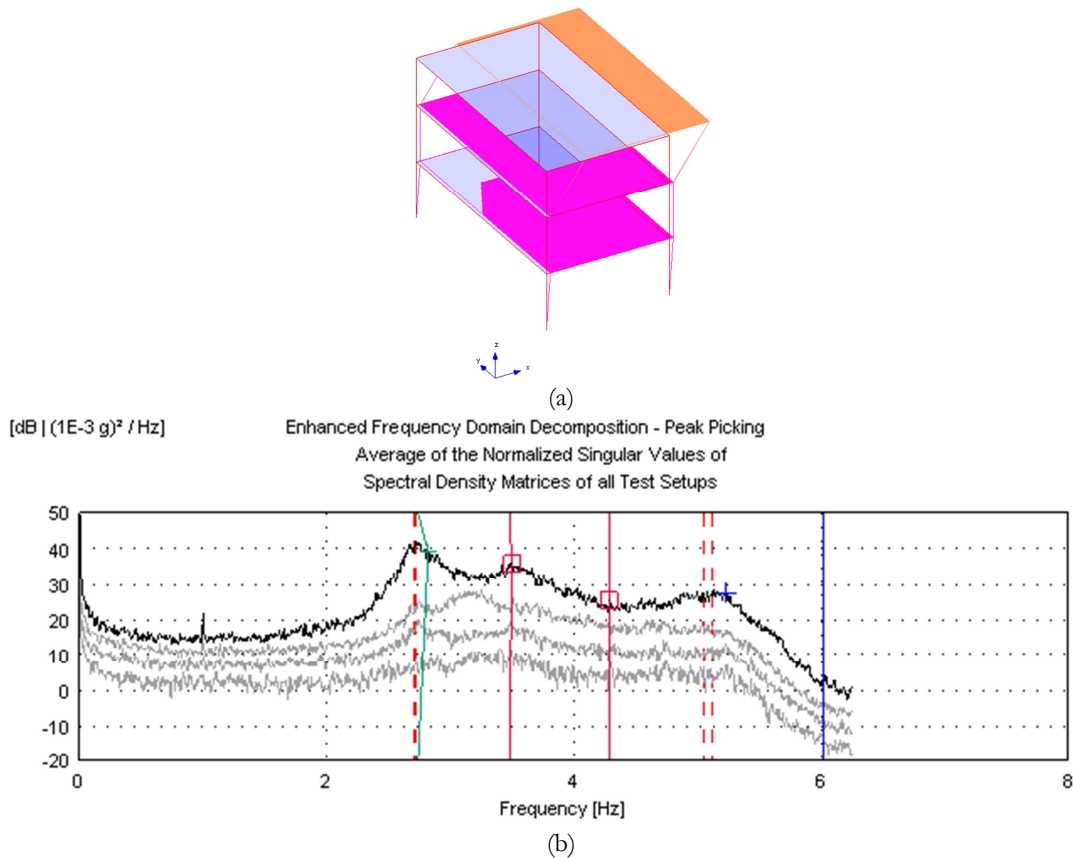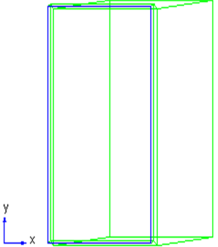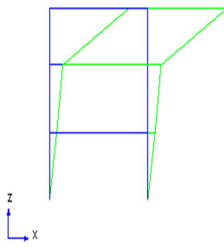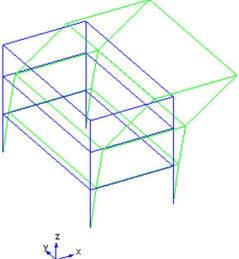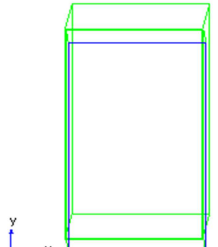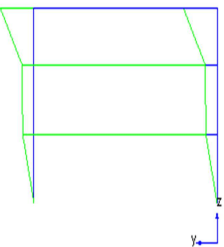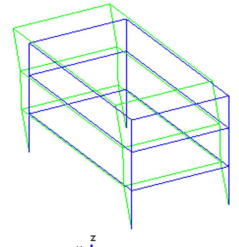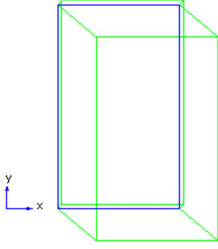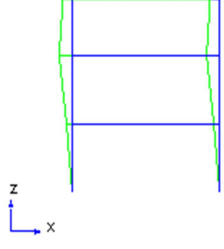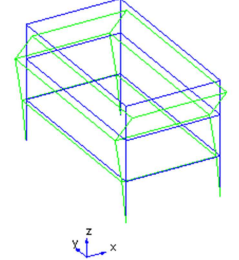
Figure 3.13 – Ambient vibration test results for the CCP2 building; (a) 3-D vibration modes, and (b) Average of the normalized singular value of spectral density matrices

The agreed structural frequencies and their corresponding vibration modes for the CCP2 building are organised in Table 3.6. As expected, the first two vibration modes were translational and third one was diagonal. The fundamental frequency and the respective modes of vibration are illustrated in top, lateral, and 3-D views. The insufficient recoded data sometimes could create difficulties in capturing pure torsional building response. The first vibration mode was observed along the X-axis, which represents the building's E–W direction and the second vibration mode was along the building's N–S direction, as clearly illustrated in Table 3.6.

Table 3.6 – Ambient vibration frequency and respective mode of vibration for the CCP2 building

Vibration mode	Fundamental frequency (Hz)	Top view	Lateral view	3-D view
First mode	2.74			
Second mode	3.47			
Third mode	4.29			

3.4 Bare Frame Structure (MRT1)

3.4.1 General introduction

The bare frame is a three-storey building located in the south-east of Bhaktapur, Suryabinayak Municipality, Nepal. The building was built in 2005 at the beginning of the MRT guideline approval and implementation. It was without infill walls and was abandoned, as observed during the site survey (see Figure 3.14). It reflects the construction practices of the locality, where initially buildings are built as a bare frame of the required storeys and after a certain time interval the infill walls are erected, beginning from the ground floor, depending upon the financial wherewithal of the owner. Based on the number of storeys, plinth area, reinforcement details for the structural elements, and section details as recorded from the site survey, it can be classified as a pre-engineered building or MRT building and named as MRT1. Some structural defects were identified during site inspections. They include the stair landing on the beam at the mid-height of the column, which could initiate short-column mechanism and discontinuity of floor beam in the stair portion, as presented in Figure 3.14 (c). Figure 3.14 (b) presents observed defects due to poor material quality, poor compactions, reinforcement exposed due to inadequate effective cover, and so on. Due to such confinement problems, the brittle failure of the structural elements cannot be ignored. In addition, the presence of large voids and swelling near the beam-column joint as recorded during site reconnaissance is most likely due to poor compaction and poor workmanship at the construction site. The MRT1 building also possesses structural plan irregularity, where structural circular columns at the ground floor are being replaced by rectangular columns in the first floor, and the lack of column at beam-beam joint also increases plan irregularity. Such joints act as the weakest point and are more likely to undergo excessive deformation and eventually decrease the floor rigidity when acted upon by lateral loads. The building was also selected due to the opportunity of having a fully characterized bare-frame building, where a different infill masonry scenario can be added, and vulnerability assessment for different dispositions can be investigated through static and dynamic analyses, discussed in detail in Chapter 5.
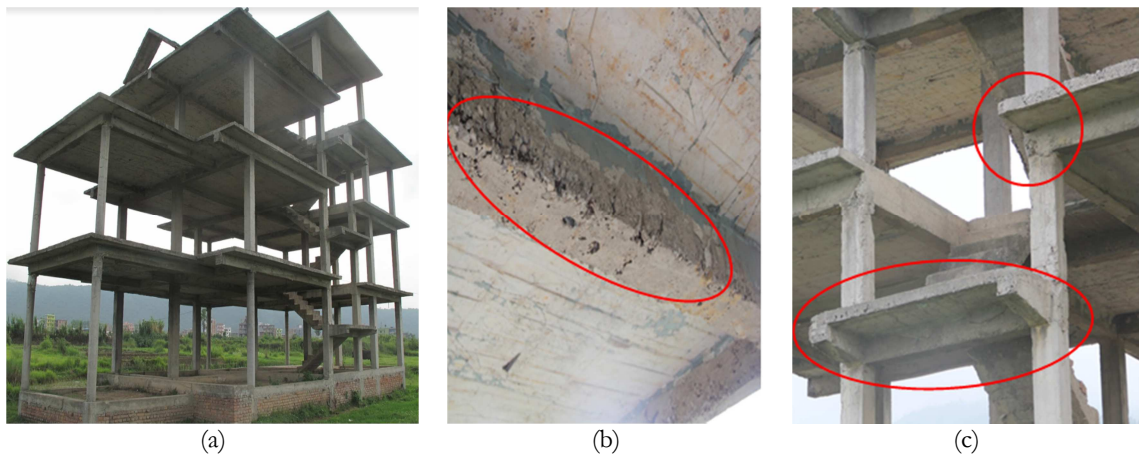
Figure 3.14 – Description of the MRT1 building as observed in site survey; (a) 3-D view, (b) Reinforcement exposed on the beam and poor concrete quality and (c) Short-column at the staircase landing and improper connection at beam-column joint

Figure 3.15 presents the geometrical plan layout, section, and reinforcement details as measured in situ. The building possesses uniform inter-storey height of 2.74 m, such that the total height of the building is 10.96 m, which includes the stair cover portion at the top floor. The building has two bays in the E-W direction with a maximum bay length of 4.7 m represented along the X-axis, and four bays in the N-S direction with a maximum bay length of 3.5 m and denoted by the Y-axis, as shown in Figure 3.15 (a). Thus the total span along the X-axis is 16 m and 8.3 m along the Y-axis, and the total plinth area of the building is approximately 100 mm². A detailed assessment of the building was carried out, which included measurement of structural section size and the detection of different column sizes, such as a rectangular section (300 x 230) mm² and (230 x 230) mm², and a circular section of Φ 230 mm. In addition, the building possesses uniform beam section (230 x 355) mm² including slab thickness of 125 mm. All the columns are reinforced with longitudinal reinforcement of (4 Φ 16) + (2 Φ 12) and with reinforced beam with top reinforcement of 3 Φ 16 and bottom reinforcement of 3 Φ 12. Furthermore, the transverse reinforcement of 2 legged Φ 6 mm is uniformly spaced at 150 mm centre throughout the beam and the column height.
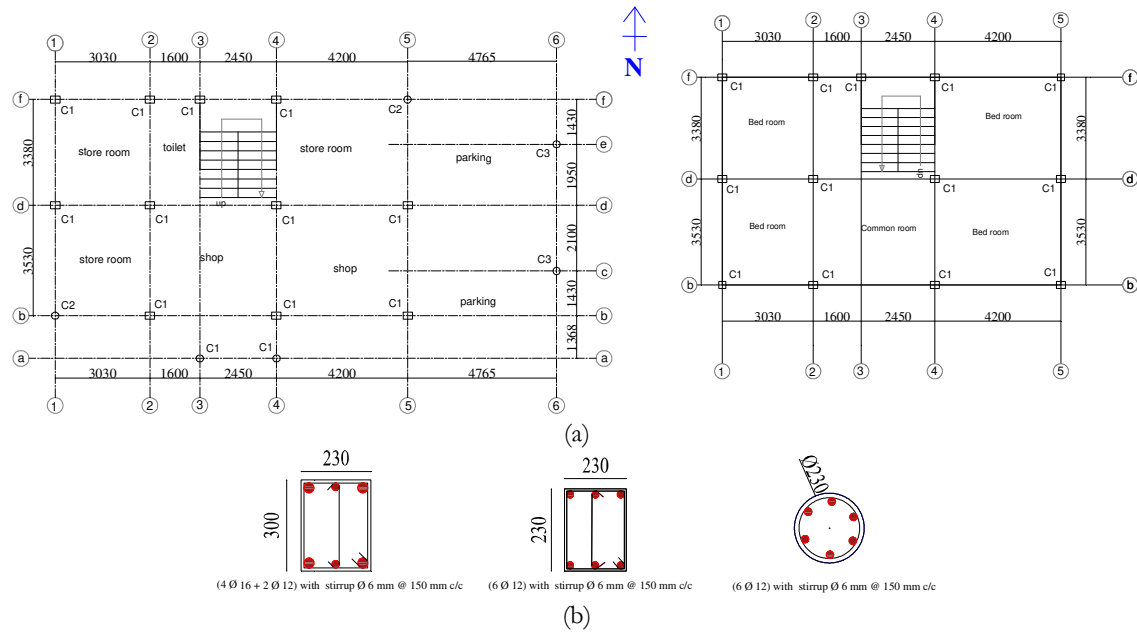
Figure 3.15 – Geometrical details and structural layout of the MRT1 building; (a) Plan and structural layout of the first and top floors, respectively, and (b) Detailing of column sizes and reinforcement (all dimensions are in mm)

3.4.2 Field tests

As discussed in the previous sections, two types of field test were performed at the site after the Gorkha earthquake, as follows.

3.4.2.1 Schmidt hammer test

For each test set, at least 16 data points were recorded in each beam, column, and slab element of the MRT1 building. Table 3.7 presents calibrated compressive strengths of concrete obtained using the correction factor presented in Table 3.2. This calibrated mean compressive strength was then rounded to the nearest value, such that the mean compressive strength for beam, column and slab elements were considered as 20 MPa, 20 MPa and 15 MPa, respectively, for further analysis.

Table 3.7 – Schmidt hammer test results of the bare frame building (MRT1)

Reading	Calibrated strength in MPa	Mean concrete strength (MPa)	Structural element
38	22.99		
41	24.53		
31	18.78	21.2	Beam
36	21.45		
33	19.75		
33	19.91		
38	22.63		
37	22.44		
32	19.28		
36	21.30	22.2	Column
39	23.49		
39	23.13		
38	22.88		
25	15.18		
24	14.14		
30	17.96	16.6	Slab
29	17.39		
29	17.32		
29	17.36		

3.4.2.2 Ambient vibration test

3.4.2.2.1   Test setups

Ambient vibration tests for the MRT1 building were performed to investigate the dynamic properties of the building that was being affected from a main shock and a series of aftershock earthquakes. Figure 3.16 illustrates the ambient vibration tests layout, which was carried out in three set-ups.
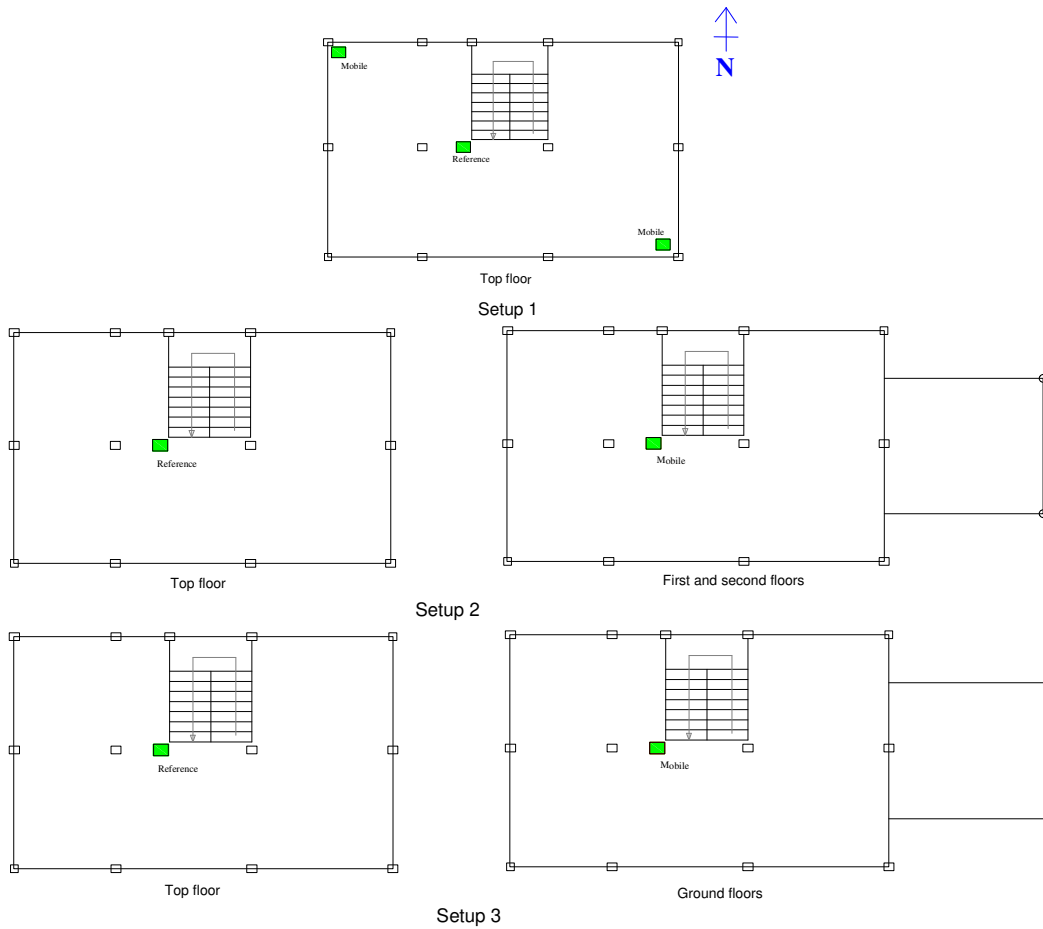
Figure 3.16 – Ambient vibration tests set-up for the MRT1 building - schematic layout (not scaled)

3.4.2.2.2   Test results

Figure 3.17 presents singular and normalized curves for the spectral matrix of all the measured seismographs. The agreed fundamental frequencies obtained by comparing peak frequencies from the singular value of the spectral density matrix with vibration modes are presented in Table 3.8. As expected, the first two mode shapes were detected as translational and the third one as diagonal. Thus obtained fundamental frequencies and respective vibration modes are shown in the form of top, elevation, and 3-D views in Table 3.8.

(a)

(b)
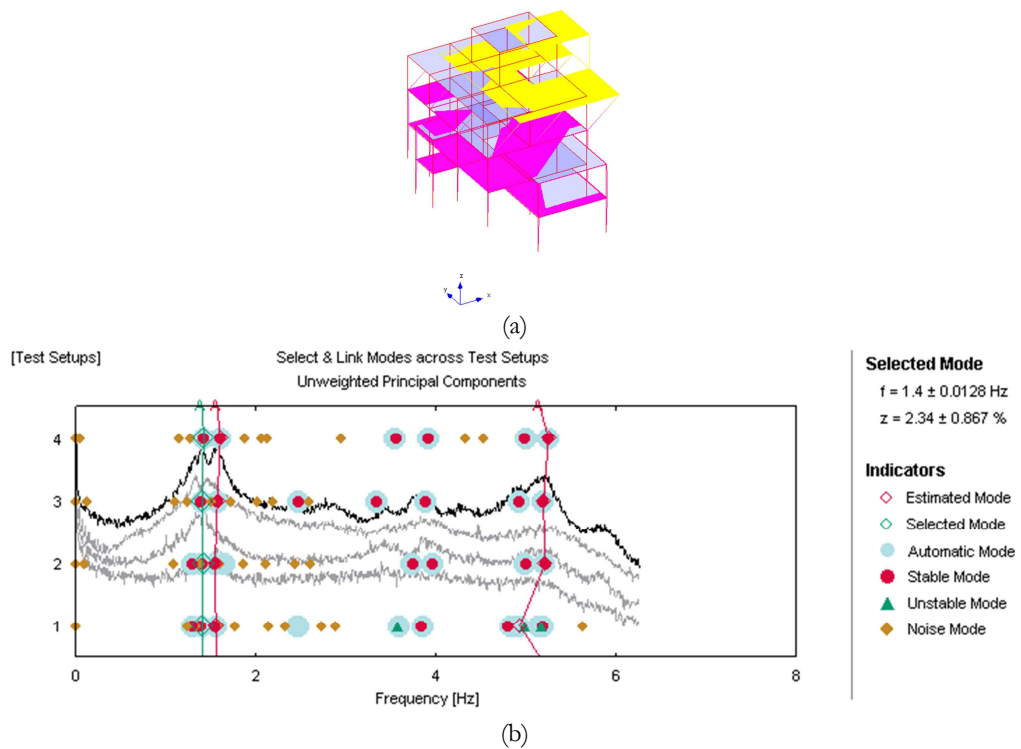
Figure 3.17 – Ambient vibration tests results for the MRT1 building; (a) Vibration mode, (b) Singular value of spectral density matrices

Table 3.8 – Ambient vibration frequency and respective mode of vibration for the MRT1 building

Vibration mode	Fundamental frequency (Hz)	Top view	Lateral view	3-D view
First mode	1.41			
Second mode	1.57			
Third mode	1.67			

3.5 Twayana House (MRT2)

3.5.1 General introduction

The Twayana house is a five-storey RC-MRF building that includes one basement and is located in Suryabinayak Municipality, Bhaktapur, Nepal. The building was constructed in 2004, which also marked the beginning of the MRT guideline implementation [20], although the structural sections, reinforcement details, number of storeys, plinth area and so on were not identical to the MRT guideline. The structural sections measured in situ represent elements relatively similar to the one defined by the NBC 205: 1994 [20] guideline; thus the building is classified as pre-engineered and named as MRT2. The primary objective of this building selection was to investigate the seismic performance of a building that was identical to the MRT guideline, and also to study an increase in vulnerability due to irregular distribution of infill walls. The large vertical irregularities were recorded in the MRT2 building after the field reconnaissance and were mainly due to irregular distribution of infill panels. The building is without internal infill walls at the basement. In addition, a complete bay on the road-facing side, i.e. the west side at the ground floor, is without external infill panel. As a result, the roadside corner columns were observed to be damaged, and repair work was being carried out on the damaged columns. In addition, new internal infill panels were being erected in the basement. Based on observed structural and non-structural damage, the MRT2 building was sub-categorized as damaged building type. Figure 3.18 illustrates the MRT2 building, with damage detected on both structural and non-structural elements and maintenance works.

Figure 3.18 – MRT2 building scenario observed in site survey; (a) East-South elevation, (b) North elevation, (c) and (d) Repair and maintenance works on the beam-column joint and (e) Diagonal cracking on infill panel

As observed, the building was considerably used for residential and commercial purposes; all rooms were rented and the roadside bay at the ground floor was utilized for commercial purposes, having shutters instead of masonry infill panels. The absence of internal infill walls at the basement and irregular distribution of infill panels throughout the building leads to the conclusion that the building is most likely to fail under soft-storey mechanism. This statement can be justified through observed corner column damage and medium to large cracking of infill walls throughout, as illustrated in Figure 3.18. This problem was further exacerbated by the absence of infill panel in a complete bay on the road-facing side at the ground floor. In addition, shear failure in the column is most likely to occur due to large openings on the external walls on all sides except the northern side of the building. The short-column could also be a dominant failure mechanism in this particular building due to the staircase landing on the beam at the mid-height of the column. Since the MRT2 building possesses many structural defects, potential failure under different mechanisms can be expected.

It possesses two types of solid masonry infill walls: external infill walls of 230 mm thickness placed at the periphery and internal infill walls of 110 mm thickness and functioning as internal partitions. No special connections between infill walls and surrounding frames

were detected, which could increase the possibility for out-of-plane collapse of the infill walls. The infill walls mostly at the basement and ground floors were observed to have minor to large cracks. Figure 3.19 presents a typical floor and beam plan layout for the MRT2 building, revealing that it is almost rectangular in plan. However, torsional behaviour can also be a dominant building response contributed by the irregular distribution of infill panels at the basement and ground floor, as discussed above. The total height of the building is 12.58 m including the basement, where the building has uniform inter-storey height of 2.52 m. It possesses two bays in the N–S direction with a maximum bay length of 2.97 m and five bays along the E–W direction having a maximum bay length of 3.58 m. The total plinth area of the MRT2 building is approximately 133 m^2, such that the total span along the N–S direction is 8.91 m and 17.9 m along the E–W direction. The MRT2 building possesses uniform column and beam sections: column section (270 x 270) mm^2 and beam section (230 x 330) mm^2 including constant slab thickness of 100 mm throughout. The building is reinforced with longitudinal reinforcements in the column containing (4 Φ 16) + (2 Φ 12), and in the beam, top reinforcement of (2 Φ 16) + (1 Φ 12) and bottom reinforcement of 2 Φ 16. The transverse reinforcement of Φ 8 mm is uniformly spaced at 150 mm centre throughout the beam and the column height. The yield strength of reinforcement was considered as 415 MPa as per NBC 205:1994 [20].

(a)

(b)
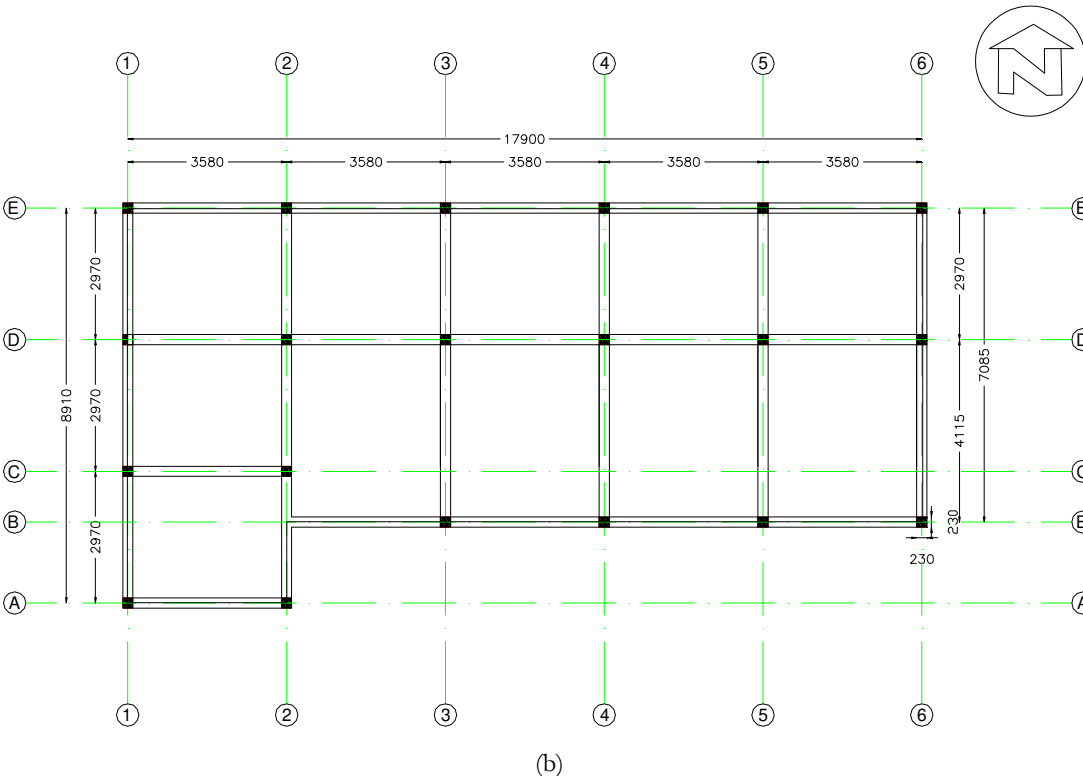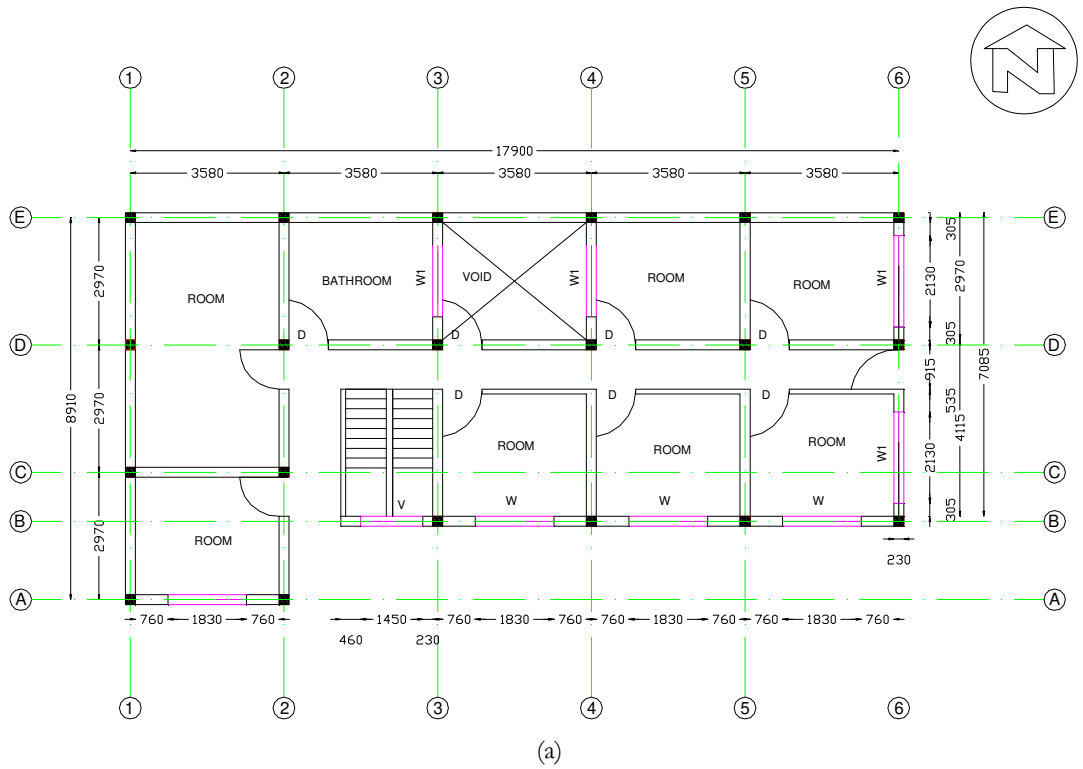
Figure 3.19 – Structural floor layout of the MRT2 building; (a) Representative layout of the floor plan and (b) Typical beam and column layout (all dimensions are in mm)

3.5.2 Field test

3.5.2.1 Schmidt hammer test

At least 20 records were recorded for each test set and largely varied data were omitted and averaged which later calibrated using correction factor as presented in Table 3.2. The rounded mean concrete compressive strengths for the beam and the slab were found to be 15 MPa and 20 MPa for the columns, as tabulated in Table 3.9. These records are only rough estimates and adjusted later through model calibration.

Table 3.9 – Schmidt hammer test results for the MRT2 building

Reading	Calibrated strength in MPa	Mean strength (MPa)	Structural element
20	13.40		
22	14.74		
17	11.39	15.60	Beam
27	18.09		
20	13.40		
30	22.50		
24	17.28		
26	18.72		
29	20.88		
30	21.60		
18	12.96		
14	8.68		
22	15.84	18.90	Column
21	15.12		
32	23.04		
24	17.28		
33	23.76		
36	25.92		
30	21.60		
30	21.60		
22	15.84		
18	12.06		
21	14.07	13.90	Slab
16	10.72		
24	17.28		
20	13.40		

3.5.2.2 Ambient vibration test

3.5.2.2.1 Test setup

The ambient tests for the MRT2 building were performed in four test set-ups, as presented in Figure 3.20. The test was conducted in four test set-ups, such that one reference seismographs fixed at the top floor and the slave seismograph shifted to the consecutive

lower floors and placed at the geometrical centre, positioned just below the reference seismograph.
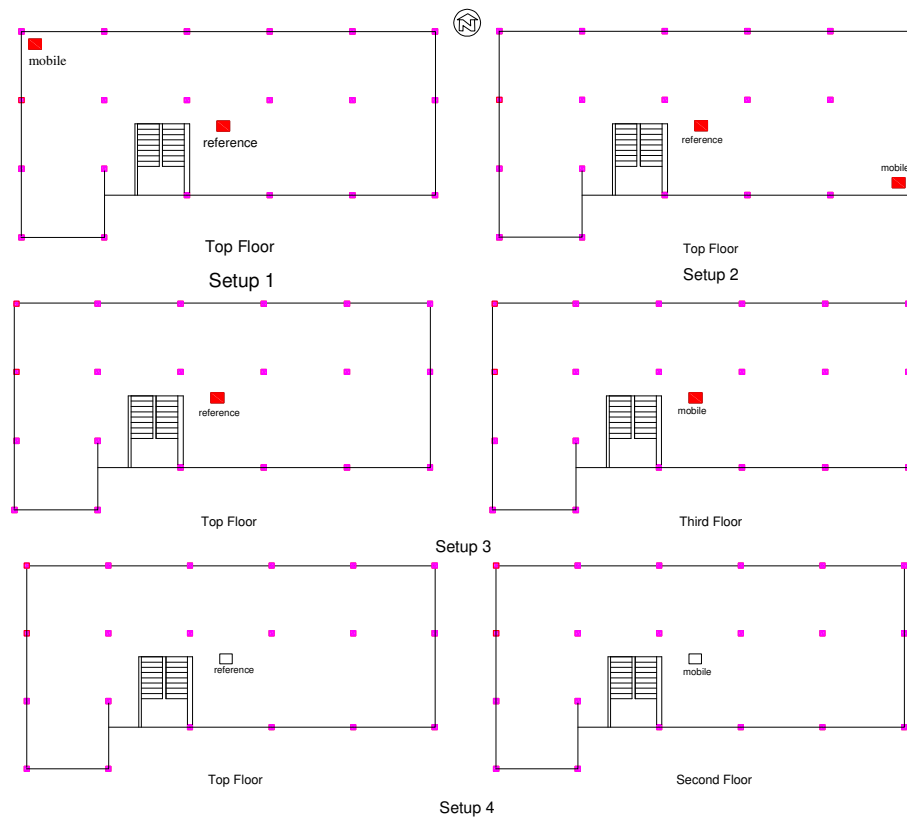
Figure 3.20 – Ambient vibration tests setup for the MRT2 building - schematic layout (not scaled)

3.5.2.2.2   Test results

The average of the normalized spectral density matrices and vibration mode is illustrated in Figure 3.21. The matched peak picked frequencies and respective vibration modes are tabulated in Table 3.10. Interestingly, the MRT2 building reveals a first vibration mode along the translational and a second vibration mode as diagonal. In addition, a third vibration mode is the mixed translational.

(a)

(b)
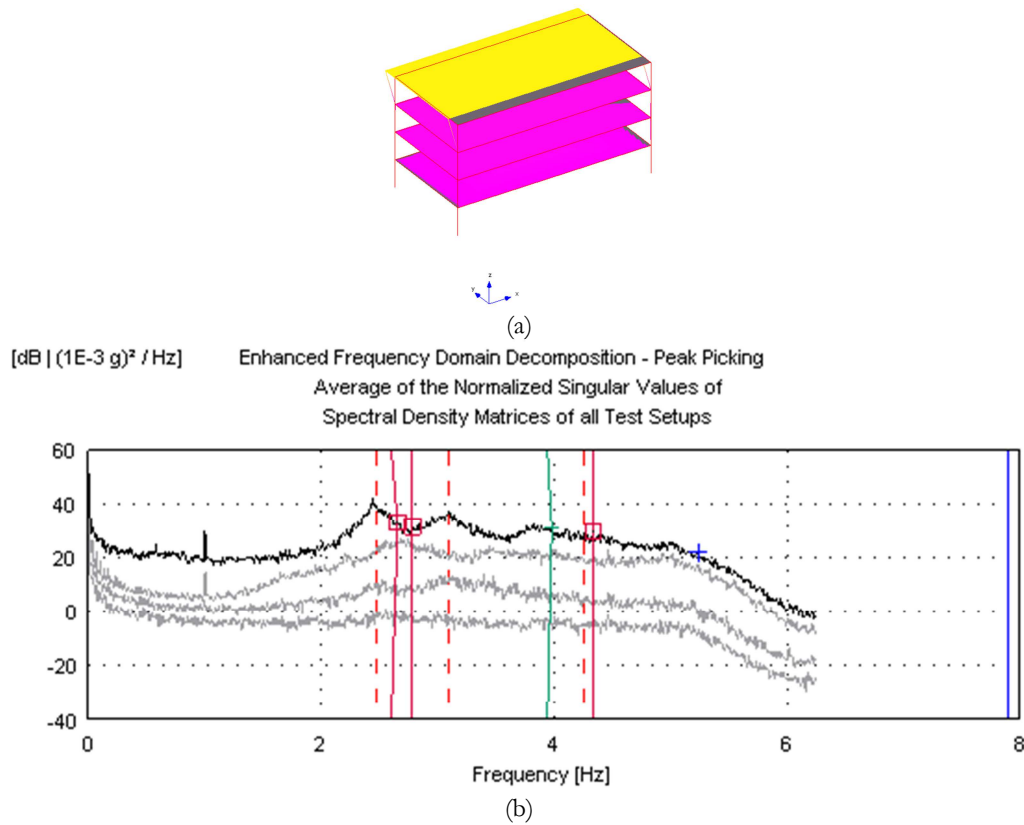
Figure 3.21 – Ambient vibration tests results for the MRT2 building; (a) Vibration mode, and (b) Average of normalized singular value of spectral density matrices of all test setups

Table 3.10 – Ambient vibration frequency and respective mode of vibration for the MRT2 building

Vibration mode	Fundamental frequency (Hz)	Plan view	Lateral view	3-D view
First mode	2.60			
Second mode	3.90			
Third mode	4.34			

3.6   Khwopa Engineering College Block 'C' (WD1)

3.6.1   General introduction

The Khwopa Engineering College Block 'C' is a five-storey building located in Libali-02, Bhaktapur, Nepal. The building was built in 2005. It is the first community-based engineering college undertaken by the Bhaktapur Municipality and is used for institutional purposes. The building was built in such a way that it attempts to combine new technology with old construction philosophy. The former adapts the concept of RC frame skeleton and the latter uses a façade, representative of a traditional building, as shown in Figure 3.22. The building is used by the engineering students and faculty members affiliated with Purwanchal University. Approximately 400 people use it during weekdays. The building was designed as a special moment-resisting frame (SMRF), whose structural elements were designed as a seismic-force-resisting system, following several design guidelines, such as NBC 105: 1994, IS 1893 (Part I): 2002, and IS 4326: 1993 [24, 30, 50] and numerical analysis using design software SAP 2000. It was designed considering response reduction factor (R) as 5 [30] and importance factor (I) as 1.5 [30], which also depends on the functional use, post-earthquake functional needs and economic importance. The ductile detailing of the structural elements was carried out using IS 13920:1993 [51]. Considering all these design considerations and philosophies, the building was classified as well-designed and named as WD1. The WD1 building possesses two types of URM as infill walls: external infill wall of 350 mm thickness and internal partition wall of 230 mm thickness. Almost all external infill walls possess wide openings for doors and windows, and the building has a slanting roof with brick tiles. The building did not suffer any structural damage, but the infill walls sustained insignificant or minor hairline cracks resulting from the Gorkha earthquake. Therefore, the building was sub-categorized as non-damaged.

(a)   (b)

Figure 3.22 – WD1 building observed in the course of field survey; (a) and (b) No structural damage and insignificant or hair line cracks on few infill panels

A representative floor layout, beam-column layout, and the structural section and reinforcement detailing layouts for the building are illustrated in Figure 3.23. The plan is rectangular with seven bays in the E–W direction (along the X-axis) and two bays in the N–S direction (along the Y-axis). The maximum bay length along the E–W direction is 6 m and 7 m along the N–S direction. The total span is 36 m along the E–W direction and 14 m along the N–S direction; thus the total plinth area of the building is approximately 423 m². The building possesses uniform inter-storey height of 3.3 m; thus the total height is 18.93 including the slanting roof.

The structural sections and detailing presented and discussed for the WD1 building were based on the structural drawings obtained from the college administration. The building possesses different column sections: rectangular column sections (400 x 600) mm² and (600 x 400) mm², and circular section Φ 500 mm. Similarly, it possesses different beam sections: (300 x 500) mm², (230 x 500) mm², and (350 x 500) mm² including uniform slab thickness of 150 mm. Although the column section is the same, the distribution of longitudinal reinforcements varies depending upon location and orientation. However, the present study considered averaged longitudinal reinforcement for the columns and beams possessing the same sections in order to simplify numerical calculations, computations, and analysis approaches. The average longitudinal reinforcement considered in the rectangular column was (14 Φ 25) + (6 Φ 20), and the circular column was 16 Φ 16, as shown in Figure 3.23 (c). Similarly, the beam is reinforced with longitudinal reinforcement with beam size (300 x 500) mm² and (350 x 500) mm² containing top reinforcement of (4 Φ 25) + (2 Φ 20) and bottom reinforcement of 3 Φ 25, and the beam size (230 x 500) mm² containing top reinforcement of (4 Φ 25) + (1 Φ 20) and bottom reinforcement of 3 Φ 25. The WD1 building is reinforced with transverse stirrups of Φ 8 mm uniformly spaced at 100 mm centre for a height of h/4 from the end face of the beam and column, and spaced at 150 mm for the remaining height (at the middle portion). The effective cover considered for the column, beam, and slab elements was 40 mm, 25 mm, and 15 mm, respectively. Furthermore, the development length allotted for tension and compression bars was 50 and 40 times the diameter of the main bars, respectively. The yield strength of the reinforcement should be at least 415 MPa conforming to IS: 1786-1985 [52], and hooks in lateral ties and stirrups bent at 135⁰ with hook length more than 10 times the stirrup diameter.

(a)

(b)

(c)
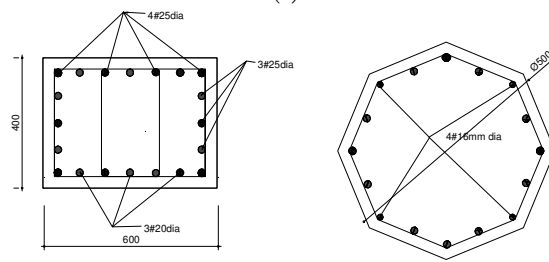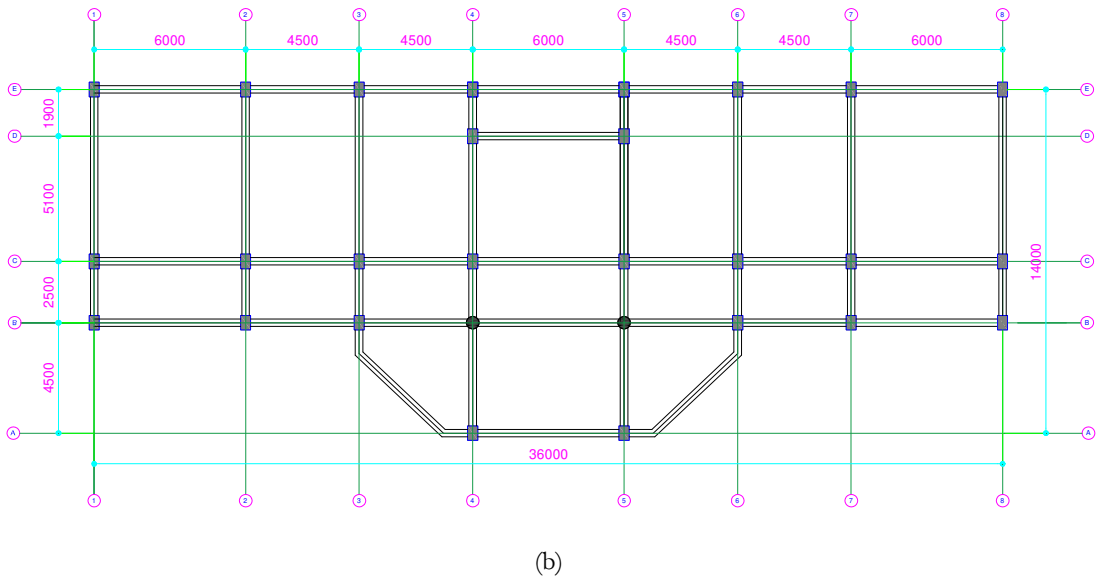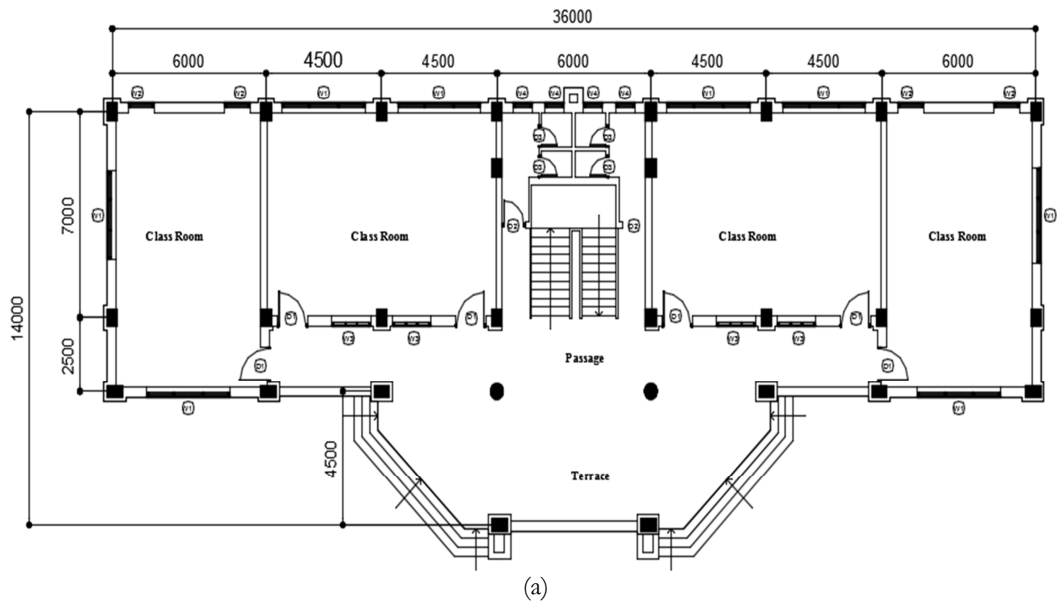
Figure 3.23 – Geometrical details and structural layout of the Khwopa Engineering College block 'C'; (a) Typical floor plan details, (b) Beam-column layout and (c) Typical column section and reinforcement details (all dimensions are in mm)

3.6.2 Field tests

The Schmidt hammer test was not carried out for this building due to various constraints at the site, i.e. related to the unavailability of exposed surface (i.e. without plaster surface) in the beam and columns. Therefore, the concrete compressive strength was predicted for various structural elements similar as specified in the authorized drawings provided by the college administration. The concrete compressive strength for the entire column, beam and slab elements were considered as 20 MPa.

3.6.2.1 Ambient vibration test

3.6.2.1.1 Test setups

Figure 3.24 presents the ambient vibration tests layout for the WD1 building. The test was carried out in three set-ups and recorded data for duration of 15 minutes in each test set-up.
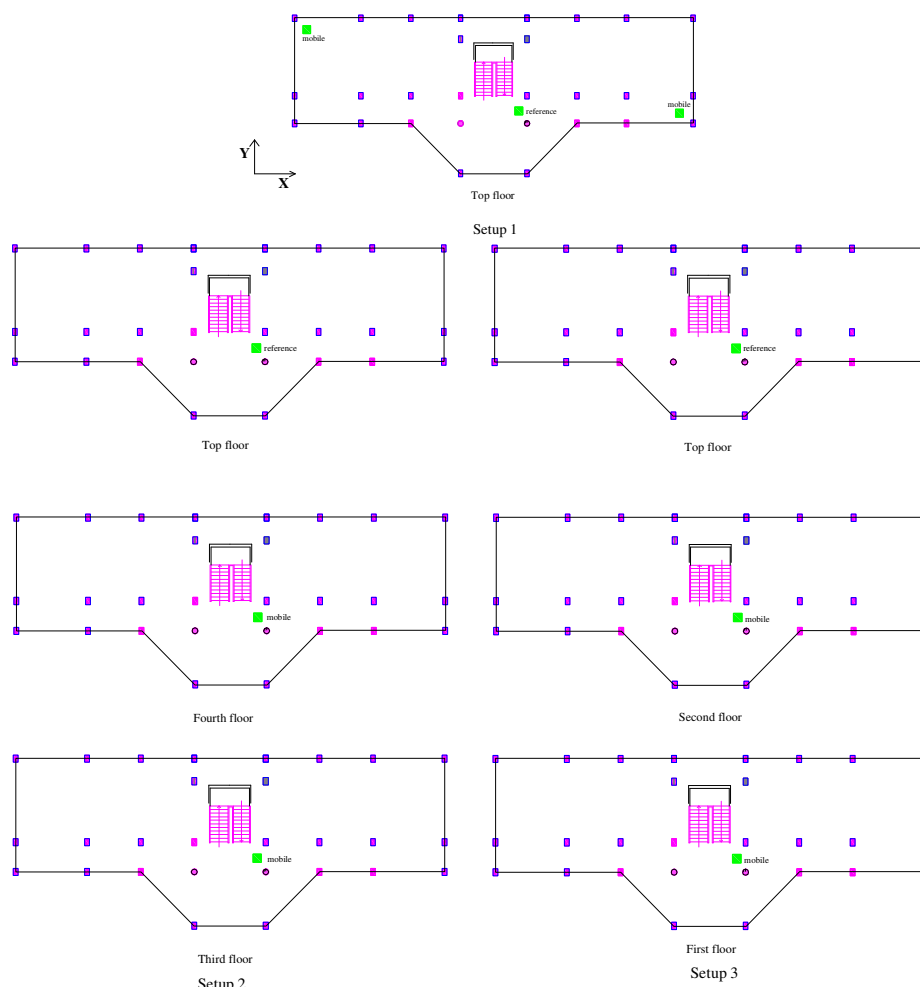
Figure 3.24 – Ambient vibration tests setup for the WD1 building - schematic layout (not scaled)

3.6.2.1.2   Test results

Figure 3.25 presents the normalized singular values of the spectral density matrices and vibration mode obtained through the EFDD method to estimate the building responses. The agreed first three fundamental frequencies and corresponding vibration modes for the WD1 building are presented in Table 3.11. It shows that the first two vibration modes were translational and third one was diagonal. While analysing data, it was identified that the seismographs stationed on the fourth and first floors had problems and were highly deviated, such that these data were not synchronized. Therefore, the reliability of the third frequency was uncertain.

(a)

(b)
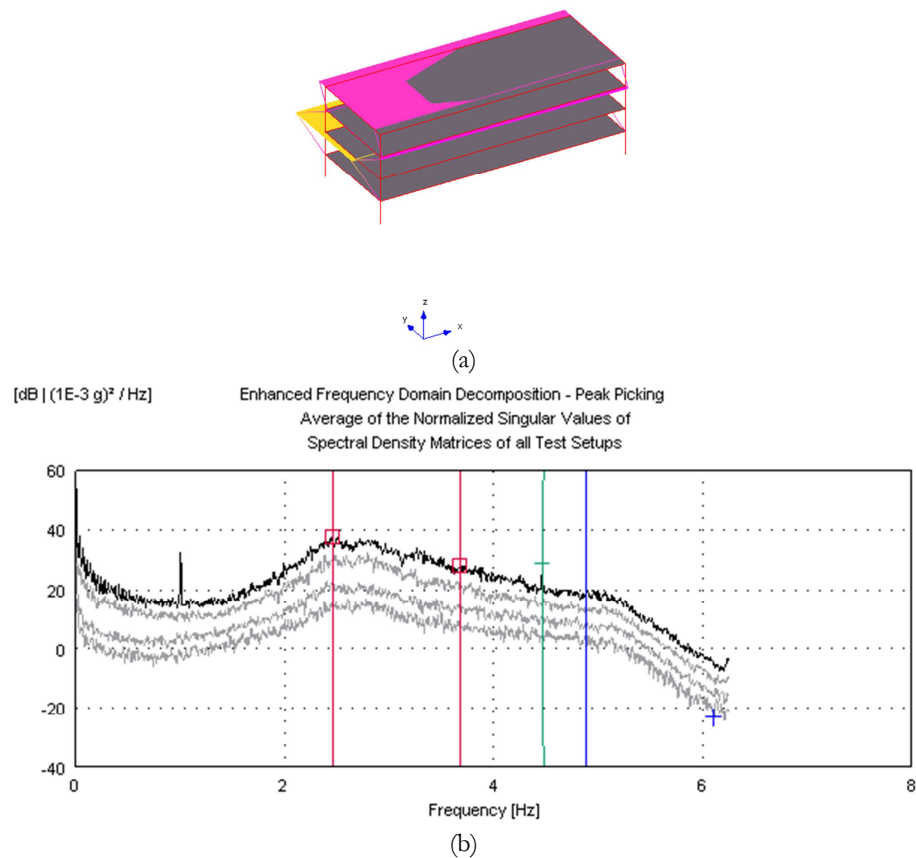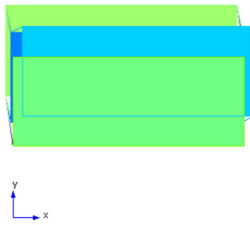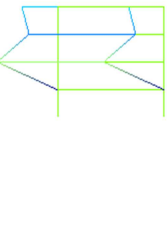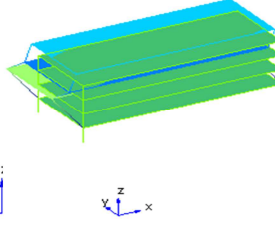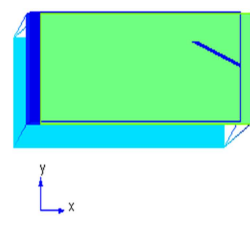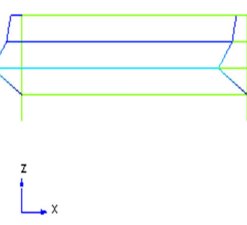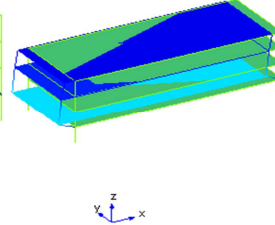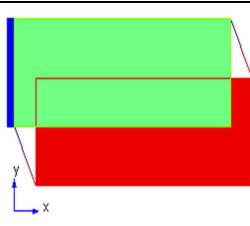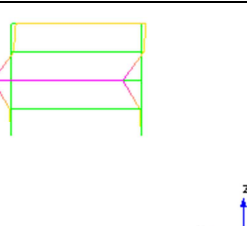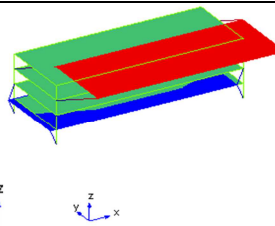
Figure 3.25 – Ambient vibration tests results for the WD1 building; (a) Vibration mode and (b) Average of the normalized singular value of spectral density matrices of all test setups

Table 3.11 – Ambient vibration test frequencies and respective mode of vibrations for the WD1 building

Vibration mode	Fundamental frequency (Hz)	Plan view	Lateral view	3-D view
First mode	2.45			
Second mode	3.68			
Third mode	4.48			

3.7 Khwopa College of Engineering Block 'E' (WD2)

3.7.1 General introduction

The Khwopa College of Engineering Block 'E' is located next to the WD1 building within the same compound. It has six storeys including a basement, as shown in Figure 3.26, and was constructed in late 2000. The building is utilized for both academic and administrative purposes, and it is being used by approximately 400 students and staff during weekdays. The college is affiliated with Tribhuvan University and is undertaken by the Bhaktapur Municipality. The building was designed and detailed similarly to that of the WD1 building; thus design codes and other parameters are not discussed in this section. The building was classified as a well-designed building and named as WD2. The site survey revealed that the building did not suffer any structural and non-structural damage; thus it was sub-categorized as non-damaged.

During inspections, the building was found to be utilized for multiple purposes. The basement is being utilized for laboratories and the ground floor for store, account, and classes. Similarly, the first and second floors are mostly used for classes, and the third and fourth floors are mainly utilized for offices and departments. The periphery of the basement has RC shear wall of floor height, whereas remaining floors possess URM infill walls: the same external and internal infill walls of 230 mm thickness. All the external infill walls have wide openings, and the external façade consists of brick cladding on all sides (see Figure 3.26 (a)). The cladding contribution was neglected in the analysis and is only used for dead load calculation. To the surprise of the team, the building possesses an irregular distribution of infill panels, where the ground floor at the entrance is without infill walls. In addition, a large difference in strength capacity between the basement and ground floors can be expected, as the former is provided with shear wall and the latter with URM infill panels. This phenomenon could contribute to a soft-storey mechanism at the ground floor. However, the present study neglected the basement effect, such that further analyses were carried out for superstructure only, i.e. the ground floor. The stair is landed on the beam at the mid-height of the column, which could initiate a short-column effect in the building. The authorized architectural drawing shows the lift details and its position, but in reality it does not exist. Therefore, the design of the lift and its influence or impact on the global performance of the building was not considered in this study.

(a)   (b)
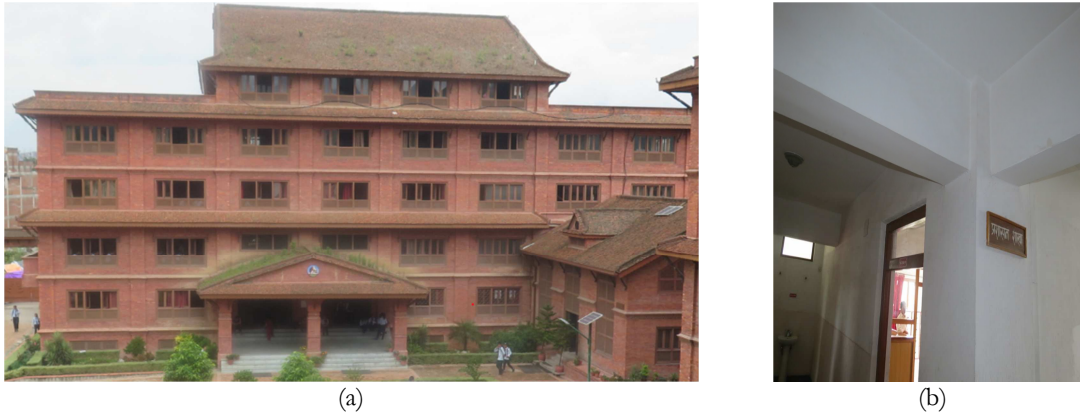
Figure 3.26 – WD2 building; (a) East elevation and (b) Beam-column connection and openings in infill panels

The building is rectangular in plan, with three bays in the E–W direction having a maximum bay length of 7 m and eight bays in the N–S direction with a maximum bay length of 4.8 m, as shown in Figure 3.27 (a) and (b). Similarly, the total span along the E–W direction is 21 m and 37.175 m along the N–S direction; thus the building plinth area is approximately 655 m². The building possesses uniform inter-storey height of 3 m throughout, so that the total height of the building is 21.5 m including the slanting roof.

The building possesses different column sections: rectangular column sections (400 x 400) mm² and (450 x 600) mm² and a circular column section Φ 600 mm. Typical column sections are shown in Figure 3.27 (d). Similarly, it possesses two types of beams that depend on orientation; beams directing along the N–S direction have a (300 x 500) mm² section and along the E–W direction have a section of (300 x 600) mm² including uniform slab thickness of 150 mm. The structural details for the beams and columns demonstrated that longitudinal reinforcement varies, although it has the same sections. Figure 3.27 (c) presents the longitudinal reinforcement distribution in the beams. The present study considered an average reinforcement area for numerical and calculation simplicities. The column section (450 x 600) mm² is reinforced with longitudinal reinforcement of (18 Φ 25) + (6 Φ 20) and column section (400 x 400) mm² reinforced with 8 Φ 16, and Φ 600 column reinforced with 20 Φ 20. It is characterized by two-legged lateral ties of Φ 8 mm uniformly spaced at 100 mm centre up at the bottom and the top one-fourth (i.e. h/4) of the beam and column height at each storey and remaining length spaced at 150 mm centre. At the overlapping portions of the beams and the columns, the stirrups were spaced at 100 mm centre up to the height of development length, where development length for tension and compression were 50 and 40 times the diameter of the main bars. The effective covers

for the column, beam, and the slab elements were 40 mm, 25 mm, and 15 mm, respectively.

The Schmidt hammer test could not be performed for this building as well; thus the concrete compressive strength for the column, beam, and the slab was assumed to be 20 MPa, as specified in the authorized architectural drawings. Similarly, the yield strength of the reinforcement bar should be at least 415 MPa conforming to IS: 1786-1985 [52]. Hooks in lateral ties and stirrups were bent at 135^0 and hook length was more than 10 times the stirrup diameter.

(a)

(b)

(c)

(d)
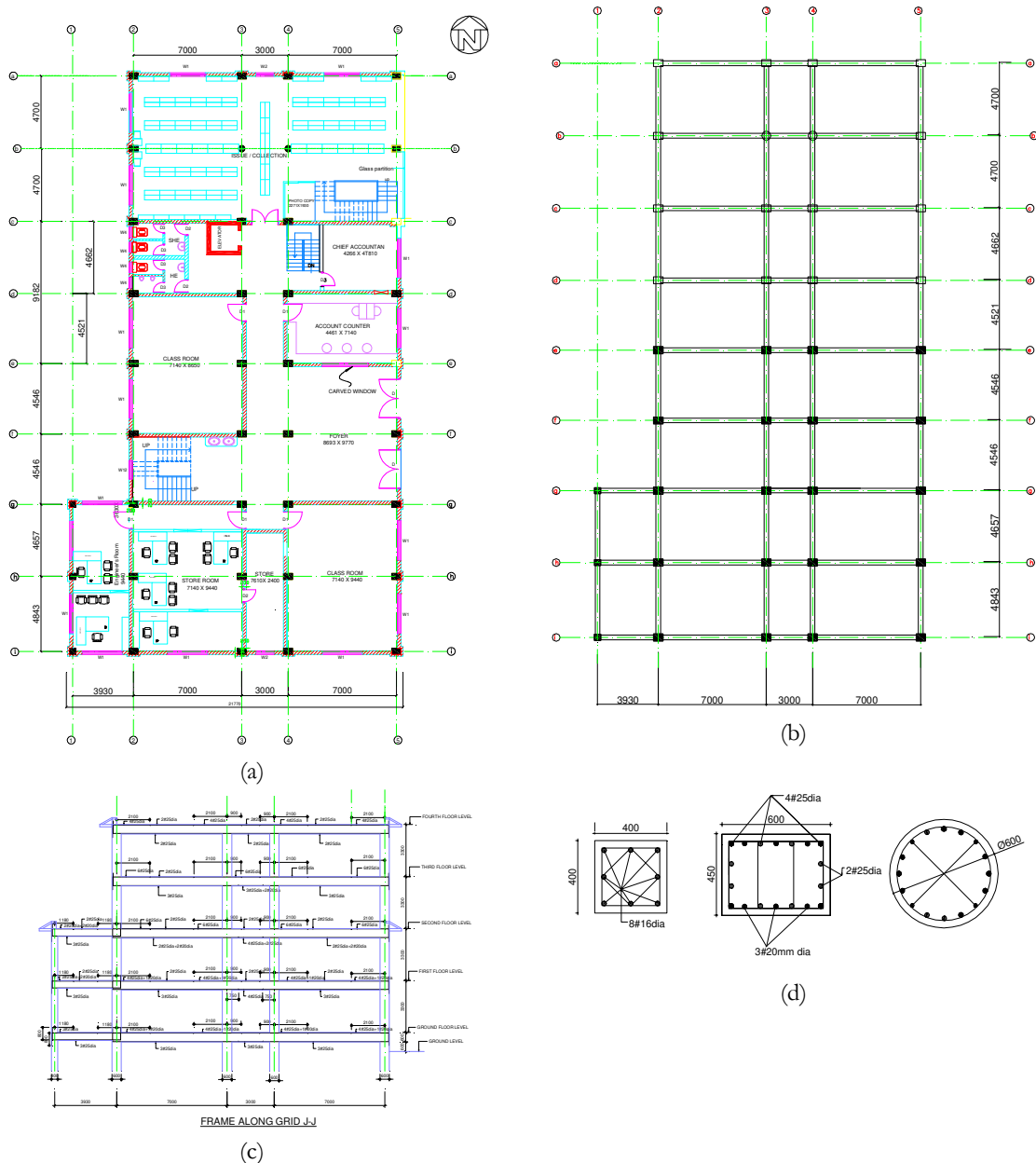
Figure 3.27 – Details and structural layout of the Khwopa College of Engineering Block 'E'; (a) Typical floor layout, (b) Representative beam and column layout, (c) Reinforcement detailing in beam and (d) Representative detailing in column and its section (all dimensions are in mm)

3.7.2 Field tests

3.7.2.1 Ambient vibration test

3.7.2.1.1 Test setups

Figure 3.28 presents the ambient vibration tests layout for the WD2 building, such that the test was performed in three test set-ups.
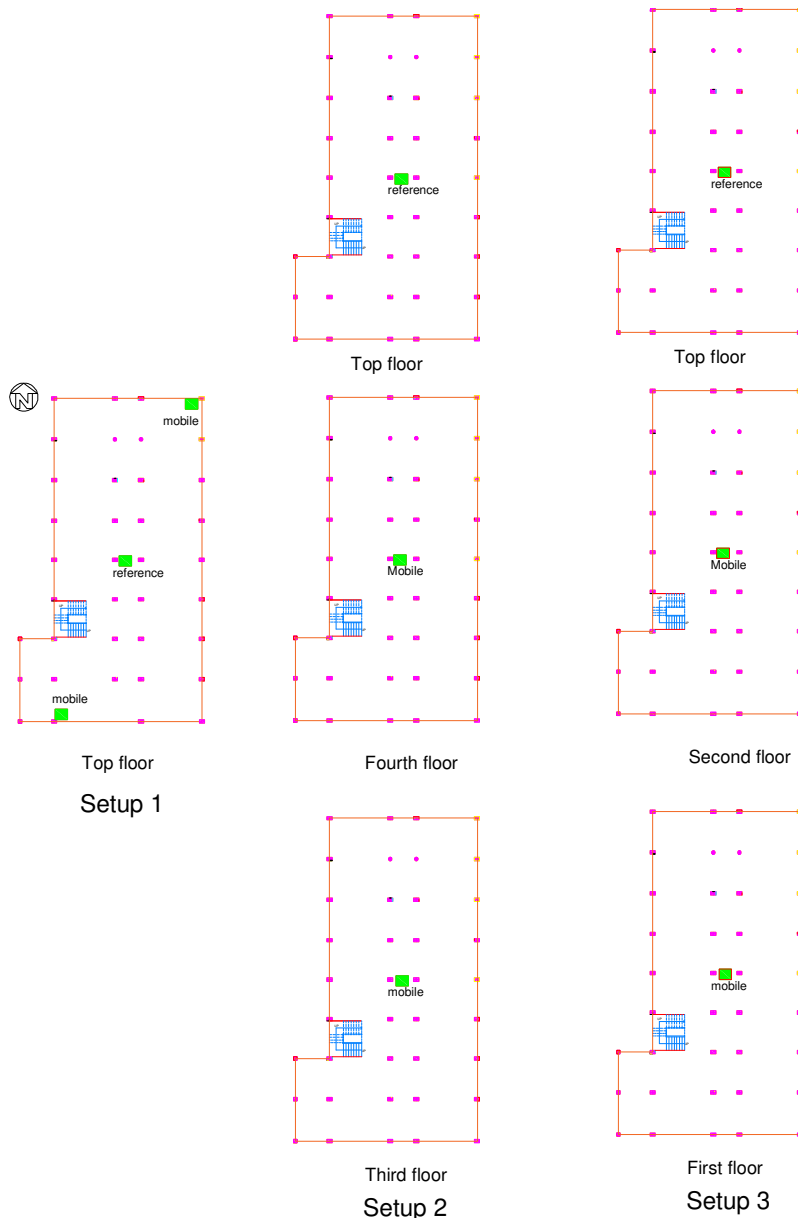
Figure 3.28 – Ambient vibration tests setup and seismographs position for the WD2 building - schematic layout

3.7.2.1.2   Test results

The modal analysis was performed using the EFDD method, where singular and normalized spectral density matrices for all set-ups were generated (shown in Figure 3.29). Interestingly, the first vibration was second order mode and second vibration as first order mode (along Y axis) and third one as third order mode (along X axis). The fundamental frequencies and corresponding vibration modes for the WD2 building are presented in Table 3.12.

(a)

(b)
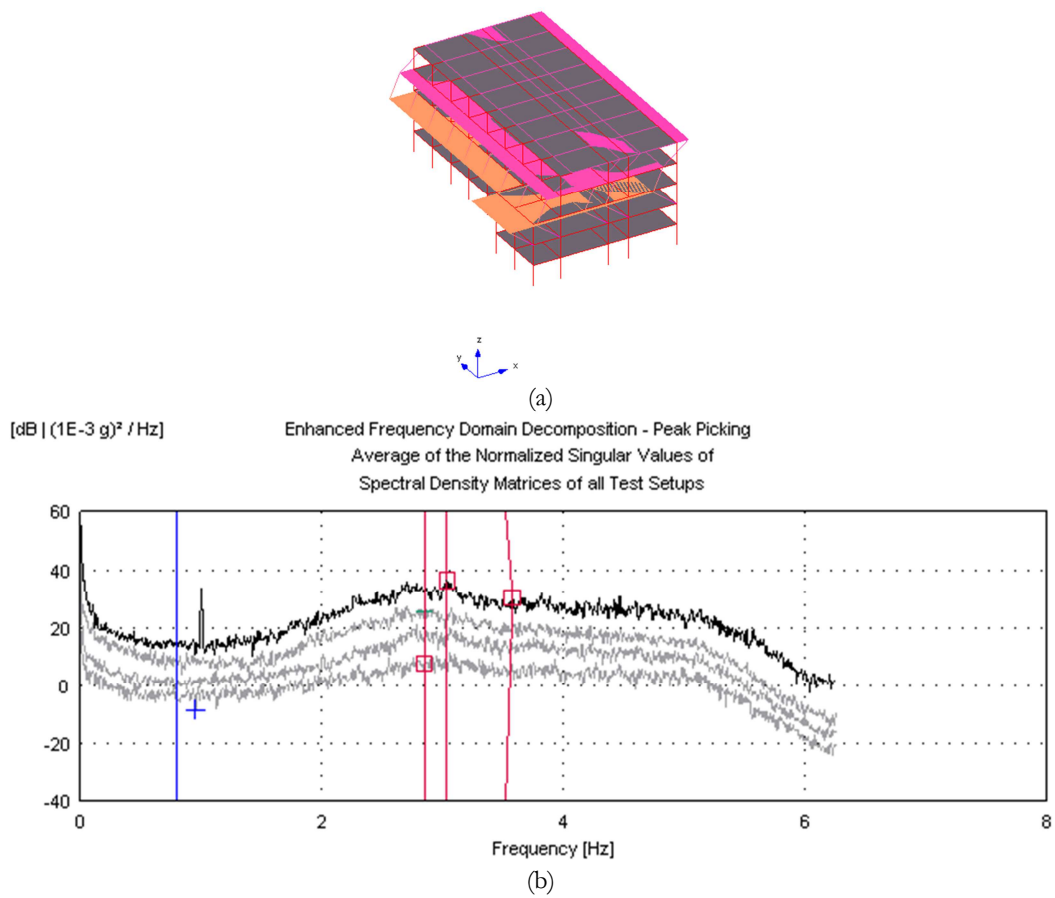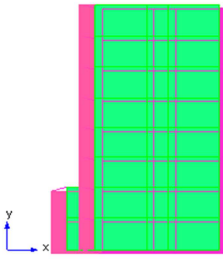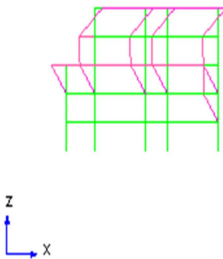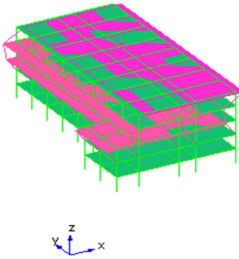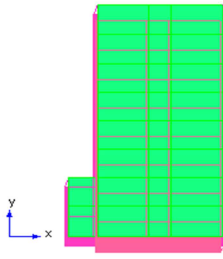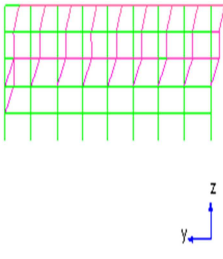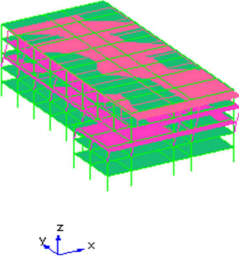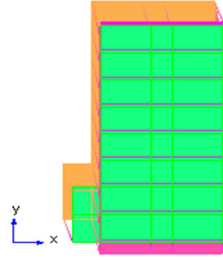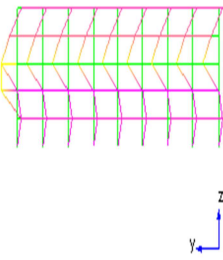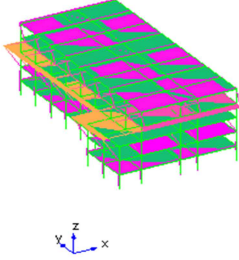
Figure 3.29 – Ambient vibration tests results for the WD2 building; (a) Vibration mode, and (b) Singular value of spectral density matrices of all test setups

Table 3.12 – Ambient vibration frequency and respective mode of vibration for the WD2 building

Vibration mode	Fundamental frequency (Hz)	Plan view	Lateral view	3-D view
First mode	2.86			
Second mode	3.04			
Third mode	4.11			

3.8 General Loading and Material Properties for Case Study Buildings

3.8.1   Material properties

The material properties constitute the prominent factor that greatly influences the performance of the building, and it varies largely for a small variation in the material contents. The standard material properties for the infill walls, steel and concrete are as shown in Table 3.13, as given by NBC 201:1994 [53]. These standard values were employed in the numerical model and, in some cases, the properties were readjusted after parametric analysis for all case-studied buildings. The design guideline NBC 201:1994 [53] also discusses the variation in the modulus of elasticity of masonry infill with respect to the cement-sand mortar ratio; thus 1:6 and 1:4 ratios are to be adopted for one-brick and half-brick walls, respectively.

Table 3.13 – Standard material properties for all case study buildings [53]

Material	Material properties	Characteristics
Steel	Yield strength, f_y	415 Mpa
	Young's modulus, E_s	200 Gpa
	Poisson' ratio, μ_s	0.3
	Unit weight	78.5 kN/m³
Concrete	Compressive strength, f_c	-
	Young's modulus, E_c	$5000\sqrt{fck}$ Mpa
	Poisson' ratio, μ_c	0.2
	Unit weight	24 kN/m³
Masonry Infill Panel	For 1:6 cement-sand mortar	
	Modulus of elasticity of brick masonry, E_m	2400 N/mm²
	Modulus of elasticity of plaster, E_{mp}	1000 N/mm²
	For 1:4 cement-sand mortar	
	E_b	3000 N/mm²
	E_p	1500 N/mm²
	Poisson' ratio, μ_b	0.15
	Unit weight	18.85 kN/m³

3.8.2   General loading consideration

All the types of load that are applied on the structure must be considered for the safety assessment of the building structures. The assessment also needs to account carefully in order to design a building that can exhibit a proper behaviour for all the actions from the load during its service life. The types of loads also depend on the geographical location, types of structures, and occupancy of the building. Generally, the present study considered only two types of loads acting on the structures: dead and live loads.

3.8.2.1   Dead loads

Dead loads are static loads that act constant over time. Some of the material properties adopted were attained from IS: 875 (Part I) -1987 [54] due to lack of experimental works and the validation and similarity of materials between Nepal and India.

3.8.2.2   Live loads

Live loads are moving loads over a short duration of time. They include loads due to occupancy of the building, the weight of movable partitions, traffic vehicle loads, distributed and concentrated loads, impact loads, snow loads, seismic loads, and other loads due to temperature changes, creep, shrinkage, differential settlement, etc. In seismic design, the live loads should be the greatest loads that will be produced by intended use or

occupancy, but should not be less than equivalent minimum loads, as specified in Table 3.14 and Table 3.15 [55].

Table 3.14 – Live loads on floor of different occupancies [55]

S. No.	Occupancy Classification	Uniformly distributed load (UDL) kN/m²
	i) Residential Buildings	
	All rooms and kitchens	2
	Toilet and bathrooms	2
	Corridors, passages, staircases including tire escapes and store rooms	3
	Balconies	3
1	*ii) Educational Buildings*	
	Class rooms and lecture rooms (not used for assembly purposes)	3
	Office, lounges and staff rooms	2.5
	Kitchens	3
	Toilet and bathrooms	2
	Store rooms	5
	Corridors, passages, lobbies, stair-cases, including fire escapes - as per the floor serviced	4
	Balconies	Same as rooms to which they give access but with a minimum of 4.0
	Floor finishes	1

Table 3.15 – Live loads on various types of roof [55]

S. No.	Types of Roof	Uniformly distributed load (UDL) kN/m²
	i) Flat, sloping or curved roof with slopes up to and including 10 degrees	
	a) Access provided	1.5
	b) Access not provided except for maintenance	0.75
1	*ii) Sloping roof with slope greater than 10 degree*	For roof membrane sheets or purlins-0.75 kN/m² less 0.02 kN/m²for every degree over 10 degrees increase in slope
	iii) Weathering course on roof	2.25

The IS 1893 (Part1): 2002 [30] stresses the need to consider only a percentage of the live loads for earthquake load calculation. Therefore, the present study estimated earthquake load as the sum of full dead load plus a percentage of live loads. The contribution of live loads considered for seismic weight calculation depends on the live loads acting on the floor area; for instance, 25% of live loads was considered if UDL is limited up to 3 kN/m² and 50% in case UDL is above 3 kN/m² [30].

3.9   Final Comments

This section provides detailed descriptions of the site survey carried out in the area after the main shock and a series of aftershocks for the 2015 Gorkha earthquake in order to investigate the performance of existing buildings built based on various design conditions: non-engineered, pre-engineered and well designed. To meet the objective, two buildings

representing each design approach were selected, including damaged and non-damaged types. All selected buildings were initially visually inspected to acquire information on the state of structural and non-structural damage and the structural configuration. Besides case-studied buildings, visual inspections were also performed for other buildings, and it was observed that most of the failure or damage in the building was related to the irregular distribution of infill walls, which leads to building collapse under the soft-storey mechanism. Most of the case study buildings were plastered and in some cases the owner hesitated to let the team to carry out such measurements. Therefore, several constraints exist and measure cross-sections for structural elements and reinforcement details might not match the real scenario, thus its cross-sections were adjusted through parametric study that will be discussed in detail in Chapter 5.

Later, these buildings were experimentally investigated through two types of test: the Schmidt hammer test and the ambient vibration test. The former is used for obtaining the existing concrete strength and the latter for obtaining dynamic properties of the buildings. The Schmidt hammer test results were averaged and calibrated with a correction factor as defined in Table 3.2, which was later rounded to the nearest value to represent the practicable strength. The ambient tests were performed for all selected buildings using seismographs containing three triaxial accelerometers. The ambient test was performed with one seismograph stationed as fixed at the top floor and the remaining seismographs shifted to the consecutive lower floors. The acquisition time for each test set-up was set as 15 minutes. The natural frequencies were selected through peak picking frequencies and compared with corresponding vibration modes through a trial-and-error method. The states of the selected buildings, calibrating existing characteristic strengths of concrete and natural frequencies, are presented in Table 3.16.

Table 3.16 – Comparative study for case study buildings

Bldg. name	No. of storey	Damage states		Compressive strength of concrete (MPa)			Exp. fundamental frequencies (Hz)		
		Damaged	Non-damaged	Beam	Column	Slab	f_1	f_2	f_3
CCP1	3		√	20	15	15	4.89	5.28	5.34
CCP2	4	√		10	15	10	2.74	3.47	4.29
MRT1	3		√	20	20	15	1.40	1.57	1.67
MRT2	5	√		15	20	15	2.60	3.90	4.34
WD1	5		√	20	20	20	2.45	3.68	4.48
WD2	5		√	20	20	20	2.86	3.04	4.11

Chapter 4.

Literature Review

4.1 General Overview

The reinforced concrete (RC) infilled with unreinforced masonry (URM) walls is one of the most common construction practices, mostly in seismically active region around the globe. Although the URM is likely to prior brittle failure, such type of construction is still intense in these countries, most likely due to easy availability of the construction material and economic status. Generally, the URM walls are constructed as a non-structural element and are not intended to resist the seismic loads. However, it considerably enhances the global stiffness and strength capacity elastically in moderate to severe earthquakes but decreases the deformation capacity of the infilled building structures. When strong lateral loads act on the infilled RC frames, infill walls tend to interact with the surrounding frames, thus contributing the load resistance but not usually accounted in the design methods. The past experimental and numerical researches demonstrated that the specimen with stronger infill walls exhibit higher loads and higher energy-dissipation capability, but their peak strength reduces more promptly with increasing displacement. For the large magnitude earthquakes and in some cases, small magnitude earthquakes with longer recorded duration results infill walls to experience the in-plane and out-of-plane damages beforehand RC frames. Therefore, the seismic loads in the last stages are to be resisted by frame alone, potentially collapse of building under soft-storey mechanism.

The present chapter is mainly divided into four main sections. The first section discusses the literature reviews on the masonry infills (both experimental and analytical), failure modes, infill properties and strengthening techniques. The second section deals with the modelling strategies for the beam/column elements and masonry infill walls. The third section discusses the nonlinear static and dynamic time history analyses in which various loading approaches are discussed. In addition, the selection of ground motion records and different threshold limit states for damage state identification is presented. And, the last section describes briefly the parameter to be considered for the development of fragility

curve. The detailed procedures stated above are presented in the flowchart, as illustrated in Figure 4.1.
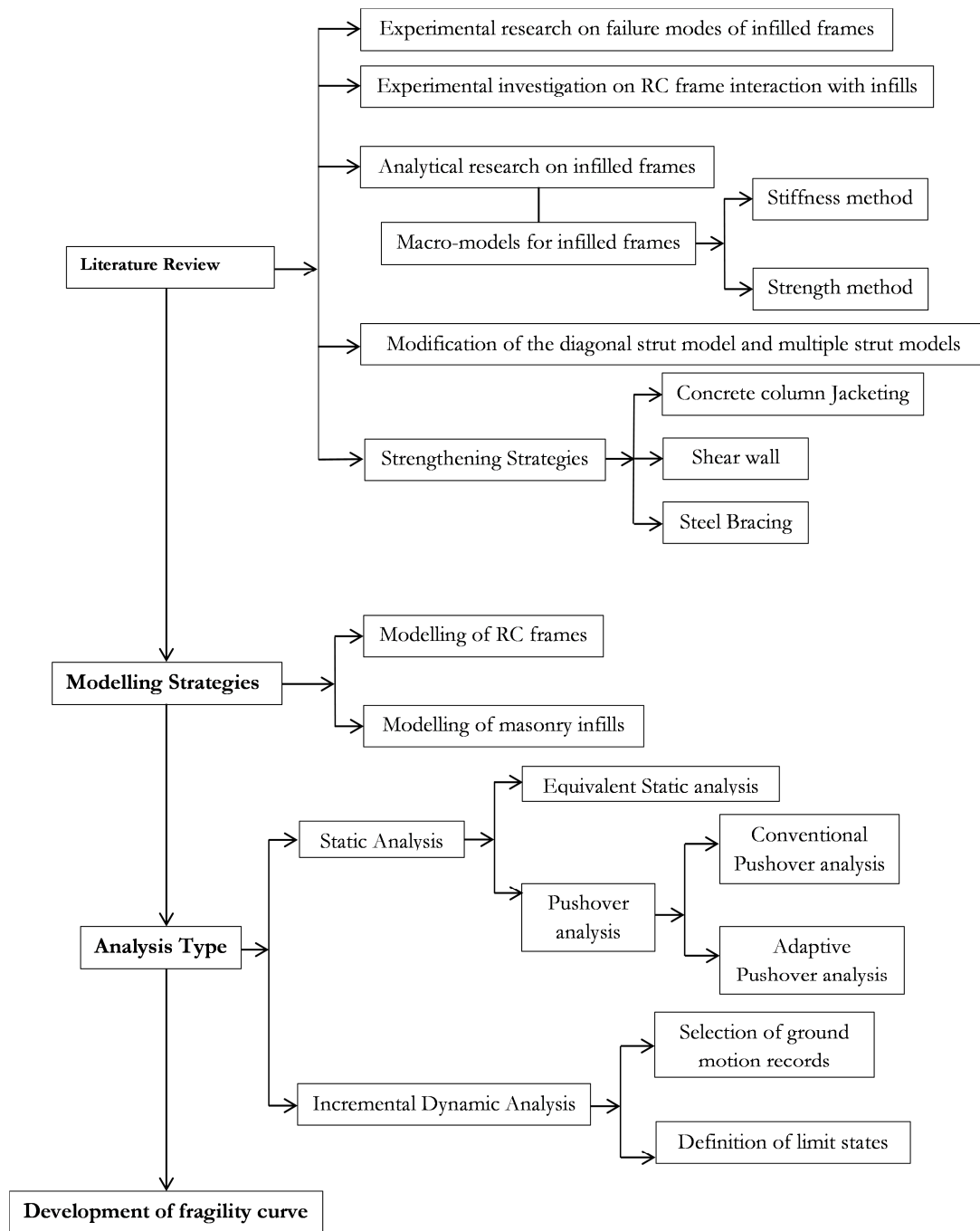
Figure 4.1 – Flowchart showing the various steps discussed in the chapter

4.2 Literature Review

4.2.1 Experimental research on failure modes of infilled frames

Although intensive experimental researches have been performed over the last six decades, a conclusive and reliable design approach has not been accepted yet. This is attributed to the large uncertainties associated with the URM and its interaction with the surrounding RC frames.

Based on the analytical and experimental studies during last six decades, El-Dakhakhni, *et al.,* (2003) [56] summarizes the in-plane failure modes of the masonry infilled frame into five distinct modes, discussed below and shown in Figure 4.2 as well.

- Corner crushing (CC) mode usually occurs in a weak infill wall "surrounded by a frame with weak joints and a strong frame". This type of failure "mode represents the crushing of infill panel in at least one of its loaded corners".

- Sliding shear (SS) mode is associated with weak mortar joints in the masonry infill panel. It can be observed by the "horizontal sliding shear failure through bed joints of a masonry infill". This type of failure mode is mainly associated with comparative "weak mortar joints in the infill" panel.

- Diagonal compression (DC) "mode is associated with a relatively slender infill, where failure results from an out-of-plane buckling instability of the infill". This type of failure mode represents the "crushing of the infill within its central region".

- Diagonal cracking (DK) failure mode is similar to CC mode, however, strong frame "members infilled with rather strong infill". Such failure mode form cracks "connecting two loaded corners".

- "Frame failure (FF) mode is seen in the form of plastic hinges in the columns or the beam-column connection". Such type of failure mode can be observed in a "weak frame or a frame with weak joints and strong members infilled with a rather stronger infill".

CC mode   SS mode   DC mode   DK mode   FF mode
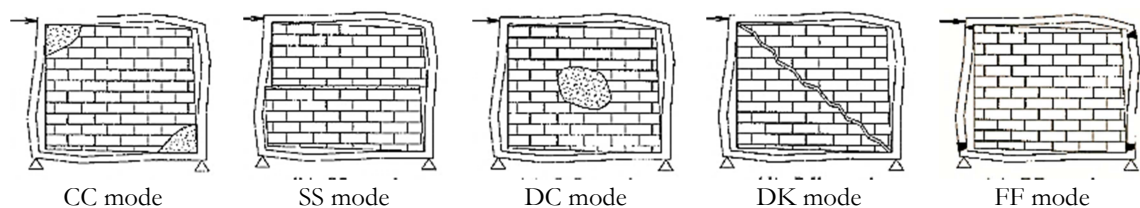
Figure 4.2 – Various in-plane failure modes of URM infilled frame as classified by El-Dakhakhni, 2003 [56]

Similarly, Mehrabi, *et al.* (1996) [7] discussed the five failure mechanisms depending upon the "relative stiffness and strength" between the frame and the infill panel. These are flexure, mid-height horizontal cracking, "diagonal crack, horizontal slip and corner crushing". In addition, Stavridis, A. (2009) [57] categorised the in-plane failure mode of the infilled frame according to three main failure mechanisms, such as horizontal sliding, diagonal cracking and panel crushing, as shown in Figure 4.3.
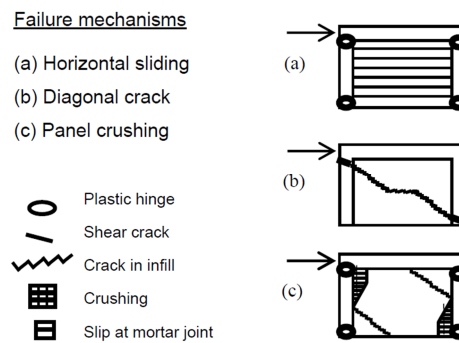
Figure 4.3 – Failure mechanisms of the infilled frame as defined by Mehrabi, 1996 [7]

However, infilled frame with opening changes infill behaviour, and as a result, it changes the failure modes different that discussed above. This type of failure mode is investigated by Asteris, *et al.* (2011) [58] through an experimental test on the partially infilled frame. Depending upon the shape, location and size of the opening, different failure mechanisms were detected. The test results concluded that the presence of opening eliminates the "well-known failure modes of Diagonal Compression (DC) and Diagonal Cracking (DK)". This reveals that the infill panel does not function as a diagonal strut or bracing. Similarly, the shear sliding failure above and below the window was also observed irrespective of the size of the opening. Furthermore, it is observed that for infill with door opening; "toe crushing due to rocking of masonry segment, internal crushing of the masonry segment" between door and column and shear sliding failure above the door [58].

4.2.2 Experimental investigation on RC frame interaction with infills

Experimental investigation is a reliable tool to understand the interaction of the RC frame with infill walls under seismic loading. Several researchers investigated and are exploring its interaction in order to improve the modelling, analysis and design approaches. Some of the earliest and important experimental investigations are discussed in brief as follows.

Thomas, F. (1953) [59] performed "a number of tests on brick walls and piers" that include the test on full scale one storey infilled frame and one-bay. The test was conducted on the steel frame with and without masonry walls, and the test result shows that there is greater influence of the infill panels on the frame-wall interaction.

Polyakov, S. (1960) [60] conducted tests on masonry infilled steel frames. The test specimen includes one-storey one-bay and three-storey three-bay subjected to a horizontal in-plane load. The researcher made an effort for analytical modelling of the infilled frames considering each panel as equivalent to the diagonal bracing. The important task of this research was the innovative consideration of the infill walls as a bracing system on the frame for analytical modelling approach that functions as compression strut. This behaviour of compressive strut as equivalent truss mechanism is represented in Figure 4.4. This approach became one of the most important preliminary approaches for the macro modelling of infill wall.
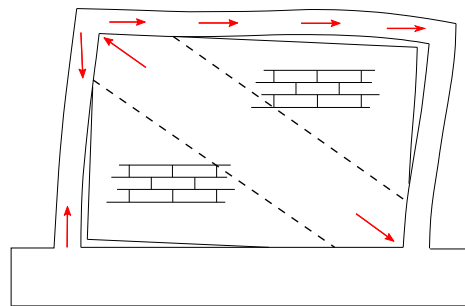
Figure 4.4 – Equivalent truss mechanism for infilled frames [60]

Sachanski, S. (1960) [61] carried out the full-scale test on the masonry infilled frame subjected to a series of monotonic static loads. He utilized the experimental data to develop theoretical tool for better understanding of the influence of infill walls on the RC frames. The test result shows that the "formation of cracks along the compression diagonal" predicted through an analytical model to "idealize the frame-wall contact forces as discrete redundant loads".

Holmes, M. (1961, 1963) [62, 63] performed small-scale and full-size tests to investigate the increase in both stiffness and strength of the steel frame when steel frame and infill walls acts compositely. In this method, equivalent diagonal strut acts as a diagonal brace to represent the wall, and the test result shows that the equivalent frame fails after exceeding the compressive strength of the strut. The method assumes that the deformations in the brace frame system as a result of elastic analysis. The test result concludes that the strength

of the frame with RC walls increases by 400%; whereas, it increases by 100% with brick masonry infills. The researcher also pointed out that the strength could reduce up to 40% in case of opening in infill walls based on the composite behaviour [62, 63]. The main limitation of the work was the consideration of steel frame only.

Smith, S. (1962) [64] performed tests on three steel frames with infill walls. The stiffness of the composite section was interpreted based on the equivalent strut concept. The effective width of the equivalent strut was estimated depending on the relative frame-wall stiffness. The composite system was replaced by a linkage of two pin-jointed diagonals, as shown in Figure 4.5, which helps in determining the stiffness of the system. In other words, it can be said his work was an extension of the equivalent strut model proposed by Polyakov (1960) [60] and compute the width of the equivalent strut to measure the stiffness of the system [64].

(a) Double arching effect   (b) Proposed equivalent model
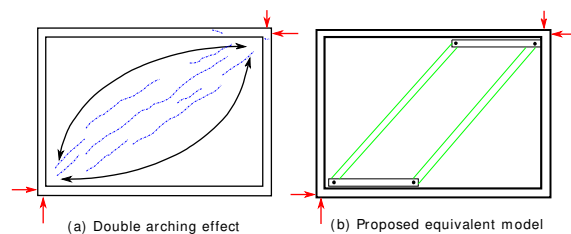
Figure 4.5 – Double arching effect and proposed equivalent model [60]

Fiorato, *et al.* (1970) [65] for the first time performed test on infilled RC frame considering the opening on the masonry infill walls. The test consists of total 26 structural models and 1 additional bare frame. The specimens were scaled at 1:8 and grouped in eight one-storey one-bay, thirteen five-storey one-bay, and six two-storey three-bay. The specimens have variation in number of storeys and bays, and amount, quality and reinforcement arrangement. Similarly, variation in vertical load, size, shape and location of openings were also assumed. The test results concluded that a considerable increase in the stiffness and strength capacity, but decrease ductility is attained with the addition of infill walls. Similarly, the test results also revealed that the shear cracks along a single joint was detected, thus separating the wall into two parts. This phenomenon concludes that the shear cracks appear depending upon the quality of the mortar in the masonry walls and the proportion of the walls. It also concluded that the opening reduces the strength, but not in the proportion to the reduction in cross-sectional area of the wall [65]. Besides infill walls immense contributions on the RC frame, there exist some limitations that includes different conditions of the mortar joints than those in real masonry walls and also does not

reinforced with transverse reinforcements, thus it does not represents the real infilled frame structures.

Mainstone, *et al.* (1972) [66] performed a full-scale test using solid brick infill panel infilled in the concrete-encased steel frames and the specimens were subjected to a cyclic load. The test results concluded that when a significant part of the infilled frame reaches its ultimate strength capacity, the frame changes the mode of deformation and as a result direct sharing of the load by the infill walls was reduced on average by the same amount as increase in the flexure strength of the frame. They proposed an empirical equation to determine the effective width of the strut [66].

Bertero, *et al.* (1983) [67] performed experiment tests to study the effects of hollow masonry panel and light weight concrete panels infilled on the RC moment resisting frame building. For this, a total of 18 test sets were considered, modelled on 1/3-scale with variation in infill layout and excitation through a series of quasi-static cyclic and monotonic loadings. The test results showed that adding infill panel significantly changes the dynamic characteristic of the building thus should be considered in the design. In addition, the building stiffness increases significantly when all the frames were infilled; such that the increase varies from 366% to 944%. This concludes that a larger variation in the stiffness and fundamental period of the structures was obtained but depends on the number of frames infilled [67].

Zarnic, *et al.* (1988) [68] experimentally tested 28 specimens and grouped into four. The Group 1 includes 1 bare frame and 3 infilled frame with clay-brick masonry in 1:2 reduced scale, Group 2 contains 1 bare frame and 8 infilled frame with concrete block masonry walls in 1:3 reduced scale, Group 3 has 6 infilled frame with concrete blocks masonry infill (includes 2 specimens having window and 2 specimens having door openings), and Group 4 includes repaired and strengthened specimen of Group 2. The repair was performed with two methods; first using epoxy-grouting of filler wall and other by the combination of epoxy-grouting and application of reinforced cement coating on both faces of the infill walls. The test results concluded that by means of epoxy-grouting of the infill walls, both lateral stiffness and load-bearing capacity of the strengthened structure can be improved moderately. Furthermore, by means of epoxy-grouting and reinforced-concrete coating of the infill walls, both the lateral stiffness and load carrying capacities can be enhanced significantly but decline extremely after attaining their maximum value [68].

In the year 1989, Dawe, *et al.* [69] carried out the experiment tests on nine large-scale concrete masonry infilled panels to investigate the out-of-plane behaviour of the infilled panel. The test results concluded that before the first major crack, the lateral load resistance of the infilled frame was governed by flexure action, and arching effect becomes dominant in the post cracking range. Similarly, it also pointed out to the need for flexible frame deformation to reflect the real behaviour of a system. The exponential increase in maximum load carrying capacity was detected for the increase in panel thickness and decreases with the increase in the panel length and the height. Furthermore, it also pointed out that relatively small central opening does not reduce the arching strength significantly [69].

Mehrabi, *et al.* (1996) [7] performed experimental tests on twelve 1/2–scale, single-storey and single-bay including two bare frames under in-plane lateral loads. For this, two frames designed based on the ACI 318-89 were selected, which includes one "weak" frame (weak columns and strong beams) and other "strong" frame (strong columns and weak beams). It also considered the solid and hollow concrete masonry panels representing strong and weak infills, respectively. The tests concluded that the addition of infill panels significantly enhances the performance of RC frames. And better performance obtained for strong frames with strong panels compared to weak frames and weak panels, in terms of strength and energy dissipation capability. Later, the test specimens were repaired and performance was again evaluated. The test results are widely used at the present for analytical researches, potentially due to availability of large comprehensive data, including data required for developing refined finite element models [7].

Crisafulli, F. (1997) [11] considered four different stages to investigate the infill walls interactions with the RC frame. This test results reveals that initially "the structure behaves as monolithic cantilever wall until separation occurs"; and later the behaviour was characterised "by composite interaction between the infill wall and the frames" although the materials remain un-cracked and followed by significant cracking of the infill walls "until maximum lateral resistance is achieved"; and finally the strength capacity decreases and "the response is mainly controlled by the frame".

Lee, *et al.* (2001) [70] carried out experiment tests in order to "investigate the effect of the masonry infills on the seismic performance of low-rise reinforced concrete frames with non-seismic detailing". For this, an infilled RC frame with two-bay three-storey modelled in 1:5-scale was selected and acted by a series of lateral forces. The test results revealed that

the infilled frames are most likely to have shear failure in masonry walls instigated by the bed-joint sliding. In addition, the increase in strength capacity was many folds greater than those induced by the inertial forces, such that the deformation capacity of the structure remains almost similar, thus it can be beneficial [70].

The two full-scale models of a four-storey with three-bay RC frame without seismic design (common practice of 40-50 years ago) was experimentally tested by Pinto, *et al.* (2002) [71]. The specimens tested under pseudo-dynamic test (PSD) where the masonry infill frames were retrofitted using shotcrete. The test results demonstrated that the bare frame building was highly vulnerable corresponding to collapse at the 3rd storey, whereas infilled frame improves the behaviour completely, but increases the storey mechanism and shear failure of the external columns. In addition, the rehabilitation of the existing infill panels using shotcrete improves the seismic performance of the walls, but cause the premature failure of the external columns by shear mechanism, which ultimately leads the premature loss of the structures. Furthermore, shotcrete was only beneficial if appropriate doweling was provided to the adjacent beams/girders.

Ghobarah, A. (2004) [72] performed five full-scale masonry block wall tests considering different opening configurations in the walls and were subjected to lateral load up to the failure. Later, these walls were again tested after strengthening with carbon fibre-reinforced polymer laminate strips. The test results concluded that the strengthened walls significantly increases the lateral load capacity by many folds and also enhances the ductility compared to unstrengthen walls [72].

Benefit on the seismic performance of infilled RC frame by using slight reinforcement was experimentally investigated by Calvi, *et al.* (2004) [73]. The experimental test was performed on a concrete frame with single-bay, single-storey, a single geometry, and a single design and a single type of masonry unit. The test results concluded that the addition of little reinforcement largely improves the response of infilled frames. In addition, the infill panel prevents damage level in a particular infilled building for a PGA between 0.15-0.30, severe damage for 0.2-0.4 PGA. However, with addition of <1% reinforcement in the mortar layer, the building undergoes occupational limit state between 0.25-0.60g and damage limit state for 0.35-0.70g. Furthermore, the steel applied as external weld mesh on both sides of the walls also increases the occurrence of damages in the building to higher PGA [73].

Karayannis, *et al.* (2005) [74] performed experimental investigation and verified analytically. For this, three specimens of single-storey, single-bay at a 1/3-scale were considered, such that two specimens were bare frame and another one infilled frame. The dominant failure mode was found to be the diagonal cracking in the infill panels. The analytical verification was carried out by modelling the infill using equivalent strut model, whose characteristics depends on the experiment results [74].

In 2008, Arulselvan and Subramanian [75] carried out experiment on the 3D RC frame infilled with URM infill and scaled at 1/5. The specimen includes two frames with three bays and central bay was provided with brick infill in the direction of loading, and another two numbers without infill in transverse direction with slab. The test specimens were constructed in such a way that plastic hinges in beam can be visualised before the failure of the columns. From the test, it was found hinge formation is developed at the beam-column interface ultimately failure by joint shear. Similarly, the first crack appears in the interface between the beam and the infill walls as a result of low shear capacity at the interface. After the diagonal cracks on the infills, it was found to be inactive [75].

Kakaletsis and Karayannis (2009) [76] experimentally investigated the influence on the seismic performance of the infilled RC frames as a result of eccentric distribution of openings on the infill walls. The specimen includes "eight 1/3-scale, single-storey, single-bay frame" and tested under cyclic pseudo dynamic horizontal loading until the drift level reaches to 40%. All the test results found that the shear strength of the columns was much higher than the cracking shear strength of the solid infill. Based on the results, it was concluded that the masonry infills walls with eccentric openings were beneficial to the bare frame in terms of strength, ductility, and energy dissipation. It also concluded that an improvement on the seismic performance of the infilled frame was observed no matter opening located near the edge of the infill [76].

Pujol and Fick (2010) [77] experimentally tested three storeys masonry infilled RC frame in a full-scale, consisting of two bays in loading direction and one-bay on other side. A bare frame specimen was originally tested to failure, which was later rehabilited by adding solid clay brick infill walls. The test results revealed that the slab-column connection fail under punching shear when specimen was without infill walls, and the repaired specimen showed increase in stiffness, strength, and drift capacity to large extent and only small cracks in the infill panel appears at 1.5% drift, such that out-of-plane failure of the infill was prevented [77].

Stavridis, *et al.* (2012) [78] performed a shake table test on three-storey two-bay RC frame with solid unreinforced masonry walls scaled to 2/3. The specimen was a non-ductile RC frame with opening in the infill walls and tested under the cyclic loads. The test results concluded that infilled RC frames with wall openings were more likely to collapse than frame with solid walls. In addition, if sufficient infill walls were considered, it behaves as a safest during strong ground motions, but the study was limited to the in-plane behaviour only [78].

Zovkic, *et al.* (2013) [79] tested ten masonry infilled RC frame with one-bay and one-storey designed according with the EC8, built in 1:2.5 scale and the specimen tested under the cyclic load. The test was performed for various types of masonry infill, such that no additional shear connection was provided between masonry and concrete blocks. The test result shows that the structure behaves as monolithic until a drift of 0.1% and reaches to its maximum capacity at 0.3% drift and maintained around 0.75% drift, and after which the structures behaviour depends on the frame only. The test results concluded that the frame demonstrates minor damage at 1% drift and it reaches up to 2% without any loss of capacity. It also pointed out the need in the "improvement of the infill provisions in the codes" considering the contributions of a masonry walls in reducing expected damage by lowering the drift levels [79].

Preti, *et al.* (2014) [80] proposed a new design approach for masonry infill walls that is capable of reducing the vulnerability under seismic actions. The specimen possesses sliding joint at the infill-frame interface and also at certain height interval. The experimental test was performed on two large-scale specimens and sub-assemblies subjected to both in- and out-of-plane loading. The sliding joint at the interface reduces the infill-frame interaction, such that reduces the stiffness and strength capacity, but increases the ductility and energy dissipation capacity of the structure. With this intervention, the test results concluded that the infill wall was capable of 2.5% in-plane drift with negligible damage without strength degradation, whereas some damage appears for the infill with openings after 1.5% drift. Remarkably, in both cases the specimens was capable to undergo 3% drift without collapse. Furthermore, this techniques reduces the stiffness by 3-10 times and strength by almost 2 times relatively compared to the specimen without sliding joint. The shear connectors were dispensed at the masonry-column interfaces to resist the out-of-plane failure mechanisms [80].

The seismic performance of deficient detailed RC frames, which was infilled with "low-shear strength masonry infills with openings" was experimentally investigated by Mansouri, *et al.* (2014) [81]. The test specimen was "six half-scale single-storey single-bay frame" tested under in-plane lateral loading. The test result indicates that the openings in the infill changes the modes of failure of the infills and increases the level of damages. It also increases the stiffness and strength capacity thus reducing the ductility capability of the infilled frames. It was also found that door opening reduces "29% in strength, 34% in the effective stiffness and 23% in the energy dissipation capacity". Similarly, the window opening leads to "average reductions of 23% in strength, 8% in effective stiffness and 11% in the energy dissipation capacity". Similarly, they proposed empirical equation for estimating the overall reductions in stiffness and strength of the infilled frames due to openings taking the effect of size, shape and location of opening [81].

The openings effect on the in-plane masonry panel in the infilled RC frame structure was experimentally studied by Sigmund and Penava (2014) [82]. The specimen was built in 1:2.5-scale, door and openings were centrically and eccentrically located. The test result illustrates that "openings did not influence the initial stiffness and strength at low drift levels". The role of openings becomes significant at higher drift that corresponds to lower energy dissipation capacity of the structure. The infill wall illustrates multiple failure mechanism depending on the opening height and its position. The positive infill contribution was attained by enhancing the overall performance of the structure [82].

Hak, S. (2014) [83] tested "full-scale, single-storey, single-bay RC frame" infilled with "strong masonry infills" to investigate the out-of-plane behaviour of the infill panel. The specimen undergoes cyclic static to observe in- and out-of-plane test on the bare frame, fully infilled, and the partially infilled RC frames. The test results concluded that if the masonry infill was strong and adherent to the RC frame then the out-of-plane stability does not present a critical issue. Based on test results, they proposed a relation for out-of-plane stiffness and strength as a function to previous in-plane drift illustrated in Figure 4.6 [83].
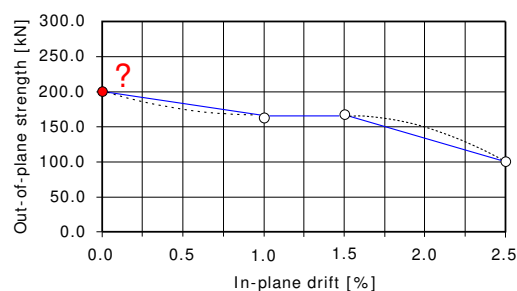
Figure 4.6 – Out-of-plane strength reduction in function of in-plane drift [83]

Gavilan, *et al.* (2015) conducted experimental study on the confined masonry walls with varying aspect ratio. They performed experiment on seven full-scale confined masonry walls with "height-to-length" aspect ratio (H/L) varied from 0.3 up to 2.2. The test result demonstrates that the failure of the walls with H/L<1 was due to combination of diagonal tension and sliding failure mechanisms. Similarly, wall deformation at failure increased with aspect ratio. The paper proposed a new expression for inclined cracking shear for wide range of aspect ratio.

Basha, *et al.* (2016) [84] performed experiment on "eleven half-scale, single-story masonry infilled RC frame". The test was performed in two stages; the initial stage includes eight specimens RC members with different reinforcement detailing infilled masonry of different brick sizes, and second stage with three specimens designed with improved form, as per IS 13920:1993 [51]. The columns failed in shear were mostly noticed although the infilled were relatively weak. The first stage test results revealed that the infilled frame greatly enhances the performance of the building, such that increase in stiffness by almost "7-10 times", increase in strength by "1.6-2.5 times", and increase in energy dissipation by almost "1-2.3 times" compared with the corresponding bare frame. Similarly, in the second stage, special confining reinforcement was ascertained to enhance the lateral load behaviour of the infilled frames, especially in enhancing post-peak load behaviour, energy dissipation and ultimate deformation capacity. Furthermore, the test results also illustrated that the initiation of shear cracks was delayed and the amount of shear cracks was also limited in the later specimens, but shear failure could not be prevented [84].

The out-of-plane behaviour of the infill masonry walls was also investigated by Furtado, *et al.* (2016) [85] through full-scale tests, which comprises the out-of-plane tests with and without previous in-plane damages in the masonry walls. The test results concluded that infill walls without previous in-plane damage illustrate maximum strength and increases by almost four times and also out-of-plane drift attained was higher. A significant reduction in the initial stiffness was detected for test specimen with previous in-plane damage [85].

Shan, *et al.* (2016) [86] examined experimentally to "simulate the failure of the structural component due to abnormal loads or design flaws". The specimen "two 1/3-scaled, four-bay, two-story RC frame" with and without infill walls was considered. The specimen is without central column in the first story and tested under the quasi-static loads under displacement control to study the collapse mechanisms of the infilled RC frame. The researchers observed that the infill walls can alters the load transfer that was originally

supported by beam only, thus improves the seismic capacity of the frame. As concluded by other researchers, the test results also revealed that the reduced deformation capacity with the addition of infill panels, and also changes the modes of failure of the infill panel and RC frame. It was also concluded that the progressive collapse of RC frames was significantly enhanced with the addition of infill walls [86].

The seismic behaviour of the masonry infilled RC frames with and without openings were experimentally investigated by Zhai, *et al.* (2016) [87]. The test specimen consists of "four full-scale, single-story and single-bay specimens tested under constant vertical loads and quasi-static cyclic lateral loads". They found that the column of infilled RC frame are mostly likely to crack for smaller drift compared to the bare frame, and the failure due to the formation of plastic hinges at the bottom of the columns was relatively low due to weak masonry. The tests result also concluded that the infilled RC frame dissipate more energy and equivalent viscous damping ratio than the bare frame. The opening in the walls increases the ductility ratio of the structure and was attributed to the uniform distribution and slow propagation of cracks due to the "force transformation of the lintel beam" [87].

The in-plane behaviour of the masonry infilled RC frame with interfacial gaps was investigated by Steeves, R. (2017) [88]. A total of five specimens were tested to failure using displacement controlled quasi-static loading, of which four were given a pre-defined interfacial gap between the infill and the RC frame, and one was a bare frame. Of the four gapped specimens, two also had window openings in the infill. "The four infilled frame specimens had the following interfacial gap scenarios: 1) a gap at the top beam-infill interface of 12 and 25 mm, respectively; 2) a gap at the column-infill interfaces of 12 mm (6 mm gap on each side); and 3) a full separation gap of 12 mm at the beam-infill and 12 mm at column-infill interfaces (6 mm gap on each side). Of the infilled specimens, two specimens also had a window opening accounting for 16% of the infill area". The test results illustrated that a significant increase in stiffness and strength was observed for the frame with gaps and infill openings compared to the bare frame but depends on its location and magnitude. The infilled frame dissipates higher energy compared to the bare frame, and infilled frame with gaps and no openings dissipates higher energy compared to specimens with gaps and window openings [88].

Pradhan, *et al.* (2017) [89] performed experimental tests to investigate the effect of adding infill walls partially on the RC frames under lateral loading. The test specimen consists of a single-storey single-bay RC frame scaled at 1/3. The test results concluded that the failure

modes of the RC frame and partially infilled RC frames under lateral loads were distinct and different. It also concluded that the failure of the bare frame and partially infilled frames occurs at joints; whereas, the columns in partially infilled frame fail at the locations where the infill walls discontinues acting as a cantilever wall due to short-column mechanism [89].

From all the above experimental investigations, it can be concluded that infill wall exhibits both positive and negative effects in the structure. All the researchers concluded that the stiffness and strength of the bare frame was significantly enhanced with the addition of masonry infill panels, i.e. strong infill panels or weak infill panels nevertheless the deformation capability reduces significantly. Similarly, the addition of infill in bare frame and introduction of openings in the infill walls alters the modes of failure of the masonry and frame structures, increases the damage level, and energy dissipation capacity of the structure. Furthermore, these tests also revealed that the behaviour of the masonry infilled frame was so fluctuating that it depends upon various aspects, such as infill wall configuration and used material, size and location of opening, aspect ratio and gap in the interface between frame-infill and so on. Hence, it is very difficult to generalize from the limited experimental data. Based on these facts, it becomes necessary for design code and design engineers to look up and understand the role of infill walls in the building structure.

Although the real buildings are multi-storey, most of the experimental researches were carried out considering a single panel only. This could create a doubt on the accuracy of the analytical results while utilizing it for numerical modelling due to large uncertainties associated with masonry infill walls. Few researches have been carried out on the multi-storey, such as Holmes, M. (1961) and Smith, B. (1962), but such tests were performed on steel structures infilled with concrete panels. Fiorato, *et al.* (1970), Arulselvan, S. (2008), Pujol, S. (2010) and Stavridis, A. (2012) investigated on multi-storey infilled RC frame, but researchers concluded that the methods proposed to analyse one story infilled frame were valid for multi-storey structures. This may be due to the fact that damage concentrates mainly at the first-storey, where the columns and masonry panels were mostly affected. Besides these, it is obligatory to investigate its effect on the upper storeys as well. Although some of the conclusions were similar, still concrete, reliable and trustworthy approaches have not been proposed until date, which raised many questions regarding the scope of the researches and their findings.

4.2.3 Research on analytical approaches for infilled frames' behaviour

4.2.3.1 General considerations

The main objective of the present section was to review different development of analytical approaches in order to capture the structural behaviour of infilled frame. The masonry walls demonstrate different directional properties with mortar joints that act as the weakest zone in the masonry panel. The three different modelling strategies that were used for modelling of infill panels based on the accuracy and simplicity, as proposed by Lourenço, P. (2002) [90] are discussed and shown in Figure 4.7.

- "detailed micro-modelling-units and mortar in the joints are represented by continuum elements whereas the unit-mortar interface is represented by discontinuum elements;

- simplified micro-modelling-expanded units are represented by continuum elements whereas the behaviour of the mortar joints and unit-mortar interface is lumped in discontinuum elements;

- macro-modelling-units, mortar and unit-mortar interface are smeared out in a homogenous continuum."
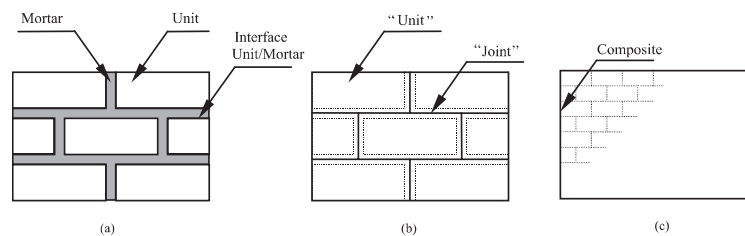
Figure 4.7 – Modelling strategies for masonry structures: (a) Detailed micro-modelling, (b) Simplified micro-modelling and (c) Macro-modelling (Lourenço, 2002) [90]

Hossameldeen, *et al.* (2017) [12] defined the detail micro-modelling approach in which "the brick and mortar joints are modelled as continuum elements and the interaction between these elements is represented by interface or contact elements", as illustrated in Figure 4.7 (a). "The behaviour of both continuum elements and interface elements are defined by nonlinear stress-strain relations". In this approach, Young's modulus, Poisson's ratio and inelastic material of both unit and mortar are considered. This method can achieve higher accuracy in representing potential crack and/or slip, expected failure patterns, and structural response as well. The micro-modelling approach requires large computational time, effort and input data. Thus in-spite of being most accurate technique, the modelling

is only limited and "feasible for small specimens, such as one-bay one-storey specimens" [90].

"In a simplified micro-modelling approach, bricks are modelled by continuum elements, but each joint consisting of mortar and two unit-mortar interfaces with bricks, which are "modelled together as a single interface element", as shown in Figure 4.7 (b). This approach assumes masonry as a set of elastic blocks bounded by potential failure/slip lines at joints. The cracking sometimes also occurs vertically between the bricks, possibly due to the dilatation effect of the mortar joints" [90]. In order to capture this mechanism, "a vertical interface can also be added between bricks" [12]. The Poisson's effect of the mortar is not considered in this approach, thus the accuracy is lost, but several researchers use this model due to the balance between accuracy and simplicity [90].

"When using macro-modelling approach, the behaviour of brick, mortar and two unit-mortar interfaces is modelled as one continuum" surface or element or modelled as single or multiple equivalent diagonal struts, assuming all materials behave as homogenous anisotropic continuum, as presented in Figure 4.7 (c). In this approach, few elements are enough to represents the effect of the whole masonry infill panels. This modelling approach is easy and requires low computational cost, time and effort. Therefore, despite less accurate, this approach is widely used for preliminary studies at the present researches [90].

In conclusion, all the modelling approaches have their own significance and the choices of modelling strategies depending on the need of the accuracy, available computational time and operation cost. Hence, it will not be justifiable to state one modelling approach preferred over the other because different application field exists for each modelling strategies. The micro-modelling approach is necessary for better understanding about the local behaviour of masonry structures and this type of modelling approach is applicable for structural details. Whereas, macro-models are applicable to large dimension structures so that the stress across macro length is necessarily uniform. Similarly, macro-modelling is extensively used and practice-oriented method, as it reduces modelling and analysis time, as well as capable to generate user-friendly meshes to represent the global infill panels. This type of modelling is essential when compromise between accuracy and efficiency is negotiable.

The present research does not intend to carry out any micro-modelling approach; therefore, only macro-modelling analytical literature reviews are discussed in the chronological order as follows.

4.2.3.2 *Macro-models for infilled frames based on strut models*

As discussed in the previous section, the macro-model approach is the most practicable approach to study the behaviour of the infilled frame structures due to simplicity and less computational cost. The concept on macro-model analytical tool as equivalent strut replacing the infill panel was studied since 1956 to date. A large number of researches have been performed to determine the properties of the diagonal struts, such as width, stiffness, strength, constitutive behaviour, and the number of struts that represents the actual behaviour. The property of the diagonal strut varies according to the type of analysis performed, i.e. linear elastic or nonlinear and loading procedure, i.e. either monotonic or pseudo-dynamic or dynamic loading. Hossameldeen, *et al.* (2017) [12] discussed the analytical methodologies defining the in-plane properties of strut models into two main approaches: i.e. stiffness and strength methods. Both of these methods represent the infill panel by equivalent strut but use different approaches to define the necessary properties of the strut. The stiffness method is based on the geometrical properties of the infill for estimating the properties of the diagonal strut in order to define the capacity of the infill. Similarly, the strength method defines the properties of the strut by quantifying the lateral forces carried by the infill walls. In this section, the literature review of both methods will be discussed in the chronological order.
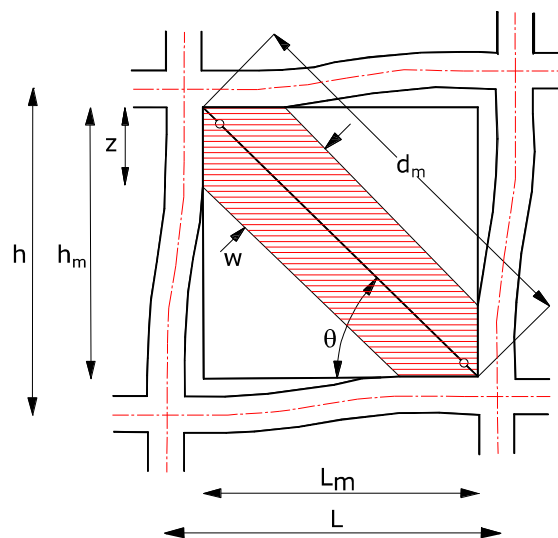
Figure 4.8 - Geometrical properties of the equivalent diagonal strut and its relevant properties (Crisafulli, 1997) [11]

4.2.3.2.1   *Stiffness method*

Polykov, S. (1956) [60] was one the first researchers who assume innovative study about the possibility of representing analytically the infill panel as an equivalent diagonal bracing. The analytical study was based on the elastic theory. Later, he concluded that the masonry panels in the frames subjected to lateral loads can be represented by an equivalent diagonal strut [60]. Later, Holmes, M. (1961) [62] adopted his idea and proposed a single diagonal strut model that works under compression only. He replaced the infill panel by single diagonal strut that has material and thickness similar to the infill panel, but the width (w) of the diagonal strut is equal to one third of the diagonal length of the panel [62], according to equation (4.1).

$$w = \frac{1}{3} d_m \tag{4.1}$$

where: d_m is the diagonal length of the masonry panel as shown in Figure 4.8. This rule was also called the one-third rule. Equation (4.1) was proposed as the first analytical approach to evaluate the equivalent strut width in the lack of experimental data [62].

Smith, S. (1962) [64] refined the approach and started a numbers of tests to examine and evaluate the best and more precise expression for the computation of the width of the equivalent diagonal strut. He reported that the ratio w/d_m varied from 0.1 to 0.25 that depends on the relative value of the length and height of the panel [64].

$$0.1 < \frac{w}{d_m} < 0.25 \tag{4.2}$$

The contact length, z between the infill panel and the frame is given by Smith, S. (1968) [91] as follows equation (4.3).

$$z = \frac{\Pi}{2\lambda_h} h \tag{4.3}$$

where: h is the height of the column between centrelines of the beams and λ_h is a dimension less parameter, which expresses as the relative stiffness of the infill panel to the frame is given by equation (4.4):

$$\lambda_h = h \sqrt[4]{\frac{E_m t \, Sin2\theta}{4E_c I_c h_m}} \tag{4.4}$$

$$\theta = \tan^{-1}\left(\frac{h_m}{L_m}\right) \tag{4.5}$$

where: t, h_m, and L_m are the thickness, height, and length of the masonry panel, respectively, and θ is the inclination of the diagonal (in degree) panel. E_m and E_c are the modulus of elasticity of the masonry and concrete, respectively, and I_c is the moment of inertia of the columns. Typically the value of λ_h varies from 3 to 10. The smaller value illustrates that the frame is much stiffer than the infill panel. The parameter λ_h was initially proposed for steel frames in which I_c can be uniquely defined. However, for the RC frames the value of I_c significantly decreased after cracking develops in the column.

Mainstone, R. (1971, 1974) [92, 93] performed series of experimental tests using two different infilled materials (concrete and masonry) surrounded by steel frame. He investigated all the variables that are likely to influence in the contribution of the infill panels to the strength of the multi-storey framed buildings. He proposed two expressions for the evaluation of w in-case of brick and concrete panels, obtained from equations (4.6) to (4.9) [92, 93].

$$w = 0.175 d_m \lambda_h^{-0.4} \qquad \text{Brick} \tag{4.6}$$

$$w = 0.115 d_m \lambda_h^{-0.4} \qquad \text{Concrete} \tag{4.7}$$

$$w = 0.16 d_m \lambda_h^{-0.3} \qquad \text{Brick} \tag{4.8}$$

$$w = 0.11 d_m \lambda_h^{-0.3} \qquad \text{Concrete} \tag{4.9}$$

The values of relative stiffness, λ_h in the equations (4.6) and (4.7) are in the range of 4-5 and the value in equations (4.8) and (4.9) is greater than 5.

Bazan and Meli (1980) [94] predicted the width of the equivalent strut given by equation (4.10).

$$w = (0.35 + 0.022\beta)h_m \tag{4.10}$$

where: β is the dimensionless parameter and define as:

$$\beta = \frac{E_c.A_c}{G_m.A_m} \tag{4.11}$$

where: A_c is the gross area of column, A_m is the area of the masonry panel in the horizontal plane, and G_m is the panel shear modulus. The value of β has some limitations as shown below:

$$0.9 \leq \beta \leq 11 \text{ and } 0.75 \leq L_m/h_m \leq 2.5$$

where: L_m and h_m are the width and height of the infill panel, respectively.

Hendry, A. (1981) (as reported by [95]) evaluated the relative stiffness, λ_b and λ_c, and corresponding contact lengths, Z_b and Z_c, separately for the beam and the column stiffness (units are in inches and ksi) is given as:

$$Z_b = \frac{\Pi}{2\lambda_b} \tag{4.11(a)}$$

$$Z_c = \frac{\Pi}{2\lambda_c} \tag{4.11(b)}$$

$$\lambda_b = \sqrt[4]{\frac{E_m t \, Sin2\theta}{4E_c I_b h_m}} \tag{4.11 (c)}$$

$$\lambda_c = \sqrt[4]{\frac{E_m t \, Sin2\theta}{4E_c I_c h_m}} \tag{4.11(d)}$$

where: I_b and I_c are the moment of inertia of the beam and column, respectively.

The effective width of the diagonal strut is calculated using the equations (4.12) and is given as:

$$w = \frac{1}{2}\sqrt{Z_b^2 + Z_c^2} \tag{4.12}$$

Tassios, T. (1984) [96] modified the relation proposed by Bazan and Meli (1980) [94] to predict the width of the equivalent strut for the case of cracking across the diagonal of the infill panel by the following expression:

$$w \cong 0.2d_m sin\theta \sqrt{\frac{E_c A_c}{G_m A_m}} \quad \text{if } 1 < \frac{E_c A_c}{G_m A_m} < 5 \tag{4.13}$$

Te-Chang, *et al.* (1984) [97] proposed semi-empirical equation to compute the width of the equivalent diagonal strut for θ in the range of 25^0 and 50^0 by the following expression:

$$w = \frac{0.95 h_m cos\theta}{\sqrt{\lambda_h}} \tag{4.14}$$

The ratio h_m/L_m assumed in equation (4.14) varies from 1.0 to 1.5.

For cracked and uncracked infill walls, Decanini, *et al.* (1987) [98] proposed two sets of expressions to evaluate the width of diagonal strut (equations (4.15) and (4.16)).

$$\text{Uncracked panel: } w = \begin{cases} \left(0.085 + \frac{0.748}{\lambda_h}\right) d_m & \text{if } \lambda_h \leq 7.85 \\ \left(0.130 + \frac{0.393}{\lambda_h}\right) d_m & \text{if } \lambda_h > 7.85 \end{cases} \tag{4.15}$$

$$\text{For Cracked panel: } w = \begin{cases} \left(0.010 + \frac{0.707}{\lambda_h}\right) d_m & \text{if } \lambda_h \leq 7.85 \\ \left(0.040 + \frac{0.470}{\lambda_h}\right) d_m & \text{if } \lambda_h > 7.85 \end{cases} \tag{4.16}$$

Moghaddam, *et al.* (1988) [99] proposed a simple relation between the length of the diagonal equivalent strut and its width given by equation (4.17).

$$w = \frac{1}{6}d_m \tag{4.17}$$

Paulay, *et al.* (1992) [100] suggested an equation for the estimation of equivalent width of the diagonal strut for seismic design purposes using the following expression:

$$w = \frac{1}{4}d_m \tag{4.18}$$

To illustrate the variation of the w/d_m for the infilled frame as a function of the parameter λ_h is presented in Figure 4.9 plotted according to the relation defined in the equations (4.1), (4.6), (4.14), (4.15), (4.16), (4.17) and (4.18). An equation (4.14) was represented in the Figure 4.9 assuming the inclination angle θ equals to 25^0 and 50^0, which represents the practicability limit values. Formulas for constant values for the w/d_m ratio are not always adequate, but they often used for their simplicity. The ratio w/d_m proposed by Holmes, M. (1961) [62], Moghaddam, *et al.* (1988) [99] and Paulay, *et al.* (1992) [100] was independent of λ_h. The constant values of w/d_m for above proposed values were 1/3, 1/6 and 1/4, respectively. The ratio w/d_m proposed by Mainstone, R. (1971) [92], Te-Chang, *et al.* (1984) [97] and Decanini, *et al.* (1987) [98] is inversely proportional to λ_h as the contact length is smaller, when the stiffness of the masonry panel is higher than that of the frame. The main advantage of Decanini, *et al.* (1987) [98] relation was that the reduction of the equivalent strut width for a cracked section of the masonry considered in the equation.
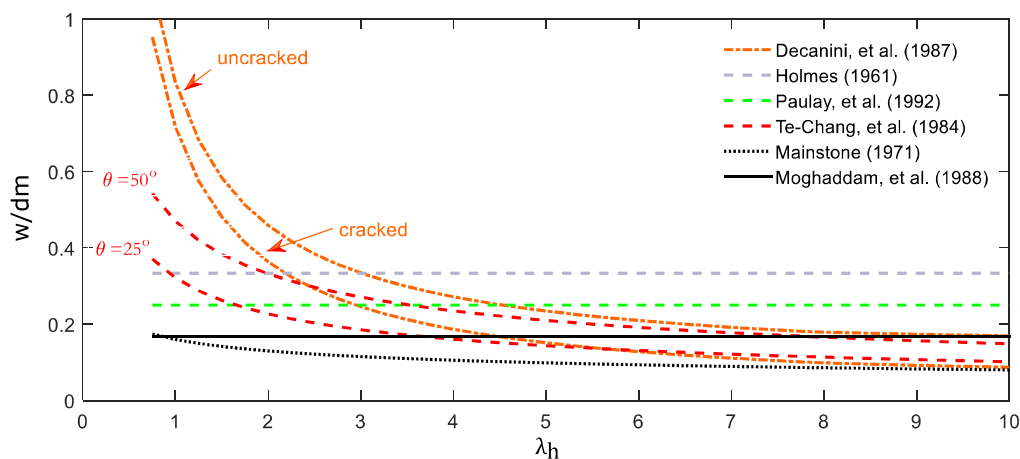
Figure 4.9 – Variation of the w/d ratio for the infilled frames as a function of the parameter λ_h (after, Hossameldeen, 2017) [12]

Durrani, *et al.* (1994) [101] proposed the semi-empirical formula to formulate the width of equivalent diagonal strut as follows:

$$w = \gamma d_m \sin(2\theta) \tag{4.19}$$

$$\gamma = 0.32 \left[\frac{h^4 E_m t_m}{m E_c I_c h_m} \right]^{-1} \left[\sqrt{\sin 2\theta} \right] \tag{4.20}$$

$$m = 6 \left(1 + \frac{6 E_b I_b h}{\Pi E_c I_c L} \right) \tag{4.21}$$

where: E_b and E_c are the Young's modulus of the beam and the column, respectively, and I_b and I_c are the moment of inertia of the beam and the column, respectively.

Bennett, *et al.* (1996) [102] proposed a linear strut width as given by equation (4.22).

$$w = \frac{\Pi}{C \lambda_m \cos \theta} \tag{4.22}$$

where: C is an empirical value dependent on the in-plane drift displacement and infill damage. The value of C varies with the type of frame and materials of the infill walls. Bennett, *et al.* (1996) [102] published values of the parameter C for steel frames with clay tile infill walls, steel frames with concrete masonry infill walls, concrete frames with concrete masonry walls, and concrete frames with brick masonry walls, which were listed from Table 4.1 to Table 4.4, respectively.

Table 4.1 – Values of C with structural clay tile in steel frames as proposed by Bennett, *et at.* (1996) [102]

C	Displacement (in)	Typical infill damage
5	0.00 - 0.05	None
7	0.05 - 0.20	Diagonal mortar joint cracking
11	0.20 - 0.40	Off diagonal mortar joint cracking
14	0.40 - 0.60	Banded diagonal mortar joint cracking
16	0.60 - 0.80	Corner mortar crushing and tile cracking
18	0.80 - 1.00	Tile faceshell splitting (primarily corner regions)

Table 4.2 – Values of C for steel frames with concrete masonry infill walls as proposed by Bennett, *et al.* (1996) [102]

C	Displacement (in)	Typical infill damage
4	0.00 - 0.10	None
5	0.10 - 0.30	Diagonal mortar joint cracking
8	0.30 - 0.65	Off diagonal mortar joint cracking
12	0.65 - 0.80	Extensive random cracking; possible corner crushing

Table 4.3 – Values of C according to Bennett, *et al.* (1996) [102] for RC frames with concrete masonry infill

C	Displacement (in)	Typical infill damage
4	0.00 - 0.10	None
5	0.10 - 0.25	Diagonal sliding mortar joint cracking
8	0.25 - 0.45	Off diagonal mortar joint cracking bed joint sliding; corner crushing

Table 4.4– Values of C according to Bennett, *et al.* (1996) [102] for RC frames with solid brick masonry infill

C	Displacement (in)	Typical infill damage
4	0.00 - 0.10	None
5	0.10 - 0.15	Diagonal sliding mortar joint cracking
8	0.15 - 0.25	Off diagonal mortar joint cracking bed joint sliding; corner crushing
10	0.25 - 0.35	Extensive random cracking; possible corner crushing

Papia and Cavaleri (2001) [103] introduced a new parameter for the estimation of relative stiffness, λ^* and is given by equation (4.23).

$$\lambda^* = \frac{E_m t\, h}{E_c A_c}\left(\frac{h^2}{L'^2} + \frac{1}{4}\frac{A_c}{A_b}\frac{L'}{h}\right) \tag{4.23}$$

where: L' is the length between the column centrelines and A_b is the gross beam area.

El-Dakhakhni, *et al.* (2003) [56] modified the single strut into three strut model to better represent the "actual distribution of forces from the infill to the frame". In this case, the total strut area was estimated as the product of the strut width obtained from equation (4.24) and the infill panel thickness.

$$w = \frac{(1-\alpha_c)\alpha_c h}{\cos\theta} \tag{4.24}$$

$$\alpha_h = \alpha_c h = \sqrt{\frac{2\left(M_{pj}+0.2M_{pc}\right)}{t f'_{m-0}}} \leq 0.4h \tag{4.25}$$

$$\alpha_l = \alpha_b l = \sqrt{\frac{2\left(M_{pj}+0.2M_{pb}\right)}{t f'_{m-90}}} \leq 0.4l \tag{4.26}$$

where: α_c= ratio between the column contact length to the height of the column

M_{pj}=minimum of the column's, the beam's or the connection's plastic moment capacity, referred to as the plastic moment capacity of the joint (kN-mm)

M_{pc}=column plastic moment capacities (kN-mm)

M_{pb}=beam plastic moment capacities (kN-mm)

f'_{m-0}=masonry strength parallel to bed joints (kN/mm²)

f'_{m-90}=compressive strength of the masonry panel perpendicular to the bed joint

The total strut area is divided among the three struts, namely, upper strut, middle strut, and lower strut. Each of the upper and lower struts consists (1/4) of the total area, while the former strut connect the upper beam with the leeward column and latter one connecting

lower beam and windward column, and the middle strut connecting the two loaded corners consisting (1/2) of the total area. The two off-diagonal struts provide better distribution of the forces between the infill panels and the frame members. The contact length of the loaded infill walls with the column can be obtained from equation (4.25) [56].

The equivalent strut width for partially infilled frame was formulated by Pradhan (2012) [104]. According to elastic strip theory, the contact length between frame and masonry walls, k_x is given by equation (4.27).

$$k_x = \frac{\pi}{2} h_y \tag{4.27}$$

where: h_y is the equivalent length of the wall that contributes in compression.

Here, the strut width is given by the equation (4.28).

$$w = \frac{\pi}{2} * 2.29 * \left[\frac{E_c I_c h_m}{E_m t h_c}\right]^{\frac{1}{3}} * \frac{L_m}{\sqrt{L_m^2 + (h_m - k_x)^2}} \tag{4.28}$$

where: h_c is the centre to centre height of the frame, h_m is the height of partial infill and parameters are illustrated in Figure 4.10.
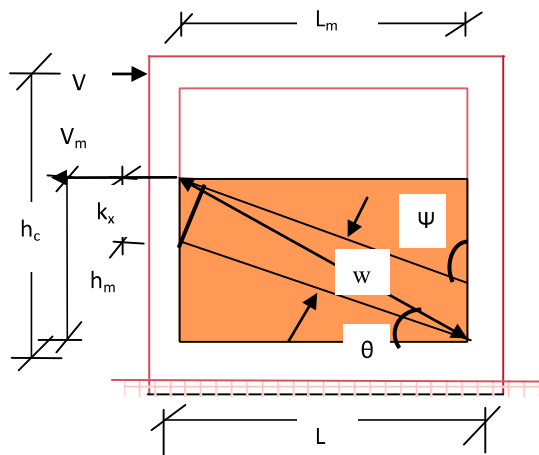
Figure 4.10 – Analytical model for equivalent strut defined by Pradhan, P. M. (2012) [104]

In 2014, Turgay, *et al.* (2014) [105] performed experimental tests, and proposed alternative and improved expression for the estimation of the stiffness, strength and deformation capability of the infilled RC frames. The equivalent width of the diagonal strut proposed given by equation (4.29).

$$w = 0.18 \frac{d_m}{\sqrt[4]{\lambda_h}} \tag{4.29}$$

The researchers conducted the entire experiment test on specimens having L_m/h_m between 1.2 and 2.

4.2.3.2.2   Strength method

The strength method defines the force-displacement relation which later relates with the area of the strut to define the constitutive behaviour of the infill walls. The force-displacement relation of the equivalent strut must be adequately defined to conduct the nonlinear cyclic or dynamic analysis. The representation of the hysteretic behaviour increases both the complexity of the analysis and uncertainties of the problem. The experimental and analytical studies on the cyclic behaviour of the masonry infilled frames was initially conducted by Klingner, *et al* (1978) [106]. The study focus on the effects of the cyclic loads tested on the portion of the multi-storey buildings and proposed three nonlinear hysteretic models for the equivalent diagonal struts. The cyclic models considered the strength and the reloading stiffness degradations, as illustrated in Figure 4.11. The envelope was represented by a linear elastic ascending branch followed by an exponential descending curve, while the unloading stiffness was assumed to be linear and equal to the initial stiffness. Although their model assumed diagonal strut contains a certain amount of tensile strength, authors ignored this component in the implementation of the model in their numerical analyses. The model calibration reveals a poor agreement between the analytical results and experimental data. This was the first model to consider the nonlinear cyclic response of the diagonal strut, thus regarded as the preliminary step for further development [106].
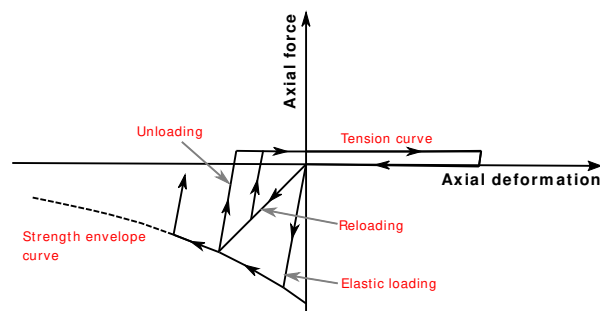
Figure 4.11 – Force-displacement response of the strut model proposed by Klingner, *et al.* (1978) [106]

The force-displacement relationship illustrating the mechanical behaviour of the diagonal struts, as proposed by Andreaus, *et al.* (1985) [107], was presented in Figure 4.12. The model does not consider any stiffness degradation effects; however, it assumes strength

degradation starts immediately after the strength of the strut reaches its maximum value. Reloading occurs when the axial deformation is equal to the plastic deformation of the previous loop.
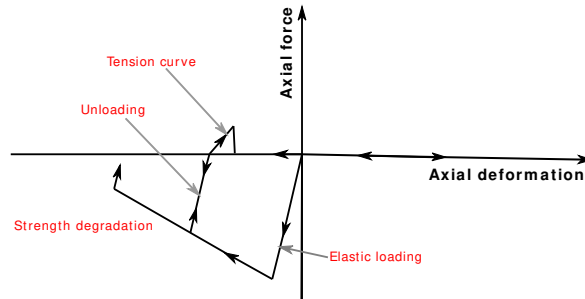
Figure 4.12 – Force-displacement response of the strut model proposed by Andreaus, *et al.* (1985) [107]

Doudoumis, *et al.* (1986) [108] proposed a nonlinear cyclic hysteretic model, as illustrated in Figure 4.13, such that no initial stress branch mainly due to shrinkage of contact zones. This model was developed and applicable for the non-integral infilled frames, where a gap between infill walls and surrounding frame normally exists. The strength degradation effect was considered in the envelope, and the hysteretic cycles demonstrated in a very simplified way such that the reloading occurs following the elastic branch [108].
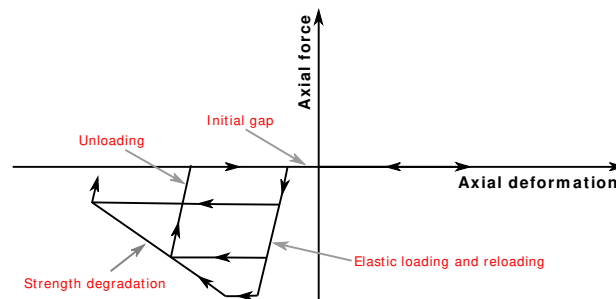
Figure 4.13 – Hysteretic model for non-integral infilled frames developed by Doudoumis, *et al.* (1986) [108]

Soroushian, *et al.* (1988) [109] proposed a different approach to derive a typical hysteretic model for the masonry shear walls that fails in shear and in flexure. The hysteretic response was modelled by combining two equations; the first equation (a logarithm exponential function) defines the strength envelope, and the second equation (a quartic polynomial function) represents the hysteretic loops, as shown in Figure 4.14. This hysteretic approach was later modified by Chrysostomou, *et al.* (1992) [110] to simulate the nonlinear behaviour of the equivalent diagonal strut model. These expressions describe the mechanical behaviour of the infill walls and were utilized to derive the force-displacement relations for

the central and off-diagonal struts of the model proposed by Chrysostomou, *et al.* (1992) [110].
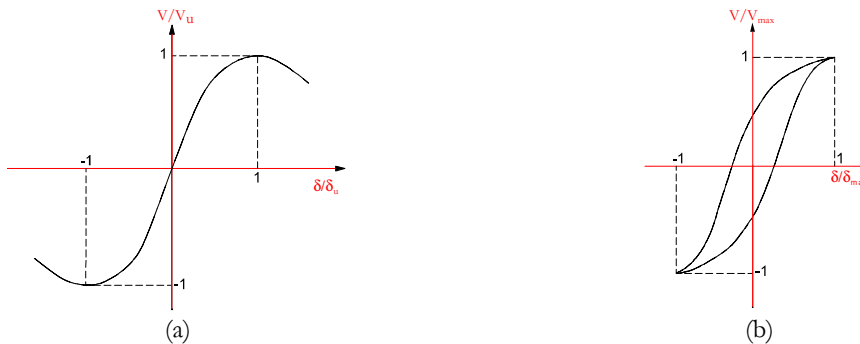
Figure 4.14 – Hysteretic model proposed by Soroushian, *et al.* (1988) [109] for masonry shear walls and adopted by Chrysostomou, et al. (1992) [111] for the diagonal strut model; (a) Strength envelope and (b) Hysteretic loop

Madan, *et al.* (1997) [112] developed a hysteretic model that combines a set of mathematical functions to develop the smooth force-displacement relationship, as demonstrated in Figure 4.15. The strength degradation, stiffness decay, and pinching of the hysteresis loops can be considered by selecting the proper values of the nine parameters included in the model. Some of the parameters are empirical, whereas the other depends on the energy dissipation considerations. The implementation of this model was not straightforward and the solution requires the numerical integration of a differential equation [112].
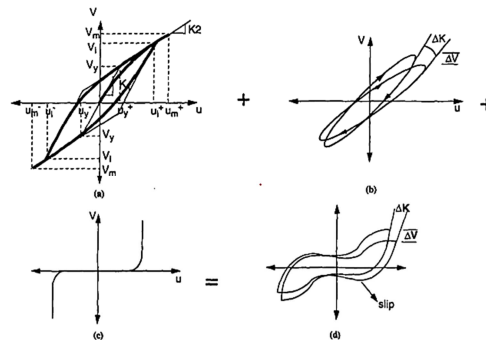
Figure 4.15 – Integrated hysteretic model for degrading pinching element according to Madan, *et al.* (1997) [112]

Crisafulli, F. (1997) [11] proposed an analytical formulation to simulate the hysteretic axial response of masonry (stress-strain relationship), and used it to define the response of the equivalent strut. He introduced some specific conditions to the hysteretic model in order to simulate the fact that the material can carry compressive stresses before the cracks were completely closed. The consideration of contact effects produces wider hysteresis loops and gradual increase of compressive stress in the reloading process. The model proposed

also includes the effect of the inner loops. For this, he conducted tests on standard concrete cylinders with different combinations of complete and inner loops. The conclusions drawn were the successive inner loops increase the reloading strain, do not affect the plastic deformation and remain inside the cycle defined for the complete unloading and reloading curves. The former can exhibit change in direction of its concavity depending on the starting point of the loading curve, while later shows no inflection point. The nonlinear response of masonry infill walls in compression, contact effects in the cracked material, and small cyclic hysteresis were considered in this model, as presented in Figure 4.16. A good agreement was obtained when compared the experimental and analytical results; however, several empirical parameters need to be defined in order to represent adequately the hysteretic response [11].
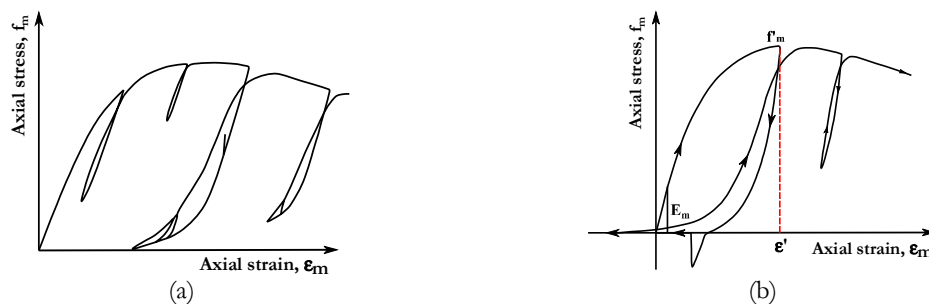
Figure 4.16 – Hysteretic model proposed by Crisafulli (1997) [11]; (a) Typical cyclic response with small cycle hysteresis and (b) Local contact effects for the cracked masonry

Several nonlinear hysteretic models were successively developed starting from different considerations. El-Dakhakhni, *et al.* (2003) [56] proposed a simplified stress-strain relation of the masonry material, employing a trilinear response model illustrated in Figure 4.17, for diagonal strut models. This hysteretic model includes an elastic, plastic (ultimate strength) and post-capping branch of the strut behaviour. This simplified model results in less solution time, especially applicable in multi-storey three-dimensional structures which have large numbers of DOF.
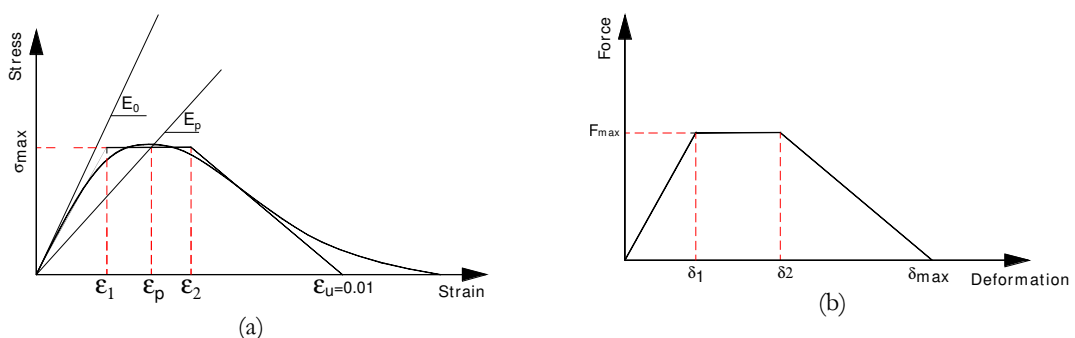
Figure 4.17 – Simplified trilinear relations of the strut proposed by Dakhakhni, *et al.* (2003) [56]; (a) Stress-strain relation of concrete masonry and (b) Typical force-displacement relation for struts

Many researches have been performed using a trilinear relation to represent the nonlinear behaviour of the masonry infills, such as those proposed by Dolsek, *et al.* (2008) [9] and Uva, *et al.* (2012) [113], etc. To define the trilinear curve, three coordinates of the three main points in terms of the forces and corresponding displacements are required. However, the available expressions to define these trilinear relations are either based on regression analysis using experimental data or adopt and combine the pre-existing expressions available from literature to get more realistic curves.

The present study considered the hysteretic model as proposed by Crisafulli, F. (1997) [11], as shown in Figure 4.18 for the modelling of masonry infill walls due to availability in SeismoStruct software [22]. The model considered the axial load struts following the masonry strut hysteresis model while the shear strut uses a bilinear hysteresis rule. A detailed modelling approach for the infill walls will be discussed in the following sections.
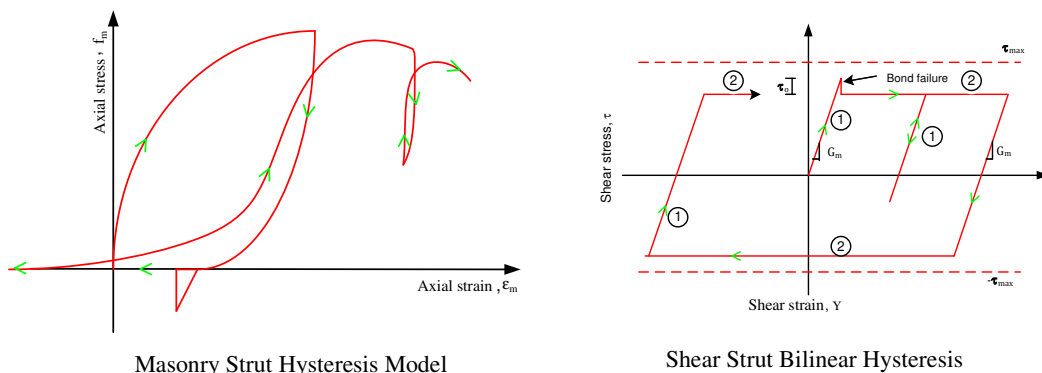
Masonry Strut Hysteresis Model   Shear Strut Bilinear Hysteresis
Figure 4.18 – Hysteretic rules adopted for the infill panel proposed by Crisafulli (1997) [11]

4.2.3.3   *Modification of the diagonal strut model and multiple struts model*

As discussed in the previous section, the interaction between the infill panel and the surrounding frames can be represented by the diagonal strut model. Initially, a single diagonal strut model was proposed which is simple and is capable to represent the interaction of masonry infill panels globally; however, it could not adequately capture the distribution of frame bending moment and shear forces, and also cannot describe the interaction of infill walls and surrounding frames in local level. Therefore, a more complex macro-model was proposed, such as two, three and multiple struts, and also modifying their arrangements in order to capture the behaviour of infilled frames in local and global levels.

Leuchars, *et al.* (1976) [114] proposed a double strut model, as shown in Figure 4.19 (a), that is capable to capture the horizontal shear sliding occurs in the masonry panel. The double strut model represents large bending moments and shear forces induced in the central zone of the columns. Furthermore, it is also possible to consider the friction mechanism that develops along the cracks, which mainly controls the strength of the system [114].

Syrmakezis, *et al.* (1986) (as reported in Siamak, S. 2013 [115]) introduced one of the early attempts to consider the infill-frame interaction by using five parallel compressive struts in each direction, as shown in Figure 4.19 (b), to study the effect of the contact length on the moment distribution of the frame [115].

Zarnic, *et al.* (1988) [68] proposed a model based on the experimental tests on the infilled frames. During the tests, they observed damages on the upper zone of the masonry panel with an offset from the diagonal. Hence, the modified diagonal strut connects to the lower zone instead of connecting at beam-column joint, as depicted in Figure 4.19 (c). This model is applicable for the masonry infill walls which are likely to develop shear failure at the top of the column. Schmid, *et al.* (1989) (as reported in Siamak, 2013 [115]) combined the idea of off-diagonal struts and increased the number of struts, proposing a strut model with offsets at both ends, as illustrated in Figure 4.19 (d). In spite of the complexity, the multi-strut models are able to represent the internal forces in the frame precisely and accurately, which is the main advantage of these models than single strut model.

| (a) | (b) | (c) | (d) |
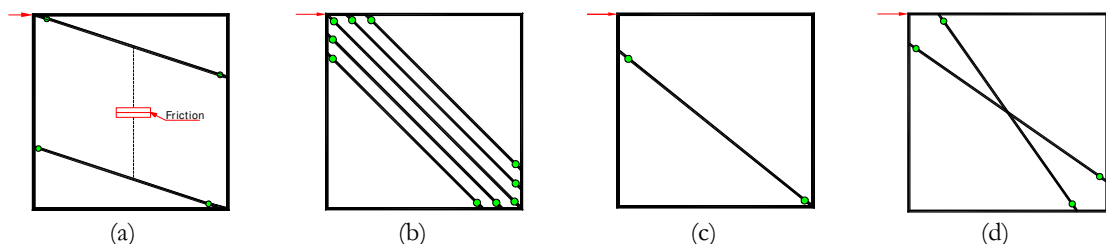
Figure 4.19 – Modification of the diagonal strut model and multiple strut models to model the frame infill interaction proposed by; (a) Leuchars, *et al.* (1976) [114], (b) Syrmakezis, *et al.* (1986) [115], (c) Zarnic, *et al.* (1988) [68] and (d) Schmidt, *et al.* (1989) [115]

A more complex multiple strut model was proposed by Thiruvengadam, *et al.* (1985) [116], where experimental test results and finite element solutions for all the considered frames holds a good agreement except for the short frames. The model comprises a number of pin-jointed diagonals and vertical struts, in which the diagonals exhibit the shear and axial stiffness of the infill walls. The partial separations were provided between the infill walls

and the surrounding frames and the contact length was calculated, and ineffective struts were removed. In a similar way, the effect of openings can be considered by removing the struts crossing the opening area. Due to the complexity and refinement involved in this multiple strut models, it can be considered as an intermediate modelling approach between the micro-models and macro-models [116].

Chrysostomou, C. (1991) [111] further altered the orientations of the strut in order to model the response of the infill panels with six diagonal strut systems, as demonstrated in Figure 4.20. The model consist a total of six struts, such that three parallel struts in each diagonal direction and off-diagonal one were positioned at critical locations along the frame members. For a given instant, the three diagonal struts were active in the direction of loading and were replaced when their compressive strength was reduced to zero. The locations of diagonal struts were specified by parameters α_h and α_l, which is associated with the position, where a plastic hinge likely to develop in a beam and column. The parameters α_h and α_l were theoretically evaluated based on Te-Chang, *et al.* (1984) [97].
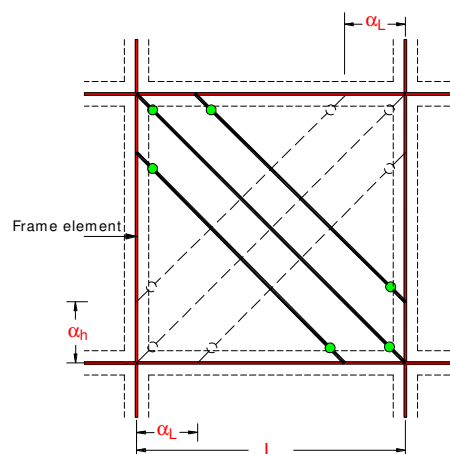
Figure 4.20 – Six-strut model for masonry infill panels in frame structures (Chrysostomou, 1991) [111]

The influence of using different number of diagonal struts on the structural response in terms of stiffness and forces in the perimeter of the frame was investigated by Crisafulli, F. (1997) [11]. The results obtained from single, double and triple struts model were compared with those obtained from a detailed finite element model, as illustrated in Figure 4.21. The single strut model underestimates the bending moment as lateral forces were primarily transferred by a truss mechanism, whereas two-strut model cause larger response values compared to that obtained with the finite element model. Similarly, a better approximation can be achieved from the three-strut model proposed by Chrysostomou, C. (1991) [111], as illustrated in Figure 4.20, although some differences arises at the ends of

both columns. In addition, Crisafulli, F. (1997) [11] recommended double strut modelling approach over three strut model as the results were accurate enough and simpler to model as well.
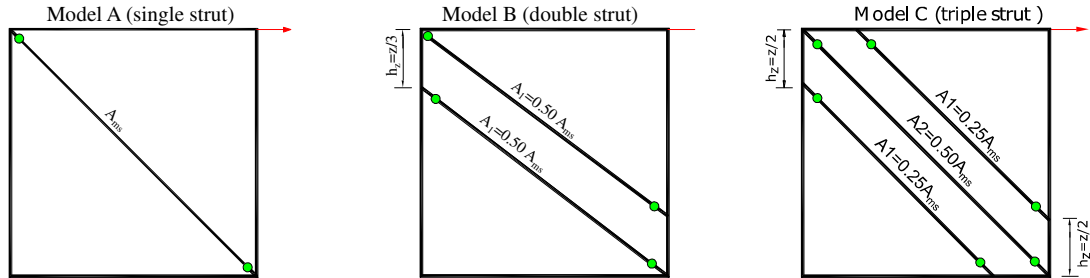
Figure 4.21 – Strut model proposed by Crisafulli, F. (1997) [11]

More recently, El-Dakhakhni, *et al.* (2003) [56] proposed a model for steel frames infilled with concrete or masonry units using two groups of strut to capture the bending moment in the columns and corner crushing of the masonry infills. Each group consists of three non-parallel struts having diagonal struts with two offset struts, as shown in Figure 4.22. The model was capable to defined the tri-linear response, which includes the elastic, plastic (ultimate strength), and post-capping branch for the strut. The total area of the proposed strut system, A, is given by the equation (4.30) [56].

$$A = \frac{(1-\alpha_c)\alpha_c h}{\cos\theta}t \tag{4.30}$$

where: α_c is the ratio between the column contact length and its height and is given by equation (4.25).
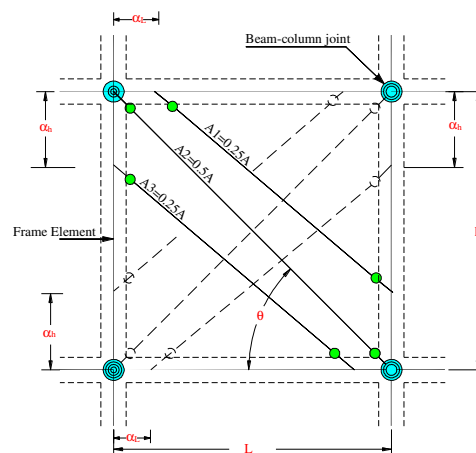
Figure 4.22 – Six-strut model for masonry infill panel in steel frame structures (El-Dakhakhni, *et al.*, 2003) [56]

In order to better represent the shear failure mechanism in the infill wall, Crisafulli, *et al.* (2007) [117] proposed a different strut model, i.e. multi-strut along with spring model, which was implemented in a 4-node element. The compressive and shear behaviour of the infill walls were internally accounted using two parallel struts and a shear-spring in each direction, as illustrated in the Figure 4.23. The shear strength of the spring was evaluated based on the shear-friction mechanism that can represent the shear strength as a function of the maximum permissible shear stress, axial load, and length and thickness of the infill. The area of the struts in this model decreases as the axial strut displacement increases, due to the reduction of the contact length between frame and infill walls and also due to cracking of the masonry infill. The offset of the struts from the diagonal, h_z, varies between $z/3$ and $z/2$, where z is the contact length between the panel and the frame which is given by equation (4.3). This struts model can adequately consider the lateral stiffness and strength of the masonry panel, particularly applicable when shear failure along the joints or diagonal tensile failure was expected. Similarly, the model was simple, easy and requires less computational time that can be applied in the analysis of large infilled frame structures. This model is useful until the masonry panel is in a plane state (in the un-deformed state) and once the infill panel is not in plane state, where other effects (shell or membrane behaviour) becomes dominant, is not considered in this model [117]. Similarly, considering the single and double strut systems for the experimental test performed by Pinto, *et al.* (2006) [118] and Asteris, *et al.* (2011) [119] concluded that double struts model was better with openings to capture the behaviour of the tested infilled frames compared to single strut model.
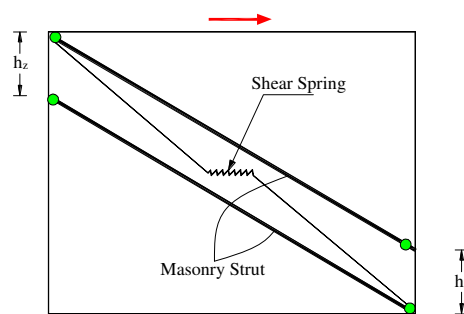
Figure 4.23 – Multi-strut proposed by Crisafulli, *et al.* (2007) [117] (only the struts and shear spring active in one direction are represented)

Rodrigues, *et al.* (2008) [120] proposed an equivalent bi-diagonal compression strut model considering the interaction of the masonry panel's behaviour in the two directions. The masonry wall is represented by four struts and a central strut element in which nonlinear

hysteretic behaviour is concentrated, as illustrated in Figure 4.24. The results concluded that the proposed model is calibrated with different experimental tests and revealed that the model is capable to represent the building's response in terms of progressive displacement, global shear drift at each storey and cumulative dissipated energy [120].
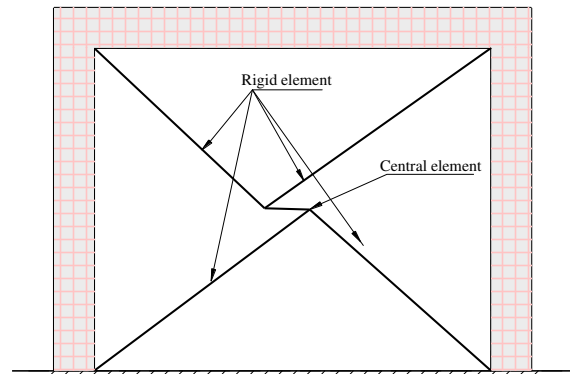
Figure 4.24 – Strut-model proposed by Rodrigues, *et al.* (2008) [120]

When the infilled RC frame building is subjected by lateral loads, the infill walls could fail either by in- or out-of-plane behaviour of the masonry infill walls. All the above discussed modelling approaches are applicable for in-plane behaviour of the infill walls and could not capture the out-of-plane behaviour. Furtado, *et al.* (2015) [121] introduced an analytical modelling approach to represent the out-of-plane behaviour of the infill walls through the location of infill mass in two central nodes, the proposed model was presented in Figure 4.25. When the model reaches the drift limits, the infill walls were removed with the help of algorithm proposed by Mosalam and Gunay (2015) [122].The out-of-plane behaviour of the infill walls follow linear elastic hysteretic curve. The model implemented the mass through the application at the central nodes, and the mass was calculated as 0.81 M, where M is the total mass of the infill walls.
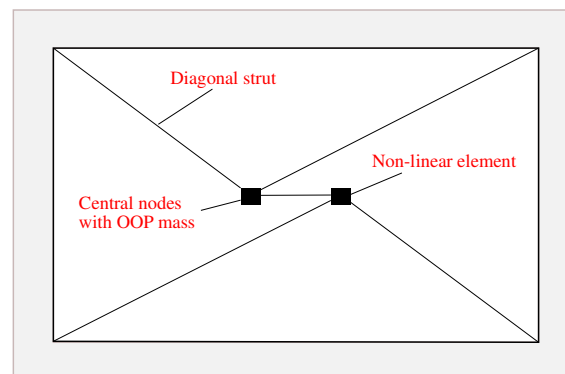
Figure 4.25 – Modelling of infill walls to capture the in- and out-of-plane behaviour Furtado, *et al.* (2015) [121]

4.2.4 RC frame strengthening strategies

The infilled RC buildings constructed in past decades do not comply with the seismic code at the present and show poor performance to the seismic actions. Hence, these existing RC buildings become often necessary to be upgraded in order to satisfy the new building code requirements or to improve seismic performance of the structures. Almost all design codes specified the structural requirements for the design of new construction; however, the design for strengthening of an existing building in most cases is based on the engineering judgement. This is due to uncertainty associated with the evaluation, lack of proper and accurate assessment of frame interaction with infill walls and also lack of reliable identification tools for the existing concrete and reinforcement condition. This is also due to limited research on the methods of strengthening and lack of assessing the structural performance of the strengthened structures. As referred by Sugano, S. (1981) [123], in early years of the World Conference on Earthquake Engineering (WCEE), the major topic in the technical session of the rehabilitation was the development of techniques to repair and strengthen the existing structures. The extensive damage to concrete and wood structures during 1968 Tokachi-Oki earthquake and 1978 Miyagi Ken-Oki earthquake have motivated Japanese researchers to carryout extensive studies on repairing of damaged structural members and retrofitting of existing buildings. The 1994 Northridge earthquake and the 1995 Kobe earthquake have strongly pushed the society to recognize the importance of earthquake countermeasures for the existing vulnerable buildings [124]. This motivates and encourages the researchers to provide more appropriate and reliable design guidelines for the rehabilitation of the existing RC structures.

In 1983, United Nations Industrial Development Organization (UNIDO) with the participation of several countries in the Balkan region developed a qualitative rehabilitation guideline for the damage assessment of common building structural systems, such as masonry load bearing walls and simple wood, steel and concrete frames (as reported by Rodrigues and Park [125]). The guideline was applicable for the repair work as it was based on the existing building codes and standards. Therefore, engineer must rely on his personal judgement in assessing areas of weakness in a structure and then develop an appropriate strengthening scheme based on that assessment. Due to the large uncertainties associated with the quality of the concrete, inadequate attention to joints during design and construction, poor workmanship, and no soil test before structural analysis have further resulted complexity in designing strengthened guidelines [125].

The present section discusses three conventional strengthening approaches adopted for the repair and maintenance of the existing case study RC buildings, representing commonly practiced in Nepal. It includes concrete column jacketing, addition of RC shear walls and steel bracing. The increased level of performances due to its intervention are discussed with the help of past experimental researches and also discussed the design guidelines followed for the design of such structural elements as follows.

4.2.4.1 Concrete column jacketing

Concrete column jacketing is one of the most popular methods of retrofitting since the design and construction procedures of RC columns and jacketing can provide protection from both the environmental effects and fire. Jacketing is the effective procedure to rehabilitate the existing structures, as it improves the lateral stiffness, strength and energy dissipation capacity [126, 127]. Similarly, RC jacketing significantly enhances the shear capacity, flexural strength and deformation capacity of damaged or weak members [8]. The addition of longitudinal reinforcement and increase of the cross-section of the existing structural elements can enhance significantly the stiffness and flexural strength [128]. Figure 4.26 presents a generalized concrete jacketing as reported by Sichko, *et al.* (2017) [129].
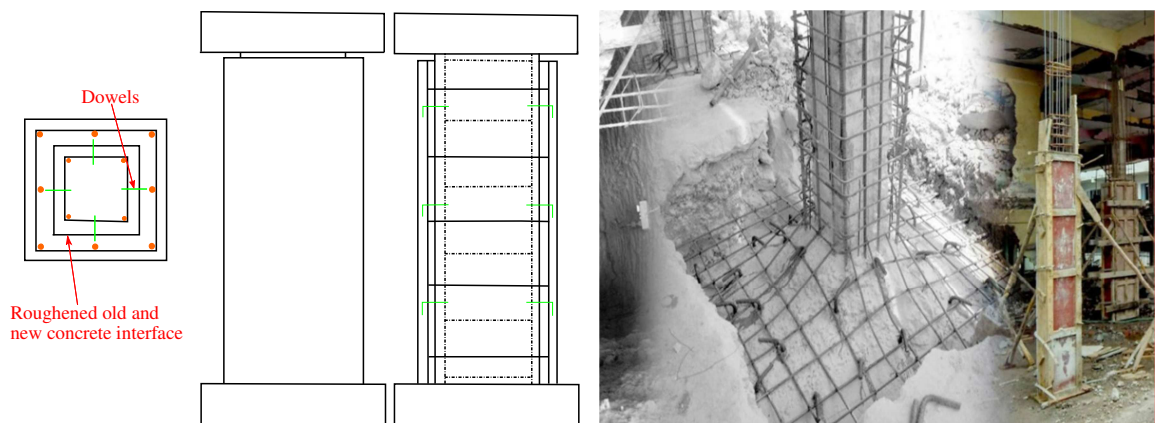
Figure 4.26 – Concrete jacketing strengthening scheme as reported by Sichko, *et al.* (2017) [129]

In 1983, UNIDO [125] illustrates an example of local strengthening of reinforced columns by jacketing which was strengthened only between the floors. The jacket consists of added concrete strengthening and longitudinal and transverse reinforcement around the existing column. It was concluded that this type of strengthening measure significantly enhances the axial, shear, and flexural strengths of the column; however, the strength of the beam-

column joint remained almost same. The procedure involves the chipping of the original concrete member and roughening its surface, so that the bond between the old and new concrete can be improved. The UNIDO guideline also describes different approaches to improve the column flexural strength. One of the techniques involves the addition of longitudinal reinforcements that is passed through the holes drilled in the slab and placing of new concrete at the beam-column joint [125].

Bett, *et al.* (1988) [130] performed the experimental tests to examine the effectiveness of jacketing techniques in enhancing the lateral load resistance. For this, the specimens considered were 2/3-scaled and other structural parameters were identical to the buildings of the U.S. in the 1950s and early 1960s. The tests were performed in two ways, such that first specimen was retrofitted with jacketing only after testing and second one is retrofitted before testing. The test results concluded that both strengthened and the repaired column show better performance compared to the original columns. The column strengthened by jacketing with and without supplementary cross-ties were stiffer and laterally stronger than the original and unstrengthen column, but the ductility capacities observed to be very poor in entire cases [130].

Alcocer, S. (1993) [127] carried out the experimental program to assess the behaviour of slab-beam-column joints rehabilitated by jacketing. The test specimen includes four full scale RC frames designed according to the American practice of the 1950's and 1960's and was not detailed for ductile behaviour. These specimens were repaired by jacketing for column only, and both column and beams. The test results concluded that jacketing is effective for the rehabilitation of the existing building, thus by enhancing the stiffness, strength and total energy dissipation characteristics compared to the existing structure. It also concluded that jacketing in the beam is uneconomical as it requires large and heavy forms and special skills as well, whereas column jacketing can be performed easily.

The seismic tests on the repair and strengthening techniques was investigated by Rodriguez, *et al.* (1994) [131]. For this, two column units representing RC column designed and constructed in New Zealand in the 1950s were tested. The test results showed that the columns designed to early seismic codes possess very low ductility. During the testing, the available displacement ductility factor of approximately 2 was found in these column units. The above tested specimens were again retrofitted by adding reinforced concrete jackets which is carried out by surface roughening through chipping the surface of the as-built columns before placing jacket. A new concrete layer of 100 mm thickness was added and

also reinforced with new longitudinal and transverse reinforcements. Results of the simulated seismic load tests revealed that the stiffness and strength of the jacketed columns increased by 3 times than that of as-built columns [131].

Vandoros, *et al.* (2006) [132] conducted experimental tests to investigate the effectiveness of interface treatment, such as surface roughening and embedding of steel dowels in the original columns and combination of both. The five specimens considered includes three strengthened, each one un-strengthened and as-built specimen, and scaled to half height and is representative of 1950's Greek code. The jacket of the strengthened specimens was constructed with shotcrete. The test results concluded that application of the proper strengthening significantly improves the stiffness and strength to a level that is comparable to monolithic behaviour. In addition, the interface treatment by surface roughening also enhances the energy absorption capacity, whereas dowel improves the ductility of the member, and combination of both techniques enhances the stiffness and also influence in the failure and cracking pattern in the members [132].

The effectiveness of RC jacketing of the substandard RC columns with short lap splices was experimentally studied by Kalogeropoulos, *et al.* (2014) [133]. The experiment was conducted for 1:1.5 scale RC rectangular column specimens to identify the feasibility and performance of a pre-earthquake specimen, representative of those found in the pre-1970. The specimen includes one with continuous longitudinal, two with lap splices of $20d_b$ length and two more with lap splices of $24d_b$ were constructed. One of the column sub-assemblages with a lap splice of $20d_b$, one with lap splice of $24d_b$ and the column with the continuous longitudinal bars were strengthened by reinforced concrete jacketing, while the lap-spliced bars of the old columns were welded. The test results concluded that the deficient members (columns) of the existing old buildings can significantly improve if proper concrete jacketing procedure was carried out. The retrofit techniques applied proved to be an effective method for the pre-earthquake strengthening of columns with deficient lap splices [133].

Based on the different investigations works and literature available on this subject; in 2002, the Central Public Works Department (CPWD) prepared a "Handbook on Repair and Rehabilitation of RCC Buildings" [134]. The document stated that the present trends of jacket retrofit are designed in such a way that new jacket behaves compositely and the new jacket elements will only take the additional loads, initially to be resisted by the original column. Some of the problems that may arise if:

- "Old concrete has reached limiting strain and is not likely to sustain any more significant strain

- Old concrete is weak and porous and started deteriorating due to weathering action and corrosion of reinforcement."

There was a big debate on the composite design approach and later a new design approach was proposed, which ensures the loads transferred to the new jacket column. For this, a perfect bond has to be created between the new and old concrete. This can be achieved providing shear keys and bond coat using epoxy resign or polymer modified cement slurry, such that its strength must not be less than new jacket concrete. A typical arrangement of the concrete jacketing and detail of shear key bars were presented in Figure 4.27 [134].
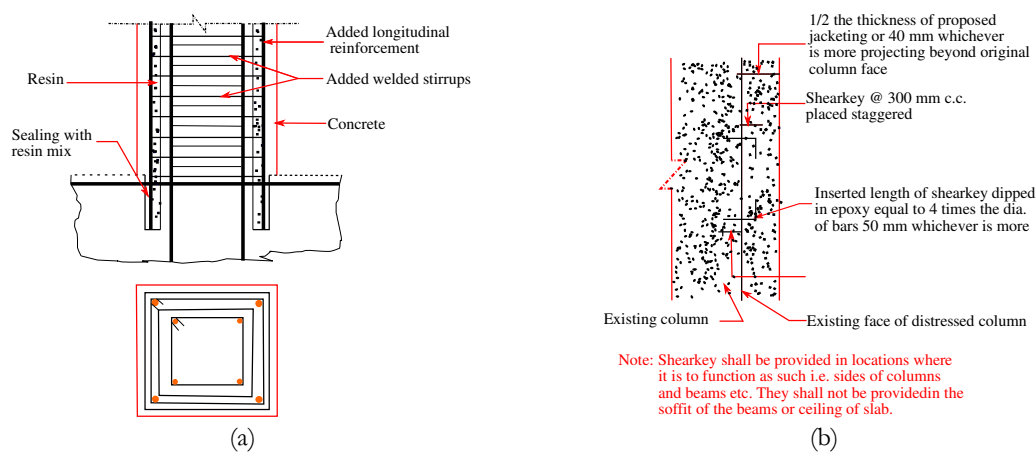
Figure 4.27 – Schematic layout of column jacketing; (a) Column strengthening concrete jacket and (b) Details of shear key bars (adopted from CPWD [134])

Since the experimental tests were performed on the individual column or plane frames, such tests cannot represent global structural behaviour and the reliability of test results will be uncertain. In the present study the design and detailing of concrete column jacketing for the existing RC buildings was carried with the help of IS 15988: 2013 [135]. This guideline is useful for the rehabilitation of the existing buildings having deficient members identified during detailed evaluation. This approach enables to enhance the seismic performance of the existing buildings related to the life-safety of the occupants. It also provides different design procedures for jacket strengthening techniques depending upon the requirements of the structural members, such as RC jacketing, steel profile jacketing and steel encasement or wrapping with FRPs and so on. The various design steps stated in the IS 15988: 2013 guideline for the concrete column jacketing are as follows [135].

1. The seismic demand on the columns, in terms of axial load 'P' and moment 'M' is obtained.

2. Column section size and details are estimated for P and M using IS 456: 2000 [136].

3. The existing column size and amount of reinforcement is deducted to obtain the amount of concrete and steel to be provided in the jacket.

4. The extra size of column cross-section and reinforcement is provided in the jacket.

5. Increase the amount of concrete and steel actually to be provided as follows to account for losses.

$$A_c = \frac{3}{2}A_c' \text{ and } A_s = \frac{4}{3}A_s' \quad\quad (4.31)$$

where:

A_c and A_s = actual concrete and steel to be provided in the jacket; and

A_c' and A_s' = concrete and steel values obtained for the jacket after deducting the existing concrete and steel from their respective required amount.

6. The lateral ties to be provided in the jacket are spaced in order to avoid flexural shear failure of the column, and provide adequate confinement to the longitudinal steel along the jacket is given as:

$$s = \frac{f_y}{\sqrt{f_{ck}}} \frac{d_h^2}{t_j} \quad\quad (4.32)$$

where:

f_y = yield strength of steel,

f_{ck} = cube strength of concrete,

d_h = diameter of stirrup, and

t_j = thickness of jacket.

7. If the transfer of axial load to new longitudinal steel is not critical then friction present at the interface shall be relied on the shear transfer, which shall be enhanced by roughening the old surface.

8. Dowels which are epoxy grouted and bent into 90^0 hooks shall also be employed to improve the anchorage of new concrete jacket.

Similarly, the design code IS 15988: 2013 [135] also provides some minimum specifications that need to be considered for the design of column jacketing are as follows.

1. "Strength of the new material shall be equal or greater than those of the existing column. Concrete strength shall be at least 5 MPa greater than the strength of the existing concrete.

2. For columns where extra longitudinal reinforcement is not required, a minimum of Φ 12 bars in the four corners shall be provided with 135^0 bend at Φ 10 leg lengths.

3. Minimum jacket thickness shall not be <100 mm.

4. Lateral support to all the longitudinal bars shall be provided by ties with an included angle of not more than 135^0.

5. Minimum diameter of ties shall be 8 mm and not less than one-third of the longitudinal bar diameter.

6. Vertical spacing of ties shall not exceed 200 mm, whereas the spacing close to the joint within a length of ¼ of the clear height shall not exceed 100 mm. The spacing of ties shall not exceed the thickness of the jacket or 200 mm whichever is less."

The sample example of concrete jacketing on the reinforced concrete column based on IS 15988: 2013 [135] is illustrated as shown in Figure 4.28.
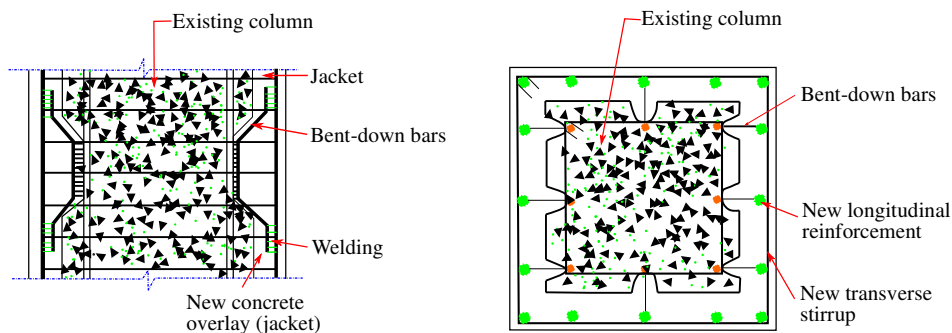
Figure 4.28 – Schematic layout of reinforced concrete jacketing as per IS 15988: 2013 [135]

The above experimental and code guidelines were considered as guidelines for the evaluation and strengthening of deficient column members in existing case study buildings. In addition, the critical columns (shear and bending) were selected for jacketing in the present study. The minimum number of reinforcements in the columns and the minimum section sizes, grade of concrete, and detailing assigned were designed based on IS 15988: 2013 [135]. The primary objective of this strengthening technique was to minimize the irregularity in the structures thereby uniformly distribute global building stiffness and strength, such that the design building is safe enough and economical in cost.

4.2.4.2 Addition of RC shear walls

The main objective of the addition of RC shear wall as a strengthening technique is to increase the lateral strength of the structure and correct eventual irregularities. The addition of the RC shear wall was one of the most common strengthening techniques used in Japan after 1968 Tokachi-Oki and 1978 Miyagiken-Oki earthquakes, where increase the lateral strength of reinforced concrete buildings was the primary objective (as referred in Rodriguez and Park, 1991 [125]). Later, this method was also used in the Mexico City for strengthening structures after 1985 Mexico earthquake but in less extent [137]. Although this method reveals many advantages, one main disadvantage is the increase in lateral resistance of the structures that is only concentrated at few places and also extremely increase in overturning moment, as a result strengthening of the existing foundation might be mandatory. This procedure increases own dead loads, therefore is not feasible where strengthening of foundation is not possible or the strengthening cost for foundation is unbearable, and in some cases where the existing information on foundation and original design is not known. In this section, some of the experimental works performed, their results and some design guidelines related to the RC shear wall strengthening are reviewed. Figure 4. 29 illustrate the reinforcement details for shear wall in the existing building.

Figure 4. 29 – Shear wall constructed in the existing building

Hayashi, *et al.* (1980) [138] initially performed experimental tests to investigate effectiveness of strengthening techniques on the existing infilled RC buildings. For this, six types of test specimens were selected. The experiment test intended to give a quantitative understanding on how infilled shear wall interacts with the existing RC frames and a role in improving the stiffness and strength of the structure as a whole. The new concrete shear wall full-infilled was added in the site with pressure inside the existing frame. The test results showed that the specimens with monolithic wall and RC frames failed in shear with numerous shear

cracks spreading over the wall. The specimen with shear connector of small concrete keys, and the concrete keys under the beam were out of place resulting punching shear failure at the top of the column and also observed rapid deterioration of load capacities. In addition, the paper also concluded that the load capacities of the RC frame infilled with shear wall increases by almost 3.5-5 times compared to frame only, and 0.55-0.72 times than that of the monolithic wall. The overall conclusion from the paper was that the infilled shear wall inside the existing frame can be remarkably effective as strengthening for the existing RC buildings that are short of stiffness and strength [138].

The experimental study and later analytical investigation on the influence of adding shear wall on RC frames as strengthening was carried out by Higashi, *et al.* (1984) [138]. A total of 13 specimens that includes one-bay one-storey RC frames (with poor web reinforcement columns) strengthened by adding various shear walls and scaled one third. The test adopted 10 types of strengthening methods and behaviour of all specimens was analysed using inelastic frame models. The test results revealed that strengthening increases the maximum strength capacity in the range of 1.31-4.30 times compared to bare frame. Similarly, in case of the frames with ductile beam and weak column exposed for severe earthquakes, it reveals the possibility of strengthening frames by adding the precast concrete panels [138].

In 1990, Bush, *et al.* [139] performed experimental tests to investigate an improvement in seismic behaviour of the non-ductile frame structures that can be attained after shear wall strengthening. The test specimen comprises two bays and three floors, scaled at 2/3 and was subjected to cyclic lateral load. The test results observed that the governing failure mechanism shifted from column shear failure to flexural hinging of the beams, and it was also detected that the strengthened frame behaves as monolithic that considerably increases both lateral stiffness and strength capacities [139].

Canbay, *et al.* (2003) [140] investigated distribution of internal forces in RC frames attained from the addition of RC walls. The experimental tests were performed on the test specimens with two storeys three bays and scaled at 1/3. Initially, the frame was subjected to lateral drift until damaged and then strengthened with two shear walls at the middle bay and again subjected to reversal drifts. The frame was displaced to a roof-drift ratio of 1.6% and the frame developed base shear capacity of approximately 14 kN, and again the strengthened frame was tested to a drift of 1.6% and strengthened frame developed a base shear capacity of approximately 53 kN [140].

Anil, *et al.* (2006) [141] conducted experimental tests on ductile RC frames with partially infill under reversed cyclic lateral loads. A total of 9 test specimens with one-bay and one-storey and scaled 1/3, and infill walls with aspect ratio (l_w/h_w, where l_w = infill length, h_w = infill height) and its configurations were the parameters of the study. From the test results, it can be concluded that the partially infilled frames also significantly increases the stiffness and strength compared to the bare frame. In addition, the test results also concluded that the increase in aspect ratio significantly increases the rigidity and strength, but it is highly governed by the connection between the frames and partially infill walls. Furthermore, the specimens with partial infill walls that were properly connected to both columns and beams demonstrated the most successful behaviour [141].

Altin, *et al.* (2008) [142] performed experimental tests on non-ductile RC frames, later strengthened with RC infills, and was tested under cyclic lateral loads. A total of six specimens were considered having one-bay, two storeys, and scaled at 1/3. Similar to previous conclusions, the test results detected significantly increased in both stiffness and strength capacities through the addition of RC infills. A major deficiency of this strengthening technique can be detected failure in the lap splices of the column. Therefore, the study also proposed three local strengthening techniques in order to overcome this deficiency and concluded that these techniques prevented local failures in the splice region of the columns. In addition, it also substantially increased both stiffness and strength of the infilled frames [142].

Kaplan, *et al.* (2011) [143] carried out investigation by adding shear wall on the exterior part of the RC buildings, includes two specimens of two-storey, three-bay in one direction and one-bay in other direction and scaled at one-third. The test results demonstrated that both external shear walls and the frames behave monolithically, thus only minor cracks was detected after 1% drift. In addition, if the dowels were well-designed then exterior shear wall behaves monolithic to the existing frame building that ultimately reduces the vulnerability of the existing buildings. This concludes that this approach enhances the seismic performance of the existing RC buildings [143].

Chrysostomou, *et al.* (2013) [144] studied the effectiveness of adding new RC infill as a seismic retrofit techniques on the multi-storey buildings, originally designed and detailed for gravity loads that is similar to buildings built in 1970's in the Cyprus. The main objective of the test includes the study of different connection details between the surrounding frames and the RC infill and the percentage of the reinforcement considered

in the RC infill. The test results concluded that the specimens can sustain an earthquake of 0.25 g PGA without any significant damages. In addition, this method can be used as the best retrofit techniques since it increases strength and ductility of the deficient structures or members [144].

Besides concrete shear wall as a retrofit methods, Akin, *et al.* (2016) [145] experimentally investigated an alternative approach through the introduction of the steel plate shear wall, and its effectiveness was studied on deficient concrete frames with hollow tile infill walls. A total of five specimens were considered with one-bay and two-storey which was scaled at 1/3, and tested under quasi-static lateral loading. The tests results indicated that considerable improvement can be attained in lateral load carrying capacity and energy dissipation capacities. However, this method increases the shear demand in the surrounding columns that might require a local strengthening in shear for deficient columns [145].

All the above discussed researches on the shear wall concluded that it increases the lateral load capacity, ductility and energy dissipation capacity of the existing non-ductile RC structures or deficient members as well. The numerical design procedures adopted for the shear wall which includes the design of section sizes, reinforcement details and design checks is based on the guideline IS 15988: 2013 [25, 135]. The design procedures followed are as follows [25, 135].

1. The concrete shear wall can be either ordinary reinforced type or ductile shear wall type depending upon suitable choices for the response reduction factor, R.

2. The thickness for ordinary shear wall shall not be less than 100 mm while for ductile shear wall, it shall not be less than 150 mm. For coupled shear walls, the minimum thickness shall be at least 200 mm.

3. All shear walls shall have aspect ratio less than 4:1, else the foundation system shall be investigated for its adequacy to resist overturning moments. Wall piers need not be considered.

4. For ordinary shear walls, the minimum reinforcement ratio shall be 0.0015 of the gross area in each direction. For ductile shear walls this value is increased to 0.0025 in the horizontal direction. The reinforcement shall be distributed uniformly across the cross-section of the wall.

5. The stirrups in all the coupling beams over openings for doors, passages, staircases, etc., shall be spaced at or less than d/2 (d = beam depth) and shall be anchored into the core with hooks of 135^0 or more.

6. Average shear stress in concrete and masonry shear walls, τ_{wall} shall be calculated as per the following equation:

$$\tau_{wall} = \left(\frac{V_j}{A_{wall}}\right) \tag{4.33}$$

where: V_j = storey shear at level j; and

A_{wall} = total area of shear walls in the direction of the loading.

For concrete shear walls, τ_{wall} shall be less than 0.40 MPa and for unreinforced masonry load bearing wall buildings, the average shear stress, τ_{wall} shall be less than 0.10 MPa. Similarly, the shear stress in the reinforced masonry shear walls shall be less than 0.30 MPa.

Based on the experimental investigations, it can be concluded that the lateral strength capacity of the existing structure can be considerably enhanced through the addition of concrete shear walls. However, the selection, location and its orientation should be done carefully. In the present study, the studied buildings were strengthened in order to minimize or avoid irregularities and additional eccentricities as much as possible. For this, at least two shear walls in each direction were provided and the section sizes and reinforcement details were designed based on the guidelines. The main objective of this strengthening technique is to increase the shear capacity and reduce drift concentration at single storey, mainly at the ground floor. However, the addition of shear walls at the ground floor shifts the seismic demand at the consecutive upper floors. Therefore, in most of the cases, the upper storeys might require retrofitting but with reduced sections so that the uniform inter-storey drifts can be attained throughout.

4.2.4.3 Addition of steel bracing

Steel bracings are diagonal members provided between beam and column to increase the global lateral stiffness, strength, ductility and energy dissipation capacities through the axial forces in their inclined braces developed due to earthquake ground motions. Bracing members are mainly designed to work in tension and compression, similar to a truss mechanism. Mostly, bracing frames are composed of the steel members and assigned in the selected bays without any disruption to the occupants. The main advantage of steel bracing

is the overall increase in strength and deformation capability of flexible and non-ductile infilled RC frames. It prevents early brittle failure of bracing elements and their connection, or of shear critical members as well. This method has been used for strengthening in some existing structures in Japan after 1968 Tokachi-Oki and 1978 Miyagiken-Oki earthquakes, and 1985 Mexico earthquake (as reported by Rodriguez and Park, 1994 [131]), respectively. The main disadvantage of this technique is the undesirable modifications to the original architectural features resulted by using exterior bracing. Additional disadvantages might be the associated costs and lack of field experiences among technicians and the proper connection to the existing RC elements [146]. Some experimental investigations carried out and then influence in enhancing the seismic performance and guideline for the design of steel bracing sections are reviewed.

Bush, *et al.* (1991) [147] performed experimental tests on the ductile RC frame, which was strengthened by steel X-bracing system at the exterior part of the frame using epoxy-grouted dowels. The test specimen includes two-bay and three storeys frame scaled to 2/3 and tested under a cyclic lateral load. The test results indicated that considerable increase in both stiffness and strength capacity. The lateral capacity of the strengthened frame was governed by the brace buckling and eventually leading to the column shear failure and connection failures. The columns attached at the side of the bracing elements also significantly increases the shear capacities [147].

A series of experimental tests was carried out by Maheri and Sahebi (1997) [148] to investigate the effect of different arrangement of diagonal bracing in the shear strength of the concrete frame and also evaluate the behaviour in tension and compression. The paper concluded that the diagonal steel bracing significantly increases the in-plane strength, i.e. increase almost four times relatively compared to unbraced frame. The bracing failure was recorded during the experimental works, mainly contributed by the weak connections that does not allow bracing to be fully utilized, which signifies the importance of proper connection in the bracing systems [148].

Massumi, *et al.* (1999) [149] performed a series of experimental tests on the performance of the steel bracings along with concrete framed structures. For this, eight specimens with one-bay one-storey and scaled at 1:2.5 was considered in order to select the easiest, quickest, and economic techniques. Two frames were not strengthened (un-braced) and were used as control specimens and six others were strengthened by X-bracing, and with five details of connection between frames and bracing. The test results observed that a

considerable increase in the lateral strength and/or displacement ductility of strengthened frames. It can be concluded that adding cross bracings to reinforced concrete frames, depending on the details of the connections, would significantly increase the frame stiffness and change its behaviour. In case, the steel bracing is not properly connected to each other in the midst for strengthening the concrete frames, it does not change the frame failure mechanism [149].

Maheri, *et al.* (2003) [150] carried out large number of experimental tests on the connection, so that eccentricity due to the brace frame in the existing structures can be minimized, and ultimately transfer the brace forces to the corner of the frame without local damage in the existing frame members. The techniques adopted in this research decreased the number of required connections in the internal bracing system, thus reducing the bracing construction costs [150].

Ghobarah, *et al.* (2005) [151] proposed two rehabilitation techniques; namely, fibre reinforced polymer (FRP), and X-steel braces, to investigate the suitability of each techniques and also to improve dynamic response of the existing infilled frame structures. The FRP was used as local strengthening to enhance mainly ductility and joint strength, whereas X-steel bracing at the middle bay throughout the height of the frame. The test results concluded that the FRP eliminates local brittle failure modes in the structure with insignificant changes in the structural response. Whereas, bracing alters the global building response, obtained through the increase in stiffness of the infilled RC structures and also reduces drastically the inter-storey drift [151].

The efficiency of using concentric internal steel bracing in the RC frames was experimentally investigated by Youssef, *et al.* (2007) [152], assuming moderately ductile RC frames and later braced with steel bracing. Similar to the previous conclusions, the bracing increases the lateral strength significantly and also provide large ductility relatively compared to the moment resisting frames. In addition, the study also claimed the first step for the development of the designing a guideline as it results acceptable seismic performance in the frame structures [152].

Gao, *et al.* (2013) [153] performed the experimental tests on the existing frame retrofitted with circular tubes steel braces along with carbon fibre reinforced polymer (CFRP) and later carried out numerical analysis to predict the axial load capacity, lateral and axial displacements, and material and geometrical nonlinearities. The test results concluded that

the failure of the steel bracing was mainly due to buckling under compression at the mid-length. Similarly, the application of CFRP layers increases the stiffness and strength of the braces and system as a whole [153].

Here in the present study, the design of steel bracing is based on IS 15988: 2013 [135]; i.e. a guideline for the seismic evaluation and strengthening of the existing reinforced concrete buildings. The influence in seismic performance due to addition of the steel bracing on the RC frame structures was carried out through the experimental and analytical researches as discussed above. The design of steel bracing, its layout, location, etc. were based on the guidelines, the braces were arranged in such a way that their centre line passes through the centres of the beam-column joints. The design criteria followed for the design of bracing elements are as follows [135]:

1. Slenderness of bracing member shall be less or equal to $2500/\sqrt{f_y}$ (f_y = yield strength of the steel in MPa)

2. The width-thickness ratio of angles sections for braces shall not exceed $136/\sqrt{f_y}$. For circular sections, the outside diameter to wall thickness ratio shall not exceed $8960/\sqrt{f_y}$.

3. The brace connection shall be adequate against out-of-plane failure and brittle fracture.

The following procedures were considered systematically for the design of bracing section similar to the design of axially loaded column as IS 800: 2007 [154] are follows:

1. First assume a suitable trial section and classify the section in accordance with the classification detailed in Table 3.1 (limiting width to thickness ratio) of chapter 3 from IS 800: 2007 [154] (use correction factor suitable if the section is slender).

2. Calculate the effective cross-section area, A_e as defined in clause 7.3.2 of IS 800: 2007 [154].

3. Calculate the effective slenderness ratio, KL/r, i.e. the ratio of effective length, KL to radius of gyration.

4. Calculate, λ i.e. slenderness ratio,

$$\lambda = \sqrt{\frac{f_y}{f_{cc}}} = \sqrt{\frac{f_y(\frac{KL}{r})^2}{\pi^2 E}} \tag{4.34}$$

5. Calculate Φ from the equation:

$$\Phi = 0.5[1 + \alpha(\lambda - 0.2) + \lambda^2] \tag{4.35}$$

where: α = imperfection for various buckling curves a, b, c and are given in the following Table 4.5.

Table 4.5 - Empirical values for buckling curves parameter

Buckling class	a	b	c	d
α	0.21	0.34	0.49	0.76

6. Calculate χ from equation:

$$\chi = \left[\frac{1}{[\Phi + (\Phi^2 - \lambda^2)^{0.5}]} \right] \tag{4.36}$$

7. Choose appropriate value of partial safety factor for material strength, γ_{mo} from Table 5.2 of chapter 5 of the IS 800: 2007 [154].

8. Calculate design stress in the compression, f_{cd}, following equation (Clause 7.1.2.1 of IS 800: 2007 [154])

$$f_{cd} = \frac{f_y / \gamma_{mo}}{\Phi + (\Phi^2 - \lambda^2)^{0.5}} = \frac{\chi f_y}{\gamma_{mo}} \leq \frac{f_y}{\gamma_{mo}} \tag{4.37}$$

9. Calculate the load P_d, that compression member can resist, $P_d = A_e . f_{cd}$.

10. Calculate the factored applied load and check whether the column is safe against the given loading. The most economical section can be arrived by trial and error method, i.e. repeating the above process.

4.3 Review of Numerical Modelling Approaches

4.3.1 Numerical modelling of the RC frame

As presented in the previous Section 4.2.3, the models were divided into different groups; namely, global models, microscopic models and discrete finite element (member) models. In global models, the nonlinear response of a structure is represented at selected degrees of freedom. This type of model can be used for a "preliminary evaluation of the inter-storey drifts and ductility demands" [155]. In microscopic finite element models, each finite element of the structures is discretized into the member and joints separately. Similarly, in discrete finite element modelling approach, the structure is modelled through inter-connected frame elements with either lumped or distributed nonlinearities. Among all, the member-type is the one of the best modelling approaches as it provides better accuracy in representing building response, reduces the computational time, effort, cost and simple to use [156].

At element level, the material nonlinearities of beam-column members are modelled from lumped plasticity formulations to distributed plasticity formulations depending on the finite methods [157], as illustrated in Figure 4.30.
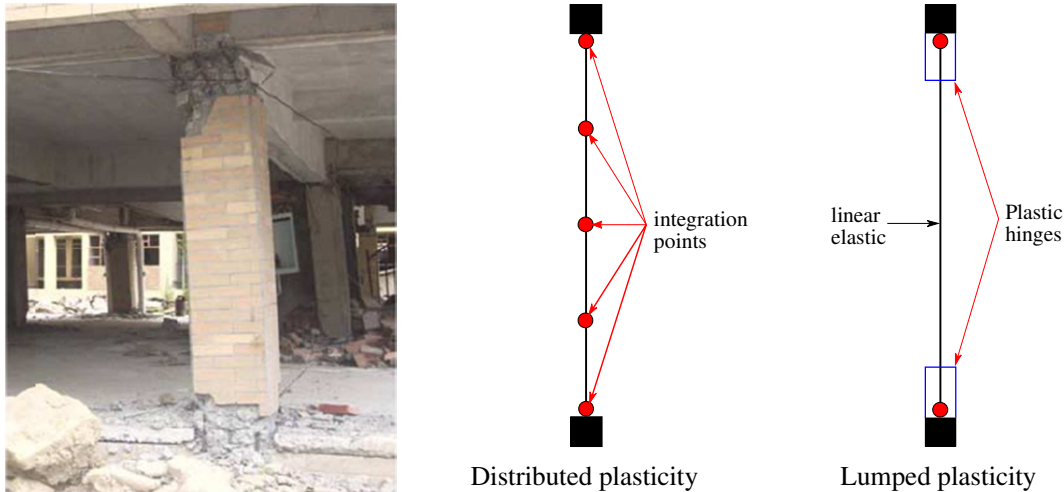
Figure 4.30 – Element model approach for nonlinear numerical modelling of RC beam/column elements (Rodrigues, H., 2012) [158]

In the lumped plasticity models, it is assumed that nonlinear behaviour of the beam-column members is concentrated at the ends or at the pre-determined sections [159]. It assumes that the nonlinear behaviour is located at the centre of the plastic hinge zone, generally located at each end of RC elements [160]. The lumped-plasticity model was initially studied by Clough, *et al.* (1965) [161], and further improvement in the model considering the bending and axial force interaction [162, 163], biaxial bending interaction [164, 165] and bending/shear interaction [163, 166]. Rodrigues, H. (2012) [158] describes the lumped-plasticity models as a simplification of the real behaviour, and therefore, so have inherent deficiencies. This modelling approach is not applicable for the RC elements like shear walls in which bending governs the structural behaviour and this type of elements are expected to possess significant shear cracks along at the mid-height. Therefore, the lumped plasticity modelling assumption for such elements are not practicable and accurate [167].

Distributed plasticity approach is associated with the distribution of nonlinearity along the element with a certain number of controlling sections, which are integrated in order to attain the global nonlinear response of the elements. Initially, the concept of distributed plasticity model was introduced by Otani, S. (1974) [168]. The major advantage of this modelling approach is that it does not consider the predetermined length, but each section

can incur the inelasticity in the whole response range (linear and nonlinear). The modelling approach requires more computational time and capacity, and it provides the results which are approximately closer to reality [169]. These formulations are extend in the work of Taucer, *et al.* (1991) [170], Spacone, *et al.* (1996) [155], and Arede, A. (1997) [156].

The literature reviewed by Rodrigues, H. (2012) [158] concluded that the member-type modelling approach are found to be accurate representations of the key features of RC elements behaviour. However, the simplified modelling approach, such as bounding surface models, spring models or lumped plasticity models have major advantage in the representation of global seismic response with less input preparation and less computer time and storage [158].

In this study, the numerical analyses were carried out through SeismoStruct software [22] for the entire case study buildings. This is a fibre based model that provides an accurate estimation in capturing the complex bi-axial behaviour under constant and varying loads. The software is also based on the finite element analysis, and the spatial frame behaviour can be predicted under various analyses, such as static or dynamic analysis, which considers the material inelasticity and geometrical nonlinearities. The program can also perform different analyses, such as nonlinear static and dynamic analysis, eigenvalue analysis, incremental dynamic analysis, adaptive and conventional pushover analysis, and non-variable static loading. The accuracy of the software was evaluated through the comparison between experimental and numerical results. For this, the software offers verification reports that contain large set of assumptions in the model and its validation with the experimental results through linear to nonlinear analyses. In addition, Smyrou, *et al.* (2011) [171] and Rodrigues, *et al.* (2012) [158] also performed large set of numerical analyses and concluded that the SeismoStruct results hold a good agreement with the experimental results. Despite large advantage, there exist several limitations in the SeismoStruct software such as it cannot capture shear failure modes of column and out-of-plane failure of infill walls.

At the element level, the lumped plasticity modelling approach was employed to introduce the beam-column nonlinearities. The cross-section behaviour is represented by the fibre-based approach, and each fibre is associated with uniaxial stress-strain relationship. The sectional stress-strain state of the beam-column element is obtained through the integration of the nonlinear uniaxial stress-strain response of the individual fibres, such that all structural elements include beam and column for all case study buildings are discretized

into five integration sections and again sub-divided into 150 section fibres, as illustrated in Figure 4.31. A minimum number of 3 Gauss-Lobatto integration sections are required to avoid under-integration, but such options will in general does not simulate the spread of inelasticity in an acceptable way. Therefore, Calabrese, *et al.* (2010) [169] concluded that each element needs to integrate a minimum of six in order to predict a stabilized local response.
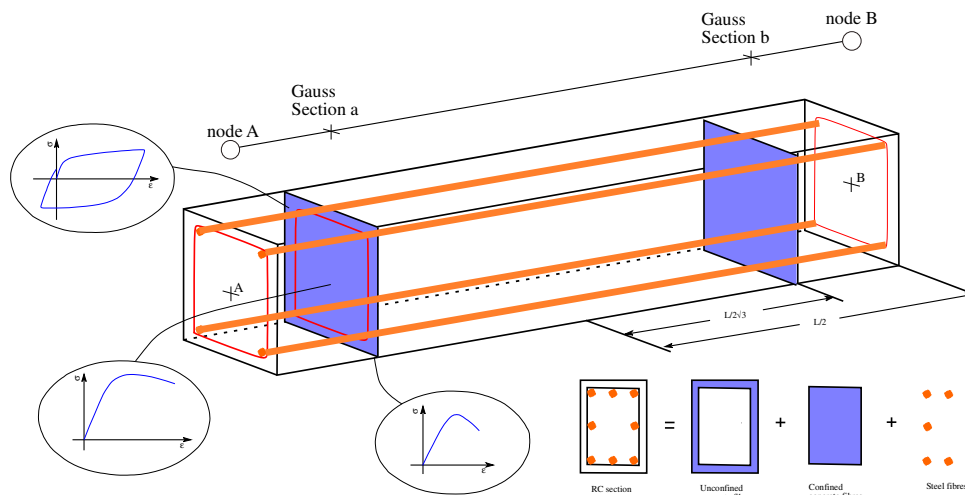
Figure 4.31 – Discretisation of typical RC cross-section (SeismoStruct, 2004) [22]

The beam and column elements were modelled as 3-D (three dimensional) inelastic force-based frame element type, connecting two adjacent nodes. These elements were discretized into 5 integration sections and at the equilibrium section level, the number of fibre was set 150. The concrete uniaxial material model is based on the constitutive relationship proposed by Mander, *et al.* (1988) [172] and cyclic rule proposed by Martinez-Rueda and Elnashai (1997) [173], initially programed by Madas and Elnashai (1992) [174] that is based on uniaxial nonlinear constant confinement model. Lateral transverse reinforcement confinement effect was incorporated by Mander, *et al.* (1993) [175], whereby constant confining pressure assumed throughout the entire stress–strain range. Uniaxial steel model as proposed by Menegotto and Pinto (1973) [176], coupled with isotropic hardening rules proposed by Filippou and Fenves (2004) [177]. The Bauschinger effect [178] considered in this model to represent the steel degradation, and consequently both the concrete and steel (i.e. column stiffness) degradation under cyclic loading, Dumaru, *et al.* (2016) [10]. Under uniaxial compression, the concrete strain corresponding to the point of unconfined peak stress was considered 0.002. For the concrete model, the tensile stress capacity was assigned as 0. The Poisson's ratio (ν_c) of concrete under uniaxial compressive stress was

assumed to be 0.2. The modulus of elasticity of concrete (E_c) was calculated using the empirical formula given by IS 456:2000 [136], i.e. $E_c = 5000\sqrt{f_{ck}}$, where f_{ck} is the concrete compressive strength at 28 days. The specific weight of the concrete material (γ_c) was assumed as 24 kN/m^3. It is to be noted that the present modelling strategy is based on fibre-based approach and does not consider the nonlinear shear behaviour. In addition, failure in RC columns may occurs under shear during seismic events and in cases, where masonry infill walls with opening possess higher potential to develop shear force and can lead to short column failure if not properly designed for shear or constructed. However, shear failure caused by the unexpected rupture of the element and total strength capacity in the elements are not examined [179].

4.3.2   Numerical modelling of the masonry infill walls

As discussed in the previous section the infill walls can be modelled through three different modelling approaches; namely, detailed micro-modelling, simplified micro-modelling and macro-modelling. However, the present study modelled the infill masonry walls through a simplified macro-model approach proposed by Crisafulli (1997) [11], where six struts model was utilized in which two pairs act as compression-tension diagonal struts that transfer the axial loads between the diagonal corners and a pair as shear struts with a shear spring to carry the shear from the top to the bottom of the infill walls, as illustrated in Figure 4.32. It consists of four internal nodes to account for the width and height of the columns and beams, respectively, whereas four dummy nodes are employed to account for the contact length between the frame and the infill panel [22]. No special intermediate bonding at the interface between the infill walls and frame elements was assumed, thus the forces (i.e. moment and shear forces, etc.) from infill walls were transferred only at the connecting end nodes of the column. All the masonry modes of failure are difficult to capture due to large uncertainties and complexity involved, thus in the present strut model common failure caused by shear was considered as utilized by Smyrou, *et al.* (2011) [171]. The diagonal strut member has same thickness as that of masonry without considering the plaster and its length equal to the diagonal length between compression corners of the frame. The effective width of the diagonal strut was estimated using the relation proposed by Holmes, M. (1961) [62]. The cross-section area obtained as the product of effective width and thickness of the strut. The opening in the infill walls were integrated by reducing

the value of strut area by a value ranged from 30% to 40%, which is comparable as one proposed by Pinho and Elnashai (2000) [180].
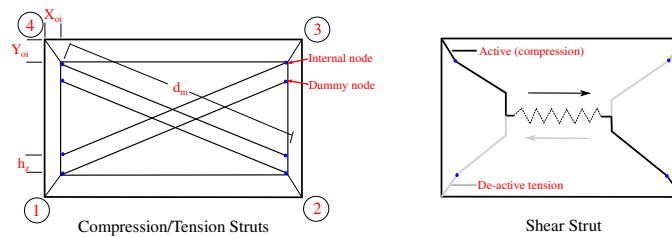
Figure 4.32 – Six struts model for the infill panel proposed by Crisafulli, 1997 [11]

The geometrical properties of the diagonal strut elements were determined using the stiffness method, as discussed in the previous section. The other important mechanical properties of the infill element, such as unit weight, modulus of elasticity, compressive strength, shear bond strength and infill panel thickness were assigned from NBC 205: 2012 [21]. All other remaining strut curve parameters and shear curve parameters were assigned default from the program. The program also allows the out-of-plane failure drift and once the out-of-plane drift in the infill panel exceeds the given threshold drift then the elements dictates as de-activation, which indicates that the panel failed and does not contribute in the building response thereafter. Table 4.6 shows the material properties adopted for the infill walls which was initially assumed and used by Chaulagain, *et al.* (2013) [23] and later by Rodrigues, *et al.* (2018) [181].

Table 4.6 – Material properties adopted for infill wall panels in the numerical model (mainly for MRT buildings)

Modulus of elasticity E_m (GPa)	Compressive strength f_m (MPa)	Diagonal tensile strength f_t (MPa)	Shear stress τ_0 (MPa)	Maximum shear stress τ_{max} (MPa)	Coefficient of friction μ	Maximum stress ε_m	Ultimate stress ε_u	Closing strain ε_{cl}
2.3	2.3	0.575	0.3	1	0.7	0.012	0.024	0.003

4.4 Analysis Type

The seismic performance of the selected buildings was evaluated through two methods; the nonlinear static method and dynamic time history analyses considering the nonlinear material response. In the dynamic time history analysis, the structures were subjected to a large number of real or artificial ground motion accelerations or earthquakes. Hence, this approach can be considered as the most reliable tools to examine the seismic performance of the buildings, but requires large computational time and it is hard to interpret the results.

4.4.1 Static analysis

The structural response in the form of demand and capacity are evaluated through the static analysis such that the strength and deformation can be attained at various limit states, i.e. elastic, yielding, ultimate, and collapse states. If the damping and inertial effects are assumed as negligible, the static analysis is also considered as a special form of dynamic analysis. The material inelasticity and geometrical nonlinearity were considered in this method. Therefore, in earthquake engineering, the static analysis is one of the most common methods used for the seismic design of the building considering the spectrum of the site, few methods were discussed as follows [182].

4.4.1.1 Equivalent static analysis

The seismic performance assessment of the RC structures can be investigated through a simplest analysis tool known as the equivalent static analysis, also referred as equivalent lateral force method (EFL). This method considered the material behave as linear elastic, i.e. material follows Hooks law, and geometrical nonlinearity which considers the second-order (P-Δ) effects [182]. In this method, the inertial forces assumed to act during earthquakes are converted to equivalent lateral loads and these equivalent forces along with the gravity loads are applied at the nodes of the frame throughout the height of the structures. In this method, generally two types of loads pattern, i.e. inverted triangular and parabolic load patterns were subjected, depending upon the fundamental period and vibration modes of the structures. The predetermined mode shapes are identified with the help of which the magnitudes of lateral forces in each storey are computed. Elnashai and Di Sarno (2008) [182] concluded that the first vibration mode is the dominant in the entire structures, and triangular load pattern considered in the equivalent static analysis for the estimation of the horizontal forces are approximately good and precise.

The steps performed for the equivalent static analysis as mentioned in Elnashai and Di Sarno (2008) [182] are as follows:

1. Assume a lateral load pattern distribution.
2. Apply the gravity and horizontal loads.
3. Evaluate displacements and hence internal forces.
4. If scaled forces are used, the ensuing displacements also require scaling.

This method is applicable for the structures when acted upon the forces until the material initiate inelasticity and the estimated deformation to this state is also approximate and quite good. However, this method could not define the important characteristics or in other words neglected, such as degradation of stiffness and strength, hysteretic effect in the infill panels, and internal forces (chord rotations and moment curvatures) in the structural elements, and so on [182].

4.4.1.2   *Static pushover analysis*

The estimation of the strength and deformation demands in the structures is evaluated through a pushover analysis and these demands are compared with the capacities to identify the various performance levels of the structures. The performance assessment can be done through building response parameters, such as roof displacement, global drift, inter-storey drift, deformation in the structural and non-structural elements, and element and connection forces. It is observed from various literatures that some of the parameters, such as estimation of inter-storey drift and its distribution throughout the height, force and displacement demands on brittle and ductile members, respectively, identification of likely failure modes, global structural behaviour due to effect of individual member strength deterioration, and so on, can be attained which cannot be obtained from advance analysis (i.e. elastic static and elastic dynamic analysis) [182].

The structural response evaluated from the pushover analysis is generated assuming the system as the equivalent single degree of freedom (SDOF) and it is found that if single mode can control the response, then it remains constant in the time history as well [183]. Based on the lateral force distribution patterns, either uniform or inverted triangular load patterns; the pushover analysis is grouped into two methods, i.e. conventional pushover and adaptive pushover analysis, where the former analysis considers the forcing function as constant during the analysis and the latter one considers the variation with respect to the vibration modes of the structure in the elastic range, which is discussed as follows.

4.4.1.2.1   *Conventional pushover analysis*

The conventional pushover analysis consists of a constant lateral force or displacement pattern type to the structures under constant gravity loads. The material inelasticity and geometrical nonlinearity is considered in this method. The pushover analysis estimates the

capacity of the structures in which certain functions acts to represent the inertial force due to earthquake ground motions. This method assumes the structures as in a static equilibrium and incremental iterative solutions are introduced. The iteration proceeds until the program fails to converge when the state can be assumed to have reached the target displacement. The capacity curve is the plot of the global base shear V_{base} plotted along the ordinate versus roof displacements, δ_{top} or global drift along the abscissa, representing the variation of the base shear capacity for corresponding roof displacements. Elnashai and Di Sarno (2008) [182] defined certain steps to carry out the conventional pushover analysis which are as follows.

1. "Apply the gravity loads in a single step.

2. Assume a lateral load pattern either in terms of displacement shape Φ or force vector **V**.

3. Select a controlling displacement node, e.g. the roof centre of mass for buildings.

4. Determine the vertical distribution of lateral forces V_i ($= m_i \, \Phi_i$), if the displacement vector Φ has been selected in 2. Conversely, determine the vertical displacement distribution Φ_i.

5. Compute the incremental - iterative solution of the static equilibrium equations. This step is repeated until the target performance level, e.g. the target displacement of the roof centre of mass, is reached. The target displacement is intended to represent the maximum displacement likely to be experienced during the expected earthquake ground motion.

6. For structures that are not symmetric about a plan perpendicular to the applied loads, the lateral load or displacement pattern should be applied in both positive and negative directions.

7. Determine the base shear V base, top displacement δ top, the storey shear V_i and storey drift δ_i .

8. Plot the system (V base versus δ top) and the storey (V_i versus δ_i / h_i) pushover curves".

Elnashai and Di Sarno (2008) [182] stated that "the uniform pattern, which is proportional to the total mass at each floor, should be used along with the modal pattern. The latter can be the inverted triangular load pattern distribution, which is when more than 85% of the total mass participates in the fundamental mode in the direction under consideration". The limitations associated with the static analysis methods can be partly overcome considering

at least two load pattern, i.e. uniform and triangular load pattern along the main axis of the structures.

4.4.1.2.2   *Adaptive pushover analysis*

The adaptive pushover analysis is a particular way to perform the static analysis, which allows changes in the inertial forces distribution along the global drift, as illustrated in Figure 4.33. This method overcomes the main limitations associated with the conventional pushover, which requires constant force throughout the analysis. Similarly, the results of the conventional pushover analysis, such as the horizontal forces and the displacements does not fully reflect the inelastic characteristics of the buildings [184].
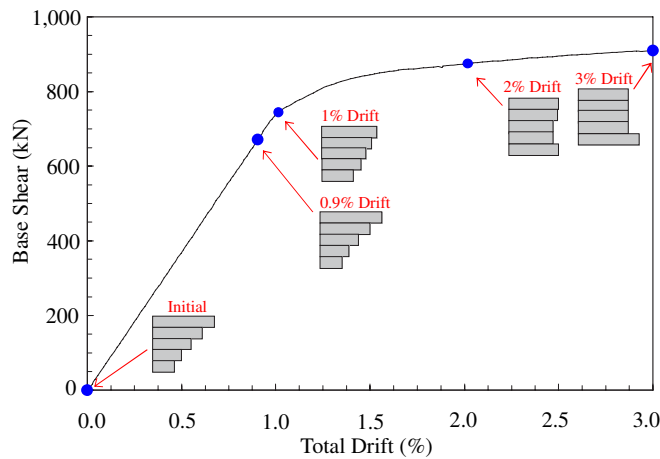
Figure 4.33 – Changes of the distribution of inertial forces in a regular framed building (adaptive force distribution) as presented by Elnashai and Di Sarno, 2008 [182]

The different types of steps to be followed to carry out the adaptive pushover analysis of the structural system, as defined by Elnashai and Di Sarno (2008) [182] are as follows.

1. Apply the gravity loads in a single step.
2. Perform an eigenvalue analysis of the structure at the current stiffness state. The elastic stiffness can be used for the initial step. Eigenvalues and eigenvectors are computed.
3. Determine the modal participation factors Γ_j for the jth mode using equation:

$$\Gamma_j = \frac{L_j}{M_i^*} \tag{4.38}$$

In which, M_i^* is the generalised mass given as:

$$M_i^* = \Phi_j^T M \Phi_j \tag{4.39}$$

$$L_j = \Phi_j^T M_i \tag{4.40}$$

4. Compute the modal storey forces at each floor level for the N modes deemed to satisfy mass participation of about $85 - 90\%$ of the total mass. These forces $F_{i,j}$ are estimated at the ith level for the jth mode (being $1 \leq j \leq N$) as given below:

$$F_{i,j} = \Gamma_j M_i \phi_{i,j} g \tag{4.41}$$

where: M_i is the seismic mass of the ith level, g is the acceleration due to gravity.

5. Perform a static pushover of the structure subjected to the storey forces computed in step 4 and corresponding to each mode independently.

6. Estimate element (or local) and structure (or global) forces and displacements by means of square root of the sum of squares (SRSS) combination of each modal quantity for the kth step of analysis. Add the above quantities, i.e. forces and displacements, to the relevant quantity of the $(k-1)^{th}$ step.

7. Compare the values established in step 6 to the limiting values for the specified performance goals at both local and global levels. Return to step 2 until the target performance is achieved.

Research to refine the adaptive pushover method is still ongoing for both buildings [185-188] and bridges [189, 190]. Figure 4.34 presents the comparison of the capacity curve for conventional and adaptive analysis, in both regular and irregular systems. The two load patterns were employed for the conventional pushovers, i.e. uniform and triangular, whereas adaptive pushover analysis closely uses the distribution of inertial forces as the time variant. It can be observed from the plot that the lateral capacity of the regular building shows the upper boundary using the conventional pushover or the uniform load distribution, which is not sufficient to capture the dynamic characteristics of the building, eventually concluding that uniform load pattern might mislead the structural response [182]. The various conclusions attained from the different literatures stated that adaptive pushover is far superior compared to the conventional pushover; however, this is not always true and not guaranteed [182-184]. Considering all these, further pushover analysis and results for the entire case studied buildings will be performed based on the adaptive pushover.
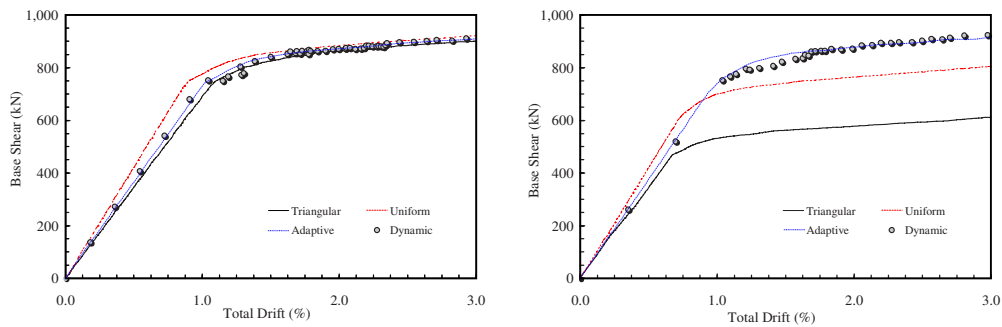
Figure 4.34 – Conventional, adaptive and dynamic pushover curves for different structural modes: regular (left) and irregular (right) systems as defined by Elnashai and Di Sarno (2008) [182]

4.4.2 Incremental dynamic time history analysis

The estimation of the demand under the seismic loading for a range of IMs through a series of nonlinear dynamic analysis is also termed as incremental dynamic analysis (IDA). This procedure was initially developed and proposed by Vamvatsikos, *et al.* (2002) [191]. The method provides information on different state of the building starting from material elasticity to yielding of various structural components, and finally the total collapse of the building. The various suites of selected ground motion records, and suitably scaled to a range of intensity measures (IMs) are applied in the structural model in order to produce large number of curves plotted for the same structure, such that the building's response are plotted along the abscissa and IMs along the ordinate, also known as IDA curves [191]. The IDA curves are similar to the static pushover curves, where the former curve provides the general information on the performance of the structure at large IMs and latter curve provides the load capacity of the structure at the corresponding displacement. The major advantage of the IDA curves is that it provides better information on the structural consequence even for rare ground motions. A sufficient number of ground motion records under multiple scaled IMs should be employed in the analysis, as the IDA curves are highly dependent upon the number of recorded sample. Hence, in this way, the uncertainty associated with the building response can be captured coming from record-to-record variability. The choice of a suitable intensity should be carefully done so that the structural response can be obtained throughout its entire range of behaviour [182]. Furthermore, the ground motion scaling levels reflect increasing level of intensity that is defined by a parameter usually termed IM [12].

The various steps considered for obtaining IDA from each earthquake record, defined by Elnashai and Di Sarno (2008) [182] are as follows:

1. Define a suitable earthquake record consistent with the design scenario.

2. Define a monotonic scaleable ground-motion intensity measure, e.g. the PGA, PGV, PGD or a combination.

3. Define a damage measure or structural state variable, which could be force-based (maximum base shear, bending moment or axial load) or deformation-based (maximum storey drifts or member rotations) parameters. Energy-based quantities, such as ductility and/or hysteretic energy are also suitable damage indices.

4. Define a set of scale factors to apply for the selected intensity measure in 2.

5. Scale the sample record in 1 to generate a set of records that will test the structure throughout its response range, from elastic response to collapse.

6. Perform response history analysis of the structural model subjected to the scaled accelerogram at the lowest intensity measure.

7. Evaluate the damage measure in 3 corresponding to the scaled intensity measure in 2.

8. Repeat step 6 to 7 for all the scaled intensity measures.

The structure's response (or demand) can be defined by any structural or non-structural parameters, where the structural response for each IM can be in the form of local state, i.e. the internal chord rotations, plastic hinge formation; whereas, in the global response, it can be maximum inter-storey height, peak roof displacement, global ductility and hysteretic energy, and maximum base shear, etc. In the performance based earthquake engineering (PBEE), it may be appropriate to represent the various structural characteristic, such as threshold limit states and mode of failure through at least two damage measures (DMs), resulted from the same nonlinear analyses [191]. In this study, the absolute maximum inter-storey drift along the height was considered as the structural demand to represent the structural behaviour or response. It would not be practical or even unnecessary to assess individual component of building damage; hence, maximum inter-storey drift demand parameter was selected, and it also provides good co-relation in estimation of structural or non-structural damages and associated economic loss. In addition, using the IDA method for large scale IMs for different ground motions, a more direct comparison of the fragility curves between the structures can be performed, since the IM is common to all.

4.4.2.1 *Ground motion records selection procedure*

The seismic vulnerability assessment of each case study building was performed using the IDA method. For this, a total of 21 recorded real ground motion earthquakes were selected from the real seismic events according to Macedo, *et al.* (2013) [192], that matches with the target response spectra of the site. The present study selected the response spectrum for the Kathmandu Valley, similar as defined in IS 1893 (Part 1): 2002 [30], for the zone V and medium type of the soil, demonstrated in Figure 4.35 (a). Thapa, *et al.* (2013) [193] estimated the PGA values at bed rocks of Nepal using a probabilistic approach. According to Thapa, *et al.* (2013) [193], the annual probability of exceedance of PGA values for a range of 0.07-0.16g is 63%, PGA between 0.21-0.62g is 10%, and between 0.38-1.1g is 2%, for earthquakes of return period 50 years. Similarly, Shrestha, S. (2014) [194] predicted the PGA values for the Kathmandu Valley. The study revealed that there is 2% annual probability of exceeding, 0.31g PGA, in 50 years that is equivalent to Modified Mercalli Intensity (MMI) of VIII. Furthermore, there is 10% annual probability of exceeding, a PGA of 0.18g, having earthquakes of 50 years return period, i.e. similar to MMI of VII. An earthquake of MMI IX that is comparable to the 1934 Nepal-Bihar earthquake of PGA between 0.5-0.55g has 0.7% annual probability of exceedance in 50 years [194]. Subedi, *et al.* (2016) [195] established that the earthquakes of 475 year return period can have maximum PGA of 0.3g for hard soil, 0.4g for medium soil, and 0.5g for soft soil.

(a)   (b)
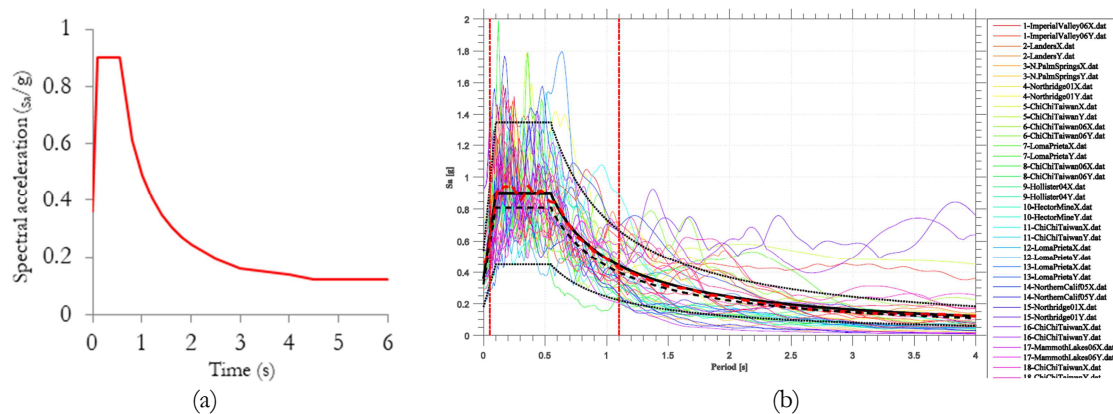
Figure 4.35 – (a) Expected response spectra for zone V and medium soil as per IS 1893:2002 and (b) elastic spectra of selected real ground motion according to Macedo (2013) [192]

The NBC 000: 1994 [24] defined an earthquake of return period 50 years for the ordinary importance residential buildings, whereas for the strengthened buildings the return period was selected as 300 years. Therefore, a return period between 50 years and 300 years could be used for defining the damage and safety limit, respectively. Considering previous

researches prediction in context of Nepal, the selected earthquakes have PGA ranges between 0.08g and 0.921g. The selected ground motion records also match the target spectrum having range of periods between 0.1 and 1.1 second that covers the fundamental periods of the entire case study and modified MRT buildings [196]. All the selected real ground motion records also ensure that for period range, the spectral values of individual natural records are within a bound defined by ± 50% of the target spectral values. These selected ground motion records were scaled at the interval of 0.1g up to 0.5g. The maximum response under two components is usually more than one component in linear and nonlinear behaviour [197, 198]. Therefore, the seismic excitation was subjected as bi-directional component of the earthquakes applied at the support of the structures for a critical angle of 0 and 90 degree to obtain the critical angle of incidence.

4.4.2.2   *Definition of drift limit states*

Limit state is related with the state of a structure beyond which it no longer fulfils the defined design criteria. In other words, it is a measure to describe the state of the structure based on predefined level of damage, such as cracking, yielding and collapse. The structure's response in the form of displacement or drift is mainly governed by the stiffness, strength and ductility factors of the particular building. Other factors that influence the deformation of the structures are applied loads, confinement and shear span. In a building, the ratio of difference of the displacements between the two adjacent floors to the respective height of the floor is represented as inter-storey drift ratio. The design and the serviceability check of the structural elements, such as that of the beams and the columns are directly related to the inter-storey drift and the damage in each floor can also be associated with the inter-storey drift of that floor. In addition, the final softening can be used as damage index to identify the global damage in the structures, in which the damage index can be either in the elements level or in the storey level [199].

Several researchers and various international guidelines proposed the threshold drift limits for the different types of buildings to define the performance limit states for RC building, such as FEMA-273 (1997) [200], SEAOCO-VISION (2000) [201], Rossetto, *et al.* (2003) [202], Ghobarah, A. (2004) [199], etc. The various performance levels associated with the overall building response in terms of inter-storey drift limits for the frame without infills (i.e. bare frame) were proposed by FEMA-273 [200], which defines three performance

levels, presented in Table 4.7, such as immediate occupancy, life safety, and collapse prevention.

Table 4.7 – Inter-storey drift limit proposed by FEMA-273 [200]

	Structural Performance Levels		
ISD_{max} (%)	Collapse Prevention	Life Safety	Immediate Occupancy
	>4%	1-2%	1%

Furthermore, the threshold inter-storey drift limits for the bare structure was also proposed by SEAOC-VISION (2000) [201], as presented in Table 4.8. Four performance levels were defined to represent the damage state of the bare frame building in the guideline, such as fully operational, operational, life safety and near collapse.

Table 4.8 – Inter-storey drift limit proposed by SEAOC-VISION (2000) [201]

	Performance level			
ISD_{max} (%)	Fully operational	Operational	Life safety	Near collapse
	1	1-2	2	4

Both FEMA-273 [200] and VISION [201] proposed inter-storey drift limits for the bare frame buildings, thus the present study scope does not matches with these guidelines, and hence, only referred as reference. Rossetto, *et al.* (2003) [202] and Ghobarah, A. (2004) [199] proposed a threshold inter-storey drift for the masonry wall infilled in the RC frame building. The threshold drift recommended by Ghobarah, A. (2004) [199] is presented in Table 4.9, which defines six limit damage states. These limit states observed more conventional and conservative, as the infilled RC buildings were expected to collapse for a drift above 1%, which does not seems practicable and is not a usual scenario with recorded previous earthquake damages and collapse of the infilled buildings around the globe. Such buildings undergo large drift before the collapse of the building, thus this approach does not appears realistic based and is not considered for the performance assessments of case study buildings in the present study.

Table 4.9 – Inter-storey drift limit proposed by Ghobarah, A. (2004) [199]

ISD_{max} (%)	No damage	Light damage	Moderate damage	Irreparable damage	Partial collapse	Collapse
	<0.1	0.2	<0.5	> 0.5	0.8	>1.0

Therefore, the present study aims to evaluate the state of the building through the comparison of threshold drift as proposed by Rossetto, *et al.* (2003) [202], as presented in Table 4.10. It defines seven damage states, i.e. ranges from none to collapse for the

structural and non-structural elements to identify building states at each IM corresponding to proposed ISD_{max} presented in Table 4.10. As observed in the table, the drift limit is applicable for large building cases, such as non-ductile MRF, infilled MRF and shear walls. The present study considered four different building cases (one bare frame and other infilled), thus for consistent comparison, the inter-storey drift associated with the all categories were considered.

Table 4.10 – Inter-storey drift ratio limit proposed by Rossetto, *et al.* (2003) [202]

Damage state	All	Non-ductile MRF	Infilled MRF	Shear-walls	Expected damage in structural and non-structural elements
None	0	0	0	0	No damage
Slight	0.13	0.32	0.05	0.26	Fine cracks in plaster partitions/infills
Light	0.19	0.43	0.08	0.34	Cracks initiates at wall-frame interfaces, diagonal cracking of walls, limited crushing of bricks at beam-column connections
Moderate	0.56	1.02	0.30	0.72	Increased brick crushing at beam-column interfaces, some diagonal shear cracking in members especially for exterior frames
Extensive	1.63	2.41	1.15	1.54	Partial failure of many infills, heavier damage in frame members, some fail in shear
Part. Collapse	3.34	4.27	2.80	2.56	Beams and/or column fail in shear causing partial collapse, near total infill failure
Collapse	>4.78	>5.68	>4.36	>3.31	Complete or impending building collapse

4.5 Development of Fragility Curves

The vulnerability assessment of the selected buildings are evaluated through the fragility curves, which is a statistical tool that represents the state of damages in the building through a conditional probability of exceedance, due to probable earthquakes of large ground intensities. The structural collapse in terms of mean annual rate can be evaluated as a combination of hazard curve for a site and the estimated fragility functions of the building [203, 204]. The fragility functions for a building can be estimated through nonlinear dynamic analyses, such that each earthquake is scaled over a range of IMs. Incremental dynamic analysis (IDA) is the most common method in which the earthquake ground motions, either real or artificially generated for the site (see Figure 4.35) are suitably scaled and applied at the supports of the building and damage states are identified until it reaches the collapse of the building [191, 205].

Various methods, such as detailed field survey to state the damage level, various types of structural analyses, i.e. static to dynamic time history analysis, and in some cases the engineering judgement can also be carried out to derive fragility functions [206-208]. In the present study, the fragility functions were established through an analytical procedure developed from nonlinear time history analyses subjected by the selected earthquakes, discussed in detail in the previous section. Padgett, *et al.* (2008) [209] performed large scale of the nonlinear dynamic analyses for bridges and proposed a methodology to generate fragility curves. This approach is simple and easy to understand the various types of parameters associated with it. "The conditional probability of the seismic demand (D) placed upon the structure exceeding its capacity (C) for a given level of IM", is given by equations (4.42) to (4.44) [209].

$$\text{Fragility} = P[D \geq C|IM] \tag{4.42}$$

And, the average value of seismic demand, S_d, is represented as:

$$S_d = aIM^b \tag{4.43}$$

where: a and b are unknown regression coefficients. The conditional probability of state for each IM is calculated assuming the seismic demand as lognormally distributed, and the relation is given by following equation:

$$P(D \geq C|IM) = 1 - \Phi\left[\frac{\ln(C) - \ln(S_d)}{\beta_{D|IM}}\right] \tag{4.44}$$

"where: $\Phi(.)$ is the standard normal cumulative distribution function, S_d is the average value of seismic demand obtained from equation (4.43), and $\beta_{D|IM}$ is the logarithmic standard deviation (dispersion) of the demand conditioned on the IM, which is estimated in the regression analysis [209]. Here, the ultimate result of developing a probabilistic seismic demand model is to provide a relationship between peak component responses and ground motion intensity through a probabilistic model".

4.6 Conclusions

Several experimental and analytical investigations have been carried out to study the infill walls interaction with the surrounding frames over the past six decades and concluded that they behave monolithic to resist the lateral seismic loads. In addition, it was also recorded that the introduction of infill walls considerably increases both stiffness and strength capacity, but the deformation capacity was largely reduced. However, due to its brittle behaviour under compressions, the infill walls are most likely to fail under various failure modes after attaining the maximum base shear capacity and the base shear is to be resisted by the frame structures only. Furthermore, the infill walls with openings changes the failure modes and also the dynamic behaviour of the infilled RC buildings. In addition to the positive contributions, the researchers also concluded its negative impact that leads to the shear cracks in the columns if strong infill panels were provided in the weak frames.

The various modelling strategies for the infill walls were discussed, such as detailed and simplified micro-modelling and macro-modelling approaches. In case, the accuracy was the primary objective, several researchers recommended a detailed micro-modelling approach, but it requires large computational time, efforts and input data, whereas the macro-modelling approach although less accurate, is mostly used for the modelling of three-dimensional structures, due to low computational cost, time and efforts. The macro-modelling of the infill walls in the three-dimensional models has been integrated as diagonal struts, which works in both tension and compression. For this, several researchers defined and proposed the infill walls modelling approaches, i.e. from single to multiple struts. The in-plane properties of the strut models were defined through two methods, i.e. stiffness and strength methods, where the former one was performed to determine the geometrical properties (i.e. width) of the diagonal struts and the latter one to define the force-displacement relationship (hysteretic) that relates with the area of the strut to define the consecutive behaviour of the infill walls. Initially, the single strut model was proposed, but could not capture the distribution of the bending moment and shear force and also could not describe the interaction of infill walls with the surrounding frames. Later, it was modified and proposed double strut model and multiple struts models. However, the present study modelled the infill wall for the entire case study buildings as six strut model as proposed by Crisafulli, F. (1997), as it could account all the tension, compressions and shear forces acting in the infill walls.

Several literature reviews in the strengthening techniques and its influence have been discussed in the study. The experimental investigations found that all the strengthening measures considerably enhances the stiffness, strength, ductility and energy dissipation capacities of the existing non-ductile RC buildings. It also enhances the strength and deformation capacities of the deficient structural members. Finally, the generation of fragility curve was discussed, through which vulnerability of the building can be identified as a conditional probability of exceeding damage states, with respect to to a threshold drift limit proposed by Rossetto, *et al.* (2003).

Chapter 5.

Numerical Analysis and Results Discussion

5.1   Introduction

The typical damage and failure modes observed in infilled RC frame buildings after the Gorkha earthquake were presented and discussed in detail in Chapter 2. A large number of infilled RC frame buildings reported light to moderate structural damage and some even collapsed. As discussed in Chapter 3, the repair and maintenance are still being carried out in existing RC buildings that had moderate to extensive structural damage. This is being done for many of them without consultation with design engineers. Such practices are likely to create a benefit of doubt about the efficiency of the repair and/or the retrofitting work.

There could be several causes for the damage and collapse of the infilled buildings. However, after the site surveys, it was clear that the main failures were associated with the soft-storey mechanism. This was mainly due to the irregular distribution of the infilled walls, insufficient structural sections and poor reinforcement detailing. After the site surveys, most of the existing RC frame buildings in Nepal, namely non-engineered and pre-engineered buildings, are unlikely to meet the seismic demands in future earthquakes. Therefore, these remained infilled buildings need immediate need strengthening. For such existing RC buildings (both damaged and non-damaged), the design engineers are encouraged to carry out detail site investigations to identify the state of the structural and non-structural elements. Later, a detail seismic performance assessment needs to be carried out to evaluate the as-built capacity and also estimate the seismic demand under nonlinear static and dynamic analyses. Due to various limitations, the present study intends to investigate the seismic performance of the buildings and focus on six case study buildings, as presented in detail in Chapter 3.

The main objective of this chapter is to analyse and discuss the numerical results obtained from the nonlinear static and dynamic time history analyses performed. The incremental dynamic analysis (IDA) was developed and utilized to generate fragility curves to ascertain the level of damage states of the study buildings. In other words, the goal was to assess the

vulnerability of the existing buildings in Nepal. In the last section of the present chapter, the case study buildings were analysed and recommended for strengthening in case these buildings demonstrate inadequate capacity than seismic demand. The detailed strengthening measures, such as retrofitting, will be discussed in Chapter 6.

In this chapter, the seismic performance of all case studied buildings that were discussed and presented in Chapter 3 were modelled using a SeismoStruct software [22]. The detail modelling approach adopted for frame elements and infill walls were discussed in Chapter 4, Section 4.3.1 and 4.3.2. In addition, the concrete and steel properties considered for all case study buildings are shown in Table 5.1 and Table 5.2. The section size of the RC elements and its detailing were similar to those measured in-situ. For the internal infilled was considered a thickness of 110 mm and 230 mm for the external infilled walls. For each case study building, the results were analysed and interpreted separately. Initially, the model calibration was performed for selected buildings, where a comparison between the experimental and numerical frequencies was carried out. The first section of the chapter deals with the detail evaluation of the bare frame (MRT1) building that was later modified with the various disposition of infilled walls (vertical irregularity) throughout the building. The primary objective of this approach was to gather overall information regarding the influence of infilled walls on the building response and compare those findings with past experimental and numerical investigations. For other case study buildings, the goal was to consider only the real case scenario, such that the infilled walls were distributed similar to those observed during the site survey and without any modifications. The later sections of the chapter will discuss, in detail, the seismic performance assessment of the CCP1 building. This will be followed by the CCP2, MRT2, WD1 and WD2 buildings.

Table 5.1 – Concrete properties adopted in the SeismoStruct software for case study buildings

Bldg. Name	Compressive strength (f_c) in MPa	Tensile strength	Modulus of elasticity (E_c) in MPa	Strain at peak stress (ε_c)	Specific weight (γ_c) in kN/m³	Confinement factor
CCP1	15		19365			
CCP2	15		19365			
MRT1	20	0	22361	0.002	24	1.2
MRT2	20		22361			
WD1	20		22361			
WD2	20		22361			

Table 5.2 – Steel properties adopted in the SeismoStruct software for case study buildings

Modulus of elasticity (E_s) in MPa	Yield strength (f_y) in N/mm²	Strain hardening parameter	Specific weight (γ_s) in kN/m³
2 x 105	415	0.005	78

5.2   Bare Frame Building (MRT1)

The bare frame building was modelled using SeismoStruct software [22] and the model was calibrated through parametric study. After the model calibration, the bare frame model was modified with the introduction of three different infilled wall distributions throughout that represent common building typologies in Nepal. The location of the infilled walls largely depends on the need of the owner and occupants. Therefore, the present study considered three dominant solid brick infilled wall distributions. The entire modified buildings were examined under nonlinear static and dynamic time history analyses. This study aims to evaluate the seismic performance of the entire modified buildings and identify the potential level of damage states with respect to IMs.

The different arrangements for the infilled walls in the frame buildings includes a bare frame (MRT1), frame without ground infilled panels (MRT1-WO-GI), frame with irregular infilled walls (MRT1-W-Irr.-I) and frame with whole infilled panels (MRT1-W-I), as presented in Figure 5.1. The various material properties considered for this building were presented in Table 3.13, Table 5.1 and live loads presented in Table 3.14 and Table 3.15. The model calibration was initiated considering the concrete compressive strength for the beam and column, which were measured in-situ and later calibrated, as discussed in Chapter 3. Therefore, the concrete compressive strength for the beam and column were considered to be 20 MPa (see Table 3.7). The modulus of elasticity for the concrete was estimated as $5000\sqrt{f_{ck}}$ [136], where f_{ck} is the compressive strength of the concrete. For solid infill walls, the material properties were adopted as presented in Table 4.6. The modulus of elasticity of infill wall was estimated as $E_m = 550\ f_m$ (f_m = compressive strength of infill) [100].

| (a) | (b) | (c) | (d) |

Figure 5.1 – 3D model assumptions for the MRT1 building with different disposition of infills; (a) MRT1, (b) MRT1-WO-GI, (c) MRT1-W-Irr.-I and (d**)** MRT-W-I

5.2.1 Parametric study

A parametric study of the bare frame building was performed to calibrate the numerical model by comparing the experimental and numerical frequencies. The study was carried out varying one parameter while the other parameters remained constant. The parameters that could have a larger influence on the global natural frequencies were varied, such as the Young's modulus of the concrete, the column cross-section dimension (reduction or uniformization, as common in Nepal) and slab thickness. Thus, different numerical models were built based on the calibrated model, and different variations were tested as follows:

- The concrete elasticity modulus was varied between 11 and 22 GPa. From the comparison with the calibrated model results (Exp. f_1 and Exp. f_2), it can be observed that for E = 22 GPa, the difference in natural frequencies was about 30% (first and second frequencies). For E = 12 GPa, the second frequency tended to coincide and the difference in natural frequencies was reduced to 2.5%. Furthermore, when E = 11 GPa, the numerical first frequency almost coincided with the experimental and the difference in the first natural frequencies was nearly <1%. The trend of the variation between the natural frequencies with respect to variation of elastic modulus of the concrete is presented in Figure 5.2.
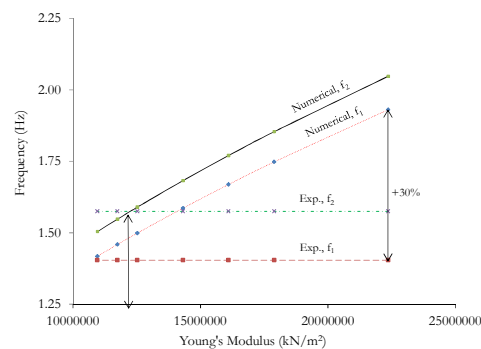
Figure 5.2 – Parametric study results regarding the influence of the concrete elasticity modulus variation

- The column cross-sections were varied. Three different column cross-sections were assigned to understand their influence on the variation of the building frequencies, as illustrated in Figure 5.3. The typical column cross-sections that were based on the common practices in Nepal were selected, namely: (230 x 230) mm², (230 x 300) mm² and (300 x 300) mm². When the compressive strength of the concrete for the beam and column were given a constant value, as obtained from the field test, it was found that actual column showed the difference in the natural

frequencies by approximately 37.5%. Similarly, the difference in natural frequencies for column sizes (230 x 230) mm², (230 x 300) mm² and (300 x 300) mm² was almost 18%, 41% and 52%, respectively.
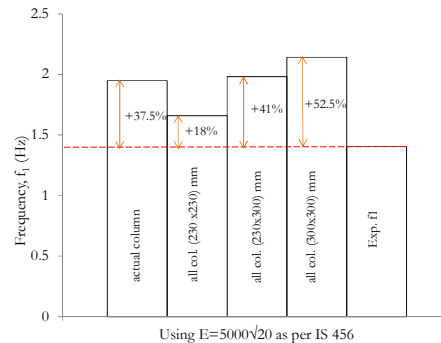
Figure 5.3 – Parametric study results regarding the influence of the variation of the column cross-sections

- The slab thickness was varied. The influence of the slab thickness variation on the natural frequencies of the building was examined, as illustrated in Figure 5.4. The thickness variations were t = 100 mm, t = 120 mm, t = 125 mm and t = 130 mm (representative of Nepal). For this, a slab thickness of 125 mm, as measured in-situ, was considered as the reference. It was observed that for a slab thickness of t = 100 mm that the first frequency increased by approximately 33% and second frequency almost 24% compared with the ambient vibration test frequencies.
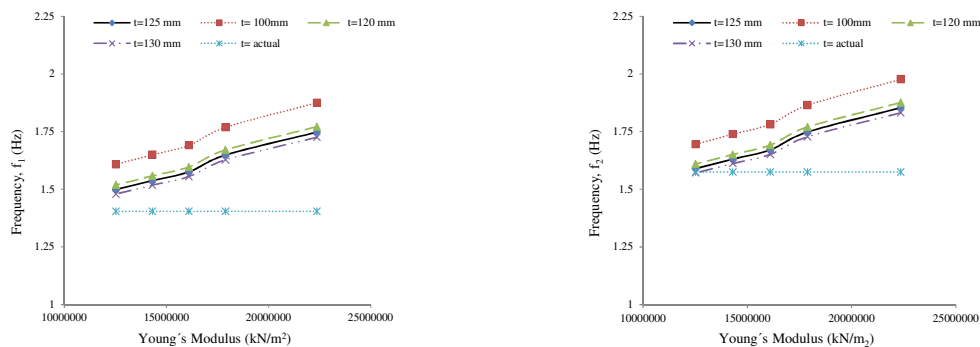
Figure 5.4 – Parametric study results regarding the influence of the building's slab thickness

The parametric study results demonstrated that upon varying the concrete elastic modulus from 22 to 11 GPa, the difference between the experimental and numerical frequencies was reduced from 30% to <1%. In addition, upon varying the column sizes, i.e. from the actual to normally practiced column sizes, the difference was reduced from 37.5% to 18%, and was a minimum for column section (230 x 230) mm². Therefore, it can be concluded from the parametric study that the concrete Young's modulus and size of the column sections are dominant parameters. For further analysis, the Young's modulus of concrete

was considered as 11 GPa, column sections as measured in-situ and other concrete and steel properties as shown in Table 5.1 and Table 5.2 and infill walls properties as presented in Table 4.6, i.e. Young's modulus of infill wall as 2.3 GPa.

5.2.2 Eigenvalue analysis

The natural frequencies and mode shapes for the entire modified buildings were analysed through eigenvalue analysis and compared, as shown in Table 5.3. The entire studied modified buildings demonstrated the first two vibration modes as translational, such that the first vibration mode was along the building's X-axis and second was along the Y-axis. This was the case for all buildings except for MRT1-W-Irr.-I, which exhibited the first vibration mode along the Y-axis and the second along the X-axis. From the above statement, it became clear that the vibration modes for a particular building may not be always constant, but they depend on the distribution, location and the percentage of openings in the infilled walls. The cumulative effective modal mass participation factor for the first two vibration modes was more than 93%. Therefore, the present study considered first two fundamental frequencies and their respective vibration modes as presented in Table 5.3. The calibrated model was also validated with scalar values, also known as model assurance criteria (MAC), that relates the degree of reliability between the analytical and experimental modal vectors [210] and is mathematically estimated using Equation (5.1) as follows:

$$\text{MAC} = \frac{\left|\{\emptyset_a i\}^T\{\emptyset_{ej}\}\right|^2}{\{\emptyset_a i\}^T\{\emptyset_a i\}\{\emptyset_{ej}\}^T\{\emptyset_{ej}\}} \tag{5.1}$$

where: $\{\emptyset_a i\}$ and $\{\emptyset_{ej}\}$ are the modal vectors of the analytical and experimental techniques, respectively.

Figure 5.5 demonstrates the graphical representation of the MAC values for the MRT1 building that were plotted using equation (5.1) and considered only the diagonal values of each mode. The attained MAC values were above 85%, such that the MAC value recorded for the first mode was 92% and was 86% for the second mode. This indicated that all results were expected to overlap and provided a good correlation between the calibrated model and experimental tests.
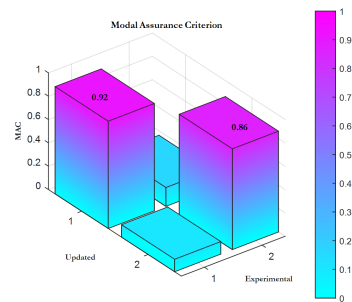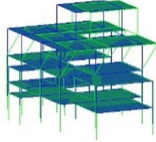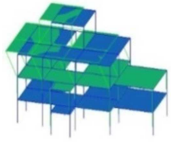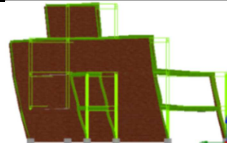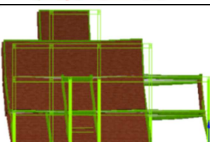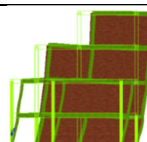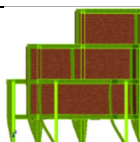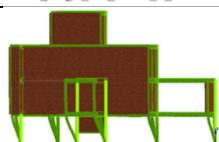
Figure 5.5 – Graphical representation of the modal assurance criteria (MAC) for the bare frame building

The eigenvalue analysis results illustrated that the fundamental frequencies of the bare frame building increased with the addition of infilled walls, such that the MRT1-W-I building exhibited higher frequencies, i.e. the first and second frequencies increased approximately 4 and 3.80 times, respectively, compared with the bare frame (MRT1). Similarly, the increase in the fundamental first frequency for the MRT1-W-Irr.-I and MRT1-WO-GI buildings was about 3.2 and 1.4 times, respectively. For these types of structures and frequency ranges, the higher frequency usually corresponds to an increase in the seismic demand based on the response spectrum for Nepal [30]. Hence, the infilled building structures are required to be designed properly to meet the potential seismic demands so as to avoid unexpected and undesirable failure and damage to the buildings.

Table 5.3 – Eigenvalue analysis results for the MRT1 building: natural frequencies and vibration modes

Modal	Frequency (Hz)		First vibration mode	Second vibration mode
	f_1	f_2		
Experimental frequency	1.40	1.56		
Existing bare frame (MRT1)	1.42	1.50		
Fully infilled (MRT1-W-I)	5.68	5.99		
Irregularly infilled (MRT1-W-Irr.-I)	4.47	5.65		
Without ground infilled or soft-storey (MRT1-WO-GI)	1.96	2.24		

5.2.3   Nonlinear static pushover analysis

As discussed in the Chapter 4, Section 4.4.1.2.2, the adaptive pushover is considered to be more accurate when compared with conventional pushovers, i.e. uniform and triangular load patterns. Therefore, the present study carried out nonlinear static analysis using adaptive pushover analysis for the entire case study buildings. This is a static method that helps to predict the nonlinear structural behaviour prompted by various types of earthquake loads. It is simple and easy in terms of numerical calculations and best in the context that better reliability of the results can be attained and less computational time is needed to predict the capacity curve of structures. The capacity curve is a plot in which the cumulative base shear at the support is plotted along the ordinate and the roof displacement or global drift is plotted along the abscissa. It provides general information about the initial stiffness, yield strength, maximum strength, ultimate strength and rupture strength with respect to the global drift of the structure.

Figure 5.6 presents capacity curves for the modified MRT1 buildings in both directions. The plot demonstrates that a considerable increase in stiffness and maximum strength capacities was attained through the introduction of infilled walls. However, this approach decreased the deformation capability with respect to the maximum base shear capacity when compared with bare framed building. The increase in the stiffness was almost 3.5-10 times and 6.5-15 times in X and Y directions, respectively, as compared to the bare frame building. In addition, the infilled building shows a steep decline in the capacity curve after attaining the maximum capacity, potentially due to in-plane cracking and crushing and out-of-plane failure of the infilled panels. If such structures were subjected to increasing lateral forces, then the lateral forces would be expected to be resisted by the frames only. This point assumed that all the infilled walls at the ground floor collapsed. Ultimately, the total collapse of the building was most likely under the soft-storey mechanism, and in some cases shear failure in the columns and short-columns. Furthermore, the maximum increase in stiffness and base shear capacity were detected for the fully infilled building. It increased almost 3.5 times more than bare frame in both directions. In contrast, the maximum base shear capacity for MRT1 and MRT1-WO-GI was approximately comparable in both directions, but the global drift occurred prior in the MRT1-WO-GI building in both directions. This phenomenon reveals that the MRT1-WO-GI building is most likely to undergo premature collapse, theoretically, under the soft-storey mechanism in comparison with the MRT1 building.
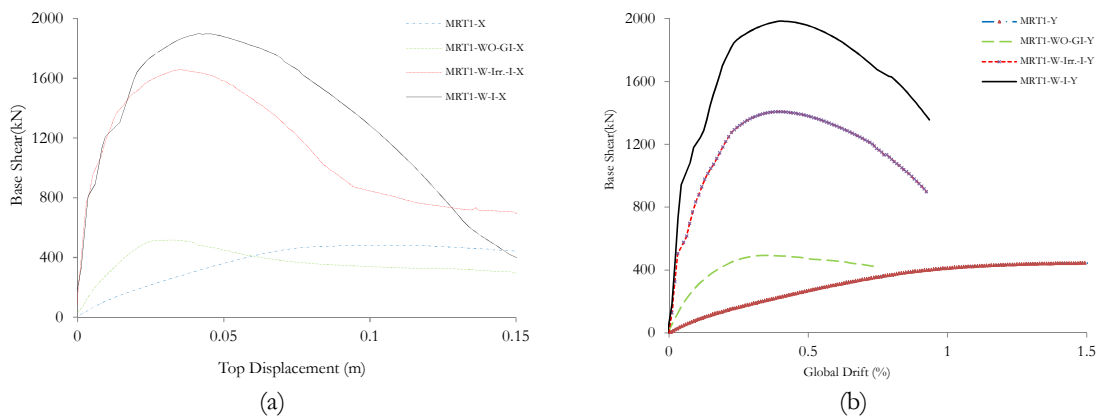
Figure 5.6 – Capacity curve for the modified bare frame building; (a) X direction and (b) Y direction

Figure 5.6 also demonstrates that both the MRT1-W-I and MRT1-W-Irr.-I buildings had a similar initial increasing trend for the capacity curves with nearly the same line until a global drift of 0.1% and 0.05% occurred in the X and Y directions, respectively. For MRT1-W-I, the maximum base shear capacity attained at a global drift of 0.37% and 0.41% in X and Y directions, respectively. Similarly, for MRT1-W-Irr.-I, it occurred at a global drift of 0.32% and 0.39% in the X and Y directions, respectively. For MRT1-WO-GI, it occurred at a global drift of 0.28% and 0.36% in the X and Y directions, respectively. Finally, for MRT1, it occurred for a global drift of 0.93% and 1.21% in the X and Y directions, respectively. The above results indicated that the bare frame building had a higher ductility, whereas the soft-storey building exhibited a lower ductility. The other was in between them. This also revealed that the structural elements of the soft-storey building underwent an early hardening and the formation of plastic hinges was likely to be dominant, most likely due to higher seismic demand concentration in a single floor. Likewise, the infilled frame buildings can be expected to have a prior brittle failure when the seismic demand overcomes the structural capacity. This is due to brittle behaviour of the infilled panels, where crushing and cracking of the infilled walls occurs and failure under different mechanisms can be expected.

5.2.4   Nonlinear time history analysis

Dynamic time history analysis is the most accurate method for the assessment of the seismic response of the structures. The precision of the results depends on number of parameters, such as the number and selection of ground motion records. In this section, the seismic performance of the entire modified building types was evaluated through non-

linear time history analyses, subjected to selected real ground motion records. As discussed in Chapter 4 and Section 4.4.2.1, a total of 21 real earthquake records were selected from natural seismic events around the globe that matches the target response spectrum. This decision was mainly due to unavailability of recorded seismic events from the past for the region. Each earthquake record was suitably scaled for a range of PGA, i.e. 0.1g to 0.5g at the interval of 0.1g. The selected earthquakes were subjected at support as bidirectional at 0^0 and 90^0 to obtain the critical angle of incidence. The seismic performance of the buildings was evaluated in terms of maximum inter-storey drift (ISD$_{max}$) as a building response and results were presented and discussed with the help of IDA and fragility curves to identify the most vulnerable building type.

5.2.4.1   *Maximum inter-storey drift profile*

The maximum inter-storey drift (ISD$_{max}$) profile illustrates the distribution of storey drift throughout the building height with respect to IM. Here, the ISD$_{max}$ attained for each storey was plotted along the abscissa and the storey along the ordinate. Figure 5.7 presents a representative ISD$_{max}$ profile for the 5-ChiChi Taiwan earthquake that had a 0.3g PGA. The plot demonstrates that all the infilled buildings exhibited the ISD$_{max}$ at the ground floor and negligible drift at the consecutive upper floors in both directions. In contrast, for the bare frame, the drift profile was observed to be relatively uniform throughout and indicated a uniform distribution of stiffness and strength. However, it is interesting to note that the recorded drift for the bare frame was relatively comparable to the ground storey drift for soft-storey model. This particular case indicated that the bare frame and soft-storey buildings are equally vulnerable, potentially due to lower stiffness and strength capacities of the bare frame. For the soft-storey building, the larger variations in stiffness and strength capacities occurred between the ground floor and consecutive upper floors. The obtained ISD$_{max}$ for the MRT1 building was approximately 1.35% and 2.1% in the X and Y directions, respectively. On the other hand, the ISD$_{max}$ for the MRT1-WO-GI building at the ground floor was about 1.42% and 2.55% in the X and Y-directions, respectively. Thus, the attained higher inter-storey drift can be minimized through the introduction of infilled walls throughout, and a uniform and negligible drift could be attained. This shows that infilled walls can improve the distribution of stiffness and strength capacities, such that uniform distribution can be recorded throughout and be true for lower to medium PGAs [8].

When the drift profile for the MRT1-W-Irr.-I and MRT1-W-I buildings were compared, the former building exhibited an ISD_{max} slightly higher at the ground floor in both directions, whereas both demonstrated an insignificant drift at the consecutive upper floors. For this particular PGA, both buildings exhibited an ISD_{max} below 0.5%. Based on the illustrated ISD_{max} profile, it can be concluded that the observed lower ISD_{max} in infilled frame buildings was perhaps due to significant contribution of infilled walls to the frame structures acting together in a monolithic way to resist the lateral loads. However, this statement holds true for low to medium PGAs until the capacity meets the seismic demand. The level of damage states in the building models can be identified based on the threshold limit, as defined in Chapter 4 and Table 4.10. Therefore, the MRT1 building can be expected to have extensive damage, the MRT1-WO-GI building can reach partial-collapse, and the MRT1-W-Irr.-I and MRT1-W-I buildings can have moderate damage. The preliminary results indicated that the MRT1-WO-GI (soft-storey) building was found to be much more vulnerable, though it can be reduced by 3-4 times through the addition of infilled walls throughout for this particular bare frame building.
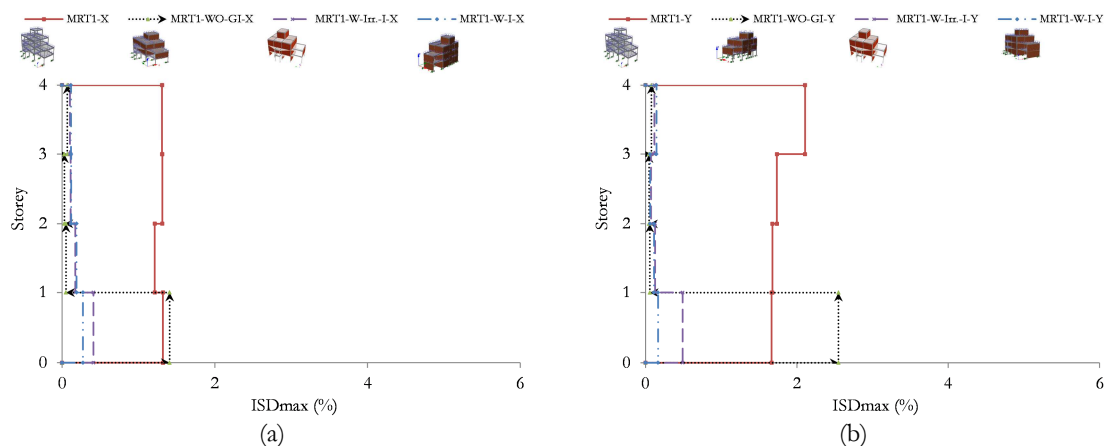
Figure 5.7 – Typical representative ISD_{max} for the modified bare frame building due to 5-ChiChi Taiwan, at 0.3g PGA; (a) X direction and (b) Y direction

5.2.4.2 IDA curves

Incremental dynamic analysis (IDA) was performed for all building types via the selected real ground motion records. These records were suitably scaled as discussed in Section 5.2.4. The IDA curve represents the evolution of ISD_{max} with respect to the IMs. The IMs are plotted along the ordinate and the building response in terms of the ISD_{max} is plotted along the abscissa. Figure 5.8 illustrates the individual IDA curves for each subjected

earthquake obtained from non-linear dynamic time history analyses. Here, the building's response with respect to IM was represented by light solid lines. A large dispersion of ISD_{max} for the same IMs was observed when subjected to different earthquakes, illustrating that the seismic demand is governed by earthquake parameters, such as its frequency contents and recorded duration. The upper and lower boundaries were enclosed to demonstrate the maximum and minimum seismic demand variations. In addition, the mean IDA curve is the average of all ISD_{max} for respective IM, which provides information on the overall building response for that IM.

Figure 5.8 presents the IDA curves for MRT1, MRT1-WO-GI, MRT1-W-Irr.-I and MRT1-W-I buildings. The entire plots revealed that the buildings exhibited larger values of ISD_{max} with respect to the increase of IMs. In some cases, particularly for MRT1-WO-GI, the building exhibited a lower ISD_{max} corresponding to higher IMs. This is possibly due to large seismic demand with respect to low IMs. When subjected to large IMs, the structural elements were most likely to undergo excessive hardening. Furthermore, all the modified buildings were predicted to be in the elastic region until 0.2g PGA. For the MRT1-WO-GI and MRT1 buildings, after 0.2g PGA, the majority of the subjected earthquakes resulted in a higher seismic demand that overcame the elastic region and non-linearity became dominant. A similar trend can be seen for the MRT1-W-I and MRT1-W-Irr.-I buildings beyond 0.3g PGA, where the majority of the subjected earthquakes caused the end of material elasticity and were expected to initiate non-linearity in the structural elements. When non-linearity becomes dominant, the MRT1-WO-GI model can be predicted to have a complete collapse due to the soft-storey mechanism. On the other hand, extensive in-plane cracking and crushing and out-of-plane failure of infilled walls can be expected for the infilled frame buildings. They may possibly undergo a soft-storey mechanism. In some cases, the shear failure in columns can be detected.
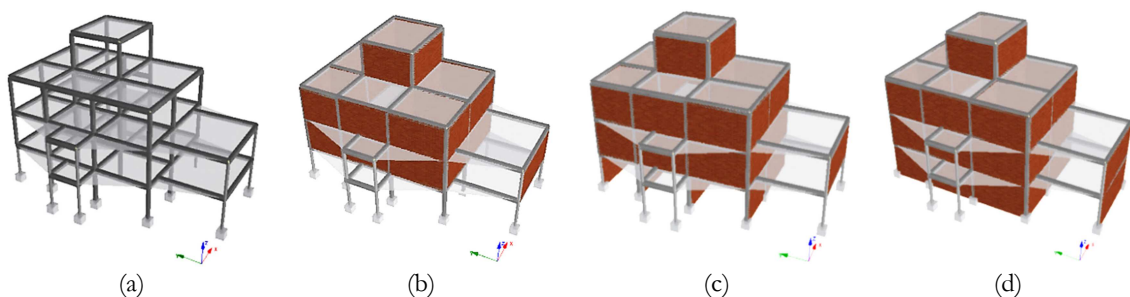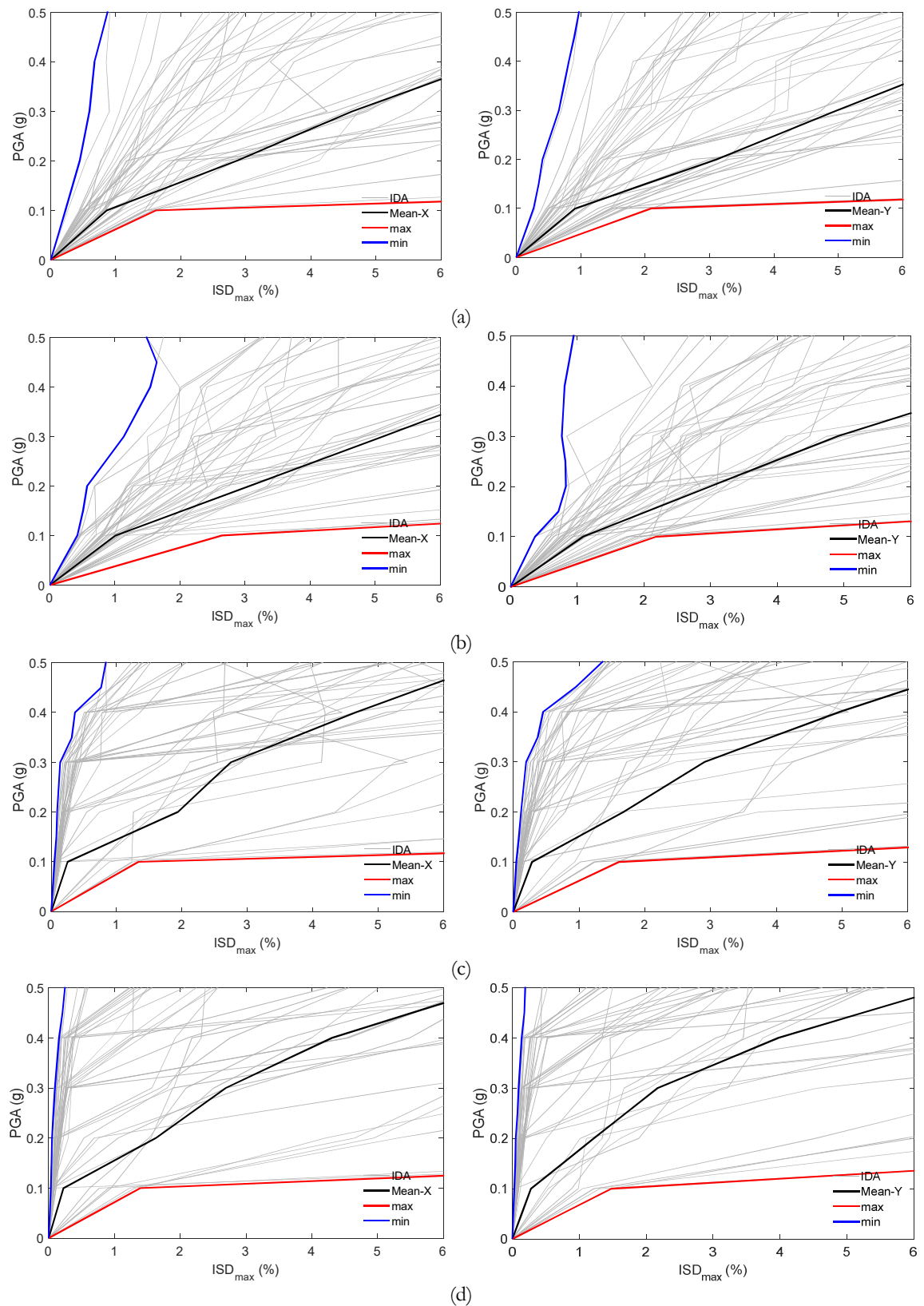
Figure 5.8 – IDA curves for the MRT1 building with different disposition of infills; (a) MRT1, (b) MRT-WO-GI, (c) MRT1-W-Irr-I and (d) MRT1-W-I in X and Y directions, respectively

Figure 5.9 presents the comparative mean IDA curves for all modified MRT1 buildings in both directions. The primary objective of this plot was to simplify and better illustrate the distribution of the building response for same IMs so that it will be easier to comprehend the likely vulnerability. As discussed above, both the MRT1 and MRT1-WO-GI buildings illustrated relatively similar mean IDA curves in both directions. The MRT1-W-I and MRT1-W-irr.-I buildings demonstrated a comparable mean IDA curve. When the overall comparison was performed for same IMs, the MRT1-WO-GI buildings always exhibited a much higher ISD_{max} relatively compared to regularly and irregularly infilled buildings and a slightly higher compared to the MRT1 building. A slight difference in the mean ISD_{max} for lower IM, i.e. until 0.1g, can be attained. Beyond this PGA, the difference becomes wider. Similarly, the mean IDA curve for the MRT1-W-Irr.-I and MRT1-W-I buildings in the Y direction revealed a similar building response for lower IM, i.e. until 0.1g PGA. Beyond this, the former one deviated highly towards the abscissa compared to the latter one.

A distinct difference can be observed beyond 0.2g PGA and the difference became even more distinct for increasing IMs. The mean IDA curves for MRT1 and MRT1-WO-GI buildings revealed that both had an approximately 1% ISD_{max} at 0.1g and more than 6% ISD_{max} at 0.3g PGA. Such a building is expected to totally collapse. When a building is regularly and irregularly infilled throughout, the drift can be reduced to a 2.9% ISD_{max} at 0.3g PGA. This PGA corresponded to the infilled buildings to possessing extensive damages, mainly in the masonry infilled walls, and in few cases, shear cracks appeared in the columns. Beyond 0.3g PGA, the infilled buildings exhibited a higher mean ISD_{max} that was comparable to the bare frame and soft-storey building. This indicated that the infilled walls failed under in-plane and out-of-plane conditions and resulted in the soft-storey mechanism.

Based on all above discussion, it can be concluded that the MRT1-WO-GI building exhibited a higher ISD_{max} than the MRT1 building, but the difference was insignificant. This revealed that both the MRT1-WO-GI and MRT1 buildings are highly vulnerable. Similarly, infilled buildings greatly enhanced the seismic performance, such that the extensive and collapsed states that were observed in the bare frame and soft-storey buildings at lower IMs can be extended to higher IMs. In addition, the dynamic results also revealed that the addition of regular infilled walls throughout could delays the collapse of the building. In other words, an enhanced seismic performance can be achieved. Furthermore, the dynamic time history analyses also revealed that longer recorded

earthquakes that have comparably large frequencies could be a dominant factor for initiating higher level damage for lower IMs.
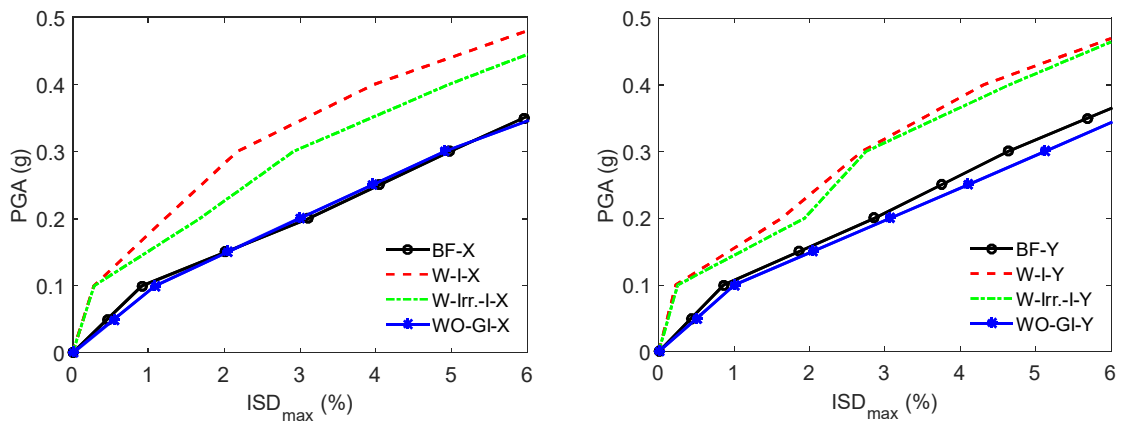
Figure 5.9 – Comparative study of mean IDA curves for the modified MRT1 buildings in the X and Y directions, respectively

5.2.4.3 Fragility curves

The fragility curves were plotted for all modified MRT1 models, as illustrated in Figure 5.10, which helps to identify the probability of exceeding the level of damage states. Both the MRT1 and MRT1-WO-GI models demonstrated peak slight and light damage below 0.1g PGA. This state of the building can be expected to exhibit minor damage in the infilled walls, such as hairline cracks. As discussed in the Chapter 4 and Section 4.3.2.1, the state of damage in the buildings was identified for earthquakes, at 0.3g PGA, which represents 475 years as the return period of large magnitude earthquakes in Nepal. Interestingly, at this PGA, both MRT1 and MRT1-WO-GI models illustrated theoretically peak damages, i.e. until the extensive damage states. Similarly, the probability of exceeding partial-collapse and collapse states for MRT1, at 0.3g PGA, was approximately 43% and 34%, respectively. For MRT1-WO-GI building, it was 93% and 42%, respectively. Similar to the bare frame and soft-storey buildings, the infilled buildings also exhibited peak lower damage states at lower IMs, i.e. below 0.2g PGA. When the building was irregularly infilled, the probability of exceeding collapse, at 0.3g PGA, can be reduced by almost 16% compared to the soft-storey building. Similarly, if the building is regularly infilled, the collapse probability can be reduced by 20% at 0.3g PGA. In addition, the probability of exceeding moderate to collapse damage for the MRT1-W-Irr.-I model, at 0.3g PGA, had a range of 62-26%, and for the MRT1-W-I model, the range was 55-22%, respectively. This

indicated that a greater reduction in the failure probability can be attained through the addition of infilled walls throughout.
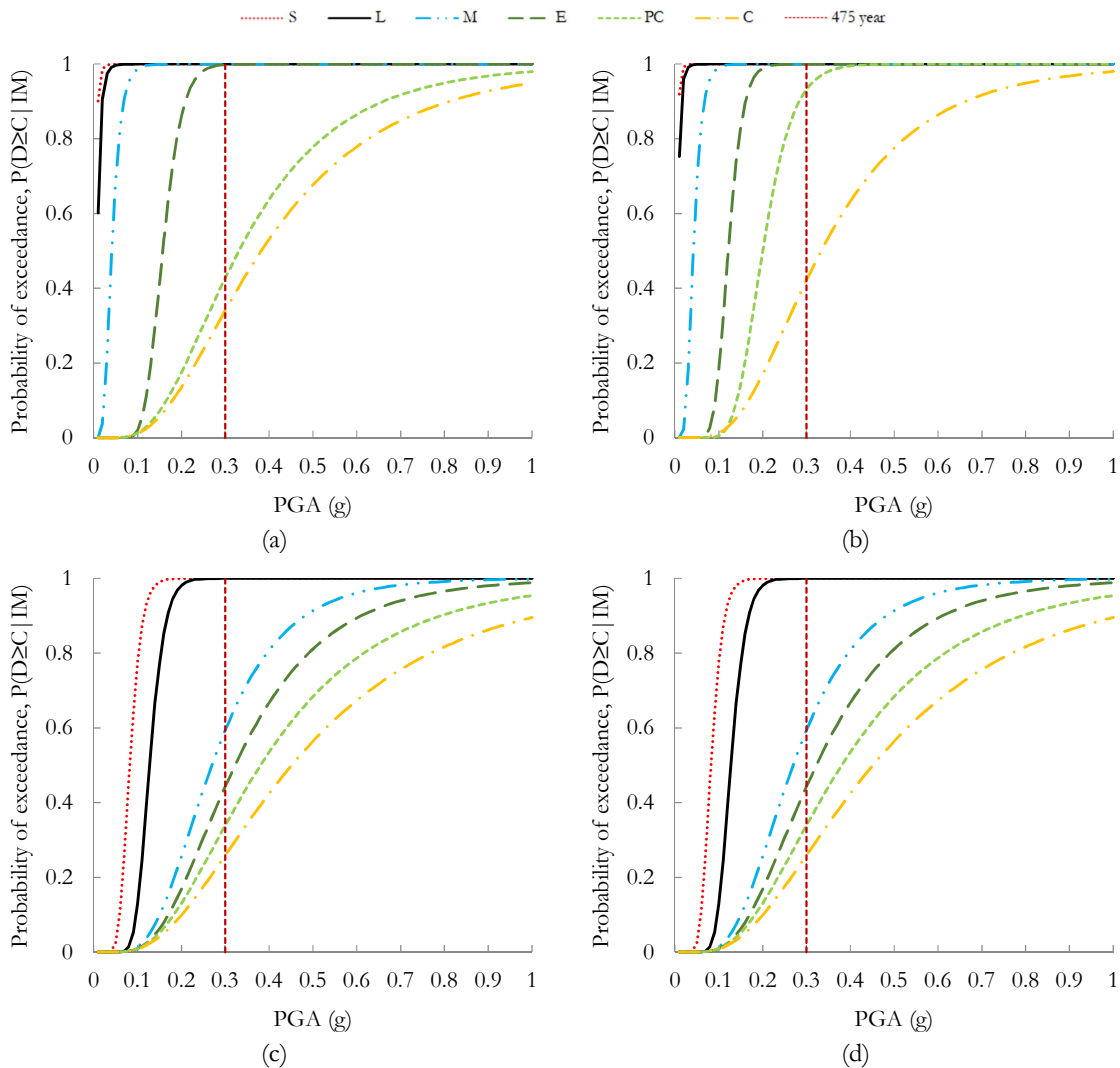
Figure 5.10 – Fragility curves; (a) MRT1, (b) MRT1-WO-GI, (c) MRT1-W-Irr.-I and (d) MRT1-W-I buildings. S – slight, L – light, M – moderate, E – extensive, PC – partial collapse, C – collapse

A better seismic performance can be investigated through the comparative study of typical higher damage states for the entire modified buildings. Figure 5.11 presents the comparative fragility curves for three higher damage states, such as extensive, partial-collapse and collapse. As discussed above, the MRT1-WO-GI model demonstrated a much higher probability of exceedance than the other infilled models when compared with the same PGA. Similarly, a regular infilled building always exhibits a lower probability of exceedance. The probability of extensive damage for the MRT1-W-Irr.-I and MRT1-W-I models, at 0.3g PGA, was approximately 44% and 40%, respectively, whereas the theoretically peak extensive damage state was recorded for both MRT1 and MRT1-WO-GI

models. Therefore, it can be stated that the addition of infilled walls could considerably reduce the extensive damage, and it was reduced to 55%.

Similarly, Figure 5.11 (b) illustrates comparative fragility curves for partial collapse. The state of the building could be predicted to exhibit shear failure in the beams and columns and almost total collapse of the infilled walls. The probability of exceeding partial collapse for the modified buildings, at 0.3g PGA, was between 93-26% with the maximum for the soft-storey and the lower value for the fully infilled building. Furthermore, Figure 5.11 (c) shows the comparative fragility curve for the collapsed state. This state of the building was assumed to have collapsed, where no repair and maintenance would be possible. The plot illustrates that the probability of exceeding collapse for MRT1, MRT1-WO-GI, MRT1-W-Irr.-I and MRT1-W-I buildings, at 0.3g PGA, was approximately 34%, 42%, 26% and 22%, respectively. The above discussion indicated that the addition of infilled walls in the bare frame model could significantly improve the partial collapse and collapse states, thus reducing the probability of partial collapse and collapse by approximately 67% and 20%, respectively.

From all above discussions, it can be concluded that MRT1-WO-GI model is the most vulnerable building type when compared with infilled buildings. This conclusion also revealed that the existing soft-storey buildings in Nepal could be the worst scenario during future earthquakes. Therefore, such buildings must be evaluated under non-linear time history analyses and if found seismically deficient, should be strengthened.
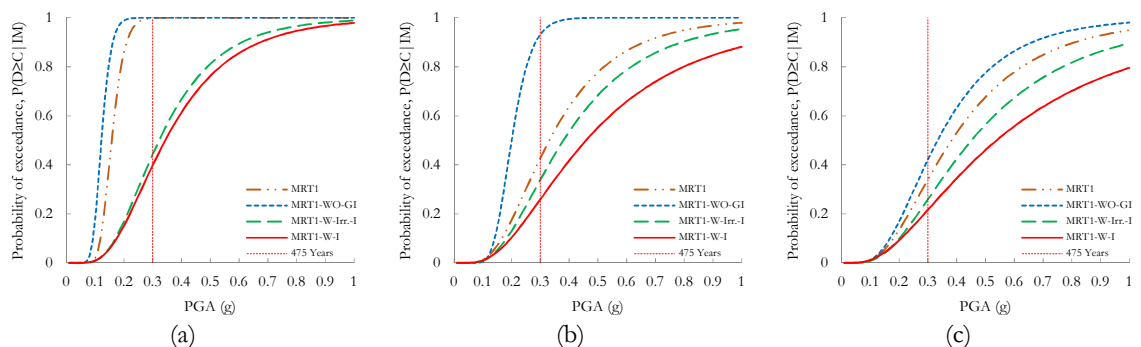
Figure 5.11 – Comparative study of different damage states for modified bare frame models; (a) Extensive, (b) Partial collapse and (c) Collapse

5.3 Mitra Chaphakhana (CCP1)

Although the CCP1 building was located in one of the damaged areas in Nepal, the field observation revealed it as a remarkably undamaged non-engineered building. Hence, the building was selected for the study to acquire the building response evidence for such types. The primary objective of the CCP1 building selection was to examine the seismic performance under nonlinear static and dynamic time history analyses. For this, the building was initially modelled in SeismoStruct software [22] using same modelling approach as discussed in Chapter 4 and Section 4.4.2. Figure 5.12 presents the real building and numerical model, where various standard material properties were assumed, as shown in Table 3.13 and Table 5.1. The concrete strength measured in-situ was used as preliminary data, and a model calibration was performed through the variation of different material properties that have a greater influence on the global building frequencies. As discussed in Chapter 3, the ambient tests were performed using only one test setup, thus it was not wise to estimate the MAC value and compare it to the numerical model. Various loading types were assumed from Chapter 3, Table 3.14 and Table 3.15. The damages observed in solid infill walls were modelled though the adjustment of Young's modulus of infill walls studied through parametric study, initially the infill properties were assumed as shown in Table 4.6. After model calibration, the non-linear static and dynamic time history analyses were performed and results were presented and discussed with the help of capacity curves, IDA curves and fragility curves. Here, the building's E-W orientation was represented along the X-axis and the N-S orientation along the Y-axis. The geometrical plan, structural sections and its detailing, numbers of storeys, storey height, etc. were identical, as discussed in Chapter 3 and Section 3.2.

(a)   (b)

Figure 5.12 – CCP1 building; (a) Real building, and (b) Numerical model

5.3.1 Parametric study

As discussed above, various material properties for infilled walls and concrete were assumed for the building model in the SeismoStruct software [22]. Therefore, the model calibration was required to validate the calibrated concrete strength and also readjust other material properties before employing it for further nonlinear static and dynamic analyses. This was carried out by comparing the experimental and numerical frequencies. The in-situ measured and later calibrated concrete compressive strength for the structural members was considered to be 20 MPa and Young's modulus of infilled walls was assumed 4125 N/mm². The present section covers the parametric study through the variation of various parameters, such as the Young's modulus of concrete and infill walls, and change of column sizes. The governing factor that had a greater influence on global building fundamental frequencies is also determined as follows:

- The variation of the Young's modulus of concretes, such as 16, 19, 22 and 25 GPa representing the compressive strength for concrete that are commonly used in Nepal were used, namely, M10, M15, M20 and M25, respectively, while other parameters remained constant. Figure 5.13 shows the variation of the numerical fundamental frequencies with respect to the Young's modulus of the concrete, which varied from 25 to 16 GPa. Assuming the reference Young's modulus of the concrete was 22 GPa, it was observed that the numerical frequency decreased by approximately 7% when Young's modulus of the concrete was changed from 22 to 16 GPa. In addition, when the Young's modulus of the concrete varied from 22 to 25 GPa, the numerical frequency increased by almost 2%. Therefore, it can be stated that the numerical frequencies varied nearly 10% when Young's modulus of the concrete changed from 25 to 16 GPa or concrete strength changed from 25 to 10 MPa.
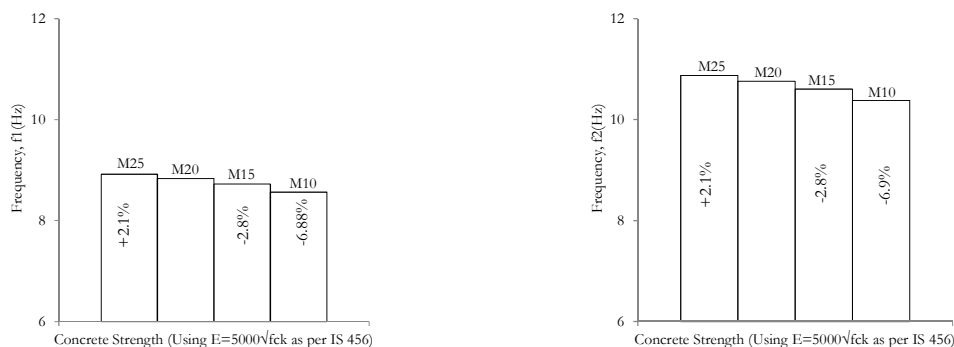
Figure 5.13 – Parametric study results for the influence of concrete elastic modulus variation for the first and second frequencies, respectively

- The variation in the column size commonly practiced in Nepal was used, namely (230 x 230) mm², (230 x 300) mm² and (300 x 300) mm², while other parameters remained constant, i.e. the concrete strength was 20 MPa and the Young's modulus of infilled walls was 4125 N/mm². Figure 5.14 presents the variation of first and second frequencies caused by changing the column sizes. The in-situ measured column size of (230 x 230) mm² was assumed as a benchmark, and it was found that with the increase in column size, the first and second numerical frequencies increased by approximately 3.75% and 4.3%, respectively.
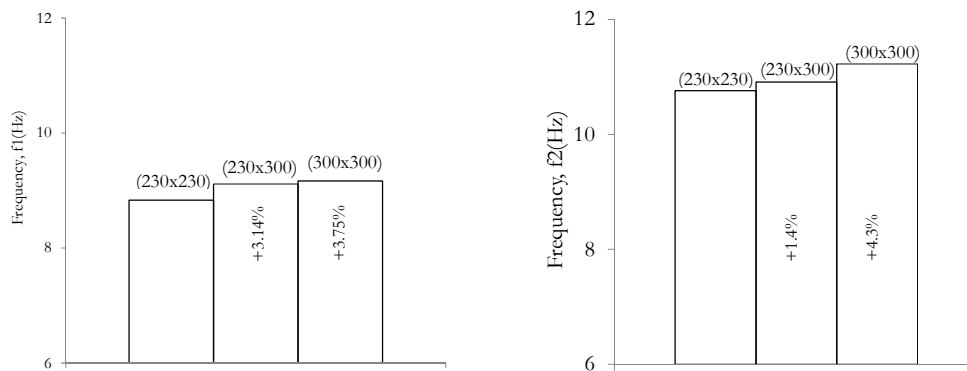
Figure 5.14 – Parametric study results regarding the influence of column size for the first and second frequencies, respectively

- The variation of the modulus of elasticity of the infilled walls was considered, such that the concrete compressive strength and in-situ measured column size remained constant. Here, the modulus of elasticity of the infilled walls was varied, namely N7.5, N5, N4, N3, N2.5, N2 and N1.5 were used. The values ranged from 4125 N/mm² to 825 N/mm², respectively, and the variation in the numerical frequencies was evaluated assuming 4125 N/mm² (i.e. N7.5) as the reference, as shown in Figure 5.15. Initially, the concrete strength was set as 20 MPa and it was found that the numerical first and second frequencies were reduced by approximately 88% and 99%, respectively, when the modulus of elasticity of the infilled walls was varied from 4125 N/mm² to 825 N/mm². Similarly, the compressive strength of the concrete was set as 15 MPa and the modulus of elasticity of the infilled walls varied from 4125 N/mm² to 825 N/mm². It was found the first and second numerical frequencies decreased almost 87% and 97%, respectively. Finally, the compressive strength of the concrete was set 10 MPa. For a similar variation in the infilled wall modulus of elasticity, the first and second numerical frequencies decreased by almost 85% and 94%, respectively. In addition, when the infilled wall modulus of

elasticity was altered from N7.5 to N5 and the compressive strength set to 10 MPa, the first and second frequencies decreased by approximately 26% and 28%, respectively. Furthermore, the difference between the numerical and experimental first frequency could be reduced from +75% to +1.2% when the modulus of elasticity of the infilled walls varied from 4125 to 1100 N/mm² (N7.5 to N2) and the concrete strength was set at 10 MPa.

(a)

(b)
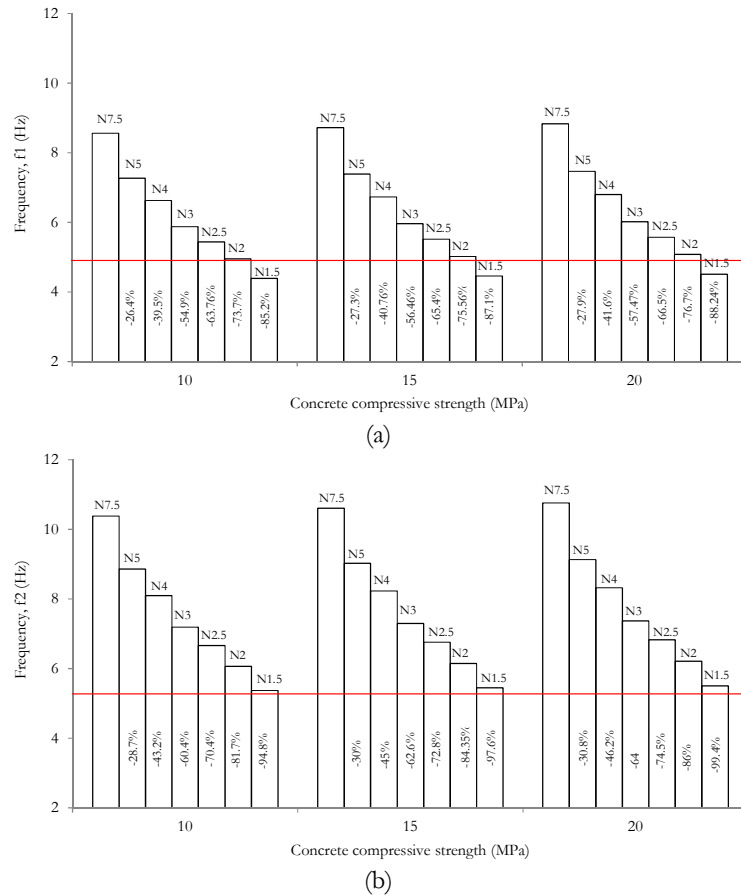
Figure 5.15 – Parametric study result regarding the influence of the Young's modulus of the masonry infilled panel as a function of the compressive strength of the concrete; (a) First frequency and (b) Second frequency
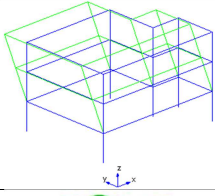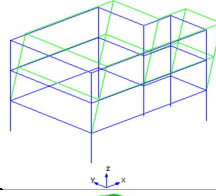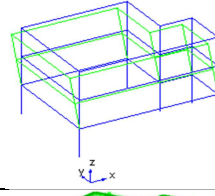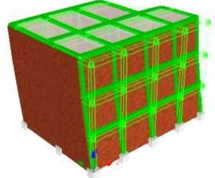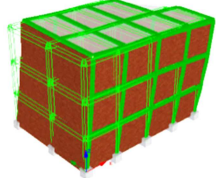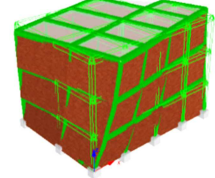
From the above discussion, it is clear that for the global frequencies, the variations introduced by the Young's modulus of concretes and column sizes were not particularly relevant when compared to the variations introduced by the infilled masonry walls. Similarly, the difference in the frequencies could be reduced from 75% to 1.2% for a concrete compressive strength of 10 MPa. The modulus of elasticity for the infilled walls decreased from 4125 N/mm² to 1100 N/mm² for a column size of (230 x 230) mm². In the end, the material properties of CCP1 were readjusted. For further analyses, the concrete strength was considered to be 10 MPa and the Young's modulus of the infilled

walls was 1100 N/mm², which corresponds to a crushing strength for the infilled walls 2 N/mm² and column size of (230 x 230) mm².

5.3.2 Eigenvalue analysis

After calibrating the numerical model, the building fundamental frequencies were evaluated through eigenvalue analysis, and the attained frequencies and corresponding vibration modes are illustrated in Table 5.4. Both experimental and numerical vibration modes were observed to be relatively similar, such that first two vibration modes were translational and third one diagonal. The numerical first fundamental frequency for the CCP1 model was 4.95 Hz along the Y-direction, the second frequency was 6.06 Hz along the X-direction and the third frequency was 6.94 Hz, i.e. torsional.

Table 5.4 – Eigenvalue analysis results for the CCP1 building: natural frequencies and respective vibration modes

Modal	Frequency (Hz)			First vibration mode	Second vibration mode	Third vibration mode
	f_1	f_2	f_3			
Experimental	4.89	5.28	5.34			
Numerical	4.95	6.06	6.94			

5.3.3 Nonlinear static analysis (Pushover analysis)

To assess the ultimate capacity of a structure considering its non-linear behaviour, different methods and approaches can be employed. However, the present section utilizes an adaptive pushover analysis, which is one of the simplest, less time consuming and computer efficient approaches, as discussed and described in detail in Chapter 4. After successive adaptive pushover analysis, the capacity curve was plotted for the CCP1 building (see Figure 5.16), where a sudden and steep increase in the stiffness and base shear capacity was observed for the lower global drift demands. The trend of an initial increase in the base shear capacity and maximum strength were approximately similar in both directions. The

plot demonstrates that the Y direction of the building revealed a slightly higher ductility in comparison to the X direction. This was illustrated through the obtained maximum base shear capacity that corresponds to a global drift of 0.6% and 0.82% in the X and Y directions, respectively.

The global drift did not designate ISD_{max}. Thus, at the maximum yielding point, the building at the ground floor can be expected to have approximately a 1.5% ISD_{max} in both directions, illustrating an extensive damage state that could cause in-plane crushing and cracking in the infilled walls. After this point, a parallel and steep decline in the base shear capacity was recorded in both directions. The capacity curve was plotted until the base shear capacity decreased and was reduced to 0.8 times of the maximum capacity, which corresponds to a global drift of approximately 1% and 1.2% in the X and Y directions, respectively. This state of the building can be expected to have reached the ultimate point and achieved ultimate capacity. This point can be predicted to exhibit an ISD_{max} of approximately 3% in both directions, where the entire infilled walls at the ground floor can be predicted to have collapsed and caused the soft-storey mechanism, a dominant failure mechanism in the URM infilled RC buildings. Furthermore, the attainment of the maximum capacity at a lower global drift also revealed that the CCP1 building could possesses lower ductility, and a steep drop in capacity represented the potential cracking and crushing of the infilled walls. After the ultimate point, it is expected that lateral force would be resisted by the frame structures alone.
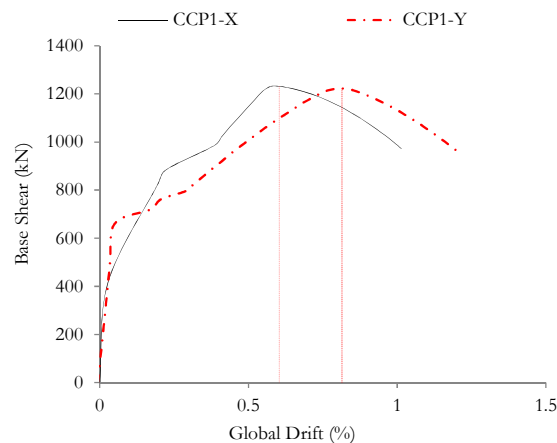
Figure 5.16 – Capacity curve for the CCP1 building in both directions

5.3.4 Nonlinear time history analysis

5.3.4.1 ISD$_{max}$ profile

Figure 5.17 demonstrates the ISD$_{max}$ profile for the CCP1 building subjected to the 8-ChiChi Taiwan earthquake that was scaled from 0.1g to 0.5g with a step of 0.1g. The plot illustrates that the maximum drift arose at the ground floor and decreased consecutively at the upper floors in both directions. An insignificant ISD$_{max}$, with almost a uniform drift profile, was observed in both directions for this particular earthquake until 0.3g PGA. This highlighted the significant contribution from the infilled walls and the frames in resisting the lateral forces. The ISD$_{max}$ was approximately 1.2% and 0.4% in the X and Y directions, respectively. This state of the building can be expected to be in a moderately damaged state, and could potentially possess moderate to extensive damage in the infilled walls. A similar ISD$_{max}$ distribution can be observed for 0.5g PGA as well, where the ground floor had the maximum ISD$_{max}$ and there was a consecutively lower drift at the upper floors in both directions, such that soft-storey mechanism may have initiated. The ISD$_{max}$ at the ground floor for 0.5g PGA corresponded to approximately 2% and 0.9% in the X and Y directions, respectively. This state of the building can be assumed to possess extensive damage in the X direction and moderate damage in the Y direction. This phenomenon revealed that this particular infilled building showed better seismic performance for low to medium IMs, and behaved as soft-storey for higher IMs.

(a)   (b)
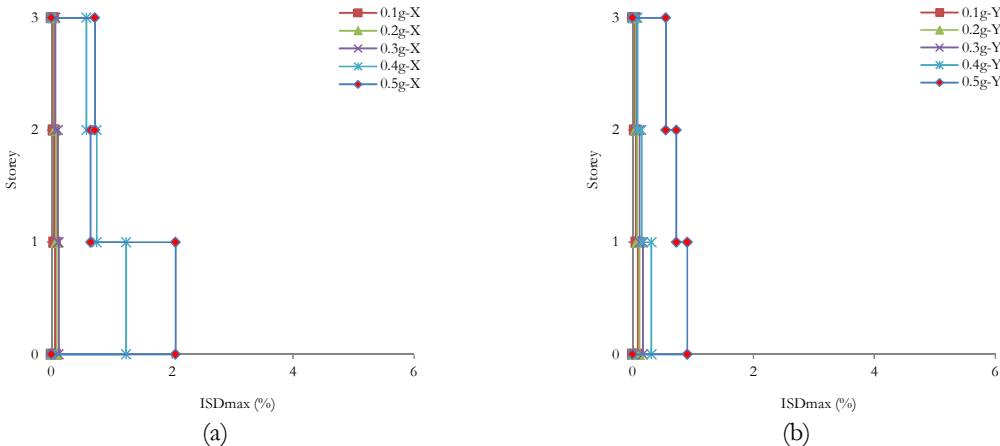
Figure 5.17 – Representative ISDmax profile for 8-ChiChi Taiwan earthquake excited by bidirectional earthquake and scaled PGA from 0.1g to 0.5g; (a) X direction and (b) Y direction

5.3.4.2 IDA curves

The IDA curves for the CCP1 building subjected to 42 ground motion records and scaled from 0.1g to 0.5g with a step of 0.1g are shown in Figure 5.18. For the majority of the subjected earthquakes, the plot reveals less scattering for the ISD_{max} until 0.3g PGA. This illustrates that the CCP1 building would be expected to meet the seismic demand elastically in both directions until 0.3g PGA. However, beyond 0.3g PGA, large dispersions in the ISD_{max} were detected and the majority of the earthquakes expected to initiate the end of elasticity and induce non-linearity in some of the structural elements and hardening became dominant. The building exhibited a higher ISD_{max} with the increase in IMs, and this was true until the building met the seismic demand. However, in some cases, the building cannot meet the seismic demand, especially when subjected to higher IMs that have a lower drift than expected. This indicates that the building could have potentially collapsed before reaching the expected drift. The mean IDA curve illustrated by the solid black line exhibits the insignificant ISD_{max} at 0.1g PGA, and a value of approximately 1.3% at 0.2g PGA in both directions. In addition, the increase in IM results in an increase in ISD_{max}. At 0.3g PGA, the observed mean ISD_{max} exceeded 2% in both directions and was approximately 4% for the 0.4g PGA in both directions. This PGA trend illustrates that the building reached a partially collapsed state, where the total collapse of the infilled walls, mostly at the ground floor, and failure of some structural elements can be predicted. Beyond 0.4g PGA, the building can be predicted to have irreparable damage and if it has not already collapsed, the building might need to be demolished.
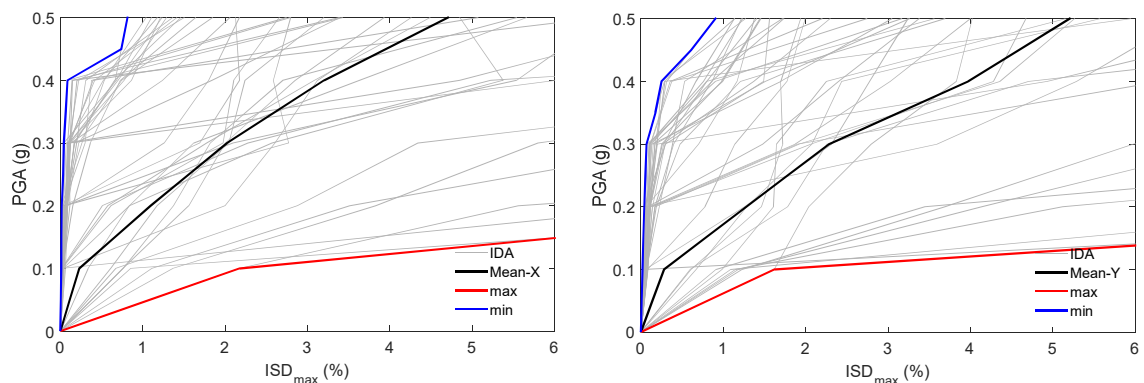
Figure 5.18 – IDA curves for the CCP1 building in X and Y directions, respectively

5.3.4.3 Fragility curves

The probability of exceeding each damage state initiated by earthquakes of different intensities can be represented by fragility curves. As defined in the previous section, 42 ground motion records were selected that matched the response spectra for the region. Initially, the seismic behaviour of the CCP1 building was investigated through incremental dynamic analysis, as discussed above. The state of the building was represented and discussed based on the conditional probability of exceeding damage states with respect to IMs, as demonstrated in Figure 5.19. The straight vertical line observed in the plot characterizes a 10% probability of exceeding a PGA of 0.3g in 50 years, which corresponds earthquakes with a return period 475 years in Nepal, as defined in Chapter 4, section 4.4.2.1. The plot illustrates that the increase in the PGA level increases the probability of exceeding damage states, such that peak slight and light damage states were attained for a range of 0.1 and 0.2g PGA. Similarly, the probability of exceeding moderate to complete collapse, at 0.3g PGA, ranged from 60% to 14%, respectively. Thus, attainment of a lower failure probability for higher damage states is potentially due to positive contribution of infilled walls. However, this was inadequate when considering the safety of the occupants and loss of the structural and non-structural elements; hence, the building was recommended for further strengthening.
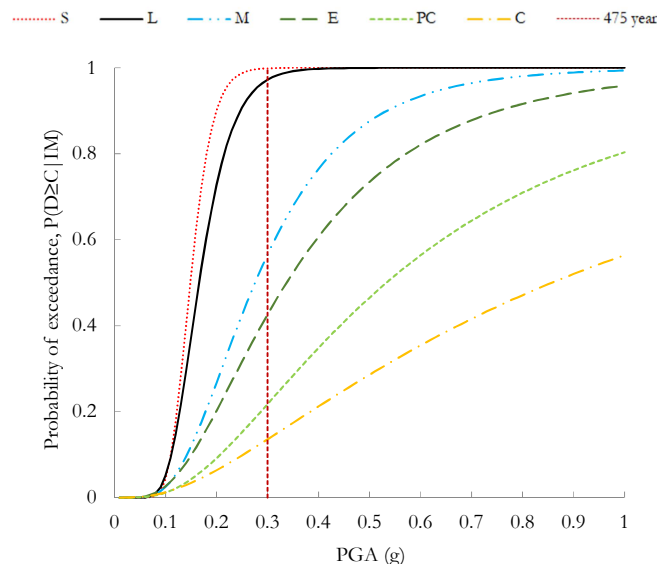
Figure 5.19 – Fragility curve for the CCP1 building. S – slight, L – light, M – moderate, E – extensive, PC – partial collapse, C – collapse

5.4   Suwal House (CCP2)

This building was selected as a damaged non-engineered building that represents common buildings built before MRT guidelines came into practice. The primary objective of this building selection was to study the seismic performance of a non-engineered building infilled irregularly throughout under seismic excitation. Strengthening measures would be recommended, if needed, so that the human and property losses can be minimized in future earthquakes. To achieve this objective, the building was analysed through different types of linear and non-linear analyses and the results will be presented and discussed with the help of capacity, IDA and fragility curves.

Initially, the building was modelled in SeismoStruct software [22], as discussed for the previous case study buildings. Various standard material properties and other parameters were assigned, except for the concrete compressive strength, which was measured in-situ. Therefore, the first step was the numerical model adjustment through parametric study. The main limitation of this software is the inability to model observed cracks in the infilled wall, which were integrated through the model calibration. The dimensions of the structural elements and their detailing were assigned in a similar way as for those measured in-situ, as discussed in detail in Chapter 3. In addition, the location and dimensions of the internal and external infilled walls were identically assigned, as observed and measured in-situ. The dead loads and live loads were assigned in the respective beam elements. All live loads acting on the building were considered to be 2.5 kN/m²; thus, only 25% of the live loads were considered in the seismic load calculation. Figure 5.20 presents the existing CCP2 building and its three-dimensional numerical model developed in the SeismoStruct [22], in which the E-W orientation of building was represented along the X-axis and N-S orientation along the Y-axis.

(a)   (b)

Figure 5.20 – CCP2 building; (a) Real building and (b) Numerical model

5.4.1 Parametric analysis

Here, the parametric analyses were performed through the variation of material properties that could have a greater influence in the global building frequencies. In addition, the observed damages in infill wall were modelled through adjustment of Young's modulus. The results were attained as follows:

- The variation in the Young's modulus of the concrete, such as 16, 19, 22 and 25 GPa that represent concrete strength of 25 MPa, 20 MPa, 15 MPa and 10 MPa, respectively, were used. These concretes are commonly used in Nepal. Figure 5.21 shows the variation of the building's fundamental frequencies attained through the variation of the Young's modulus of concrete while other infilled and column sections remained constant. The in-situ modulus of elasticity for concrete that was 19 GPa (M15) was set as a reference and the variation was recorded. When the Young's modulus concrete varied from 19 to 16 GPa, a decrease in first frequency was observed to be approximately 2%. Similarly, when the Young's modulus of the concrete was modified from 19 to 25 GPa, an increase in frequencies was observed, such that the first, second and third frequencies varied approximately 2.5%, 1.3% and 1.6%, respectively. In addition, the first, second and third frequencies increased approximately 5%, 3% and 3%, respectively, when the Young's modulus of the concrete varied from 16 to 25 GPa (i.e. 10 to 25 MPa).
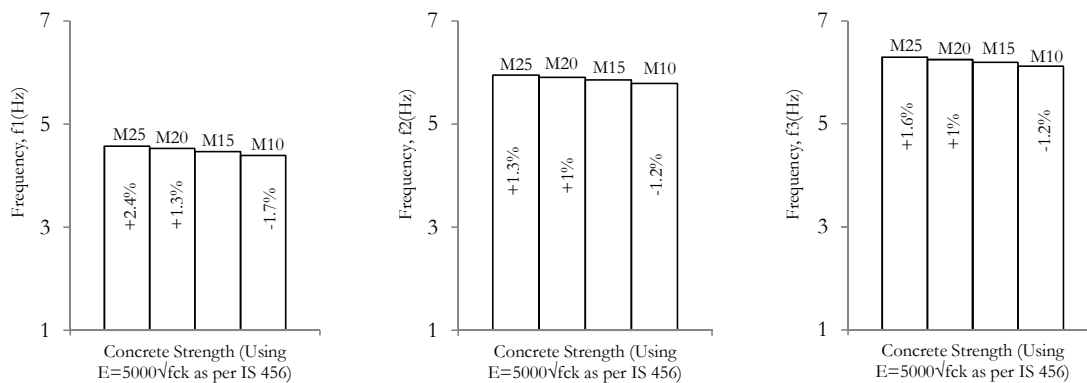
Figure 5.21 – Parametric study results for the influence of the Young's modulus of the concrete on the first, second and third frequencies, respectively

- The parametric analysis was done through the variation of column sizes, namely (230 x 230) mm², (230 x 300) mm² and (300 x 300) mm². The variation of numerical frequencies is shown in Figure 5.22. The increase in the frequencies can be observed with the increase in column size, but it was not as expected. When the

column size varied from (230 x 230) mm² to (230 x 300) mm²; the first, second and third frequencies increased by almost 2%, 2.5% and 2.5%, respectively. Similarly, when the section increased to (300 x 300) mm², the increase in the frequencies was about 8%, 3.5% and 3.5%, respectively. These variations seem quite low (less than 10%). Thus, it can be stated that the column sections did not have significant effect on the global frequency behaviour of the infilled frame building.
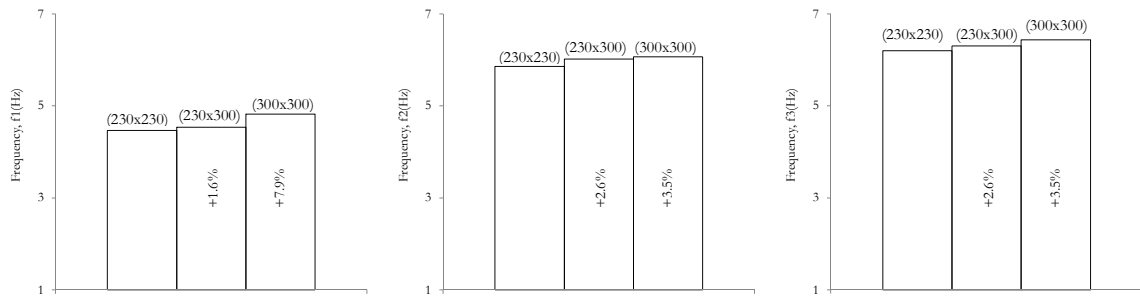
Figure 5.22 – Parametric study results for the influence of column section on the first, second and third frequencies, respectively

- The variation of the modulus of elasticity of the infilled walls was considered, namely N4, N3, N2.5, N2 and N1.5 that varies from 2200 to 825 N/mm². The concrete strength was set to 10, 15, and 20 MPa to investigate the influence on the global building frequencies by varying the crushing strength of the infilled walls. Figure 5.23 presents the variation in the first three fundamental frequencies. In the beginning, the modulus of elasticity of the infilled walls was set to 2200 N/mm², as a reference for this particular building, and variations in frequencies were discussed. When the modulus of elasticity of the infilled walls was varied from N4 to N3 and the concrete strength set 10 MPa, the first, second and third frequencies reduced by approximately 16%, 19% and 16%, respectively. Similarly, the reduction in the frequency was about 48%, 57% and 48%, respectively, when the modulus of elasticity was modified from N4 to N1.5. In addition, when the compressive strength of the concrete set at 15 MPa and the modulus of elasticity changed from N4 to N1.5, the first, second and third frequencies were reduced by almost 49%, 57% and 48%, respectively. Furthermore, when the concrete compressive strength was set to 20 MPa and modulus of elasticity of the infilled walls changed from N4 to N1.5, the first, second and third frequencies reduced to nearly 48%, 57% and 48%, respectively. In doing so, it was noted that the difference in modal and experimental frequencies could be reduced from 60% to 10% when the modulus of

elasticity of the infilled walls changed from N4 to N1.5. Therefore, it can be concluded that a better and closer approximation between the frequencies could be attained for a modulus of elasticity of infilled 825 N/mm² for the infilled walls, which is equivalent to a crushing strength of 1.5 N/mm², concrete compressive strength of 10 MPa and column section of (230 x 230) mm².
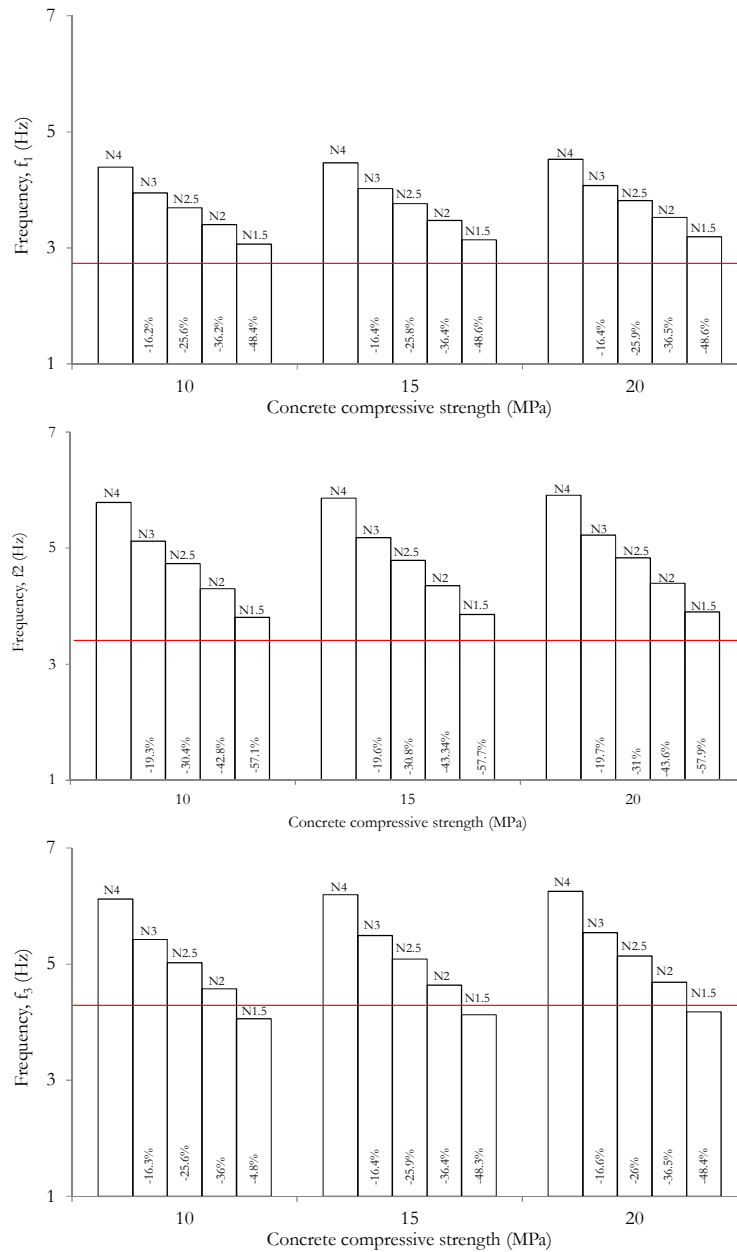
Figure 5.23 – Parametric study results regarding the influence of the Young's modulus of the infilled panel on the first, second and third frequencies, respectively

From the parametric study performed for the CCP2 building, it can be summarized that the change in the concrete strength and column sizes did not have a significant effect on the global frequency variation (which as less than 10%) when compared with the influence

of the infilled walls. The difference in the frequencies can be reduced to approximately 10% for a modulus of elasticity of infilled 1.5 N/mm² for the infilled walls, a concrete strength set to 10 MPa and a column section of (230 x 230) mm². These adjusted material properties along with properties presented in Table 5.1 and Table 5.2 were adopted for further analyses.

5.4.2 Eigenvalue analysis

Table 5.5 presents the first three fundamental frequencies and their respective vibration modes for the CCP2 building obtained from the eigenvalue analysis. It can be observed that both experimental and numerical vibration modes were reasonably comparable, such that first two vibration modes were translational and third one was diagonal. The observed first modal frequency was 3.06 Hz with vibration mode along the building's X-axis. The second frequency was 3.80 Hz along the Y-axis and the third frequency was 4.06 Hz with a torsional vibration mode.

The MAC values obtained from Equation (5.1) is graphically represented in Figure 5.24, which recorded MAC values in the range between 89% and 93%. The higher MAC values revealed the accuracy of the calibrated model. Thus, the obtained numerical mode shapes are likely to overlap with the experimental vibration modes. Therefore, the calibrated model can be justified to represent the original CCP2 building.
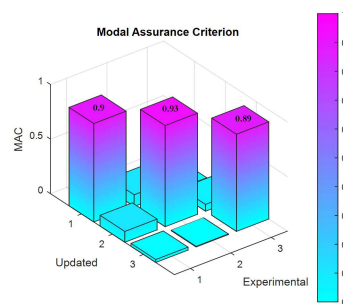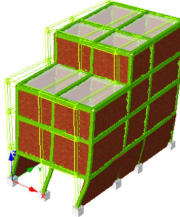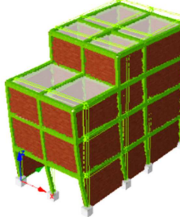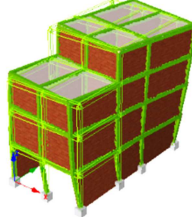
Figure 5.24 – Graphical representations of MAC values for the CCP2 building

Table 5.5 – Eigenvalue analysis results for the CCP2 building: natural frequencies and respective vibration modes

Modal	Frequency (Hz)			First vibration mode	Second vibration mode	Third vibration mode
	f_1	f_2	f_3			
Experimental	2.74	3.47	4.29			
Numerical	3.07	3.80	4.06			

5.4.3   Pushover analysis

Figure 5.25 presents the capacity curve for the CCP2 building in both directions, and it was plotted until the base shear capacity reduced to 80% of the maximum capacity. This point was indicated as the ultimate point. As observed, a sudden and steep increase in initial stiffness can be observed in both directions. This state of the building can be predicted to be in the elastic region, where entire structural elements are assumed to meet the seismic demand elastically, and the estimated maximum inter-storey drift could be less than 0.5%. In addition, the Y direction of the building had the maximum base shear capacity relatively compared with its X direction. However, it occurred at a prior global drift, illustrating that it possessed a slightly lower ductility than the X direction. The point for the maximum base shear capacity was represented as a yielding point that corresponds to a global drift of approximately 0.52% and 0.39% in the X and Y directions, respectively.

This global drift at a yield point can be expected to exhibit an inter-storey drift greater than 1%, and it was most likely at the ground floor. This point also revealed that the contribution of the infilled panels to the frame structures reached the peak level in resisting the lateral forces. Beyond this, the seismic force was resisted by the frame alone. The attained lower global drift in both directions illustrated the lower deformation capability of the infilled CCP2 building. Furthermore, a sudden and steep decrease in base shear capacity was observed after attaining the yield point. The descending branches were

identical in both directions. At the ultimate point, the infilled walls were expected to completely collapse, mostly at the ground floor, which would result in the failure of the building under the soft-storey mechanism. The ultimate point corresponds to an ISD_{max} of more than 3% in both directions, where the building can be predicted to have reached partial collapse or/and collapse states in both directions.
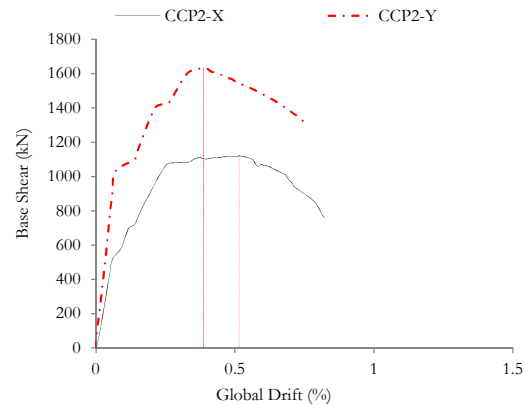
Figure 5.25 – Capacity curve for the CCP2 in both directions

5.4.4   Nonlinear time history analysis

5.4.4.1 ISD_{max} profile

Figure 5.26 presents typical ISD_{max} profile for the 5-ChiChi Taiwan earthquake, plotted for a suitably scaled PGA that ranges from 0.1g to 0.5g with steps of 0.1g. Similar to the CCP1 and infilled MRT1 buildings, a uniform drift profile along the storey for lower PGA was recorded in both directions. This revealed that the building capacity to uniformly distribute stiffness and strength throughout was largely due to the regular distribution of infilled walls. This building exhibited a larger ISD_{max} even for lower IMs, highlighting the higher level of vulnerability. A potential soft-storey mechanism can be expected in the building beyond 0.2g and 0.3g PGA in X and Y directions, respectively, such that maximum drift was primarily concentrated at the ground floor. The larger vulnerability along the X direction was mainly due to the irregular distribution of the infilled walls, where one complete bay was without infilled walls. From the above discussion, it can be concluded that the CCP2 building had a seismically deficient and poor seismic performance.
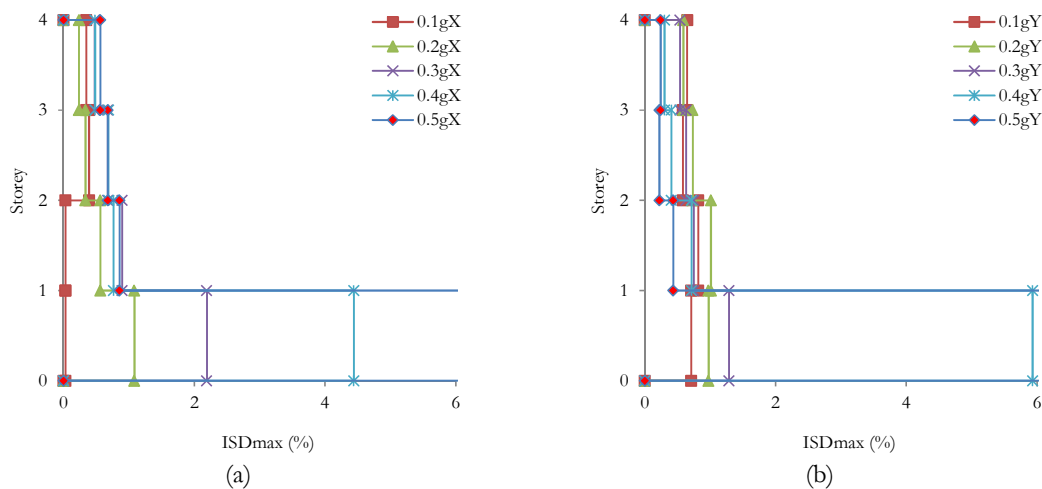
Figure 5.26 – Representative ISD_{max} for the CCP2 building, subjected by 5-ChiChiTaiwan earthquake, suitably scaled for a range of PGA between 0.1 and 0.5g; (a) X direction and (b) Y direction

5.4.4.2 IDA curves

The seismic performance of the CCP2 building was evaluated through IDA curves excited by 42 ground motion records, suitably scaled for a range of PGA between 0.1 and 0.5g with a step of 0.1g. Figure 5.27 presents the individual IDA curve excited by each earthquake. The plot demonstrates large scatter in the building response for the same IM, i.e. the larger variation of ISD_{max} with respect to IMs. The increase in the IMs exhibited a higher ISD_{max}, as expected. In some cases, earthquakes with a comparable higher frequency and longer period cause a higher seismic demand as compared to building capacity, even at lower IMs. As a result, some of the structural elements are expected to experience hardening. The building can be predicted to behave elastically until 0.2g PGA for the majority of subjected earthquakes, where the mean ISD_{max} attained was below 1% in both directions. Beyond this PGA, non-linearity became dominant and some of the column elements were expected to form plastic hinges and result in premature collapse of the building. The ISD_{max} recorded through the mean IDA curves, at 0.3g PGA, corresponded to approximately 1.5% and 2% in X and Y directions, respectively. Furthermore, the CCP2 building can be expected to reach partial collapse and/or collapse states beyond 0.3g PGA in both directions, such that the observed ISD_{max} was approximately 3.2% and 3.5% in X and Y directions, respectively.
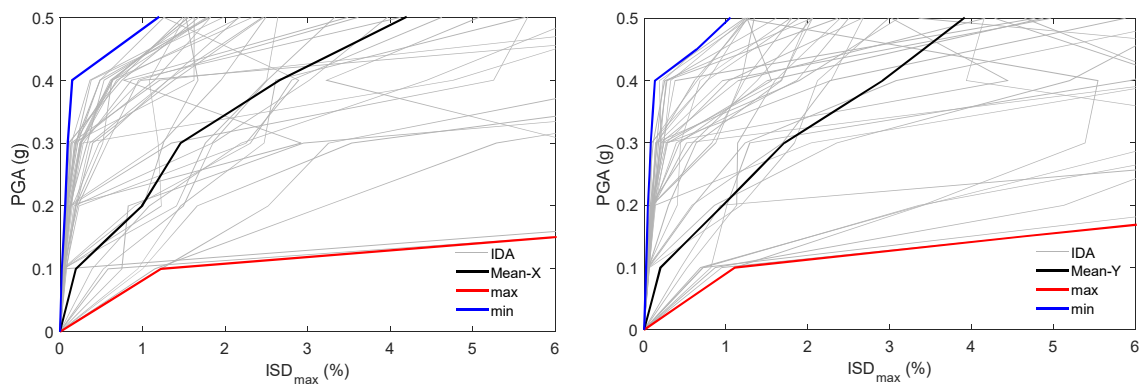
Figure 5.27 – IDA curves for the CCP2 building in X and Y directions, respectively

5.4.4.3 Fragility curves

Figure 5.28 presents the fragility curves for the CCP2 building and represents the conditional probability of exceeding several damage states with respect to the PGA. The plot illustrated that the peak slight, light and moderate damage states occurred below 0.3g PGA. Considering an earthquake with a return period 475 years, i.e. 0.3g PGA, the conditional probability of exceeding extensive, partial collapse and complete collapse ranged from 44 to 20%. This revealed that the particular CCP2 building is highly susceptible to larger damage states. The entire dynamic analyses and results revealed that the CCP2 building illustrated poor seismic performance. Thus, a detailed seismic performance that introduces different strengthening measures is required.
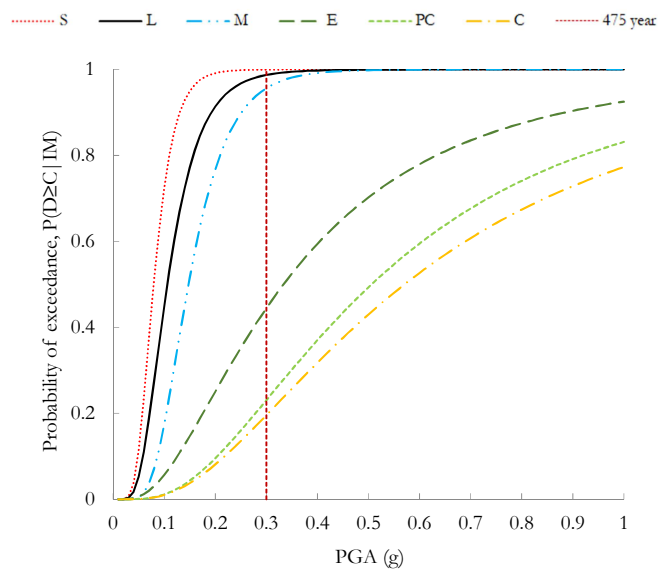
Figure 5.28 – Fragility curve for the CCP2 building for different damage states. S – slight, L – light, M – moderate, E – extensive, PC – partial collapse, C – collapse

5.5   Twayana House (MRT2)

The MRT2 building was classified as a damaged pre-engineered building, whose structural section sizes, infilled wall distributions and locations were presented in detail in Chapter 3 and Section 3.5. The primary objective of this building selection was to explore the seismic performance of buildings that were built in the early stages of the NBC guidelines. The obtained results and conclusions drawn after the detailed seismic performance assessment of this particular building were expected to provide information of similar buildings located in the area. As discussed in Chapter 3, the real building possesses a large and irregular distribution of infilled walls, such that they were placed only at the periphery in the basement. However, during the in-situ test, it was detected that new infilled walls were being constructed; hence, this was considered in the numerical model. The real building and its numerical model were generated using SeismoStruct software [22] are presented in Figure 5.29. Here, the building's E-W orientation was modelled numerically along X-axis and N-S orientation along Y-axis. The various standard material properties were considered as defined in Chapter 4. Therefore, before utilizing the numerical model in the detailed seismic performance assessment, it must be calibrated and the material properties must be adjusted. The observed cracks in the infilled walls of the MRT2 building were integrated in the model through a variation of the Young's modulus. Initially, the calibrated concrete compressive strength of 20 MPa for the columns and 15 MPa for the beams was considered. The crushing strength of the infilled walls was set to 4 N/mm². Uniform live loads of 2.5 kN/m² and floor finishes of 1 kN/m² were considered for numerical simplicity.

(a)   (b)
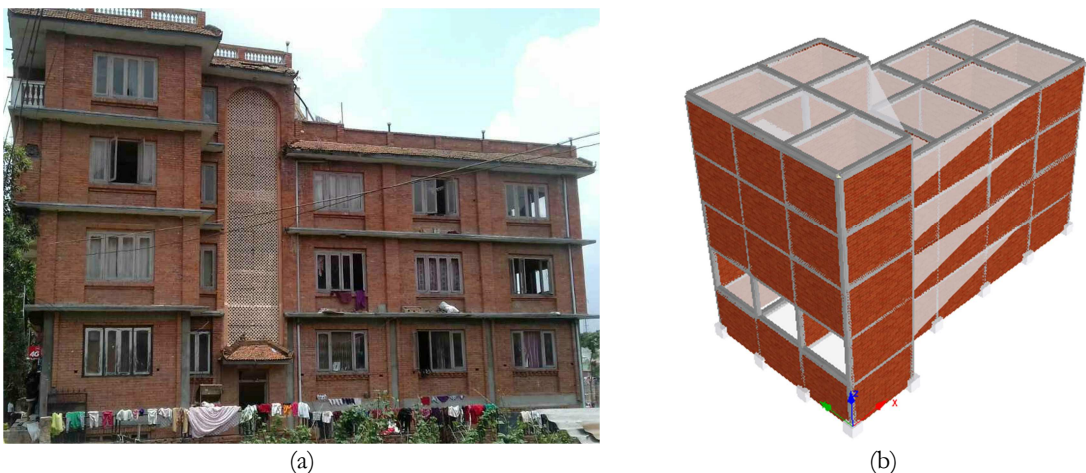
Figure 5.29 – MRT2 building; (a) Real building and (b) Numerical model

5.5.1 Parametric study

This parametric study was performed primarily through the variation of the elastic modulus of concrete, column sections and modulus of elasticity of the infilled walls. A similar procedure was followed to that used for the previously discussed case study buildings. The parametric study was conducted through the variation of the various material properties and its effect on the modal frequencies. Finally, the difference between the modal and experimental frequencies achieved as follows:

- Initially, the numerical frequencies were attained through the variation of the Young's modulus of concrete, namely 16, 19, 22 and 25 GPa representing concrete strength of 25 MPa, 20 MPa, 15 MPa and 10 MPa, respectively. The Young's modulus of infilled walls was set 2200 N/mm² and other parameters remained constant. Figure 5.30 presents the variation of the first, second and third modal frequencies with respect to the variation of Young's modulus of the concrete. The plot shows that when the Young's modulus of concrete changed from 19 to 16 GPa, a decrease in frequencies of approximately 1% was attained. In addition, when the Young's modulus of concrete varied from 19 to 25 GPa, the frequency increased by approximately 2%. In addition, when Young's modulus of concrete varied from 16 to 25 GPa, the frequency increased by approximately 5%. Thus, its effect on the global building frequencies was irrelevant, mainly for the infilled RC buildings.
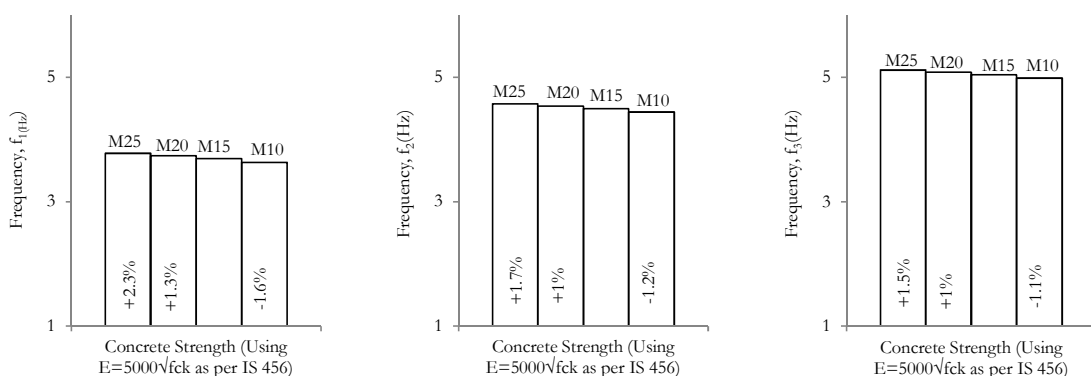
Figure 5.30 – Parametric study results for the influence of the compressive strength of the concrete on the first, second and third frequencies, respectively

- Here, the modal frequencies were compared through the variation of column sizes, namely (230 x 230) mm², (230 x 300) mm² and (300 x 300) mm², and the results are plotted in Figure 5.31. The results revealed that the first modal frequency increased

by almost 6% when the column size varied from (230 x 230) mm² to (230 x 300) mm². It increased by about 8% for a column size of (300 x 300) mm². A similar frequency variation was observed for the second and third frequencies, but it was irrelevant.
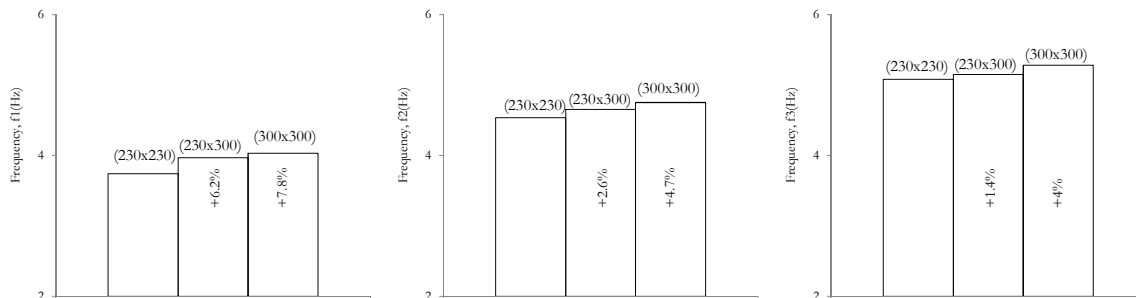
Figure 5.31 – Parametric study results for the influence of the column section on the first, second and third frequencies, respectively

- The modal calibration was done through the variation of the modulus of elasticity of the infilled walls from 2200 to 825 N/mm² (N4 to N1.5), which is equivalent to crushing strength of infilled walls 4 to 1.5 N/mm², respectively, while other parameters remained constant. In the first step, the concrete strength was set at 15 MPa and the variation in the modal frequencies was evaluated, as demonstrated in Figure 5.32. The plot illustrates that a decrease in modal frequencies by almost 13% was recorded when the modulus of elasticity of the infilled walls was varied from N4 to N3. Similarly, when they were varied from N4 to N1.5, the entirety of the frequencies was reduced by approximately 38%. In the second step, the concrete strength was set 10 MPa and the variation in the modal frequencies was examined while varying the modulus of elasticity of infilled wall. It was found that a decrease in the modal frequencies, i.e. the first, second and third frequencies, by approximately 41 to 38% occurred upon varying the modulus of elasticity from N4 to N1.5. Finally, the variation in modal frequency was investigated for the concrete strength of 20 MPa and a similar variation of the infilled wall modulus of elasticity. A decrease in the first, second and third modal frequencies by almost 41%, 37% and 38%, respectively, was observed when the modulus of elasticity of the infilled walls varied from N4 to N1.5. Furthermore, the modal calibration also revealed that the difference in frequencies was reduced from 41% to <1% when the modulus of elasticity of the infilled walls was set to 825 N/mm² that is equivalent

to crushing strength 1.5 N/mm², the compressive strength of the concrete was 15 MPa and other in-situ measured structural dimensions and sizes remained constant.
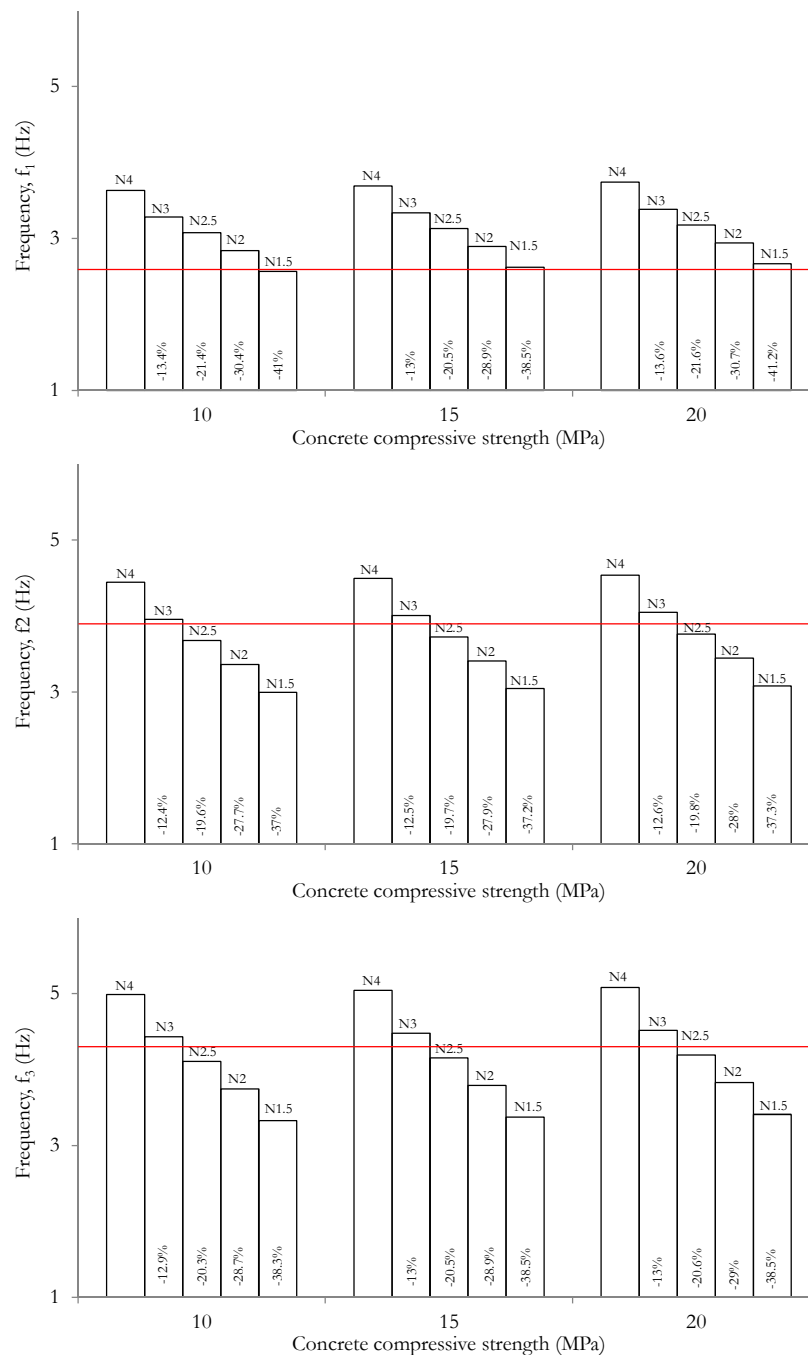
Figure 5.32 – Parametric study results regarding the influence of the Young's modulus of infilled panel on the first, second and third frequencies, respectively

The parametric study results for the MRT2 building illustrated that the material properties of the concrete and column sizes may not be governing factors in influencing the global building's frequencies. However, the variation in crushing strength of the infilled walls had a greater influence on the global building frequencies, such that the difference in

frequencies can be reduced to <1% for concrete with a compressive strength of 15 MPa and a modulus of elasticity of the infilled walls of 825 N/mm². These values were selected for further analyses along with measured structural size. Through these calibration procedures, the model was able to integrate the observed cracks in the infilled walls and other damage in the RC elements.

5.5.2   Eigenvalue analysis

The present section estimated the fundamental frequencies of the MRT2 building through the eigenvalue analysis considering the material properties and frame sections defined from the parametric study. The first three fundamental frequencies and relevant vibration modes attained for the MRT2 building are presented in Table 5.6. This particular building demonstrated its second mode as diagonal, which was unexpected. The first vibration mode was translational, i.e. along Y-axis. The vibration modes were relatively similar to the one obtained from the ambient vibration tests. In addition, the obtained third vibration mode shape was the combination of translational and torsional modes. This indicated that the building's vibration modes were mainly governed by the distribution, location and percentage of openings in the infilled walls. This type of infilled wall distribution had a dominant effect on the stiffness and strength of the building.

Figure 5.33 presents a graphical representation of the MAC values for the first three vibration modes for the experimental and numerical cases. It can be observed that the MAC value varied from 85% to 93%, and the maximum MAC value indicated that the calibrated model was relatively identical to the original MRT2 building. This can be used as a tool to validate the reliability of the model calibration. The observed MAC values revealed that the entire mode shapes can be expected to overlap and showed a good correlation between the experimental and numerical vibration modes.
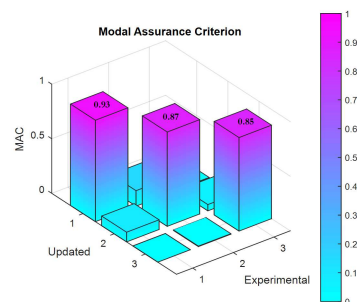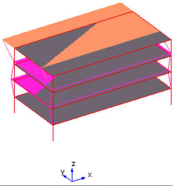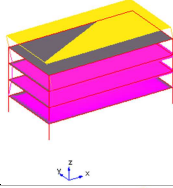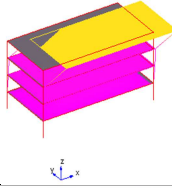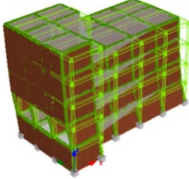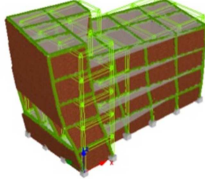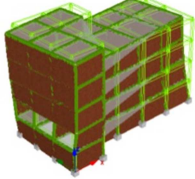
Figure 5.33 – Graphical representation of MAC values for the MRT2 building

Table 5.6 – Eigenvalue analysis results for the MRT2 building: natural frequencies and respective vibration modes

Modal	Frequency (Hz)			First vibration mode	Second vibration mode	Third vibration mode
	f_1	f_2	f_3			
Experimental	2.60	3.90	4.34			
Numerical	2.90	3.41	3.79			

5.5.3   Pushover analysis

Figure 5.34 illustrates the capacity curve for the MRT2 building plotted in both directions. Initially, a steep increase in the stiffness and strength in both directions can be observed, largely in the X direction of the building. The initial strength was assumed to be largely due to the combined effects of the infilled walls and frame structures. The maximum yielding occurred at a global drift of approximately 0.62% and 0.43% in X and Y directions, respectively, and highlighted that the deformation capacity of the infilled building was comparatively lower. The recorded global drift was very small in both directions, but the ISD_{max} might be much higher than expected from its configuration. The ISD_{max} of 1.5%-2% in both directions can be predicted. This state of the building corresponded to moderate to extensive damage in the infilled frame building. After attaining a maximum yielding point, a steep decline in the base shear capacity was recorded in both directions and revealed the in-plane and out-of-plane failure of the infilled walls. In some cases, shear failure in columns can be predicted.
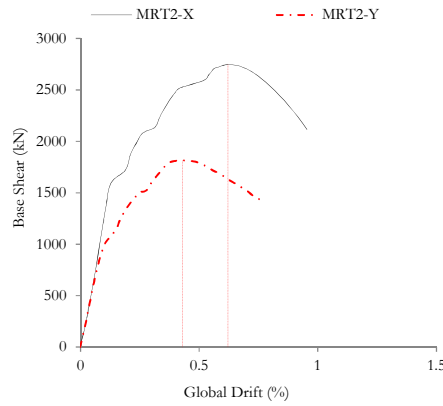
Figure 5.34 – Capacity curve for the MRT2 building in both directions

5.5.4 Nonlinear time history analysis

5.5.4.1 ISD$_{max}$ profile

The variation of inter-storey drift along the height of the building under seismic excitation scaled for a range of IMs was analysed and presented for a particular earthquake, as shown in Figure 5.35. Remarkably, the MRT2 building illustrated a larger drift even when subjected to lower IMs of 0.1g PGA for this particular earthquake, where the attained ISD$_{max}$ was about 0.5% in both directions. This state of the building predicted light to moderate damage in the infilled walls. It exhibited an ISD$_{max}$ higher than 1% in both directions and was mainly concentrated at a single floor (ground floor) and experienced an insignificant drift in the upper storeys when subjected to 0.2g PGA. Furthermore, when the building was subjected to higher IMs, i.e. beyond 0.3g, it exhibited an ISD$_{max}$ greater than 4% in both directions, revealing that the building collapsed under the soft-storey mechanism.
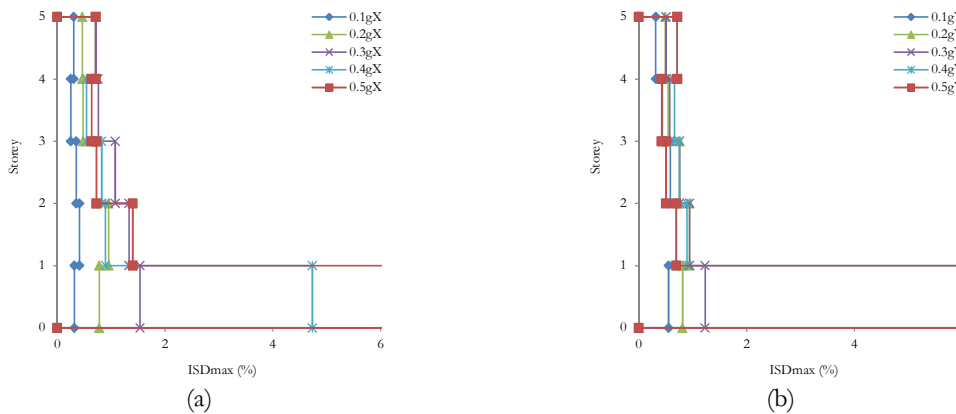
Figure 5.35 – ISD$_{max}$ profile for the MRT2 building, subjected by 8-ChiChi Taiwan earthquake scaled for range of PGA between 0.1 to 0.5g; (a) X direction and (b) Y direction

5.5.4.2 IDA curves

Figure 5.36 presents the IDA curves for the MRT2 building in both directions when subjected to 42 earthquakes, as represented by light solid lines, and where a larger dispersion of the building response for the same IMs was obtained. For low IMs up to 0.2g PGA, the building exhibited a lower ISD_{max} and was expected to behave elastically for the majority of the selected earthquakes in both directions. The increase in the IMs also increased the seismic demand and exhibited a higher ISD_{max}. However, a greater discrepancy was recorded even subjected to same IMs. This was due to the phenomenon that selected earthquakes that have a series of higher frequencies, even for short durations, are most likely to induce maximum building response in comparison to lower frequency content earthquakes recorded for a longer duration. The obtained mean drift, at 0.3g PGA, was more than 2% and 3%, respectively. This state of the building can be reported to have reached an extensive to partial collapse state. Beyond 0.3g PGA, the building can be predicted to have collapsed with mean drift more than 4% in both directions. From the above discussion, it can be concluded that the MRT2 building demonstrated a higher seismic demand and exhibited a higher vulnerability, where structural failure was likely by the dominant soft-storey mechanism.
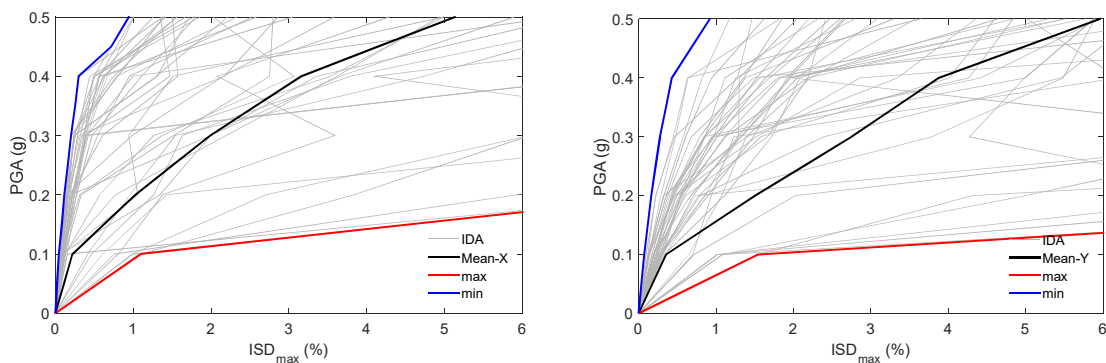
Figure 5.36 – IDA plot for the MRT2 building along X and Y directions, respectively

5.5.4.3 Fragility curves

Figure 5.37 presents the fragility curve for the MRT2 building and shows the probability of exceeding different damage states with respect to PGA. The plot demonstrates that peak slight, light and moderate damage states occurred below 0.3g PGA. In addition, the probability of exceeding extensive, partial collapse and collapse, at 0.3g PGA, ranged between 47% and 22%. Therefore, it can be concluded that the MRT2 building was found

to be highly vulnerable, where larger damage states can be observed even subjected to lower PGA. Thus, the building is recommended for further seismic performance assessment using different strengthening measures.
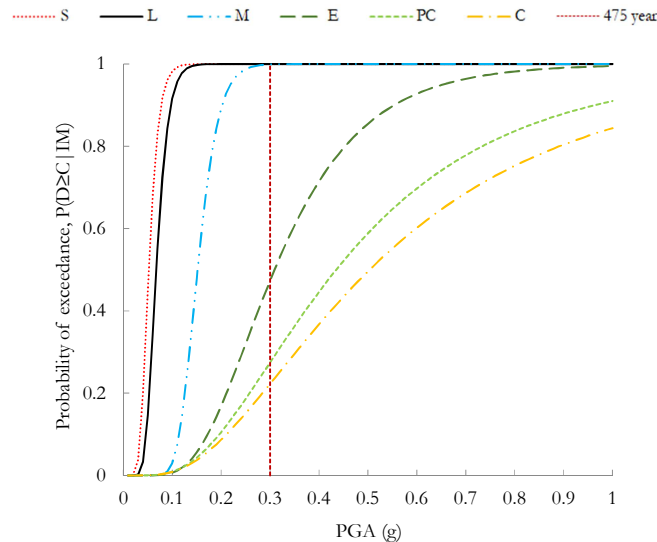
Figure 5.37 – Fragility curve for the MRT2 building. S – slight, L – light, M – moderate, E – extensive, PC – partial collapse, C – collapse

5.6   Khwopa Engineering College Block 'E' (WD1)

In the previous sections, the detailed seismic performance assessment of both non-engineered and pre-engineered buildings was performed and presented. The present section describes the detailed seismic performance of a well-designed building, namely WD1 that was classified as non-damaged to identify the level of damage states that is likely in this type of building. Initially, the building was input into the SeismoStruct software [22], and the existing building and its numerical model are presented in Figure 5.38. The building's east-west orientation was represented along the X-axis and the north-south orientation along Y-axis. The calibrated characteristic strength of the concrete was 20 MPa, the crushing strength of the infilled walls set to 7 N/mm² and the other standard material properties, as discussed in Chapter 4, were initially assigned as a reference, which were adjusted after the model calibration. The geometrical layout and structural sections and locations were similar to the authorized drawings. The dead loads of the assigned elements, such as beams, columns and the infilled walls were estimated by the program through defined sections and the corresponding unit weight of the materials. Whereas other dead loads, such as the slabs, cantilever walls, parapet walls, staircases, etc. were assigned to the

respective beam in the form of UDL and point loads. In addition, a constant live load of 4kN/m² was assumed throughout for load calculation simplicity. Hence, the seismic load was calculated considering 50% of the live load contribution.

Figure 5.38 – WD1 building; (a) Real building and (b) Numerical model

5.6.1 Parametric study

The numerical model assumed various parameters, thus the model required calibration, which was done through the comparison between the numerical and experimental frequencies. The model calibration in the present section was performed by varying the dominant parameters that highly influence the global building frequencies. They included the Young's modulus of the concrete and infilled walls. The study was performed in such a way that the one of the parameters was varied at a time such that other parameters remained constant. The various procedures employed and results attained were as follows:

- Initially, the study was conducted with a variation in the Young's modulus of concrete, namely 16, 19, 22 and 25 GPa representing concrete strength 10 MPa, 15 MPa, 20 MPa and 25 MPa, respectively. The structural sections were assumed to be as defined in the drawings and the Young's modulus of the infilled walls was 4125 N/mm². Figure 5.39 presents the variations in the modal frequencies obtained through the modification of the Young's modulus of concrete. The plot illustrates that when the Young's modulus of concrete was modified from 22 to 25 GPa, the first, second and third frequencies increased by approximately 1%. On the other hand, a decrease in first frequency by about 5% and almost 2.5% in second and third frequencies was estimated when the Young's modulus of concrete varied from 22 to 16 GPa. In addition, a total frequency reduction of about 7% was attained when the Young's modulus of concrete changed from 25 to 16 GPa. This

illustrates that the Young's modulus of concrete was found to be irrelevant on the global model frequencies for infilled RC buildings.
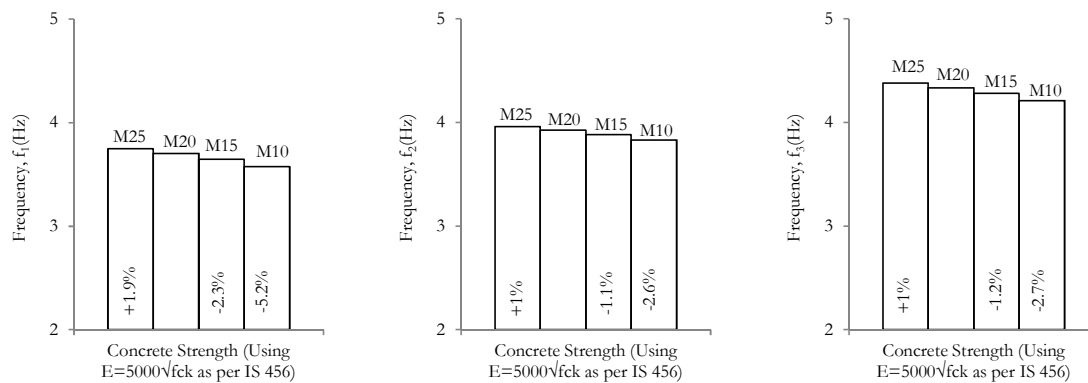
Figure 5.39 – Parametric results for the influence of compressive strength of concrete in the first, second and third fundamental frequencies, respectively, for the WD1 building

- Here, the variation in modal frequencies introduced by the adjustment of the modulus of elasticity of the infilled walls was studied, where the modulus of elasticity of the infilled walls was modified ranges 4125 to 1100 N/mm² representing crushing strength of infilled walls ranges between 7 N/mm² and 2 N/mm², respectively. Figure 5.40 presents the variation of the first three model frequencies obtained through the variation of the modulus of elasticity of the infilled walls with respect to the concrete strength. In the first stage, the concrete strength was set to be 20 MPa and the modal frequencies decreased when the modulus of elasticity of infilled wall was varied from N7 to N5. The decrease in the first, second and third frequencies were almost 17%, 13% and 12%, respectively. Similarly, a 50% to 34%reduction in the frequencies was obtained when the modulus of elasticity of the infilled walls was altered from N7 to N2. In the second and third stages, the concrete strength was set at 15 and 25 MPa successively and similar conclusions were obtained. When the modulus of elasticity of infilled wall was varied from N7 to N2, a 50% to 34%decrease in the frequencies was attained. In addition, it was also observed that when one modal frequency tended to coincide with an experimental frequency, the other frequencies deviated largely. Due to this phenomenon, the present study intended to calibrate the model mainly focusing on the first fundamental frequency, which was a dominant frequency in the buildings. Based on this assumption, the difference in the first frequencies could be reduced to <1% for a concrete compressive strength of 20 MPa and modulus of elasticity of the infilled walls of 1100 N/mm² (i.e. equivalent to 2

N/mm²) while the other structural sections and details remained similar to the authorized drawings, as discussed in Chapter 3.
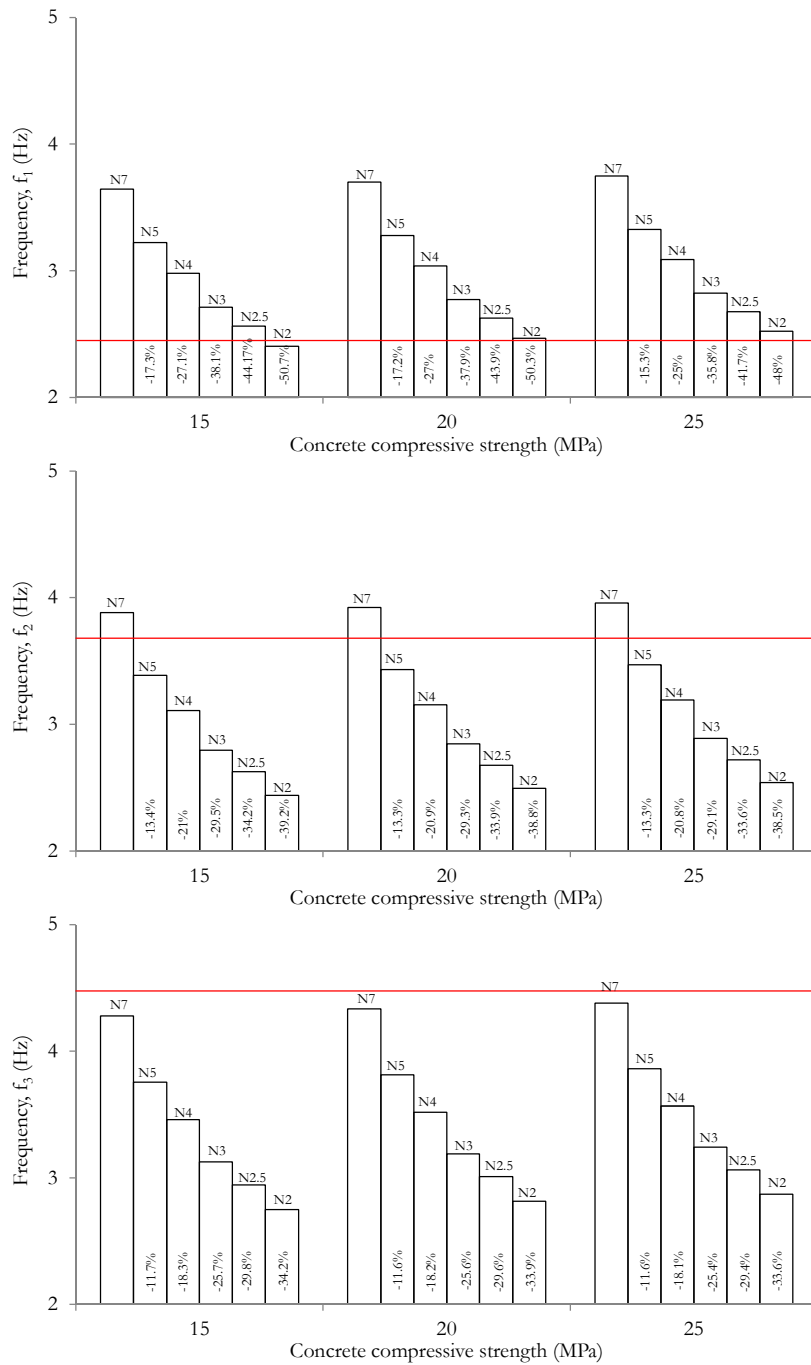
Figure 5.40 – Parametric results regarding the influence of the Young's modulus of infilled panels in the first, second and third fundamental frequencies, respectively, for the WD1 building

The parametric study results for the WD1 building was aligned with the other case study buildings, and it concluded that the modulus of elasticity concrete did not have significant influence on the global building frequency when compared with the parameters of the infilled walls. The difference in the frequencies was reduced to <1% for the concrete

strength of 20 MPa, an adjusted modulus of elasticity for the infilled walls of 1100 N/mm² and structural sections similar to the authorized drawings.

5.6.2 Eigenvalue analysis

Table 5.7 presents the three fundamental frequencies and corresponding vibration modes obtained from the eigenvalue analysis. It demonstrates that the first two vibration modes were translational and third one diagonal. The results are reasonably similar to those obtained from ambient vibration tests. The first, second and third numerical frequencies were 2.47, 2.49, and 2.82 Hz, respectively. A large difference between the experimental and numerical frequencies was recorded for the second and third fundamental frequencies.

The reliability of the calibrated model was verified through the estimation of the MAC values, obtained from Equation (5.1). Figure 5.41 shows the attained MAC values for the WD1 building where the MAC values for first three mode shapes were in the range of 79% to 94%. The obtained MAC value for the first frequency was higher than 90%. This indicated that the first mode between the experimental and analytical results were expected to overlap; thus, it can be stated that a better correlation was attained. On the other hand, the third mode shape had a lower MAC value, and thus a poor correlation was attained between them.
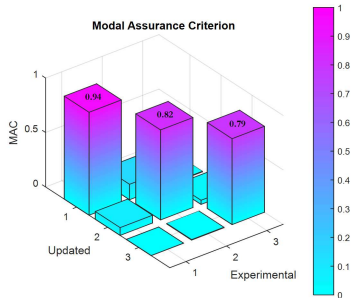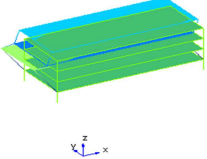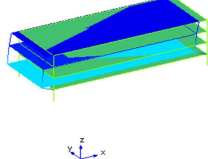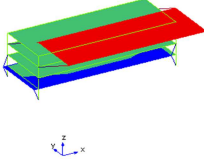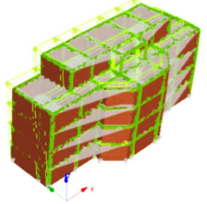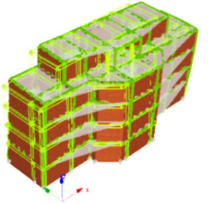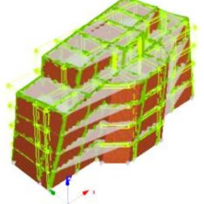
Figure 5.41 – Graphical representation of MAC values for the WD1 building

Table 5.7 – Eigenvalue analysis results for the WD1 building: natural frequencies and respective vibration modes

Modal	Frequency (Hz)			First vibration mode	Second vibration mode	Third vibration mode
	f_1	f_2	f_3			
Experimental	2.45	3.68	4.48			
Numerical	2.47	2.49	2.82			

5.6.3   Pushover analysis

Figure 5.42 presents the capacity curve for the WD1 building in both directions showing a higher initial stiffness and strength. The attained maximum base shear capacity was comparable in both directions, whereas the maximum capacity occurred at an early global drift in the X direction. The maximum capacity occurred at a global drift of around 0.57% and 0.94% in the X and Y directions, respectively. At this point, the building can be expected to exhibit an ISD_{max} below 1% in both directions, such that most infilled walls would exhibit light to moderate damage. The yielding point illustrated the maximum contribution of the infilled walls to the frame structures that behaved like a monolith in resisting seismic loads. If the structure is subjected to lateral loads beyond this point, moderate to extensive damage can be expected to appear on the infilled walls and its contribution would decrease. However, it was observed that the degradation of capacity curves was more uniform in both directions, highlighting that the building possesses higher ductility and can behave elastically for a large deformation. The ultimate point was attained at larger global drift; thus, an ISD_{max} of around 1.5% in both directions can be predicted. This building has larger sections for structural elements than are actually necessary, and thus the collapse of the WD1 building is unlikely.
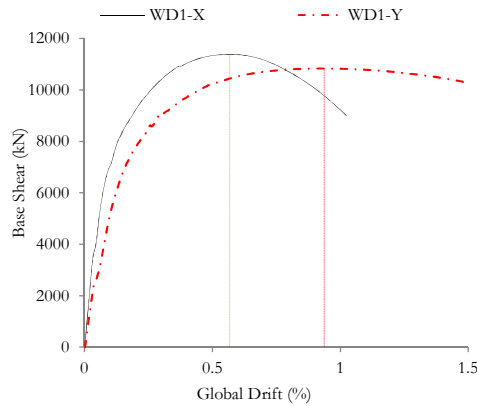
Figure 5.42 – Capacity curve for the WD1 building

5.6.4 Nonlinear time history analysis

5.6.4.1 ISD$_{max}$ profile

A typical ISD$_{max}$ profile for the WD1 building is illustrated in Figure 5.43, which demonstrates the distribution of the drift along the height of the building. For this particular earthquake, the building exhibited a relatively uniform and lowered ISD$_{max}$, i.e. <1%, up to a 0.2g PGA. A significant increase in the ISD$_{max}$ was recorded at 0.3g PGA in both directions and was mainly concreted in a single storey at the ground floor. The ISD$_{max}$ recorded at the ground floor, at 0.4g PGA, was approximately 4.8% and 2.2% in X and Y directions, respectively. This revealed that the WD1 building collapsed in X direction, most likely under the soft-storey mechanism. On the other hand, in-plane cracking and crushing of the infilled walls can be expected in Y direction. This revealed that a slight increase in IM can considerably increase the seismic demand, and as a result, substantially increase in ISD$_{max}$ attained in both directions.

(a)   (b)
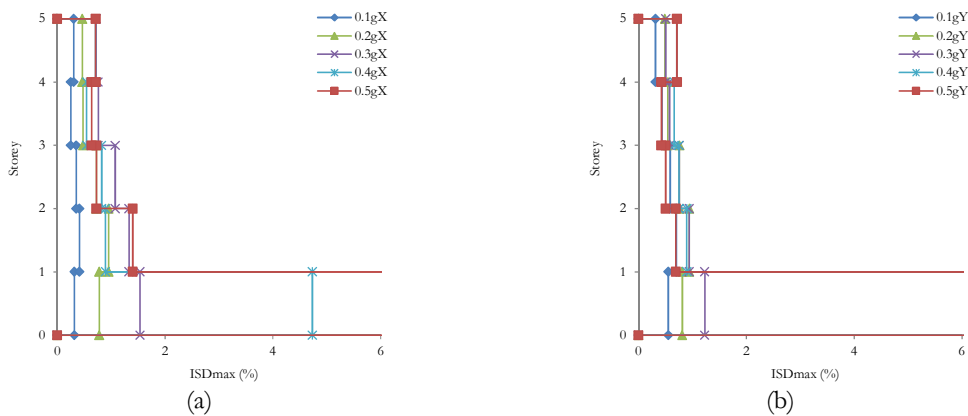
Figure 5.43 – ISD$_{max}$ profile for the WD1 building, subjected by 16-ChiChiTaiwan earthquake scaled for range of PGA between 0.1 and 0.5g; (a) X direction and (b) Y direction

5.6.4.2 IDA curves

Figure 5.44 presents the IDA curves for the WD1 building and demonstrates the distribution of the building response in terms of maximum inter-storey drift with respect to the IMs due to selected 42 ground motion records. The WD1 building behaved elastically for the majority of the subjected earthquakes until a 0.3g PGA was reached in both directions. This IM potentially initiated slight to moderate damage in the infilled walls in both directions. The mean IDA curves at 0.4g PGA exhibits a mean ISD_{max} of approximately 1.2% and <1% in X and Y directions, respectively. Similar to the previous case studies, some of the IDA curves exhibit a lower ISD_{max}, even for increasing IMs. This highlighted that a few earthquakes reveal a tremendously higher seismic demand. This type of phenomenon develops when buildings subjected to higher IMs are already in a collapsed state or do not meet the seismic requirement for lower IMs. The building response can be expected to end elasticity beyond 0.4g PGA, and the non-linearity would become dominant for the majority of the subjected earthquakes. The recorded ISD_{max} from mean IDA curve, at 0.5g PGA, corresponds 2% and 1.5% in X and Y directions, respectively. This state of the building was predicted to have extensive damage in the infilled walls. The lower ISD_{max} recorded from the mean IDA curves in both directions, even subjected to higher IMs, revealed that the infilled walls and frames behaved as a monolith in resisting the seismic force.
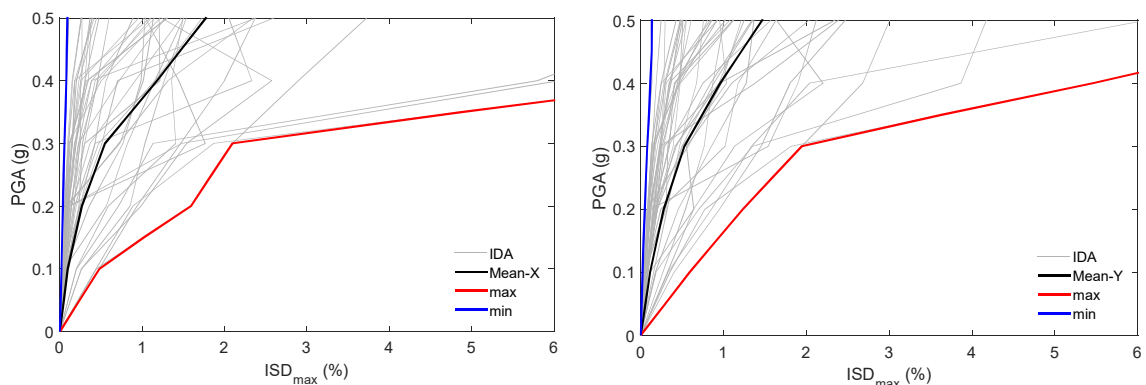
Figure 5.44 – IDA curves for the WD1 building along X and Y directions, respectively

5.6.4.3 Fragility curves

The fragility curve for the WD1 building is demonstrated in Figure 5.45 and shows the probability of exceeding various damage states with respect to IMs. The fragility curve illustrates the conditional probability of exceeding each damage state, such that peak slight

and light damage states occur below 0.3g PGA. Similarly, the conditional probability of exceeding higher damage states, such as extensive, partial collapse and collapse, at 0.3g PGA, was approximately 7.4%, 3.6% and 2.3%, respectively. Furthermore, the fragility curve for the WD1 building also revealed a remarkable result, where the probability of exceeding moderate, extensive, partial collapse and collapse damage at 1g PGA ranged 95% to 27%, respectively. This indicated that this particular WD1 building would likely withstand higher IMs and the potential damage would also be quite lower than initially predicted. This indicated that the WD1 building exhibited superior performance and would not be recommended for further strengthening measures.
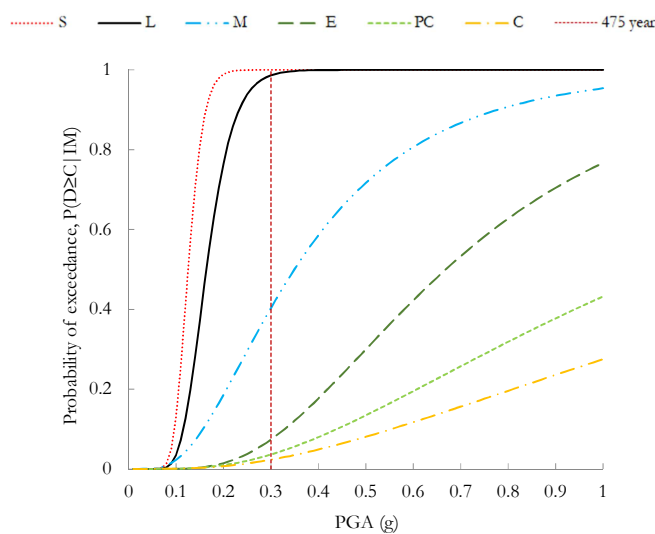
Figure 5.45 – Fragility curves for the WD1 building. S – slight, L – light, M – moderate, E – extensive, PC – partial collapse, C – collapse

5.7   Khwopa College of Engineering Block 'E' (WD2)

The WD2 building was also well-designed and classified as non-damaged, as presented in detail in Chapter 3. The primary objective of this building selection was to evaluate the seismic performance of another well-designed building under non-linear static and dynamic time history analyses, and also to reinforce the results and conclusions acquired from the previous WD1 building. It was interesting to investigate the seismic performance of such a well-designed building under several earthquakes because it had an irregular distribution of the infilled walls. The existing WD2 building and its numerical model developed using SeismoStruct software [22] are demonstrated in Figure 5.46. The east-west orientation of the building was represented along the X-axis and north-south orientation along the Y-axis. The material properties of the structural elements and infilled walls were initially assumed

and then later adjusted through the model calibration. Other geometrical layout and structural sections and its detailing were assigned as recorded in the authorized drawings. The dead and live loads that were considered were similar to the WD1 building. The estimated loads were assigned to the respective beams in the form of UDL and point loads. The seismic performance assessment of the building was analysed and presented with the help of IDA and fragility curves.

(a)   (b)
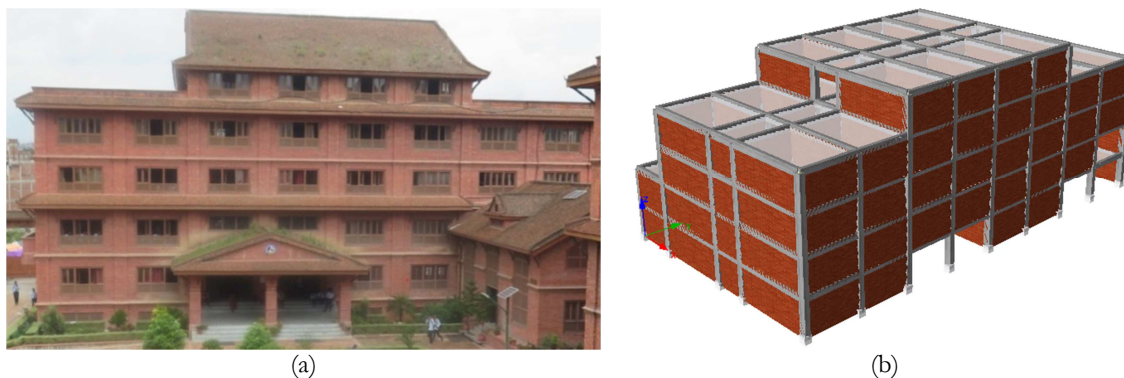
Figure 5.46 – WD2 building; (a) Real building and (b) Numerical model

5.7.1   Parametric analysis

The numerical model was developed in which various parameters were assumed, thus it was required to calibrate the model before employing it for non-linear static and dynamic analyses. If employed without model calibration, the reliability and accuracy of the attained results would be uncertain and ambiguous. Therefore, in the first stage, the model calibration was carried out by varying the Young's modulus of the concrete and infilled walls. The obtained building frequency was then compared with the ambient frequencies. The procedure continued until the difference between the frequencies was reduced below 10%. The parametric study performed and obtained results were as follows:

- The influence of Young's modulus of concrete on the fundamental frequencies was investigated, where a commonly used concrete strength was considered. The Young's modulus of strengths included ranges 25 to 16 GPa represented as M25, M20, M15 and M10, respectively, and the modulus of elasticity of infilled walls was set 4125 N/mm² while other parameters remained constant. Figure 5.47 presents the variation of the modal frequencies that were obtained through the adjustment of the Young's modulus of concrete. An increase in the first modal frequency by around 2.5% was observed when the Young's modulus of concrete varied from 22

to 25 GPa. In addition, when the Young's modulus of concrete was modified from 22 to 16 GPa, the first frequency was reduced by approximately 6.3%, whereas the second and third frequencies were reduced by almost 4.4%. Furthermore, the first frequency was increased by almost 10% when the Young's modulus of concrete improved from 16 to 25 GPa. In this way, the difference between the first frequencies could be reduced to 16.5% for a Young's modulus of concrete of 16 GPa and crushing strength of infilled 7 N/mm² for the infilled walls.
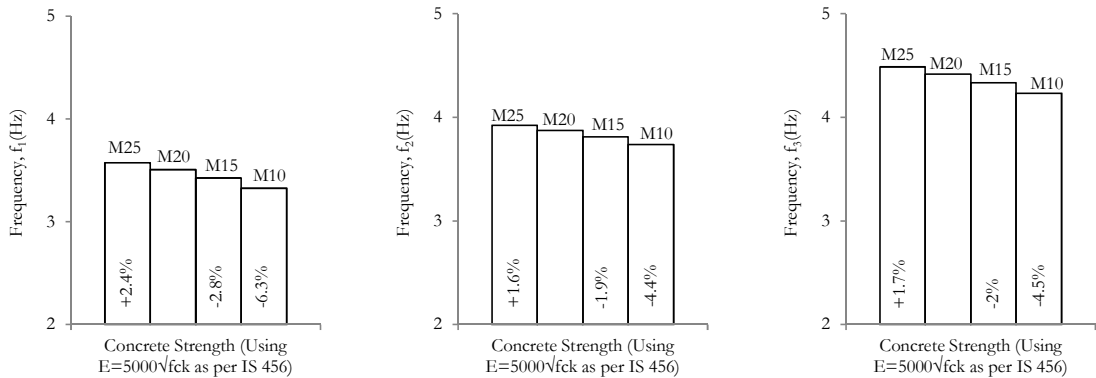
Figure 5.47 – Parametric results for the influence of Young's modulus of the concrete on the first, second and third frequencies, respectively

- In this section, the parametric study was carried out varying the modulus of elasticity of the infilled walls and investigating its influence in the global building frequencies. The modulus of elasticity for the infilled walls included ranges 4125 to 1375 N/mm² represented by N7.5, N5, N4, N3 and N2.5, respectively, whereas the concrete strength and other parameters remained constant. In the first step, the concrete strength was set to be 20 MPa and the modulus of elasticity of infilled wall was varied, as defined above. Figure 5.48 presents the variation of the building fundamental frequencies obtained due to the variation of the modulus of elasticity of the infilled walls. When the modulus of elasticity of the infilled walls varied from N7 to N2.5, a decrease in the fundamental frequencies was recorded, such that the first, second and third frequencies were reduced from 27% to 26%. Similarly, in the second stage, the concrete strength was set 15 MPa and the first frequency decreased by around 27% when the modulus of elasticity of the infilled walls varied from N7 to N2.5. Furthermore, for a concrete strength of 25 MPa and modulus of elasticity of the infilled walls from 4125 to 1375 N/mm², the first frequency decreased by almost 26%. Therefore, the difference in first frequency (between modal and experimental) was reduced below 1% for a modulus of elasticity of the

infilled walls of 1650 N/mm² and concrete strength set as 20 MPa while other parameters remained constant.
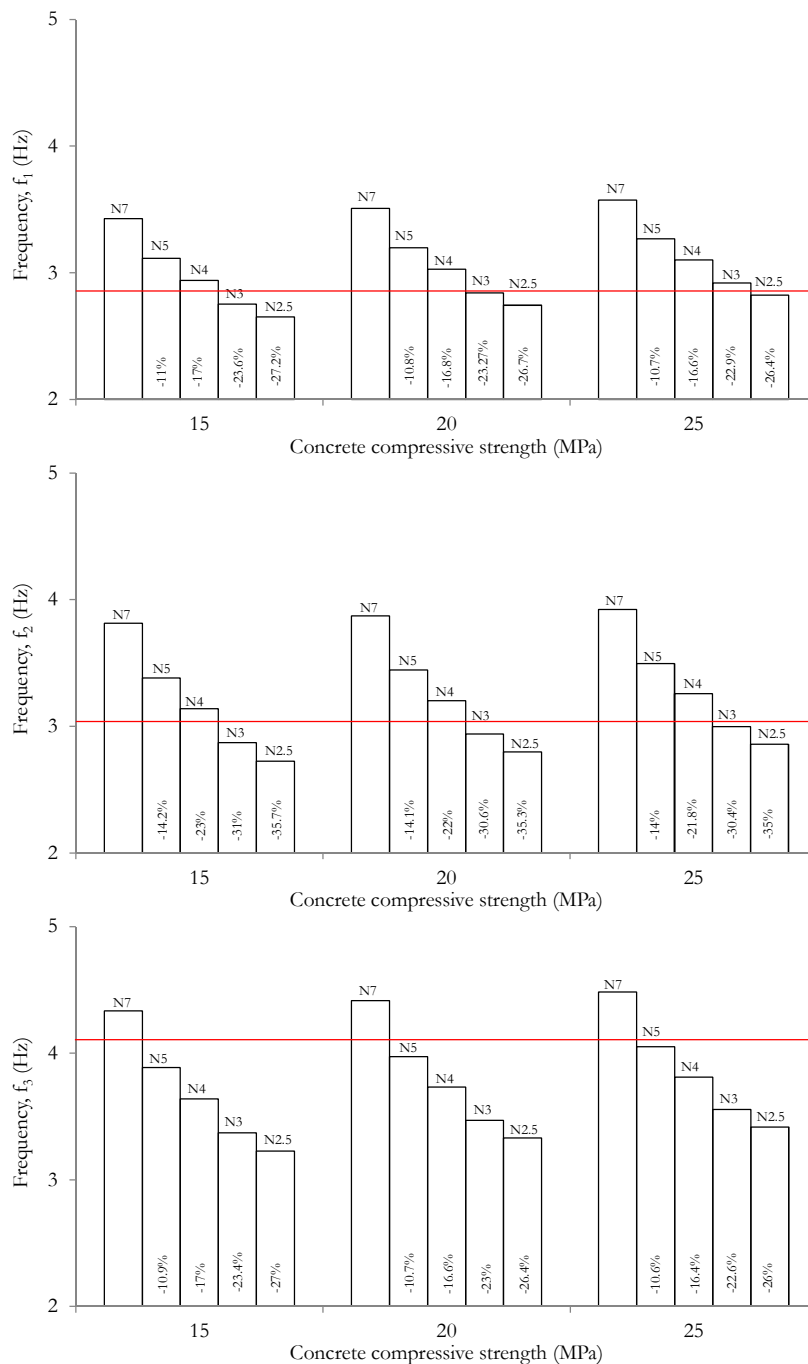
Figure 5.48 – Parametric results regarding the influence of Young's modulus of infilled panels on the first, second and third frequencies, respectively

From above discussion, it can be concluded that the modulus of elasticity of concrete was not a governing factor in influencing global frequencies of the infilled frame building, which might have been a dominant factor if the structure was bare framed. The modulus of

elasticity of the infilled walls was found to have greater impact in influencing the frequencies. The difference in the first frequency was reduced below 1%.

5.7.2 Eigenvalue analysis

The eigenvalue analysis was performed for the calibrated model in which the compressive strength of the concrete was 20 MPa and crushing strength of the infilled walls was set 3 N/mm^2, as obtained in the parametric study. Table 5.8 presents the experimental and numerical fundamental frequencies and their corresponding vibration modes. As expected, the first two vibration modes were recorded as translational and the third one as diagonal, which is reasonably comparable to the ambient vibration modes. In addition, the experimental and numerical frequencies obtained were also relatively similar, where the first model fundamental frequency was 2.84 Hz along the X-axis, the second frequency was 2.94 Hz along the Y-axis and the third frequency was 3.47 Hz.

The calibrated model was again investigated through the MAC values that help to characterize the correlation between the analytical and experimental mode shapes for the WD2 building, as shown in Figure 5.49. The first three modes were compared between the calibrated models and experimental results, and the attained MAC values ranged between 90% and 94%. The attained MAC values indicated that the mode shapes nearly overlapped and the correlation between them was also satisfactory.
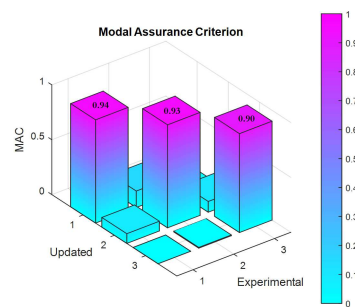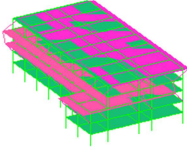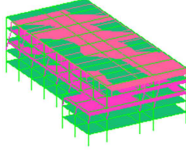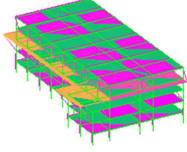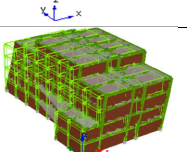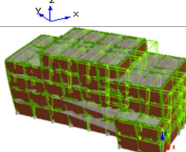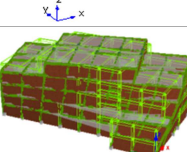
Figure 5.49 – Graphical representation of MAC values for the WD2 building

Table 5.8 – Eigenvalue analysis results for the WD2 building: natural frequencies and respective vibration modes

Modal	Frequency (Hz)			First vibration mode	Second vibration mode	Third vibration mode
	f_1	f_2	f_3			
Experimental	2.86	3.04	4.11			
Numerical	2.84	2.94	3.47			

5.7.3   Pushover analysis

Figure 5.50 demonstrates the capacity curve for the WD2 building in both directions, and it was observed that the initial stiffness and strength were reasonably similar and appeared as a single line. A slightly higher maximum base shear capacity and higher global drift was observed along the X direction of the building. The global drift that corresponded to the maximum capacity was approximately 1.14% and 0.9% in the X and Y directions, respectively. This point reveals the maximum contribution of the infilled walls to the frame structures, where minor hair line cracks are likely to be visible in the infilled walls. It is well known that the global drift does not represent the maximum inter-storey drift that had occurred at this point, thus it can be expected to have an ISD_{max} <1% in both directions. This building has light to moderate damages in the infilled walls. A steep degradation of the capacity curves was observed beyond the yielding point in both directions. This can be predicted mainly due to in-plane and out-of-plane failure of the infilled walls. The ultimate point corresponds to a global drift of approximately 1.4% and 1.2% in the X and Y directions, respectively. The ISD_{max} can be expected to be in the range of 1.5-2% in both directions. The building possesses moderate to extensive damage in the infilled walls and in some cases crushing of the infilled walls can be observed.
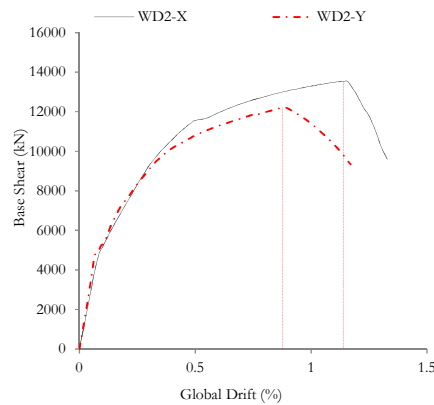
Figure 5.50 – Capacity curve for the WD2 building

5.7.4   Nonlinear time history analysis

5.7.4.1   ISD$_{max}$ profile

A typical ISD$_{max}$ profile for the WD2 building is illustrated in Figure 5.51, in which the distribution of the ISD$_{max}$ along the height with respect to IMs is shown. The lower IMs exhibited a considerably uniform and lower drift throughout and held true for PGA until 0.2g. This also illustrates the uniform distribution of stiffness and strength throughout, which was mainly due to the un-cracked infilled walls that resisted the seismic action. When the IMs increased to 0.3g and above, the seismic demand increased significantly and failure of the building under the soft-storey mechanism became dominant. The maximum drift was observed to be concentrated at the ground floor, most likely due to in-plane and out-of-plane failure of the ground infilled walls. Therefore, a single storey drift concentration was observed at the ground floor and consecutively lower drift at the upper storeys for this particular earthquake.

(a)   (b)
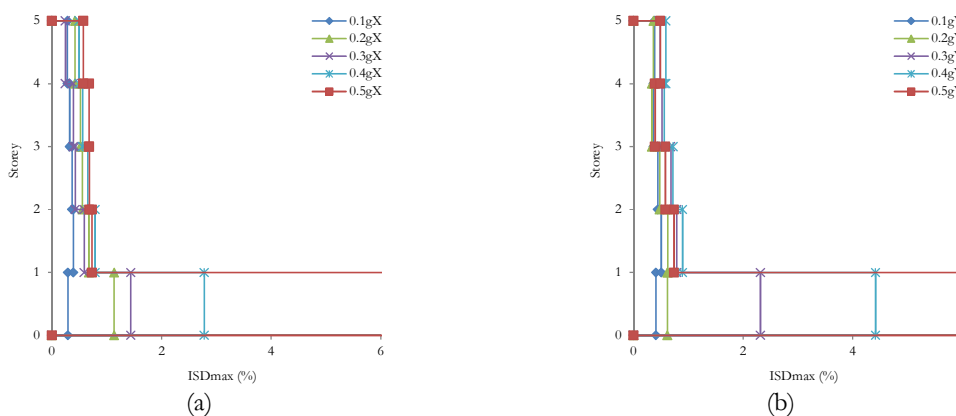
Figure 5.51 – Typical ISD$_{max}$ profile for the WD2 building, subjected by 18-ChiChiTaiwan earthquake scaled for range of PGA between 0.1 and 0.5g; (a) X direction and (b) Y direction

5.7.4.2   IDA curves

Figure 5.52 presents the IDA curves for the WD2 building in both directions obtained from the dynamic time history analyses, per the procedure defined in Chapter 4. Each IDA curve is characterized by light solid lines that represent the building response to the subjected earthquake and suitably scaled IMs. A narrow dispersion of ISD_{max} was recorded until 0.2g PGA in both directions, which indicates that the building components were in the elastic region and behaved elastically. The corresponding ISD_{max} detected from the mean IDA curves was <0.5% in both directions. Similarly, for the majority of subjected earthquakes, the IDA curve indicated elastic behaviour for the considered range of IMs along the X direction. A larger scattering of ISD_{max} was recorded beyond 0.3g PGA along the Y direction, and the building was expected to undergo non-linearity with hardening in the structural members. From the above discussion and plot, it can be concluded that the building illustrated superior seismic performance for medium to higher IMs for the majority of the selected earthquake ground motions and considered IMs.
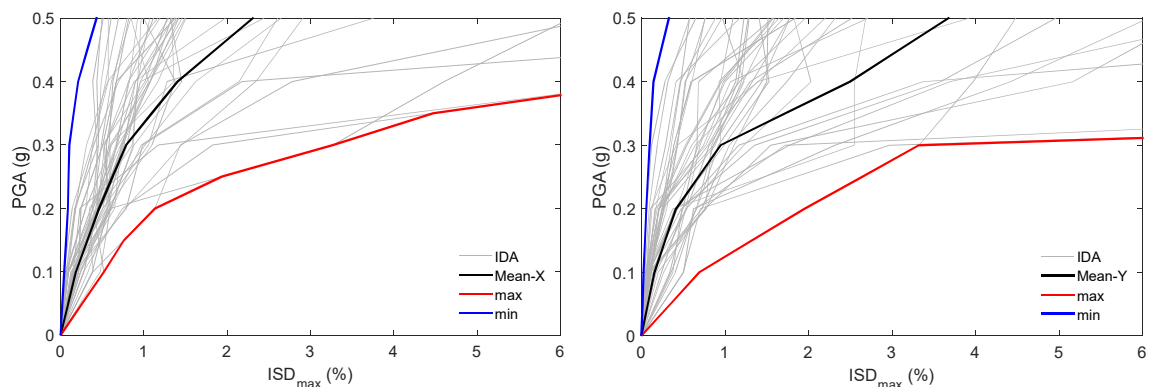
Figure 5.52 – IDA curves for the WD2 building along X and Y directions, respectively

5.7.4.3   Fragility curves

Figure 5.53 illustrates the fragility curve that shows the probability of exceeding each damage state with respect to the PGA. The plot shows that the peak slight, light and moderate damage states occurred below 0.4g PGA. Similarly, the probability of exceeding higher damage states, such as extensive, partial collapse and collapse states, at 0.3g PGA, ranged 18% to 5.3%, respectively. In addition, the vulnerability of the building was investigated at 1g PGA such that the probability of exceeding extensive, partial collapse and collapse states ranged from 79% to 28%, respectively. This also indicated that the

WD2 building shows enhanced seismic performance and is capable of experiencing higher IMs than actually predicted for Nepal.
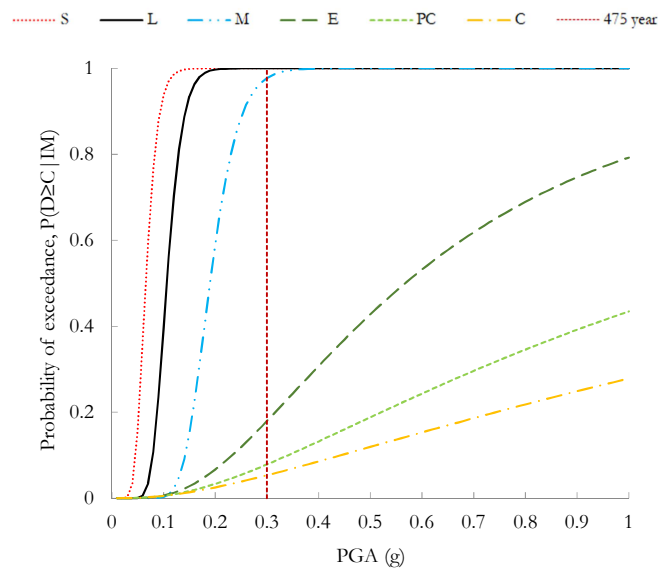
Figure 5.53 – Fragility curve for the WD2 building. S – slight, L – light, M – moderate, E – extensive, PC – partial collapse, C – collapse

5.8   Global Comparative Analysis

The present section considers the three building design approaches, where the results obtained above for each design approach were combined. The results are presented and interpreted in terms of the inter-storey drift profile and fragility curves. Table 5.9 presents a quick overview of all case study buildings that were presented in detail in Chapter 3 and analysed in the present Chapter. The damaged and non-damaged non-engineered buildings were grouped together and represented by building name CCP. Similarly, pre-engineered buildings with damaged and non-damaged states were grouped together and characterized by building name MRT. Finally, the well-designed buildings were grouped and denoted by building name WD.

Table 5.9 – General description of various construction approaches

Bldg. name	Bldg. typology	No. of storey	Damage state	Remarks
CCP	CCP1	3	non-damaged	The building has regular infilled orientation and some hair line cracks on the infilled panels only
	CCP2	4	damaged	Two corner column were damaged and retrofit carried out during the site survey and cracks in the infill panels
MRT	MRT1	3	non-damaged	Structural irregularity, lack of column at the beam-beam joint, no floor beam at the stair portion
	MRT2	5	damaged	No internal infill panels at the basement, irregular distribution of infilled panels throughout, corner column damaged
WD	WD1	5	non-damaged	some hair line cracks on the infilled panels
	WD2	5	non-damaged	some hair line cracks on the infilled panels

5.8.1 Inter-storey drift profile

Figure 5.54 presents the ISD_{max} profile for buildings based on the three designs that were subjected to the 8-ChiChi Taiwan earthquake, at 0.3g PGA. A single storey drift concentration with a maximum drift at the ground floor and an insignificant drift at the consecutive upper floors was recorded for the MRT1-WO-GI building. Similarly, both non-engineered buildings exhibited a maximum ISD_{max} at the ground floor and comparatively lower drift at the consecutive upper floors in both directions. The higher drift at the ground floor revealed the in-plane cracking and out-of-plane crushing of the infilled walls, potentially leading to failure of the building under the soft-storey mechanism. Finally, the well-designed buildings demonstrated a relatively smaller drift and comparatively uniform drift throughout. The entire drift profile for the infilled buildings revealed a uniform distribution of stiffness and strength throughout. The attained drift profile indicated that the well-designed buildings demonstrated an enhanced seismic performance compared to the pre-engineered and non-engineered buildings. In addition, the pre-engineered buildings were found to be relatively much more vulnerable than non-engineered buildings. This was potentially due to the irregular distribution of the infilled walls and added number of storeys.
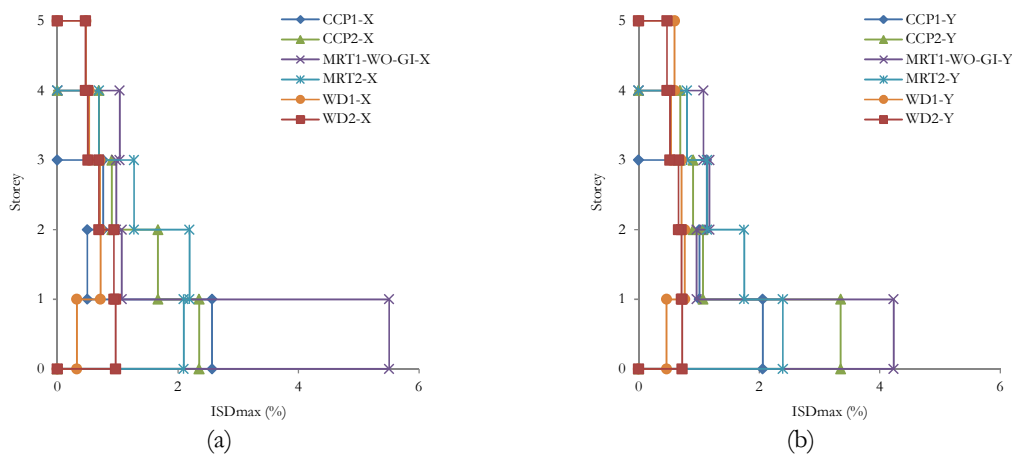
Figure 5.54 – Comparative ISD$_{max}$ profile for various design approaches, plotted for 8-ChiChi Taiwan earthquake of 0.3g PGA; (a) X direction and (b) Y direction

5.8.2 Fragility curves

Figure 5.55 presents the fragility curves for the three building design approaches to examine and conclude the probability of exceeding damage states with respect to the PGA. The vulnerability of the buildings was compared considering four higher damage states, namely moderate, extensive, partial-collapse and collapse. Figure 5.55 (a) illustrates the comparative fragility curve for the moderate damage state. The plot shows that the probability of exceeding the peak moderate damage state was approximately similar for all design approaches. This revealed that all the building design approaches are likely to initiate light to minor cracks in the infilled walls. Similarly, Figure 5.55 (b) presents the fragility curves for the extensive damage state. The plot shows that the probability of exceeding extensive damage for each PGA was always higher for the MRT building in comparison to the CCP and WD buildings. The probability of the extensive damage state for CCP, MRT and WD buildings at 0.3g PGA was approximately 42%, 45% and 17%, respectively. Furthermore, Figure 5.55 (c) shows the comparative fragility curves for the partial collapse state. The probability of exceeding partial collapse w.r.t PGA was always greater for the MRT building. The probability of partial collapse for the CCP, MRT and WD buildings at 0.3g PGA was approximately 24%, 31% and 8.2%, respectively. Finally, Figure 5.55 (d) shows the fragility curves for total collapse. Similar to the other damage states, the MRT building is more likely to collapse. The probability of exceeding collapse for the CCP, MRT and WD buildings at 0.3g PGA was approximately 18.5%, 24% and 4%, respectively.

The entirety of the discussions and findings indicated that the case study MRT buildings were found to be more vulnerable when compared to the CCP buildings, which was unexpected. However, it is to be noted that the buildings classified as pre-engineered buildings were built before the MRT guidelines were implemented and do not comply with the guidelines. The positive conclusion that can result from the present study is that vertical irregularity and different arrangements of infilled walls largely influences the behaviour of the buildings. Hence, its orientation and location should be regular as much as possible. Furthermore, the well-designed buildings demonstrated a satisfactory level of enhanced seismic performance.
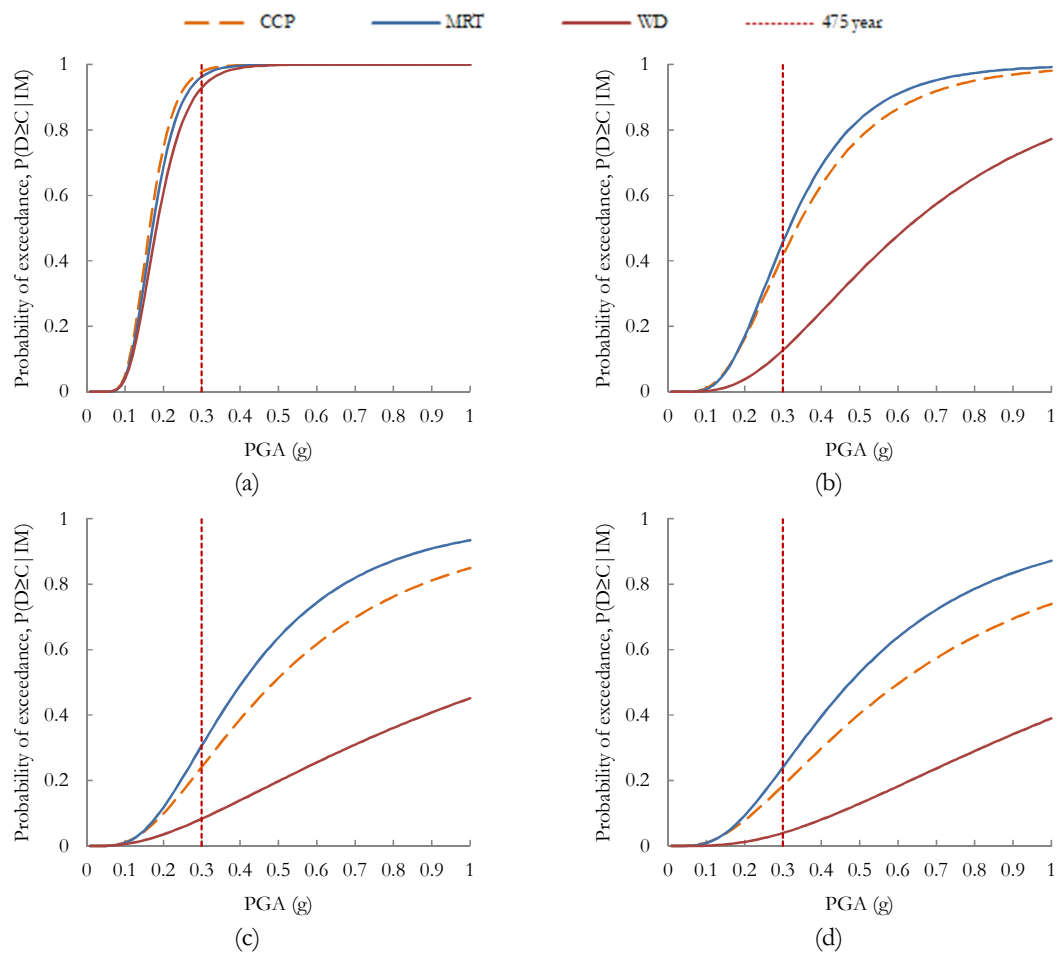
Figure 5.55 – Comparative fragility curves for various design approaches; (a) Moderate, (b) Extensive, (c) Partial collapse and (d) Collapse states

5.9   Conclusion

The seismic performance assessment of the buildings that were built based on three different design approaches were evaluated in this chapter. All the case studied buildings were initially modelled using SeismoStruct software. Initially, the model was calibrated by varying the compressive strength of the concrete, column sections and crushing strength of the infilled walls. Table 5.10 summarizes the material properties adopted after the model calibration. The calibrated models were also validated through MAC values, where comparisons between the experimental and analytical models were carried out. The obtained MAC values indicated that in most of the cases, the higher MAC values revealed the overlap between the original and calibrated models.

Table 5.10 – Summary of the material properties adopted after model calibration

Bldg. name	Experimental frequencies (Hz)			Numerical frequencies (Hz)			Young's modulus	
	f1	f2	f3	f1	f2	f3	Concrete (GPa)	Infill wall (N/mm²)
CCP1	4.89	5.28	5.34	4.95	6.06	6.94	16	1100
CCP2	2.74	3.47	4.29	3.07	3.80	4.06	16	825
MRT1	1.40	1.56	-	1.42	1.50	-	16	-
MRT2	2.60	3.90	4.34	2.90	3.41	3.79	19	825
WD1	2.45	3.68	4.48	2.47	2.49	2.82	22	1100
WD2	2.86	3.04	4.11	2.84	2.94	3.47	22	1650

Initially, the influence of the infilled walls on the frame structures was studied considering the MRT1 building with various dispositions of the infilled panels. The study concluded that for this particular building, the infilled structure increased the frequency almost four times compared to the bare frame. In addition, the inter-storey drift for the infilled structure was relatively uniform throughout the building for low to medium IMs. For low damage states (i.e. slight, light, moderate and extensive), the MRT1 and MRT1-WO-GI buildings illustrated a similar behaviour. The performance of the MRT1-W-Irre.-I model also demonstrated a similar behaviour to the MRT1-W-I model. The fully infilled building can reduce the partial collapse at 0.3g PGA by around 70% in comparison to the soft-storey and bare frame buildings. Similarly, the collapse was reduced by almost 20%. This indicated that the addition of infilled walls can enhance the seismic performance for low to medium earthquakes, but other constraints related to the infilled wall construction and connection with the frames are considered ideal.

The comparison of buildings built based on three design approaches were also investigated through the fragility curves. The MRT buildings selected in this study did not obey the

MRT guidelines, such as a limitation on number of storeys, irregularity and so on. The performance of all case study buildings was found to be similar for lower damage states (i.e. slight and light). However, for the moderate damage state, the performance of CCP was poor and likely to initiate damage earlier than the MRT and WD buildings. For extensive, partial collapse and collapse states, interestingly the performance of the MRT buildings was observed to be far inferior in comparison to the CCP and WD buildings. This conclusion could mislead perceptions. The main reason behind its poor performance was the vertical irregularity and number of added storeys. The CCP buildings considered had regular infilled walls and a limited number of storeys. Hence, taking only the positive information, it can be concluded that the regularly infilled CCP structures can exhibit better seismic performance than irregularly infilled and disorganized MRT buildings, and vice-versa. Based on the above conclusions, further study was carried out on the CCP1, CCP2, MRT1 and MRT2 buildings with the addition of different retrofit measures.

Chapter 6.

Seismic Retrofitting of the Case Study Buildings

6.1   Introduction

The four case study buildings (non-engineered and pre-engineered) revealing poor seismic performance, as analysed and discussed in Chapter 5, was further studied. Three retrofit measures were used in each case study building, and their effectiveness in enhancing seismic performance were evaluated. The retrofit measures included concrete column jacketing, circular hollow section (CHS) steel bracing and addition of an RC shear wall, commonly practiced in Nepal. Based on the trend of retrofit practice, concrete column jacketing was recorded to be the most used retrofitting technique, followed by RC shear wall and steel bracing. Concrete column jacketing was performed by enlarging the existing column size by adding a new layer of confining concrete reinforced with longitudinal and transverse reinforcements. This method was particularly used for the repair and maintenance of damaged columns and beams in the building. As reviewed in Chapter 4, the method not only increases the stiffness and strength capacities of the existing building structures but also improves ductility at the member level.

These retrofit techniques were employed for the selected case study buildings. The primary objective of introducing retrofit measures is to minimise structural irregularities in order to correct discontinuities and obtain a regular structure for improving seismic performance. For each case study building, the infill walls observed at the site were modelled along with retrofit strategies, such that the performance of the building could be evaluated by the combination of both existing infill walls and newly added structural elements. Taghavi and Miranda (2003) [211] revealed that the total monetary loss caused by damage to the non-structural components accounts for approximately 62%, 70% and 48% of the total investment in office, hotel and hospital buildings, respectively. In the present study, the retrofit measures were mainly employed for the structural elements and did not focus on the reduction of the collapse of non-structural elements. However, the reduction of the

seismic demand, namely the inter-storey drift, will cause a direct reduction of the non-structural drift. One of the main aims of the present work was to enhance the seismic performance of the case study buildings to reduce the number of injuries and fatalities. In addition, the study also attempted to reduce large drift concentration in a single storey, primarily recorded in the existing RC buildings, so that the uniform distribution of stiffness and strength can be obtained to avoid the soft-storey mechanism.

6.2   General Procedure Adopted for Retrofit

This section discusses three retrofit approaches considered for the existing non-engineered and pre-engineered buildings under study, namely concrete column jacketing, addition of RC shear walls and use of steel bracings.

6.2.1   Concrete column jacketing

One of the initial questions considered was related to the selection of columns for jacketing. Mostly critical columns (critical in shear force and bending moments), such as corner columns and short-columns, were selected for jacketing. The procedures for RC jacketing elements design followed the guidelines IS 15988: 2013 [135] and Section 8.5.1.1, and are also discussed in Chapter 4. The compressive strength and crushing strength of concrete in infill walls assigned for each case study building after model calibration are presented in detail in Chapter 5. The IS 15988: 2013 [25] design code specifies that the concrete compressive strength of the new material should be at least 5 MPa greater than existing column strength. However, the present study considered the new concrete strength for jacketing to be 20 MPa for the entire buildings selected; i.e. for some buildings this was increases by 10 MPa and in few buildings it was increased by at least 5 MPa. In addition, RC jacketing was defined as when a new concrete layer with a minimum thickness of 100 mm was added to either face of the existing columns. In most of the case study buildings, the designed jacketed columns were of small sections than actually employed, is mainly due to least section to be provided as specified in the guidelines.

The jacketing procedure begins with surface preparation, where rigorous surface roughness was not performed for undamaged and sound elements, whereas in case of damaged elements the surface was initially roughened using hand chipping, electric hammering, etc., followed by sand-blasting or water demolition techniques. A two-component epoxy resin

was used as a binding agent. Steel connectors were considered only in the case of short-columns to improve the stiffness and strength under lateral loading. The holes were drilled on the footings and cleaned using the vacuum cleaner for anchoring of the added longitudinal reinforcements. Longitudinal bars can be efficiently anchored to the footing by applying a two-component epoxy resin. If continuity of longitudinal bars in jacketing was needed between floors, holes were drilled in the slab to pass them through. This method helps to increase column shear strength and ductility [212]. The jacketing elements were reinforced with longitudinal bars of minimum diameter of Φ 16. In addition, lateral ties were reinforced with a minimum diameter of Φ 8, anchored at 135° and uniformly spaced at 100 mm centred throughout the height. The number of columns required to be jacketed in each floor and number of storeys was evaluated through the attained building response, i.e. in terms of maximum inter-storey drift as an engineering demand parameter (EDP) with respect to intensity measures (IMs).

6.2.2 Steel bracing

A steel bracing system enhances the seismic performance of the existing structures by increasing the building's global stiffness and strength, as discussed in Chapter 4, Section 4.2.5.2. The bracing elements are provided externally, thus they are easy to apply and do not disturb the occupants during its maintenance. Different types of steel bracing can be applied, such as K type, channel type, X type, diagonal braced, inverted V-braced type and so on. However, the present study concerns X type steel bracing of CHS for each selected building. The hollow section was considered in the present study due to some advantages over the solid one, which includes economic in cost, strength adjustment without enlarging outer-diameter, higher resistance to bending or deflection and load required to buckle is same around circular-section. The outer diameter and thickness of CHS for each case study building varied and the designs followed the procedure specified in the standard steel code, IS 800: 2007 [154], taking into account safety against buckling failure that is mainly caused by axial force and also verifying if the design section was safe against the given loading.

The procedure for steel bracing layout was applied from the ground storey. Its location and orientation was concluded in such a way to minimise eccentricity caused by the irregular distribution of infill walls and structural members, reduce or eliminate internal torsional-rotation effects and maximise damping. Similarly, the necessity of bracing in the consecutive upper floors was evaluated through the attained inter-storey drift along the

height for the subjected IMs. The present study employed bracing elements in upper floors as well, due to drift shift in consecutive, unbraced upper floors introduced by the lower braced floor. The modulus of elasticity and yield strength of the steel bracing was assumed to be 2 x 10^5 MPa and 355 MPa, respectively.

6.2.3 RC shear wall

A RC shear wall can be introduced as a new structural wall on the existing structure to control the inter-storey drift, acting as a combined structural configuration against seismic loads. The addition of this new element highly increases the global lateral stiffness and strength of the buildings and, if properly located, also reduces plan irregularities to help enhance the building's seismic performance. A minimum of two shear walls in each direction were assigned to minimise eccentricities. The design of a shear wall begins with assumed width and thickness, such that the minimum thickness should not be less than 150 mm, whereby various design checks were carried out with reference to IS 13920: 1993 [51]. The RC shear walls were reinforced with longitudinal reinforcements in two curtains and transverse reinforcements distributed uniformly in the plane of the wall. A minimum reinforcement of 0.25% of the gross area in each direction was provided and distributed uniformly across the cross-section of the wall. A constant concrete compressive strength of 20 MPa and yield strength of reinforcements of 415 N/mm^2 were assumed in the study.

The location and orientation of an RC shear wall depends on the existing building's geometry and also the orientations of structural and non-structural elements within the existing building. These elements were prioritised in large structurally deficient joints or areas of the building. Generally, these elements were placed between the columns, but in the present study they were provided at the face of the column; where the centre of the column coincide with the centre of the shear wall and its width extended equally on both ends. Similarly, the number of storeys and the sections of the shear wall required to be provided was mainly governed by the respective floor inter-storey drift. Here, the shear walls extended throughout having constant thickness but the width of the shear wall was reduced along the height to meet the seismic demand and to attain uniform drift throughout. This strategy could highly control the drift concentration in each storey, such that comparable stiffness and strength in each storey could be attained throughout.

6.3   Retrofit Modelling Strategies for Case Study Buildings

The retrofit strategies described above will be modelled for each case study building using SeismoStruct software [22]. The modelling of jacketing elements followed the same methodology used for original beam and column elements, where these elements were modelled as an inelastic forced-based frame element type. The elements were discretised into 5 integration points and at the section level discretised into 150 section fibres. Lumped plasticity model was used to model at the element level to introduce its nonlinearity. The nonlinear concrete model was based on the consecutive relationship proposed by Mander, *et al.* (1988) [172]. The adopted material properties were discussed in Section 4.3.1 and 4.3.2 and also presented in Table 5.1 and Table 5.2. As discussed in the previous Section 6.2.1, the concrete compressive strength for RC jacketing was set at 20 MPa. The initial section was later modified depending upon the seismic demand and allowable serviceability criteria. The RC jacketing layout for each case study building will be discussed in detail in their respective sections.

The steel bracing was modelled using the nonlinear, finite element based software SeismoStruct [22]. The steel material was modelled as an uniaxial, bilinear stress-strain model with kinematic strain hardening, whereby the elastic range remained constant throughout the various loading stages, and the kinematic hardening rule for the yield surface was assumed as a linear function of a increment of plastic strain. The steel bracing elements were modelled as an inelastic, forced-based element type taking into account the integration of material response over the cross-section and integration of the section response along the length of the element. These elements were discretised into 5 integration sections and 200 section fibres at the section level, adopted a mesh cross-section for accurate representation of inelastic strains. The centre line of cross bracing passed through the centre of the beam and column joints. The modulus of elasticity and yield strength of the steel bracing were assigned to be 2×10^5 N/mm^2 and 355 MPa, respectively. The location, orientation and sections of the steel bracing for each selected building will be discussed in detail in the respective sections.

The RC shear walls were assigned as rectangular in geometry and at least two were provided in each direction to minimise the eccentricity and also ensure the stiffness centre matched the shear centre. The RC shear walls were modelled as forced-based, inelastic frame elements with 5 integration sections. The number of fibres used in section

equilibrium was set at 200. At the element level, RC shear walls were modelled with a distributed plasticity approach as the lumped plasticity model did not hold as practicable and accurate for elements in which bending governs the structural behaviour. The Mander, *et al.* (1988) [172] concrete model was employed for defining the concrete material used in shear walls. Each element was represented by two boundaries nodes, one at the top and another at the bottom. The concrete compressive strength was assigned as 20 MPa. The peak stress under uniaxial compression was considered to be 0.002. The Menegotto-Pinto steel model was employed to define the steel material for the shear wall [71]. Young's modulus of elasticity of reinforcement was considered to be 2×10^5 N/mm² and yield strength to be 415 MPa. The dimensions and reinforcement distribution in the shear wall for each building case studied was designed and specified using IS 13920: 1993 [51] and IITK-GSDMA guidelines [31]. Different shear wall sections were obtained and assigned to the models within the same building on different storeys and will be discussed in detail in the respective sections. Figure 6.1 presents the representative CCP1 building modelled for each retrofit strategy using SeismoStruct software [22].

| (a) | (b) | (c) |
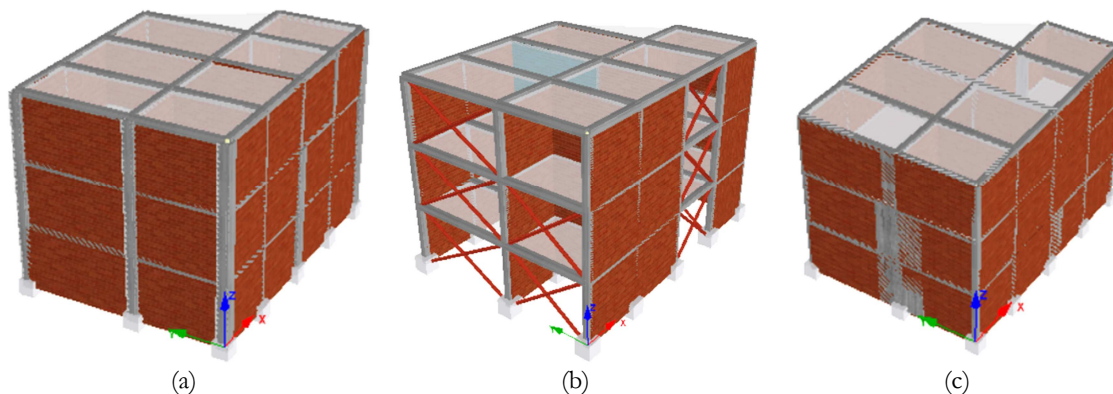
Figure 6.1 – Representative retrofit model in the SeismoStruct software [22]; (a) Jacketing, (b) Bracing and (c) Shear wall

6.3.1   CCP1 building

The initial seismic performance assessment of the CCP1 building presented in detail in Chapter 5 revealed that the building behaves elastically for the selected earthquakes until 0.2 g PGA and nonlinearity becomes dominant beyond this PGA. In addition, the fragility curves revealed that the peak lower damages occur below 0.2 g PGA and the possibility of damages from moderate to collapse was prominent with the probability of exceeding them from 60% to 14%, respectively, at 0.3 g PGA. In order to enhance the seismic demand of the existing CCP1 building and decrease the probability of large damage states in future

earthquakes, the present study aimed to strengthen the existing building and evaluate the degree to which damage level that can be reduced through intervention. And also check the feasibility and suitability of the adopted retrofit techniques.

In the first stage, concrete jacketing was introduced to the existing building, whose floor layout illustrating the position and number of columns jacketed in each floor, and its sections and reinforcement details are presented in Figure 6.2. The building was assigned with uniform jacketed column sections of (430 x 430) mm² throughout. It was reinforced with four Φ 20 longitudinal bars at the corners and four Φ 16 bars at the intermediate. The lateral ties of Φ 10 were uniformly spaced at 100 mm from centre and assigned throughout the column height. A total of 9 out of 14 columns were jacketed on the ground and first storeys. They included three columns from grid c-c, two from grid b-b and four columns from grid a-a, represented by enlarged column sections (see Figure 6.2). The first-floor jacketing layout was replicated on the second floor, but jacketing columns from grid c-c and three intermediate columns from grid a-a were removed. A typical jacketing column layout and reinforcement detail is presented in Figure 6.2.
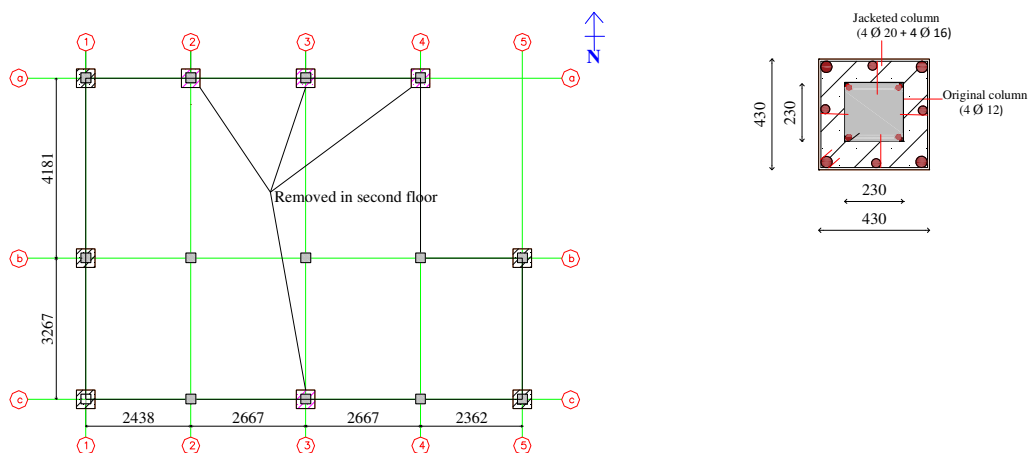
Figure 6.2 - Jacketing plan layout and reinforcement details of new jacketed column in the CCP1 building (all dimensions are in mm)

In the second stage, a CHS was adopted as a steel bracing element. The building was considered to have uniform CHS throughout for numerical simplicity. The assigned CHS had 130 mm outer diameter and 8 mm thickness, and the yield strength considered to be 355 MPa. Figure 6.3 presents the bracing floor layout, where the ground and first storeys have a similar layout; such that two bays from grid 1-1 and grid 4-4 and an additional one bay from grid a-a and grid c-c were braced, represented by a dumbbell hatched surface. In addition, the first-floor layout was reproduced on the second storey, but one bracing each

from grid 1-1 and grid 4-4 were removed, indicated by the solid hatched surface in Figure 6.3.
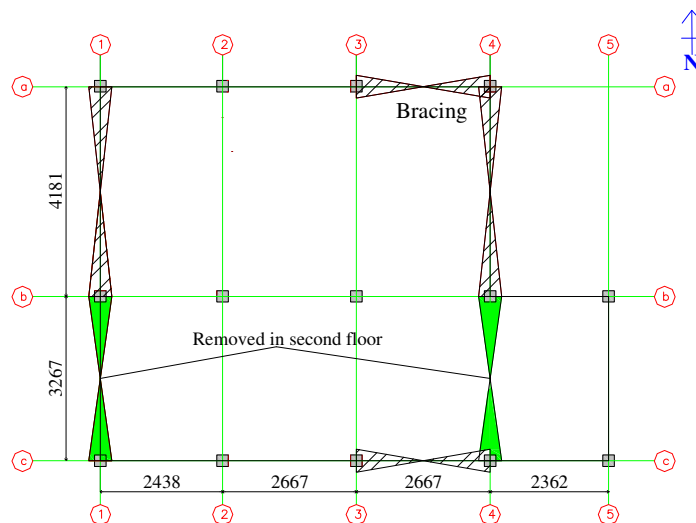
Figure 6.3 - Bracing layout in the CCP1 building (all dimensions are in mm)

The new RC shear walls were introduced in the CCP1 building at the exterior periphery of the building, due to availability of construction space and easier construction. Figure 6.4 presents the shear wall layout, illustrating its orientation, section size and reinforcement details. A total of four shear walls were considered in each storey, two in each direction so as to minimise the irregularities due to addition of new structural elements. They included two types of shear walls, i.e. S1 and S2, whose section sizes and reinforcement details are shown in Figure 6.4. Both shear walls possessed 150 mm thickness, whereas the widths of S1 and S2 were 2 m and 1.5 m, respectively. In addition, both shear walls were reinforced in two layers with Φ 12 longitudinal bars that were uniformly spaced; such that the number of longitudinal bars that comprised S1 and S2 were 16 and 12, respectively. Furthermore, transverse reinforcements of Φ 12 bars uniformly spaced at 200 mm from centre throughout were assigned in both shear walls. The ground and first storeys of the CCP1 building were considered to have four shear walls of the same section, i.e. S1. The first storey layout was extended in the second storey but Shear wall 1 was replaced with S2.
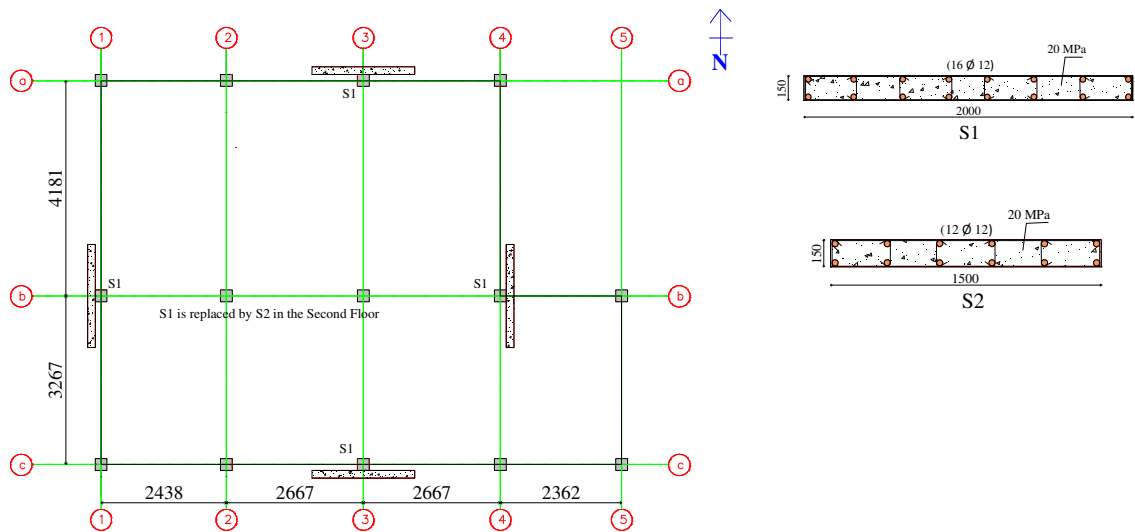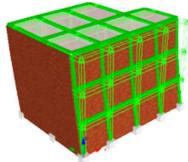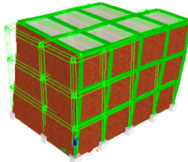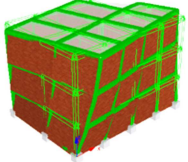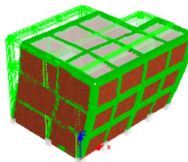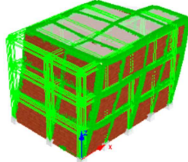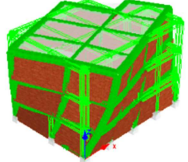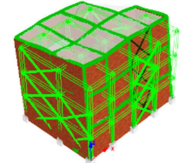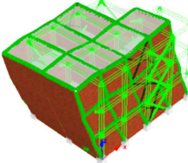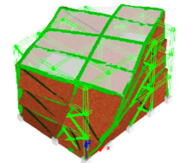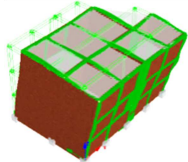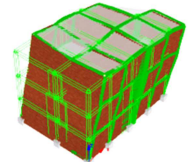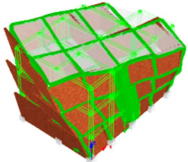
Figure 6.4 - Shear wall layout and reinforcement details in the CCP1 building (all dimensions are in mm)

6.3.1.1 Analysis and interpretation of results

6.3.1.1.1 Eigenvalue analysis

The fundamental frequencies of the retrofitted buildings were obtained through eigenvalue analysis and compared with the original building. Table 6.1 demonstrates the first three fundamental frequencies and corresponding vibration modes. The analytical results for all retrofitted buildings revealed that the first two vibration modes were translational and third one torsional, thus justifying the proper arrangement of newly added elements in the CCP1 building. The vibration modes were also identical with the original CCP1 building, where first vibration mode was along building's Y-axis. The effective modal participation factors corresponding to the first vibration mode for retrofitted buildings was more than 85%. This illustrates that the first fundamental frequency in each retrofit technique was relatively dominant compared with the second and third frequencies. The entire retrofit techniques relatively increased fundamental frequencies compared to the original building as shown in Table 6.1. The maximum increase was attained for the steel braced building, and followed by shear wall and jacketed buildings, respectively. The increase in fundamental frequencies ranged from 1.5 to 2 times more than the original CCP1 building. The steel braced building is expected to attract higher seismic demand based on the response spectrum of the region, and result in a reduction in the fundamental period.

Table 6.1 - Eigenvalue analysis results: natural frequencies and respective vibration modes for the CCP1 building with and without retrofit techniques

Mode	Frequency (Hz)			First vibration mode	Second vibration mode	Third vibration mode
	f_1	f_2	f_3			
CCP1	4.95	6.06	6.94			
Jacketing	7.63	9.35	10.11			
Bracing	9.67	10.00	13.05			
Shear wall	9.03	10.56	12.58			
Mode type	Trans.	Long.	Torsional			

6.3.1.1.2   *Capacity curves*

The seismic performance of the CCP1 building with and without intervention using retrofit measures were initially investigated using adaptive pushover analysis. Figure 6.5 presents capacity curves for original and retrofitted buildings in both directions, such that the descending branch was plotted until the capacity attained 80% of the maximum base shear capacity. This point was indicated as the ultimate point. The capacity curves revealed that a considerable enhancement in stiffness, strength and ductility capacities in the existing building could be attained after retrofitting. A significant and steep increase in stiffness and strength was recorded in both directions. Interestingly, the increase in initial stiffness and strength capacities between retrofitted buildings were found to be comparable in the X direction. Whereas in the Y direction, steel bracing exhibited extensive increases in both stiffness and maximum base shear capacity, and was observed to be comparable between jacketing and shear wall retrofitting. The increase in stiffness ranged from 5–6.7 times in the X direction and 3.5–7 times in the Y direction compared to the original CCP1 building.

In addition, the maximum base shear capacity also increased by almost 2 to 3 times in the X direction and 1.5 to 5 times in the Y direction. In all cases, the maximum increase was recorded for steel braced construction and followed by shear wall and jacketing, respectively. Likewise, the steel braced building demonstrated larger global drift w.r.t maximum base shear capacity and the degradation branch was also uniform. This phenomenon signifies higher ductility acquired in the original building through this intervention. Furthermore, the descending branches for the other retrofit techniques also revealed a uniform or slight fall in the capacity curve, which revealed that the retrofit techniques introduced a large displacement capability to the original building, which will ultimately prevent the collapse of the building, thereby, undergoing large deformation. The conclusion is that such intervention measures can prevent the collapse of the building ensuring the safety of the occupants, and also prevent or minimise other structural and non-structural losses.

Figure 6.5 - Capacity curve for the CCP1 building with and without retrofit techniques; (a) X direction and (b) Y direction

6.3.1.1.3   *Nonlinear time history analysis*

6.3.1.1.3.1   *Maximum Inter-storey drift (ISD_{max}) profile*

The seismic performance of the existing building after introducing the retrofit strategies was evaluated through the comparison of inter-storey drift profiles. Figure 6.6 presents the distribution of inter-storey drift for construction with and without retrofit measures in the CCP1 building, subjected to an 11-ChiChi Taiwan earthquake, at 0.3 g PGA. The observed maximum inter-storey drift (ISD_{max}) concentration in a single floor at ground floor in the

original building was significantly reduced after retrofit measures, where uniform distribution along the height in both directions was attained. This indicates that uniform distribution of stiffness and strength was attained through the additions, a primary objective of the present study. For this typical earthquake of specified IM, steel braced construction was found to considerably reduce the drift to lower values in both directions, as expected. In addition, both jacketing and shear wall measures also reduced drift and were comparable along the building in the X direction, whereas in the Y direction the shear wall was found to be more efficient. It reduced the ISD_{max} by almost 5–10 times in the X direction and 2–4 times in the Y direction compared to the original building. From the global demands, it can be seen that steel bracing could be the more effective retrofit technique, followed by shear wall and jacketing, respectively. In addition, bracing significantly increased the shear and axial forces on the existing columns at the ground floor; hence, proper retrofitting at the foundation might be required.
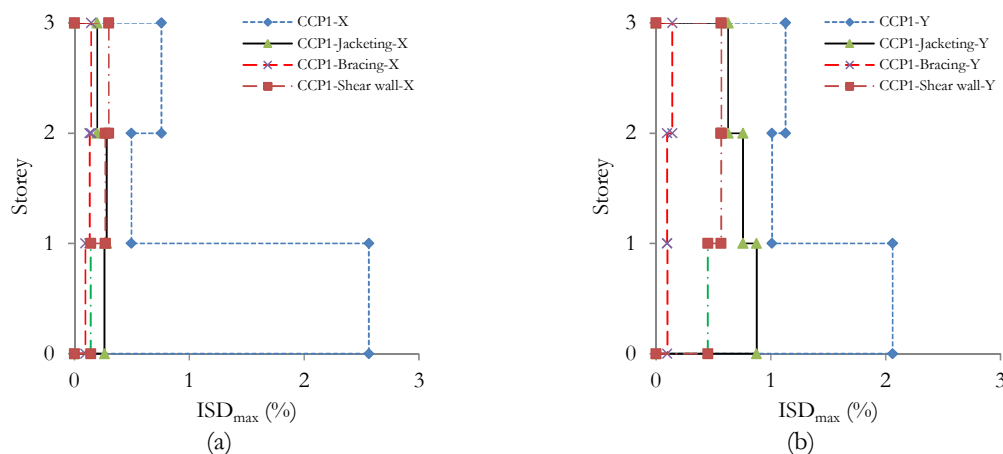
Figure 6.6 – A representative inter-storey drift profile for the CCP1 building with retrofit techniques due to 11-ChiChi Taiwan earthquake, at 0.3 g PGA; (a) X direction and (b) Y direction

6.3.1.1.3.2   IDA curves

The seismic performance of the CCP1 building after retrofit measure interventions was examined through IDA curves. For this, retrofitted CCP1 building were subjected to dynamic time history analyses, which were subjected to 21 real ground motion records and acted on bidirectionally at 0° and 90°, and suitably scaled to a range of IMs from 0.1 g to 0.5 g at steps of 0.1 g. The IDA curves were plotted between IMs and their corresponding ISD_{max} values and, finally, investigated for the vulnerability of the strengthened buildings. Figure 6.7 (a to c) presents the IDA curves for the existing building retrofitted with

jacketing, steel bracing and shear wall, respectively. The IDA curve for each subjected earthquake is represented by the light solid line, illustrating the variation of ISD_{max} with respect to IMs. In addition, the intermediate dark solid line represents the mean IDA curve, which gives the average building response when subjected to a large number of earthquakes at specified IMs. The large dispersion of ISD_{max} was recorded for the same IMs, which signifies that the building's response primarily depends on the selected earthquake frequency contents and recorded durations. Generally, increased IMs also exhibit increased seismic demand; hence, a higher ISD_{max} was recorded. However, in some special earthquakes, a decrease in ISD_{max} was recorded even for increasing IMs, potentially due to hardening of some structural elements, most likely in the non-retrofitted structural members or frames nearby newly added elements. In other words, such phenomena observed in buildings having seismic demand already exceed the capacity, and if such structure persists to higher IMs the building no longer meets the seismic demand. The potential failure of some structural elements on such buildings lowers the building response, as the building was expected to have collapsed already. Remarkably, the IDA curves for the steel braced building exhibited lower discrepancies of ISD_{max} even when subjected to higher IMs, when compared to jacketing and shear wall. The IDA curves for jacketing illustrate that the building was expected to be in elastic region until 0.3 g and 0.2 g PGA in the X and Y directions, respectively. Similarly, the IDA curves for steel braced construction are likely to be in the elastic region for the selected earthquakes and studied range of IMs in both directions. Whereas, few IDA curves in the X direction could be expected to initiate nonlinearity. Furthermore, the IDA curves for shear wall construction demonstrate highly scattered ISD_{max} and the building can be predicted to behave elastically until 0.2 g PGA in both directions. Beyond this PGA, the building is most likely to develop plastic hinges in the surrounding frames and potentially experience partial collapse to collapse, and failure of the retrofitted building under the soft-storey mechanism can be expected. Based on the above discussions, it can be concluded that steel bracing was found to be relatively more effective in enhancing the seismic performance of the existing CCP1 building, and other retrofit techniques were also found suitable and relevant for improving the existing building performance.
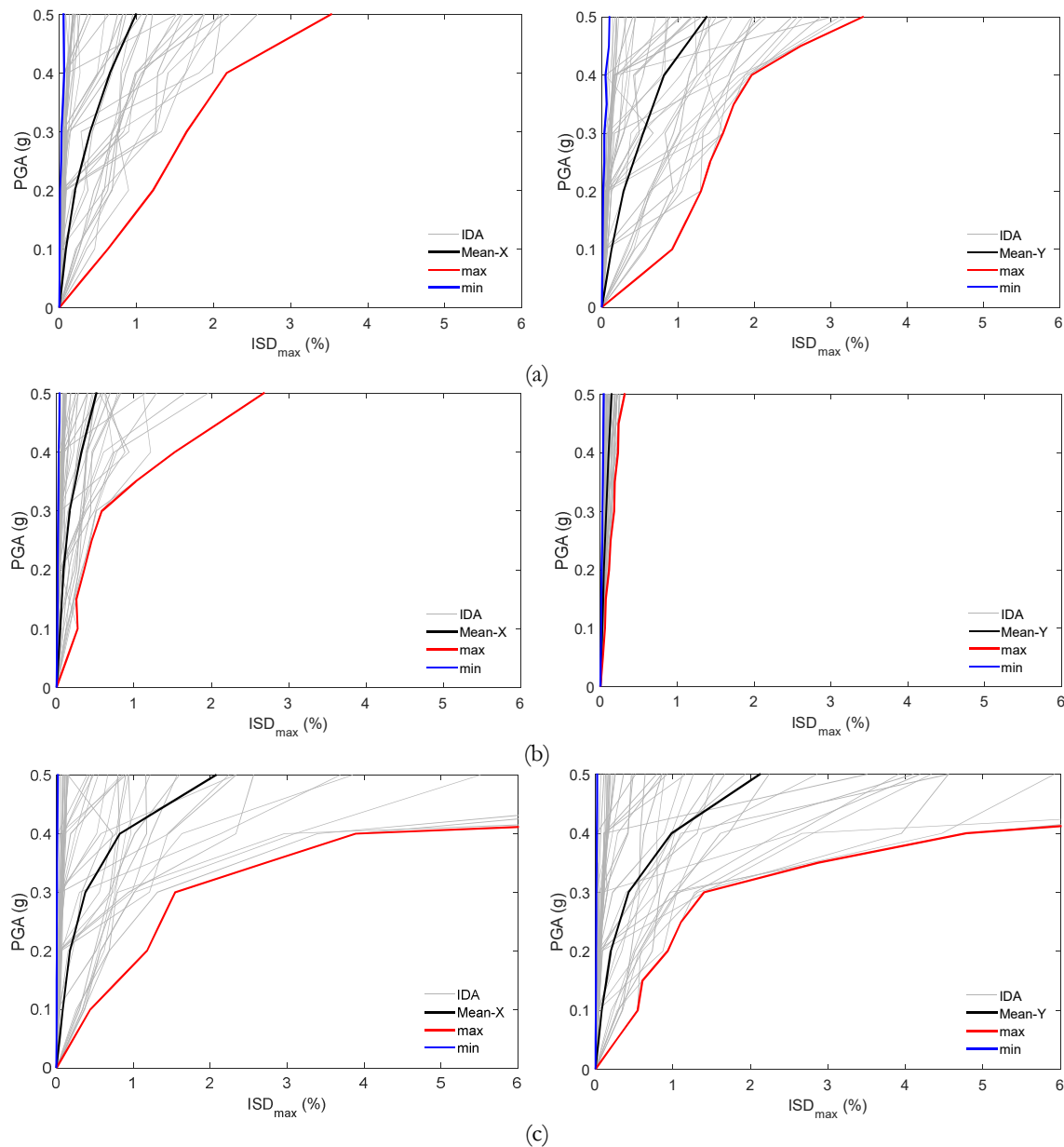
Figure 6.7 - IDA curves for the CCP1 building; (a) Jacketing, (b) Bracing and (c) Shear wall

The vulnerability assessment of the existing CCP1 building with and without retrofit can be investigated in more a generalised form through the comparison of mean IDA curves presented in Figure 6.8. The indices used in the plots indicate the existing building retrofitted with jacketing (J), steel bracing (Br.) and shear walls (Sh.). The plot illustrates that the entire retrofit measures were effective in reducing the mean ISD_{max} in comparison to original building with respect to chosen IMs. This statement can be justified through the values attained, where the mean IDA curves for the original CCP1 building, at 0.5 g PGA, exhibited approximately 5% ISD_{max} in both directions, whereas it was reduced below 2% ISD_{max} in both directions using retrofit measures. In addition, when the effectiveness of

the proposed retrofit techniques were investigated, it could be observed that the existing building with jacketing and shear walls illustrated similar mean IDA curves until 0.4 g PGA, and beyond this the building with RC shear walls exhibited slightly higher mean ISD_{max} in both directions. Whereas, in the case of steel braced construction, the recorded mean ISD_{max} was considerably lower in both directions. The observed ISD_{max}, at 0.5 g PGA, for building with steel bracing was lower than 0.5% in both directions. All the above results and discussions led to the conclusion that steel bracing was relatively more effective in improving the seismic performance, followed by jacketing and shear wall, respectively.
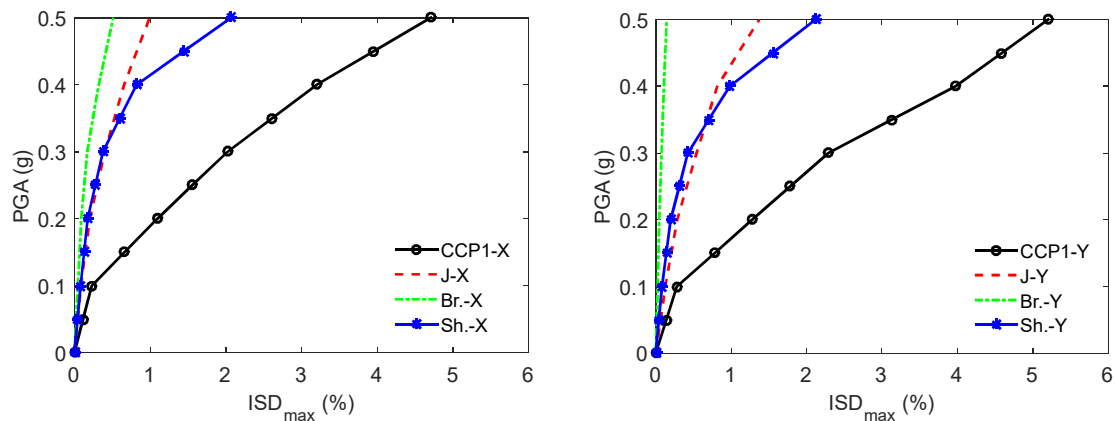
Figure 6.8 – Comparative mean IDA curves for the CCP1 building with and without retrofit measures in the X and Y directions, respectively. J – jacketing, Br. – bracing, Sh. – shear wall

6.3.1.1.3.3   *Fragility curves*

The levels of damage for different building types at certain IMs can be evaluated with the help of fragility curves plotted using incremental dynamic analyses, as discussed in Section 6.3.1.1.3.2. Figure 6.9 (a to b) and Figure 6.10 shows the comparative fragility curves between the existing CCP1 building with and without retrofit measures. The fragility curves were plotted for six damage states, i.e. slight, light, moderate, extensive, partial collapse and collapse, represented as S, L, M, E, PC and C, respectively, which was proposed by Rossetto, *et al.* (2003) [202] as shown in Table 4.10. The fragility curves for all the retrofit strategies demonstrate that the damage level can be reduced when compared with original building. Only insignificant improvement was attained for reducing the peak in lower damage states through shifting its occurrence to higher IMs, whereas substantial improvement was recorded for higher damage states. For the existing building, the probability of exceeding collapse, at 0.3 g PGA, was approximately 14% and was reduced to theoretically zero with the introduction of jacketing and steel bracing. A similar

conclusion was recorded with shear walls, where the probability of exceeding collapse, at 0.3 g PGA, was reduced to below 2%. The analytical results concluded that all retrofit techniques introduced in the existing CCP1 building were highly efficient in enhancing the seismic performance.

(a)

(b)
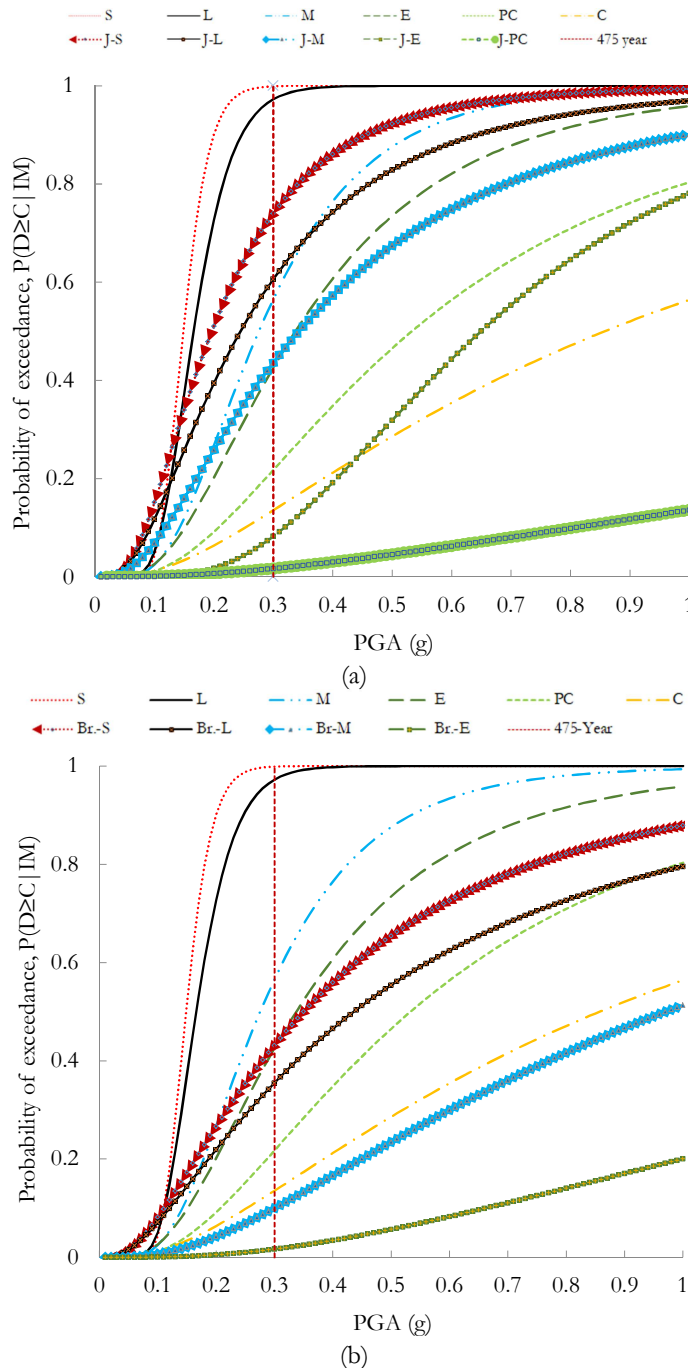
Figure 6.9 – Comparative fragility curves for the CCP1 building after introducing retrofit techniques; (a) Jacketing and (b) Bracing. J – jacketing, Br. – bracing, Sh – shear wall, S – slight, L – light, M – moderate, E – extensive, PC – partial collapse, C – collapse
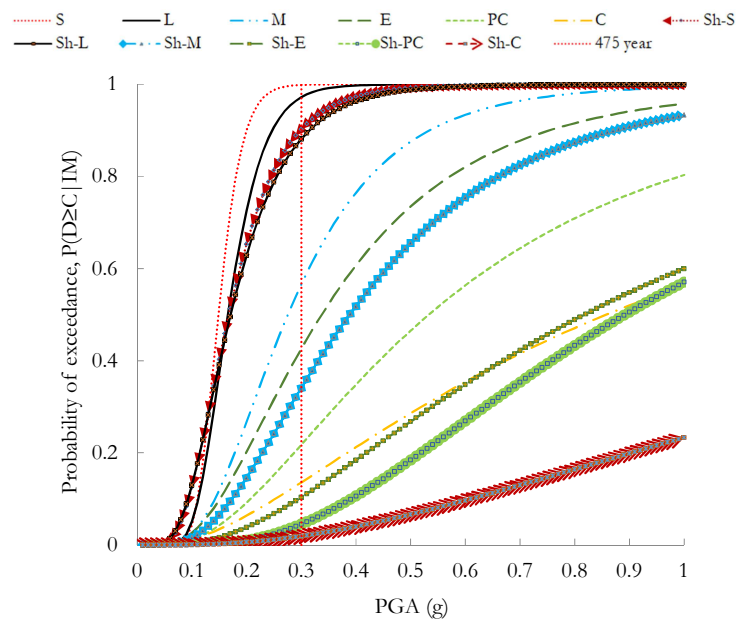
Figure 6.10 – Comparative fragility curves for the CCP1 building after introducing Shear wall. J – jacketing, Br. – bracing, Sh – shear wall, S – slight, L – light, M – moderate, E – extensive, PC – partial collapse, C – collapse

An extensive study on the seismic performance of the CCP1 building after introducing the retrofit measures was performed through the comparison of fragility curves, especially for higher damage states. In addition, the study was conducted with the objective of identifying the most suitable retrofit measures for this particular building, CCP1. Figure 6.11 presents the comparative fragility curves for four damage states; i.e. medium, extensive, partial collapse and collapse. The entire plot reveals that steel braced construction exhibits a lower relatively probability of exceeding certain damage states compared with other retrofit techniques. For the moderate damage state, the steel braced measures were found to be considerably effective in reducing the failure probability, whereas the effect of other techniques was insignificant. The expected probability of a moderate damage state, at 0.3 g PGA, can be reduced by almost 50% using steel bracing. In addition, the probability of exceeding extensive damage for the existing building, at 0.3 g PGA, was almost 43%, and was reduced to 10% to 2% through the addition of retrofit techniques. Similarly, in the case of partial collapse, the bracing retrofit revealed theoretically zero failure probability, and most interestingly, jacketing displayed better seismic performance than shear wall. The probability of exceeding partial collapse for the existing building, at 0.3 g PGA, was almost 22% and was reduced to 8% to 4% with intervention using retrofit techniques. Furthermore, the probability of exceeding collapse for buildings with steel bracing and jacketing was theoretically zero. The probability of collapse for the existing CCP1 building,

at 0.3 g PGA, was 14% and was reduced to 2% with RC shear walls. Therefore, based on the comparison fragility curve results, it can be concluded that the steel braced technique illustrates superior seismic performance.

Figure 6.11 - Comparative study of fragility curves for the CCP1 building with different damage states; (a) Moderate, (b) Extensive, (c) Partial collapse and (d) Collapse. J – jacketing, Br. – bracing, Sh – shear wall

6.3.2 CCP2 building

The detailed seismic performance of the existing CCP2 building under nonlinear static and dynamic time history analyses was performed and presented in detail in Chapter 5, with the objective to evaluate whether the building met the seismic demand for future earthquakes, and recommend retrofit measure(s) if seismic deficiency was exhibited. The IDA and fragility curves concluded that the CCP2 building could potentially undergo nonlinearity beyond 0.2 g PGA in both directions, and the probability of exceeding partial collapse and

collapse, at 0.3 g PGA, corresponded to approximately 27% and 22%, respectively. This indicates that the existing CCP2 building needs strengthening and to have its performance evaluated, so that the loss due to structural collapse and resulting loss of human life can be minimized. The present study evaluated the detailed seismic performance of the CCP2 building with three retrofit techniques under nonlinear static and dynamic time history analyses. The three retrofit approaches employed in the building are demonstrated in Figure 6.12 to Figure 6.14. Initially, the design of retrofit measures, their reinforcement details and other parameters were based on the procedures specified in design codes [31, 50, 51, 135, 154]. The procedure of introducing retrofit measures adopted from the ground storey and could be replicated to the consecutive upper storeys depending upon the attained inter-storey drift on the non-retrofitted upper floors. The primary objectives of introducing retrofit techniques in the CCP2 building was to minimise the eccentricity due to irregular distribution of the infill walls and structural elements, neutralise the structural deficit joints and members, and uniformization of drift throughout.

Initially, concrete column jacketing was employed in the CCP2 building. Two types of concrete column jacketing were considered; namely J1 and J2. Figure 6.12 shows the jacketing layout and section details in which a total of 7 columns were jacketed out of 12 columns on the ground floor and was continued on the first and second floors of the building. The jacketed columns include all the columns of grid a-a and grid d-d, and the central column of grid b-b, as represented by enlarged column sections. More columns were jacketed on the southern face of the building in order to counterbalance eccentricity developed by the irregular distribution of infill walls and also to compensate the damage observed in corner columns of grid a-a, mainly on the ground floor. Similarly, on the top floor (i.e. stair cover portion) the central column of grid b-b and all the columns of grid d-d were jacketed, as presented in Figure 6.12 (b). The newly jacketed columns were enlarged by a minimum thickness of 100 mm on each side of the original column, a minimum requirement specified in design codes [135]. Jacketed columns J1 and J2 have section sizes of (430 x 430) mm^2 and (430 x 530) mm^2, respectively. In addition, both jacketed columns were reinforced with eight Φ 20 longitudinal bars and lateral ties of Φ 10 bars uniformly spaced at 100 mm from centre throughout.
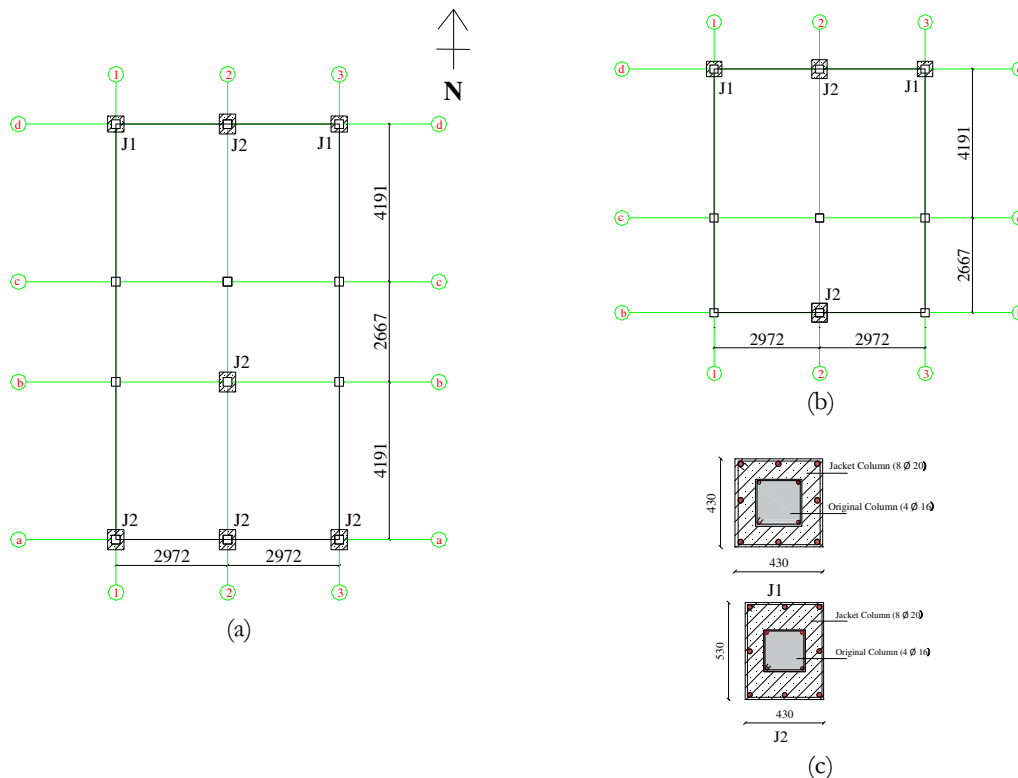
Figure 6.12 - Jacketing layout and reinforcement detailing in the CCP2 building; (a) Ground, first and second floors plan, (b) Top floor plan and (c) Section and reinforcement details (all dimensions are in mm)

As an alternative retrofit method for the existing CCP2 building, cross steel bracing was proposed to evaluate its influence in improving the seismic performance. Figure 6.13 presents the steel bracing layout, where entire bays of grid a-a were braced at the ground floor to eliminate or minimise the soft-storey mechanism observed in the existing building. The ground floor bracing also included each bay of grid b-b-2-3, grid d-d-2-3, grid b-c-1-1 and grid b-c-3-3, as illustrated in Figure 6.13 (a), represented by hatched surface. The ground floor bracing layout was reproduced for the first and second storeys, but the entire bracing from grid a-a was removed (represented by alternative solid hatching) demonstrated in Figure 6.13 (a). Similarly, Figure 6.13 (b) shows the bracing layout for the top floor of the CCP2 building, which was similar to the floor below, i.e. second floor. A uniform circular hollow section of outer diameter 100 mm and 5 mm thickness was assigned throughout and its yield strength was considered as 355 MPa.
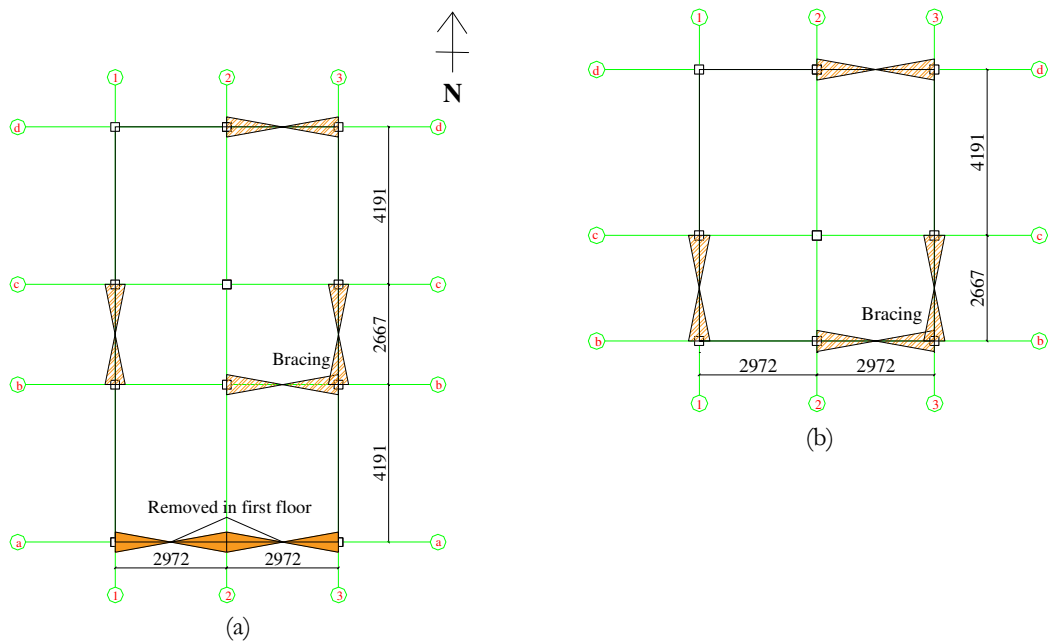
Figure 6.13 – Cross steel bracing layout in the CCP2 building; (a) Ground, first and second floors plan, (b) Top floor plan (all dimensions are in mm)

RC shear walls were introduced as a third alternative retrofit measure for the existing CCP2 building to investigate the seismic performance enhancement and its influence on reducing vulnerability. Figure 6.14 presents the shear wall layout for different floors and section details. Two types of shear walls were designed and considered, i.e. one as a bar bell type (i.e. S1) and other one simple shear wall (i.e. S2), which differed in sections and distribution of reinforcement bars. The total width of the bar bell type shear wall was 2 m, and consisted of column-like sections of 300 x 300 mm at both ends, and the middle portion was a rectangular section having 1400 mm width and 230 mm thickness. The end section of S1 was reinforced with six Φ 12 longitudinal bars and confined with transverse reinforcements of Φ 12 bars uniformly spaced at 200 mm from centre. In addition, the middle portion of the shear wall contained two curtains of longitudinal bars, reinforced with six Φ 12 bars in each curtain. Furthermore, the width of S2 was 1250 mm and 230 mm thickness, which was reinforced with total of 12 Φ 12 longitudinal bars distributed in two layers. The E-W direction at the ground floor was reinforced with three shear walls and two shear walls were added in the N-S direction of the building. The extra shear wall was assigned to balance deficiency and eccentricity produced by the irregular distribution of the infill walls, where the complete bay of grid a-a was without infill walls and corner columns were also observed to be damaged. The layouts of the upper floors (first, second

and top) were similar to the ground floor but lacked S2 from grid a-a after the ground storey.
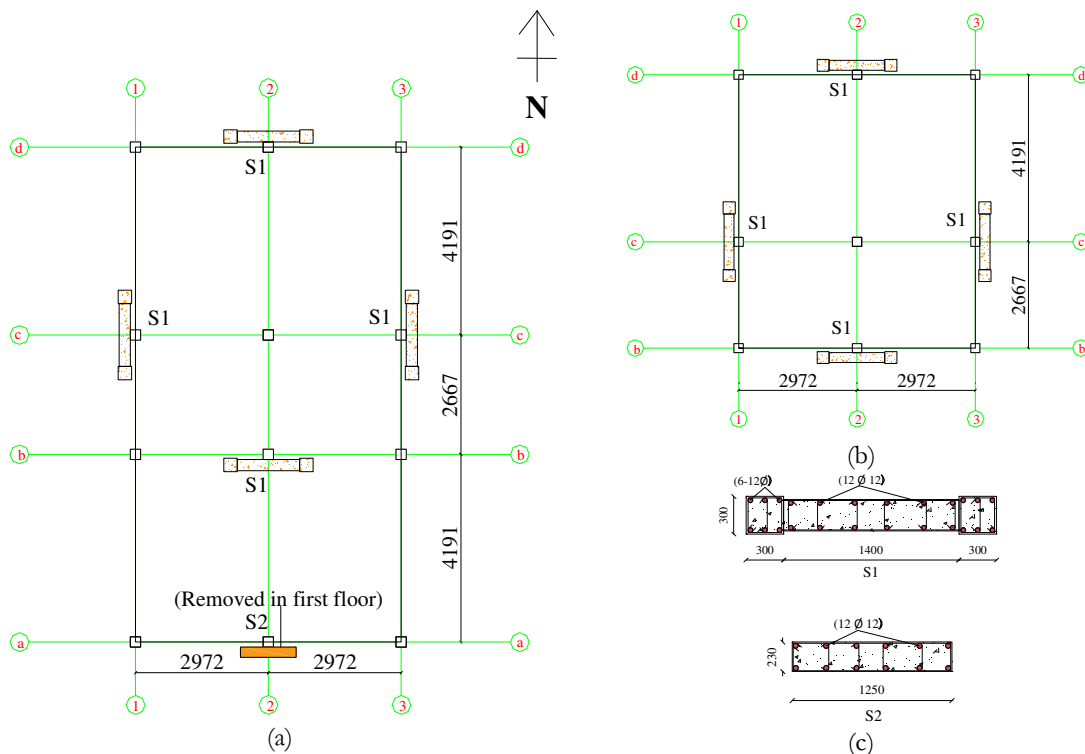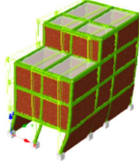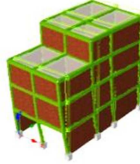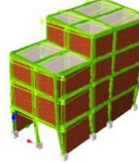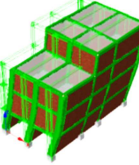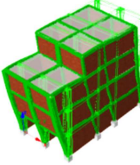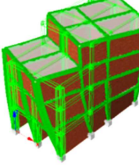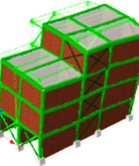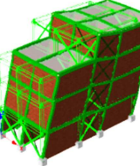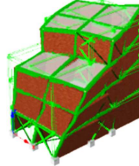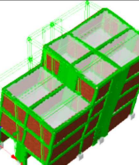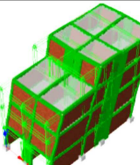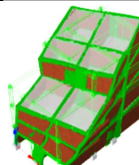
Figure 6.14 - Shear wall layout in the CCP2 building; (a) Ground, first and second floor plan, (b) Top floor plan and (c) Section and reinforcement details of shear wall (all dimensions are in mm)

6.3.2.1 Analysis and interpretation of results

6.3.2.1.1 Eigenvalue analysis

Table 6.2 presents the eigenvalue analysis results for the CCP2 building with and without retrofit measures, demonstrating the first three fundamental frequencies and corresponding vibration modes. The increase in the fundamental frequencies was recorded for retrofitted construction as compared with the original building. For this particular building, the highest frequency was obtained for the building retrofitted with shear walls, followed by bracing and jacketing, respectively. The increase in first frequency ranged from 2–2.2 times, relatively compared with the existing CCP2 buildings. In addition, all the retrofit measures demonstrate the first two vibration modes as translational and third one as torsional, which were identical to the original CCP2 building. The first effective modal mass participation factor for the CCP2 building with jacketing, bracing and shear walls corresponded to 86%, 75% and 77%, respectively.

Table 6.2 - Eigenvalue analysis results: natural frequencies and respective vibration modes for the CCP2 building with and without retrofit techniques

Mode	Frequency (Hz)			First vibration mode	Second vibration mode	Third vibration mode
	f_1	f_2	f_3			
CCP2	3.06	3.80	4.06			
Jacketing	5.84	6.46	7.28			
Bracing	6.54	6.89	8.95			
Shear wall	6.72	7.06	8.65			
Mode type	Trans.	Long.	Torsional			

6.3.2.1.2   Capacity curves

The increase in maximum base shear capacity in the existing CCP2 building after adding retrofit techniques was evaluated through adaptive pushover analysis. Figure 6.15 presents the capacity curves for the CCP2 building with and without retrofit techniques in both directions. The plot revealed that the trend of increasing initial stiffness was approximately similar for all retrofitted buildings and considerable improvement was attained compared to the original CCP2 building. The initial stiffness was increased by almost 1.5–2.5 times along the X direction and 1.2–1.8 times along the Y direction in comparison to the original building. The retrofit measures not only increased the stiffness, but it also significantly enhanced the base shear capacity. The increase in the maximum base shear capacity ranged from 2–3.5 and 1.5–2.6 times in the X and Y directions, respectively, compared to the original CCP2 building. The maximum base shear capacity was recorded in the steel braced building in both directions. The global drift corresponding to maximum base shear capacity

illustrates the yielding point. This point reveals the maximum contribution of the infill walls to the frame structures after which it undergoes in-plane and out-of-plane failure. In some cases, shear cracks were recorded on some structural elements, especially nearby non-retrofitted columns that were more likely to initiate formation of plastic hinges. Remarkably, the maximum base shear capacity for the all the retrofit measures was attained for approximately similar global drifts, highlighting that all retrofitted buildings can undergo comparable deformations. The uniform decrease in capacity curves were recorded after introduction of retrofit measures, which illustrates larger improvement in ductility.
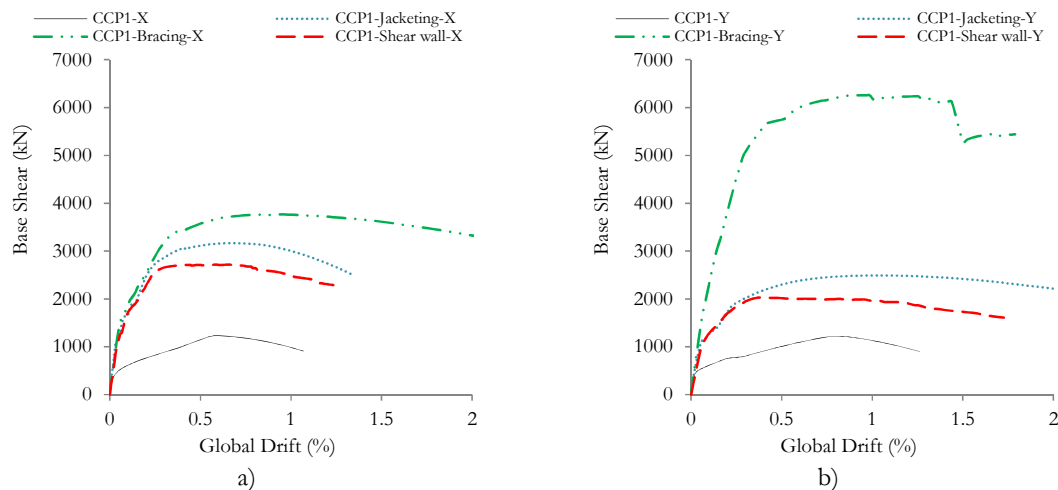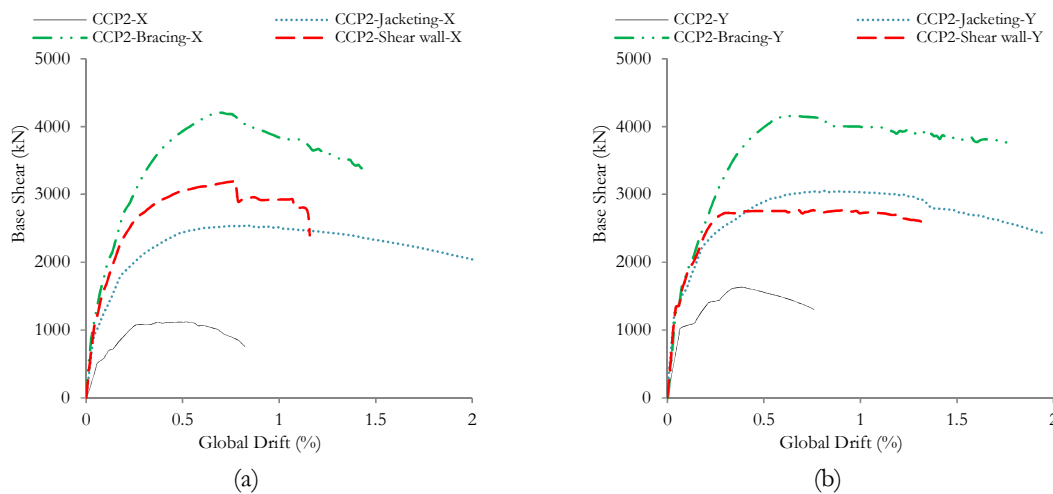

Figure 6.15 - Capacity curves for the CCP2 building with and without retrofit techniques; (a) X direction and (b) Y direction

6.3.2.1.3   Nonlinear time history analysis

6.3.2.1.3.1 ISD_{max} profile

Figure 6.16 presents a typical comparative inter-storey drift profile for the CCP2 building with and without retrofit measures, subjected to a 5-Chi Chi Taiwan earthquake at 0.3 g PGA. The plot revealed that the ISD_{max} was considerably reduced after retrofit intervention and distribution of the drift profile was also largely improved throughout. These techniques eliminated the single storey drift concentration recorded in the original building whereby a uniform drift profile was recorded throughout. This indicates that properly assigned retrofit techniques can uniformly distribute stiffness and strength throughout the height, which was one of the primary objectives of the present study. For this particular earthquake and IM, steel bracing was found to highly reduce ISD_{max} to lower values, i.e. < 0.5% in both directions. A similar building response was recorded in the case

of a shear wall along the X direction, whereas in the Y direction the recorded ISD_{max} was approximately 1%. In addition, the building with concrete jacketing also reduced the ISD_{max} but not as expected. This state of the building potentially would have moderate and extensive damages to the infill walls. The retrofit measures reduced the ISD_{max} by almost 2.5–5 times in the X direction and 3–7 times in the Y direction compared with the original CCP2 building. This phenomenon signifies the suitability and applicability of the retrofit measures in this particular building.
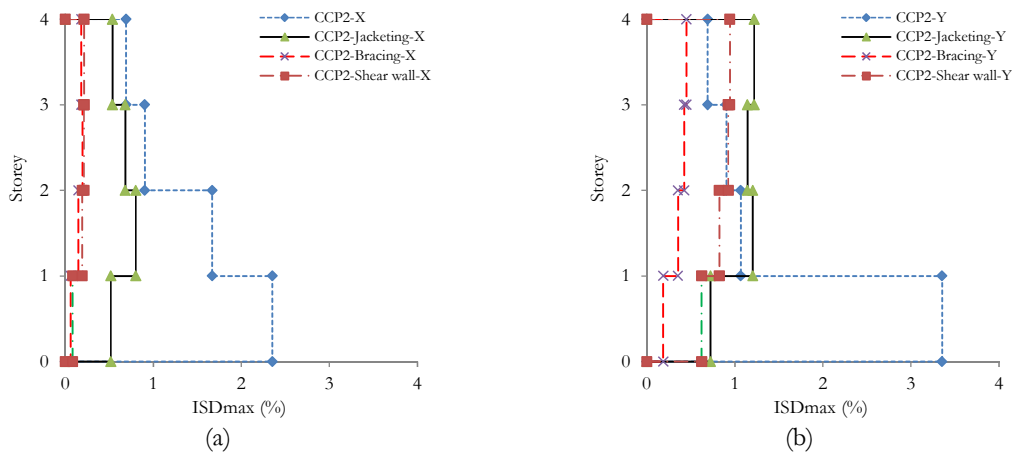
Figure 6.16 - Typical comparative ISD_{max} profile for the CCP2 building with and without retrofit strategies, subjected to a 5- ChiChi Taiwan earthquake, at 0.3 g PGA; (a) X direction and (b) Y direction

6.3.2.1.3.2   *IDA curves*

The IDA curves were plotted for the retrofitted CCP2 building obtained through dynamic time history analysis. Figure 6.17 presents the IDA curves for the CCP2 building with jacketing, steel bracing and shear walls in both directions. The IDA curve for each earthquake and range of IMs are represented by a light solid line, such that it provides information on the building response with respect to IMs. All the plots illustrated that the large dispersion of ISD_{max} for the same IM was observed due to large variation in seismic demand for the same IMs. For the majority of selected earthquakes, jacketed construction exhibited an elastic region until 0.4 g and 0.3 g PGA in the X and Y directions, respectively. Beyond this PGA, the building is expected to attain nonlinearity and hardening occurs in some non-retrofitted structural elements. In the case of the steel braced building, it is likely to behave elastically for the subjected IMs in the X direction demonstrating a lower ISD_{max} even at 0.5 g PGA; whereas, in the Y direction the building can be predicted to be in the elastic range until 0.3 g. Beyond this PGA, the seismic

demand increases considerably and the majority of earthquakes would potentially cause adjacent structural components to partially collapse or collapse. In the case of the building retrofitted with shear walls, the elastic region was expected until 0.4 g and 0.3 g PGA in the X and Y directions, respectively, and beyond this PGA, the building exhibits higher ISD_{max} where large damage states can be recorded.
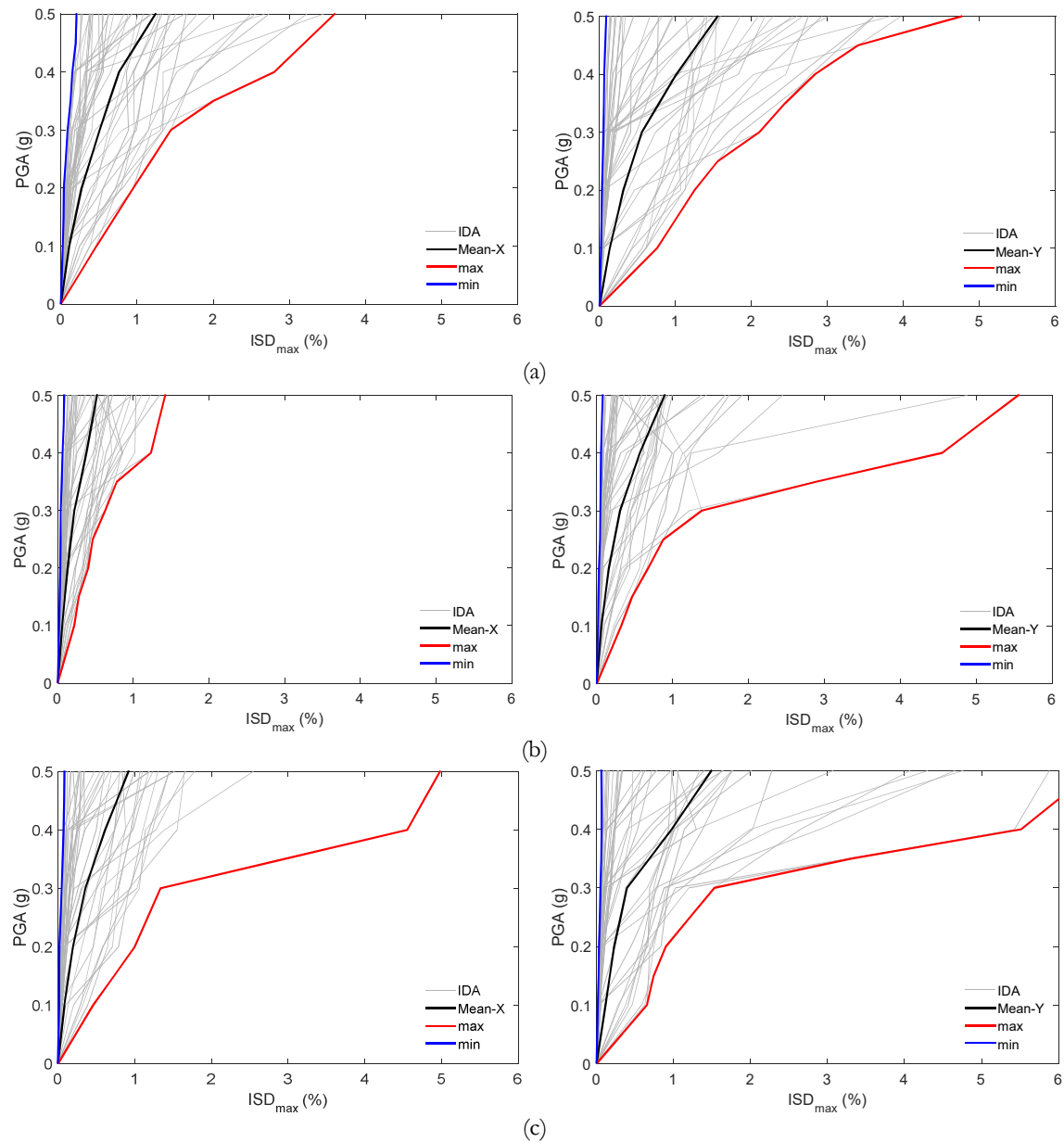
Figure 6.17 - IDA curves for the CCP2 building; (a) Jacketing, (b) Bracing and (c) Shear wall

It is very difficult to generalise conclusions through individual IDA curves. Therefore, the present section aimed to compare the building response with the help of the mean IDA curves obtained for each retrofit technique in both directions and, finally, evaluate the most effective retrofit techniques. Figure 6.18 presents the comparative mean IDA curves for

the building with and without retrofit techniques, and observed that the seismic vulnerability of the existing CCP2 building could be considerably reduced to a lower level than initially expected. The dynamic results revealed that steel bracing was found to be highly effective in reducing the ISD_{max} in both directions, when compared with other retrofit measures. In addition, concrete jacketing and RC shear walls demonstrated comparable mean building responses for the assumed IMs. The retrofit measures could reduce the mean drift by almost 3–4 times in both directions compared to the original building, at 0.5 g PGA. From all the plots it can be concluded that all retrofit techniques considered for the study would be effective in enhancing seismic performance of the existing CCP2 building, but steel bracing was found to be more effective.
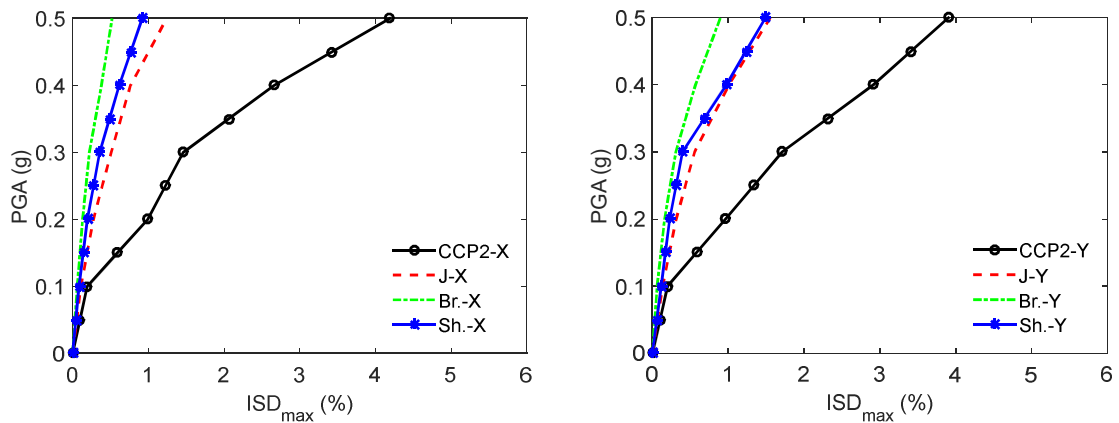
Figure 6.18 – Comparative mean IDA curves for the CCP2 building with and without retrofit measures. J – jacketing, Br. – bracing, Sh. – shear wall

6.3.2.1.3.3   *Fragility curves*

In this section, comparative fragility curves were plotted between the existing CCP2 building with and without retrofit techniques. The aim of the plot was to benefit researchers and readers in identifying the reduced levels of damage that can be attained through the interventions, explained through the probability of exceeding each damage state. Figure 6.19 (a to b) and Figure 6.20 presents comparative fragility curves for building with jacketing, steel bracing and shear wall, respectively. For lower damage states, such as slight and light, the retrofit measures were found to be inefficient. Whereas, in cases of higher damage states, a substantial reduction in failure probabilities can be obtained through retrofit measures, which also justifies their suitability in the existing CCP2 building.

(a)

(b)

Figure 6.19 - Fragility curves for the CCP2 building; (a) Jacketing and (b) Bracing. J – jacketing, Br. – bracing, Sh – shear wall, S – slight, L – light, M – moderate, E – extensive, PC – partial collapse, C – collapse

Figure 6.20 - Fragility curves for the CCP2 building with Shear wall. J – jacketing, Br. – bracing, Sh – shear wall, S – slight, L – light, M – moderate, E – extensive, PC – partial collapse, C – collapse

A more simplified and informative approach to evaluate the reduced levels of damage states that can be obtained after the introduced retrofit measures to the existing CCP2 building was investigated with the help of comparative fragility curves for higher damage states. Figure 6.21 presents the comparative fragility curves, where comparison was carried out between the existing and retrofitted buildings. All of the plots illustrate that a considerable reduction in the failure probabilities was recorded after the addition of retrofit measures. In addition, it was found that the steel braced building exhibited minimal failure probability at all IMs when compared to other techniques. The fragility curve for moderate damage illustrates that the all the retrofit techniques would minimise the probability of exceedance but insufficiently, where the peak was attained beyond 0.7 g PGA. The retrofit measures could reduce the probability of moderate damage by almost 20–70% compared to the original building, at 0.3 g PGA. In the case of extensive damage, the failure probability was reduced to almost 30–40%, at 0.3 g PGA. Similarly, the comparative fragility curves for partial collapse exhibit large reductions in failure probability with retrofit techniques. Remarkably, a change in the fragility pattern was recorded for partial collapse, where the jacketing revealed better seismic performance than the shear wall technique. The probability of partial collapse was reduced, at 0.3 g PGA, by approximately 25%. The comparative fragility curves for the collapse state show a remarkable reduction in failure probability, which reduces to theoretically zero for all retrofit techniques. The probability

of exceeding collapse for the existing building, at 0.3 g PGA, corresponded to 22% and retrofitted buildings could reduce this to below 1.5%. From all the above discussions, it can be stated that addition of retrofit techniques would be more effective in reducing the higher damage states. This also indicates that retrofit techniques are effective in reinstating the existing building to its original form so that it does not require heavy repairs and maintenance work after future earthquakes. This ultimately minimises the loss due to human injuries and fatalities, and also minimises the structural and non-structural loss, the objectives of the present study. All the above discussions conclude that steel bracing was found to be much more effective in improving the seismic performance for this particular CCP2 building.
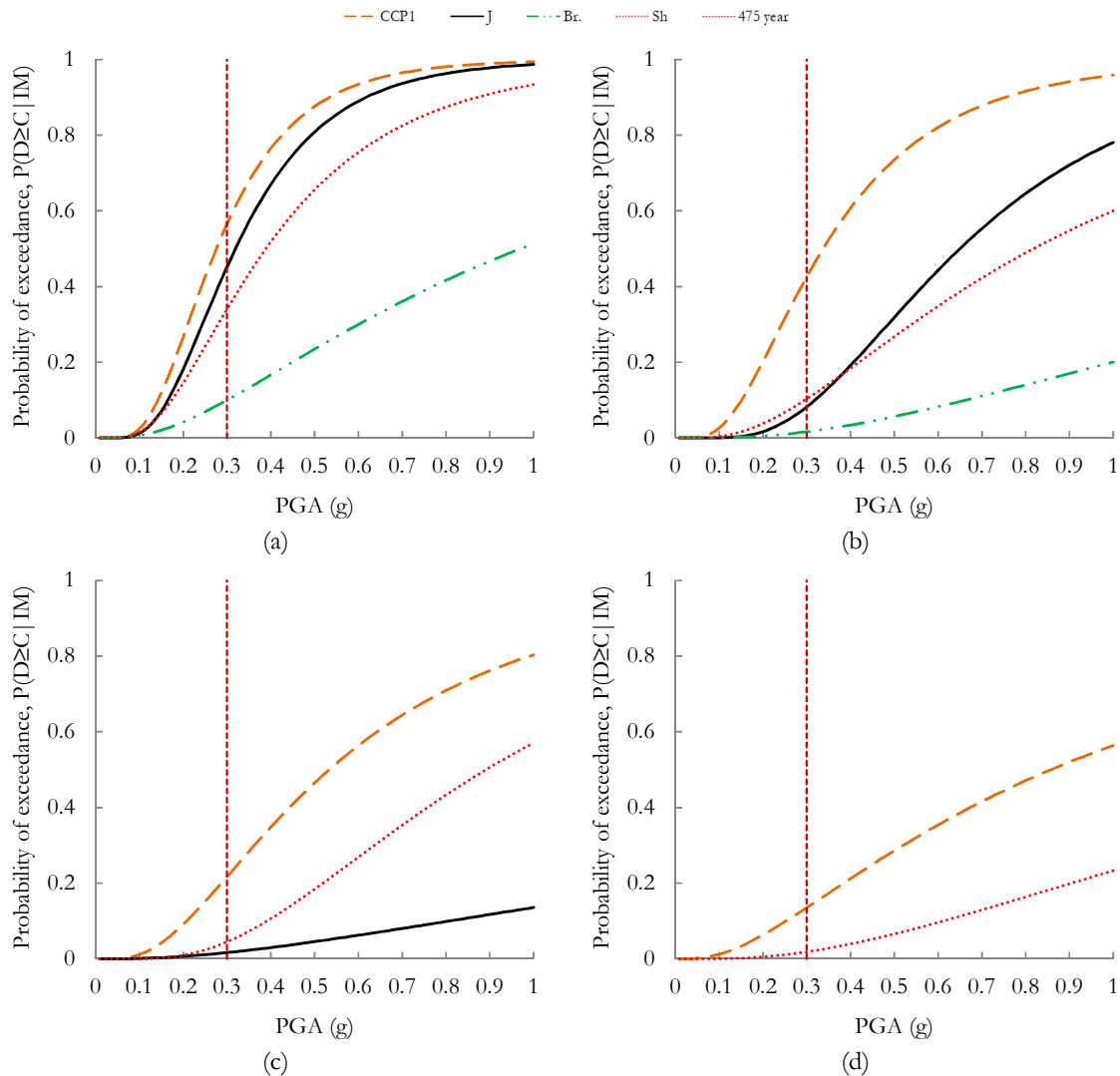

Figure 6.21 - Comparative fragility curves for the CCP2 building with various damage states; (a) Moderate, (b) Extensive, (c) Partial collapse and (d) Collapse. J – jacketing, Br. – bracing, Sh – shear wall

6.3.3 MRT1-WO-GI building

The detailed seismic performance evaluation of the bare frame building along with various arrangements of infill walls was analysed and presented in detail in Chapter 5, which included the bare frame, soft-storey, irregularly infilled and fully infilled buildings. After series of static and dynamic time history analyses and the obtained results, it was concluded that the soft-storey building was found to be the most vulnerable in which drift was concentrated in a single storey, i.e. only on the ground floor. The probability of exceeding partial collapse and collapse, at 0.3 g PGA, was approximately 93% and 42%, respectively. This conclusion also aligned with the field observation, where most of the collapsed infilled RC buildings were observed to be due to a soft-storey mechanism, also discussed in Chapter 2. This was the motivation for the need for retrofit measures in this building, so that the performance could be improved to a certain extent that will ultimately benefit the safety of the occupants and the owners, and also prevent property losses in future earthquakes. Therefore, the present study aimed to instill retrofit measures in the MRT1-WO-GI building (soft-storey) that are expected to largely reduce the vulnerability of such buildings. The three retrofit methods discussed above were employed and, further, seismic performance was investigated under nonlinear static and dynamic time history analyses.

Initially, concrete jacketing was adopted as a retrofit technique, as it is the most commonly practiced retrofit measure at the construction site and does not require innovative ideas and highly skilled man power. The newly added concrete jacketing layout on each floor, section sizes and reinforcement details are presented in Figure 6.22, shown with enlarged column sections. Three types of jacketing elements were assigned (see Figure 6.22 (c)); namely, J1, J2 and J3. The jacketing column J1 had section sizes of (480 x 550) mm², such that new concrete of 125 mm thickness was added on either side of the existing column element. Similarly, both J2 and J3 jacketed columns had section sizes (530 x 530) mm², where J3 column had new concrete of 115 mm thickness added along the longer face and 150 mm thickness enlargement on the shorter side of the existing column. In addition, all the jacketing sections were reinforced with eight Φ 20 longitudinal bars and lateral ties of Φ 10 bars uniformly spaced at 100 mm from centre throughout the column height. The yield strength of the reinforcements and Young's modulus of elasticity were considered to be 415 N/mm² and 2 x 10⁵ N/mm², respectively.

A total of 9 columns out of 17 columns were jacketed on the ground floor, which included two end columns from grid 5-5, three columns from grid 4-4, one column from grid 3-3, one central column from grid 2-2 and two end columns from grid 1-1, as shown in Figure 6.22 (a), illustrated by enlarged column sections. A large number of columns were jacketed near the staircase to counterbalance the effect of large seismic force due to the potential of short-column mechanism. The ground floor jacketing layout was replicated on the first and second storeys, but a column from grid 4-4-B-B (i.e. B-5) was removed, as shown in Figure 6.22 (b).
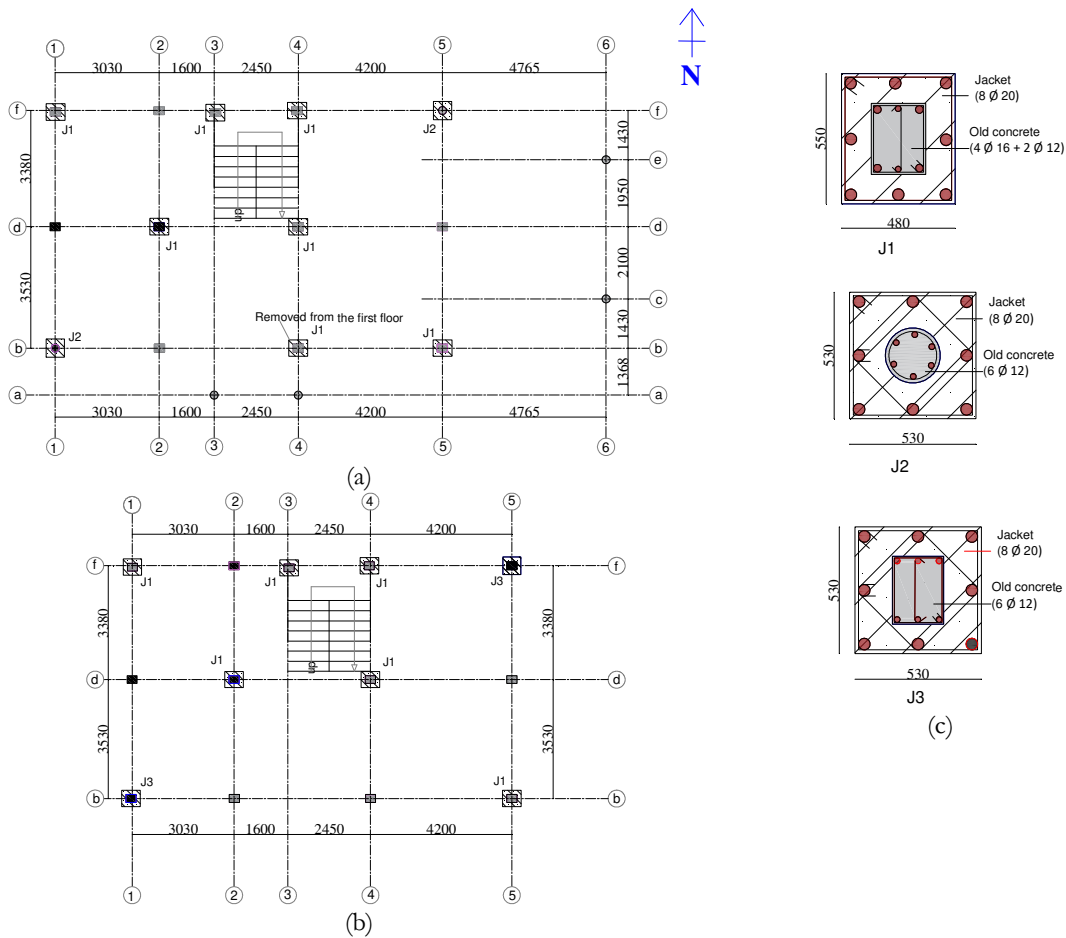
Figure 6.22 - Jacketing layout and section details in the MRT1-WO-GI building; (a) Ground and first floors, (b) Second floor and (c) Section and reinforcement details (all dimensions are in mm)

As an alternative retrofit method, steel bracing was introduced in the MRT1-WO-GI building to investigate its effectiveness in enhancing the seismic performance of the building. Figure 6.23 presents the steel bracing layouts for the different storeys. The present study considered four types of CHS; namely, B1, B2, B3 and B4. The cross-section of the steel bracing elements were: B1 had 130 mm outer diameter and 8 mm thickness, B2 had 120 mm outer diameter and 8 mm thickness, B3 had 100 mm outer diameter and 7

mm thickness and B4 had outer diameter of 70 mm and 5 mm thickness. Different outer diameters and thicknesses for steel bracing were considered to counterbalance drifts for the upper storeys, such that small diameter steel bracing might be sufficient in the upper floors. The steel bracing layout was similar throughout, where the entire bays of grid 1-1 and grid 5-5, and end bays of grid B-B and grid F-F were braced, represented by the hatched surfaces in the Figure 6.23. As the study building was soft storey on the ground floor, large numbers of steel bracing of larger diameter were provided due to potential buckling failure. The ground floor was assigned with steel bracing B1 and B2 along the N-S and E-W directions, respectively. Similarly, the first floor was braced with bracing element B3, and on the second floor it was replaced with bracing element B4. Furthermore, all the bracing elements had the same material properties, and yield strength of the steel bracing element was considered to be 355 MPa.

(a)

(b)
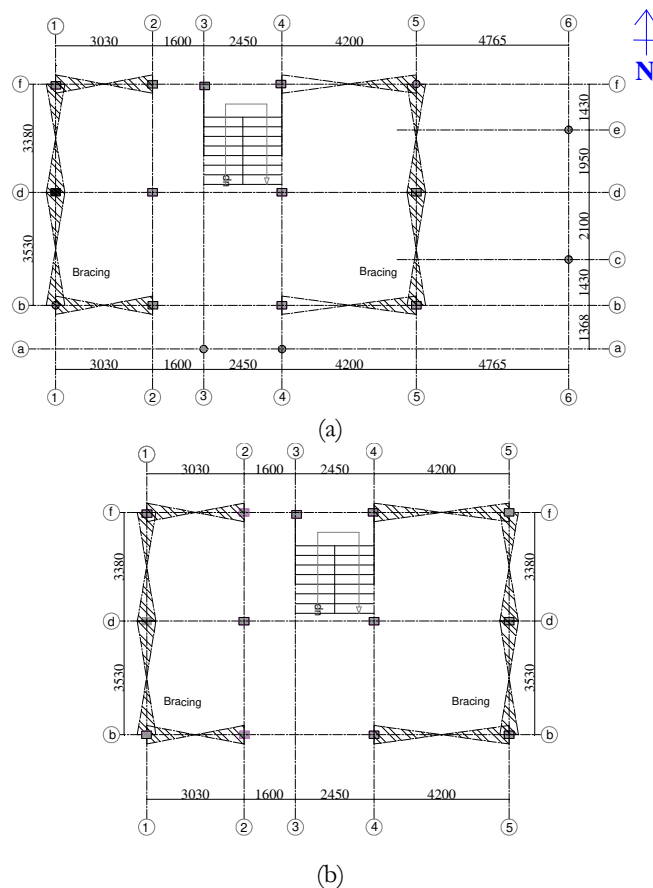
Figure 6.23 - Bracing layout in the MRT1-WO-GI building; (a) Ground and first floors, (b) Second floor (all dimensions are in mm)

Finally, the third retrofit technique introduced in the MRT1-WO-GI building was the addition of RC shear walls, to evaluate the degree of seismic performance improvement

that can be attained after this intervention. The RC shear wall layout illustrating its orientation, sections sizes and reinforcement details are demonstrated in Figure 6.24. Two types of shear walls were considered, i.e. S1 and S2. The height of the shear walls was similar to the height of the respective storeys. The width of S1 and S2 were 2 m and 1.2 m, respectively, and both had 230 mm thickness. The longitudinal reinforcements were distributed in two curtains and each curtain was reinforced with ten Φ 12 bars in S1 and six Φ bars 12 in S2. Both shear walls were reinforced with transverse reinforcements of Φ 12 bars distributed uniformly at 200 mm from the centre along the width of the shear wall. The ground floor was provided with four shear walls (i.e. S1); two in each opposite direction. A shear wall of the same section was assigned in order to minimise potential irregularities due to newly added structural elements (shear wall) and also to neutralise or minimise the eccentricities in the existing building. This included two shear walls constructed at the external face and remaining two shear walls internally, as illustrated in Figure 6.24 (a). A similar shear wall layout was extended to the first and second storeys; however, in the first floor the S1 adjacent to the staircase was substituted by S2, as presented in Figure 6.24 (a and b).
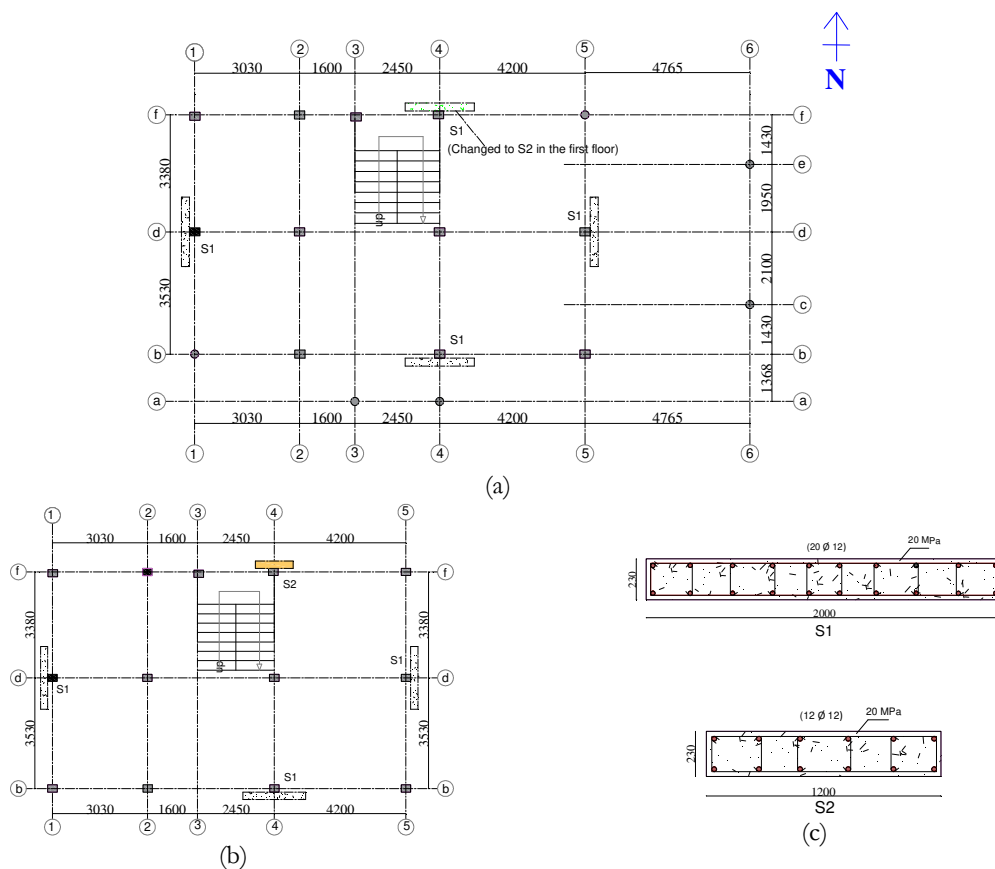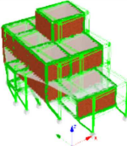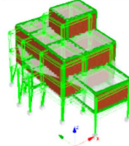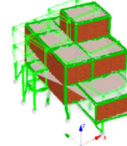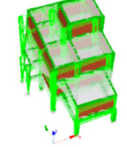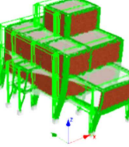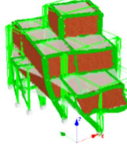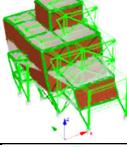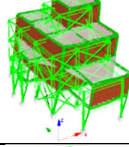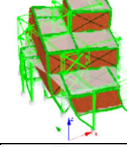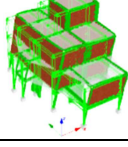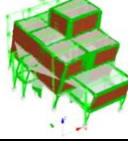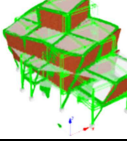
Figure 6.24 - Shear wall layout in the MRT1-WO-GI building; (a) Ground and first floors, (b) Second floor and (c) Detailing of reinforcement in shear wall (all dimensions are in mm)

6.3.3.1 Analysis and interpretation of results

6.3.3.1.1 Eigenvalue analysis

Table 6.3 presents the first three fundamental frequencies for the MRT1-WO-GI building with and without retrofit measures evaluated using eigenvalue analysis. The eigenvalue analysis results revealed that all the retrofitted buildings illustrate the first two fundamental frequencies as translational and third one torsional, except steel braced building that demonstrates translational modes in opposite direction. The first mode effective modal mass participation factors for building with jacketing, bracing and shear wall was approximately 73%, 79% and 80%, respectively. As recorded in previous case study buildings, the retrofit measures increased the fundamental frequencies of the existing MRT1-WO-GI building. When compared between retrofitted buildings, the building with shear wall demonstrates maximum increase in frequency. The increase in the first frequency was almost (2.25-3) times than original building.

Table 6.3 - Eigenvalue analysis results: natural frequencies and respective vibration modes for the MRT1-WO-GI building with and without retrofit techniques

Mode	Frequency (Hz)			First vibration mode	Second vibration mode	Third vibration mode
	f_1	f_2	f_3			
MRT1-WO-GI	1.97	2.24	2.98			
Jacketing	4.40	4.66	5.83			
Bracing	5.48	5.59	7.44			
Shear wall	5.75	6.02	7.56			

6.3.3.1.2   *Capacity curves*

The change in base shear capacity of the existing MRT1-WO-GI building after the addition of retrofit techniques was evaluated and interpreted with the help capacity curves, obtained from the adaptive pushover analysis. Figure 6.25 presents the capacity curves for the building with and without retrofit techniques. The plot illustrates that all retrofit techniques tremendously increased stiffness, strength and deformation capabilities of the existing MRT1-WO-GI building. The maximum increase in stiffness and strength capacities in both directions was recorded in steel braced buildings, and it was followed by reinforcement with RC shear walls and jacketing, respectively. The stiffness increased by 3.5–7 times along the X direction and 4–8 times along the Y direction relatively compared with original building. In addition, the maximum base shear capacity increased by 4–10 times in both directions. The building retrofitted with shear walls and RC jacketing exhibited comparable maximum base shear capacity in both directions. The extreme increase in stiffness and strength capacities was largely contributed to the lack of infill walls on the ground floor in the original building. The increasing patterns of stiffness and strength capacities also revealed that newly added retrofit measures can generate more strength than infill walls. All the plots showed that higher ductility was attained with retrofit measures in both directions. Furthermore, the descending branches of the capacity curve were uniform in the X direction, whereas in the Y direction a steeper degradation branch can be observed with steel braced building. This reveals that the Y direction of the steel braced building can undergo early brittle failure.
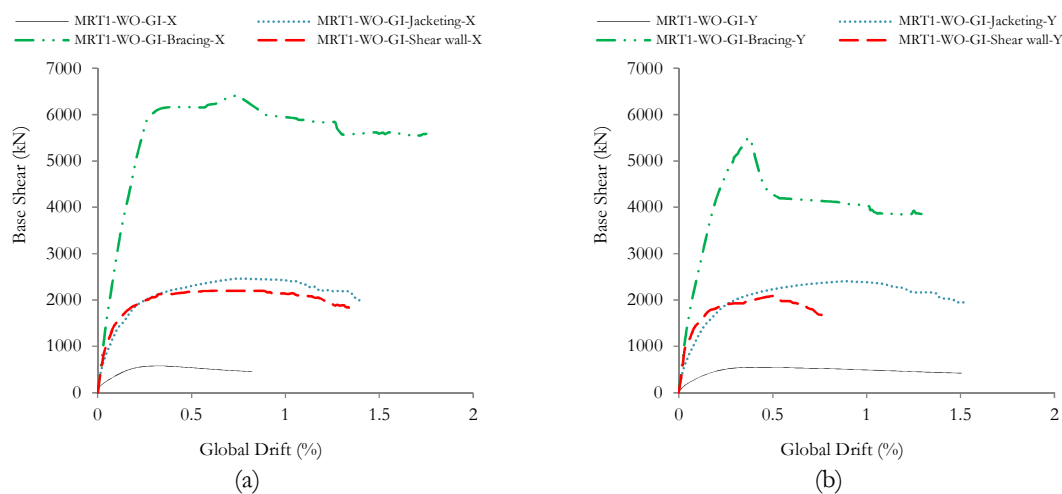
Figure 6.25 – Comparative capacity curves for the MRT1-WO-GI building using different retrofit approaches; (a) X direction and (b) Y direction

6.3.3.1.3   Nonlinear time history analysis

6.3.3.1.3.1   ISD$_{max}$ profile

Figure 6.26 presents a typical inter-storey drift profile for the MRT1-WO-GI building with and without retrofit measures, subjected to a 5-Chi Chi Taiwan earthquake, at 0.3 g PGA. The application of retrofit measures in the original building drastically reduced the ISD$_{max}$ to a minimum value and also modified its distribution, such that drift concentration on the ground floor in the original building was later modified to uniform distribution throughout. The attained drift profile revealed that all retrofit measures adopted satisfied one of the primary objectives of the present study, i.e. the uniform distribution of stiffness and strength throughout. The reduced ISD$_{max}$ for this particular IM ranged from 4–10 times in the X direction and 1.3–4 times in the Y direction compared with the original building. The drift attained in the original building shows that the building was in a collapse state, but with the application of the retrofit measures the building can be predicted to have moderate to extensive damage states. This concludes that after retrofitting the original building, it can be utilised for future earthquakes and potential loss of life and property can be minimized. Although all retrofit techniques were equally effective in significantly reducing the ISD$_{max}$ to minimum values, it can be stated that the steel bracing was reasonably more effective in both directions.

(a)   (b)
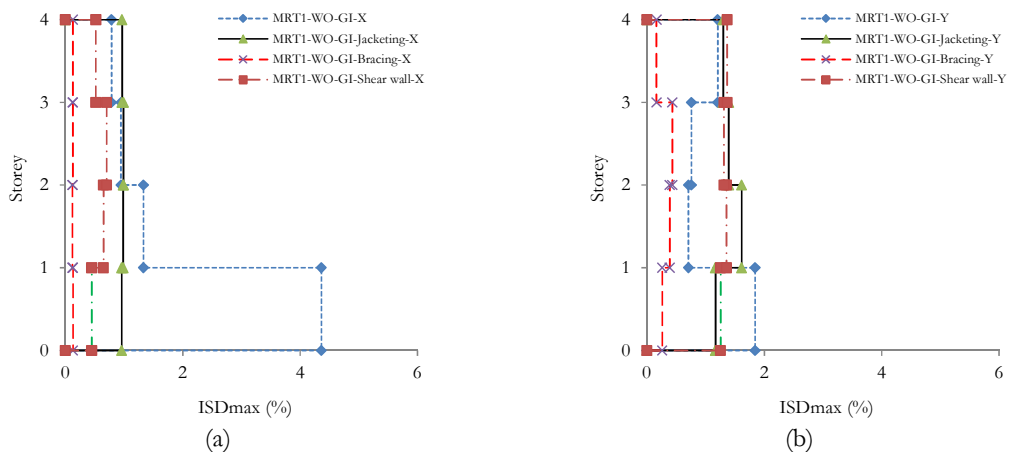
Figure 6.26 - Typical representative inter-storey drift profile for the MRT1-WO-GI building using retrofit techniques, subjected to a 5- ChiChi Taiwan earthquake, at 0.3 g PGA; (a) X direction and (b) Y direction

6.3.3.1.3.2   IDA curves

Figure 6.27 presents the IDA curves for the MRT1-WO-GI building retrofitted with jacketing, steel bracing and shear walls, which were obtained from nonlinear dynamic time history analyses. A larger dispersion of ISD_{max} was recorded for the same IMs, most likely due to variation in seismic demands mainly influenced by the different parameters of the subjected earthquakes. The seismic demand increased with the increase in IMs as expected, but at one point the building would undergo nonlinearity and formation of plastic hinges in the structural members might be dominant even for lower IMs. In such cases, if the building was subjected to higher IMs, it may not meet the seismic demand and potentially exhibit lower ISD_{max}, as observed in a few IDA curves. The IDA curves for jacketing and shear wall retrofits illustrate that it behaves elastically, until 0.3 g PGA. Such buildings are dominated by nonlinearity behaviour with formation of plastic hinges, perhaps in the non-jacketed columns and nearby shear wall columns, beyond 0.3 g PGA. Whereas, in case of steel braced retrofitting the building behaves elastically for the subjected IMs and selected earthquakes.
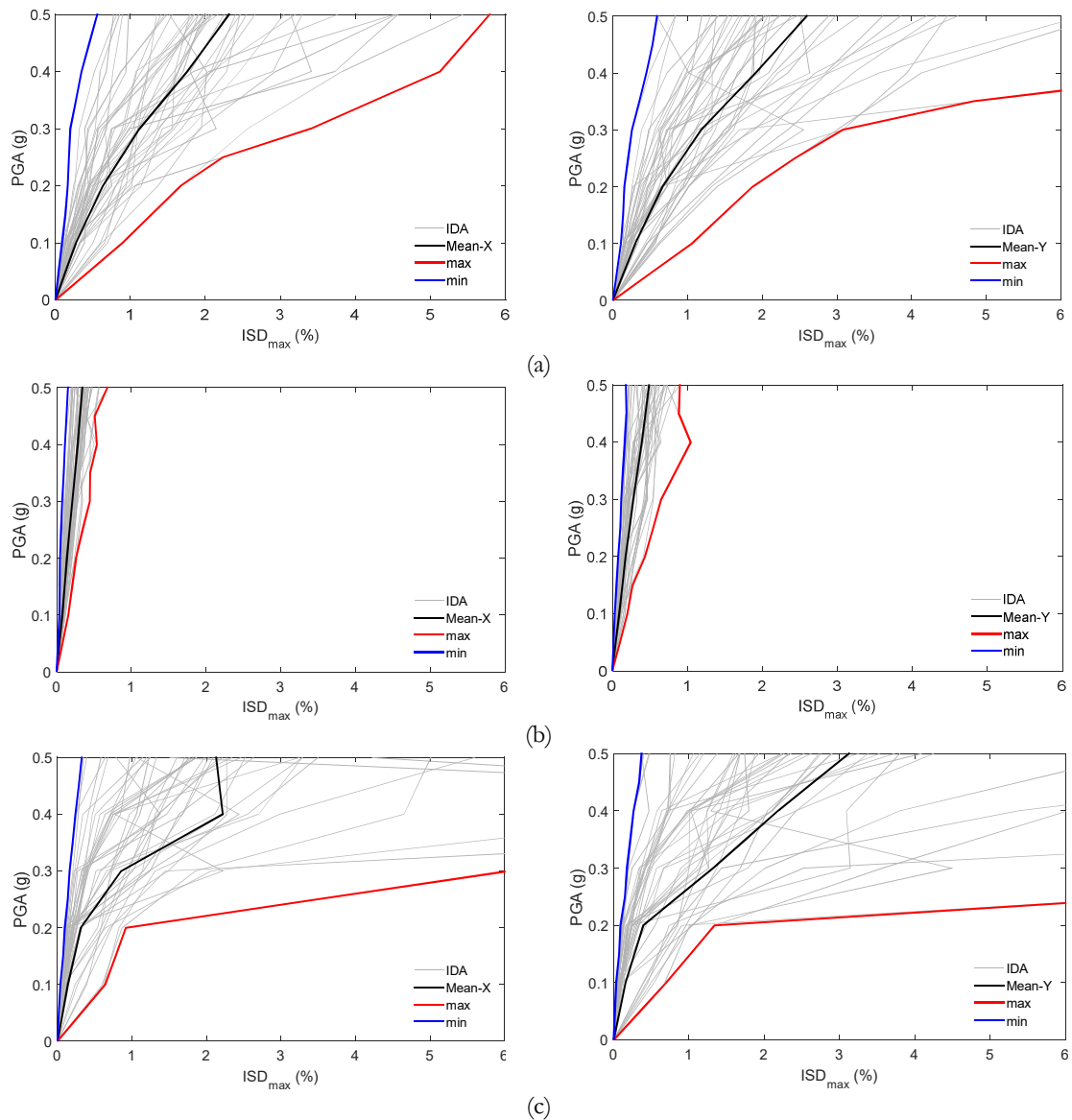
Figure 6.27 – IDA curves for the MRT1-WO-GI building showing large dispersions of building response in the X and Y directions, respectively; (a) Jacketing, (b) Bracing and (c) Shear wall

The IDA curves discussed above might be beneficial to provide an overview of the discrete distributions of the building's response with respect to IM, but it is difficult to generalise and draw a conclusion regarding the selection of the most effective retrofit measures. To overcome this limitation, the present study aimed to plot and compare mean IDA curves that attempt to illustrate the mean seismic demand corresponding to IM. Figure 6.28 presents the comparative mean IDA curves for the building with and without retrofit techniques, and observed that all the retrofit techniques considerably reduced the mean drift to minimum values. In addition, steel braced reinforcement was found to be relatively much more effective in both directions compared to other measures. The attained mean

drift, at 0.3 g PGA, for the MRT1-WO-GI building was more than 6%, which predicts the collapse of the building and such drift was reduced below 1.5% using retrofit measures. This indicates that the potential collapse of the original building can be avoided using retrofit measures leading to moderate to extensive damage states. Furthermore, the building with retrofit measures, at 0.5 g PGA, revealed an average drift of approximately 2.5% and 3% in the X and Y directions, respectively. This state of the building would potentially have extensive to partial collapse, but the life loss could be prevented or reduced due to its large deformation capability before collapse. All the above discussions concluded that the retrofit measures were found to be equally effective in reducing the drift to lower levels and, thereby, reduce the possible damages to the building, but the most effective was found to be steel bracing for this particular building.
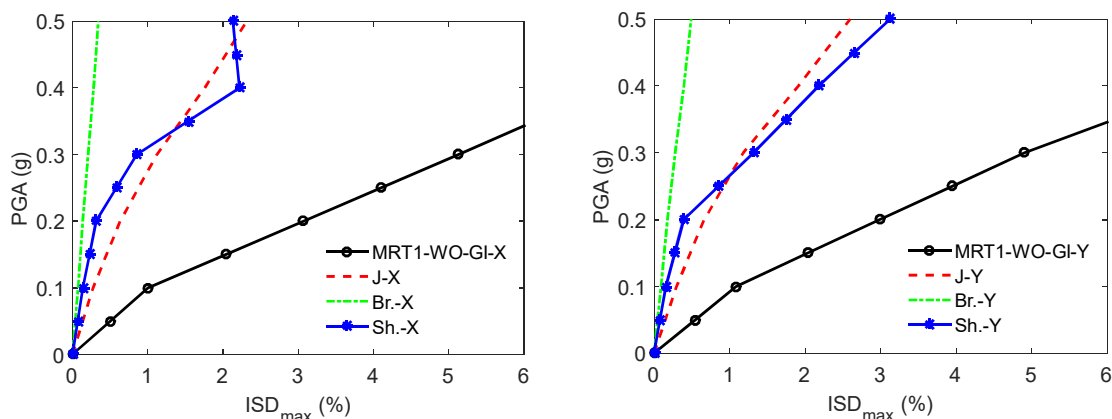
Figure 6.28 – Comparative mean IDA curve for the MRT1-WO-GI building with and without retrofit measures in the X and Y directions, respectively. J – jacketing, Br. – bracing, Sh. – Shear wall

6.3.3.1.3.3   *Fragility curves*

This section investigates and discusses the degree of damage that can be reduced through intervention with retrofit techniques, which was interpreted in terms of probability of exceeding each damage state. Figure 6.29 (a to b) and Figure 6.30 presents the comparative fragility curves for the MRT1-WO-GI building with and without retrofit measures. Such retrofit measures slightly improved the failure probability of lower damage states but insignificantly. Whereas, a drastic and significant improvement was recorded beyond the moderate damage state, such that in some cases the building with retrofit measures exhibited theoretically null damage. The probability of exceeding extensive, partial collapse and collapse damages for the original building, at 0.3 g PGA, ranged from 99–42% and with the adoption of jacketing, bracing and shear walls, it was reduced to 38–1%, 20–1%

and < 1%, respectively. The objective of these retrofit technique interventions in the original building was not to prevent the total collapse but to delay its occurrence and also to control or minimise the lower damage states (associated with damage in the infill walls). Therefore, the obtained results from the comparative fragility curves revealed that this objective was met by the assigned retrofit measures in this particular building.
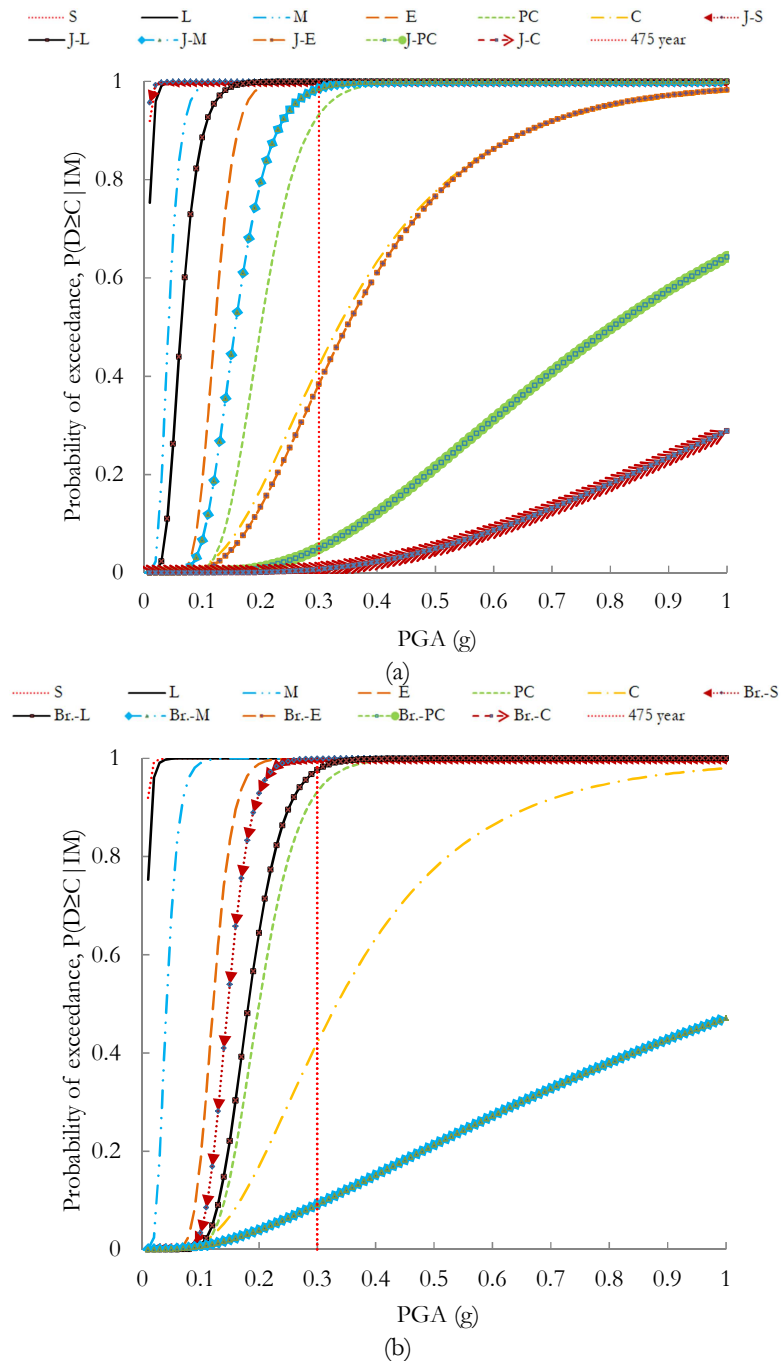
Figure 6.29 - Fragility curves for the MRT1-WO-GI building; (a) Jacketing and (b) Bracing. J – jacketing, Br. – bracing, Sh – shear wall, S – slight, L – light, M – moderate, E – extensive, PC – partial collapse, C – collapse
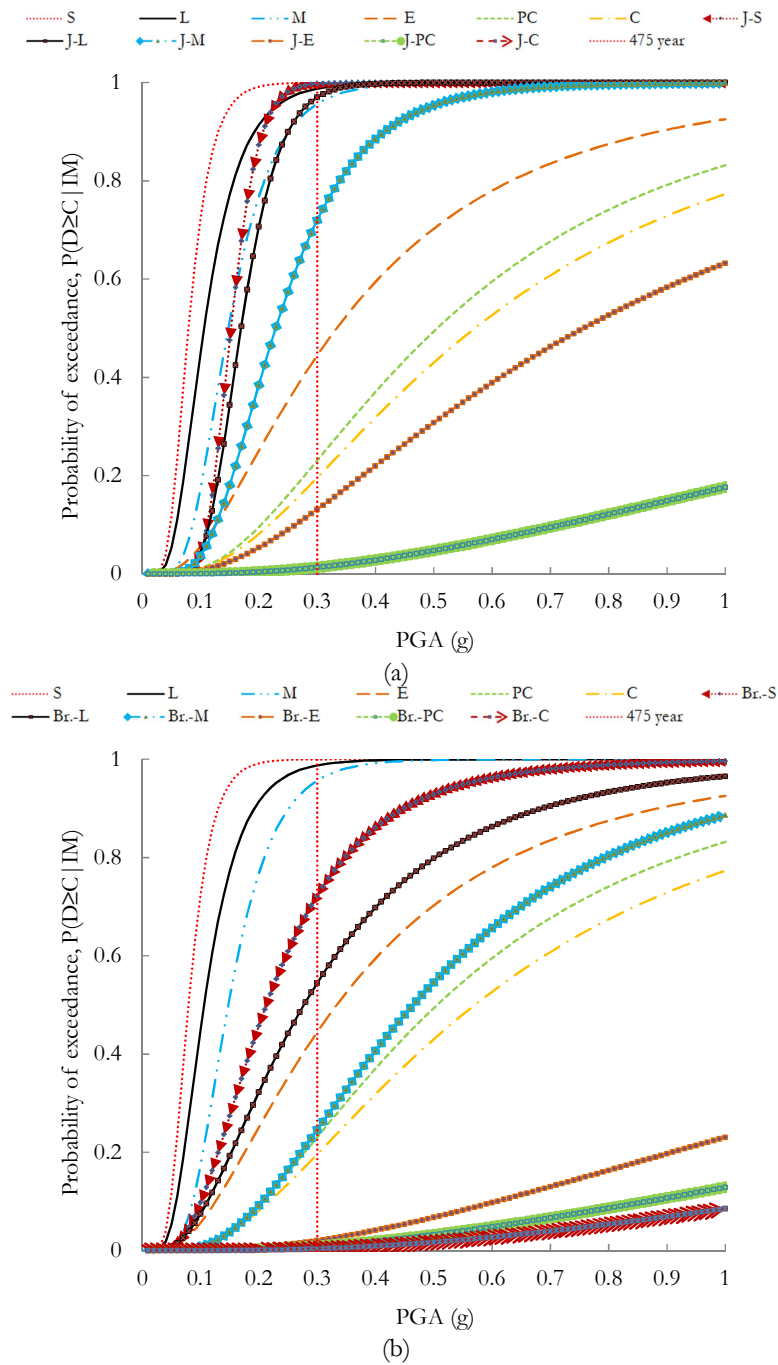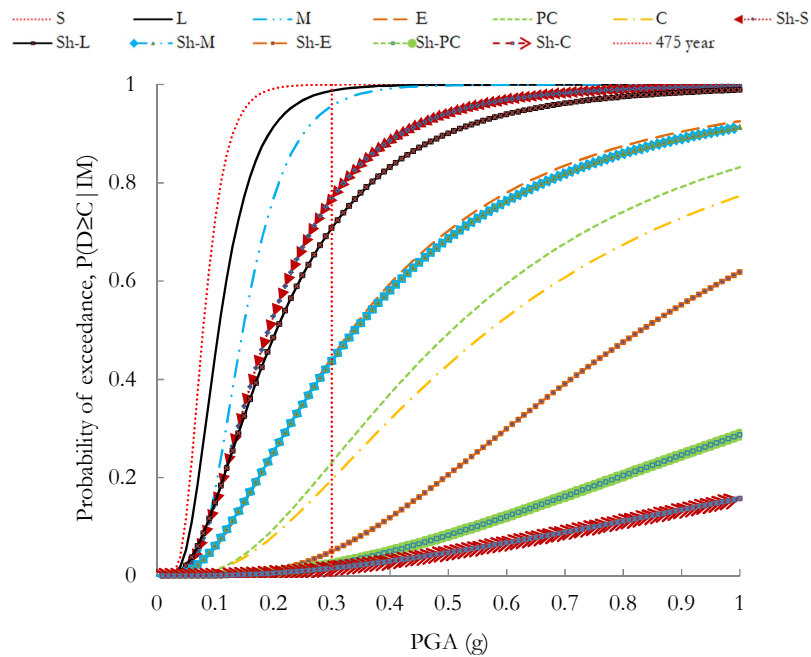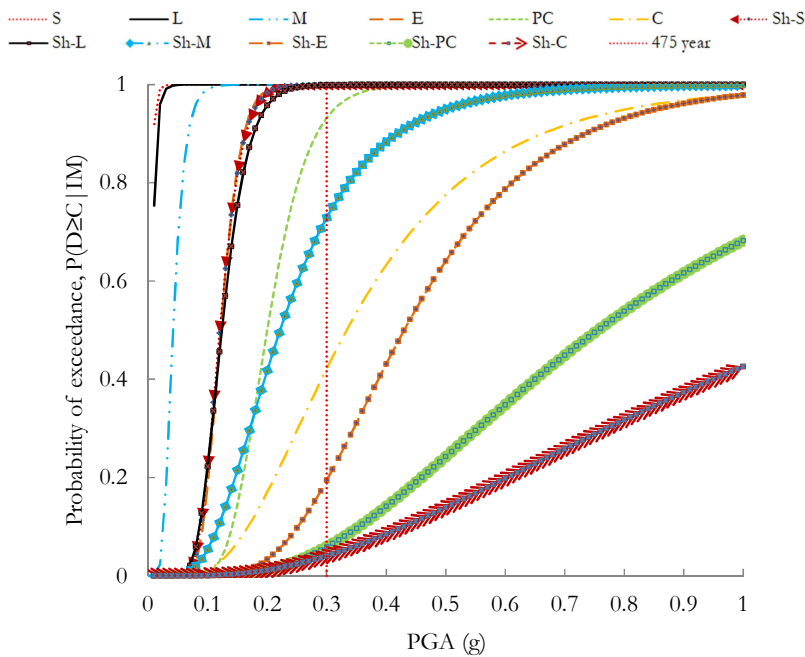
Figure 6.30 - Fragility curves for the MRT1-WO-GI building with Shear wall. J – jacketing, Br. – bracing, Sh – shear wall, S – slight, L – light, M – moderate, E – extensive, PC – partial collapse, C – collapse

The suitability of each retrofit technique for various damage states can be evaluated by comparing the fragility curves. Figure 6.31 presents the comparative fragility curves for higher damage states. All of the plots illustrated that steel braced reinforcement was the most effective in reducing the failure probabilities. The comparative fragility curves for moderate damage reveals that peak damage initially occurred below 0.1 g in the case of the original building, and its occurrence was shifted beyond 0.5 g with addition of retrofit measures. Interestingly, the comparative fragility curves for steel braced retrofitting beyond the moderate damage state revealed theoretically null failure probability. The probability of exceeding extensive damage state, at 0.3 g PGA, could be reduced by 60–80% using retrofit measures in the original building. In addition, the probability of exceeding partial collapse and collapse, at 0.3 g PGA, could also be reduced by 90% and 35–40%, respectively. Summarising all the attained results, it can be concluded that the steel bracing was found to be the most effective in improving the seismic performance of the existing MRT1-WO-GI building, followed by concrete jacketing and RC shear wall, respectively.
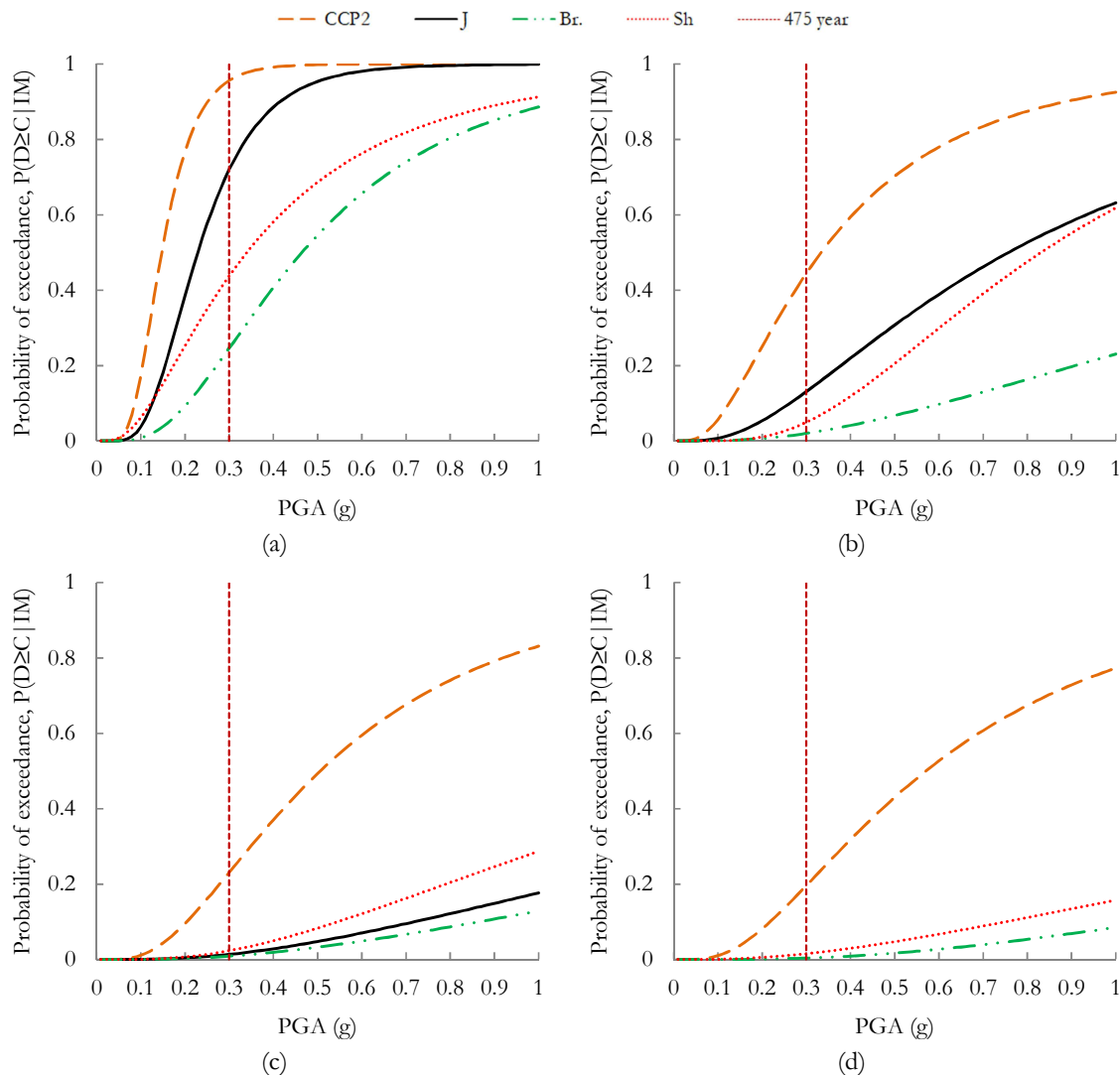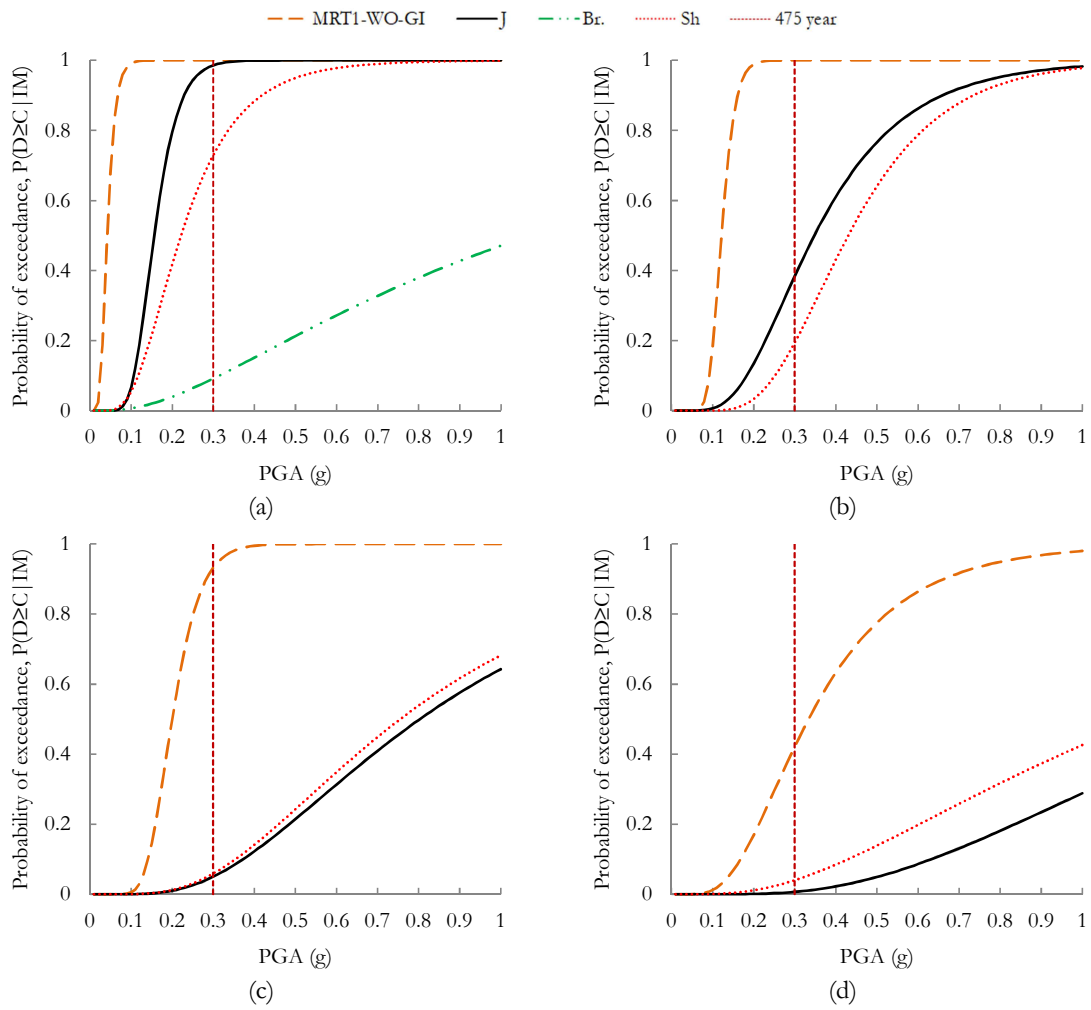
Figure 6.31 – Comparative fragility curves for the MRT1-WO-GI building with different damages; (a) Moderate, (b) Extensive, (c) Partial collapse and (d) Collapse. J – jacketing, Br. – bracing, Sh – shear wall

6.3.4 MRT2 building

The detailed seismic performance assessment of the existing MRT2 building was performed and presented in detail in Chapter 5. The attained results led to the conclusion that the MRT2 building is more likely to have higher damage states and failure of the building is expected under the soft-storey mechanism. The probability of exceeding partial collapse and collapse, at 0.3 g PGA, for the existing MRT2 building was 27% and 22%, respectively. This indicates the necessity for intervention with retrofit measures in the existing building. The three retrofit methods discussed above were employed in the MRT2 building and its detail seismic performance was examined under nonlinear static and dynamic time history analyses.

In the first stage, concrete column jacketing was employed as it is the most commonly practiced retrofit measure in Nepal. Figure 6.32 illustrates the jacketing layout, with section sizes and reinforcement details. The critical columns (critical in shear and flexural and in some cases, structural deficit elements) were identified and selected for jacketing. The study aimed to minimise and rectify structural deficit joints, reduce irregularity due to distribution of infill walls and structural elements, and achieve proper load path distribution. The MRT2 building had a uniform jacketing section of (500 x 500) mm², such that the new concrete of 115 mm thickness was added on either face of the existing columns. The jacketed column was reinforced with eight Φ 20 longitudinal bars and transverse reinforcement of Φ 10 bars uniformly spaced at 100 mm from centre throughout.

A total of 13 columns out of 20 columns were jacketed in the basement, including all columns from grid 1-1 and grid 6-6, three columns from grid 2-2, one central column from grid 3-3 and two end columns from grid 4-4 represented by enlarged column sections, as shown in Figure 6.32 (a). The basement floor layout was reproduced for the ground floor, where one of the columns from grid 2-2-C-C was not jacketed. Similarly, the jacketing layout was replicated on the first floor, where one central column from grid 3-3 was removed. Furthermore, the first-floor jacketing layout was repeated on the second floor, where the jacketed column from grid 3-3-D-D was removed. Finally, the top floor was jacketed, which consisted of two end columns from grid 1-1 and grid 2-2, as shown in Figure 6.32 (b).
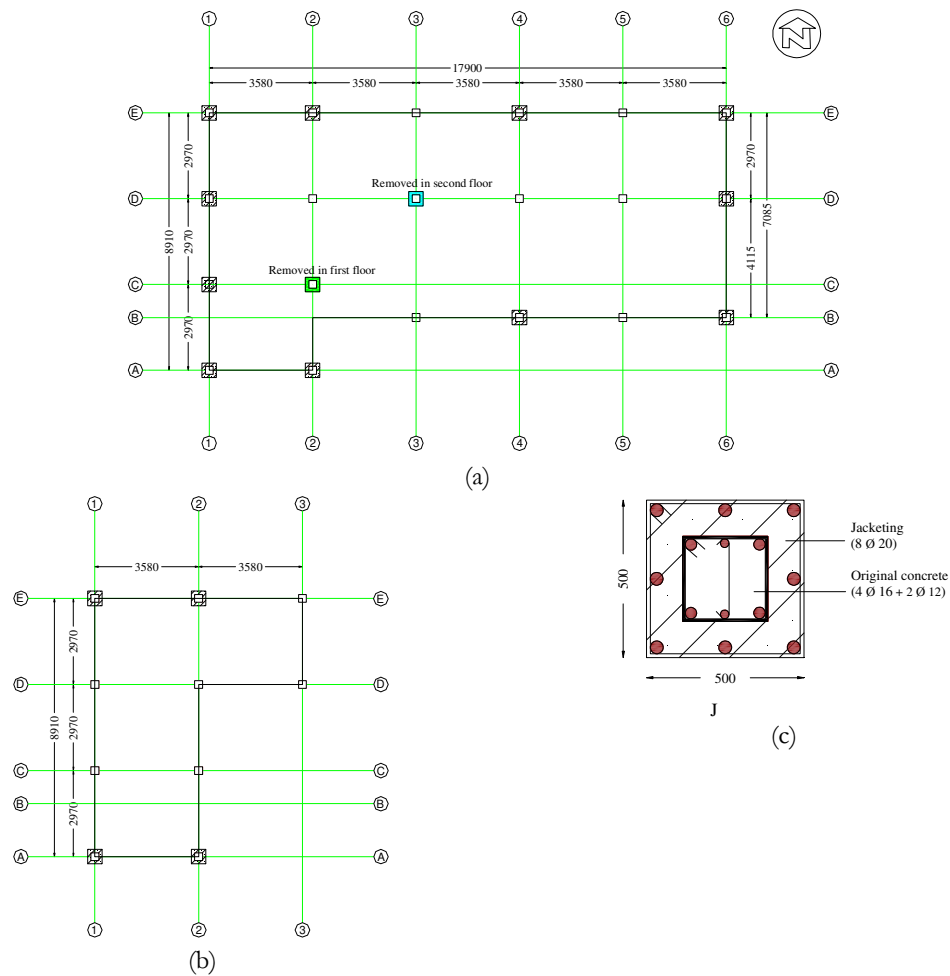
Figure 6.32 - Jacketing layout in the MRT2 building; (a) Plan for basement, ground, first and second floors, (b) Top floor plan and (c) Section and reinforcement details of jacketing (all dimensions are in mm)

As an alternative retrofit technique, CHS steel bracing was adopted, with the layout presented in Figure 6.33, represented by hatched dumbbell shapes. The building considered two types of CHS; namely, B1 and B2. The steel bracing B1 had an outer diameter of 100 mm and 5 mm thickness, and B2 had 140 mm outer diameter and 7 mm thickness. A constant material property was assigned for the bracing, where the yield strength of the steel material was assumed to be 355 MPa. The steel bracing B1 was assigned along the building's N-S direction and B2 along the E-W direction. The bracing layout was identical for the basement and ground storeys, which included all bays from grid 1-1, mid-bay from grid 2-2, one bay from grid 6-6, two bays from grid E-E and also each bay from grid A-A and grid B-B. The bracing layout for the first and second floors were also similar to that of the ground floor, but bracing from end bays of grid 1-1 was removed, shown by a different hatched surface (see Figure 6.33 (a)). Finally, the top floor consisted of four bracings,

which included one bay each from grid 1-1, grid 2-2, grid A-A and grid E-E, as illustrated in Figure 6.33 (b).
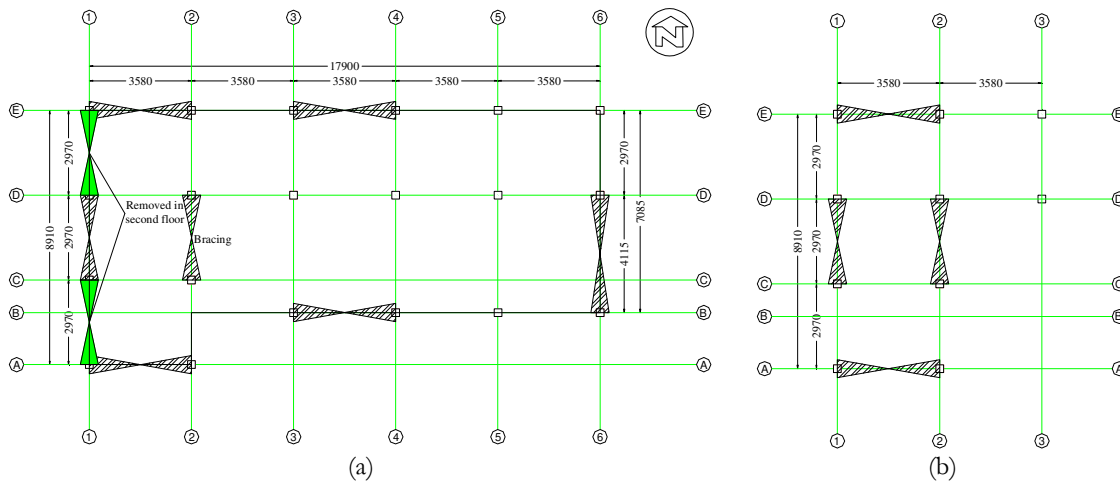
Figure 6.33 - Bracing layout in the MRT2 building; (a) Plan for the basement, ground, first and second floors, (b) Top floor plan (all dimensions are in mm)

Finally, the third stage of retrofit measures included the addition of new RC shear wall elements in the existing MRT2 building, and the seismic performance was investigated to evaluate the reduced levels of damage states. Figure 6.34 presents the RC shear wall layout, orientations, section sizes and reinforcement details. The present study positioned the shear walls in such a way that the centre of the shear walls coincided with the centre of the column. Three types of RC shear walls were considered and assigned, namely S1, S2 and S3. All the shear walls possessed the same thickness of 250 mm. Similarly, the widths of S1, S2 and S3 were 2.5 m, 1.8 m and 1.4 m, respectively. All the shear walls had two curtains of longitudinal reinforcements, such that S1, S2 and S3 were reinforced with a total of 24 Φ 12, 18 Φ 12 and 14 Φ 12 longitudinal bars, respectively. It was reinforced with transverse reinforcements of Φ 12 bars uniformly spaced at 200 mm from the centre throughout. Three shear walls were provided (two external and one internal) along the N-S direction and two along the E-W direction of same section, i.e. S1 on the basement and ground floors. A similar shear wall layout was extended to the first and second floors, where S1 was modified to S3 along the N-S direction and S2 along the E-W direction. Furthermore, the top floor was provided with two shear walls only in the N-S direction, as shown in Figure 6.34 (c).
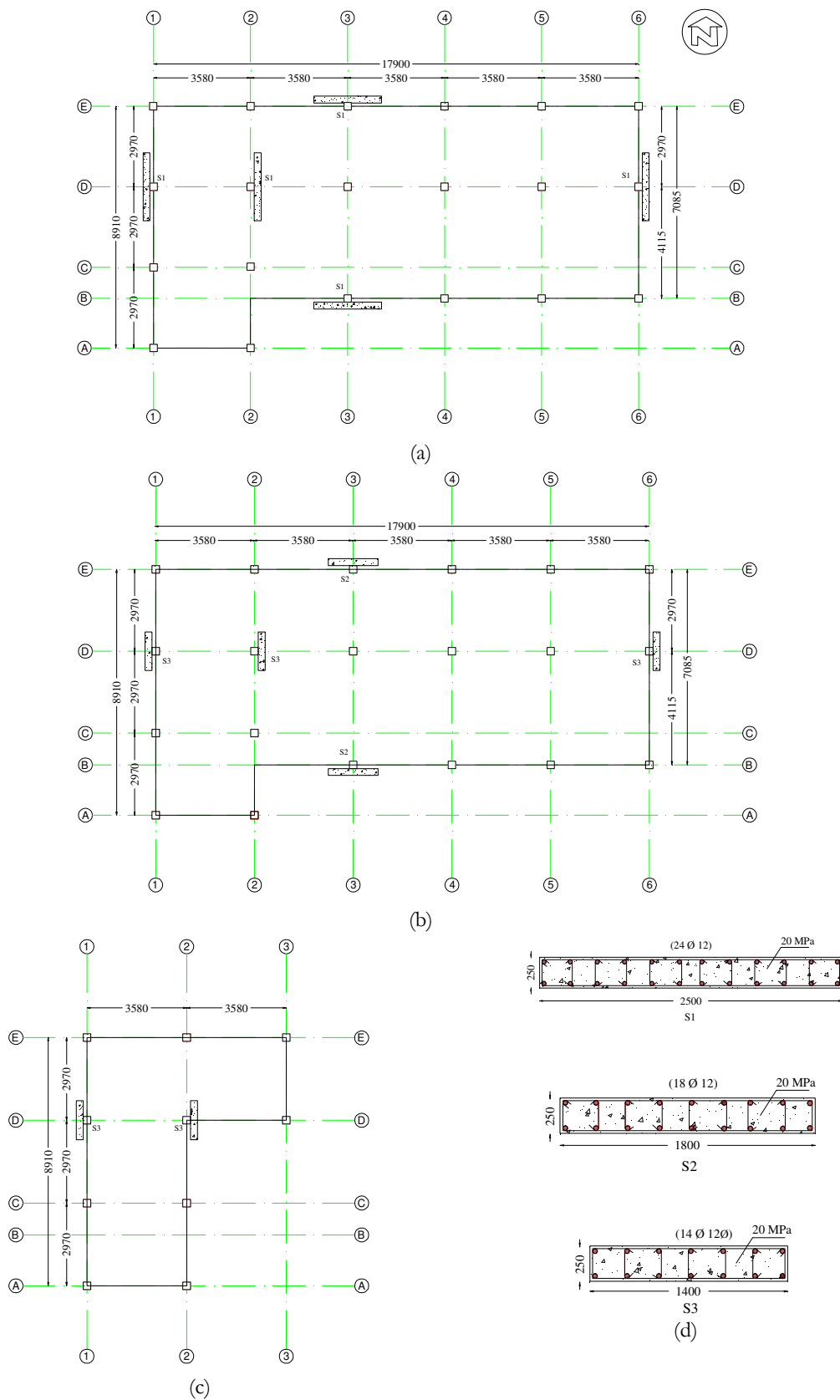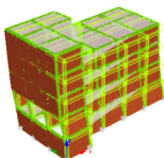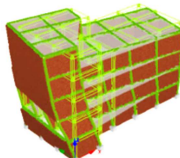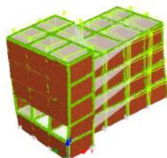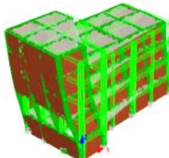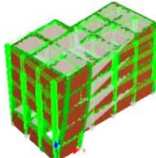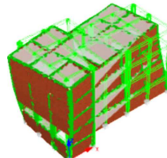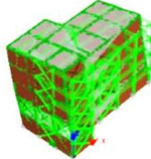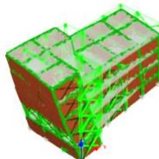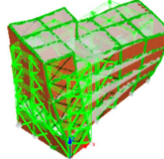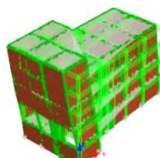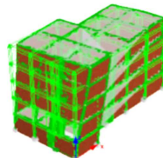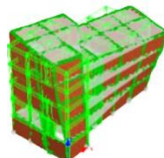
Figure 6.34 - Shear wall layout and section details in the MRT2 building; (a) Plan for the basement and ground floors, (b) Plan for the first and second floors, (c) Top floor plan and (d) Detailing of shear walls (all dimension are in mm)

6.3.4.1 Analysis and interpretation of results

6.3.4.1.1 Eigenvalue analysis

Table 6.4 presents the first three fundamental frequencies and their respective vibration modes for the original and retrofitted MRT2 buildings obtained from eigenvalue analysis. As expected, all the retrofitted buildings demonstrated the first two vibration modes as translational and the third one as torsional, which was relatively similar to the original building. The percentage of effective modal mass participation factors for the first mode for the building with jacketing, steel bracing and RC shear wall were approximately 82%, 82% and 79%, respectively. The eigenvalue analysis results also revealed that all the retrofit measures significantly increased the fundamental frequencies of the building. The highest increase in frequency was recorded for the building retrofitted with RC shear walls. The retrofit measures increased the first frequency by 1.7–1.9 times the original MRT2 building.

Table 6.4 - Eigenvalue analysis results: natural frequencies and respective vibration modes for the MRT2 building with and without retrofit techniques

Mode	Frequency (Hz)			First vibration mode	Second vibration mode	Third vibration mode
	f_1	f_2	f_3			
MRT2	2.90	3.41	3.79			
Jacketing	5.01	5.27	5.85			
Bracing	5.39	5.97	6.83			
Shear wall	5.54	5.99	6.78			

6.3.4.1.2   Capacity curves

Figure 6.35 presents the capacity curves for the MRT2 building with and without retrofit measures, obtained from adaptive pushover analysis. This helps to investigate the changes in stiffness and strength capacities in the original building after the addition of retrofit measures. Substantial increases in stiffness, strength and ductility capacities were recorded in both directions as compared with that of the MRT2 building. The maximum increases in stiffness and strength capacities were recorded for steel bracing in both directions. With the addition of retrofit measures, the increase in stiffness ranged from 2–3 times in the X direction and 1.5–3 times in the Y direction compared to the original MRT2 building. The maximum base shear capacity for the building retrofitted with shear walls and concrete jacketing was comparable. In addition, the increase in maximum base shear capacity ranged from 1.3–2.3 times in the X direction and 1.5–3 times in the Y direction. The degradation branch was observed to be uniform, which indicates that besides increases in stiffness and strength capacities, it also largely increased the deformation capability of the original building. This indicates that the retrofitted buildings can undergo large deformation, thus preventing the collapse of the building, as a result the loss of life and other damages can be minimized.
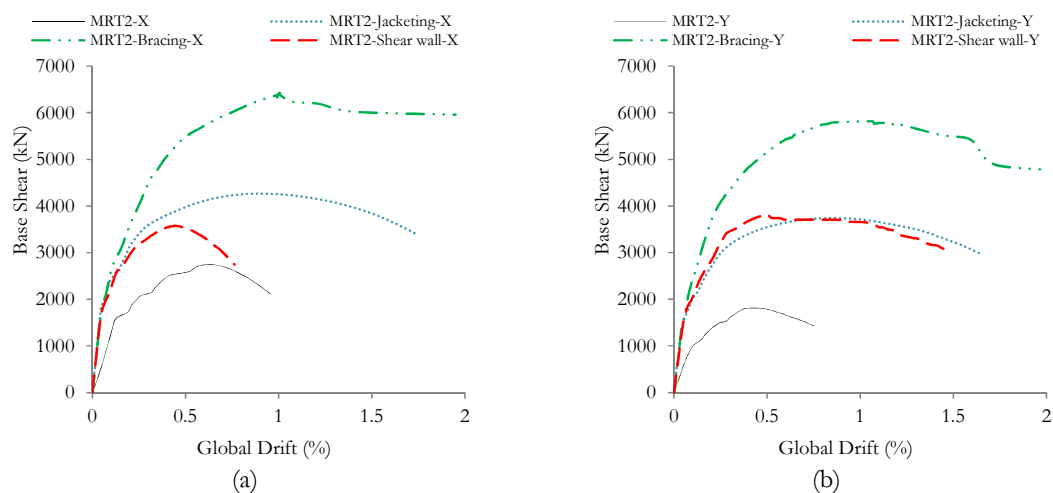
Figure 6.35 - Comparative capacity curves for the MRT2 building using different retrofit strategies; (a) X direction and (b) Y-direction

6.3.4.1.3   Nonlinear time history analysis

6.3.4.1.3.1 ISD_{max} profile

The effectiveness of the retrofit techniques in the existing MRT2 building can also be evaluated through the distribution of drift along the height. Figure 6.36 presents a representative inter-storey drift profile, subjected to a 5- Chi Chi Taiwan earthquake, at 0.3 g PGA, to examine the modification in drift distributions after introducing retrofit techniques. The retrofitted buildings had significantly reduced ISD_{max} and also uniform distribution of the drift throughout. This approach eliminated a single storey drift concentration recorded mostly in the basement of the original MRT2 building. This is due to the ability of proper retrofit techniques to uniformly distribute stiffness and strength throughout, which was one of the primary objectives of the present study. The addition of retrofit measures largely reduced the ISD_{max}, with reductions of 4–7 times in the X direction and 3.5–7 times in the Y direction. This particular drift revealed that the original building would have collapsed but using the retrofit measures the building exhibited moderate to extensive damage states only.
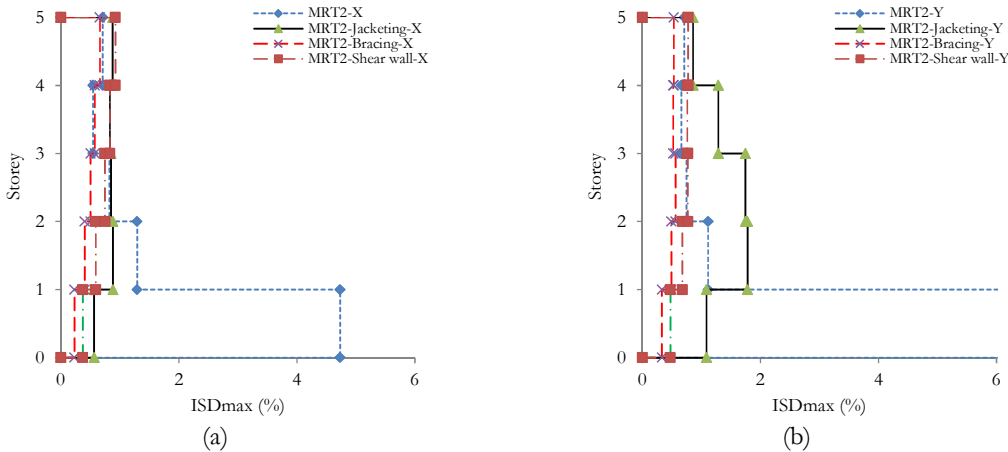
Figure 6.36 - Typical representative inter-storey drift profile for the MRT2 building considering retrofit techniques, subjected to a 5- ChiChi Taiwan earthquake, at 0.3 g PGA; (a) X direction and (b) Y direction

6.3.4.1.3.2   IDA curves

Figure 6.37 presents IDA curves for the retrofitted MRT2 buildings obtained from nonlinear dynamic time history analyses. All the IDA curves illustrate that the increase in IMs resulted in an increase in ISD_{max}, as expected. However, some earthquakes having large comparable frequency and recorded for a longer duration exhibited higher seismic

demand even for low IMs, and such buildings if subjected to higher IMs exhibits lower IMs as the structure was expected to have collapsed, illustrating lower drift than estimated. The IDA curves for the building retrofitted with jacketing demonstrated large scattering of the building response for the same IM in both directions. The jacketed building showed elastic behaviour until 0.2 g and 0.3 g PGA in the X and Y directions, respectively, and thereafter nonlinearity can be expected to be dominant. Similarly, the steel braced MRT2 building also revealed a large dispersion of ISD$_{max}$ and the building could be expected to behave elastically until 0.4 g PGA. A more dispersed ISD$_{max}$ for same the IMs was more clearly visible for the building retrofitted with RC shear walls. This phenomenon was recorded beyond 0.3 g, thus it was predicted to behave elastically until 0.3 g PGA and nonlinearity would become dominant beyond this PGA.
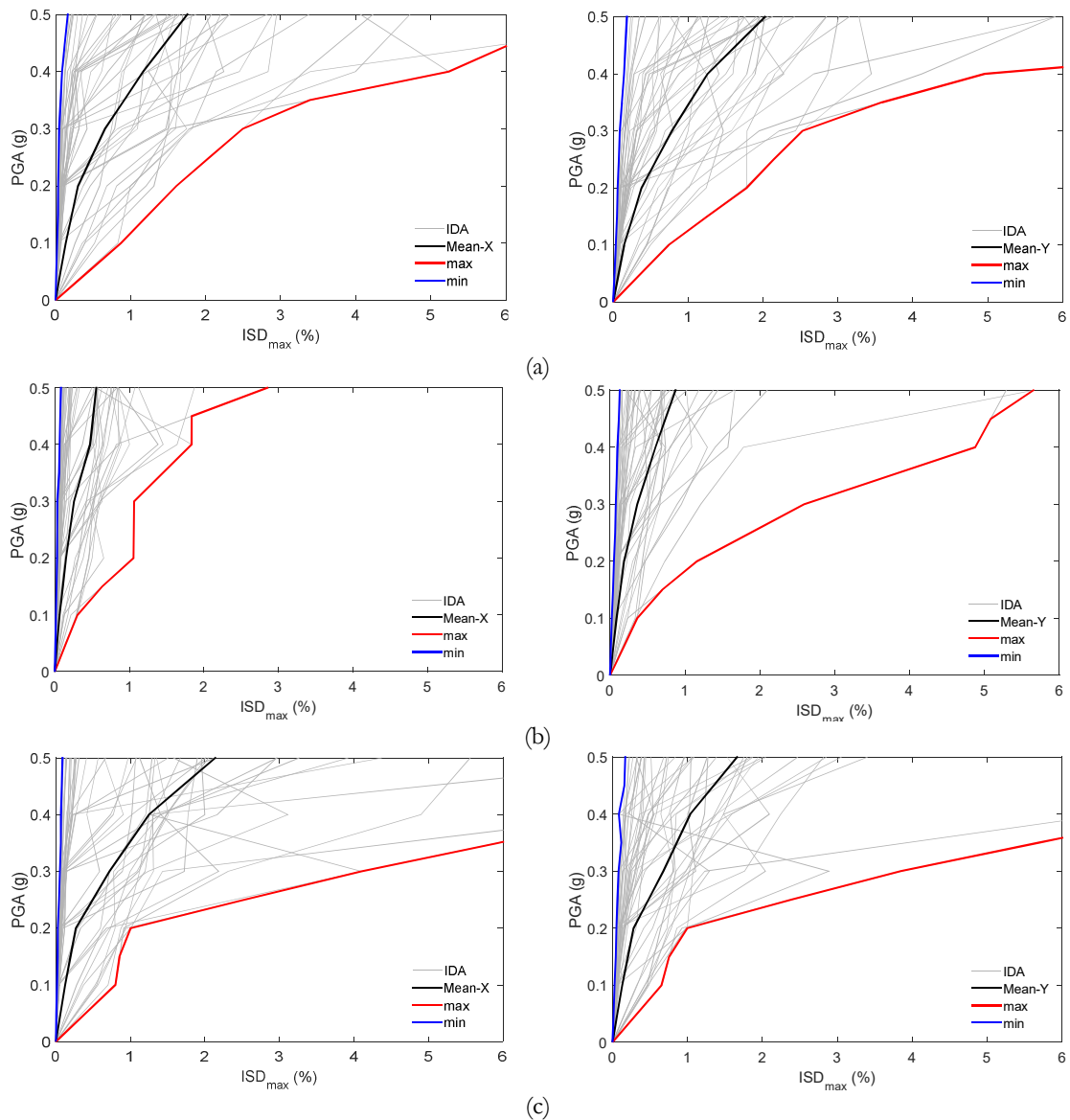
Figure 6.37 – IDA curves for the MRT2 building showing large dispersion of building response at various IMs; (a) Jacketing, (b) Bracing and (c) Shear wall

The behaviour of the MRT2 building with and without retrofit techniques under dynamic time history analyses can be evaluated more clearly through a more suitable and simplified approach, i.e. plotting comparative mean IDA curves. Figure 6.38 presents the mean IDA curves for the MRT2 building with and without retrofit techniques. All the retrofit measures were found to reduce the mean ISD_{max} to minimum values. It was observed that steel bracing exhibited the lowest mean ISD_{max} for the considered IMs, when compared with other measures. In addition, the MRT2 building with shear walls and jacketing was observed to exhibit comparable mean IDA curves in the X direction; whereas, in the Y direction shear wall measures exhibited slightly lower mean ISD_{max} than the jacketed building. The original MRT2 building exhibited more than 5% mean ISD_{max}, at 0.3 g PGA, such that it experienced total collapse. After introducing retrofit techniques, the mean ISD_{max} was reduced to below 2% in both directions, where the buildings had moderate to extensive damage states. Summarising all the above analytical results and discussions, it can be concluded that all the adopted retrofit techniques in this particular building significantly enhanced the seismic performance, thus satisfying the seismic demand even for higher IMs. In addition, the building with steel bracing was found to be much more effective than other techniques.
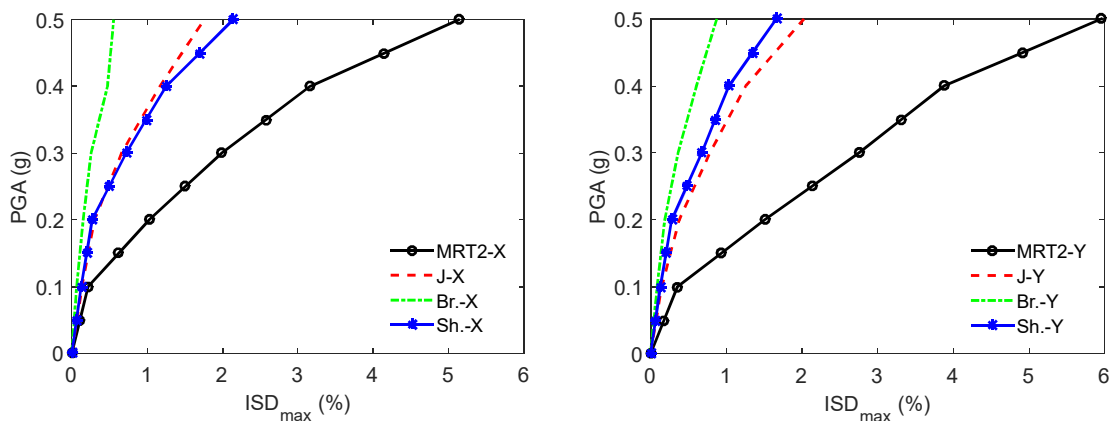
Figure 6.38 – Comparative mean IDA curves for the MRT2 building with and without retrofit techniques. J – jacketing, Br. – bracing, Sh. – shear wall

6.3.4.1.3.3   Fragility curves

The viability and suitability of all retrofit measures in the original building were evaluated with the help of fragility curves, which analytically illustrate the seismic vulnerability of the retrofitted MRT2 building and also improvement attained in the level of damage states. Figure 6.39 and Figure 6.40 (a to b) presents the comparative fragility curves between the

original building and retrofitted buildings for six damage states. Similar to the other study buildings, no significant improvement was attained for lower damage states, i.e. slight and light; where its occurrence was below 0.1 g in the original building and later shifted at 0.4 g using retrofit techniques. In cases of higher damage states, a significant improvement was attained similar to other study buildings discussed in previous sections. The probability of exceeding partial collapse and collapse, at 0.3 g PGA, could be reduced to 2% and < 1%, respectively. The lower damages could not be prevented though such damages can be recovered with simple maintenances, whereas higher damages that require extensive efforts, time and money could be reduced to lower levels. Finally, the human injuries and fatalities could be minimized to lower values, a primary objective of the present study. Therefore, it can be concluded that all retrofit techniques were suitable and efficient in enhancing the seismic performance of the existing MRT2 building.
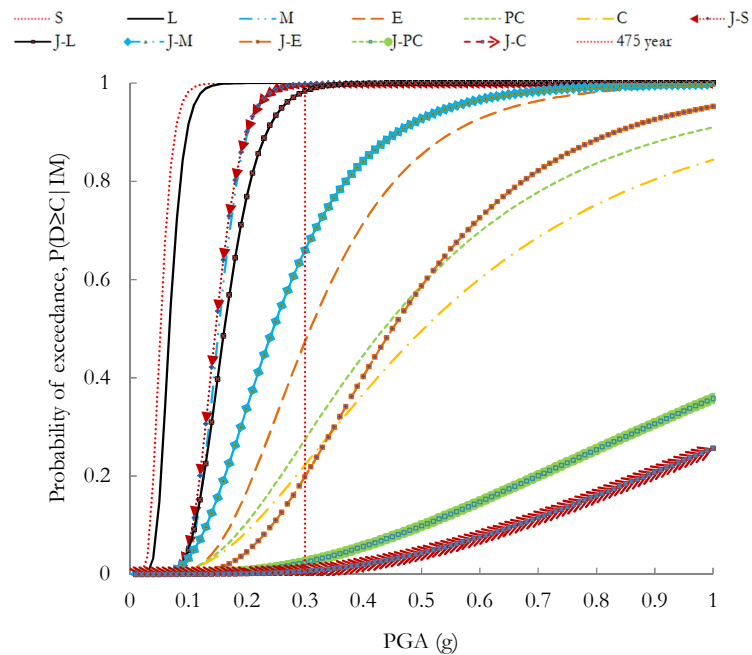
Figure 6.39 - Fragility curves for the MRT2 building with Jacketing. S – slight, L – light, M – moderate, E – extensive, PC – partial collapse, C – collapse
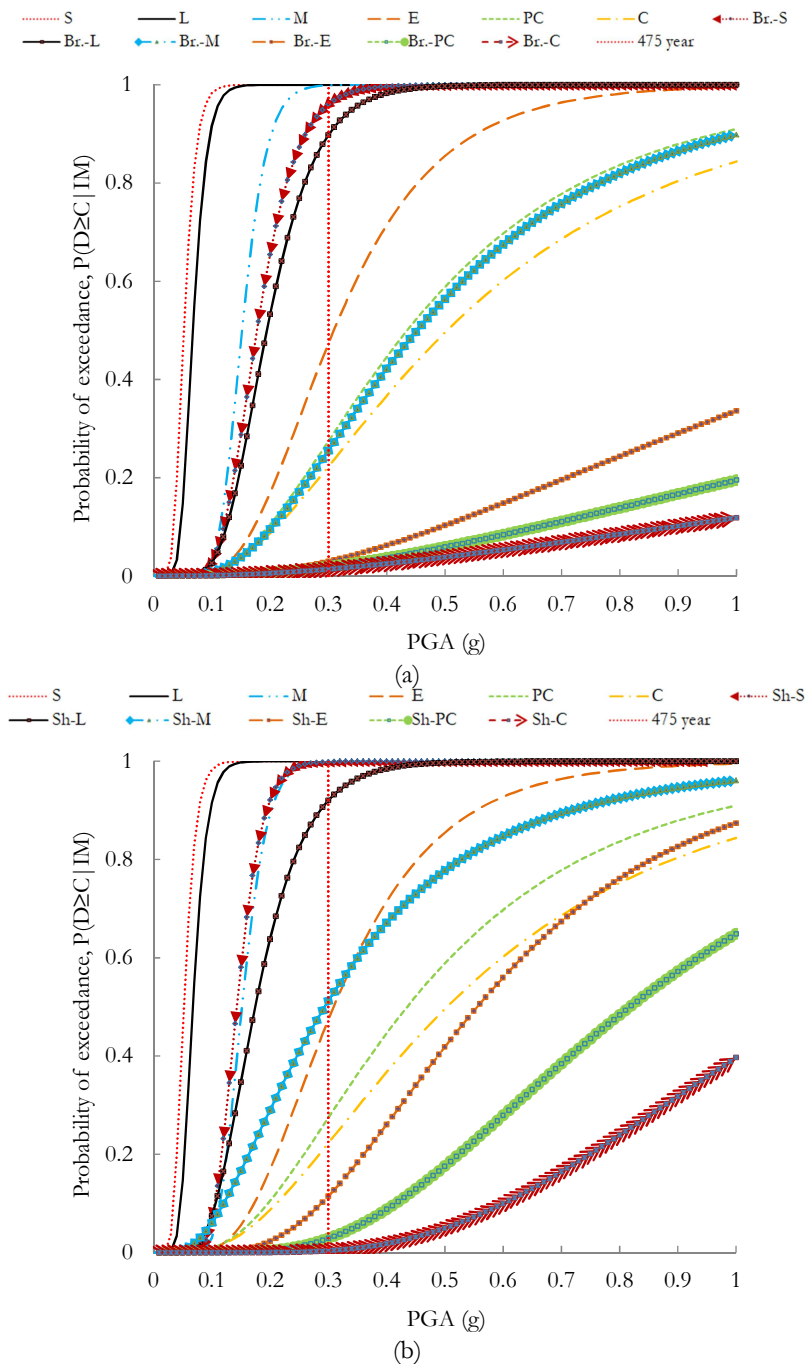
Figure 6.40 - Fragility curves for the MRT2 building; (a) Bracing and (b) Shear wall. J – jacketing, Br. – bracing, Sh – shear wall, S – slight, L – light, M – moderate, E – extensive, PC – partial collapse, C – collapse

The most effective and efficient retrofit techniques for the MRT2 building and the levels of damage that could be reduced after their intervention can be interpreted through the comparative fragility curves, plotted between the original MRT2 building and retrofitted buildings and shown in Figure 6.41. For the selected damage states, the steel braced building was observed to demonstrate lower failure probabilities. Similarly, when comparing between the buildings retrofitted with RC shear walls and concrete jacketing, it

was found that shear walls were found slightly more effective in moderate and extensive damage states. Whereas, jacketing displayed better seismic performance for partial collapse and collapse states than shear walls. The failure probability of moderate damage, at 0.3 g PGA, could be reduced by 35–75% from the original building. Similarly, the probability of exceeding extensive damage, partial collapse and collapse, at 0.3 g PGA, was reduced by 25–40%, 25% and more than 20%, respectively, compared with the original building. Theoretically, the probability of exceeding partial collapse and collapse was reduced to lower values, i.e. < 2% and < 1%, respectively. Summarising all the obtained results, it can be concluded that steel bracing was found to be relatively more effective in enhancing seismic performance.
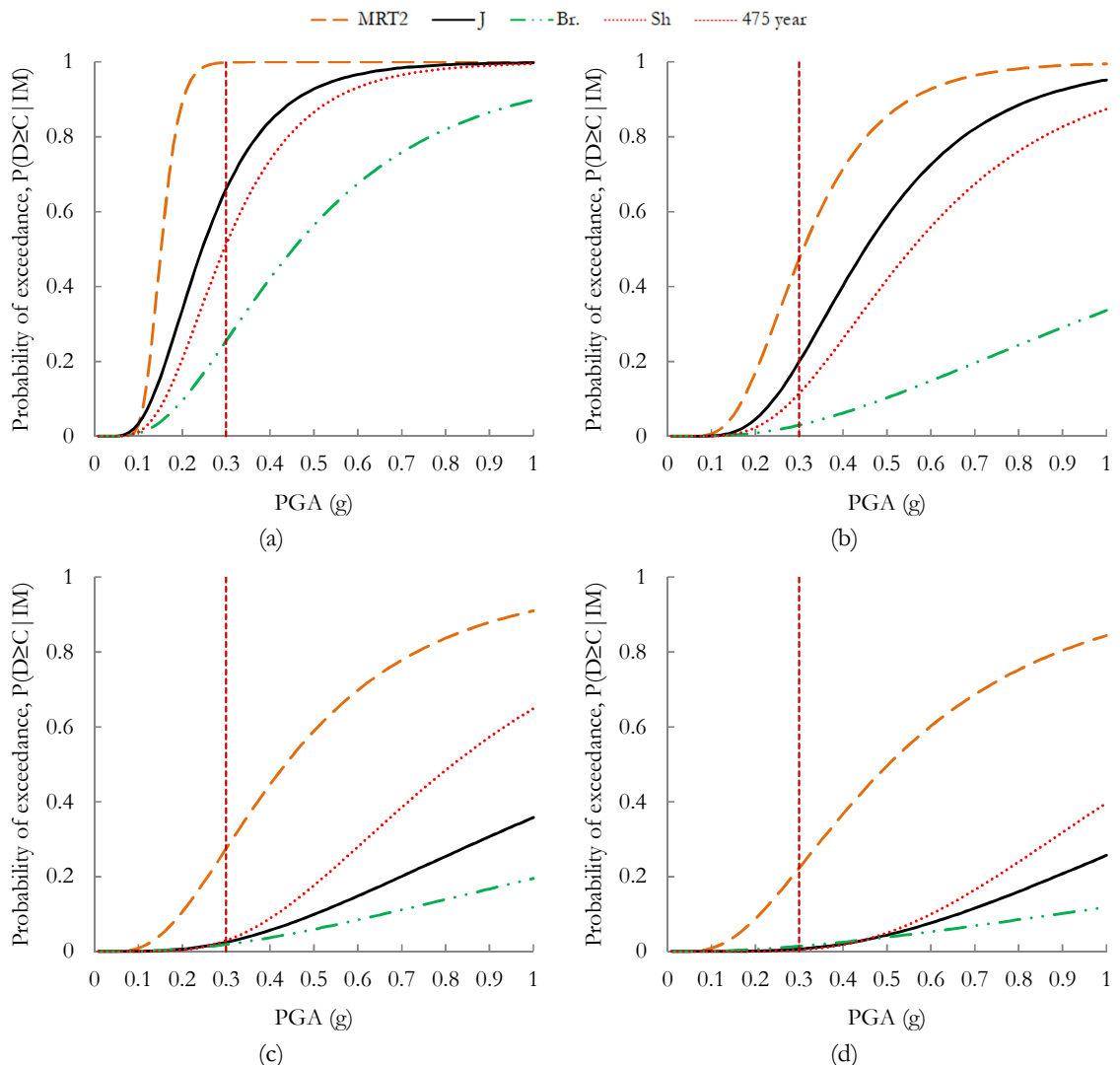
Figure 6.41 - Comparative fragility curves for the MRT2 building with various damage states; (a) Moderate, (b) Extensive, (c) Partial collapse and (d) Collapse. J – jacketing, Br. – bracing, Sh – shear wall

6.4   Conclusion

The preliminary detailed investigations concluded that the case study non-engineered and pre-engineered buildings were found to be seismic deficiencies, as analysed and discussed in detail in Chapter 5. Therefore, the present chapter discussed the potential increase in seismic performance through the addition of retrofit measures that are commonly practiced in Nepal. The selection of concrete column jacketing was very difficult; however, the columns that were critical in shear and flexure were selected for jacketing, including corner columns and short-column. In addition, the retrofit location and number of storeys to be retrofitted depends upon the attained inter-storey drift in each floor. The eigenvalue analysis results showed that all the retrofit measures increased the fundamental frequencies and the building vibration modes were also similar to the original building.

In the second stage, the adaptive pushover results revealed that all the retrofit measures considerably increased the stiffness, strength and deformation capabilities compared to the existing buildings. In all case study buildings, steel braced building was found to highly increase stiffness and strength capacities. For the CCP1 building, the increase in stiffness was 4–7 times in both directions, and the increase in strength was 2–3 times in the X direction and 1.5–5 times in the Y direction more than the existing CCP1 building. Similarly, for the CCP2 building, the increase in stiffness ranged from 1.5–2.5 and 1.2–1.8 times in the X and Y directions, respectively, and the increase in maximum base shear capacity was 2–3.5 and 1.5–2.5 times in the X and Y directions, respectively. In addition, the MRT1-WO-GI building illustrated an increase in stiffness by 3.5–7 times in both directions and strength was increased by 4–10 times compared to the existing building. Furthermore, the MRT2 building showed an increase in stiffness of 1.5–3 times in both directions and increase in strength ranged from 1.3–2.3 times in the X direction and 1.5–3 times in the Y direction. All the retrofit techniques showed uniform degradation capacity curves signifying that the retrofit measures not only increased the stiffness and strength, but also increased ductility in the existing buildings, and steel bracing was reported to exhibit high ductility. Similarly, retrofit techniques considerably reduced the ISD_{max} and also attained uniform drift distribution throughout. In addition, they also eliminated drift concentration in a single storey that was common in the existing buildings.

Dynamic time-history analyses concluded that the large dispersion of building response (ISD_{max}) was attained for same IMs revealing that the building response depends on

various parameters of the earthquakes to which they were subjected, such as frequency contents and recorded durations. The mean IDA curves were compared between retrofit techniques and original buildings and revealed that, in most cases, the steel braced building exhibited comparatively lower drift than other techniques. This concludes that steel bracing is much more effective in improving the seismic performance of the existing buildings. In addition to the IDA curves, the suitability of the selected retrofit measures were also evaluated through the comparative fragility curves. The fragility curves revealed that in most of the case study buildings, steel bracing was found to significantly reduce the probability of exceeding damage states compared to other techniques. When comparing between the seismic performance of shear walls and jacketing, interestingly a consistent conclusion was not established, such that for lower damage states shear walls illustrated better performance but for higher damage states, jacketing revealed lower failure probability. Therefore, it can be concluded that the retrofit technique suitable for one building type may not be applicable to other buildings. Hence, the study recommends the design engineers evaluate the detailed seismic assessment of the building. The practical suitability and feasibility of the studied retrofit techniques largely depends on the associated cost and benefit that can be obtained, i.e. cost-benefit analysis, and is discussed in detail in Chapter 7.

Chapter 7.

Cost-benefit Analysis of Retrofitted Non-engineered and Pre-engineered Buildings using Probabilistic Approach

7.1   Introduction

Past earthquakes around the globe demonstrated large destructions and typical damages to the structural components, such as beams and columns, and non-structural components, including infill walls, finishing, other machinery, etc. associated with the buildings. This is more prominent in non-engineered or pre-code buildings since these are not designed to resist lateral loads under large seismic ground excitations. Liel, *et al.* (2010) [213] investigates the seismic performance evaluation through comparison between the modern reinforced concrete frame and non-ductile RC frame. They concluded that the non-ductile frames are highly susceptible to collapse, i.e. 40 times higher (in terms of annualized risk) than code conforming ductile RC frames [213]. These buildings undergo slight to collapse damage states causing social and economic disturbances. This includes various types of direct losses (i.e. repair and replacement cost), indirect losses (i.e. rental loss, relocation loss and economic loss due to business interruption), and life safety (i.e. number of injuries and fatalities) [213]. Liel, A. (2008) [204] concludes the likelihood of the older RC frame being more susceptible to be damaged leading to more costly repairs compared to the modern RC frames.

Almost 9,000 people were killed and more than 22,000 people injured resulted by more than 600,000 fully damaged buildings (includes masonry, wooden and RC frame buildings), as recorded in 25th April 2015, Gorkha earthquake, Nepal [19]. It includes 6,613 collapsed and 16,971 partially damaged RC frame buildings [214]. The failure mechanisms of RC buildings recorded after in-situ site survey was presented and discussed in detail in Chapter 2. The typical damage and failure in the RC buildings causing large number of injuries and fatalities motivated to carry out the cost-effective strengthening on the existing non-ductile moment resisting frames. Other literatures and analytical results presented in Chapter 6

revealed that strengthening adopted in the existing infilled RC buildings could significantly enhance the seismic performance and will be able to resist future earthquakes without major building damages and likely human loss can be prevented and/or minimized. The strengthening (i.e. retrofitting) of the case study buildings (non-engineered and pre-engineered) using three common construction practices was presented in detail in Chapter 6. It was concluded that such measures highly reduces drift demand and lower the failure probabilities. However, cost is a governing factor that motivates owners, stakeholders and other concerned parties to invest the money for carrying out the retrofit on the existing buildings. Therefore, the present study carries out the comparative life time cost benefit analysis for each case study building using the probabilistic approach and the most cost effective retrofit measures for the particular building will be established. The cost effectiveness will be investigated through the unexpected loss in the structure either in the form of expected annual loss, life cycle loss and sensitivity analysis.

7.2   Overview of Previous Works

The performance based earthquake engineering (PBEE) method has been used to investigate the building's life cycle cost (LCC). The seismic performance of the structural and non-structural components was evaluated through the PBEE method under seismic excitation so as to attain the recommended performance goals. The goals can be at the local levels (i.e. probability of structural and non-structural member cracking and crushing, etc.) or at the global level including the life safety (i.e. probability of structural collapse and resulting fatalities), and economic losses (i.e. probability of various damage states, such as slight, light, extensive and so on). Figure 7.1 presents the conceptualized procedures of the PBEE method, where the building was subjected lateral forces resulting nonlinear response and subsequent damages. The relationship between the structural responses (e.g. inter-storey drifts, inelastic member deformations and member forces) and performance levels, such as Immediate Occupancy (IO), Life Safety (LS) and Collapse Prevention (CP) were established.
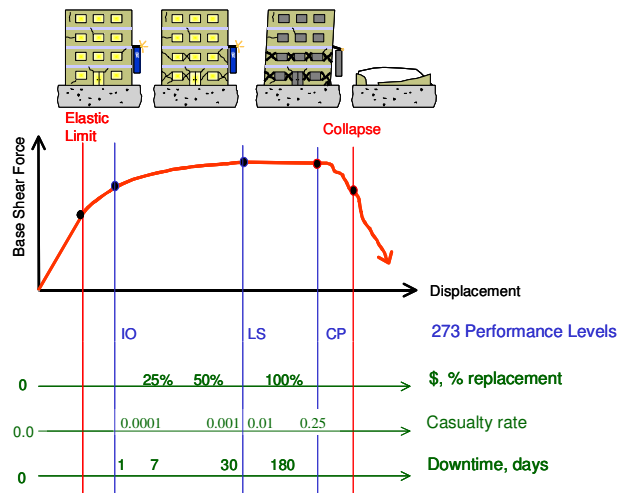
Figure 7.1 – A visualization of performance-based earthquake engineering (after Moehle, 2003 [215])

In 1992, Federal Emergency Management Agency (FEMA 227) published first user's manual on "A Benefit-Cost Model for the Seismic Rehabilitation of Hazardous Buildings" [216]. This methodology provides guidelines for design professionals and encourages the decision makers and other interested groups to undertake decision to mitigate the risks possessed by the existing hazardous buildings in case of an earthquake. It provides two intended applications of benefit-cost models. The first application helps in decision making, whether the particular seismic rehabilitation program is economically feasible depending upon the seismic site of the building. The second application provides a guideline to perform detail analyses with the help of first application if the rehabilitation is economically justifiable for further consideration. Cost-benefit analyses provide useful guidance; for example, depending on acceptable seismic risk, rehabilitation programs might include or exclude some classes of buildings, occupancies or uses.

Initially the concept of PBEE was documented in the VISION 2000 report [201] in which performance-based earthquake design (PBED) for various hazard levels were defined. The hazard level includes frequent intensity level that has probability of exceedance of 50% in 30 years, occasional intensity level with 50% probability of exceedance in 50 years, rare intensity level with 10% probability of exceedance in 50 years, and 10% probability of exceedance in 100 years for very rare intensity level [201]. The VISION 2000 [201] classified the performance levels into four; such as fully operational, operational, life safety, and near collapse to define damages to the structural and non-structural elements and its impacts to the occupants. VISION 2000 [201] also provides a relationship between seismic hazard and performance levels based on the type of the structures. The performance level

for each building type was defined based on the requirement of the client or owner; the designer designs the structure which varies for private to public and commercial buildings. For private buildings, high performance level may not be concerned as the owner may not be interested in investing big money. The risk is borne by the owner himself; hence, the performance level is determined mutually between client and design engineer. However, the risk cannot be accepted or comprised for hospital, school buildings and other important public buildings, where public life safety is the major concern. Hence, such type of buildings should be designed for higher performance levels [201].

In 1996, Applied Technology Council (ATC) prepared a report on "Seismic Evaluation and Retrofit of Concrete Buildings Volume 1" [217]. The main purpose of ATC-40 reports is to provide "state-of-the-practice recommendations to address current needs for the seismic retrofit provisions and seismic risk decision tools" mainly focusing on vulnerable concrete buildings. In 1997, FEMA 273 published a guidelines on "NEHRP Guidelines for the Seismic Rehabilitation of Buildings" [200], concluding manifestation obtained from the effort of more than 13 years. The proper and effective rehabilitation technique limits the earthquake damage in the building to a range corresponding to the ground shaking and check if design professionals utilized the design guidelines properly. FEMA 273 addresses the rehabilitation of the existing structures, later revised and updated by the joint effort of American Society of Civil Engineers (ASCE) and FEMA with the outcome of most comprehensive guidelines of PBEE to date, i.e. FEMA 356 (2000) – "Prestandard and Commentary for the Seismic Rehabilitation of Buildings" [218]. FEMA 356 (2000) guidelines was planned to encourage the wider use of the "NEHRP Guidelines for the Seismic Rehabilitation of Buildings", i.e. FEMA 273, by converting it to a user-friendly language. It also provides a basis for American National Standards Institute (ANSI) approved standard, a nationally recognized standard that integrates the design and its construction practice [218]. The existing buildings can be rehabilitated in an appropriate way using this procedures and it is even more applicable for the new buildings that are built under new codes. The target performance levels and seismic hazard levels are similar to as defined in the VISION 2000. The structural performance levels are selected from "four discrete performance levels and two intermediate structural performance ranges". The former levels include Immediate Occupancy (S-1), Life Safety (S-3), Collapse Prevention (S-5) and Not Considered (S-6). Similarly, the intermediate structural performance ranges are the "Damage Control Range (S-2) and the Limited Safety (S-4)". The five discrete non-structural performance levels for a building are selected, such as; "Operational (N-A),

Immediate Occupancy (N-B), Life Safety (N-C), Hazards Reduced (N-D), and Not Considered (N-E)" [218].

The facilities that are damaged by earthquake hazard, whose performance can be assessed by methodology proposed by Moehle, J. (2003) [215]. This methodology addresses the shortcoming of the first generation PBEE methods. It is intended to serve as performance engine that could be useful for detail assessment of the facilities. The second methodology is intended to calibrate the simplified procedures for the beneficial for future building guidelines [215]. In 2005, "a second generation performance-based earthquake engineering (PBEE-2) developed by Pacific Earthquake Engineering Research Centre (PEER)" published a report on "PEER Testbed Study on a Laboratory Building: Exercise Seismic Performance Assessment" [219]. The PEER PBEE methodology was exercised in various structures. The PEER performance-based methodology linked between the analytic stages with hazard analysis, structural analysis, damage probabilities, and loss calculations, which has direct relation with the interest of the stakeholders. The main characteristics of the PBEE approach is the calculation of various performance levels through probabilistic methodology devoid of expert opinion [219]. Bommer and Abrahamson (2006) [220] discusses about the uncertainty related to aleatory variability which is related to ground motion predication equations that has greater influence on evaluated hazards. They concluded that estimating high seismic hazard is due to either complete negligence or artificially reduced the ground-motions variability. The identification and ranking of significant sources of uncertainties and structural components with respect to the seismic demand of RC structural systems was performed by Lee and Mosalam [221]; "accordingly, uncertainties in earthquake intensities, ground motion characteristics, structural response, physical damage, and economic and human losses" were considered. Mitrani-Reiser, *et al.* (2006) [222] developed an analytical procedure to incorporate various uncertainties; such as shaking intensity, facility mechanical properties, and the damage uncertainty and facility unit cost. Porter, *et al.* (2007) [208] utilize PBEE method for developing the fragility curve through which each damage in the form of probability for a building response or other EDP can be calculated, such that it is intended to the design professionals who uses PBEE methodology. Rojas, *et al.* (2011) [223] utilize the PEER framework to develop algorithm for "optimized and automated design of steel frame" system. Gunay and Mosalam (2013) [224] summarized the "PEER PBEE methodology in a simplified manner", so that it will be easier to adopt by practicing engineers. They concluded that the methodology could be

utilized not only for the design of traditional building types but also applicable for the sustainable and innovative design and also retrofit design as well [224].

Taghavi and Miranda (2003) [211] investigated the non-structural seismic performance, which recorded that the structural costs contribute only 20% of the whole building cost and the rest is spent for the non-structural components and contents. They considers only the direct structural loss and found that all the retrofit measures were suitable, however, only for the short life span of the structures [211]. Aslani and Miranda (2005) [225] develops a methodology for the economic lost estimation probabilistically, and revealed that the non-structural component damages are the primary causes of the losses in the building. The expected annual losses are produced primarily by moderate earthquakes; however, significant losses are produced by high probability of collapse for low deformation capacity structure [225]. The direct approach for estimating benefit-cost analysis for the selected residential buildings was carried out by Erdurmus, S. (2005) [226]. He concluded that in the mitigation activities, the discount rate and time period are related and affects each other. A very high discount rate implies that the mitigation work is only feasible for low service life structures [226]. Tonekaboni, M. (2006) [227] pointed out the limitations of the current retrofit code as the economic criteria is ignored. Hence, he proposed a novel approach for probabilistic cost-benefit analysis considering the seismic hazard and the fragility curve to estimate the economic feasibility index (EFI) for the rehabilitation approach. The economic assessment was also performed after retrofitting pre-code RC building. The paper also concluded that the retrofit method economically applicable for a building may not be applicable for a similar building located in other areas, illustrating that EFI is highly site dependent [227].

Ramirez and Miranda (2009) [228] proposed a simplified lost estimation model based on storey-based to evaluate the seismic performance assessment, an alternative and computationally less expensive compared to the previous PEER approach. This approach was implemented as user-friendly computer tool to estimate economic losses as a metric of structural performance [228]. Padgett, *et al.* (2010) [229] proposed a cost-benefit analysis model for the loss estimation of non-seismically designed bridges, which is located in areas of varying seismicity. They concluded that the expected loss and cost-benefit does not only depend on the location, but also depends on local seismic hazard. The results also concluded that the particular retrofit strategies cannot be expected to be applicable for other cases due to relative damage states based on the location and the nature of seismic hazard [229]. Ramirez, *et al.* (2012) [230] investigated the predictable earthquake damages

and repair costs in code-conforming structures based on the PBEE framework, "which integrates the site-specific seismic hazard, structural response, damage to building components and contents, and the resulting repair cost". They found that for highly seismic site in California, the expected annual loss (EAL) is approximately 1% of the replacement cost of the RC building [230]. The cost-effectiveness of retrofitting of the older concrete buildings can be beneficial, if the cost of retrofit is less than 50% of the replacement cost of the building as concluded by Liel and Deierlein (2012) [231]. Bai, *et al.* (2014) [232] discusses the scenario-based earthquake damage statement considering only the direct losses. The study concluded that for the scenario based earthquake event, large numbers of RC buildings are likely to have heavy damage and many other buildings are expected to complete collapse state [232].

Cardone and Perrone (2017) [233] researches on the damage and loss assessment, and found that the earthquake loss in the Pre-70 RC frame buildings is due to damage and loss of the non-structural components which covers 80% of the loss. Hence, they suggests for the improvement of the fragility curves and loss functions of the infill walls, partition-like components and internal partitions [233]. Dyanati, *et al.* (2017) [234] concluded from the analytical study that the loss associated with the drift sensitive is lower and loss associated with acceleration sensitive is higher attained from the study of 6-storey and 10-storey self-centring concentrically braced frames (SC-CBF). The paper also concluded that SC-CBF is not economically beneficial for tall buildings, as the total expected annual loss (EAL) is higher for 10-storey buildings compared to 6-storey buildings [234]. Dynati, *et al.* (2017) [235] concluded that all the impact considered (i.e. ground motion, the chosen engineering demand parameter formulation, adopted seismic hazard) have significant impact on the building response and expected annual loss, such that it enhances the seismic performance of the building. Furthermore, when two IMs are involved, more accurate performance evaluation can be obtained when using a suite ground motion using vector valued demand models compared to scalar-valued demand models, and joint hazard formulations [235]. Cardone, *et al.* (2017) [236] and Sousa and Monteiro (2018) [237] proposed alternative retrofit strategies for non-structural elements (e.g. infills) to reduce the monetary loss. The time-based assessment approach was proposed for EAL for pre and post rehabilitated RC frame buildings. The paper concluded that the strengthening of the existing infills or their replacement with the new infills are inapplicable (considering an economic view point) for undamaged structures. Furthermore, the break-even time of above 30 years was needed for

the interventions based on the strengthening of masonry infills for this particular case study building [237].

7.3 Overview on Seismic Loss Assessment Framework

A schematic layout of the procedure to obtain the seismic loss through the probabilistic approach as defined by PEER PBEE is illustrated in Figure 7.2, which consists of four steps, such as hazard analysis, structural analysis, damage analysis, and loss analysis. Baker and Cornell (2008) [238] proposed four steps to estimate the life cycle loss estimation similar to the PEER PBEE methodology, considering both model and aleatory uncertainty in each stage of this method. These steps include; (i) "determining earthquake occurrence and intensities (hazard analysis)", (ii) "evaluating the seismic responses of the building" at each intensity measures (structural analysis), (iii) determining various types of damage states (damage analysis), and (iv) loss estimation for associated damages (loss analysis). In the first step, the hazard analysis was estimated, such that the future earthquake occurrence of different hazards based on past earthquake scenario and possible active sources was evaluated at the site of the study area. The potential seismic hazard at a site is identified by the probabilistic seismic hazard analysis and mapping hazard curve. The hazard analysis depends on various factors, such as source-site distance, condition of the site, predication of ground motion and its relationships, faults, their magnitude-frequency, etc. The hazard curve is the graphical representation of the intensity measures (e.g. peak ground acceleration, peak spectral velocity, peak spectral displacement, etc.) and its mean annual frequency of exceedance [220, 238]. The hazard curve can be utilized to predict the potential future earthquakes occurring and to select suites of ground motions at the building site.
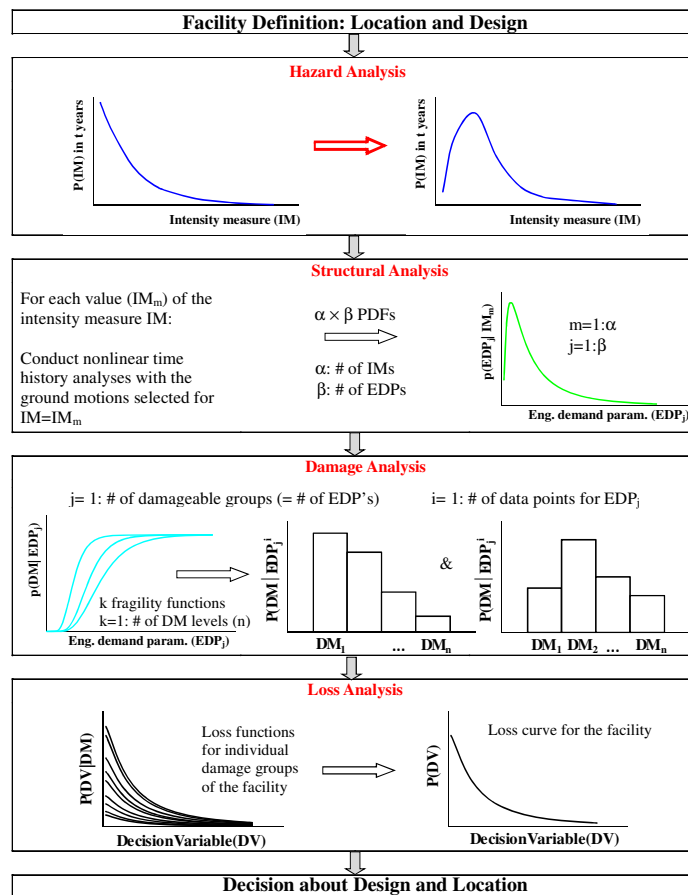
Figure 7.2 – Loss assessment methodology proposed by the PEER PBEE (after Mosalam, 2013 [224])

The present work considered the probabilistic hazard curve developed for Kathmandu, Nepal by Shrestha, S. (2014) [194] for determining the mean annual frequency of exceedance. For this, the author considered ten independent seismic source zones laying in the vicinity which is in reality are active faults. The paper considered Conrell, *et al.* (1968) [239] attenuation relationship to estimate the earthquake ground motion and its probability of exceedance in a given future period of time. The mean annual occurrence rate of earthquake and earthquakes of various magnitude are assumed to be distributed following Gutenberg-Ritcher model [240]. The earthquake temporal occurrence is assumed to be independent with respect to time and space and its occurrence is assumed to follow Poisson's model. The probability of exceedance at least once in 't' year of a certain PGA is defined by the relation as follows [194]:

$$P\ (N \geq 1) = 1 - e^{-\lambda t} \tag{7.1}$$

where: λ is the mean annual frequency of exceedance.

Figure 7.3 presents the hazard curve for the Kathmandu Valley, as developed by Shrestha, S. (2014) [194]. The seismic hazard curve revealed that there is 2% probability of exceeding 0.31g PGA in 50 years which is comparable to the earthquake intensity of VIII. Similarly, in 50 years, an earthquake of PGA 0.18g has 10% probability of exceeding that is similar to earthquake intensity VII. It is also concluded that PGA between 0.5-0.55g has 0.7% probability exceeding in 50 years that is comparable to the earthquake intensity of IX, which is also identical to 1934 AD earthquake in Nepal. The seismic hazard curve is used for the hazard analysis assuming the probability of exceeding PGA level at least once in 1 year, 50 years and 100 years, as illustrated in Figure 7.3 [194].
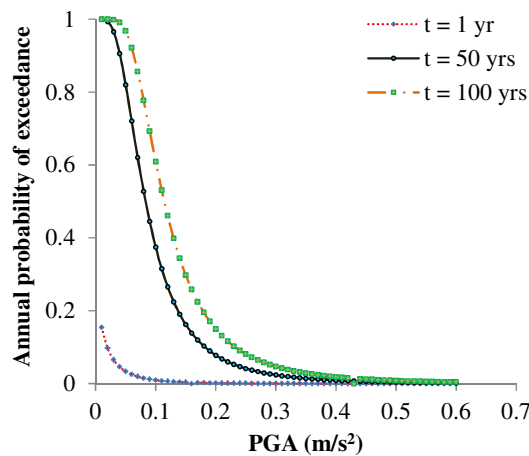
Figure 7.3 – Seismic hazard curve for Kathmandu Valley (Shrestha, 2014) [194]

The second stage of the PEER PBEE framework deals with the structural analysis, where structural response is evaluated with respect to IMs. The present study selected 21 real ground motions and scaled to suitable IMs ranges between 0.1-0.5g at the step interval of 0.1g PGA. Therefore, each case-study building was subjected to approximately 210 nonlinear time history analyses were conducted to the buildings as bi-directional at the support analysed and presented in detail in Chapter 5 and Chapter 6. Uncertainties in material properties and section sizes in the model were calibrated through parametric analysis performed through the variation of relevant properties that has greater influence in the global building frequencies, as discussed in detail in Chapter 5. For each IM, the corresponding building's response is estimated in terms of EDP, as shown in Figure 7.4. The EDP varies for different earthquakes even for same IM. The resulting plot between EDP and corresponding IMs generates the fragility curve, represents the probability of exceeding each damage state corresponding to IMs, as depicted in Figure 7.4. Typically, the maximum inter-storey is used as EDP for the structural elements; whereas, the peak floor acceleration is used as EDP for the non-structural elements [213, 228, 230, 234, 236]. In

addition, in some cases, the peak "inter-storey drift and peak floor acceleration" is used as EDP for the non-structural components [234]. The present study considered absolute maximum inter-storey drift as EDP parameter, neglecting the peak floor acceleration effect of the non-structural elements even though previous studies pointed out its significance in the total loss of the building value.
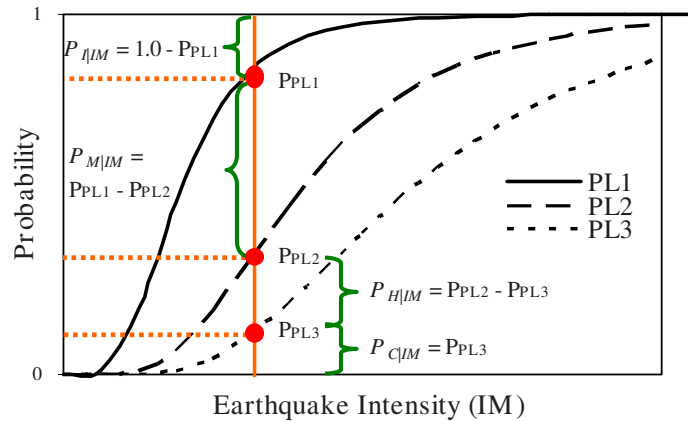
Figure 7.4 – Fragility curve representing the probability of each damage state at respective IMs [241]

The third stage in the PEER PBEE framework is related with the damage analysis of the building. In this stage, fragility functions are used to describe probabilistically the level of damage to the building components defined through damage measures (DM), as a function of the EDP. For each building, the probability of exceeding each damage state is generally calculated as a function of EDP threshold models. As discussed in the previous chapter, six damage states were assumed as proposed by Rossetto, *et al.* (2003) [202], as presented in Table 4.10. This represents the damage states for each building that helps to identify the state of the building and needs of the repair efforts to reinstate to its original undamaged state. The main objective of the damage analysis is the estimation of the damage levels and effort required to repair and maintenance of the structural components in order to restore to its original conditions [242]. Figure 7.5 illustrates the proportion of each damage measure obtained from the fragility curves for each IMs [243].
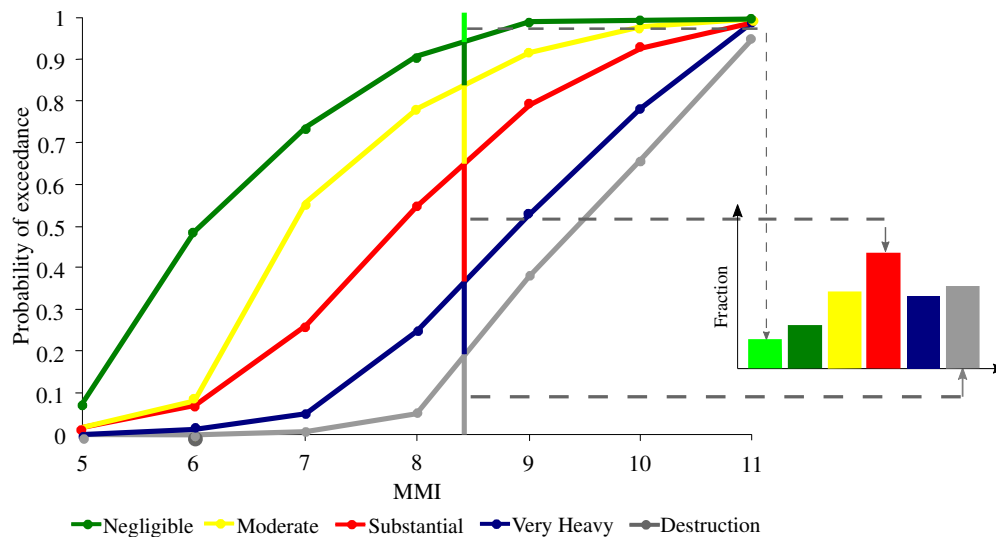
Figure 7.5 – Fragility proportions for each damage state at particular intensity level (Romao, 2014 [243])

ATC-13 [244] defines different mean damage factors for the fraction of injuries and fatalities in case of the existing and rehabilitated buildings, as illustrated in Table 7.1 and Table 7.2, respectively. Both tables define seven damage states, each representing different DMs for the structural and non-structural (mainly infills) elements. The slight damage state represents the limited minor damage, which do not require repair, light damage showing substantial damage with repair not required, moderate state as damage to many components requiring repair, heavy state correspond extensive damage that requires major repairs of the structural and non-structural components, major damage represents the large cracking in the structural elements and complete damage of infills that results either demolish or require huge maintenance, destroyed damage state where either repair is possible or require huge investment, thus total demolition is better option than the repair and maintenance [244]. Mitrani-Reiser, *et al.* (2006) [222] defines three damage states to represent the state of structural elements, such as light, moderate, and severe (or collapse). The damage states define depending upon the need of various retrofit measures, i.e. injection of epoxy, mostly in jacketing retrofit, and in some cases, element replacement, respectively. In addition, for the non-structural elements, such as dry partitions walls, various damage states are defined, such as visible cracking, significant cracking that requires patching, and partition replacement, respectively [222].

Table 7.1 – ATC-13 damage states and corresponding mean damage factors and fraction injured and death for existing building [244]

Damage state	Equivalent damage state	Damage factor (%)	Mean damage factor (%)	Fraction injured		Fraction death
				minor	serious	
None	None	0	0	0.00	0.00	0.00
Slight	Slight	0-1	0.5	0.00003	0.000004	0.000001
Light	Light	1-10	5.5	0.0003	0.00004	0.00001
Moderate	Moderate	10-30	20	0.003	0.0004	0.0001
Heavy	Extensive	30-60	45	0.03	0.004	0.001
Major	Partial collapse	60-100	80	0.30	0.04	0.01
Destroyed	Collapse	100	100	0.40	0.40	0.20

Table 7.2 – ATC-13 Damage states and corresponding mean damage factors and fraction injured and death for rehabilitated building [244]

Damage state	Equivalent damage state	Damage factor (%)	Mean damage factor (%)	Fraction injured		Fraction death
				minor	serious	
None	None	0	0	0.00	0.00	0.00
Slight	Slight	0-1	0.5	0.00000	0.00	0.000000
Light	Light	1-10	5.5	0.00000	0.00	0.000000
Moderate	Moderate	10-30	20	0.00000	0.00	0.000000
Heavy	Extensive	30-60	45	0.00003	0.000004	0.000001
Major	Partial collapse	60-100	80	0.0003	0.00004	0.00001
Destroyed	Collapse	100	100	0.003	0.0004	0.0001

The calculation of the loss analysis is the last step of the PEER PBEE framework, where the damage measures (DMs) are converted to the final decision variables (DVs); such as death, dollars and downtime (the 3 Ds). The most commonly used decision variables are fatalities (number of deaths caused by the damage of building property), economic loss (i.e. the loss associated with the rental income and business income at the time of repair and replacement of the damaged components of the building and in some cases replacement of building), repair duration (time for the duration of maintenance), and injuries (number of injuries to the occupant). In some case, the structural and non-structural elements are grouped as separate damage, which is not practicable, which might result in different DVs although DMs is same [224]. The expected loss is the summation of product of fragility proportion (as defined in Figure 7.5 for each damage state) and the repair cost for each IM.

7.4   Summary on Seismic Life Cycle Cost Formulation

Kang and Wen (2000) [245] proposed a life cycle cost (LCC) model for the building structures considering three parameter functions. These are; (i) cost functions: includes the

initial construction cost, repair and maintenance cost and failure cost of design variables (failure cost includes damage cost, replacement cost of structural and non-structural components, loss of various contents in the building, economic loss, and death and injuries costs), (ii) important system parameters: it includes discount rate, lifetime, occurrence rate and intensity of hazards, and (iii) multiple limit states for severe natural hazards [245]. Dyanati, *et al.* (2017) [234] summarizes the Kang and Wen (2000) [245] approach and proposed simplified approach. They defined the LCC of a building which is the summation of initial construction cost (C_0), "life cycle loss (LCL) of the building, and operation/maintenance costs (C_m) during the life cycle of the building". Mathematically,

$$LCC\,(t, x) = C_0(x) + LCL\,(t, x) + C_m(x) \tag{7.2}$$

where: t = life time of the structure and x = vector of design variables for the structure.

The initial construction cost includes the structural and non-structural elements cost. It can be found from the expert opinion or R.S. Means Square Foot Costs (RS Means, 2013a) [246]. The LCL estimation includes the loss due to structural and non-structural damage to the components during the service life of the building, loss associated with content damage in the building, loss due to relocation, economic loss (i.e. income and business loss during maintenance and replacement period of the building), injury loss, human fatalities loss, and so on. The above defined loss varies from place to place within the country and also varies from country to country. Hence, the LCL calculation is a complex procedure. The loss in the building is uncertain and vague and the cost associated with life of the people is also uncertain which again makes the calculation more complex [234]. Dyanati, *et al.* (2017) [234] utilizes the expected annual loss (EAL) as proposed by Porter, *et al.* (2004) [247] for computing the expected LCL of the building structure as follows:

$$E[LCL(t, x)] = \frac{(1 - e^{-\gamma t})}{\gamma}\,EAL \tag{7.3}$$

where: γ is the constant discount rate per year and t is the expected life of the building. The present value of the future loss is calculated with the use of the discount rate. Assuming the Poisson's distribution of earthquake occurrence, the LCC formulation was implemented to derive the EAL of the building [229, 247, 248]. Mathematically, it can be represented as:

$$EAL = \sum_{j=1}^{k} -\varphi_j \big[\ln(1 - P_{aj}) - \ln(1 - P_{aj+1})\big] \tag{7.4}$$

where: φ_j = cost associated with j^{th} damage state and obtained as the product of each damage factor and their respective replacement cost of the building, as illustrated in Figure

7.6, and k is the number of damage states. Figure 7.6 considered four damage states (DS1 to DS4), i.e. slight, moderate, extensive and complete collapse. It should be noted that the equation (7.4) can be used separately to find each type of loss occurred (i.e. rental loss, structural and non-structural losses, fatalities loss and so on). P_{aj} is the annual probability of exceeding j^{th} damage state, obtained from the seismic hazard curve and fragility curve.
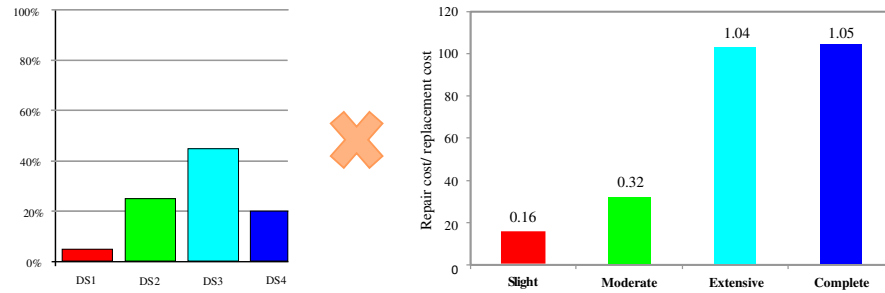
Figure 7.6 – Relationship between cost of each damage state and replacement cost by Romao, *et al.* (2014) [243]

Dyanati, *et al.* (2017) [234] proposed a relationship to compute the annual probability of exceeding damage states, P_{aj} with the help of seismic hazard curve and fragility functions (uses inter-storey drift as EDP for both structural and non-structural elements, and for non-structural elements, EDP is peak floor acceleration). Therefore, P_{aj} can be evaluated as follows:

$$P_{aj} \ = \ \int_{im=0}^{\infty} P(D > C_j | im) \left| \frac{d\lambda_{(im)}}{dim} \right| dim \qquad (7.5)$$

where: D = seismic demand (obtained from EDP model); C_j = capacity of EDP of interest associated with j^{th} damage state; im = intensity measure (IM) of interest; $P(D > C_j | im)$ = seismic fragility function; and $\lambda_{(im)}$ = probability of mean annual frequency of exceeding a given IM obtained from the hazard curve at the site [239]. Mathematically, it can be obtained as follows:

$$\lambda(s) = 1 - \exp[-(im/\mu)^{-k}] \qquad (7.6)$$

where: μ and k are the location and slope of the distribution, respectively.

The risk based LCC of the building is evaluated with the help of more simplified approach proposed by Padgett, *et al.* (2010) [229], which integrates the seismic hazard curve of the site, the structural response, cost associated with each damage, and the cost of each retrofit. The study mainly focuses on the LCC of the bridge; however, the relation can be utilized in the RC frame building as well. The study emphasised on the cost-benefit of seismic retrofit

due to potential cost as a result of damage in the structure without considering maintenance cost. They assumed the earthquake occurrence as a Poisson's distribution, such that the seismic damage to the structural and non-structural elements are estimated as expected life-cycle costs and expressed as follows [229]:

$$E[LCC] = \frac{1}{\alpha T}(1 - e^{-\alpha T})\sum_{j=1}^{4}\left(-C_j\left[\ln(1 - P_{Tfj}) - \ln(1 - P_{Tfi+1})\right]\right) \qquad (7.7)$$

where: α is the discount rate to represent the future cost into present value, which motivates the decision makers the worth of the property in the future, T is the remaining service life of the structure, j is the damage state (in this case four damage states were considered, so j varies from 1 to 4), C_j is the cost corresponding to damage state j, and P_{Tfi} is the T-year probability of exceeding damage state j, and it can be formulated from following relation as:

$$P_{Tfi} = 1 - (1 - P_{Af})^T \qquad (7.8)$$

where: P_{Af} is the annual probability of exceeding j^{th} damage state, which is calculated by integration of the product of fragility functions and hazard curve for each IM.

$$P_{Af} = \int_{im=0}^{\infty} P[DS \geq ds|PGA = im]\left|\frac{dH(im)}{dim}\right|dim \qquad (7.9)$$

where: im represents the intensity measure of the earthquake ground motions suitably scaled to range of IMs. In some cases, lower PGA or IMs up to 0.1g are neglected in the result interpretation assuming the damage in the building initiates after 0.1g. Here, DS represents the demand at each intensity and ds the capacity of the structure (i.e. the threshold for assumed damage state: such as light, slight, extensive and so on). The relation $P[DS \geq ds|PGA = im]$ is the probability of exceeding different damage levels caused by IMs and is obtained from the fragility curve as follows:

$$P[DS \geq ds|PGA = im] = \Phi\left(\frac{\ln(PGA)-\ln(\mu)}{\sigma}\right) \qquad (7.10)$$

where: μ is the mean value obtained from the fragility curve of the system in units of g PGA, σ is the logarithmic standard deviation of the considered system, and $\Phi(.)$ is the standard normal cumulative distribution function of the considered system [229].

Tonekaboni, M. (2006) [227] proposed a new probabilistic based model to compute the "Economic Feasibility Index (EFI)" which is used for the economic assessment of the structures with retrofit method. The method is simple and the calculation steps for EFI are discussed as follows [227].

The first calculation involves the development of the seismic hazard curve for a site, plotted using the return period along the ordinate versus the magnitude of the spectral accelerations at the fundamental structural period $[Sa\,(T1)]$ along the abscissa. The propose considered approximation of hazard curve, "as a linear function on a log-log scale for wide range of intensities" which is demonstrated as follows [249]:

$$\lambda\big(Sa(T1)\big) = k_0[Sa(T1)]^{-k} \tag{7.11}$$

where: $\lambda\big(Sa(T1)\big)$ is the mean annual exceedance frequency of $[Sa\,(T1)]$, and k_0 and k are the parameters defining the shape of the hazard curve. The second step is the development of fragility curves which is similar to the equation (7.10) [227].

The third step involves the calculation of total damage factor (TDF); which is the summation of the product of the probability of damage states and corresponding damage factors. The empirical damage state values in the fragility curve can be obtained as difference between the conditional probabilities of the bounding fragility curve, as demonstrated in Figure 7.4. It represents the fraction of repair cost required to rehabilitate the building [227]. The TDF is given by:

$$TDF\big(Sa(T1)\big) = \sum_i^4 DF_i x P(DS_i|Sa(T1)) \tag{7.12}$$

where: $TDF(Sa(T1))$ is the total damage factor at a given $Sa(T1)$, DF_i is the damage factor that corresponds to i^{th} damage state, and $P(DS_i|Sa(T1))$ is the probability of ith damage state at a given $Sa(T1)$.

The final step is the calculation of "annual loss expectancy (ALE)", which is estimated by the summation of the integration of the TDF with the hazard curve of the site and is computed as follow.

$$ALE = R \int_{Sa(T1)=0}^{\infty} TDF(Sa(T1))\nu(Sa(T1)) \tag{7.13}$$

where: R is the total replacement cost of the building including the demolition cost and $\nu(sa(T1)$ is the average annual frequency and it can be obtained as [227]:

$$\nu(Sa) = -\frac{d\lambda(Sa)}{dSa} \tag{7.14}$$

A more complex expression for computing expected annual loss considering the loss for each building component, PEER frame work implementation was proposed by Ramirez, *et al.* (2009) [230]. The MDLA toolbox is used for the estimation of the loss and the damage

[250]. The expected value of decision variable, $E[DV]$ for a specific IM are expressed as follows [250]:

$$E[DV|IM] = E[DV|NC, IM] . (1 - P[C|IM] + E[DV|C, IM]P[C|IM]E[DV|NC, IM])$$

$$= \sum_{i=1}^{na} \int \sum_{j=1}^{nds_i} E[DV|DM_j]p[DM_j|EDP]p[EDP|IM]dEDP \qquad (7.15)$$

where: DV is the total cost associated with repair and replacement of building components to retain its original state, $E[DV|IM]$ is the expected total repair cost for a specific ground motion IM, na is the total number of damageable assemblies in the building and nds_i is the number of damage states in the ith component. The total repair cost is associated with the damage measure (DM), engineering demand parameter (EDP) and intensity measure (IM), obtained by summation for all damage states over all damageable building elements for each hazard level. It should be noted that for each damage state, given EDP is assumed to be conditionally independent.

After the calculation of expected value of loss for each IM, expected annual loss (EAL) is computed by integrating over the hazard levels to estimate the losses. The EAL for all possible values of ground motion intensities can be obtained as follows (after [230]):

$$\lambda[DV] = EAL = \lambda_0 \int E[DV|IM]p(IM|IM \geq im_0)dIM \qquad (7.16)$$

where: im_0 is the threshold of IM value below which the repair cost are assumed to be zero, λ_0 is the mean annual rate of occurrence with $IM \geq im_0$ obtained from the seismic hazard curve at the building location, and $p(IM|IM \geq im_0)$ is the probability density function of damaging IM values, given the structure experiences a ground motion of $IM \geq im_0$ [250].

7.5   Summary on Risk-based Life-cycle Cost-benefit Analysis

The feasibility of enhancing the seismic response of a structure is calibrated with the help of the cost-benefit analysis. Different type of seismic retrofit strategies: such as steel bracing, concrete or CFRP column jacketing, shear wall, base isolation, etc. can be adopted for the structural element, and disconnection using sliding connections and seismic gap, wire mesh, etc. can be intervened in the infill panels (for the non-structural elements). The suitability of retrofit options varies for each building, thus depending on the cost of each retrofit technique and its cost-benefit attained in the future determines the selection of retrofit methods.

Dyanati, *et al.* (2017) [234] proposed an equation to evaluate the expected economic benefit of retrofit over the existing building, $E[B_R]$ as follows:

$$E[B_R] = E[LCC_E] - E[LCC_R] \qquad (7.17)$$

where: LCC_E and LCC_R are the life cycle cost of the existing and retrofitted buildings, respectively. The initial retrofit cost ($C_{0,R}$) is higher compared to the cost of the building without ($C_{0,E}$); hence, assume $C_{0,R} = a\,C_{0,E}$ (a = coefficient >1). Similarly, assuming maintenance cost for both types remain same, the expected economic benefit equations (7.2) and (7.3) can be modified as follows:

$$E[B_R] = (1-a)C_{0,E} + \frac{1-e^{-\gamma t}}{\gamma}(EAL_E - EAL_R) \qquad (7.18)$$

From the above equation (7.18), initially the expected benefit expected to be negative as the initial cost of retrofit is always higher than without and expected annual loss for both cases are insignificant. Over the time, it can be expected $EAL_E > EAL_R$ as retrofit building shows enhanced seismic performance. The **EAL** for existing and retrofit can be calculated from equation (7.4). The time when $E[B_R] = 0$, i.e. the cost of retrofit and loss incurred after retrofit equals to cost of the building and loss incurred due to seismic action (or in other words the investment is paid back), is called the break-even point or pay-off time and after this point, it can be expected always benefit over the life of the building.

Padgett, *et al.* (2010) [229] derive the equation for finding the benefit of a particular retrofit over the building without, similar to one proposed by Dyanati, *et al.* (2017) [234]. The benefit of adding a particular retrofit in the structure is evaluated as the difference between the expected LCC of the as-built and with retrofit, represented by $LCC_{as\text{-}built}$ and LCC_r, respectively, and mathematically, it is represented as follows.

$$Benefit_r = E[LCC_{as-built}] - E[LCC_r] \qquad (7.19)$$

The value of LCC for as-built and retrofit can be obtained from the equations (7.7) – (7.10). According to authors, the cost benefit ratio (**CBR**) is defined to evaluate the best suitable retrofit techniques. The **CBR** is nothing but the ratio of benefit of retrofit (**Benefit_r**) to the retrofit cost (**Cost_r**):

$$CBR_r = \frac{Benefit_r}{Cost_r} \qquad (7.20)$$

A positive return on the investment is obtained when the **CBR** values are greater than 1, i.e. cost of initial investment is lower than the loss caused otherwise, after certain duration of

the building life. Similarly, a greater value of **CBR** indicates the maximum expected saving, which otherwise would have been loss during the remaining service life of the structure. In certain cases, the ratio of less than one can be achieved, mainly important cultural heritages, which has no monetary comparison [229].

Tonekaboni, M. (2006) [227] uses economic feasibility index (EFI) as a parameter to justify the benefit of seismic retrofit strategy. The **EFI** is the difference of annual loss expectancy between as-built and after retrofit using inflation discount rate as follows:

$$\text{EFI} = \frac{(\text{ALE} - \text{ALE}_R)(1 - e^{-\gamma T})}{\gamma C} \qquad (7.21)$$

where: **ALE** and **ALE_R** are the annual loss expectancy before and after seismic retrofit of the building, which can be obtained from equations (7.11) – (7.14), **T** is the expected remaining life or the investment period, γ is the discount rate, and **C** is the retrofit cost. A positive economic benefit can be achieved for higher value of **EFI** and vice-versa. From the equation (7.21), higher **EFI** can be achieved by increasing the return period of the investment or decreasing the interest rate. In some cases, **EFI** less than 1 indicates the retrofit method is economically non feasible [227].

Sousa and Monteiro (2018) [237] used benefit cost ratio (**BCR**) as a tool for evaluating time in years necessary to reach break-even point. "The **BCR** at the time, **T** (in years) after the initial retrofit investment is calculated by dividing the change in net present value (NPV) of the **EAL** by the total cost of the retrofit". Mathematically,

$$\text{BCR(T)} = \frac{\text{NPV}_{\text{as-built}} - \text{NPV}_{\text{retrofit}}}{C_{\text{retrofit}}} = \frac{\sum_{t=1}^{T} \frac{\text{EAL}_{\text{as-built}}}{(1+\gamma)^t} - \sum_{t=1}^{T} \frac{\text{EAL}_{\text{retrofit}}}{(1+\gamma)^t}}{C_{\text{retrofit}}} \qquad (7.22)$$

where: **EAL_as-built** and **EAL_retrofit** are the expected annual loss before and after retrofit in the building, obtained from equation (7.16).

Cardone, *et al.* (2017) [236] employed net present value (**NPV**) as a cost-benefit tool for evaluating and compare between different retrofit strategies. The expression is given as follows:

$$\text{NPV} = \sum_{t=1}^{T} \frac{\Delta \text{EAL}}{(1+\gamma)^t} - C_{\text{retrofit}} \qquad (7.23)$$

where:

- C_{retrofit} is the initial cost of the retrofit;

- ΔEAL is the difference of the expected annual loss before and after retrofit methods;

- γ is the discount rate;

- T is the remaining life of the building.

If NPV > 0, it signifies the attractiveness of the retrofit strategy as the benefits overtakes the costs. If NPV = 0, represents the break-even point.

FEMA 227 [251] provides three cost-benefit models to justify the economic feasibility of the retrofit for a group of buildings as follows:

- Expected net present value model without the value of life

- Expected net present value model with the value of life

- Benefit/cost ratio

Expected net present value model without the value of life

The expected net present value of the investment on the retrofit can be obtained as the summation of the benefit obtained during the planning period and at the end of the design life of the building (salvage value) and minus the rehabilitation or retrofit cost. Mathematically, it can be expressed as follows [251]:

$$NPV = -INV + \frac{B1}{1+i} + \frac{B2}{(1+i)^2} + \cdots + \frac{B_T}{(1+i)^T} + \frac{V_T}{(1+i)^T} \tag{7.24}$$

where: INV is the initial cost of the retrofit or rehabilitation, B_T is the expected benefit over the planning period, t in year (i.e. $t = 1, 2,\ldots, T$ years), V_T is the salvage value of the building at the end of planning period, T is the expected life or planning period of the building (usually taken as 50 years for new built), and i is the discount rate. FEMA 227 recommends a discount rate between 3-6%, and revealed that if discount rate is increased; it lowers the benefit/cost ratio. Similarly, longer planning period results high present value of benefits; hence, assumed to be 20-30 years for the existing building [251]. If the expected benefit is assumed to be constant over the planning period, equation (7.24) is modified as:

$$NPV = -INV + B_T \left[\frac{1-(1+i)^{-T}}{i} \right] + \frac{V_T}{(1+i)^T} \tag{7.25}$$

Generally, at the end, the salvage value of the investment on the retrofit is a small part of the retrofit cost, thus have non-significant impact on B/C ratio and can be neglected.

The expected annual benefit can be obtained as the sum of expected avoided building component damages (i.e. structural and non-structural damages), rental losses, relocation expenses, personal and proprietor's losses, business inventory losses, and personal property losses [251].

$$B_T = \sum_{m=VI}^{XII} EAE^m \left[\sum_{S=1}^{S} \sum_{f=1}^{F} BD_{sf}^m + RT_{sf}^m + REL_{sf}^m + Y_{sf}^m + INV_{sf}^m + PP_{sf}^m \right] \qquad (7.26)$$

where:

EAE^m = Expected number of Earthquakes Annually by Modified Mercalli Intensity (MMI) ranging from VI-XII;

BD_{sf}^m = Building Damage avoided by Social function and Facility class, and MMI;

RT_{sf}^m = Rental losses avoided by Social function and Facility class, and MMI;

REL_{sf}^m = Relocation losses avoided by Social function and Facility class, and MMI;

Y_{sf}^m = Personal and Proprietors' income loss avoided by Social function and Facility class, and MMI;

INV_{sf}^m = Business Investment losses avoided by Social function and Facility class, and MMI; and

PP_{sf}^m = Personal Property losses avoided by Social function and Facility class, and MMI.

Building damage avoided (BD_{sf}^m) is the product of floor area, replacement value, expected mean damage factor for the facility class and MMI, and the expected effectiveness in reducing building damage is expressed as follows [251].

$$BD_{sf}^m = FA_{sf} RV_{sf} MDF_f^m ERE_f^m \qquad (7.27)$$

where:

FA_{sf} = Floor Area in square foot by social function and facility classes;

RV_{sf} = Building Replacement value per square foot;

MDF_f^m = Mean Damage Function by facility classification and MMI; and

ERE_f^m = Expected Rehabilitation Effectiveness by facility class and MMI.

Rental losses can be obtained as the product of floor area, rental rate, loss of function, and expected rehabilitation effectiveness. It can be expressed as follows:

$$RT_{sf}^m = FA_{sf}RR_{sf}LOF_s^mERE_f^m \tag{7.28}$$

where:

RR_{sf} = Rental Rate per square foot per day by social function and facility classe; and

LOF_s^m = Loss of Function in days by social function and MMI.

Relocation expenses avoided is defined as the product of floor area, relocation cost, loss of function and expected rehabilitation effectiveness. Mathematically;

$$REL_{sf}^m = FA_{sf}RC_sLOF_s^mERE_f^m \tag{7.29}$$

where: RC_s is the relocation costs per square foot per day by social function class.

Income losses avoided are calculated as follows:

$$Y_{sf}^m = FA_{sf}INC_sLOF_s^mERE_f^m \tag{7.30}$$

where:

INC_s = Personal and Proprietors' income generated per square foot per day.

Similarly, business investment losses are defined as:

$$INV_{sf}^m = FA_{sf}SALES_sBI_sMDF_f^mERE_f^m \tag{7.31}$$

where:

$SALES_s$ = Annual gross sales per square foot or production: and

BI_s = Investment as a percent of gross sales or production.

Personal property losses are computed as follows:

$$PP_{sf}^m = FA_{sf}RV_{sf}PPROP_sMDF_f^mERE_f^m \tag{7.32}$$

where: $PPROP_s$ = Personal Property (building contents) as a percentage of building replacement value.

Expected net present value model with the value of life

In this section, the value of life (includes the injury and casualties) due to damages in the structural and non-structural elements in the building is incorporated in the above equations to formulate B/C ratio. The main factor that determines the higher value of B/C ratio is the consideration of the value of life that can be avoided. When the value of life is included, the expected net present value is redefined as follows [251].

$$NPV^{vol} = NPV + VDAT\left[\frac{1-(1+i)^{-T}}{i}\right] \tag{7.33}$$

where:

NPV = Expected Net Present Value excluding the value of life; and

VDAT = Annual Value of Expected Deaths Avoided by rehabilitating buildings to life safety standards.

The annual value of expected death avoided by earthquake loss is assumed as the product of building occupancy times the difference in expected death rates between un-retrofit and retrofit buildings, times the dollar value of human life. It can be mathematically expressed as [251]:

$$VDAT = \sum_{m=VI}^{XII}[(EAE^m)(OCC)(DR^m - DRR^m)](VOL) \tag{7.34}$$

where:

(OCC) = average Occupancy of the building;

DR^m = expected Death Rate by central damage factor, according to ATC-13 [244];

DRR^m = expected Death Rate of Rehabilitated buildings by central damage factor; and

VOL = dollar Value Of one human life.

Ratio of benefit and cost of the retrofit

The benefit/cost (B/C) ratio is an alternative method of comparing and prioritizing the rehabilitation projects. It is simply calculated as the ratio of expected present value of future benefits to the retrofit costs. If B/C is greater than one, it corresponds to positive expected net present value while the B/C ratio less than one corresponds to negative expected net present values. The B/C ratio provides an important guidance for economic justification of various retrofit methods [251]. ATC-13 [244] provides an expert-opinion model to estimate the earthquake damage and corresponding loss for the existing buildings, industrials, hospitals and so on. The procedures followed in FEMA 227 are as follows [244]:

- Identification of most appropriate earthquake shaking characterization for damage and loss estimation.
- Development of facility classification.
- Development of earthquake damage and loss estimate with respect to earthquake shaking characterization selection and facility class identification.

Earthquake shaking characterization

The Modified Mercalli Intensity (MMI) scale (Wood and Newmann, 1931) [252] has been considered as the most appropriate shaking characterization. The upper value of MMI and intensity description is summarized in Table 7.3.

Table 7.3 – Modified Mercalli Intensity (MMI) scale [251]

MMI	Description
VI	Felt by all, many frightened and run outdoors. Some heavy furniture moved a few instances of fallen plaster or damaged chimneys; damage slight.
VII	Everybody runs outdoors. Damage slight to moderate in well-built ordinary structures; some chimneys broken. Noticed by persons driving cars.
VIII	Alarm approaches panic. Damage considerable in ordinary substantial buildings with partial collapse. Fall of chimneys, factory stacks, columns, monuments, walls. Heavy furniture overturned; disturbing to persons driving cars.
IX	Panic general. Damage great in substantial buildings with partial collapse. Well-designed frame structures thrown out of plumb. Buildings shifted off foundations. Ground cracked conspicuously.
X	Some well-built wooden structures destroyed; most masonry and frame structures destroyed. Ground badly cracked. Landslides considerable from river banks and steep slopes.
XI	Few if any masonry structures remain standing. Bridges destroyed. Broad fissures in ground. Earth slumps and land slips in soft ground.
XII	Damage total. Waves seen on ground surface. Lines of sight and level distorted. Objects thrown upward into the air.

Development of facility classification

ATC-13 [244] presented the facility classification into 78 classes, out of which 40 are for buildings. The selected facility classes must have unique seismic performance and facility numbers were assigned for each facility classes. The ATC-13 facility classification for buildings is presented in Table 7.4.

Facility Class	Facility Numbers
Wood Frame (Low Rise)	1
Light Metal (Low Rise)	2
Unreinforced Masonry (Bearing Wall)	
a. Low Rise (1-3 Stories)	75
b. Medium Rise (4-7 Stories)	76
Unreinforced Masonry (with Load Bearing Frame)	
a. Low Rise	78
b. Medium Rise	79
c. High Rise (8+ Stories)	80
Reinforced Concrete Shear Wall ((with Moment-Resisting Frame)	
a. Low Rise	3
b. Medium Rise	4
c. High Rise	5
Reinforced Concrete Shear Wall ((without Moment-Resisting Frame)	
a. Low Rise	6
b. Medium Rise	7
c. High Rise	8
Reinforced Masonry Shear Wall (without Moment-Resisting Frame)	
a. Low Rise	9
b. Medium Rise	10
c. High Rise	11
Reinforced Masonry Shear Wall (with Moment-Resisting Frame)	
a. Low Rise	84
b. Medium Rise	85
c. High Rise	86
Braced Steel Frame	
a. Low Rise	12
b. Medium Rise	13
c. High Rise	14
Moment-Resisting Steel Frame (Perimeter Frame)	
a. Low Rise	15
b. Medium Rise	16
c. High Rise	17
Moment-Resisting Steel Frame (Distributed Frame)	
a. Low Rise	72
b. Medium Rise	73
c. High Rise	74
Moment-Resisting Ductile Concrete Frame (Distributed Frame)	
a. Low Rise	18
b. Medium Rise	19
c. High Rise	20

Table 7.4 – Facility classes and numbers for buildings [251]

Moment-Resisting Non-Ductile Concrete Frame (Distributed Frame)

a. Low Rise	87
b. Medium Rise	88
c. High Rise	89
Precast Concrete (other than Tilt-up)	
a. Low Rise	81
b. Medium Rise	82
c. High Rise	83
Long Span (Low Rise)	91
Tilt-up (Low Rise)	21
Mobile Homes	23

Physical damage caused by ground shaking

ATC-13 [244] developed and proposed a relationship to obtain damage factor, which is expressed as the percentage of dollar loss to the replacement value of the building.

$$\text{Damage factor (DF)} = \frac{\text{Dollar Loss}}{\text{Replacement Value}} \qquad (7.35)$$

Expected damage (in $ Damage) for a given facility is calculated as:

$$\$ \text{ Damage} = \text{DF x (Replacement Value)} \qquad (7.36)$$

The possible cases of damages in the buildings are correlated with the DFs. The central damage factor (CDF) along with the fatalities and injuries for each damage state were defined for built up building and retrofit building are presented in Table 7.1 and Table 7.2, respectively.

7.6 Review on Damage States and Damage Factors Distributions

Cardone and Perrone (2017) [233] derive a fragility function for number of damage states (DSs) to evaluate the state of damage and corresponding loss of typical Italian pre-1970 RC framed buildings using FEMA P-58 [253]. It defines four different damage states to represent fragility functions, i.e. DS1 (light cracking), DS2 (concrete spalling), DS3 (concrete crushing) and DS4 (complete collapse or loss of vertical members). The DS0 (none damage) and DS4 are not considered in the loss assessment as in real practice none damage is difficult to realize and complete collapse repair cost is very high. The detail

description of each damages state and repair techniques for each damage state along with the unit cost in '€' are illustrated in Table 7.5 [233].

Table 7.5 – Damage states of RC components with plain rebars, its repair actions, and corresponding unit cost (Cardone and Perrone 2017) [233]

Damage states	Damage description	Repair actions	Unit costs/m² (in €)
DS1	Light cracking at beam-column joint (< 1-1.5 mm), yielding of beam bars	Clean area adjacent to cracks	6.61
		Prepare cracks to be injected	27.01
		Inject cracks with epoxy resin	156
DS2	Severe cracking (≥ 3-5 mm), wide crack at the interface of beam-column joint. Possible concrete cover spalling	Clean area adjacent to cracks and remove loosened concrete	6.61
		prepare cracks/surface to be injected/patched	27.01
		Inject cracks with epoxy resin	156
		Patch spalled concrete (if any) with mortar mix	88.35
DS3	Spalling of concrete cover, possible crushing of concrete at beam/column-joint interface. Possible buckling of column rebars	Clean area adjacent to cracks and remove damaged and potentially damaged concrete	6.61
		Prepare cracks/surface to be injected/patched	27.01
		Inject cracks with epoxy resin	156
		Replace damaged concrete with rheoplastic concrete mix or high-performance mortar mix	109.26
		Replace distort bars (if any)	50

The feasibility of pre-earthquake strengthening of building was investigated by Kappos and Dimitrakopoulos (2008) [254] defining five damage states (DS1-DS5) and no damage state (DS0). Table 7.6 shows various types of considered damage states, its label, and range of loss index including the central damage factors. The range of loss considered in the paper were similar to the one proposed by ATC-13 [244], slightly different in central damage index assumptions was recorded.

Table 7.6 – Damage states, central loss indices, nomenclature for the used building (Kappos and Dimitrakopoulos 2008) [254]

Damage state	Damage state label	Range of loss index-R/C	Central damage index (%)	Height	Structural system	Seismic code
DS0	None	0	0			
DS1	Slight	0-1	0.5	L-low rise	InfFr-infilled frame	LC-low code
DS2	Moderate	1-10	5	M-Medium	PilFr-pilotis frame	HC-high code
DS3	Substantial to heavy	10-30	20	H-high	PilDu-dual with pilotis	
DS4	Very heavy	30-60	45	e.g. LlnfFrLC: low-rise, infilled frame low-code		
DS5	Collapse	60-100	80	building		

Table 7.1 and Table 7.2 presents various damage states for the existing buildings and corresponding damage factor as proposed by ATC-13 [244], which defines seven damage states that ranges from none damage to complete collapse for the existing and retrofit buildings, including most likely fatalities and injuries for each damage state. Bai, *et al.* (2009) [241] modified the proposed ATC-13, and selected Table 7.1 model in their study for appropriate mapping. Later, they proposed a new relationship between thus defined overall damage states, such as insignificant (I), moderate (M), heavy (H), and complete (C). Table 7.7 present damage states and corresponding ATC-13 damage categories along with central damage factors. The proposed damage states: Insignificant damage matches ATC-13 none and slight damage state, Moderate damage equals to light and moderate, Heavy damage state resembles to extensive and a part of partial damage states. The partial damage state of ATC-13 is broken down into two ranges, i.e. 6a and 6b (to which a linear function was applied) and complete collapse includes ATC-13, part of partial-collapse and collapse [241].

Table 7.7 – Relationship between proposed damage states and ATC-13 damage categories (Bai, *et al.*, 2009) [241]

Proposed damage state	ATC-13 damage category	ATC-13 damage factor range
Insignificant (I)	1,2	0, 0-1
Moderate (M)	3,4	1-10, 10-30
Heavy (H)	5,6a	30-60, 60-80
Complete (C)	6b, 7	80-100, 100

For each damage state, the central damage factor (CDF) for Greek earthquake damage data has been proposed by Eleftheriadou and Karabinis (2011) [255]. The damage data base consists of 180,945 damaged buildings; classified on several earthquake types, such as based on seismic codes, materials, and construction techniques in the Southern Europe. Table 7.8 present a CDF defined for various damage states assuming relationship that "half of the undamaged buildings have a CDF equal to 0.125 and others equal to 0.50". It is stated that the damage states were based on physical damage to the main structural components of the RC buildings [255].

Table 7.8 – Central damage factor for various damage states (Eleftheriadou and Karabinis (2011)) [255]

Damage state		Definition	Central damage factor (%)
None	DS0	No damage	$(0.125+0.5)*N/2$
Green	DS1	Slight damage	0.5
Yellow	DS2	Light-Moderate damage	15
Red	DS3	Extensive damage-Partial collapse	65
Black	DS4	Collapse	100

where: 'N' in the CDF is the percentage of the buildings nearly undamaged

Eleftheriadou and Karabinis (2013) [256] listed the comparison of recorded damage state, where different code comparison was performed in tabular form. The damage factor comparison was performed for VISION 2000 [201], FEMA 273 [200], HAZUS99 [257], EMS98 [258], ATC-13 [244], EPPO (2001 & 2006) [259] and proposed EPPO [256], as shown in Table 7.9, to use for correlation analysis.

Table 7.9 – Comparison between the damage states and damage factors ranges based on previous studies (after Eleftheriadou and Karabinis 2013)

VISION 2000		FEMA 273		HAZUS		EMS98		ATC-13		EPPO (2001 & 2006)		Proposed EPPO	
Damage states (1)	Damage factors (2)	1	2	1	2	1	2	1	2	1	2	1	2
						None (0)							
Fully operational	0-2	Operational	0-1	None	0-2	Grade 1	0-1	Slight	0-1	Slight	0-1	Green	0-1
Operational	2-10	Immediate Occupancy	1-10	Slight	2-10	Grade 2	1-11	Light	1-10	Light	1-10		
Life Safety	10-50	Life safety	10-30	Moderate	10-50	Grade 3	11-50	Moderate	10-30	Moderate	10-30	Yellow	1-30
Near Collapse	50-100	Collapse Prevention	30-100	Extensive	50-100	Grade 4	50-100	Heavy	30-60	Heavy	30-60		
												Red	30-100
						Collapse (100)		Major	60-100	Major	60-100		

7.7 Literature Review on the Summary of the Losses as a Result of Damages in the Building

The direct and indirect economic losses incurred in the building and investment required to return back to its undamaged state is discussed in this section with the help of several literatures. The first major study on damage and loss estimates was performed by Algermissen, *et al.* (1972) [260], considering six scenario earthquakes in the San Francisco bay area (on the San Andreas and Hayward Faults, with magnitude of 8.3, 7.0 and 6.0 on each fault), to estimate the seismic induced losses. The study mainly focuses on the injuries and casualties, but the economic losses were also evaluated mainly for the wood frame structures. Whitman, *et al.* (1973) [261] were the pioneers to introduce the probabilistic loss estimation methods to estimate the seismic loss in the monetary terms. The damage probability matrices were developed for five storeys building, which includes RC moment frames, RC shear walls and steel moment frames. They proposed mean damage ratio for the existing buildings, located at San Francisco Bay area and the Boston area [261]. Park and Ang (1985) [262] proposed an energy based damage index to investigate the damage in the structural elements, whereas inter-storey drift and peak floor accelerations were used to evaluate non-structural damage. Strategies to map these damages to monetary losses developed including a probabilistic approach, but this paper used expert opinion deterministic mapping for the example buildings [262]. Gunturi and Shah (1993) [263] developed a scenario-based loss estimation approach, where the damage to building components were classified as the structural, non-structural and element contents in the building. The structural response was evaluated at each storey level analysed from the nonlinear time history analyses by suitably scaling the records to PGA 0.4g, 0.5g and 0.6g. The damages for each components and losses were calculated per storey, later summed to obtain the total building loss [263].

A component-based approach was proposed by Aslani and Miranda (2005) [225] to estimate the effect of the building collapse in terms of monetary loss and estimate the probability of collapse for increasing IMs. Zareian and Krawinkler (2006) [264] included the building-specific economic losses in a simplified version of PEER's performance-based design framework. The monetary loss was computed by grouping the components of the building into subsystem (either at the storey level or the building level) instead of losses per component, such that the components belonging to the same subsystem can be represented by a single structural response parameter. The main limitation of this approach

is the assumptions about the relationships between structural response and economic loss in order to evaluate the performance due to limited damage estimation and loss of data at the time the research was published [264]. Mitrani-Reiser, J. (2007) [265] considers four decision variables: direct and indirect losses associated in the building to evaluate probabilistically its seismic performance. The direct losses are related to the repair costs for the earthquake-induced damages in the building. Similarly, indirect losses are associated with the economic loss due to business interpretation, delayed in repair time, building safety and corresponding downtime, i.e. safety tagging (investigated buildings are assigned safety tags, such as green, yellow and red representing the severity of building state), and life safety, which is related with the number of injuries and fatalities caused by the state of the building after seismic excitation [265]. Mitrani-Reiser, J. (2007) [250] also suggested the increase in the EAL by 30% due to downtime for the code-conforming RC moment frame structures. Dyanati, *et al.* (2017) [234] considered seven type of losses associated with the building, which includes both structural and non-structural damages. It includes: L_1 – loss associated to the structural damage, i.e. includes the cost related to the repair and replacement cost of the building; L_2 – repair and replacement cost related to the non-structural damages (i.e. drift and acceleration sensitive components); L_3 – cost associated with the replacement of damaged elements; L_4 – cost related to the relocation due to damaged building; L_5 – loss of income during the repair and replacement; L_6 – loss caused by injury to the occupants and L_7 – loss associated with the human fatalities of the building occupants [234].

FEMA 227 [251] utilizes the five losses used as the secondary data entry screens for the computations of B/C ratio. It includes: i. Scenario damages and economic losses; ii. Expected annual damages and economic losses; iii. Expected annual damages and economic losses avoided; iv. Total benefit and costs and v. Expected death losses. The scenario damages and economic losses are the expected damages and losses per earthquake with intensity varying from VI to XII of MMI. It includes expected building damages, rental losses, other income losses, relocation costs, business inventory losses, personal property losses and total scenario losses. The expected annual damages and losses due to all expected earthquakes events, considering the probability of earthquakes of various MMIs. It represents the best estimate of future economic impacts, which would have occurred in the building without rehabilitation. The expected damages and economic losses avoided includes the loss that can be avoided by retrofit program and help to estimate the

effectiveness of the retrofit program and annual economic benefit that can be achieved after the strengthening program. The total expected benefit and cost includes the estimation of B/C with and without the value of life, ultimately indicates the significance of including the value of life in the economic analysis of the particular buildings and occupancies under consideration. The last loss estimate is the death losses, which evaluates the expected average annual fatalities due to the building remaining in weak state and the expected annual deaths avoided by considering the seismic rehabilitation program.

Hazus MH, 2003 [266] integrated in GIS platform to estimates the possible losses in the building related to the earthquake and other natural phenomenon. The software discretizes the losses in the building into three, such as societal losses, economic losses and indirect economic losses.

7.8   Application to the Case Studies

From the previous presented cases studies, four strengthened buildings were selected (two with non-engineered and two with pre-engineered design approaches), analysed and discussed in detail in Chapter 6. This Chapter is mainly focused on the economic feasibility assessment of the adopted retrofit measures evaluated through EAL, LCL, and cost-benefit analysis. The most suitable and feasible retrofit methods for each building was evaluated through loss assessment. The procedures followed for the calculation of cost-benefit ratio in the present study are as follows:

1. Selection of case study buildings, retrofit strategies, and numerical modelling

2. Probabilistic assessment of fragility curves for selected buildings

3. Selection of hazard curve for a site

4. Define expected life time of retrofit structure and discount rate

5. Calculate the probability of exceeding each damage state

6. Cost estimates

7. Evaluate expected annual loss (EAL) and life cycle loss (LCL)

8. Calculate and compare cost-benefit ratio (CBR) for design period and perform sensitivity analysis

7.8.1 Selection of the case study buildings

A detail description of the case study buildings have been presented in Chapter 3 and its seismic performance was analysed and presented in Chapter 5. Furthermore, the enhanced seismic performance after introducing the retrofit measures was analysed and discussed in Chapter 6. Therefore, the present section intends to provide only a brief introduction of the selected buildings. The four case study buildings selected for the cost benefit analysis represents pre-code (i.e. CCP1 and CCP2) and MRT buildings (i.e. MRT1 and MRT2) [20]. Thus, selected buildings were classified to each building class based on the section of the beam, column, and reinforcement details on the structural elements. The various in-situ tests conducted at the site, geometrical layout description, and structural section sizes and reinforcement details were discussed in detail in Chapter 3. The MRT1 is a bare frame building that was later modified with various arrangements of infill walls which concluded that the soft-storey effect at the ground floor was the most vulnerable building type and also a representative building of the one commonly practiced at the site. The three retrofit measures introduced in the existing case study buildings that represent a commonly practiced, includes concrete column jacketing, steel bracing, and RC shear wall. The numbers, orientations, reinforcement details and number of storeys required to retrofit depends on the building response (inter-storey drift) under seismic excitations and desired performance level. In addition, the structural sections, reinforcement details and thickness should meet the rehabilitation guidelines. Also the detail retrofit modelling approached using SeismoStruct software [22] was also discussed in detail in Chapter 4 and Chapter 6.

The dynamic response of the case-study buildings were evaluated through dynamic time history analyses subjected by 21 real ground motion records having response spectra similar to the site, seismic zone-V and medium soil condition [30], also presented and discussed in detail in Chapter 5 and Chapter 6. The present study adopted maximum inter-storey drift as EDP the building response needed for the probabilistic model.

7.8.2 Probabilistic assessment of fragility curves for each selected buildings

The fragility curves provide general information about the probability of exceeding particular damage states with respect to the defined IM. Six damage states were selected; such as slight, light, moderate, extensive, partial-collapse and collapse with respect to the threshold inter-storey drift, as proposed by Rossetto, *et al.* (2003) [202] presented in Table

4.10. As stated above, the building responses in term of inter-storey drift as EDP were considered with respect to IMs obtained from the non-linear time history analyses and the structural performance was evaluated for the as-built and retrofitted buildings. This was later utilized to develop the probabilistic seismic EDP models, which was further protracted to compute the probability of exceeding damage states. The fragility curve for the as-built buildings were presented and discussed in detail in Chapter 5. In addition, the retrofit measures and improvement in the fragility curves obtained were presented in Chapter 6.

7.8.3   Selection of hazard curve for a site

The cost effectiveness and life cycle loss (LCL) of the retrofit strategies was evaluated for the four case study buildings based on the equation (7.3). The hazard curve illustrates seismic intensity parameter along the abscissa and its annual probability of exceedance along the ordinate. The hazard curve revealed the information of frequent occurrence of small or moderate magnitude earthquakes and only occasional occurrence of large magnitude or disastrous earthquakes. In other words, the annual probability of exceedance of small IMs earthquake is frequent, whereas the annual probability of exceedance of large IM earthquake is occasional. The mapping of hazard curve for the site was beyond the scope of the present study, thus it was utilized the hazard curve developed by Shrestha, S. (2014) [194], as shown in Figure 7.3. The hazard curve was developed for Kathmandu Valley considering 10 independent seismic source zones in the vicinity of the area. The study presented three curves indicating the annual probability of exceeding range of PGA levels at least once in 1 year, 50 years and 100 years [194]. The present study considered a hazard curve having annual probability of exceedance PGA at least once in 50 years for further investigation on the cost-benefit analysis and LCC.

7.8.4   Define the expected life time of retrofitted structures and discount rate

The expected service life of the RC buildings varies for different class of the buildings, as discussed in the literature above. Therefore, the present study assumed the service life of the retrofit structures as 25 years as the case-study buildings were over 20 years by the time of the study; such that the time horizon for the concrete material could be assumed approximately 50 years [251]. Similarly, the interest rate has greater impact on the cost-benefit estimation, i.e. higher discount rate lowers the cost/benefit ratio and vice-versa.

FEMA 227 [251] recommends a discount rate of 3-6% and other literatures also presented their researches considering lower discount rate. According to the statistical data since 1964 until 2018 AD, the inflation rate in Nepal averaged 8.26 percent [267]. In addition, the commercial and development banks in Nepal are providing higher interest rate of more than 10% on fixed deposit, if deposited a minimum of three months [268]. These obliged the present study to consider a discount rate of 10% p.a. as a reference aligned with the current market rate and inflation trend. In order to validate the cost-benefit evaluation works and provide a greater assurance to the investors and owners, the present study also performed cost-benefit sensitivity analysis varying the discount rate such that the service life of the retrofit structure remains constant and vice-versa. Finally, the cost-benefit ratio for different retrofit techniques were compared, results verified and a clearer picture of the need of retrofit was ensured for the stakeholders, client, owner and concerned parties.

7.8.5 Calculate the probability of exceeding each damage state

The annual probability of exceeding a particular damage state was evaluated from equation (7.9), in which the fragility curves and seismic hazard curve were multiplied for each IM. The fragility curves were considered until 0.5g PGA, which represents 0.7% annual rate of exceeding in 50 years (probably occur once in a century in Kathmandu) [194]. Assuming the service life of the retrofitted buildings as 25 years, the T-year probability of exceeding particular damage states was obtained from equation (7.8).

7.8.6 Cost estimates

The cost of each building was estimated with the help of present unit cost of the building materials, skilled and unskilled labour costs, formworks, finishing works, and other material costs. The price of the materials differs from one district to other (for example, the price of labour in Kathmandu was different than in other places of Nepal). Therefore, the price considered for the detail estimations was based on the local market price of Bhaktapur in 2017/18. The whole sum rate for the as-built building was considered approximately 215 dollar per square metre (i.e. $ 215/m²). It includes 5% fees for sanitary works, electrical works, consultancy, and contingency fees. The total construction cost of the building was estimated by multiplying total built-up area (in m²) times cost per m² rate. The replacement cost is the sum of construction cost and demolition cost (includes the cost for demolish,

cost for clearing the site, and so on). Here, the demolition cost was assumed as 10% of the construction cost.

The detail structural analysis was performed for the super-structure, thus in the present study, the retrofit cost estimation was only carried out for super-structures assuming similar retrofit costs for the sub-structures. The estimated retrofit cost for the RC jacketing was approximately $ 560 per column, which includes materials, labours, technical, and other needed equipment charges. Similarly, the cost of steel bracing element was estimated approximately $ 1.5/kg including all extra charges. Furthermore, the estimated cost for the RC shear wall was approximately $ 200/m^2, including all material costs, labour costs and other technical and equipment charges. The estimated replacement and retrofit costs for the entire case study buildings are presented in Table 7.10. For each case study building, the projected retrofit cost was less than 40% of the building replacement cost presented in Table 7.10, thus it signifies economic feasibility of the proposed retrofit techniques [231]. The above statement will be verified through the cost-benefit ratio analysis, which will be discussed in the following sections.

Table 7.10 – Building replacement cost, retrofit cost, and % of replacement cost for four case study buildings

Building Type	Replacement cost ($)	Retrofit cost (in $)			% of replacement cost		
		Jacketing	Bracing	Shear wall	Jacketing	Bracing	Shear wall
CCP1	49,974	17,003	20,632	10,140	34.02	41.29	20.29
CCP2	59,980	17,710	17,695	12,215	29.53	29.50	20.37
MRT1	60,035	19,840	20,495	16,394	33.05	34.14	27.31
MRT2	156,450	36,132	39,315	27,460	23.09	25.13	17.55

The central damage factor (CDF) for each damage state was considered from ATC–13 [244], as shown in Table 7.1 and Table 7.2 for the as-built and retrofitted buildings, respectively. The replacement cost for each building type is illustrated in Table 7.10, based on local cost at the site. Similarly, Table 7.11 presents the loss incurred in each building with respect to each damage state as a fraction of replacement cost. It should be noted that the present study estimate the loss that was related to direct loss to the structural elements in the building without considering the losses of the non-structural elements although previous studies concluded that the major portion of the monetary loss was due to non-structural damages in the building, is mainly due to time limitations [234, 236, 237].

Table 7.11 – Central damage factor from ATC–13 [244] and loss of each damage state

Damage states	Central damage factor	Loss for each damage state ($)			
		CCP1	CCP2	MRT1	MRT2
None	0	0.00	0.00	0.00	0.00
Slight (S)	0.5	249.87	299.89	300.17	782.23
light (L)	5.5	2748.55	3298.78	3301.84	8604.57
moderate (M)	20	9994.71	11995.56	12006.68	31289.36
extensive (E)	45	22488.11	26990.01	27015.02	70401.06
Partial-collapse (PC)	80	39978.86	47982.25	48026.70	125157.44
Collapse (C)	100	49974.00	59980.00	60035.00	156450.00

7.8.7   Evaluate expected annual loss (EAL) and life cycle loss (LCL)

The expected annual loss for each building type with and without retrofit measures was evaluated using the equation (7.4). The T-year probability of exceeding each damage state was assumed to be lognormally distributed. For each intensity level of the parameter representing the hazard, fragility proportions for each damage state were extracted, as illustrated in Figure 7.5. The EAL was evaluated as a sum of the product of loss for each damage state (presented in Table 7.11) and corresponding lognormal T-year probability of exceeding each damage state for PGA that varies from 0.1g to 0.5g, obtained by substituting in equation (7.4).

Figure 7.7 presents the EAL comparing the losses for each damage state between the as-built and the retrofitted buildings. All the case study building results revealed that the EAL with respect to damage states are significantly reduced considering the retrofit techniques. Figure 7.7 (a) presents the EAL plot for the CCP1 building, where only minor loss (possibly negligible loss) was observed for slight damage. It can be also observed that the EAL for the RC shear wall and concrete jacketing was significantly higher than the as-built building in case of light and moderate damage states, respectively. Whereas, for higher damage states (from E to C), the as-built building exhibits much higher EAL in comparison with retrofitted buildings, thus signifying that a considerable improvement can be attained in reducing unexpected structural losses in the as-built CCP1 building. Figure 7.7 (b) illustrates the EAL plot for the CCP2 building with and without retrofit techniques. It reveals that the maximum losses for all damage states were observed in case of the as-built building compared to the retrofitted buildings. In addition, the maximum loss occurs in the moderate damage state, followed by collapse and extensive damage states. The EAL for moderate damage state was compared between the as-built and the retrofitted CCP2

building. Similar to CCP1 and CCP2 buildings, the EAL in the MRT1 building was reduced in the retrofitted buildings, which prevents the structural losses in the as-built building represented in Figure 7.7 (c). In addition, insignificant losses were observed for slight and light damage states in case of the as-built building, and maximum loss corresponding to higher damage states. The maximum EAL can be observed for moderate damage state, and followed by extensive, collapse and partial collapse damage states for the as-built MRT1 building. Finally, the EAL for the as-built MRT2 building depicts higher losses for light, moderate and collapse states in comparison to retrofit MRT2 building, as presented in Figure 7.7 (d).

Summarizing all the above results, it can be concluded that the structural losses can be significantly reduced with the application of retrofitting techniques in existing buildings.
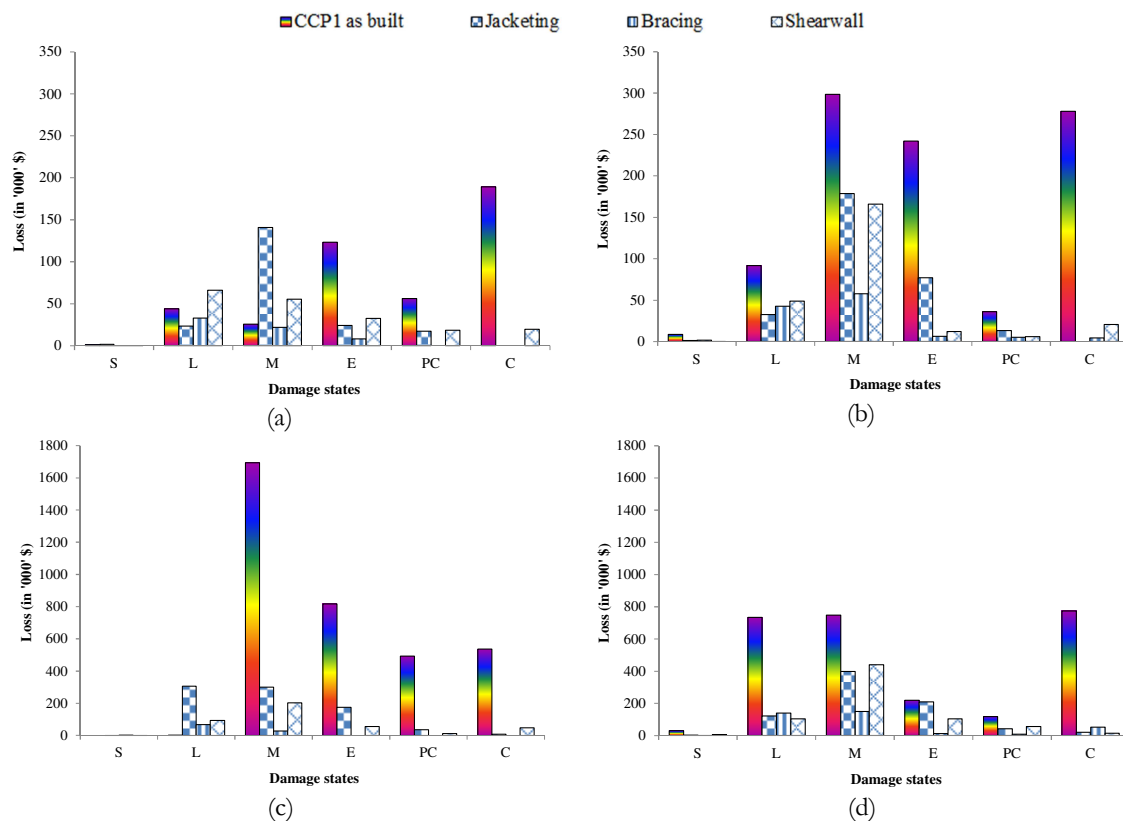
Figure 7.7 – EAL for assumed damage states for the as-built and retrofit models during the service life of the buildings; (a) CCP1, (b) CCP2, (c) MRT1 and (d) MRT2

The discrete and cumulative distribution of EAL as a function of IMs was also investigated for all case study buildings with and without retrofit measures. Figure 7.8 presents the discrete and cumulative distribution trends of EAL with respect to IMs, where the left vertical column represents the discrete distribution and right vertical column characterizes the cumulative distribution. The entire discrete plots illustrate that the maximum EAL

occurs at lower PGA; i.e. ensues between 0.1-0.2g for as-built CCP1 and CCP2 buildings, whereas in case of as-built MRT1 and MRT2 buildings, it arises below 0.1g PGA. Similar trend of the EAL distribution can be detected for retrofitted buildings as well, but the incurred loss can be extremely reduced so that the highest reduction was obtained in the MRT1 building. These results shows that frequent earthquakes of low to medium magnitude have larger influence on the losses when compared with rare earthquakes of larger magnitude, also aligned with the conclusion of Aslani and Miranda (2005) [225]. In particular, the discrete distribution of EAL for the CCP1 building with shear wall demonstrates slightly higher loss below 0.1g PGA compared to as-built building. This is aligned with the above discussions that the CCP1 building with shear wall has higher EAL than as-built building for light damage state. The results demonstrated that the maximum EAL was recorded in case of the as-built MRT1 building, and followed by MRT2, CCP2, and CCP1 buildings, respectively. In addition, the retrofit measures in the MRT2 building shifts the maximum EAL between 0.1-0.2g, which initially falls at 0.1g PGA.

The cumulative distribution of losses demonstrated that an increase in the EAL was observed for a slight increase in PGA, i.e. from 0.1g to 0.2g, which was valid for all case study buildings with and without retrofit techniques. The extreme increase in cumulative loss was recorded in the MRT1 and CCP2 buildings, where extensive and moderate damage states are highly dominant. A slight increase in the EAL continues until 0.4g PGA for the CCP1 and CCP2 buildings; whereas, it continues until 0.3g for the MRT buildings. The EAL becomes more uniform beyond 0.3g PGA. The application of retrofit measures significantly reduces the cumulative EAL; and a greater reduction can be achieved with the steel braced retrofitting solutions, followed by jacketing, and shear wall, respectively, and valid for all studied buildings. The retrofit measures minimized the maximum EAL for the CCP1, CCP2, MRT1 and MRT2 buildings by 2-7, 3-11, 7-50, and 3-7 times, respectively, compared to the as-built buildings. This concludes that the proposed retrofit techniques are highly feasible in the existing buildings, and observed EAL also signifies the prior need of strengthening.
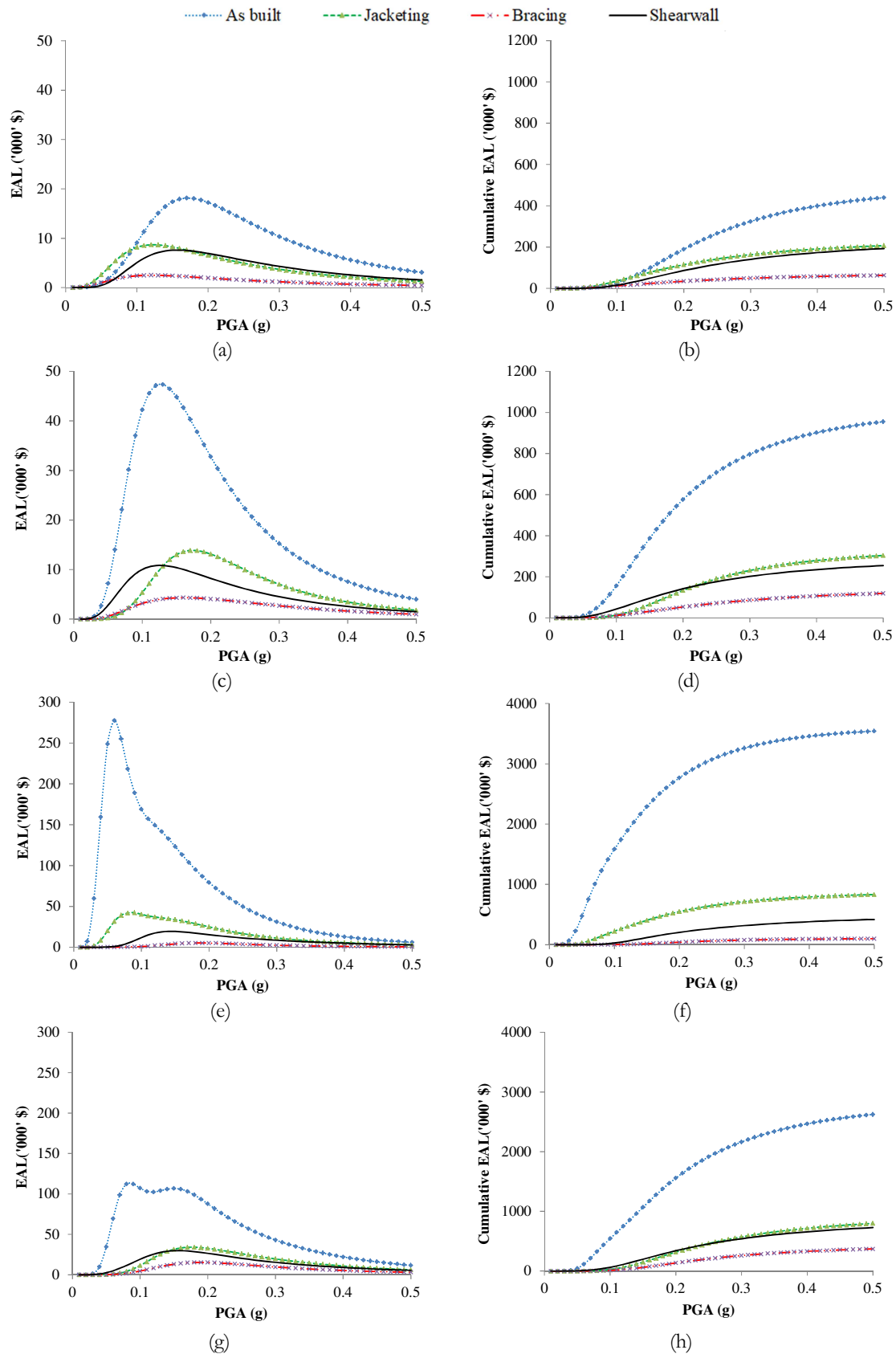
Figure 7.8 – Comparison expected annual loss (EAL); left column represents discrete distribution and right column cumulative distribution: (a) and (b) – CCP1, (c) and (d) – CCP2, (e) and (f) – MRT1, and (g) and (h) – MRT2

Figure 7.9 presents the risk curve for the case study buildings, plotted annual probability of exceedance and LCL (shown in $ value). The LCL was calculated with equation (7.3), assuming that the expected life of the retrofitted buildings as 25 years and a discount rate of 10% p.a. Each plot provides information about the LCL for as-built building and the amount of LCL that can be minimized using retrofit techniques during the expected service life of the building. As stated above, the study does not include the loss due to human injuries and fatalities. For all case study buildings, the maximum LCL was recorded for the lower annual probability of exceedance, and it decreases exponentially for the increase in annual probability of exceedance. This concludes that the maximum LCL was due to the occasional earthquakes of larger magnitude that is expected to occur once in the life time of the structures, whereas the minimum LCL was recorded for the frequent earthquakes of low to medium earthquakes. The maximum LCL was observed in the as-built MRT1 building, and followed by the MRT2, CCP2, and CCP1 buildings, respectively. In addition, it can be recorded that all retrofit techniques minimize the LCL to satisfactory lower values in all case study buildings. The most suitability of the retrofit techniques can be detected through the MRT1 building, where the LCL was reduced by almost 4 times than the as-built building. Furthermore, the steel bracing retrofit reduces the LCL to minimum values as compared to other techniques and is valid for all selected buildings.

The maximum LCL for the as-built CCP1 building with 0.4% annual probability of exceedance in 50 years was approximately $ 450,000, many folds higher compared to corresponding replacement cost. Similarly, the maximum LCL for the as-built CCP2, MRT1, and MRT2 building corresponding to 0.4% annual probability of exceedance in 50 years was approximately $ 950,000, $ 3,600,000, and $ 2,600,000, respectively. The retrofit measures expected to reduce the LCL below $ 55,000$, $ 115,000, $ 80,000, and $ 340,000 for the CCP1, CCP2, MRT1, and MRT2 buildings, respectively. This concludes that the LCL for the as-built buildings during the expected service life of the structure and considered discount rate was many folds higher than replacement cost, and can be reduced drastically to minimum value with the intervention of retrofit measures.
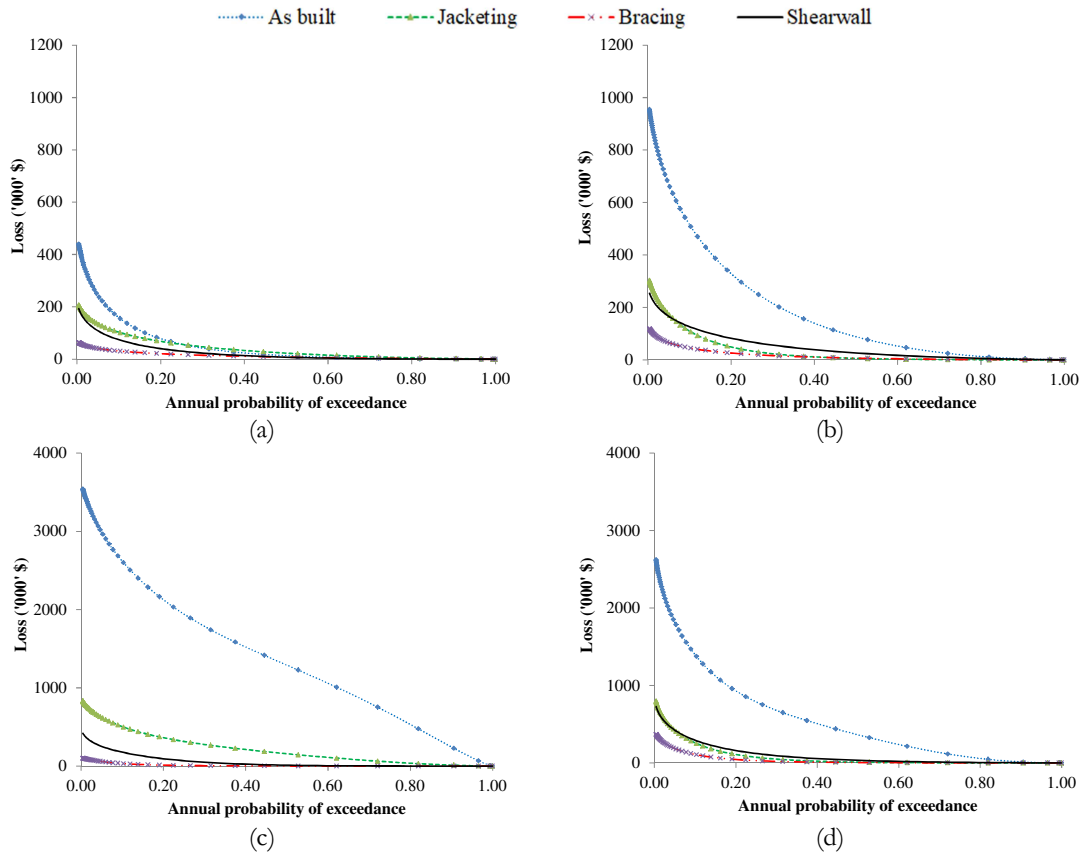
Figure 7.9 – Risk curve for the case study buildings; (a) CCP1, (b) CCP2, (c) MRT1 and (d) MRT2

7.8.8 Cost-benefit ratio

The economic feasibility of the retrofit techniques adopted was investigated with the help of cost-benefit analysis using the equation (7.20). The adopted retrofit measures are beneficial if $EAL_r < EAL_{as\text{-}built}$, as discussed in the previous section. Initially, the obtained the cost-benefit ratio (CBR) was less than one, is mainly due to the cost of retrofit was higher than the benefit attained from retrofitted buildings. With time the LCL for the as-built building increases than retrofitted building and positive return on investment can be expected. The time in year when Benefit_r becomes zero is called the break-even point or pay-off time and after this point, it can be expected to have benefits over the life of the building. A CBR value greater than one indicates a positive return in investment, which otherwise would have been loss during the service life of the structure. When a discount rate of 10% p.a. and service life of the structures was considered as 25 years from the time of retrofit, the CBR (obtained from equation (7.20)) for the CCP1 building with retrofit strategies, i.e. jacketing, steel bracing, and RC shear wall was approximately 1.37, 1.8, and 2.43, respectively. Similarly, the recorded CBR values for the CCP2 building with jacketing,

bracing and shear wall corresponds 3.7, 4.7, and 5.7, respectively. In addition, the CBR values attained for the MRT1 building was 13.65, 16.8, and 19, respectively; and for the MRT2 building, it corresponds 5.05, 5.73, and 6.9, respectively. Therefore, based on the obtained CBR values, it can be concluded that for all the studied buildings, the use of RC shear wall as a retrofitting solution is the more economically beneficial, followed by steel bracing and concrete jacketing.

7.8.9   Sensitivity Analysis

The economic feasibility of each retrofit measures were investigated based on the CBR values considering the expected life of the structures as 25 years and discount rate as 10% p.a.. The present section intend to study the influence of the variation of CBR values due to the modification in the service life of the structure (varies from 0 to 50 years), such that the discount rate (assumed as 10% p.a.) remains constant and vice versa. The previous studies concluded that a higher CBR can be achieved by increasing the service life of the structure or decreasing the interest rate [234].

Figure 7.10 presents the variation of CBR values with respect to the increase in service life of the structure, such that discount rate remains constant. The horizontal line in the plot indicates as datum (i.e. CBR=1), the boundary below which it is expected that the retrofit measures are not feasible, and above illustrates economically viable. Initially for few years, all retrofit methods demonstrated lower CBR, i.e. CBR<1, as expected, illustrating that the initial cost of the retrofit dominates over the benefit. However, the EAL for as-built building recorded higher than retrofit cost over time, such that benefit can be attained after certain duration of time. Figure 7.10 (a) depicts the sensitivity plot for the retrofitted CCP1 building. The plot shows that higher CBR values (i.e. CBR>1) was obtained for the CCP1 building with jacketing, steel bracing, and RC shear wall after 19 years (CBR=1.04), 14 years (CBR=1.02), and 11 years (CBR=1.07), respectively. This concludes that the CBR>1 can be achieved prior for building with RC shear wall, thus can be concluded that it is economically more beneficial retrofit measure for this particular CCP1 building. Figure 7.10 (b) presents the sensitivity plot for the CCP2 building, demonstrating early benefits could be achieved than in case of the CCP1 building. The CBR>1 can be achieved for the CCP2 building with jacketing, steel bracing and RC shear wall after 7 years (CBR=1.03), 6 years (CBR=1.13), and 5 years (CBR=1.15), respectively. This concludes that early benefit

attained with RC shear wall, i.e. shear wall provides prior return on the investments relatively compared with other retrofit measures for this particular CCP2 building.

Figure 7.10 (c) illustrates the sensitivity plot for the MRT1 building, where CBR>1 was attained in less time in years than initially expected. This is potentially due to high tendency of unexpected losses in the as-built MRT1 building, which was minimized largely using the retrofit techniques. The results for MRT1 building with jacketing, bracing, and shear wall recorded CBR>1 after 2 years (CBR=1.1), 2 years (CBR=1.36), and 2 years (CBR=1.54), respectively. This reveals that the existing MRT1 building is highly vulnerable and total collapse of the building was expected for low to medium earthquakes, thus the retrofit measures intervention are essential for this building. Although all the retrofit techniques demonstrate positive CBR in similar years, shear wall was preferred to be much more economically viable option since higher CBR value was recorded, and followed by steel bracing and jacketing, respectively. Finally, the sensitivity plot for the MRT2 building is shown in Figure 7.10 (d), where early return on investment was obtained than initially predicted. The CBR>1 for the MRT2 building with jacketing, steel bracing, and shear wall was attained after 5 years (CBR=1.01), 5 years (CBR=1.15), and 4 years (CBR=1.1), respectively. Similar to other selected buildings, it was found that the RC shear wall as the most economically beneficial and viable retrofit technique for this particular MRT2 building, followed by steel bracing and jacketing, respectively.
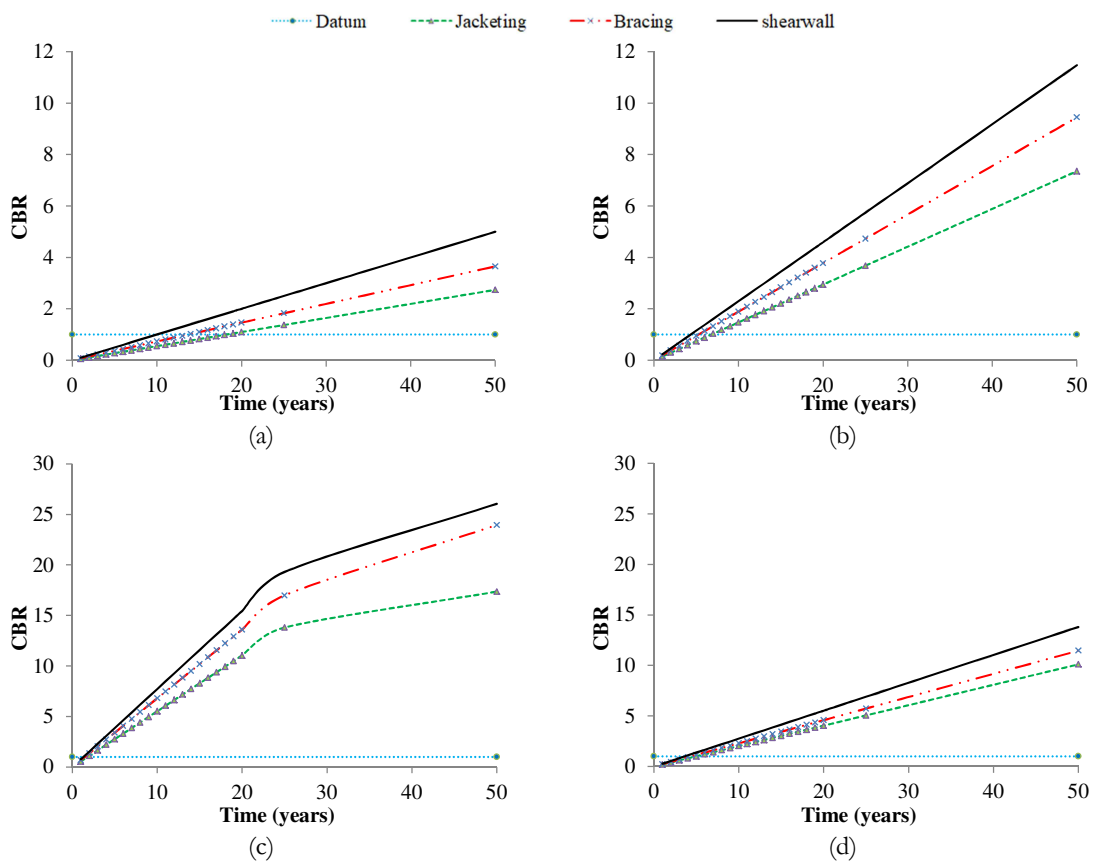
Figure 7.10 – Cost-benefit ratio for the case study buildings with different retrofit strategies showing the variation with service life assuming constant discount rate; (a) CCP1, (b) CCP2, (c) MRT1 and (d) MRT2

The sensitivity analysis was also carried out through the variation of discount rates to investigate its influence in the modification in the CBR values for the selected buildings. Figure 7.11 presents the sensitivity plots for the CCP1, CCP2, MRT1 and MRT2 buildings, where higher CBR values were recorded for lower discount rate and vice-versa, such that the service life of the retrofitted buildings, i.e. 25 years remain constant. The CBR value greater than 1 can be achieved for selected building even a maximum discount rate of 15% p.a. was selected. The sensitivity plot for the CCP1 building with and without retrofit measures is presented in Figure 7.11 (a). The lower the discount rate, higher the CBR value was achieved also aligned with the conclusion drawn by Dyanati, *et al.* (2017) [234]. The variation of CBR values for the CCP1 building retrofitted with jacketing, steel bracing, and shear wall, respectively, considering 1% discount rate was 13.68, 18.24, and 24.34, respectively. This result also aligned the above finding that the RC shear wall could be much more economically feasible option for the CCP1 building. Similar comparison was carried out for the CCP2 building, as shown in Figure 7.11 (b). This shows that the maximum benefit can be obtained with retrofit techniques or in other words, losses can be

controlled to lower level through retrofit techniques. When 1% discount rate was assumed, the CBR value for the CCP2 building retrofitted with jacketing, bracing, and shear wall corresponds 36.8, 47.24, and 57.4, respectively. Figure 7.11 (c) presents the sensitivity plot for the MRT1 building, where for 1% discount rate, i.e. the CBR value with jacketing, bracing, and shear wall was approximately 136.5, 167.9, and 190.4, respectively. These values were extremely high, and confirm the serious need of retrofit techniques on one hand and also signify the influence of discount rate in the CBR. Similar results can be obtained for the MRT2 building as shown in Figure 7.11 (d), where the CBR attained for 1% discount rate with jacketing, steel bracing, and RC shear wall was almost 50.5, 57.3, and 69, respectively.
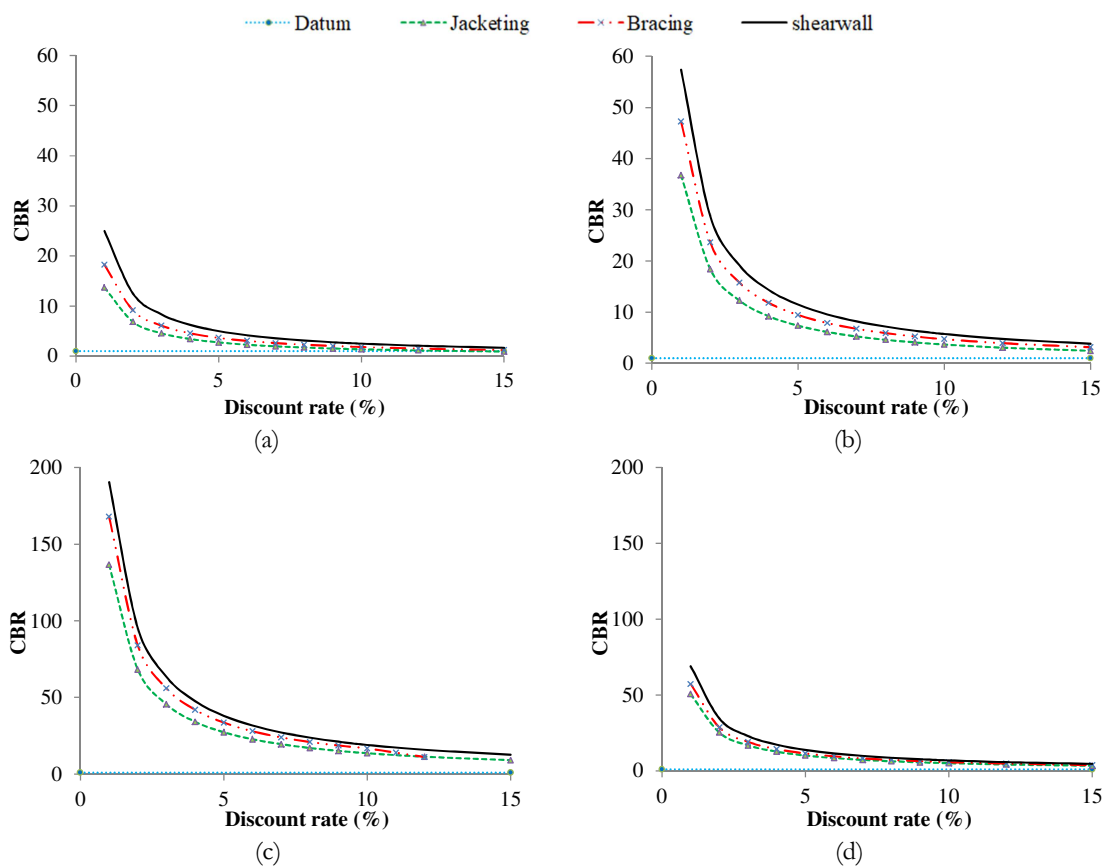
Figure 7.11 – Cost-benefit ratio for case study buildings with different retrofit strategies showing the variation with discount rate assuming constant service life of the structures; (a) CCP1, (b) CCP2, (c) MRT1, and (d) MRT2

Summarizing all the above findings, it can be concluded that CBR increases with decrease in discount rate and vice-versa, and also increases with the increase in the life time of the retrofit structures. The present study does not consider the effect of human injuries and fatalities in the CBR and sensitivity analysis. Therefore, if these losses along with other non-structural losses would have considered in the analysis, it can be expected to attain

unpredictable higher CBR values. This intends to support the benefit and need of retrofit measures addition in the selected buildings. Beside many limitations, constraints and uncertainties, it can be revealed that for the majority of buildings considered for the study concluded that the RC shear wall as much more economically beneficial and feasible retrofit techniques.

7.9 Final comments

The probabilistic cost benefit analysis was performed to support and motivate in decision making in order to upgrade the seismic performance of the existing buildings with limited investment. This method integrates probabilistic hazard models of the area, fragility curves for the as-built and retrofit buildings over a range of damage states, central damage factors, and associated cost for respective damage states. The results and conclusions obtained from the study can be expected to encourage the decision makers, owners, investors and concerned stakeholders to invest money on retrofit, and also help to identify and select the best retrofitting measures. The several conclusions attained are as follows.

- The retrofitting costs were less than 40% of the total replacement cost for the selected buildings. This reveals that the retrofit measures adopted for the existing buildings can be stated beneficial, as it aligned with the conclusion stated by the Liel and Deierlein (2012).

- The retrofit measures drastically reduced the EAL especially for higher damage states (i.e. moderate to collapse states). For lower damage states, such as slight and moderate, remarkably it was found that retrofit building exhibits slightly higher EAL compared to as-built building, is mainly observed in the CCP1 and MRT1 buildings.

- The maximum EAL in the as-built buildings was recorded in moderate, collapse and extensive damage states and can be lowered to minimum with retrofit measures. The steel bracing largely minimizes the EAL, followed by shear wall and jacketing.

- The discrete distribution of EAL for as-built building reveals that the maximum EAL occurs between 0.1g and 0.2g PGA for non-engineered buildings and below 0.1g PGA for pre-engineered buildings. This concludes that the frequent earthquakes of lower magnitude exhibit maximum EAL, whereas the occasional

earthquakes having larger magnitude exhibits lower EAL. This is also true for building with retrofit as well, but the level of EAL was significantly reduced.

- The retrofit measure highly reduces the potential maximum EAL and was observed to reduce by 2-11 times for non-engineered buildings and 3-40 times in case of pre-engineered buildings.

- The risk curve reveals that the maximum LCL occurs at the lower annual probability of exceedance and decreases with the increase in annual probability of exceedance. The maximum LCL was recorded for the as-built MRT1building, and followed by the MRT2, CCP2, and CCP1 buildings, respectively. These unexpected losses can be considerably minimized through the introduction of retrofit techniques; where the LCL can be minimized to one fifth of that as-built building.

- When service life of the retrofitted buildings were considered as 25 years and a discount rate of 10% p.a., the CBR values recorded for the CCP1, CCP2, MRT1 and MRT2 ranges 1.3-2.4, 3.7-5.7, 13.6-19 and 5-6.9, respectively. The maximum CBR was mainly reported for the building retrofitted with RC shear wall, and followed by steel bracing and concrete jacketing.

- The sensitivity analysis performed through the variation of service life of the retrofitted structure and constant discount rate of 10% p.a. reveals that increase in the service life of the structure increases the CBR value. The positive return on investment can be obtained through the addition of retrofit measures, i.e. CBR>1 was attained for the CCP1, CCP2, MRT1 and MRT2 buildings after 11-19 years, 5-7 years, 2 years and 4-5 years, respectively.

- The sensitivity analysis carried out through the variation of discount rate, assuming the constant service life of the structure as 25 years found that the decrease in the discount rate increase the CBR values and vice-versa. For a discount rate of 5% p.a., the CBR value recorded for the CCP1, CCP2, MRT1 and MRT2 buildings ranges 3-5, 8-12, 25-40 and 17-22, respectively.

- Based on the seismic performance enhancement, minimizing the EAL and LCL, it was found that the steel bracing was more effective; whereas, based on the cost-benefit ratio, RC shear wall found to be more economic beneficial.

Chapter 8.

Seismic Fragility Assessment of Revised MRT Buildings considering typical Construction changes

8.1   Introduction

Intensive experimental and numerical research has been performed on infilled RC structures in the past six decades in order to understand the influence of infill walls (either masonry or concrete) on the local and global behaviour of RC frame structures [2, 7, 10, 11, 68, 71, 92, 93, 175]. However, a conclusive and reliable design approach has not been proposed yet, most likely due to large uncertainties associated with the properties of unreinforced masonry (URM). RC buildings infilled with URM are common construction practice around the globe. This type of construction is mostly found in the under-developed and developing countries. It is one of the most common building construction types found in highly seismic regions, potentially due to the easy availability of the construction material, lower construction cost, easy availability of labour and technicians and so on.

The use of masonry infill walls in the RC frame structure can have positive and negative effects under the action of earthquakes. The positive contribution could be the considerable increase in the global stiffness and strength capacities of infilled RC buildings, when compared to bare frame buildings. If infill walls are not considered in the design of an RC building, it could lead to unexpected behaviour in RC buildings or changes in the dynamic behaviour of infilled RC buildings [8, 269]. This statement is aligned with the findings derived from the past experimental and numerical research [2, 7, 10, 11, 68, 71, 92, 93, 175]. Holmes' [62, 63] test results showed that the strength of a steel frame infilled with RC walls increases by 400%, whereas it increases by 100% if infilled with brick masonry. Similarly, Bertero and Brokken (1983) [67] concluded that a building's stiffness increases from 366% to 944% depending upon the variation in the layout of the infill walls. For larger magnitude earthquakes, the structure is most likely to collapse under the soft-storey

mechanism, as reported after the Gorkha earthquake and is dominant due to the brittle behaviour of the infill walls, where in- and out-of-plane failures are more prominent. In few cases, structural collapse occurs due to shear cracks and the short-column mechanism. Figure 8.1 presents both non-engineered and pre-engineered buildings that collapsed during the Gorkha earthquake, mainly caused by the in-plane crushing and out-of-plane failure of the infill walls, thus leading to soft-storey and in some cases, short-column and shear cracks in columns and so on.

| (a) | (b) | (c) |

Figure 8.1 – Representative damaged buildings due to the distribution of infill walls observed after Gorkha earthquake; (a) Total in-plane crushing of the infill walls, (b) Soft-storey building along with pounding mechanism and (c) Soft-storey mechanism and out-of-plane failure of the infill walls

8.2   Limitation of Design Codes and Scope of the Work

The design guidelines adopted for the ordinary residential buildings were discussed in detail in Chapter 2 and Section 2.3.1 and 2.3.2. As stated above, although infill walls demonstrate both positive and negative influences on the global building performance, the above-defined guidelines cannot materialize their contribution to the design of RC buildings. Both NBC 205: 1994 [20] and the latter revised NBC 205: 2012 [21] guidelines stated in Clause 4.1 that the building should be designed as a bare frame to resist earthquake forces excluding the influence of infill walls, but in reality the bare frame building does not exist. On the other hand, NBC 201: 1994 [53] attempts to integrate the interaction of infill walls in carrying the horizontal loads by equivalent compressive strut action, modelled together with the surrounding frames (assumed as pin-jointed), as presented in Figure 8.2. A limitation exists in NBC 201: 1994 [53], where Clause 4.2 (i) states that only infill walls with opening less than 10% of the gross panel area should be considered in resisting seismic loads. This does not correlate with the actual RC building construction practice in Nepal,

where almost 30–40% of openings are usually observed, mostly in the external infill walls (see Figure 8.1). In addition, these guidelines are suitable for RC buildings up to three storeys. But in reality, the owner or stakeholders utilize them only for design and drawing approval from the concerned authorities, and later modify them by adding more storeys. This can be justified from the buildings observed during the site survey after the Gorkha earthquakes in Nepal, illustrated in Figure 8.1. Also, Chaulagain, *et al.* (2013) [23] reported that most of the RC buildings in urban areas of Nepal were 2–6 storeys. This demonstrates that past and present construction practices do not comply with both guidelines in relation to the number of storeys and infill walls openings and their distribution. Similarly, Chaulagain, *et al.* (2013) [23] studied and published excellent work on the regular three-storey prototype building, modelled as a bare frame and designed based on different design approaches. They concluded that NBC buildings were highly vulnerable to earthquakes. Furthermore, Chaulagain, *et al.* (2016) [269] also studied a three-storey building designed which was based on three approaches whose structural sections were identical with NBC 205: 1994 [20]. In this case, the building analysed was bare framed and fully infilled, and they concluded that infill walls increase the stiffness and strength capacity and also the seismic performance of the building, hence, its influence should not be neglected.

Taking account of all these considerations, the present study aims to investigate the seismic performance assessment of the revised MRT building, also an extension of the previous work carried out by Chaulagain, *et al.* (2013, 2016) [23, 269]. The primary objective of the present study is to examine the seismic performance of the prototype building, whose structural sections and reinforcement details were initially defined for a three-storey bare frame building, and later modified with different arrangements of infill walls (the three cases considered) and finally additional storeys (four and five storeys). In this manner, the study aims to integrate the past and present construction scenario, i.e. modification to the building, and thus attained results and conclusions that are expected to be beneficial to convince and make owners, concerned authorities, stakeholders and clients aware of the likely increase in vulnerability from such building modifications.
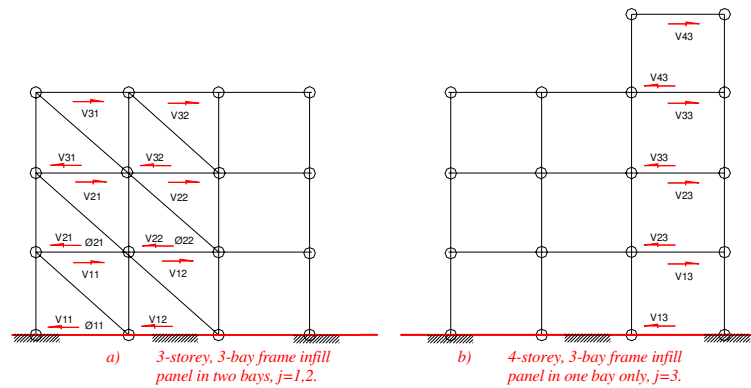
Figure 8.2 – Strut action of infill panels with RC frames (NBC 201, 1994) [53]

8.3   Description of the Case Study Building

8.3.1   General description

As stated earlier, the primary objective of the present study is the vulnerability assessment of the prototype building designed based on revised NBC 205: 2012 [21] and later modified by adding storeys and different dispositions of infill walls. The revised MRT guideline was implemented as mandatory only in 2015 after the Gorkha earthquake, so it was challenging to find real buildings. However, the present research findings can be used to generalize and also help to check the adequacy of the structural section sizes and reinforcement details as specified in the guideline. To meet the objective, initially a regular three-storey building was selected, having three bays in the longer direction represented along the X-axis and two bays in the shorter direction represented along the Y-axis, as illustrated in Figure 8.3. The second stage deals with different arrangements of infill walls throughout the building. Although there are large arrays of infill wall configurations, the present research considers only the three most dominant arrangements, representing most of the building types found in urban and rural areas of Nepal. This includes a building without infill walls at the ground floor (WO-GI) that resembles commercial buildings where the ground floor is used for storage and parking purposes; a building with one complete bay without infill walls, also known as an irregularly infilled building, representing vertical irregularity (W-Irre.-I), which is common practice in residential building, utilizing the road-facing side for commercial purposes; and finally a building fully infilled as a regular building (W-I). All the external walls were assumed to have openings of around 30% of the gross panel area and placed at the periphery of the building, whereas the internal infill walls were used as partitions. The

third and final stage was the investigation of the buildings' seismic performance when a number of storeys were added. To attain this objective, buildings were classified into three groups, i.e. 3-storey (MRT-3), 4-storey (MRT-4) and 5-storey (MRT-5), representing the majority of building types in Nepal. Therefore, a total of 12 building models were considered for the present study and are presented in Table 8.1.

Table 8.1 – Building classification based on number of storey and distribution of infill walls

Number of Storey	Building Group	Sub-Group (Building Type)	
3	MRT-3	BF	
		WO-GI	
		W-Irre.-I	
		W-I	
4	MRT-4	BF	
		WO-GI	
		W-Irre.-I	
		W-I	
5	MRT-5	BF	
		WO-GI	
		W-Irre.-I	
		W-I	

8.3.2 Geometrical and material properties

Figure 8.3 presents a typical layout of the prototype building along with the structural dimensions and section details. The present study assumed a regular plan layout and all structural dimensions and cross-sections were assumed similar for the study building groups. Each span in the longer direction (X-axis) was assumed to be equal and the considered bay length was 3.75 m, whereas the short direction (Y-axis) has a bay length of 3.5 m. A constant inter-storey height of 2.75 m was assumed, thus the total height of the MRT-3 model was 8.25 m, MRT-4 was 11 m and MRT-5 was 13.75 m. In addition to the

similar geometrical plan and section, all the building groups have similar geometrical and material properties, loading conditions, the same structural section sizes and reinforcement details and so on. As previously stated, these assumptions were based on the past and present construction scenario across Nepal, as a consequence of some representative damaged/collapsed RC buildings recorded during the site survey after the Gorkha earthquake, as presented in Figure 8.1. External infill walls of 230 mm thickness having 30% openings were considered and placed at the periphery of the building. In addition, internal infill walls of 110 mm thickness were considered and placed internally, functioning as the partition walls in the building. It is to be noted that the infill walls were composed of heavy solid bricks of size 240 x 115 x 57 mm^3 along with 10 mm horizontal and vertical mortar joints. The entire column sections were similar, having a section (300 x 300) mm^2 and uniform beam section of (230 x 355) mm^2 including 125 mm slab thickness [21]. Depending upon the position of the columns and the beams, the reinforcement details were assigned as defined in the revised NBC 205: 2012 [21], as presented in Table 8.2 and Table 8.3. The positions of the columns were characterized as corner, intermediate and interior. Similarly, the beams were classified into two groups, namely, end and intermediate. The lateral reinforcements were two-legged, of Φ 8 uniformly spaced at 100 mm between centres throughout the column and beam height. All the stirrups were hooked at 45^0 with a length of 75 mm at each end. The effective cover for the columns and beams provided was 40 mm and 25 mm, respectively. Furthermore, a layout and section details similar to three storeys was repeated to obtain the four- and five-storey building configurations.
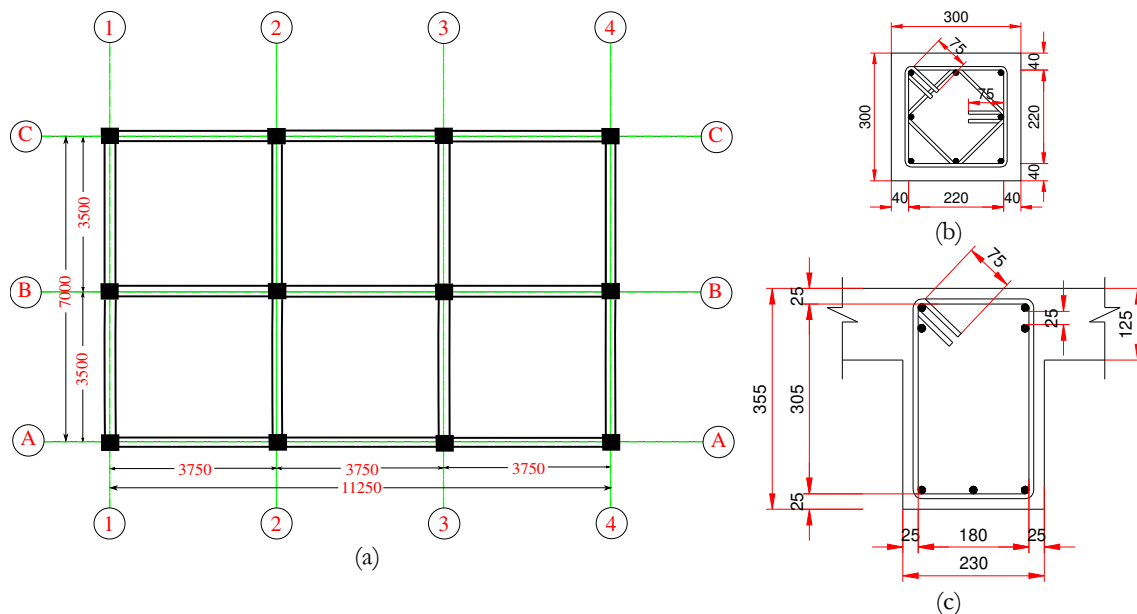
Figure 8.3 - Typical floor layout and structural details; (a) Beam and column, (b) Column detail and (c) Beam detail (all dimensions are in mm)

Table 8.2 – Columns position layout, its sections and longitudinal reinforcement details for the MRT-3 building as per NBC 205:2012 [21]

Column position	Storey	Cross-section of Column (mm²)	Longitudinal reinforcement
	1st	300 x 300	4 Φ 16 + 4 Φ 12
	2nd	300 x 300	4 Φ 16 + 4 Φ 12
	3rd	300 x 300	8 Φ 12
	1st	300 x 300	4 Φ 16 + 4 Φ 12
	2nd	300 x 300	4 Φ 16 + 4 Φ 12
	3rd	300 x 300	8 Φ 12
	1st	300 x 300	4 Φ 16 + 4 Φ 12
	2nd	300 x 300	4 Φ 16 + 4 Φ 12
	3rd	300 x 300	8 Φ 12

Table 8.3 - Beam position layout and longitudinal reinforcement details at the support and mid-span for MRT-3 building as per NBC 205:2012 [21]

Beam	Storey	At Support	At mid-span
	1st	3Φ16 ___ 2Φ16 + 1Φ12	2Φ16 ___ 2Φ16
	2nd	2Φ12 + 1Φ16 ___ 2Φ12 + 1Φ16	2Φ12 ___ 2Φ12
	3rd	2Φ12 ___ 2Φ12	2Φ12 ___ 2Φ12
	1st	3Φ16 ___ 2Φ16 + 1Φ12	2Φ16 ___ 2Φ16
	2nd	2Φ12 + 1Φ16 ___ 3Φ12	2Φ12 ___ 3Φ12
	3rd	2Φ12 ___ 2Φ12	2Φ12 ___ 2Φ12
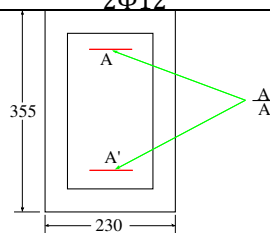
Typical beam cross-section illustrating top and bottom longitudinal reinforcement

In addition to using similar geometrical layouts, section and reinforcement details, the material properties for the concrete, infill walls and reinforcement, and loading conditions were also assumed to be similar for the variable number of storeys (three, four and five). The material properties considered for the entire building types were presented in Table 3.13, obtained from the guidelines (IS1893 (Part 1): 2002 [30]; NBC 201: 1994 [53]; NBC 205: 2012 [21]). In addition, Table 3.14 and Table 3.15 also summarize the different types

of live loads assigned in the model. Furthermore, additional material properties for the infill walls considered were shown in Table 4.6.

8.3.3   Numerical modelling

The selected buildings were modelled using SeismoStruct software (2004) [22], which is based on finite element analysis and is capable of predicting large displacement behaviour of space frames under static or dynamic loading considering material inelasticity and geometrical nonlinearities. The detail of the modelling approach was discussed and presented earlier in Chapter 4. The detailed frame elements modelling approach used was similar to that stated in Section 4.3.1 and the modelling was as stated and discussed in Section 4.3.2.

Figure 8.4 presents a typical 3-D numerical model for the MRT-3 building, which includes a bare frame model and the other three infilled RC models with different distributions of the infill walls, illustrating common and dominant construction typology of the area [23, 32]. In addition, Figure 8.5 and Figure 8.6 demonstrate 3-D models for the MRT-4 and MRT-5 buildings, respectively, each with a bare frame model and the remaining three models provided with different orientations of infill walls. Initially, the building was modelled as a bare frame, such that only the beam and column elements were assigned. The floor constraint was assigned at each floor level, such that all the nodes of the storey are predicted to undergo similar displacement under lateral loads. Later, the bare frame model was modified through the introduction of external and internal infill walls. The area of the strut for external infill walls in the building's shorter direction was reduced by 30% to integrate the openings for windows and doors, and external infill walls in the longer direction were assumed to be fully infilled. Similarly, the internal infill walls were assumed to be fully infilled. One of the modified prototype buildings was modelled as soft-storey at the ground storey in order to investigate the seismic performance of this building type under seismic excitations. Another includes the irregular distribution of infill walls, where one complete bay in the longer direction was without infill walls. Furthermore, the study also aims to evaluate the effect of introducing the vertical irregularity contributed by the infill walls; hence, one complete bay in the longer direction was without infill walls at the ground floor.
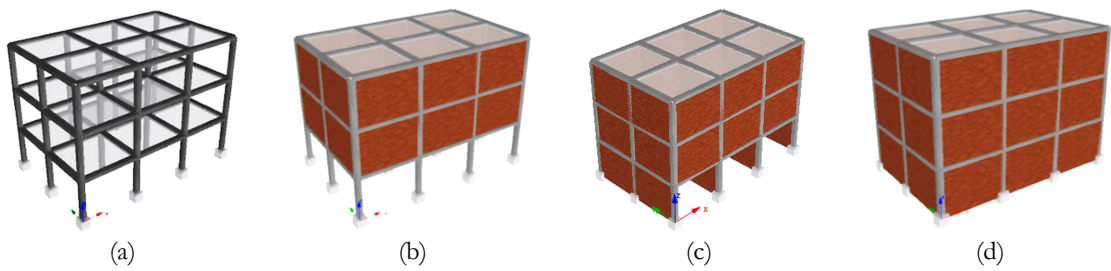
Figure 8.4 – MRT-3 3D models considering different dispositions of infill walls: (a) BF, (b) WO-GI, (c) W-Irre.-I, and (d) W-I
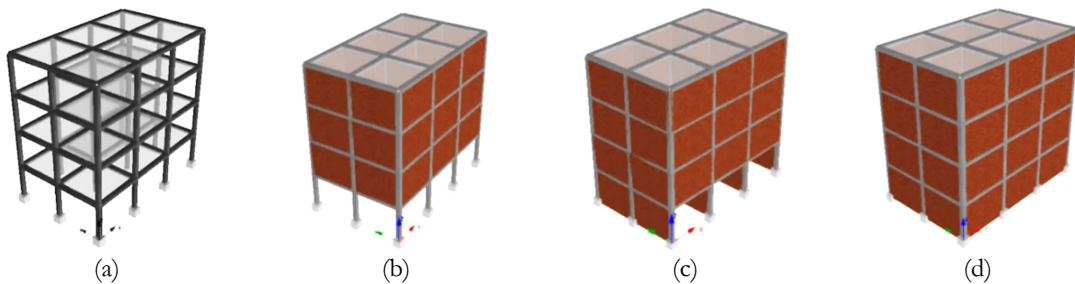
Figure 8.5 – MRT-4 3D models considering different dispositions of infill walls: (a) MRT-4-BF, (b) MRT-4-WO-GI, (c) MRT-4-W-Irre.-I, and (d) MRT-4-W-I
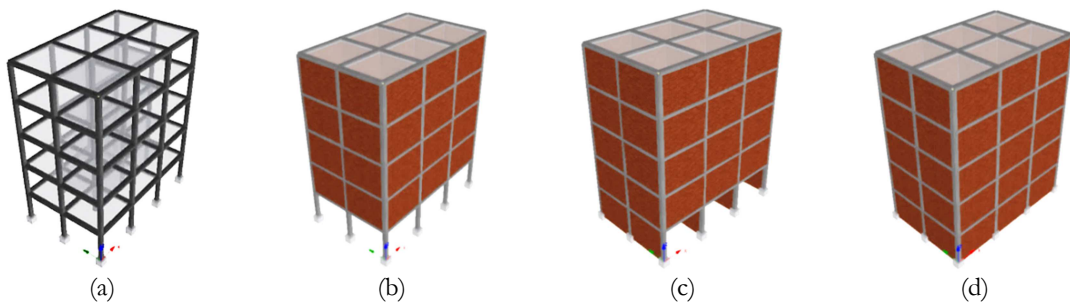
Figure 8.6 – MRT-5 3D models considering different dispositions of infill walls: (a) BF, (b) WO-GI, (c) W-Irre.-I, and (d) W-I

8.4 Vulnerability Assessment

Different types of analysis were implemented on each building type, such as eigenvalue analysis, adaptive pushover analysis and nonlinear time history analyses. A precise and accurate vulnerability assessment for the building types was performed through nonlinear time history analyses, where the results were presented and evaluated with the help of the inter-storey drift profile, IDA curves and fragility curves. The detailed analysis and interpretation of the results are discussed in the following sections.

8.4.1 Eigenvalue analysis

Table 8.4 presents the first three fundamental frequencies for all the building types evaluated through the eigenvalue analysis. Although the dynamic behaviour of the building changes with the introduction of the infill walls, the observed vibration modes were identical for the studied infill wall configurations, i.e. the first two vibration modes along the translational and third one torsional. As expected, the infilled prototype buildings increased the fundamental frequencies by almost 4 times compared to the corresponding bare frame. The maximum increase can be observed for the fully infilled building, followed by the irregularly infilled and soft-storey building, respectively. This holds true in the case of four- and five-storey buildings as well. Similarly, the building fundamental frequencies decrease with the increase in the number of storeys and are found to be reduced by almost 25% and 50% for four and five storeys, respectively. The higher frequency corresponds to the lower period of the structure, thus it attracts large seismic force particularly for low-rise buildings, as obtained from the site response spectra defined in IS1893 (Part1): 2000 [30], as shown in Figure 4.35. Therefore, low-rise infilled buildings should be properly designed and detailed to counteract large seismic forces, which is the primary objective of the present study.

Table 8.4 – Natural frequencies (Hz) for various MRT buildings with modification in infill walls distribution and number of storeys

Building type	MRT-3			MRT-4			MRT-5		
	1st	2nd	3rd	1st	2nd	3rd	1st	2nd	3rd
BF	1.96	2.00	2.33	1.44	1.47	1.72	0.93	0.95	1.06
WO-GI	3.47	3.54	4.04	2.38	2.42	2.65	1.98	2.04	2.24
W-Irre.-I	5.89	7.89	8.58	5.07	5.22	6.47	3.44	3.55	4.40
W-I	7.13	7.89	9.27	5.77	6.04	7.05	3.55	3.97	4.52
Mode Type	Transv	Long	Torsional	Transv	Long	Torsional	Transv	Long	Torsional

8.4.2 Static pushover analysis

The influence on the base shear capacity of the building as a result of the different dispositions of infill walls and due to the added number of storeys was analysed through the adaptive pushover analysis, utilizing the response spectra as shown in Figure 4.35. Figure 8.7 presents capacity curves for all the modified prototype buildings in both directions. The plot illustrates that the addition of infill walls in the RC frame building considerably increases the stiffness and strength compared to the bare frame. The

maximum increase can be obtained for fully infilled and the minimum for soft-storey buildings. The increase in stiffness for the three-storey building is in the range of 4–20 and 4–16 times in the X and Y directions, respectively, compared to the bare frame building. In addition, the increase in stiffness for four storeys varies from 6–21 and 6–-17 times in the X and Y directions, respectively. Furthermore, the increase in stiffness for the five-storey building was 8–25 and 8–20 times in the X and Y directions, respectively.

Similarly, the capacity curves also demonstrate a significant increase in the maximum base shear capacity of the building after the addition of infill walls, but depend upon its distribution. As expected, the maximum increase in base shear capacity was observed for the fully infilled building, and it increased by almost 4 and 3 times in the X and Y directions, respectively. In the case of four- and five-storey buildings, a similar increase in the base shear capacity was recorded. By contrast, a slight increase in the base shear capacity was recorded for the soft-storey building but this was comparable to the bare frame building in both directions. When comparing the different numbers of storeys, no significant variation in the maximum base shear capacity was recorded, i.e. they were very similar, as illustrated in Figure 8.7. Although the infill wall increases the stiffness and strength capacity in the building, it was recorded that the addition of the infill wall reduced the deformation capability and overall ductility of the infilled buildings. The maximum base shear capacity was attained at lower global drift, which is most likely due to brittle behaviour of the masonry infill walls in comparison to RC frames. At the maximum point, the infill walls were predicted to contribute fully along with the surrounding RC frames behaving monolithically in resisting lateral forces. This state of the building can be expected to possess minor cracks in the infill walls. This point can be predicted to attain a maximum inter-storey drift of around 1.2% in both directions. After attaining the maximum capacity, a steep decline in the capacity curve was observed, similar to the case study buildings studied in detail in Chapter 5. A steep descending branch was recorded in fully infilled and irregularly infilled RC buildings. This is potentially due to the failure of infill walls under in-plane crushing and in some cases, out-of-plane, resulting in the failure of the infilled building under the soft-storey mechanism.

From the above discussions and the capacity curves obtained, it can be concluded that the variation in base shear capacity is mainly due to the distribution of the infill walls, their positions and the percentage of openings, and is independent of the varying number of storeys when all remaining parameters are assumed constant.
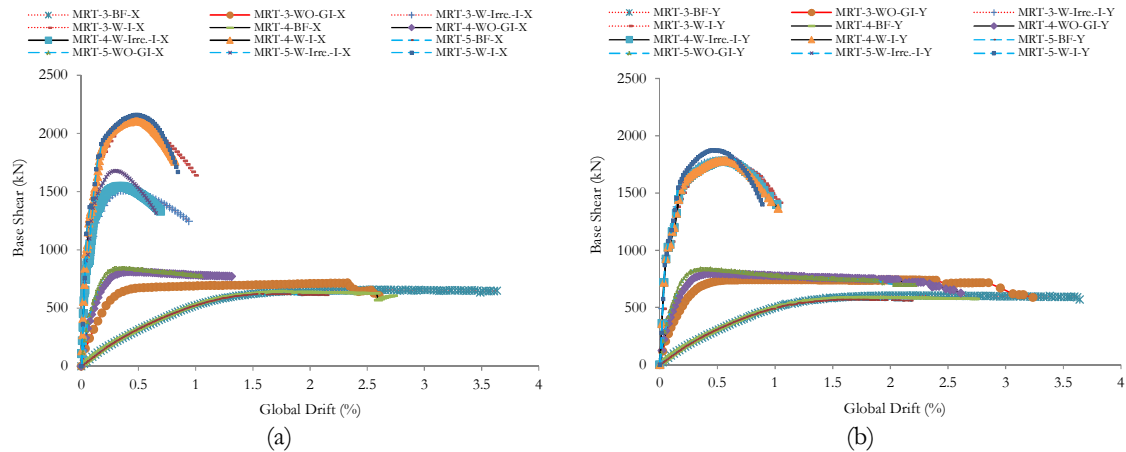
Figure 8.7 – Capacity curves for prototype MRT building influenced by different infill walls configurations and variable number of storeys; (a) X direction and (b) Y direction

8.4.3   Nonlinear dynamic time history analysis

The seismic vulnerability of all the modified prototype MRT buildings was assessed through nonlinear time history analyses. The procedure for the dynamic time history analyses was discussed in detail in Chapter 4 and the present study was carried out through selecting 21 real ground motion records acting bidirectionally, and suitably scaled between 0.1g and 0.5g at the interval of 0.1g [192]. To determine the critical angle of incidence, the selected earthquakes were subjected at 0 and 90 degrees. For each set of earthquakes, 10 scaled IMs were subjected, thus almost 210 nonlinear time history analyses were carried out for each prototype building, and a total of 2400 analyses were performed in the prototype building, whose results are presented and discussed in the following.

8.4.3.1   ISD$_{max}$ profile

The present section considers the building response as ISD$_{max}$ utilized as EDP with respect to IMs, attained from the dynamic time history analyses. The level of damage states that ensued in the building was identified comparing the obtained ISD$_{max}$ with the threshold drift limit proposed by Rossetto & Elnashai (2003) [202], and the detailed table was presented in Chapter 4 and Table 4.10.

8.4.3.1.1   *Influence due to different arrangements of infill walls*

Representative comparative inter-storey drift profiles for the MRT-3, MRT-4, and MRT-5 buildings modified with various dispositions of infill walls, affected by the 5-Chi-Chi

(Taiwan) earthquake, at 0.3g PGA, are shown in Figure 8.8 to Figure 8.10, respectively. The entire plots demonstrated that the soft-storey building exhibits the maximum inter-storey drift (ISD$_{max}$) mainly at the ground floor and insignificant drift at the consecutive upper floors, as expected. This is potentially due to the lower stiffness and strength capacity at the soft-storey as compared to the consecutive upper infilled storeys; as a consequence, it becomes a much more susceptible building type. By contrast, the bare frame building exhibits a uniform drift profile throughout, thus illustrating the uniform distribution of global stiffness and strength. Although the drift was uniformly distributed in the bare frame building, the recorded ISD$_{max}$ was comparable to the maximum drift in the soft-storey building. The regularly and irregularly distributed infill wall not only reduces the ISD$_{max}$ to lower values but also uniformly distributes it throughout. For this particular earthquake and IM, the infilled frame building reduces the maximum drift to one tenth less than the soft-storey and BF buildings in both directions. When comparing the infilled buildings' drift profiles, it was found that the fully infilled RC building exhibits lower drift than the irregularly infilled one. Furthermore, the uniform drift profile observed in the infilled building highlighted the uniform distribution of stiffness and strength, but was valid for low to moderate magnitude earthquakes and also aligned with the conclusions of Varum, H. 2003 [8]. The ISD$_{max}$ for the MRT-3, MRT-4 and MRT-5 buildings for soft-storey buildings corresponds to approximately 2.7%, 3% and 3.2%, respectively, in the Y direction, and for fully infilled buildings was reduced to below 0.7%, 0.5% and 0.9%, respectively. This particular earthquake of specified IM revealed that the soft-storey buildings have extensive to partial collapse in relation to Table 4.10, and exhibit only a moderate damage state after the intervention of infill walls.
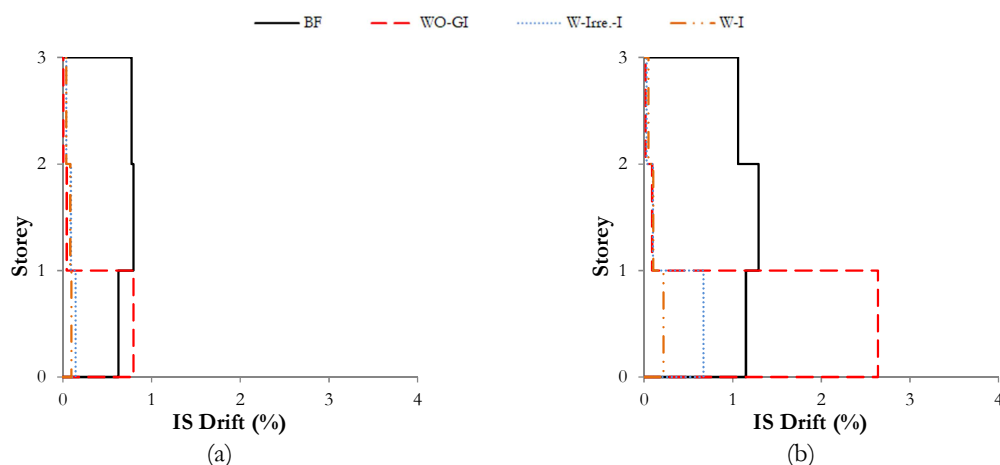
Figure 8.8 – Typical ISD$_{max}$ profile for MRT-3 with disposition of infill panels, subjected by 5-ChiChi Taiwan earthquake, at 0.3 g PGA; (a) X direction and (b) Y direction

(a)   (b)
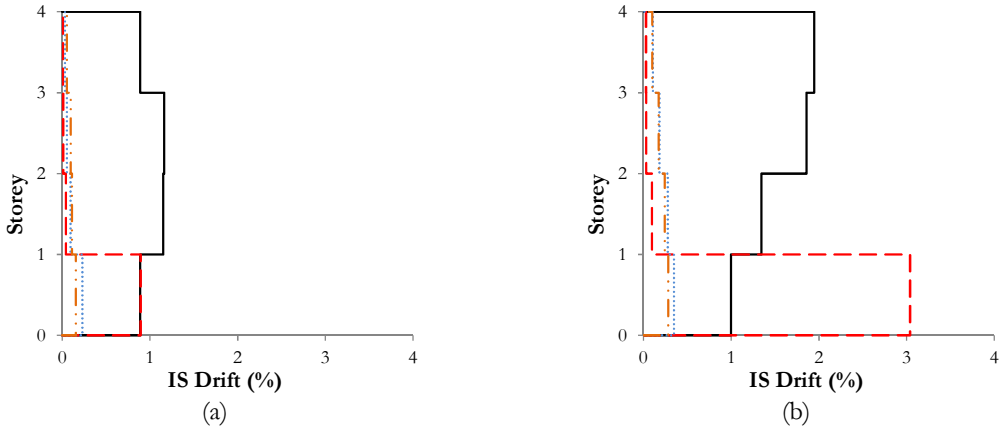
Figure 8.9 - Typical ISD$_{max}$ profile for MRT-4 with disposition of infill panels, subjected by 5-ChiChi Taiwan earthquake, at 0.3 g PGA; (a) X direction and (b) Y direction

(a)   (b)
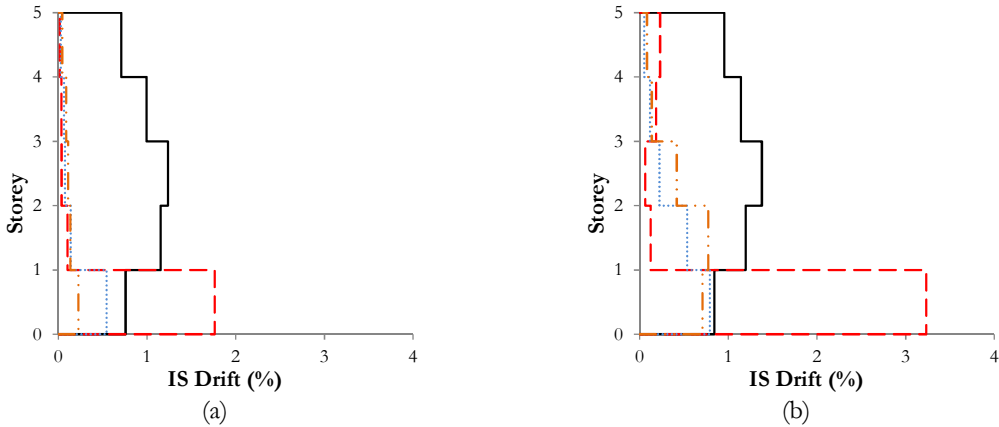
Figure 8.10 - Typical ISD$_{max}$ profile for MRT-5 with disposition of infill panels, subjected by 5-ChiChi Taiwan earthquake, at 0.3 g PGA; (a) X direction and (b) Y direction

8.4.3.1.2 *Influence of number of storeys*

Figure 8.11 to Figure 8.14 present representative comparative ISD$_{max}$ profiles for various infill wall configurations to investigate the influence of adding storeys to the prototype building. As expected, the entire plots illustrate a higher building response, i.e. they exhibit a larger ISD$_{max}$ corresponding to the added number of storeys, except in the case of the bare frame building, where the four-storey building exhibits slightly higher drift at the upper floors compared to the five-storey one. In the case of the soft-storey building, the drift increases by almost 100% and 20% in the X and Y directions, respectively, when modified from three to five storeys. Similarly, the drift increased by more than twice in both directions for the irregularly infilled model when the storeys increased from three to five. Furthermore, the fully infilled building with five storeys exhibits higher drift, i.e. almost 2 and 3 times higher than three storeys. This demonstrates that the vulnerability

increased with the added number of storeys, particularly in buildings initially designed and detailed for three storeys and later modified with added storeys.

(a)   (b)
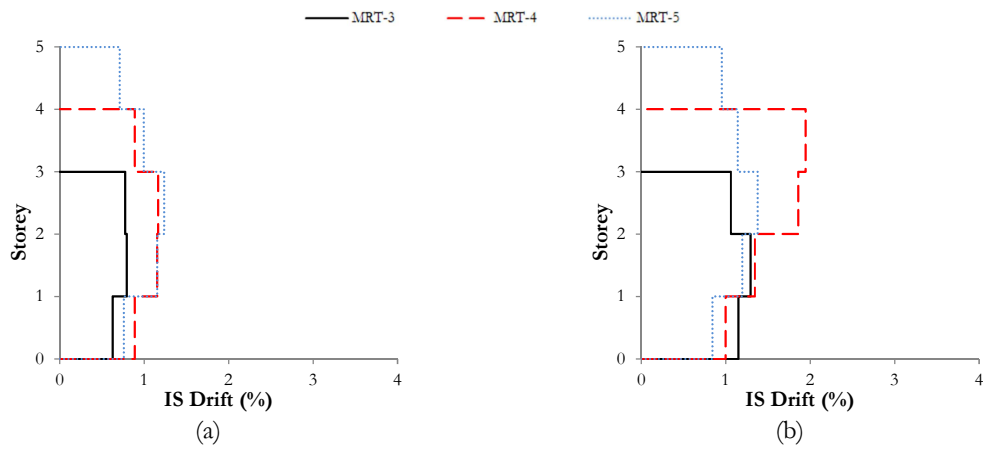
Figure 8.11 – Comparative ISD_{max} profile for BF with respect to number of storey, subjected by 5-ChiChi Taiwan earthquake, at 0.3g PGA; (a) X direction and (b) Y direction

(a)   (b)
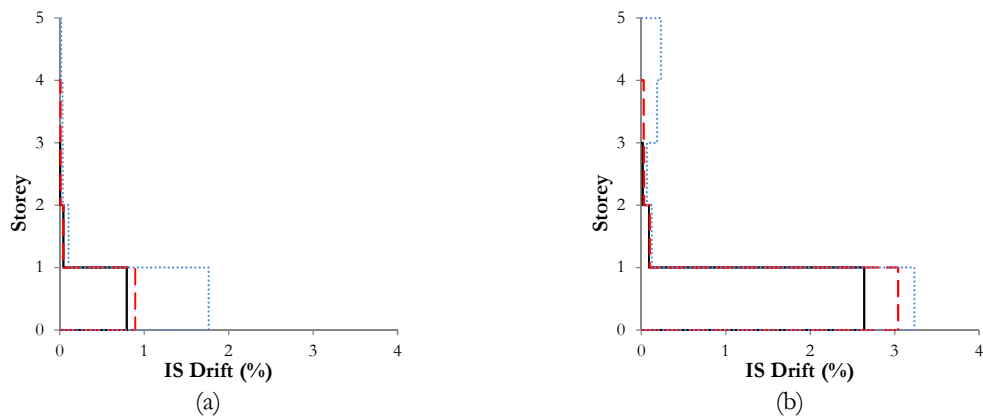
Figure 8.12 - Comparative ISD_{max} profile for WO-GI with respect to number of storey, subjected by 5-ChiChi Taiwan earthquake, at 0.3g PGA; (a) X direction and (b) Y direction

(a)   (b)
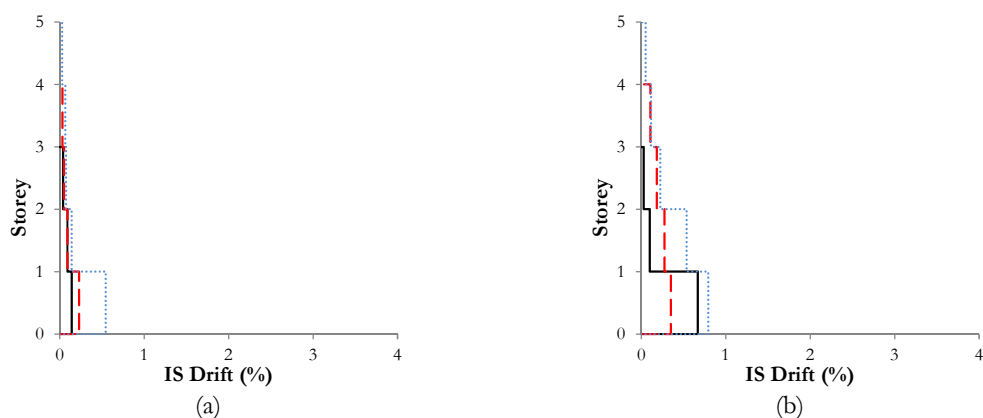
Figure 8.13 - Comparative ISD_{max} profile for W-Irre.-I with respect to number of storey, subjected by 5-ChiChi Taiwan earthquake, at 0.3g PGA; (a) X direction and (b) Y direction
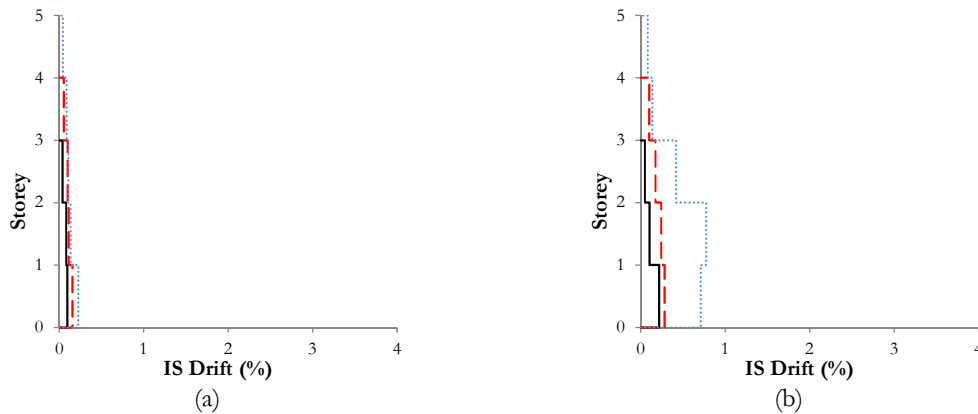
Figure 8.14 - Comparative ISD_{max} profile for W-I with respect to number of storey, subjected by 5-ChiChi Taiwan earthquake, at 0.3g PGA; (a) X direction and (b) Y direction

8.4.3.2   IDA curves

8.4.3.2.1   Influence due to different arrangements of infill walls

The results obtained from the dynamic time history analyses discussed in the above sections were used to plot the IDA curves, which helps to examine the seismic performance of the prototype MRT buildings. Figure 8.15 (a to d) presents the statistical distributions of building responses as a function of IMs for the three-storey building contributed by different arrangements of infill walls, and represented by the boundary of the minimum, maximum, and mean IDA curves. The light solid lines represent an individual IDA curve for each earthquake experienced, illustrating variation of the seismic demands with respect to increasing IMs. As predicted, the entire IDA plot exhibits an increase in ISD_{max} with increase in IMs, such that the building can be expected to behave elastically for lower IMs, i.e. until 0.2g PGA for both bare frame and soft-storey buildings, and until 0.3g PGA in the case of regularly and irregularly infilled buildings. However, in some cases, a decrease in ISD_{max} with increase in IMs was mostly recorded in the soft-storey and bare frame buildings. This state of the building response was related to the early hardening of the structural elements for lower IMs. Such buildings, when affected by earthquakes of large IMs, are unable to meet the seismic demand; as a result, the building collapses, exhibiting lower drift. This state of the building is predicted to reach partial collapse and collapse states. For lower IMs, i.e. until 0.2g, a relatively large dispersion of drift was recorded in the soft-storey and the bare frame buildings compared to the fully and irregularly infilled buildings. In addition, with a slight increase in the IMs beyond 0.3g

PGA, the irregularly infilled building also demonstrates a comparable ISD_{max} to that of the bare frame and soft-storey buildings. This is potentially due to the brittle failure of the infill walls, where both in-plane and out-of-plane failures of an infill wall result in the soft-storey mechanism, and in some cases short-column and shear failures in structural columns. In the case of the fully infilled building, nonlinearity becomes dominant beyond 0.4g PGA and the failure of infilled buildings under soft-storey mechanisms becomes dominant.
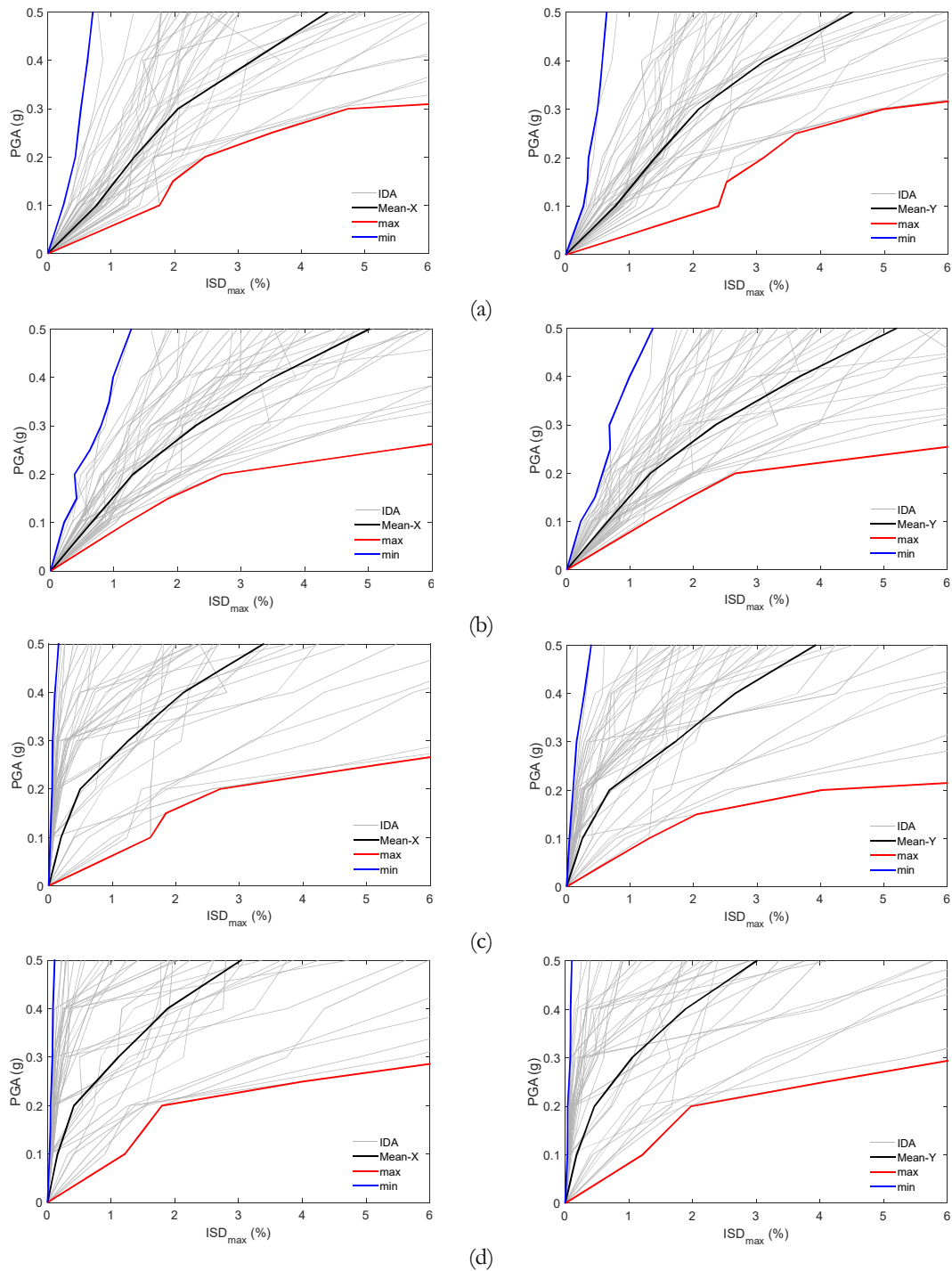
Figure 8.15 – IDA curves for MRT-3 with different structural configurations in X and Y directions, respectively; (a) BF, (b) WO-GI, (c) W-Irre.-I, and (d) W-I

A better investigation of the seismic performance building influenced by various orientations of infill walls can be evaluated through a more simplified approach, i.e. comparison of the mean IDA curves. Figure 8.16 presents the comparative mean IDA curves, illustrating that both the bare frame and soft-storey building exhibit comparable mean drift in both directions, which supports the previous conclusion stated above. Similarly, both fully and irregularly infilled buildings demonstrated a similar mean drift in the X direction for the IMs experienced, whereas in the Y direction a distinct ISD_{max} was recorded beyond 0.2g PGA. The mean ISD_{max} obtained for the three-storey building with bare frame and soft-storey, at 0.3g PGA, was almost 2.2%, and was reduced to below 1.2% with the addition of infill walls throughout. It can be concluded that the seismic performance of the prototype building was found to be improved through the addition of infill walls, thus their contribution cannot and should not be neglected by design professionals and guidelines. However, it should be noted that the above conclusion was based on the analytical results; the reality might be different as it is governed by various factors, such as connection details between the infill wall and the surrounding frames, construction methods and poor workmanship.
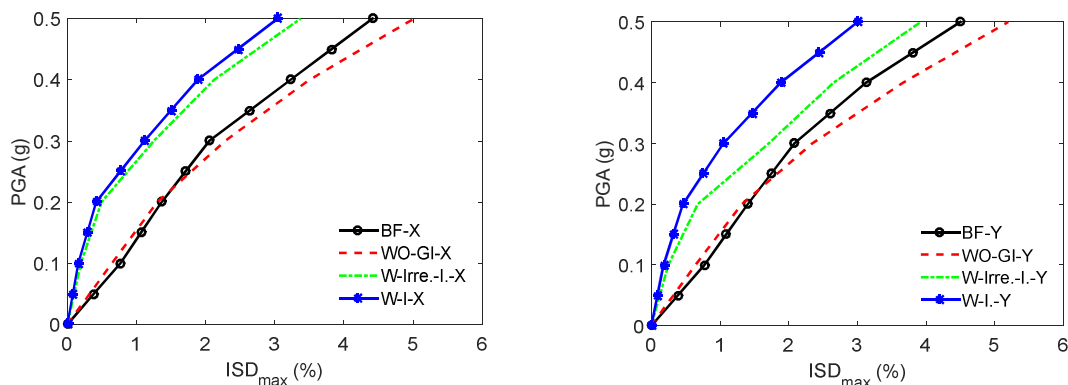
Figure 8.16 – Comparative mean IDA curves for MRT-3 with different structural configurations in X and Y directions, respectively

Figure 8.17 (a to d) presents the IDA curves for the MRT-4 building with BF, WO-GI, W-Irre.-I, and W-I, respectively, in both directions. Similarly to the three-storey MRT building's behaviour, a large dispersion of building response can be recorded for the same IMs. In addition, a larger increase in the inter-storey drift for lower IMs can be detected for the soft-storey and bare frame buildings, whereas in the case of fully and irregularly infilled buildings, a lower drift was detected. The inter-storey drift increases with the increase in IMs, i.e. beyond 0.3g PGA, the irregularly infilled building exhibits a comparable drift to the bare frame and soft-storey buildings. Such higher and comparable drifts were recorded

in the fully infilled building beyond 0.4g PGA, where the failure of the building potentially under the soft-storey mechanism is highly predicted.
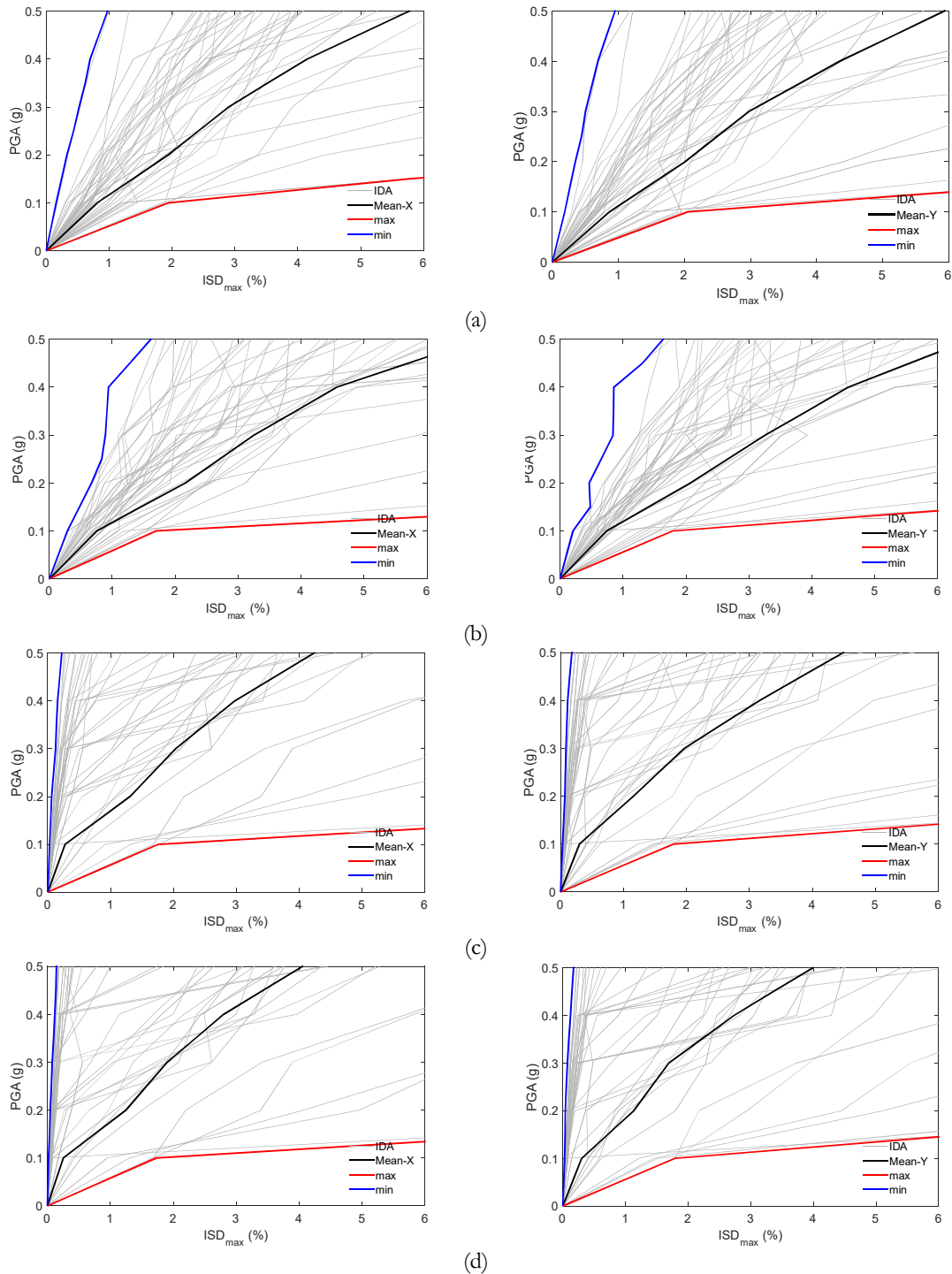
Figure 8.17 – IDA curves for MRT-4 with different structural configurations in X and Y directions, respectively; (a) BF, (b) WO-GI, (c) W-Irre.-I, and (d) W-I

Figure 8.18 presents the comparative mean IDA curves for the MRT-4 building with different distributions of infill walls in both directions. Similarly to the three-storey MRT

building, both bare frame and soft-storey buildings demonstrate similar drift in both directions. Similarly, the regularly and irregularly infilled buildings also demonstrate a similar drift in the X direction, whereas the difference widens beyond 0.2g along the Y direction. The observed mean ISD_{max} for the MRT-4 building with BF, WO-GI, W-Irre.-I and W-I, at 0.3g PGA, was almost 3%, 2.7%, 2% and 2%, respectively, in both directions. When the building response obtained was compared with the threshold drift as defined in Table 4.10, the state of the BF and WO-GI buildings can be predicted to be in extensive to partial collapse states, whereas the irregularly and fully infilled buildings are likely to have moderate to extensive damage.
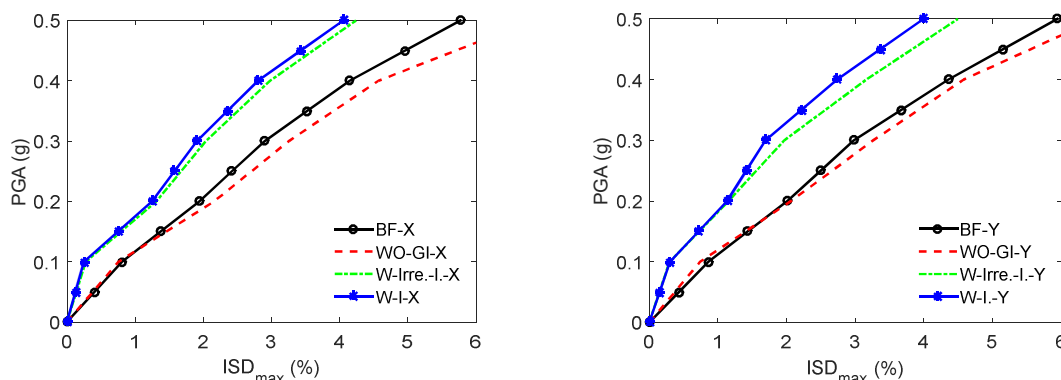
Figure 8.18 – Comparative mean IDA curves for MRT-4 with different structural configurations in X and Y directions, respectively

Figure 8.19 (a to d) presents the IDA curves for the MRT-5 building with various configurations of infill wall, such as BF, WO-GI, W-Irre.-I and W-I, respectively. For this building, larger dispersions of inter-storey drift were recorded, such that nonlinearity becomes dominant beyond 0.1g PGA for the soft-storey and bare frame buildings. By contrast, for irregularly and fully infilled buildings, the elastic behaviour can be predicted until 0.2g and 0.3g, respectively, beyond which hardening is most likely to be dominant and, with the formation of plastic hinges in the structural elements, ultimately the building will collapse. The former building exhibits slightly higher ISD_{max} for lower IMs and higher drift beyond 0.2g PGA. This revealed that the regular infill significantly enhances the seismic performance of the building, but in most cases for low to medium magnitude earthquakes only. Therefore, as in the previous cases, it can be concluded that the contribution of infill walls should not be neglected in the seismic design of infilled RC buildings, on which more research needs to be carried out to increase the ductility in the infill walls, ultimately preventing them from failure/collapse.
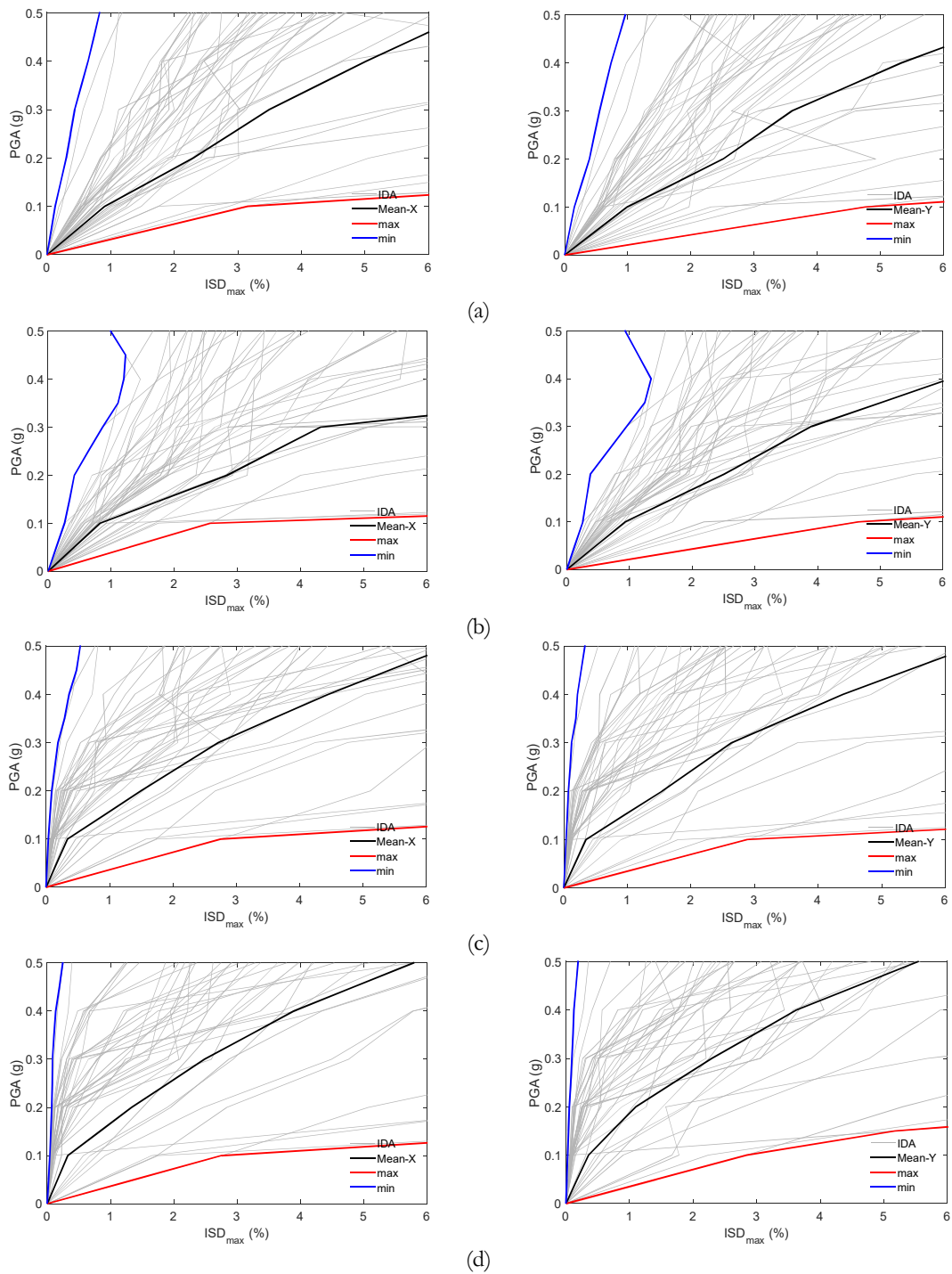
Figure 8.19 – IDA curves for MRT-5 with different structural configurations in X and Y directions, respectively; (a) BF, (b) WO-GI, (c) W-Irre.-I, and (d) W-I

It is complex to generalize the conclusion through the individual IDA curves from the above discussion; therefore, the comparative mean IDA curves were plotted to compare the different infill wall configurations, as illustrated in Figure 8.20. The plot demonstrated that both the bare frame and soft-storey buildings exhibit a similar mean ISD_{max} until 0.2g

in both directions. Remarkably, the difference widens and more distinct mean ISD$_{max}$ values were recorded beyond 0.3g PGA, such that the soft-storey building is the most vulnerable building typology. Similarly, for irregularly and regularly infilled buildings, both shows similar mean IDA curves in the X direction, whereas more distinctive building responses were recorded beyond 0.1g, such that the former illustrates a higher drift than the latter. The mean ISD$_{max}$ for the MRT-5 building with BF, WO-GI, W-Irre.-I and W-I, at 0.3g PGA, was approximately 4%, 3.5%, 2.5% and 2.4%, respectively. It can be concluded that the BF and WO-GI buildings are the most likely to reach partial collapse and collapse states, whereas infilled buildings exhibit moderate to extensive damage states.
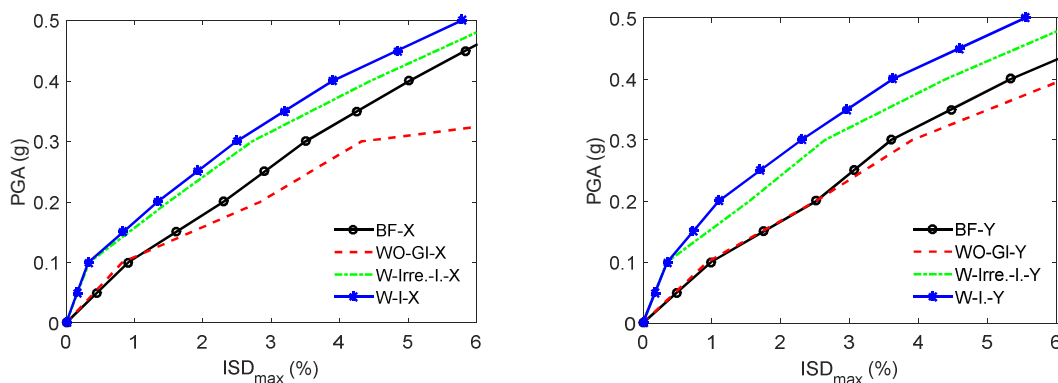
Figure 8.20 – Comparative mean IDA curves for MRT-5 with different structural configurations in X and Y directions, respectively

8.4.3.2.2   Influence of number of storeys

The vulnerability of the prototype MRT building initially designed for three storeys and later modified by adding more storeys was investigated through the mean IDA curves obtained. Figure 8.21 (a to d) presents the comparative mean IDA curves for the bare frame, soft-storey, irregularly infilled and fully infilled buildings, respectively, in both directions. The entire plot demonstrates that the vulnerability (in terms of inter-storey drift) increases with the number of storeys added when compared for the same IMs. For the considered infill walls arrangements, the IDA plots demonstrated similar behaviour of the mean IDA curves. In each configuration, all the considered storeys exhibit approximately the same mean drift until 0.1g PGA, and the difference widens with the increase in the IMs. The four-storey model always exhibits an intermediate building response between three and five storeys. The mean IDA curve for the bare frame and soft-storey buildings, at 0.3g PGA, illustrated that the vulnerability increased almost twofold, when modified from three to five storeys. Similarly, the vulnerability was increased by almost 50% when the

building was modified from three to four storeys. Similarly, in the case of both irregularly and regularly infilled buildings, at 0.3g PGA, the mean drift increases more than twofold when the number of storeys varies from three to five. Furthermore, when the number of storeys is modified from three to four, both infilled buildings exhibit drift that is almost 100% higher than the three-storey mean drift. This result revealed that fully and irregularly infilled buildings could also be the worst case scenario when subjected to higher IMs, as the susceptibility increased greatly with the increase in the number of storeys.

Summarizing all the above results and discussion, the conclusion can be drawn that the prototype MRT building reveals improved seismic performance when the building is infilled rather than as a bare frame. However, if it is built as soft-storey, it could potentially experience higher damage states and be highly susceptible to partial collapse and collapse states. Also, if the same guideline-defined sections were utilized for five storeys, it is most likely that they would exhibit higher damage levels, and partial collapse to collapse states can be predicted beyond 0.3g PGA.
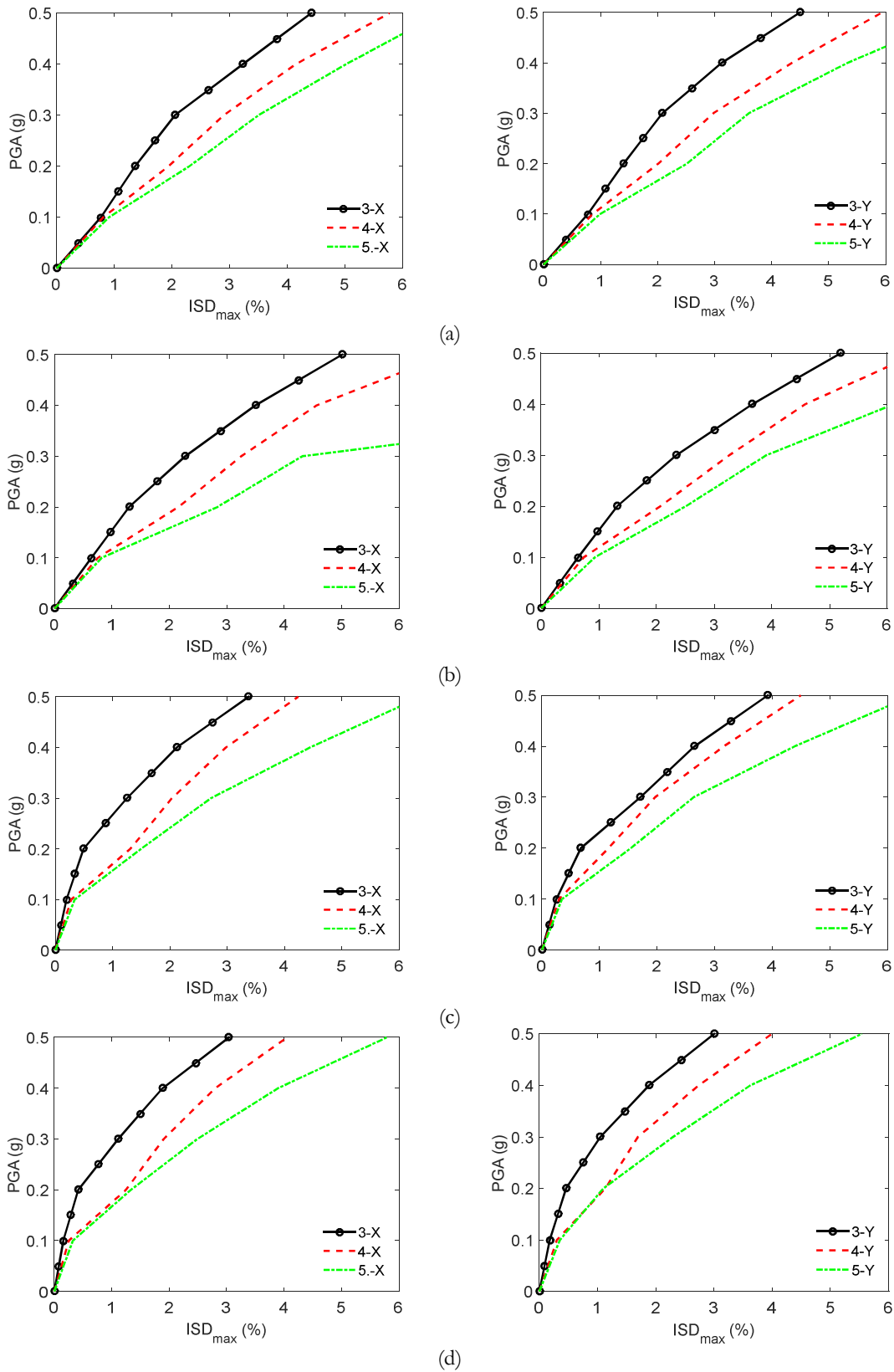
Figure 8.21 – Comparative mean IDA curves for MRT building of different storeys in X and Y directions; (a) BF, (b) WO-GI, (c) W-Irre.-I, and (d) W-I

8.4.3.3 Fragility curves

The fragility curve is a statistical tool that helps to understand the likely vulnerability of each building typology. In other words, the fragility of a structure is defined as the probability of exceeding a given damage state conditional on a certain curve of the intensity measure which accounts for the record–record variability. Here, fragility curves were developed considering the ISD_{max} as a building response parameter, as obtained from the nonlinear dynamic time history analyses. The damage states with respect to IMs were compared with the threshold drift proposed by Rossetto and Elnashai (2003) [202], as presented in Table 4.10. The building response in terms of ISD_{max} was assumed as a seismic demand and log-normally distributed. The procedure for the development of fragility curves was discussed in detail in Chapter 4. In this section, the probability of exceeding damage states influenced by the distribution of infill walls and due to the number of added storeys was investigated through fragility curves.

8.4.3.3.1   Influence due to different arrangements of infill walls

Figure 8.22 presents the fragility curves for the prototype MRT-3 building to examine the seismic performance of the prototype MRT building influenced by different dispositions of infill walls. The fragility curves for the BF and WO-GI buildings reveal that the peak slight and light damage states occur below 0.1g PGA, whereas they shift between 0.1g and 0.2g for irregularly and fully infilled buildings, respectively. In addition, the entire plots demonstrated the occurrence of peak moderate and extensive damage states but at different IMs. The probability of exceeding E, PC and C damage at 0.3g PGA for the BF building was approximately 96%, 21%, and 12%, respectively; for the WO-GI building it was 99%, 30%, and 16%, respectively; for the W-Irre.-I building it was 84%, 16%, and 9%, respectively; and in the case of the W-I building it was approximately 77%, 14%, and 8%, respectively. From the above discussion, it can be concluded that the addition of infill walls slightly improves lower damage states, whereas significant enhancement can be recorded for higher damage states. In addition, in most cases, both soft-storey and bare frame buildings exhibit comparable damage states but demonstrate a higher level of damage compared with infilled RC buildings. This reveals that the soft-storey and bare frame buildings were predicted to be much more vulnerable than the infilled buildings, considering the same structural sections and details specified by the guideline NBC 205: 2012 [21].
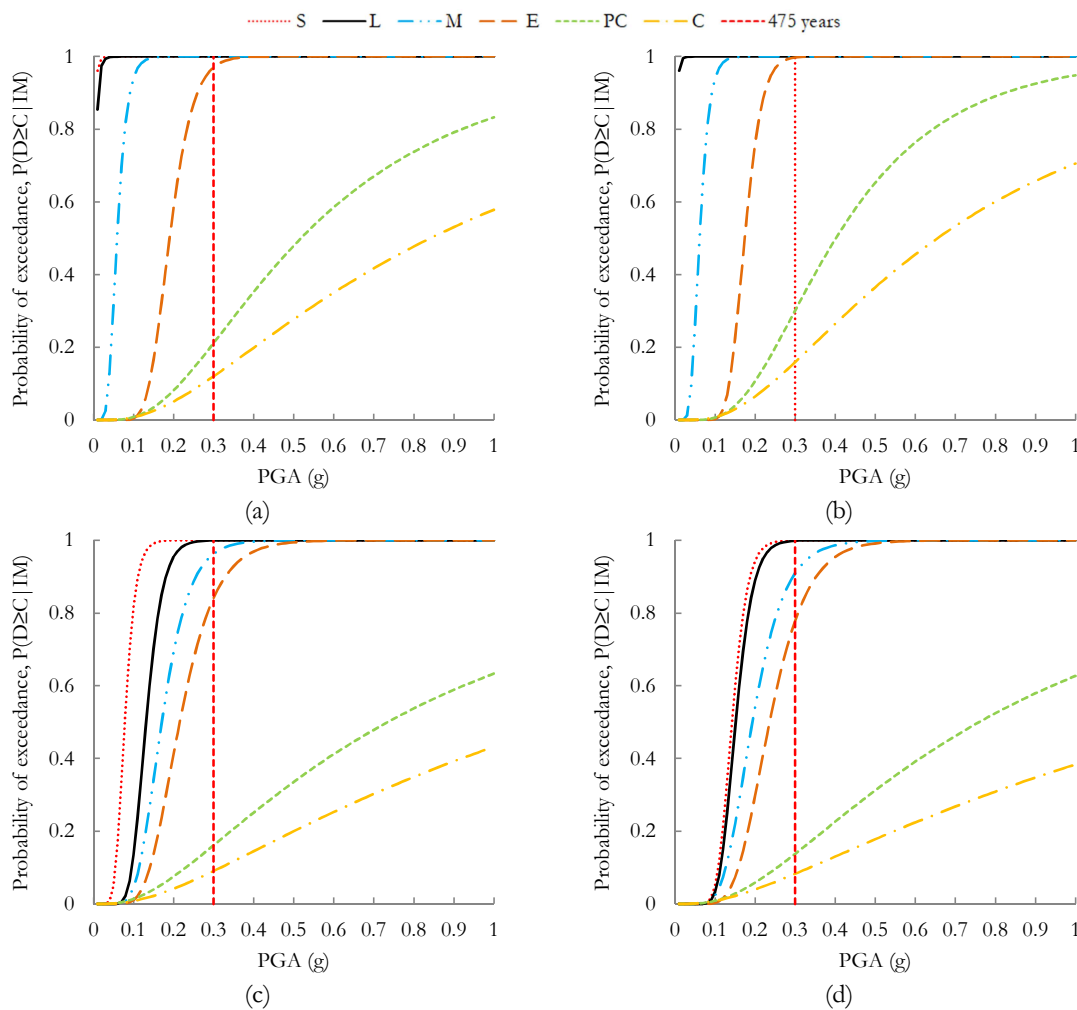
Figure 8.22 – Fragility curves for MRT-3 with various dispositions of infill panel; (a) BF, (b) WO-GI, (c) W-Irre.-I, and (d) W-I. S – slight, L – light, M – moderate, E – extensive, PC – partial collapse, C – collapse

In a similar approach, the vulnerability of the MRT-4 buildings was also investigated for the influence of different arrangements of infill walls with the help of fragility curves, as shown in Figure 8.23. Similarly to the MRT-3 building, the MRT-4 building with BF and WO-GI demonstrates the peak slight, light, moderate and extensive damage states between 0.1g and 0.3g PGA, whereas both the W-Irre.-I and W-I buildings exhibit their occurrence at larger PGA values, i.e. ranging from 0.2g to 0.6g. The probability of exceeding the E, PC and C states, at 0.3g PGA for the MRT-4 building, for BF corresponds to 99%, 27%, and 15%, respectively; for the WO-GI building was 100%, 34%, and 17% respectively; for the W-Irre.-I building was almost 82%, 19%, and 12%, respectively; and finally for the W-I building equals 79%, 19%, and 11%, respectively. Therefore, similar conclusions to those drawn for the MRT-3 building can be drawn, where the soft-storey building was found to be a much more vulnerable building type and the infilled building provides better seismic

performance. Furthermore, the observed probability of exceeding damage states revealed that the assigned structural section sizes and reinforcement details are inadequate for seismic consideration.
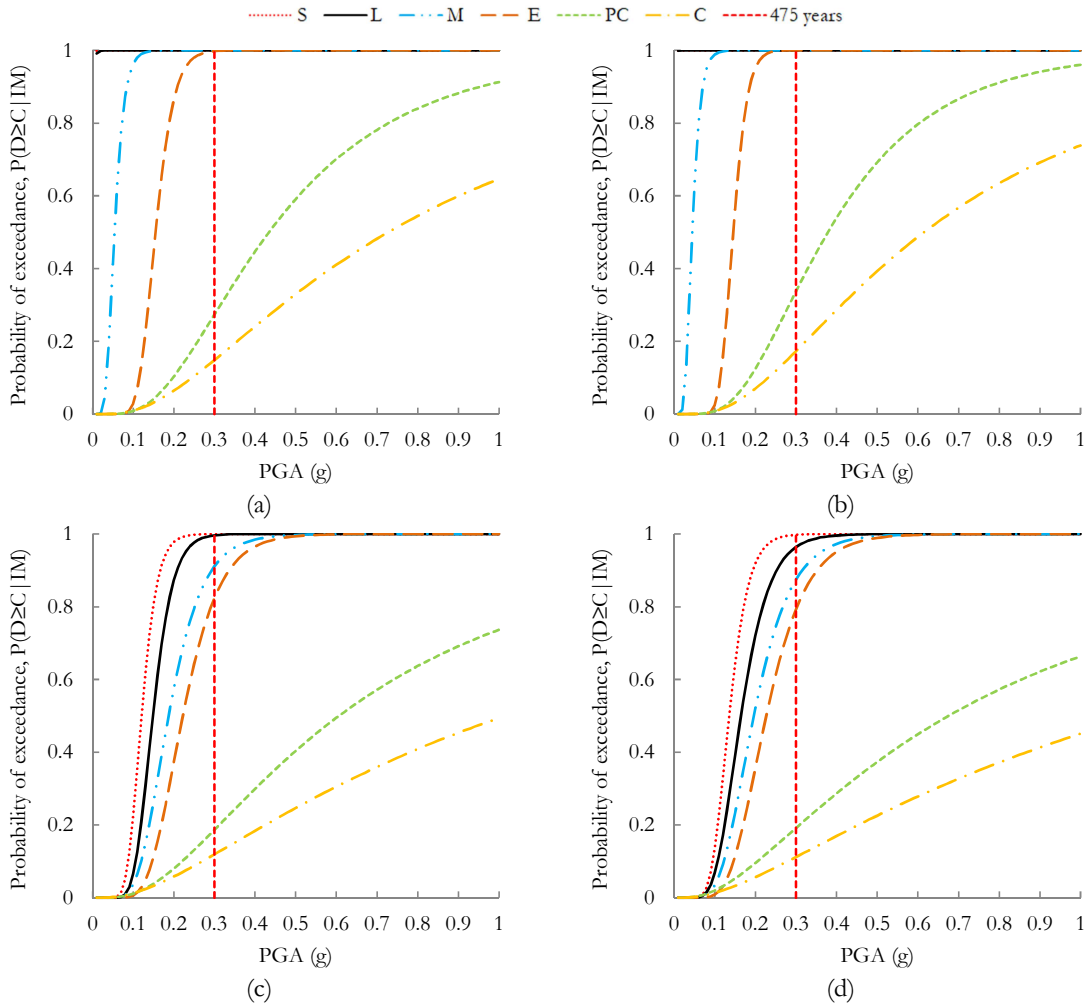
Figure 8.23 - Fragility curves for MRT-4 with various dispositions of infill panel; (a) BF, (b) WO-GI, (c) W-Irre.-I, and (d) W-I. S – slight, L – light, M – moderate, E – extensive, PC – partial collapse, C – collapse

Finally, the fragility curves for the MRT-5 building with various orientations of infill walls are presented in Figure 8.24. The entire plot illustrates that the peak slight, light, moderate and extensive damage states occur below 0.2g PGA for both the BF and WO-GI buildings, whereas, for the W-Irre-I and W-I buildings, they range between 0.1g and 0.6g. Similarly, for the infilled RC buildings, the higher probability of exceedance reveals that it is most likely that infill walls have an extensive risk of collapse damage below 0.3g PGA. Remarkably, both BF and WO-GI demonstrate comparable damage states for all IMs. The probability of exceeding E, PC and C damage for the MRT-5 building, at 0.3g PGA: for the BF corresponds to 100-17%; for the WO-GI building is in the range 100-21%; for the

W-Irre.-I building, varies from 86-17%; and for the W-I building, ranges from 80 to 27%. From all the results obtained and the discussion, it can be concluded that the soft-storey and bare frame buildings were found to exhibit poor seismic performance and should thus be considered the most vulnerable building types. By contrast, infilled RC buildings exhibit better seismic performance, but the higher damage states with reference to the higher IMs reveal that the assigned structural sections and reinforcement details were observed to be inadequate.
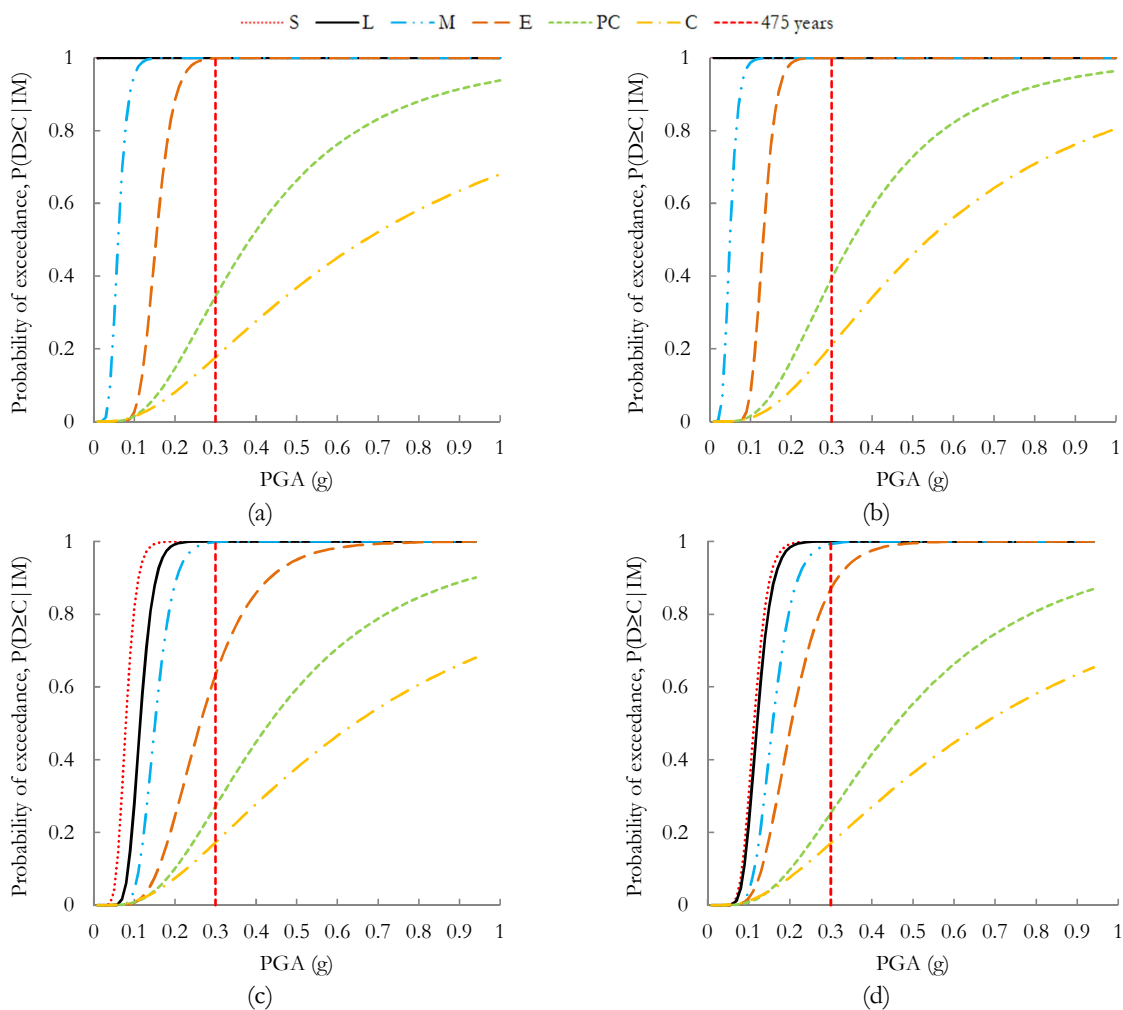
Figure 8.24 - Fragility curves for MRT-5 with various dispositions of infill panel; (a) BF, (b) WO-GI, (c) W-Irre.-I, and (d) W-I. S – slight, L – light, M – moderate, E – extensive, PC – partial collapse, C – collapse

The influence of the infill walls on the MRT-3 prototype building can be simply and clearly interpreted by comparing the various infill walls configurations (BF, WO-GI, W-Irre.-I, and W-I) considering higher damage states. Figure 8.25 presents the fragility curves for the three-storey MRT building. Overall, the plots demonstrated the soft-storey building to be the most susceptible, as expected and also as concluded in the above sections. Remarkably,

both the W-Irre.-I and W-I buildings display a similar conditional probability of exceedance. In addition, no significant improvement was attained in reducing the probability of extensive damage, but the failure probability of collapse was reduced to one half when the building was fully and irregularly infilled. The probability of exceeding collapse, at 0.3g PGA, for the MRT-3 building with BF, WO-GI, W-Irre.-I and W-I was approximately 12%, 16%, 9% and 8% respectively.
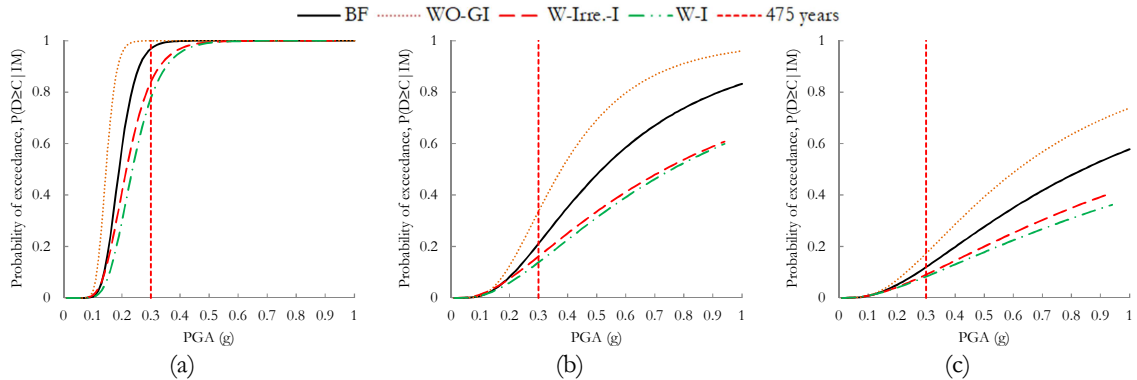
Figure 8.25 – Comparative fragility curves for MRT-3 building typology for different damage states; (a) Extensive, (b) Partial collapse, and (c) Collapse

In a similar manner, Figure 8.26 presents the comparative fragility curves for the MRT-4 building to examine the influence of the various arrangements of infill wall on the building seismic performance. It was observed that the soft-storey building is most likely to have a higher failure probability for the same PGA, as expected. In the case of extensive damage, both the bare frame and soft-storey buildings, and the fully and irregularly infilled buildings have relatively similar probabilities of exceedance. When the buildings were infilled, it was recorded that the extensive damage, at 0.3g PGA, was reduced by 20%, whereas partial collapse and collapse reduced by almost 80% and 50%, respectively.
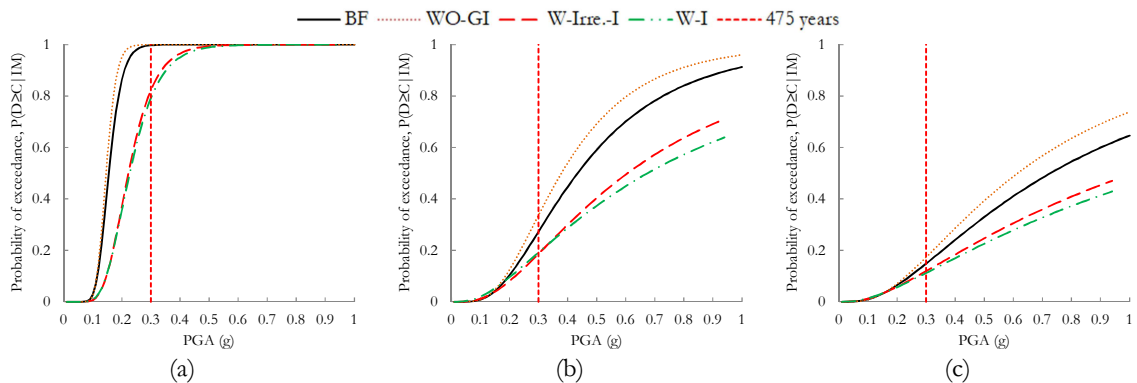
Figure 8.26 - Comparative fragility curves for MRT-4 building typology for different damage states; (a) Extensive, (b) Partial collapse, and (c) Collapse

Furthermore, Figure 8.27 presents the comparative fragility curves for the MRT-5 building, illustrating the level of failure probability, which can be reduced with the addition of infill walls throughout. The probability of exceeding extensive damage, at 0.3g PGA, was reduced by almost 35% and 15% when fully and irregularly infilled, respectively. In the case of partial collapse, both the soft-storey and bare frame buildings, and the fully and irregularly infilled buildings have almost the same failure probability. Furthermore, the entire building configuration reveals a quite similar failure probability of collapse, at 0.3g PGA, such that the failure can be reduced by only 3% for infilled buildings compared to soft-storey. This shows that the potential collapse of the MRT-5 building is comparable for all the considered infill wall configurations. Therefore, the infill walls have an insignificant influence for higher IMs, so the vulnerability increased when storeys were added to the initially designed three storeys.
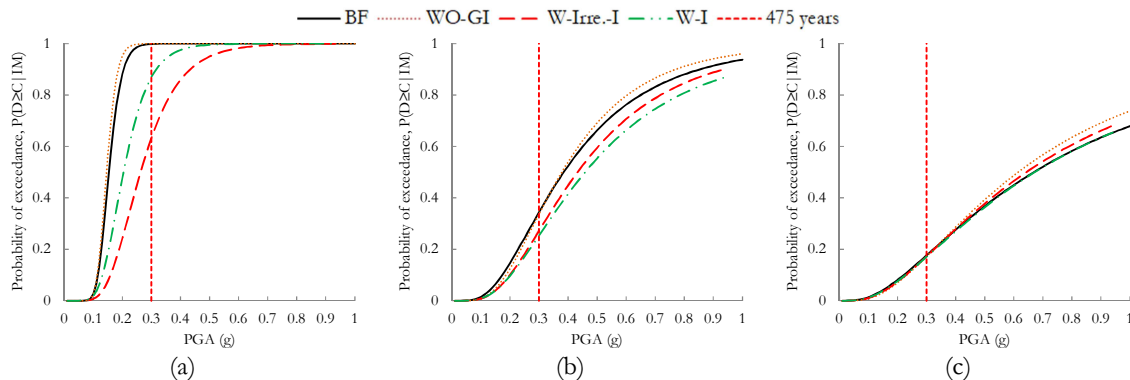
Figure 8.27 - Comparative fragility curves for MRT-5 building typology for different damage states; (a) Extensive, (b) Partial collapse, and (c) Collapse

8.4.3.3.2   Influence of number of storeys

This section intends to determine the variation in the probability of failure as a result of the number of storeys added beyond the initially designed three storeys. Figure 8.28 presents the fragility curve for the bare frame building. As expected, the maximum failure probability increased with the number of added storeys. For extensive damage, the four- and five-storey buildings have almost the same probability of failure, at 0.3g PGA, which is almost 10% greater than for three storeys. In the case of partial collapse, the failure probability, at 0.3g PGA, was almost doubled when the storeys increased from three to five. Finally, the probability of collapse, at 0.3g PGA, was increased by almost 10% and 20% with the increase to four and five storeys, respectively.
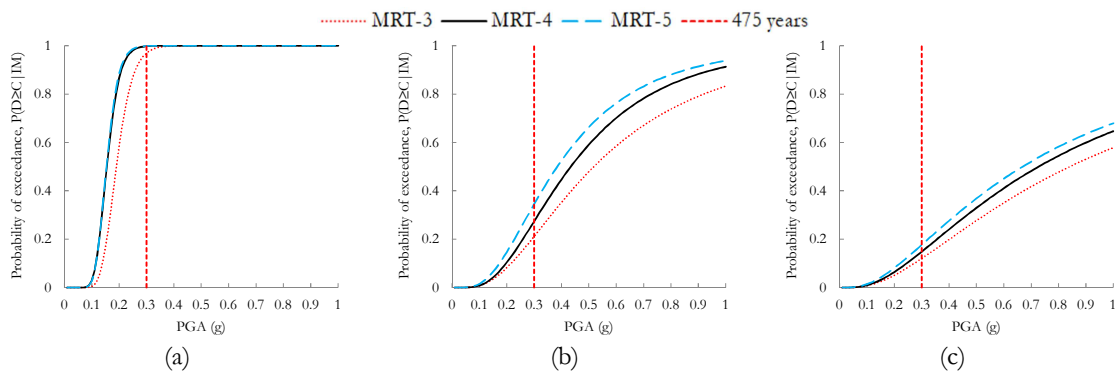
Figure 8.28 - Comparative fragility curves for BF due to addition of number of storey in MRT building for different damage states; (a) Extensive, (b) Partial collapse, and (c) Collapse

Figure 8.29 presents the comparative fragility curves for a soft-storey building influenced by the number of storeys added. Overall, the plots show a comparable failure probability for all storeys. For extensive damage, all the different storey numbers have peak exceedance at 0.3g PGA. The probability of partial collapse increased by almost 15% and 25% when the number of storey increased to four and five, respectively. Furthermore, the probability of collapse, at 0.3g PGA, increased by almost 5% and 20% when the number of storey increased to four and five, respectively.
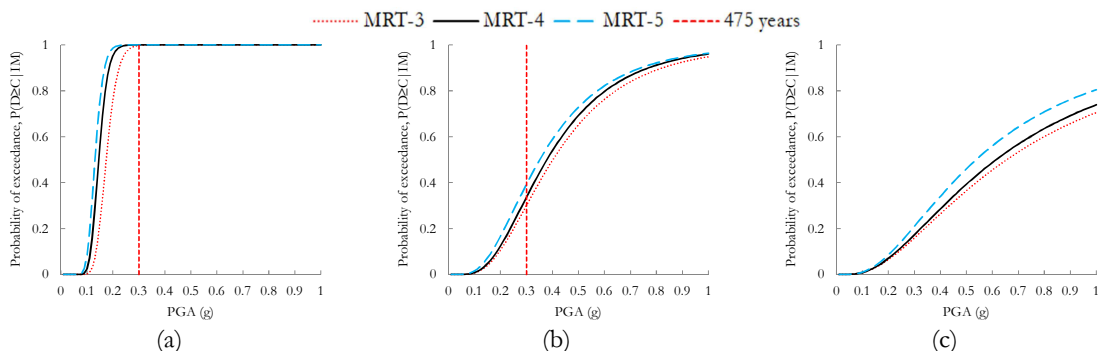
Figure 8.29 – Comparative fragility curves for WO-GI due to addition of number of storey in MRT building for different damage states; (a) Extensive, (b) Partial collapse, and (c) Collapse

Figure 8.30 demonstrates the comparative fragility curves for the irregularly infilled building influenced by the number of storeys added. Both the four- and five-storey buildings have almost the same probability of failure, at 0.3g PGA, which increased by almost 30% compared with three storeys. In the case of partial collapse, at 0.3g PGA, the five- and four-storey buildings increased the vulnerability by about 55% and 20%, respectively. Furthermore, the probability of collapse, at 0.3g PGA, increased by nearly 80% and 30% for five and four storeys, respectively.

(a)   (b)   (c)
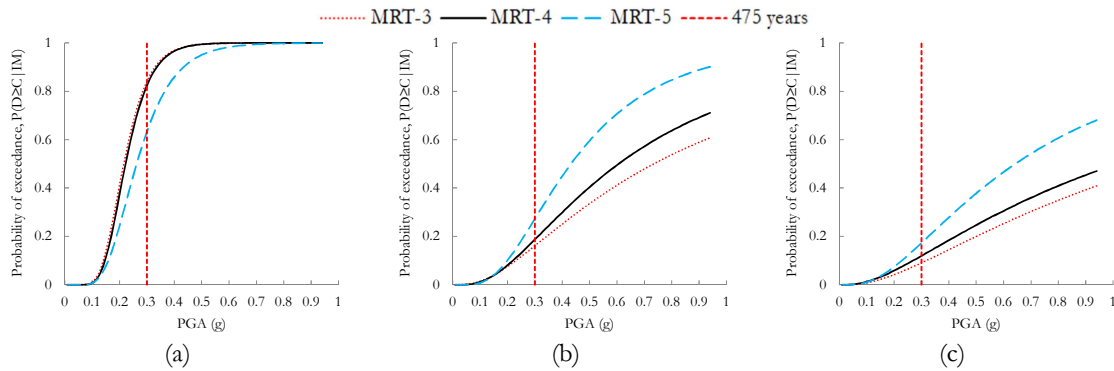
Figure 8.30 - Comparative fragility curves for W-Irre.-I due to addition of number of storey in MRT building for different damage states; (a) Extensive, (b) Partial collapse, and (c) Collapse

Furthermore, Figure 8.31 illustrates the comparative fragility curves for the fully infilled buildings to investigate the probability of exceeding the damage states influenced by the number of storeys added. For the extensive damage state, the various storey numbers exhibit a similar probability of failure. For the four- and five-storey building, the probability of failure for partial collapse, at 0.3g PGA, was increased by almost 25% and 50%, respectively. Similarly, the failure probability in case of collapse, at 0.3g PGA, was increased by almost 60% and 40% when the number of storey increased to five and four, respectively.

(a)   (b)   (c)
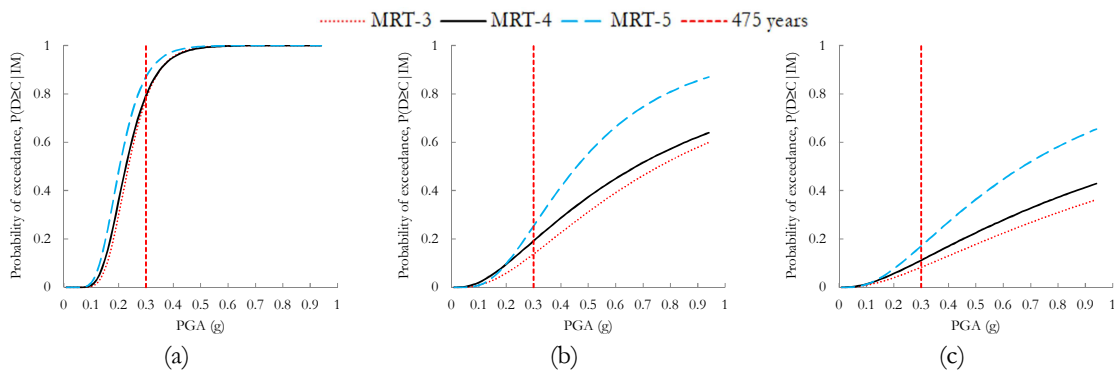
Figure 8.31 - Comparative fragility curves for W-I due to addition of number of storey in MRT building for different damage states; (a) Extensive, (b) Partial collapse, and (c) Collapse

8.5   Conclusions

The prototype MRT building initially designed and detailed for three storeys was later modified with a number of added storeys and also different configurations of infill walls throughout to investigate its influence on the seismic performance of the building before and after the modifications. The various findings obtained from the linear to nonlinear dynamic time history analyses are as follows:

- The application of infill walls was found to increase the fundamental frequencies by almost 4 times compared to the bare frame building. In addition, the frequencies decreased with the increase in the number of storeys, and reduced by almost 25% and 50% for four and five storeys, respectively.

- The infilled frame increased the global building stiffness, such that the increases for three, four and five storeys were almost 4–20, 6–21 and 8–25 times, respectively, more than the corresponding bare frame building.

- The addition of infill walls also increases the strength capacity and the maximum was recorded for fully infilled buildings. It increased by nearly 4 times compared to the bare frame in both directions. The maximum base shear capacity does not change with the number of storeys added.

- The addition of infill walls minimized or largely eliminated a single drift concentration as recorded in soft-storey building. Infill walls not only reduce the inter-storey drift but also uniformly distribute drift throughout.

- At 0.3g PGA, fully infilled building was recorded to reduce the maximum inter-storey drift by almost 4 times in comparison to soft-storey building.

- When the number of storey increased from three to five in the case of the soft-storey building configuration, the inter-storey drift increased by almost 100% and 20% in the X and Y directions, respectively. The drift increased more than twofold in both directions for irregularly infilled, and 2-3 times in the case of fully infilled buildings, whereas only a slight increase in inter-storey drift was recorded when the number of storey increased from three to four.

- Larger scattering of the inter-storey drift was observed with the added number of storeys. In the case of fully infilled, the three-storey building was observed to

behave elastically until 0.4g PGA, whereas in the case of five storeys, it behaves elastically until 0.2g PGA. From this it can be concluded that the vulnerability increases with the increase in the number of storeys and this holds true for the considered infill wall configurations.

- For three-storey building, the partial collapse and collapse states, at 0.3g PGA, were reduced to below half for fully and irregularly infilled compared to the bare frame. For four storeys, the partial collapse and collapse damage was reduced by almost 80% and 50%, respectively. Furthermore, for the five-storey building, the extensive damage was reduced by almost 35% and 15% for the regularly and irregularly infilled buildings, respectively.

- For the bare frame and soft-storey buildings, the probability of exceedance does not vary significantly when the storeys increase from three to five. However, the vulnerability increased in the case of irregularly infilled buildings, where the partial collapse probability, at 0.3g PGA, was increased by almost 55% and 20% for five and four storeys, respectively. Similarly, the collapse probability was increased by 80% and 30% for five and four storeys, respectively, compared with three storeys. Similar conclusions were also obtained for the fully infilled building, where the failure probability of partial collapse, at 0.3g PGA, increased by almost 25% and 50% for four and five storeys, respectively and total collapse by 40% and 60% for four and five storeys, respectively.

Chapter 9.

Final comments and Future Research

The main scope of the present thesis was to give an additional contribution to the study of the seismic performance of the existing RC buildings in Nepal, built based on three different approaches. The research was also set to explore the influence of solid infill walls on the seismic behaviour of these RC building, which is being neglected in the actual design guidelines, and details. The seismic assessment was carried out through the selection of three storeys bare frame building, later investigated through the adoption of different dispositions of the solid infill walls, representing common building practices in Nepal. A few open questions motivated the present study; namely: the need for designer consider the effect of the infill walls in new buildings and in the assessment of existing ones, to know the vulnerability of existing RC buildings and if there are ways to mitigate the consequences in future earthquakes, what is the potential cost, and finally to verify the RC buildings behaviour designed according to the revised NBC 205: 2012.

9.1 Main Conclusions

9.1.1 Field survey and vulnerability assessment of the existing RC buildings

A total of six existing RC buildings were selected following the reconnaissance survey after Gorkha earthquake, representing three main design approaches, such as non-engineered (as CCP1 and CCP2), pre-engineered (as MRT1 and MRT2) and well-designed (as WD1 and WD2). The seismic performance of these selected buildings was investigated under nonlinear static and dynamic time history analyses. The main conclusions drawn from field survey and experimental tests and numerical analyses are summarized as follows:

- The collapse of the RC structures as observed after Gorkha earthquake in Nepal were mostly associated with non-engineered buildings and few pre-engineered buildings. Most of the failure mechanisms were related with irregular distribution of solid infill walls in the RC framed buildings, i.e. mostly soft-storey failure, and followed by pounding, a dominant collapse mechanism, and other includes the shear failure in column and short-column failure.

- Most of the non-engineered buildings having regular distribution of solid infill walls presented only minor damage in the infill walls without any structural damage.

- The parametric study performed on the existing buildings revealed that concrete strength and column sections have a greater influence in global building behaviour in case of bare frame building, whereas in case of infilled buildings, its influence was observed to be irrelevant and the building response was found to be governed by the properties of infill wall (mainly Young's modulus).

- Addition of infill wall considerably increases both stiffness and strength capacity, the increase in stiffness and maximum base shear capacity was almost 3-10 times and 3-4 times, respectively, in comparison to bare frame building.

- A single drift concentration mainly in the soft-storey building was eliminated or minimized with the addition of solid infill wall, such that uniform drift profile can be attained for lower to medium magnitude earthquakes. This concludes that the addition of infill walls could uniformly distribute the stiffness and strength throughout.

- The statistical distribution of the inter-storey drift for the bare frame building illustrates that both bare frame and soft-storey buildings exhibits comparatively higher drift compared to the infilled buildings, when compared to same IMs. In addition, the bare frame and soft-storey buildings were recorded to behave elastically until 0.1g PGA, whereas 0.3g PGA in case of infilled buildings. This concludes that infill wall can acts as one of the strengthening techniques if other uncertainty parameters related to infill walls were assumed to be ideal.

- The soft-storey and bare frame buildings showed relatively higher probability of failure for the selected damage states as compared to the infilled buildings, such that the superior seismic performance can be attained with infill walls throughout.

9.1.2 Seismic performance of the existing buildings after retrofit and cost-benefit analysis

As discussed above, the existing case studies non- and pre-engineered buildings demonstrated poor seismic performance. Therefore, these structures were strengthened with the common practice retrofit techniques with the objective of enhancing the seismic performance. In addition to the seismic performance improvement, the study also intends to identify and select more economic feasible retrofit techniques performed through series

of probabilistic cost-benefit analyses and sensitivity analyses. The main conclusions obtained are summarized as follows:

- The addition of retrofit techniques on the existing buildings not only reduces the ISD_{max} to minimum values but also uniformly distribute throughout. This revealed that the proper strengthening selections, locations, numbers and section details along the building can uniformly distribute the global building stiffness and strength throughout.

- A narrow dispersion of inter-storey drift was recorded after the introduction of retrofit measures, such that the elastic behaviour can be extended for larger IMs. All of the retrofit measures were found to be effective in enhancing the seismic performance of the selected buildings, but the steel bracing was observed to be more efficient, followed by the RC shear wall and concrete column jacketing.

- All of the retrofit measures recorded only a slight improvement for lower damage states, such as slight and light for the entire selected non- and pre-engineered buildings, while a considerable improvement can be recorded for higher damage states, i.e. extensive, partial collapse and collapse. The probability of partial collapse and collapse states can be theoretically reduced to null using steel bracing. In most of the case study buildings, the steel bracing was found to be much more effective in reducing such failure probabilities.

- The maximum EAL occurs for lower IMs for the existing buildings with and without retrofit measures. This concluded that the maximum EAL is most likely due to frequent earthquakes of lower to moderate magnitude earthquakes rather than occasional earthquakes of higher magnitude, which occurs once in the life time of the building structures.

- The risk curves illustrate that the LCL for the existing CCP1, CCP2, MRT1 and MRT2 buildings having 0.4% annual probability of exceedance was approximately $ 450,000, $ 950,000, $ 3,600,000, and $ 2,600,000, respectively. This was many folds higher compared to the replacement cost of the respective buildings and decreases with increase in annual probability of exceeding. These unpredictable and unexpected losses can be significantly reduced with the addition of retrofit measures, such that the LCL for the CCP1, CCP2, MRT1,

and MRT2 buildings was limited to approximately $ 55,000, $ 115,000, $ 80,000, and $ 340,000, respectively.

- The probabilistic cost-benefit analysis concluded that a positive return in investment can be attained considering the service life of the building after retrofit as 25 years and 10% p.a. discount rate. The CBR value for the CCP1 building with jacketing, bracing, and shear walls: was approximately 1.37, 1.8, and 2.43, respectively; for the CCP2 building corresponds 3.7, 4.7, and 5.7, respectively; for the MRT1 building was about 13.65, 16.8, and 19, respectively; and for the MRT2 building was nearly 5.05, 5.73, and 6.9, respectively.

- All of the retrofit techniques adopted in the case study buildings were economically feasible, but comparative CBR study revealed that RC shear walls as the most economic beneficial.

- The sensitivity analysis results demonstrated that the higher CBR values were observed for the increase in the service life of the structures or lowering the discount rate and vice-versa. Initially for few years a negative CBR was recorded, is most likely due to the cost of retrofit was greater than the benefit obtained from its intervention. For all the case-study buildings, a positive payback in the investment was achieved in early years than initially expected.

9.1.3 Seismic performance assessment of a prototype building designed based on revised NBC 205: 2012 guidelines

A prototype MRT building was defined initially designed and detailed for three-storey based on the revised NBC 205: 2012 guideline. The primary objective of the study was to investigate the seismic performance of the building considering two conditions: i) the influence due to different arrangements of infill wall, and ii) influence due to added number of storeys. The structural sections and reinforcement details provided in the design guideline has clearly stated for the bare framed RC buildings; hence, the conclusion was discussed comparing each criteria with the bare frame considered as the original RC building highlighted as follows.

- The addition of infill wall in the building changes the dynamic behaviour of the RC frame buildings. It increases the initial stiffness and strength capacities but reduces the ductility as compared to the bare frame.

- Both the soft-storey and bare frame buildings exhibits comparable inter-storey drift, but a single storey drift concentration was recorded in the soft-storey building and was improved through infill wall addition, such that uniform drift profile was attained throughout.

- For lower IMs, i.e. until 0.3g PGA the infilled buildings minimized the maximum inter-storey drift by almost 4 times relatively compared to bare framed and soft-storey buildings.

- The IDA curves for soft-storey and bare frame buildings illustrated comparable mean inter-storey drift, and also irregularly and fully infilled buildings showed similar mean inter-storey drift but for low IMs. For higher PGA, the irregularly infilled exhibits slightly higher mean drift compared to fully infilled building.

- The probability of peak lower damage states was slightly improved after the intervention of infill walls (fully and irregularly) relatively compared to bare frame and soft-storey buildings. However, a significant improvement can be recorded for extensive to collapse states, such that the failure probabilities were considerably reduced for regularly distributed solid infill walls.

- Although the seismic performance of the building could be enhanced through addition of solid infill wall, but the level of recorded damages for higher IMs concluded that the structural sections specified by the MRT guidelines found to be inadequate. Thus the present study recommends and motivates the design professional and concerned authorities to the need solid infill wall consideration in the design of RC frame buildings.

9.2   Recommendations for Future Developments

This research was primarily focused on the influence of infill walls on the RC framed structures and seismic performance assessment of the existing buildings, its retrofit and cost-benefit analysis, and further investigations on the performance assessment of designed RC buildings based on revised NBC 205: 2012 due to various orientations of infill walls and added storeys. However, this research requires numerous improvements that enhance the accuracy and reliability of the obtained results, as various parameters and methods were not able to address in this dissertation. The further research should be performed as described herein:

- The research was performed for six existing buildings only, hence, the research can be extended for large number of buildings and it would be better, if the results could be generalized for each set of building categories.

- Further research should be experimental investigated on the full scaled solid infill walls encased in the portal frame and examine in- and out-of-plane behaviour of infill walls. Thus obtained result should be initially utilized for model calibration.

- With respect to the modelling strategy, the present research could not model directly the damages observed in the infill walls, could not capture the out-of-plane failure of the infill walls, could not model damages associated at the beam-column and column-column joint, and could not account the shear failure in the column that might occur in the columns and so on. Hence, it is necessary to consider the stated problems in the future numerical model.

- The strengthening of the existing buildings was performed considering only three methods, so it is recommended to develop more local based approach, which utilizes the available local materials and techniques and finally its experimental test for verification.

- The cost-benefit analysis was limited to the structural damages only, hence it is highly recommended to investigate for the acceleration and drift sensitive non-structural elements and also the value of life should be considered.

- A simplified probabilistic cost-benefit model should be developed, so it can be an easy tool for engineers that will help to convince owners to retrofit or demolish the existing buildings.

- The prototype building selected should be extended to common construction building, i.e. the analysis should be extended for building geometry with large eccentricity and different geometry, such that only one bay in one direction and large number of bays in other direction, change in height of the storey, and so on.

References

[1] K. Oven, D. Milledge, A. Densmore, H. Jones, S. Sargeant, and A. Datta, "Earthquake science in DRR policy and practice in Nepal," retrieved from https://www.odi.org/sites/odi.org.uk/files/resource-documents/10638.pdf (accessed 1st September 2016).

[2] H. Chaulagain, "Seismic assessment and retrofitting of existing buildings in Nepal," PhD, Civil Department, University of Aveiro, 2015.

[3] BCDP, "Building Code Development Project: Seismic hazard mapping and risk assessment for Nepal," K. UNDP/UNCHS (Habitat) Subproject: NEP/88/054/21.03. Ministry of Housing and Physical Planning, Ed., ed, 1994.

[4] EERI, "EERI earthquake reconnaissance team report: M7.8 Gorkha, Nepal Earthquake on April 25, 2015 and its Aftershocks," Oakland, California, 2016.

[5] A. Dixit, L. Dwelley-Samant, M. Nakarmi, S. B. Pradhanang, and B. Tucker, "The Kathmandu valley earthquake risk management project: an evaluation," *Asia Disaster Preparedness Centre: http://www. iitk. ac. in/nicee/wcee/article/0788. pdf,* 2000.

[6] List of earthquakes in Nepal. Retrieved from https://en.wikipedia.org/wiki/List_of_earthquakes_in_Nepal (Accessed November 23rd, 2016)

[7] A. B. Mehrabi, P. Benson Shing, M. P. Schuller, and J. L. Noland, "Experimental evaluation of masonry-infilled RC frames," *Journal of Structural Engineering,* vol. 122, pp. 228-237, 1996.

[8] H. Varum, "Seismic assessment, strengthening and repair of existing buildings," PhD, Civil Department, Universidade de Aveiro, 2003.

[9] M. Dolšek and P. Fajfar, "The effect of masonry infills on the seismic response of a four-storey reinforced concrete frame — a deterministic assessment," *Engineering Structures,* vol. 30, pp. 1991-2001, 2008.

[10] R. Dumaru, H. Rodrigues, A. Furtado, and H. Varum, "Seismic vulnerability and parametric study on a bare frame building in Nepal," *Frontiers in Built Environment,* vol. 2, p. 31, 2016.

[11] F. J. Crisafulli, "Seismic behaviour of reinforced concrete structures with masonry infills," PhD, Department of Civil Engineering, University of Canterbury, 1997.

[12] H. M. A. Mohamed, "Seismic risk assessment of reinforced concrete frames with masonry infill," PhD, Department of Civil Engineering, Universidade do Porto, 2017.

[13] G. Aguilar, R. Meli, and A. R. Vasquez-del-Mercado, "Influence of horizontal reinforcement on the behavior of confined masonry walls," presented at the 11th World Conf. Earthquake Engineering, Acapulco, paper no. 1380, 1996.

[14] S. Alcocer and R. Meli, "Test program on the seismic behaviour of confined masonry walls," *The Masonry Soc. J.* (Boulder) 13 (2)*, pp. 68-76, 1995.

[15] R. Meli, "Behavior of masonry walls under lateral loads," *presented at the Fifth world Conference on Earthquake Engineering,* Tokyo-Kyoto, Japan, 1973.

[16] K. Yoshimura, K. Kikuchi, Z. Okamoto, and T. Sanchez, "Effect of vertical and horizontal wall reinforcement on seismic behaviour of confined masonry walls," presented at the 11th World Conf. Earthquake Engineering, Acapulco, 1996.

[17] M. Tomazevic and I. Klemenc, "Behavior of confined masonry walls," *Earthquake Engineering and Structural Dynamics,* vol. 26, pp. 1059-1071, 1997.

[18] S. Pujol, A. Benavent-Climent, M. E. Rodriguez, and J. P. Smith-Pardo, "Masonry infill walls: an effective alternative for seismic strengthening of low-rise reinforced concrete building structures," in *The 14th World Conference on Earthquake Engineering*, pp. 1-8, 2008.

[19] 2015 Nepal earthquake: Facts, FAQ, and how to help. Retrieved from https://www.worldvision.org/disaster-relief-news-stories/2015-nepal-earthquake-facts, 2016.

[20] NBC 205:1994 (1994). Mandatory Rules of Thumb, Reinforced Concrete Buildings without Masonry Infill. HMG/Ministry of Housing and Physical Planning, Department of Building, Kathmandu, Nepal, 1994.

[21] NBC 205:2012. Mandatory Rules of Thumb, Reinforced Concrete Buildings without Masonry Infill. HMG/Ministry of Housing and Physical Planning, Department of Building, Kathmandu, Nepal, 2012.

[22] Seismosoft (2006), SeismoStruct - a computer program for static and dynamic nonlinear analysis of framed structures [online]," available from URL: http//www.seismosoft.com.

[23] H. Chaulagain, H. Rodrigues, J. Jara, E. Spacone, and H. Varum, "Seismic response of current RC buildings in Nepal: a comparative analysis of different design/construction," *Engineering Structures,* vol. 49, pp. 284-294, 2013.

[24] NBC 000:1994 (1994). Requirements for state-of-the art design an introduction. HMG/Ministry of Housing and Physical Planning, Department of Building, Kathmandu, Nepal, 1994.

[25] IS 15988:2013. Preliminary seismic evaluation aid for reinforced concrete framed structures. Bureau of Indian Standards, ManakBhavan, 9 Bahadur Shah ZafarMarg, New Delhi, 2013.

[26] T. Pokharel and H. M. Goldsworthy, "Lessons learned from the Nepal earthquake 2015," *Australian journal of structural engineering,* vol. 18, pp. 11-23, 2017.

[27] K. Goda, T. Kiyota, R. M. Pokhrel, G. Chiaro, T. Katagiri, K. Sharma*, et al.*, "The 2015 Gorkha Nepal earthquake: insights from earthquake damage survey," *Frontiers in Built Environment,* vol. 1, p. 8, 2015.

[28] R. M. Parameswaran, T. Natarajan, K. Rajendran, C. Rajendran, R. Mallick, M. Wood*, et al.*, "Seismotectonics of the April–May 2015 Nepal earthquakes: An assessment based on the aftershock patterns, surface effects and deformational characteristics," *Journal of Asian Earth Sciences,* vol. 111, pp. 161-174, 2015.

[29] N. P. Commission, "Nepal earthquake 2015: Post disaster needs assessment," *Vol. A: Key Findings. Government of Nepal, National Planning Commission,* 2015.

[30] IS 1893 (Part1):2002. Indian Standard Criteria for Earthquake Resistant Design Structures (fifth Revision). Bureau of Indian Standards, ManakBhavan, 9 Bahadur Shah ZafarMarg, New Delhi, 2002.

[31] D. C. Rai, "Review of documents on seismic evaluation of existing buildings," *Department of Civil Engineering, Indian Institute of Technology Kanpur India,* 2005.

[32] H. Varum, A. Furtado, H. Rodrigues, J. Dias-Oliveira, N. Vila-Pouca, and A. Arêde, "Seismic performance of the infill masonry walls and ambient vibration tests after the Ghorka 2015, Nepal earthquake," *Bulletin of Earthquake Engineering,* vol. 15, pp. 1185-1212, 2017.

[33] D. Gautam, H. Rodrigues, K. K. Bhetwal, P. Neupane, and Y. Sanada, "Common structural and construction deficiencies of Nepalese buildings," *Innovative Infrastructure Solutions,* vol. 1, p. 1, 2016.

[34] M. Shakya and C. K. Kawan, "Reconnaissance based damage survey of buildings in Kathmandu valley: An aftermath of 7.8 Mw, 25 April 2015 Gorkha (Nepal) earthquake," *Engineering Failure Analysis,* vol. 59, pp. 161-184, 2016.

[35] S. Mindess and J. F. Young, "Concrete Prentice-Hall," *Englewood Cliffs, NJ,* vol. 481, 1981.

[36] J.-C. Liu, M.-L. Sue, and C.-H. Kou, "Estimating the strength of concrete using surface rebound value and design parameters of concrete material," 淡江理工學刊, vol. 12, pp. 1-7, 2009.

[37] A. Brencich, G. Cassini, D. Pera, and G. Riotto, "Calibration and reliability of the rebound (Schmidt) hammer test," *Civil Engineering and Architecture,* vol. 1, pp. 66-78, 2013.

[38] F. Aydin and M. Saribiyik, "Correlation between Schmidt Hammer and destructive compressions testing for concretes in existing buildings," *Scientific Research and Essays,* vol. 5, pp. 1644-1648, 2010.

[39] A. De Sortis, E. Antonacci, and F. Vestroni, "Dynamic identification of a masonry building using forced vibration tests," *Engineering Structures,* vol. 27, pp. 155-165, 2005.

[40] S. S. Ivanovic, M. D. Trifunac, and M. Todorovska, "Ambient vibration tests of structures-a review," *ISET Journal of Earthquake Technology,* vol. 37, pp. 165-197, 2000.

[41] R. Marshall, L. Phan, and M. Celebi, "Full scale measurement of building response to ambient vibration and the Loma Prieta earthquake," in *Proceedings of 5th US National Conference on Earthquake Engineering*, vol. 11, pp. 661-670, 1994.

[42] V. R. Mclamore, G. C. Hart, and I. R. Stubbs, "Ambient vibration of two suspension bridges," *Journal of the Structural Division,* vol. 99, pp. 2567-2582 1900.

[43] C. Ventura, A. Felber, and S. Stiemer, "Experimental investigations of dynamics of Queensborough bridge," *Journal of performance of constructed facilities,* vol. 9, pp. 146-155, 1995.

[44] J. Rodrigues, R. Brincker, and P. Andersen, "Improvement of frequency domain output-only modal identification from the application of the random decrement technique," in *Proc. 23rd Int. Modal Analysis Conference, Deaborn, MI*, pp. 92-100, 2004.

[45] A. Cunha and E. Caetano, "Experimental modal analysis of civil engineering structures," pp. 12-20, 2006.

[46] P. Gueguen, M. R. Gallipoli, M. Navarro, A. Masi, C. Michel, B. Guillier*, et al.*, "Testing buildings using ambient vibrations for earthquake engineering: A European review.", *Second European Conference on earthquake engineering and seismology*, Istanbul Aug. 25-29, 2014.

[47] C. Koukoura, A. Natarajan, and A. Vesth, "Identification of support structure damping of a full scale offshore wind turbine in normal operation," *Renewable Energy,* vol. 81, pp. 882-895, 2015.

[48] R. Brincker, C. Ventura, and P. Andersen, "Damping estimation by frequency domain decomposition," in *19th International Modal Analysis Conference*, pp. 698-703, 2001.

[49] ARTeMIS Extractor Pro,"Structural Vibration Solutions," Aalborg, Denmark, 2009.

[50] IS 4326:1993. Code of practice for earthquake resistant design and construction of buildings [CED 39: Earthquake Engineering]. Bureau of Indian Standards, ManakBhavan, 9 Bahadur Shah ZafarMarg, New Delhi, 1993.

[51] IS 13920:1993. Ductile detailing of reinforced concrete structures subjected to seismic forces-code of practice. Bureau of Indian Standards, ManakBhavan, 9 Bahadur Shah ZafarMarg, New Delhi, 1993.

[52] IS 1786:1985. Specification for High Strength Deformed Steel Bars and Wires for concrete reinforcement. Bureau of Indian Standards, ManakBhavan, 9 Bahadur Shah ZafarMarg, New Delhi, 1985.

[53]   NBC 201:1994 (1994). Mandatory Rules of Thumb, Reinforced Concrete Buildings with Masonry Infill. HMG/Ministry of Housing and Physical Planning, Department of Building, Kathmandu, Nepal, 1994.

[54]   IS: 875 (Part1)-1987. Indian Standard Code of Practice for Design of loads (other than earthquake) for Buildings and Structures. Bureau of Indian Standards. Second Edition, 1987.

[55]   IS: 875 (Part2)-1987. Code of Practice for Design Loads (Other than Earthquake) for Buildings and Structures. Bureau of Indian Standards. Second Edition, 1987.

[56]   W. W. El-Dakhakhni, M. Elgaaly, and A. A. Hamid, "Three-strut model for concrete masonry-infilled steel frames," *Journal of Structural Engineering,* vol. 129, pp. 177-185, 2003.

[57]   A. Stavridis, "Analytical and experimental study of seismic performance of reinforced concrete frames infilled with masonry walls," PhD, Civil Department, University of California, San Diego, 2009.

[58]   P. Asteris, D. Kakaletsis, C. Chrysostomou, and E. Smyrou, "Failure modes of in-filled frames," *Electronic Journal of Structural Engineering,* vol. 11, pp. 11-20, 2011.

[59]   F. Thomas, "The strength of brickwork," *The Structural Engineer,* vol. 31, pp. 35-46, 1953.

[60]   S. Polyakov, "Masonry in framed buildings: An investigations into the strength and stiffness of masonry infilling," *Moscow (In English translation),* (1957).

[61]   S. Sachanski, "Analysis of earthquake resistance of frame buildings taking into consideration the carring capacity of the filling masonry," in *Proceedings of the 2nd World Conference on Earthquake Engineering,* vol. 138, pp. 1-15, 1960.

[62]   M. Holmes, "Steel frames with brickwork and concrete infilling," *proceedings of the Institution of civil Engineers,* vol. 19, pp. 473-478, 1961.

[63]   M. Holmes, "Combined loading on infilled frames," *Proceedings of the Institution of Civil Engineers,* vol. 25, pp. 31-38, 1963.

[64]   B. S. Smith, "Lateral stiffness of infilled frames," *Journal of the Structural Division,* vol. 88, pp. 183-226, 1962.

[65]   A. E. Fiorato, M. A. Sozen, and W. L. Gamble, "An investigation of the interaction of reinforced concrete frames with masonry filler walls," Retrieved from http://hdl.handle.net/2142/14303, 1970.

[66]   R. J. Mainstone and G. Weeks, "The influence of a bounding frame on the racking stiffness and strengths of brick walls: Building Research Station," pp. 165-171, 1972.

[67]   V. Bertero and S. Brokken, "Infills in seismic resistant building," *Journal of Structural Engineering,* vol. 109, pp. 1337-1361, 1983.

[68]   R. Zarnic and M. Tomazevic, "An experimentally obtained method for evaluation of the behavior of masonry infilled RC frames," in *Proceedings of the 9th World Conference on Earthquake Engineering,* vol. 6, pp. 163-168, 1988.

[69]   J. Dawe and C. Seah, "Out-of-plane resistance of concrete masonry infilled panels," *Canadian Journal of Civil Engineering,* vol. 16, pp. 854-864, 1989.

[70]   H. S. Lee and S. W. Woo, "Effect of masonry infills on seismic performance of a 3-storey R/C frame with non-seismic detailing," *Earthquake engineering & structural dynamics,* vol. 31, pp. 353-378, 2002.

[71]   A. Pinto, H. Varum and J. Molina, "Experimental assessment and retrofit of full-scale models of existing RC frames," *12th European Conference on Earthquake Engineering Paper Reference 855,* 2002.

[72] A. Ghobarah and K. El Mandooh Galal, "Out-of-plane strengthening of unreinforced masonry walls with openings," *Journal of Composites for Construction,* vol. 8, pp. 298-305, 2004.

[73] G. M. Calvi, D. Bolognini, and A. Penna, "Seismic performance of masonry-infilled RC frames: benefits of slight reinforcements," *Invited lecture to Sísmica,* vol. 6, pp. 14-16, 2004.

[74] C. G. Karayannis, D. Kakaletsis, and M. Favvata, "Behavior of bare and masonry infilled R/C frames under cyclic loading: Experiments and analysis," *WIT Transactions on The Built Environment,* vol. 81, pp. 429-438, 2005.

[75] S. Arulselvan and K. Subramanian, "Experimental investigation on three dimensional RC infilled frame–RC plane frame interactions with slab for seismic resistance," *American Journal of Applied Sciences,* vol. 5, pp. 328-333, 2008.

[76] D. J. Kakaletsis and C. G. Karayannis, "Experimental investigation of infilled reinforced concrete frames with openings," *ACI Structural Journal,* vol. 106, p. 132, 2009.

[77] S. Pujol and D. Fick, "The test of a full-scale three-story RC structure with masonry infill walls," *Engineering Structures,* vol. 32, pp. 3112-3121, 2010.

[78] A. Stavridis, I. Koutromanos, and P. B. Shing, "Shake-table tests of a three-story reinforced concrete frame with masonry infill walls," *Earthquake Engineering & Structural Dynamics,* vol. 41, pp. 1089-1108, 2012.

[79] J. Zovkic, V. Sigmund, and I. Guljas, "Cyclic testing of a single bay reinforced concrete frames with various types of masonry infill," *Earthquake engineering & structural dynamics,* vol. 42, pp. 1131-1149, 2013.

[80] M. Preti, L. Migliorati, and E. Giuriani, "Experimental testing of engineered masonry infill walls for post-earthquake structural damage control," *Springer,* vol. 13, pp. 2029-2049, 2014.

[81] A. Mansouri, M. S. Marefat, and M. Khanmohammadi, "Experimental evaluation of seismic performance of low-shear strength masonry infills with openings in reinforced concrete frames with deficient seismic details," *The Structural Design of Tall and Special Buildings,* vol. 23, pp. 1190-1210, 2014.

[82] V. Sigmund and D. Penava, "Influence of openings, with and without confinement, on cyclic response of infilled rc frames—an experimental study," *Journal of earthquake engineering,* vol. 18, pp. 113-146, 2014.

[83] S. Hak, P. Morandi, and G. Magenes, "Out-of-plane experimental response of strong masonry infills," in *2nd European Conference on Earthquake Engineering and Seismology*, 2014.

[84] S. H. Basha and H. B. Kaushik, "Behavior and failure mechanisms of masonry-infilled RC frames (in low-rise buildings) subject to lateral loading," *Engineering Structures,* vol. 111, pp. 233-245, 2016.

[85] A. Furtado, H. Rodrigues, A. Arêde, and H. Varum, "Experimental evaluation of out-of-plane capacity of masonry infill walls," *Engineering Structures,* vol. 111, pp. 48-63, 2016.

[86] S. Shan, S. Li, S. Xu, and L. Xie, "Experimental study on the progressive collapse performance of RC frames with infill walls," *Engineering Structures,* vol. 111, pp. 80-92, 2016.

[87] C. Zhai, J. Kong, X. Wang, and Z. Chen, "Experimental and finite element analytical investigation of seismic behavior of full-scale masonry infilled RC frames," *Journal of Earthquake Engineering,* vol. 20, pp. 1171-1198, 2016.

[88] R. Steeves, "In-plane behaviour of masonry infilled RC frames with interfacial gaps subjected to quasi-static loading," M. Tech Dissertation, Civil Department, Dalhousie University, 2017.

[89]   P. M. Pradhan, R. K. Maskey, and P. L. Pradhan, "Experimental study of partially masonry infilled reinforced concrete frame under lateral loading," in *Advanced Engineering Forum*, vol. 21, pp. 22-32, 2017.

[90]   P. B. Lourenço, "Computations on historic masonry structures," *Progress in Structural Engineering and Materials,* vol. 4, pp. 301-319, 2002.

[91]   B. S. Smith, "Model test results of vertical and horizontal loading of infilled frames," in *Journal Proceedings*, vol. 65, pp. 618-625, 1968.

[92]   R. J. Mainstone, "Summary of paper 7360. on the stiffness and strengths of infilled frames," *Proceedings of the Institution of Civil Engineers,* vol. 49, p. 230, 1971.

[93]   R. J. Mainstone, "Supplementary note on the stiffnesses and strengths of infilled frames: Building Research Establishment, Building Research Station," Paper 7360, pp. 57-90, 1974.

[94]   E. Bazan and R. Meli, "Seismic analysis of structures with masonry walls," in *Proc., 7th World Conf. on Earthquake Engineering*, vol. 5, pp. 633-640, 1980.

[95]   T. Nicola, C. Leandro, C. Guido, and S. Enrico, "Masonry infilled frame structures: state-of-the-art review of numerical modelling," *Earthquakes and Structures,* vol. 8, pp. 225-251, 2015.

[96]   T. Tassios, "Masonry infill and RC walls, (An invited state-of-the-art report)," in *Third International Symposium on Wall Structures*, 1984.

[97]   L. Te-Chang and K. Kwok-Hung, "Nonlinear behaviour of non-integral infilled frames," *Computers & structures,* vol. 18, pp. 551-560, 1984.

[98]   L. Decanini and G. Fantin, "Modelos simplificados de la mampostería incluida en porticos," *Caracteristicas de stiffnessy resistencia lateral en estado limite. Jornadas Argentinas de Ingeniería Estructural,* vol. 2, pp. 817-836, 1986.

[99]   H. Moghaddam and P. J. Dowling, "Earthquake resistant design of brick infilled frames," *Brick and Block Masonry (8th IBMAC) London, Elsevier Applied Science,* vol. 2, pp. 774-784, 1988.

[100]   T. Paulay and M. N. Priestley, "Seismic design of reinforced concrete and masonry buildings," Published by John Wiley & Sons, Inc., 1992.

[101]   A. J. Durrani and Y. Luo, "Seismic retrofit of flat-slab buildings with masonry infills," in *Technical Report*, ed: National Center for Earthquake Engineering Research, pp. 1-8, 1994.

[102]   R. Bennett, W. Fischer, R. Flanagan, and M. Tenbus, "Evaluation and analysis of the performance of masonary infills during the Northridge earthquake," Oak Ridge National Lab., TN (United States), Vol. 1, 1996.

[103]   A. Papaila, "Seismic fragility curves for reinforced concrete buildings," M. Tech Dissertation*,* University of Patrax, Greece, 2011.

[104]   P. M. Pradhan, "Equivalent strut width for partial infilled frames," *Journal of Civil Engineering Research,* vol. 2, pp. 42-48, 2012.

[105]   T. Turgay, M. C. Durmus, B. Binici, and G. Ozcebe, "Evaluation of the predictive models for stiffness, strength, and deformation capacity of RC frames with masonry infill walls," *Journal of Structural Engineering,* vol. 140, p. 06014003, 2014.

[106]   R. E. Klingner and V. V. Bertero, "Earthquake resistance of infilled frames," *Journal of the structural division,* vol. 104, pp. 973-989, 1978.

[107]   U. Andreaus, M. Cerone, P. D'Asdia, and F. Iannozzi, "A finite element model for the analysis of masonry structures under cyclic actions," in *Proc., 7th Int. Brick Masonry Conf,* vol. 1, pp. 479-488, 1985.

[108] I. Doudoumis and E. Mitsopoulou, "Non-linear analysis of multistorey infilled frames for unilateral contact conditions," in *Proc., 8th European Conf. on Earthquake Engineering*, pp. 63-70, 1986.

[109] P. Soroushian, K. Obaseki, and K.-B. Choi, "Nonlinear modeling and seismic analysis of masonry shear walls," *Journal of Structural Engineering,* vol. 114, pp. 1106-1119, 1988.

[110] E. Abel and JF, "Nonlinear seismic response of infilled steel frames," *Earthquake Engineer 10th World,* vol. 8, p. 4435, 1992.

[111] C. Z. Chrysostomou, "Effects of degrading infill walls on the nonlinear seismic response of two-dimensional steel frames," PhD, Civil Department, Cornell University, 1991.

[112] A. Madan, A. Reinhorn, J. Mander, and R. Valles, "Modeling of masonry infill panels for structural analysis," *Journal of Structural Engineering,* vol. 123, pp. 1295-1302, 1997.

[113] G. Uva, D. Raffaele, F. Porco, and A. Fiore, "On the role of equivalent strut models in the seismic assessment of infilled RC buildings," *Engineering Structures,* vol. 42, pp. 83-94, 2012.

[114] J. Leuchars and J. Scrivener, "Masonry infill panels subjected to cyclic in-plane loading," *Bulletin of the New Zealand National Society for Earthquake Engineering,* vol. 9, pp. 122-131, 1976.

[115] S. Sattar, "Influence of masonry infill walls and other building characteristics on seismic collapse of concrete frame buildings," PhD, Civil Department, University of Colorado at Boulder, 2013.

[116] V. Thiruvengadam, "On the natural frequencies of infilled frames," *Earthquake engineering & structural dynamics,* vol. 13, pp. 401-419, 1985.

[117] F. J. Crisafulli and A. J. Carr, "Proposed macro-model for the analysis of infilled frame structures," *Bulletin of the New Zealand Society for Earthquake Engineering,* vol. 40, pp. 69-77, 2007.

[118] A. Pinto and F. Taucer, "Assessment and retrofit of full-scale models of existing RC frames," *Advances in earthquake engineering for urban risk reduction,* Vol. 66, pp. 353-367, 2006.

[119] P. Asteris, S. Antoniou, D. Sophianopoulos, and C. Chrysostomou, "Mathematical macromodeling of infilled frames: State of the Art," *Journal of Structural Engineering,* vol. 137, pp. 1508-1517, 2011.

[120] H. Rodrigues, H. Varum, and A. Costa, "A non-linear masonry infill macro-model to represent the global behaviour of buildings under cyclic loading," *International Journal of Mechanics and Materials in Design,* vol. 4, pp. 123-135, 2008.

[121] A. Furtado, H. Rodrigues, A. Arede, and H. Varum, "Simplified macro-model for infill masonry walls considering the out-of-plane behaviour," *Earthquake Engineering and Structural Dynamics,* vol. 45, pp. 507-524, 2015.

[122] K. M. Mosalam and S. Günay, "Progressive collapse analysis of reinforced concrete frames with unreinforced masonry infill walls considering in-plane/out-of-plane interaction," *Earthquake Spectra,* vol. 31, pp. 921-943, 2015.

[123] S. Sugano, "Seismic strengthening of existing reinforced concrete buildings in Japan," *Bulletin of the New Zealand National Society for Earthquake Engineering,* vol. 14, pp. 209-222, 1981.

[124] H. Fukuyama and S. Sugano, "Japanese seismic rehabilitation of concrete buildings after the Hyogoken-Nanbu Earthquake," *Cement and Concrete Composites,* vol. 22, pp. 59-79, 2000.

[125] M. Rodriguez and R. Park, "Repair and strengthening of reinforced concrete buildings for seismic resistance," *Earthquake Spectra,* vol. 7, pp. 439-459, 1991.

[126] S. Goel and H. Lee, "Seismic strengthening of RC structures by ductile steel bracing system," *Proc. 4th US NCEE,* Vol. 12, pp. 645-666, 1990.

[127] S. M. Alcocer, "RC frame connections rehabilitated by jacketing," *Journal of Structural Engineering,* vol. 119, pp. 1413-1431, 1993.

[128] CEN (2004). Design of structures for earthquake resistance; Part 1: General Rules, seismic actions and rules for buildings. CEN, Brussels, 2004.

[129] A. Sichko, "Review and Evaluation of Reinforced Concrete Member Retrofit Methods," Master Dessertion, The Ohio State University, 2017.

[130] B. J. Bett, R. E. Klingner, and J. O. Jirsa, "Lateral load response of strengthened and repaired reinforced concrete columns," *Structural Journal,* vol. 85, pp. 499-508, 1988.

[131] M. Rodriguez and R. Park, "Seismic load tests on reinforced concrete columns strengthened by jacketing," *Structural Journal,* vol. 91, pp. 150-159, 1994.

[132] K. G. Vandoros and S. E. Dritsos, "Interface treatment in shotcrete jacketing of reinforced concrete columns to improve seismic performance," *Structural Engineering and Mechanics,* vol. 23, pp. 43-61, 2006.

[133] G. I. Kalogeropoulos and A. G. Tsonos, "Effectiveness of R/C jacketing of substandard R/C columns with short lap splices," *Structural Monitoring and Maintenance,* vol. 1, pp. 273-292, 2014.

[134] CPWD, *HandBook on Repairs and Rehabilitation of RCC Buildings*, First ed.: Director General (Works), Central Public Works Department, Government of India, Nirman Bhawan, 2002.

[135] IS 15988:2013. Seismic Evaluation and Strengthening of Existing Reinforced Concrete Buildings. Bureau of Indian Standards, ManakBhavan, 9 Bahadur Shah ZafarMarg, New Delhi, 2013.

[136] IS 456-2000. Plain and Reinforced Concrete Code of Practice. Bureau of Indian Standards. Fourth Revision, 2000.

[137] J. Aguilar, H. Juarez, R. Ortega, and J. Iglesias, "The Mexico earthquake of September 19, 1985—Statistics of damage and of retrofitting techniques in reinforced concrete buildings affected by the 1985 earthquake," *Earthquake Spectra,* vol. 5, pp. 145-151, 1989.

[138] T. Hayashi, H. Niwa, and M. Fukuhara, "Strengthening methods of the existing reinforced concrete buildings," in *Proceedings of the seventh world conference on earthquake engineering,* pp. 89-97, 1980.

[139] T. D. Bush, C. R. Talton, and J. O. Jirsa, "Behavior of a structure strengthened using reinforced concrete piers," *Structural Journal,* vol. 87, pp. 557-563, 1990.

[140] E. Canbay, U. Ersoy, and G. Ozcebe, "Contribution of reinforced concrete infills to seismic behavior of structural systems," *ACI Structural Journal,* vol. 100, pp. 637-643, 2003.

[141] Ö. Anil and S. Altin, "An experimental study on reinforced concrete partially infilled frames," *Engineering Structures,* vol. 29, pp. 449-460, 2007.

[142] S. Altin, Ö. Anil, and M. E. Kara, "Strengthening of RC nonductile frames with RC infills: An experimental study," *Cement and Concrete Composites,* vol. 30, pp. 612-621, 2008.

[143] H. Kaplan, S. Yilmaz, N. Cetinkaya, and E. Atimtay, "Seismic strengthening of RC structures with exterior shear walls," *Sadhana,* vol. 36, pp. 17-34, 2011.

[144] C. Z. Chrysostomou, M. Poljansek, N. Kyriakides, F. Taucer, and F. J. Molina, "Pseudo-dynamic tests on a full-scale four-storey reinforced concrete frame seismically retrofitted with reinforced concrete infilling," *Structural Engineering International,* vol. 23, pp. 159-166, 2013.

[145]   E. Akın, S. Z. Korkmaz, H. H. Korkmaz, and E. Diri, "Rehabilitation of infilled reinforced concrete frames with thin steel plate shear walls," *Journal of Performance of Constructed Facilities,* vol. 30, p. 04015098, 2016.

[146]   M. Badoux and J. O. Jirsa, "Steel bracing of RC frames for seismic retrofitting," *Journal of Structural Engineering,* vol. 116, pp. 55-74, 1990.

[147]   T. Bush, E. Jones, and J. O. Jirsa, "Behavior of RC frame strengthened using structural steel bracing," *Journal of Structural Engineering,* vol. 117, pp. 1115-1126, 1991.

[148]   M. Maheri and A. Sahebi, "Use of steel bracing in reinforced concrete frames," *Engineering Structures,* vol. 19, pp. 1018-1024, 1997.

[149]   A. Tasnimi and A. Masoomi, "Evaluation of response of reinforced concrete frames strengthened with steel bracing," in *Proceedings of the third international conference on seismology and earthquake engineering*, 1999.

[150]   M. Maheri, R. Kousari, and M. Razazan, "Pushover tests on steel X-braced and knee-braced RC frames," *Engineering Structures,* vol. 25, pp. 1697-1705, 2003.

[151]   T. El-Amoury and A. Ghobarah, "Retrofit of RC frames using FRP jacketing or steel bracing," *Journal of Seismology and Earthquake Engineering,* vol. 7, p. 83, 2005.

[152]   M. Youssef, H. Ghaffarzadeh, and M. Nehdi, "Seismic performance of RC frames with concentric internal steel bracing," *Engineering Structures,* vol. 29, pp. 1561-1568, 2007.

[153]   X. Gao, T. Balendra, and C. Koh, "Buckling strength of slender circular tubular steel braces strengthened by CFRP," *Engineering structures,* vol. 46, pp. 547-556, 2013.

[154]   IS 800-2007. General Construction in Steel-Code of Practice. Bureau of Indian Standards. Third Revision, 2007.

[155]   E. Spacone, F. C. Filippou, and F. F. Taucer, "Fibre beam-column model for non-linear analysis of R/C frames: Part I. Formulation," *Earthquake engineering and structural dynamics,* vol. 25, pp. 711-726, 1996.

[156]   A. J. C. D. Arêde, "Seismic assessment of reinforced concrete frame structures with a new flexibility based element," PhD, Civil Department, Univarsidade de Porto (Portugal), 1997.

[157]   M. H. Scott, G. L. Fenves, F. McKenna, and F. C. Filippou, "Software patterns for nonlinear beam-column models," *Journal of Structural Engineering,* vol. 134, pp. 562-571, 2008.

[158]   H. F. P. Rodrigues, "Biaxial seismic behaviour of reinforced concrete columns," PhD, Civil Department, Universidade de Aveiro (Portugal), 2012.

[159]   H. Rodrigues, H. Varum, A. Arêde, and A. Costa, "Comparative efficiency analysis of different nonlinear modelling strategies to simulate the biaxial response of RC columns," *Earthquake Engineering and Engineering Vibration,* vol. 11, pp. 553-566, 2012.

[160]   M. N. Aydınoğlu and G. Önem, "Evaluation of analysis procedures for seismic assessment and retrofit design," in *Earthquake Engineering in Europe*, ed: Springer, vol. 7, pp. 171-198, 2010.

[161]   R. W. Clough, K. Benuska, and E. Wilson, "Inelastic earthquake response of tall buildings," in *Proceedings, Third World Conference on Earthquake Engineering, New Zealand*, vol. 2, pp. 68-89, 1965.

[162]   C. Coelho, "Análise sísmica de estruturas tridimensionais de edifícios de betão armado," MSc, Departamento de Engenharia civil, FEUP, Porto, 1997.

[163]   K. E. Galal and A. Ghobarah, "Flexural and shear hysteretic behaviour of reinforced concrete columns with variable axial load," *Engineering Structures,* vol. 25, pp. 1353-1367, 2003.

[164]   H. Takizawa and H. Aoyama, "Biaxial effects in modelling earthquake response of R/C structures," *Earthquake Engineering & Structural Dynamics,* vol. 4, pp. 523-552, 1976.

[165]   M. G. Sfakianakis and M. N. Fardis, "Bounding surface model for cyclic biaxial bending of RC sections," *Journal of engineering mechanics,* vol. 117, pp. 2748-2769, 1991.

[166]   A. D'Ambrisi and F. C. Filippou, "Modeling of cyclic shear behavior in RC members," *Journal of Structural Engineering,* vol. 125, pp. 1143-1150, 1999.

[167]   H. Sezen, "Seismic behavior and modeling of reinforced concrete building columns," PhD, Civil Department, University of California, 2004.

[168]   S. Otani, "Inelastic analysis of R/C frame structures," *Journal of the Structural Division,* vol. 100, pp. 1433-49, 1974.

[169]   A. Calabrese, J. P. Almeida, and R. Pinho, "Numerical issues in distributed inelasticity modeling of RC frame elements for seismic analysis," *Journal of Earthquake Engineering,* vol. 14, pp. 38-68, 2010.

[170]   F. Taucer, E. Spacone, and F. C. Filippou, "A fiber beam-column element for seismic response analysis of reinforced concrete structures: *Earthquake Engineering Research Center,*" vol. 91, 1991.

[171]   E. Smyrou, C. Blandon, S. Antoniou, R. Pinho, and F. Crisafulli, "Implementation and verification of a masonry panel model for nonlinear dynamic analysis of infilled RC frames," *Bulletin of Earthquake Engineering,* vol. 9, p. 1519, 2011.

[172]   J. B. Mander, M. J. Priestley, and R. Park, "Theoretical stress-strain model for confined concrete," *Journal of structural engineering,* vol. 114, pp. 1804-1826, 1988.

[173]   J. E. Martínez-Rueda and A. Elnashai, "Confined concrete model under cyclic load," *Materials and Structures,* vol. 30, pp. 139-147, 1997.

[174]   P. Madas and A. Elnashai, "A new passive confinement model for the analysis of concrete structures subjected to cyclic and transient dynamic loading," *Earthquake engineering & structural dynamics,* vol. 21, pp. 409-431, 1992.

[175]   J. B. Mander, B. Nair, K. Wojtkowski, and J. Ma, "An experimental study on the seismic performance of brick-infilled steel frames with and without retrofit," in *Technical Report,* ed: National Center for Earthquake Engineering Research (NCEER), 1993.

[176]   M. Menegotto and P. Pinto, "Method of analysis for cyclically loaded rc frames including changes in geometry and non-elastic behaviour of elements under combined normal force and bending," in *IABSE Congress Reports of the Working Commission,* pp. 15-22, 1973.

[177]   F. Filippou and G. Fenves, "Methods of analysis for earthquake-resistant structures," vol. 6, pp. 6.1-6.65, 2004.

[178]   J. Bauschinger, "Variations in the elastic limit of iron and steel," *J Iron Steel Inst,* vol. 12, pp. 442-444, 1887.

[179]   A. Furtado, H. Rodrigues, A. Arêde, H. Varum, M. Grubišić, and T. K. Šipoš, "Prediction of the earthquake response of a three-storey infilled RC structure," *Engineering Structures,* vol. 171, pp. 214-235, 2018.

[180]   R. Pinho and A. Elnashai, "Dynamic collapse testing of a full-scale four storey RC frame," *ISET Journal of earthquake Technology,* vol. 37, pp. 143-163, 2000.

[181]   H. Rodrigues, A. Furtado, N. Vila-Pouca, H. Varum, and A. R. Barbosa, "Seismic assessment of a school building in Nepal and analysis of retrofitting solutions," *International Journal of Civil Engineering,* pp. 1-17, 2018.

[182]   A. S. Elnashai and L. Di Sarno, *Fundamentals of earthquake engineering:* Wiley New York, 2008.

[183] H. Krawinkler and G. Seneviratna, "Pros and cons of a pushover analysis of seismic performance evaluation," *Engineering structures,* vol. 20, pp. 452-464, 1998.

[184] A. S. Elnashai, "Do we really need inelastic dynamic analysis?," *Journal of Earthquake Engineering,* vol. 6, pp. 123-130, 2002.

[185] S. Antoniou and R. Pinho, "Development and verification of a displacement-based adaptive pushover procedure," *Journal of Earthquake Engineering,* vol. 8, pp. 643-661, 2004.

[186] V. K. Papanikolaou and A. S. Elnashai, "Evaluation of conventional and adaptive pushover analysis I: Methodology," *Journal of Earthquake Engineering,* vol. 9, pp. 923-941, 2005.

[187] A. S. Elnashai, "Advanced inelastic static (pushover) analysis for earthquake applications," *Structural engineering and mechanics,* vol. 12, pp. 51-70, 2001.

[188] A. K. Chopra and R. K. Goel, "A modal pushover analysis procedure for estimating seismic demands for buildings," *Earthquake Engineering & Structural Dynamics,* vol. 31, pp. 561-582, 2002.

[189] C. Casarotti and R. Pinho, "An adaptive capacity spectrum method for assessment of bridges subjected to earthquake action," *Bulletin of Earthquake Engineering,* vol. 5, p. 377, 2007.

[190] K. Shakeri, M. A. Shayanfar, and T. Kabeyasawa, "A story shear-based adaptive pushover procedure for estimating seismic demands of buildings," *Engineering structures,* vol. 32, pp. 174-183, 2010.

[191] D. Vamvatsikos and C. A. Cornell, "Incremental dynamic analysis," *Earthquake Engineering & Structural Dynamics,* vol. 31, pp. 491-514, 2002.

[192] L. Macedo, M. Araújo, and J. Castro, "Assessment and calibration of the Harmony Search algorithm for earthquake record selection," in *Proceedings of the Vienna Congress on Recent Advances in Earthquake Engineering and Structural Dynamics*, 2013.

[193] T. D. Ram and G. Wang, "Probabilistic seismic hazard analysis in Nepal," *Earthquake Engineering and Engineering Vibration,* vol. 12, pp. 577-586, 2013.

[194] S. Shrestha, "Probabilistic seismic hazard analysis of Kathmandu city, Nepal," *International Journal of Engineering Research and General Science,* vol. 2, pp. 24-33, 2014.

[195] B. Subedi and H. R. Parajuli, "Probabilistic seismic hazard analysis of Nepal," in *Proceedings of IOE Graduate Conference*, pp. 265-270, 2016.

[196] P. Ricci, M. T. De Risi, G. M. Verderame, and G. Manfredi, "Procedures for calibration of linear models for damage limitation in design of masonry-infilled RC frames," *Earthquake Engineering & Structural Dynamics,* vol. 45, pp. 1315-1335, 2016.

[197] F. Khoshnoudian and M. Poursha, "Responses of three dimensional buildings under bi-directional and unidirectional seismic excitations," in *Proceedings of the 13th World Conference on Earthquake Engineering*, paper no. 55, pp. 1-6, 2004.

[198] O. A. Lopez, A. K. Chopra, and J. J. Hernandez, "Critical response of structures to multicomponent earthquake excitation," *Earthquake engineering & structural dynamics,* vol. 29, pp. 1759-1778, 2000.

[199] A. Ghobarah, "On drift limits associated with different damage levels," in *International workshop on performance-based seismic design*, pp. 321-332, 2004.

[200] FEMA-273 (1997). NEHRP guidelines for the seismic rehabilitation of buildings. Report No. FEMA 273. Federal Emergency Management Agency, Washington D.C., USA, 1997.

[201] SEAOC (1995). Vision 2000, Performance based seismic engineering ofbuildings, vols. I and II: Conceptual framework. Sacramento(CA): Structural Engineers Association of California, 1995.

[202] T. Rossetto and A. Elnashai, "Derivation of vulnerability functions for European-type RC structures based on observational data," *Engineering structures,* vol. 25, pp. 1241-1263, 2003.

[203] L. F. Ibarra and H. Krawinkler, *Global collapse of frame structures under seismic excitations*: Pacific Earthquake Engineering Research Center Berkeley, CA, report no. 152, 2005.

[204] A. B. Liel, "Assessing the collapse risk of California's existing reinforced concrete frame structures: metrics for seismic safety decisions," PhD, Civil Department, Stanford University, 2008.

[205] J. W. Baker, "Efficient analytical fragility function fitting using dynamic structural analysis," *Earthquake Spectra,* vol. 31, pp. 579-599, 2015.

[206] R. Kennedy and M. Ravindra, "Seismic fragilities for nuclear power plant risk studies," *Nuclear Engineering and Design,* vol. 79, pp. 47-68, 1984.

[207] G. M. Calvi, R. Pinho, G. Magenes, J. J. Bommer, L. F. Restrepo-Vélez, and H. Crowley, "Development of seismic vulnerability assessment methodologies over the past 30 years," *ISET journal of Earthquake Technology,* vol. 43, pp. 75-104, 2006.

[208] K. Porter, R. Kennedy, and R. Bachman, "Creating fragility functions for performance-based earthquake engineering," *Earthquake Spectra,* vol. 23, pp. 471-489, 2007.

[209] J. E. Padgett and R. DesRoches, "Methodology for the development of analytical fragility curves for retrofitted bridges," *Earthquake Engineering & Structural Dynamics,* vol. 37, pp. 1157-1174, 2008.

[210] R. J. Allemang, "The modal assurance criterion–twenty years of use and abuse," *Sound and vibration,* vol. 37, pp. 14-23, 2003.

[211] S. Taghavi and E. Miranda, "Response assessment of nonstructural building elements," Pacific Earthquake Engineering Research Center, 2003.

[212] E. Júlio, F. Branco, and V. Silva, "Structural rehabilitation of columns with reinforced concrete jacketing," *Progress in Structural Engineering and Materials,* vol. 5, pp. 29-37, 2003.

[213] A. B. Liel, C. B. Haselton, and G. G. Deierlein, "Seismic collapse safety of reinforced concrete buildings. II: Comparative assessment of nonductile and ductile moment frames," *Journal of Structural Engineering,* vol. 137, pp. 492-502, 2010.

[214] N. P. Commission, "Nepal earthquake 2015: Post disaster needs assessment," *Vol. A: Key Findings. Government of Nepal, National Planning Commission,* 2015.

[215] J. Moehle, "A Framework for Performance-Based Earthquake Engineering. ATC-15-9, Workshop on the Improvement of Building Structural Design and Construction Practices," paper no. 679, 2003.

[216] FEMA-227 (1992). A benefit-cost model for the seismic rehabilitation of buildings. Federal Emergency Management Agency, Washington D.C., USA, 1992.

[217] ATC-40, (1996). Seismic Evaluation and Retrofit of Concrete Buildings. Applied Technical Council, California Seismic Safety Commission, Redwood City, California, 1996.

[218] FEMA-356 (2000). Pre-standard and commentary for the seismic rehabilitation of buildings. Federal Emergency Management Agency, Washington D.C., USA, 2000.

[219] M. C. Comerio, J. C. Stallmeyer, R. Smith, N. Makris, D. Konstantinidis, K. Mosalam*, et al.,* "PEER testbed study on a laboratory building: exercising seismic performance assessment," *PEER Report 2005/12,* 2005.

[220] J. J. Bommer and N. A. Abrahamson, "Why do modern probabilistic seismic-hazard analyses often lead to increased hazard estimates?," *Bulletin of the Seismological Society of America,* vol. 96, pp. 1967-1977, 2006.

[221] T. Lee and K. Mosalam, "Probabilistic seismic evaluation of reinforced concrete structural components and systems. Report 2006/04, Pacific Earthquake Engineering Research Center," *University of California, Berkeley, USA Google Scholar,* 2006.

[222] J. Mitrani-Reiser, C. Haselton, C. Goulet, K. Porter, J. Beck, and G. Deierlein, "Evaluation of the seismic performance of a code-conforming reinforced-concrete frame building-Part II: Loss estimation," in *8th National Conference on Earthquake Engineering (100th Anniversary Earthquake Conference)*, , pp. 18-22, 2006.

[223] H. A. Rojas, C. Foley, and S. Pezeshk, "Risk-based seismic design for optimal structural and nonstructural system performance," *Earthquake Spectra,* vol. 27, pp. 857-880, 2011.

[224] S. Günay and K. M. Mosalam, "PEER performance-based earthquake engineering methodology, revisited," *Journal of Earthquake Engineering,* vol. 17, pp. 829-858, 2013.

[225] H. Aslani and E. Miranda, "Probabilistic earthquake loss estimation and loss disaggregation in buildings," report no. 157, Stanford University Stanford, CA, 2005.

[226] S. B. Erdurmuş, "Benefit-cost analysis for retrofitting of selected residential buildings in Istanbul," Master Thesis, Middle East Technical University, 2005.

[227] M. Tonekaboni, "Probabilistic based economic feasibility assessment of seismic retrofit methods for structures," *ARPN Journal of Engineering and Applied Sciences*, vol. 9, pp. 2057-2063, 2006.

[228] C. M. Ramirez, "Building-specific loss estimation methods & tools for simplified performance-based earthquake engineering," report no. 171, Stanford University, 2009.

[229] J. E. Padgett, K. Dennemann, and J. Ghosh, "Risk-based seismic life-cycle cost–benefit (LCC-B) analysis for bridge retrofit assessment," *Structural Safety,* vol. 32, pp. 165-173, 2010.

[230] C. Ramirez, A. Liel, J. Mitrani-Reiser, C. Haselton, A. Spear, J. Steiner*, et al.*, "Expected earthquake damage and repair costs in reinforced concrete frame buildings," *Earthquake Engineering & Structural Dynamics,* vol. 41, pp. 1455-1475, 2012.

[231] A. B. Liel and G. G. Deierlein, "Cost-benefit evaluation of seismic risk mitigation alternatives for older concrete frame buildings," *Earthquake Spectra,* vol. 29, pp. 1391-1411, 2013.

[232] J.-W. Bai, M. B. D. Hueste, and P. Gardoni, "Case study: Scenario-based seismic loss estimation for concrete buildings in Mid-America," *Earthquake Spectra,* vol. 30, pp. 1585-1599, 2014.

[233] D. Cardone and G. Perrone, "Damage and loss assessment of pre-70 RC frame buildings with FEMA P-58," *Journal of Earthquake Engineering,* vol. 21, pp. 23-61, 2017.

[234] M. Dyanati, Q. Huang, and D. Roke, "Cost-benefit evaluation of self-centring concentrically braced frames considering uncertainties," *Structure and Infrastructure Engineering,* vol. 13, pp. 537-553, 2017.

[235] M. Dyanati, Q. Huang, and D. Roke, "Sensitivity analysis of seismic performance assessment and consequent impacts on loss analysis," *Bulletin of Earthquake Engineering,* vol. 15, pp. 4751-4790, 2017.

[236] D. Cardone, G. Gesualdi, and G. Perrone, "Cost-benefit analysis of alternative retrofit strategies for RC frame buildings," *Journal of Earthquake Engineering,* pp. 1-34, 2017.

[237] L. Sousa and R. Monteiro, "Seismic retrofit options for non-structural building partition walls: Impact on loss estimation and cost-benefit analysis," *Engineering Structures,* vol. 161, pp. 8-27, 2018.

[238] J. W. Baker and C. A. Cornell, "Uncertainty propagation in probabilistic seismic loss estimation," *Structural Safety,* vol. 30, pp. 236-252, 2008.

[239] C. A. Cornell, "Engineering seismic risk analysis," *Bulletin of the seismological society of America,* vol. 58, pp. 1583-1606, 1968.

[240] B. Gutenberg, *Seismicity of the earth and associated phenomena*: Read Books Ltd, 2013.

[241] J.-W. Bai, M. B. D. Hueste, and P. Gardoni, "Probabilistic assessment of structural damage due to earthquakes for buildings in Mid-America," *Journal of structural engineering,* vol. 135, pp. 1155-1163, 2009.

[242] K. A. Porter, "An overview of PEER's performance-based earthquake engineering methodology," in *Proceedings of ninth international conference on applications of statistics and probability in civil engineering,* 2003.

[243] X. Romão, R. Delgado, and A. Costa, "Probabilistic performance analysis of existing buildings under earthquake loading," *Journal of Earthquake Engineering,* vol. 18, pp. 1241-1265, 2014.

[244] ATC-13 (1985). Earthquake Damage Evaluation Data for California, Applied Technical Council, California Seismic Safety Commission, Redwood City, California, 1985.

[245] Y.-J. Kang and Y. Wen, "Minimum life-cycle cost structural design against natural hazards," University of Illinois Engineering Experiment Station, retrieved from http://hdl.handle.net/2142/14245, 2000.

[246] R. M. Company, *Square foot costs*: RS Means Company, 2003.

[247] K. A. Porter, J. L. Beck, R. V. Shaikhutdinov, S. K. Au, K. Mizukoshi, M. Miyamura*, et al.,* "Effect of seismic risk on lifetime property value," *Earthquake Spectra,* vol. 20, pp. 1211-1237, 2004.

[248] B. R. Ellingwood and Y. K. Wen, "Risk-benefit-based design decisions for low-probability/high consequence earthquake events in Mid-America," *Progress in Structural Engineering and Materials,* vol. 7, pp. 56-70, 2005.

[249] F. Jalayer and C. A. Cornell, "A technical framework for probability-based demand and capacity factor (DCFD) seismic formats," 2003.

[250] J. Mitrani-Reiser and J. Beck, "Incorporating losses due to repair costs, downtime and fatalities in probabilistic-based earthquake engineering," *Proceedings, Computational Methods in Structural Dynamics and Earthquake Engineering,* 2007.

[251] FEMA-227 (1992). A benefit-cost model for the seismic rehabilitation of buildings. Federal Emergency Management Agency, Washington D.C., USA, 1992.

[252] H. O. Wood and F. Neumann, "Modified Mercalli intensity scale of 1931," *Bulletin of the Seismological Society of America,* vol. 21, pp. 277-283, 1931.

[253] FEMA 58-1 (2012) Seismic performance assessment of buildings (volume 1-Methodology)," *Federal Emergency Management Agency, Washington,* 2012.

[254] A. J. Kappos and E. Dimitrakopoulos, "Feasibility of pre-earthquake strengthening of buildings based on cost-benefit and life-cycle cost analysis, with the aid of fragility curves," *Natural Hazards,* vol. 45, pp. 33-54, 2008.

[255] A. K. Eleftheriadou and A. I. Karabinis, "Development of damage probability matrices based on Greek earthquake damage data," *Earthquake Engineering and Engineering Vibration,* vol. 10, pp. 129-141, 2011.

[256]   A. K. Eleftheriadou and A. I. Karabinis, "Correlation of structural seismic damage with fundamental period of RC buildings," *Open Journal of Civil Engineering,* vol. 3, p. 45, 2013.

[257]   FEMA-99 (1999). HAZUS Technical manual. Federal Emergency Management Agency, Washington D.C., USA, 1999.

[258]   J. Schwarz, M. Raschke, and H. Maiwald, "Seismic risk studies for Central Germany on the basis of the European Macroseismic Scale EMS-98," in *Proc. 12th European Conference on Earthquake Engineering*, paper no. 295, 2002.

[259]   E. Planning Protection Organization (EPPO), "*Guidelines and Forms for Immediate Post-Earthquake Screening of Reinforced Concrete Buildings (in Greek),*" *Athens,* 1997.

[260]   S. T. Algermissen, W. Rinehart, and J. W. Dewey, *A study of earthquake losses in the San Francisco Bay Area: Data and analysis*: US Department of Commerce, National Oceanic & Atmospheric Administration. Environmental Research Laboratories, 1972.

[261]   R. V. Whitman, J. W. Reed, and S. Hong, "Earthquake damage probability matrices," in *Proceedings of the Fifth World conference on earthquake engineering*, , pp. 2531-2540, 1973.

[262]   Y.-J. Park and A. H.-S. Ang, "Mechanistic seismic damage model for reinforced concrete," *Journal of structural engineering,* vol. 111, pp. 722-739, 1985.

[263]   S. K. V. Gunturi, "Building-specific earthquake damage estimation," PhD, Civil Department, Stanford university, 1993.

[264]   F. Zareian and H. Krawinkler, "Simplified performance-based earthquake engineering," report no. 169, Stanford University Stanford, CA, USA, 2006.

[265]   J. Mitrani-Reiser, "An ounce of prevention: Probabilistic loss estimation for performance-based earthquake engineering," PhD, Civil Department, California Institute of Technology, 2007.

[266]   FEMA-443 (2003). HAZUS-MH 2.1 Technical Manual. Federal Emergency Management Agency, Washington D.C., USA, 2003.

[267]   Interest rate in Nepal. Retrieved from https://tradingeconomics.com/nepal/interest-rate

[268]   Interest rate in Nepal Investment Bank Ltd. Retrieved from https://nibl.com.np/index.php?option=com_content&view=article&id=48&Itemid=32.

[269]   H. Chaulagain, H. Rodrigues, E. Spacone, and H. Varum, "Seismic safety assessment of existing masonry infill structures in Nepal," *Earthquake Engineering and Engineering Vibration,* vol. 15, pp. 251-268, 2016.